

Applications of Fluorinated Aryl Boronates in Organic Synthesis

Dissertation zur Erlangung des naturwissenschaftlichen Doktorgrades
der Julius-Maximilians-Universität Würzburg

vorgelegt von

Yudha Prawira Budiman

aus Bandung, Indonesia

Würzburg 2020



Eingereicht bei der Fakultät für Chemie und Pharmazie am

Gutachter der schriftlichen Arbeit

1. Gutachter: Prof. Dr. Dr. h. c. Todd B. Marder
2. Gutachter: Prof. Dr. Udo Radius

Prüfer des öffentlichen Promotionskolloquiums

1. Prüfer: Prof. Dr. Dr. h. c. Todd B. Marder
2. Prüfer: Prof. Dr. Udo Radius
3. Prüfer: Prof. Dr. Dirk G. Kurth

Datum des öffentlichen Promotionskolloquiums

Doktorurkunde ausgehändigt am

Die Experimente zur vorliegenden Arbeit wurden in der Zeit von Oktober 2016 bis September 2020 am Institut für Anorganische Chemie der Julius-Maximilians-Universität Würzburg unter der Aufsicht von Prof. Dr. Dr. h. c. Todd B. Marder und Prof. Dr. rer. nat. habil. Udo Radius durchgeführt.

Acknowledgements

First and foremost, I would like to thank Allah for the helps during all my life and for giving me the power to finish this dissertation.

I would like to express my deepest thanks to my supervisors, Profs. Todd Marder and Udo Radius who have accepted me to join their group researches and guided me to finish this dissertation. In term of guidance, both my supervisors have patiently checked the various draft manuscripts, correcting the language, and gave me stylistic suggestions to make my dissertation into the final shape. Along with both supervisors, deepest thanks also addressed to Prof. Dr. Stephen Westcott who had patiently corrected the Chapter 1 into final shape. Special thanks to Dr. Arumugam Jayaraman my collaborator for the DFT calculation and for the patience in discussion thus led the Chapter 3 into final shape and has been published. All those helps made all parts of the dissertation have been submitted and/or published in some leading journals.

Special thanks to Dr. Alexandra Friedrich and Dr. Florian Kerner for measuring the crystal structures and solving the problems. I gratefully acknowledge Dr. Alexandra Friedrich and Dr. Krzysztof Radacki for teaching the crystallography courses to me. Thanks also to Dr. Rüdiger Bertermann and Marie-Luise Schäfer for their kind helps with NMR spectroscopy, and Sabine Timmroth and Liselotte Michels for the elemental analysis measurements. Special thanks also addressed to Julia Merz, who did German translation of the summary and Sabine Lorenzen who synthesized some stocks of useful metal catalysts. Great thanks addressed to Zhiqiang Liu, who has the most similarity topic with me in the group and had spent times making some starting materials together.

I would like to gratefully acknowledge Dr. Laura Kuehn, Dr. Florian Kerner, Dr. Maximilian Kuntze-Fechner for the introduction and gave some training to work in the institute in the beginning of my study. Thanks also to Christoph Mahler and Robert Ricker for the HRMS analysis of my countless samples. Thanks to Dr. Julia Merz, Dr. Florian Kerner, Dr. Yaming Tian, and Dr. Florian

Acknowledgements

Rauch for the discussion and suggestion how to deal with a dissertation submission. Special thanks to Dr. Ying-Ying Chia, who picked me in the train station when I firstly arrived in Wuerzburg. Dr. Chia was helping me to find an apartment and showed the city for the first time! Thanks to Maria Eckhardt the secretary of Prof. Marder for carrying many of my administration documents with patience. Also great thanks to Hildegard Holzinger for taking my chemical order requests with patience. Thanks to my other friendly colleagues in the group during the above times : Dr. Wenbo Ming, Dr. Xiaoning Guo, Dr. Xiaocui Liu, Mingming Huang, Jan Maier, Zhu Wu, Johannes Krebs, Jiang He, Matthias Ferger, Sarina Berger, Dr. Goutam Kumar Kole, Dr. Jörn Nitsch, Dr. Shishir Ghosh, Dr. Stephanie Griesbeck, Dr. Xiangqing Jia, and Prof. Xiaoling Luo.

Very important to be mentioned, I also gratefully acknowledge my wife, Elok Wulandari, who has been extremely supportive throughout my PhD study. Along with her I want to acknowledge my two sons, Abdurrahman and Ibrahim who support me through their own ways and make my entire life more colorful and meaningful. I am proud of having sons! Very very special thanks I give to my Dad and Mom, who give unlimited support to me.

Lastly, I gratefully acknowledge the Indonesia Endowment Fund for Education (LPDP) for the scholarship and their funding through 4 years and 3 months. Thanks also to the Indonesian Society in Würzburg city for their supports, helps, and social activities during my life in Würzburg.

List of Publications

The publications listed below are reproduced in this dissertation with permission from American Chemical Society and Wiley-VCH. The table itemizes at which position in this work the paper has been reproduced.

Publication	Position
Y. P. Budiman, S. A. Westcott*, U. Radius*, T. B. Marder*, <i>Adv. Synth. Catal.</i> Submitted.	Chapter 1
Y. P. Budiman, A. Friedrich, U. Radius*, T. B. Marder*, <i>ChemCatChem</i> 2019 , <i>11</i> , 5387–5396.	Chapter 2
Y. P. Budiman, A. Jayaraman, A. Friedrich, F. Kerner, U. Radius*, T. B. Marder*, <i>J. Am. Chem. Soc.</i> 2020 , <i>142</i> , 6036–6050.	Chapter 3
Y. P. Budiman, S. Lorenzen, Z. Liu, U. Radius*, T. B. Marder*. <i>Chem. Eur. J.</i> Submitted.	Chapter 4

Further publications:

1. W. Ming, X. Liu, A. Friedrich, J. Krebs, Y. P. Budiman, M. Huang, T. B. Marder*, *Green Chem.* **2020**, *22*, 2184–2190.
2. Z. Liu, Y. P. Budiman, Y. Tian, A. Friedrich, S. A. Westcott, U. Radius*, T. B. Marder*, *Chem. Eur. J.* **2020**, DOI: 10.1002/chem.20200288

List of Abbreviations

aq	Aqueous
B ₂ (OH) ₄	Tetrahydroxydiboron
B ₂ pin ₂	Bis(pinacolato)diboron
bpy	2,2'-Bipyridine
cod	1,5-Cyclooctadiene
CyJohnPhos	2-(Dicyclohexylphosphino)biphenyl
DABCO	1,4-Diazabicyclo[2.2.2]octane
dan	1,8-Diaminonaphthalene
DavePhos	2-Dicyclohexylphosphino-2'-(<i>N,N</i> -dimethylamino)biphenyl
dba	Dibenzylideneacetone
DCM	Dichloromethane
DFT	Density functional theory
DMAP	4-Dimethylaminopyridine
DMF	<i>N,N</i> -Dimethylformamide
DMSO	Dimethyl sulfoxide
dppf	1,1'-Bis(diphenylphosphino)ferrocene
dppp	1,3-Bis(diphenylphosphino)propane
dtbpy	4,4'-Di- <i>tert</i> -butyl-2,2'-dipyridyl
EDA	Energy decomposition analysis
Et ₃ N	Triethylamine
EtOAc	Ethyl acetate
equiv	Equivalents
GC-MS	Gas chromatography-mass spectrometry
HPLC	High-performance liquid chromatography
HRMS	High-resolution mass spectrometry
ICy	1,3-Dicyclohexylimidazol-2-ylidene

List of Abbreviations

IMes	1,3-Dimesitylimidazol-2-ylidene
IPr	1,3-Bis(2,6-diisopropylphenyl)imidazol-2-ylidene
JohnPhos	2-(Di- <i>tert</i> -butylphosphino)biphenyl
KO <i>t</i> -Bu	Potassium <i>tert</i> -butoxide
LED	Light-emitting diode
Me ₂ Im	1,3-dimethylimidazolidine-2-ylidene
MeCN	Acetonitrile
MIDA	Trivalent <i>N</i> -methyliminodiacetic acid
MOF	Metal-organic frameworks
MTBE	Methyl <i>tert</i> -butyl ether
NHC	<i>N</i> -Heterocyclic carbene
NMR	Nuclear magnetic resonance
NOCV	Natural orbitals for chemical valence
P(<i>o</i> -tol) ₃	Tris(<i>o</i> -tolyl)phosphine
P(OEt) ₃	Triethoxyphosphine
PCy ₃	Tricyclohexylphosphine
PMe ₃	Trimethylphosphine
PN	<i>o</i> -(di- <i>tert</i> -butylphosphino)- <i>N,N</i> -dimethylaniline
PPh ₃	Triphenylphosphine
P <i>t</i> Bu ₃	Tri- <i>tert</i> -butylphosphine
Q-Phos	1,2,3,4,5-Pentaphenyl-1'-(di- <i>tert</i> -butylphosphino)ferrocene
rt	Room temperature
SMe ₂	Dimethyl sulfide
SPhos	2-Dicyclohexylphosphino-2',6'-dimethoxybiphenyl
TET	Triplet energy transfer
TFA	Trifluoroacetic acid
THF	Tetrahydrofuran

List of Abbreviations

XantPhos	4,5-Bis(diphenylphosphino)-9,9-dimethylxanthene
XPhos	2-Dicyclohexylphosphino-2',4',6'-triisopropylbiphenyl

Table of Contents

1 Fluorinated Aryl Boronates as Building Blocks in Organic Synthesis.....	2
1.1 Abstract	2
1.2 Introduction	2
1.3 Synthesis of Fluorinated Aryl Boronates	5
1.3.1 Traditional Methods	5
1.3.2 Catalytic C–H Borylation	6
1.3.3 Catalytic C–F Borylation.....	16
1.3.4 Catalytic C–X Activation (X = Cl, Br, I, OTf)	22
1.4 Protodeboration of Fluorinated Aryl Boronates	25
1.5 Applications of Fluorinated Aryl Boronates in Organic Synthesis	31
1.5.1 Intermediates for the Introduction of Functional Groups	31
1.5.2 Homocoupling Reaction	42
1.5.3 Suzuki-Miyaura Cross-Coupling	45
1.5.4 C–N Cross-Coupling	60
1.5.5 C–O Cross-Coupling	64
1.5.6 C–C(O) Cross-Coupling	65
1.5.7 C–C(alkyne) Cross-Coupling	69
1.6 Conclusion and Perspective	71
1.7 References	73
2 Copper-Catalyzed Suzuki-Miyaura Cross-Coupling of Highly Fluorinated Aryl Boronate Esters with Aryl Iodides and Bromides and Fluoroarene-Arene π -Stacking Interactions in the Products .	84
2.1 Abstract	84

Table of Contents

2.2 Introduction	84
2.3 Result and Discussion	88
2.3.1 Optimization of Reaction Conditions	88
2.3.2 Investigation of Reaction Scope	91
2.3.3 Gram Scale Reaction	95
2.3.4 Molecular and Crystal Structures: Intermolecular $\pi \cdots \pi$ Stacking Interactions	95
2.4 Conclusions	100
2.5 Detailed Experiments and Characterization Data	101
2.5.1 General Information	101
2.5.2 Synthesis and Characterization of Pentafluorophenyl Boronic Acid Pinacol Ester	102
2.5.3 General Procedure for Suzuki-Miyaura Cross-Coupling Reactions.....	103
2.5.4 Competition Reaction of 4-Iodotoluene and 4-Iodobenzotrifluoride	103
2.5.5 Gram Scale Reaction Procedure: Synthesis and Characterization Data of 2,3,3',4,4',5,5',6-Octafluoro Biphenyl (2_3p)	104
2.5.6 Experimental Procedures and Characterization of Products	105
2.5.7 Single-Crystal X-ray Diffraction Data.....	124
2.6 References	126
3 Palladium-Catalyzed Homocoupling of Highly Fluorinated Aryl Boronates: Studies of the Influence of Strongly vs. Weakly Coordinating Solvents on the Reductive Elimination Process .	134
3.1 Abstract	134
3.2 Introduction	134
3.3 Results and Discussion	138
3.3.1 Experimental Studies.....	138

Table of Contents

3.3.2 Crystal and Molecular Structures of the Fluorinated Biaryl Products: Intermolecular $\pi \cdots \pi$ Stacking Interactions.	145
3.3.3 Computational Studies.....	148
3.3.4 Catalytic Cycle of the Homocoupling Reaction.....	162
3.4 Conclusions	163
3.5 Detailed Experiments and Characterization Data	164
3.5.1 General Information	164
3.5.2 Synthesis of <i>cis</i> -[Pd(MeCN) ₂ (C ₆ F ₅) ₂] (3_3a).....	166
3.5.3 Synthesis of <i>cis</i> -[Pd(MeCN) ₂ (2,4,6-C ₆ F ₃ H ₂) ₂] (3_3b)	167
3.5.4 Synthesis of <i>cis</i> -[Pd(MeCN) ₂ (2,6-C ₆ F ₂ H ₃) ₂] (3_3e).....	168
3.5.5 General Procedure for Homocoupling of Fluorinated Aryl Boronic Acid Pinacol Esters (ArF _n -Bpin)	169
3.5.6 Experimental Procedures and Characterization of Products	169
3.5.7 A Test for the Possibility of C–F Oxidative Addition.....	174
3.5.8 Single Crystal X-ray Diffraction Data	176
3.6 Detailed Description of Computational Details	178
3.6.1 Computational Details	178
3.6.2 EDA-NOCV Analysis Results.....	179
3.7 References	190
4 Base-Free Pd-Catalyzed C–Cl Borylation of Fluorinated Aryl Chlorides	198
4.1 Abstract	198
4.2 Introduction	198
4.3 Results and Discussion	201

Table of Contents

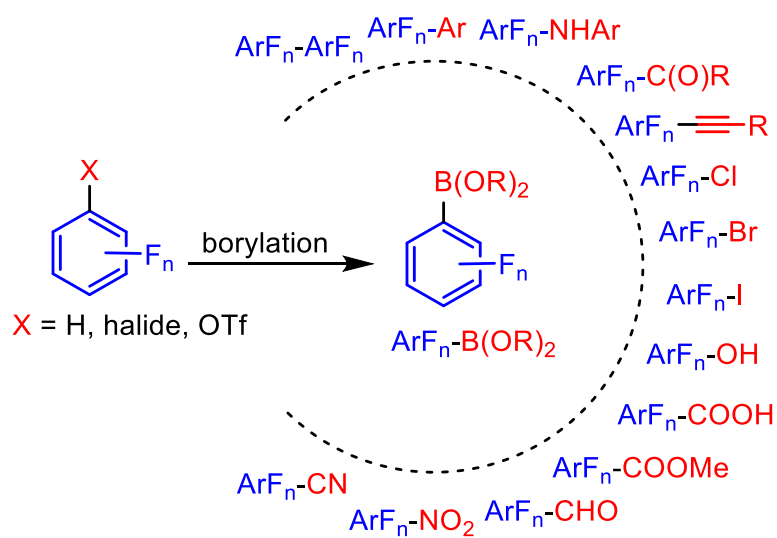
4.4 Conclusions	206
4.5 Detailed Experiments and Characterization Data	207
4.5.1 General Information	207
4.5.2 General Procedure for Pd-Catalyzed C–Cl Borylation	208
4.5.3 Characterization (GC-MS, NMR and HRMS data) of Products	208
4.6 References	212
5 Summary	216
Chapter 1	216
Chapter 2	217
Chapter 3	219
Chapter 4	222
6 Zusammenfassung	224
Kapitel 1	224
Kapitel 2	225
Kapitel 3	227
Kapitel 4	230
7. Appendix	233
7.1 NMR Spectra for Chapter 2	234
7.2 NMR Spectra for Chapter 3	305
7.3 XYZ Coordinates for Chapter 3	336
7.4 NMR Spectra for Chapter 4	396
Permission of Wiley-VCH	420
Permission of American Chemical Society	421

Table of Contents

Affidavit	423
Eidesstaatliche Erklärung	423

Chapter 1

Fluorinated Aryl Boronates as Building Blocks in Organic Synthesis



1 Fluorinated Aryl Boronates as Building Blocks in Organic Synthesis

1.1 Abstract

Organoboron compounds are well known building blocks for many organic reactions. However, under basic conditions, polyfluorinated aryl boronic acid derivatives suffer from instability issues that are accelerated in compounds containing an *ortho*-fluorine group, which result in the formation of the corresponding protodeboronation products. Therefore, a considerable amount of research has focused on novel methodologies to synthesize these valuable compounds while avoiding the protodeboronation issue. This review summarizes the latest developments in the synthesis of fluorinated aryl boronic acid derivatives and their applications in cross-coupling reactions and other transformations.

1.2 Introduction

Interest in fluorinated organic compounds has increased in recent years as these remarkable compounds have a vast array of important applications, including but not limited to, material science, pharmaceutical and agricultural chemistry, specialty chemical industries, and catalysis. Indeed, fluorine-containing organic molecules constitute one-third of the pharmaceuticals on the market today.^[1-8] To the best of our knowledge, there are no known examples of naturally occurring aryl fluorides; therefore, these molecules must be accessed through chemical synthesis. The integration of fluorine groups has several physiological advantages such as decreased metabolism, solubility (deliverability), hydrophobicity and decreased negative side effects. For example, the fluoroarene-containing molecules Vemuravenib (Figure 1-1, left) and Sitagliptin (Figure 1-1, right) are used for the treatment of late-stage of melanoma and diabetes, respectively.^[1] Some fluorinated organic and

fluorinated organometallic compounds have also shown promise as antiproliferative agents against HT29 (colon carcinoma) and MCF-7 (breast adenocarcinoma).^[9] Fluorine-containing organic compounds have also shown tremendous potential in other areas of science and industry as polyfluorobiphenyls show significant promise for use in organic light emitting diodes (Figure 1-2),^[10-13] electron-transport materials (Figure 1-3),^[14] crystal engineering,^[15-17] metal-organic frameworks (MOFs),^[18] supramolecular chemistry,^[21] and low-dimensional semi-conducting materials (Figure 1-4).^[20,21] As such, there is a growing demand for the development of novel synthetic methodologies for the generation of these valuable compounds.^[22,23]

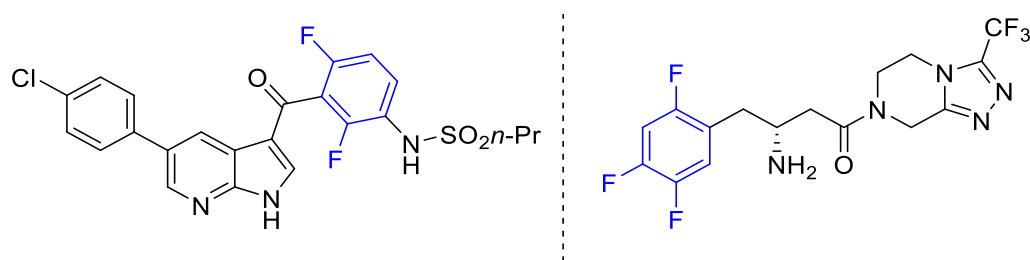


Figure 1-1. Fluoroarene-containing drugs: Vemurafenib (left) used for treatment of late-stage of melanoma. Sitagliptin (right) is used in the treatment of diabetes.^[1]

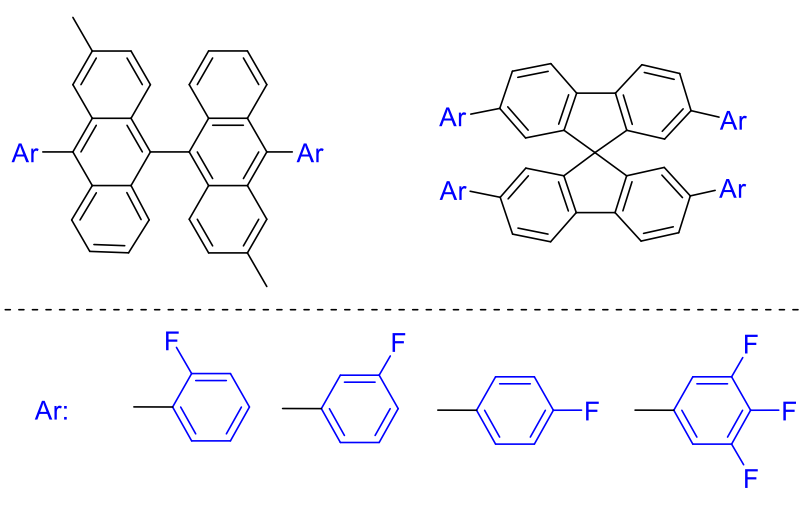


Figure 1-2. Fluoroarenes in materials science I: Fluorinated 3,3'-dimethyl-9,9'-bianthracene (left) and 9,9'-spirobifluorenes (right) derivatives for OLEDs.^[13]

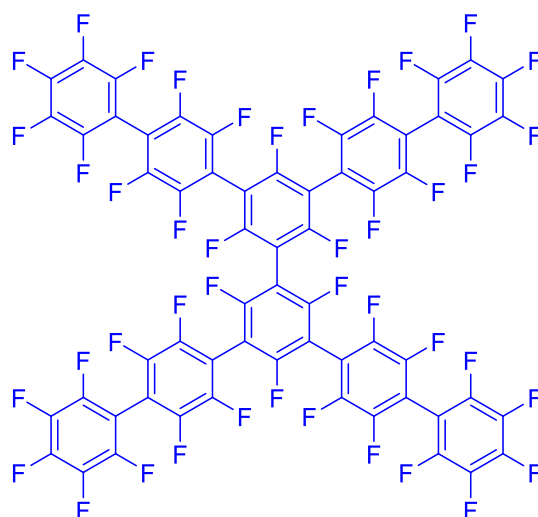


Figure 1-3. Fluoroarenes in materials science II: perfluorinated phenylene dendrimers for electron transport materials.^[14]

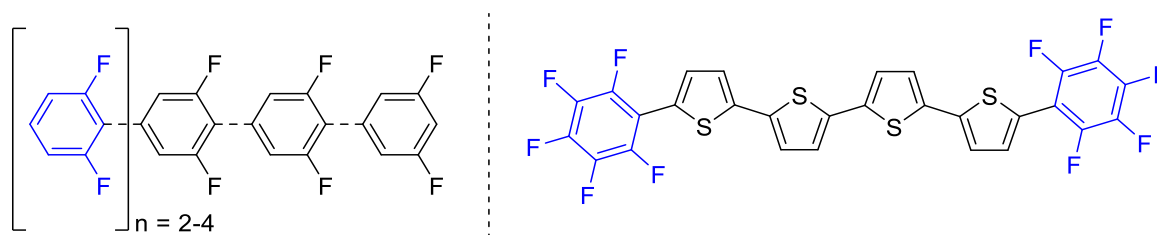


Figure 1-4. Fluoroarenes in materials science III: 2,6-difluorinated oligophenyls (left) and fluoroarene-thiophene oligomer (right) for semi-conductors.^[20,21]

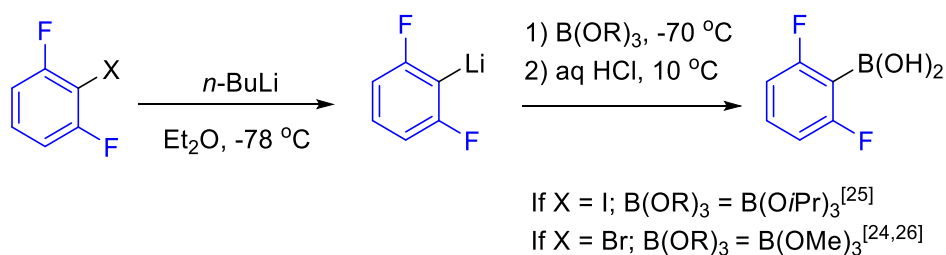
One promising methodology that has emerged recently for generating functionalized fluorine-containing organic compounds incorporates borylation chemistry, whereupon the resulting boron group can be transformed into a vast array of functional groups. Methods to generate fluorinated aryl boronate esters in catalytic process have been developed over the last 2 decades, including C–H, C–F, C–X (X = Cl, Br, I) borylations using iridium, rhodium, cobalt, platinum, palladium, and nickel metal catalyst systems. Unfortunately, some of the resulting boron-fluorine-containing products are prone to decomposition that limits their applicability in organic synthesis. For example, the employment of fluorinated aryl boronates in the Suzuki-Miyaura cross-coupling reaction to generate fluorinated biaryl compounds has been a significant challenge over the past 20 years. Applications of fluorinated aryl boronates in other cross-coupling reactions such as Chan-Evans-Lam aminations and etherification reactions have also been limited by decomposition pathways. In this review we summarize the latest developments regarding the synthesis of

fluorinated aryl boronate derivatives, discuss the stability issue of these molecules, and highlight the latest developments in the applications of fluorinated aryl boronates in organic synthesis.

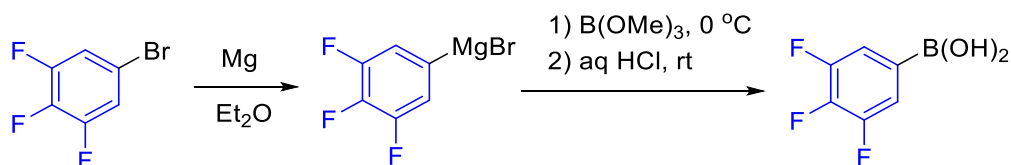
1.3 Synthesis of Fluorinated Aryl Boronates

1.3.1 Traditional Methods

Procedures to generate fluorinated aryl boronic acids traditionally involved stoichiometric processes *via* conversion of fluorinated aryl halides into aryl lithium^[24-26] (Scheme 1-1) or aryl Grignard reagents^[24,26] (Scheme 1-2) followed by addition of trialkoxyborates to yield fluorinated aryl trialkoxyborates. Subsequent addition of HCl resulted in the formation of the corresponding boronic acid. Unfortunately, these early methodologies suffered from harsh reaction conditions, low yields, and the formation of stoichiometric metal salts which made isolation of the desired products problematic. However, borylation methods for the synthesis of fluorinated aryl boronates have been developed *via* catalytic processes that can be carried out under much milder conditions and with improved yields.



Scheme 1-1. Synthesis of 2,6-fluorophenyl boronic acid using a lithium reagent.^[24-26]



Scheme 1-2. Synthesis of 3,4,5-trifluorophenyl boronic acid using a Grignard reagent.^[26]

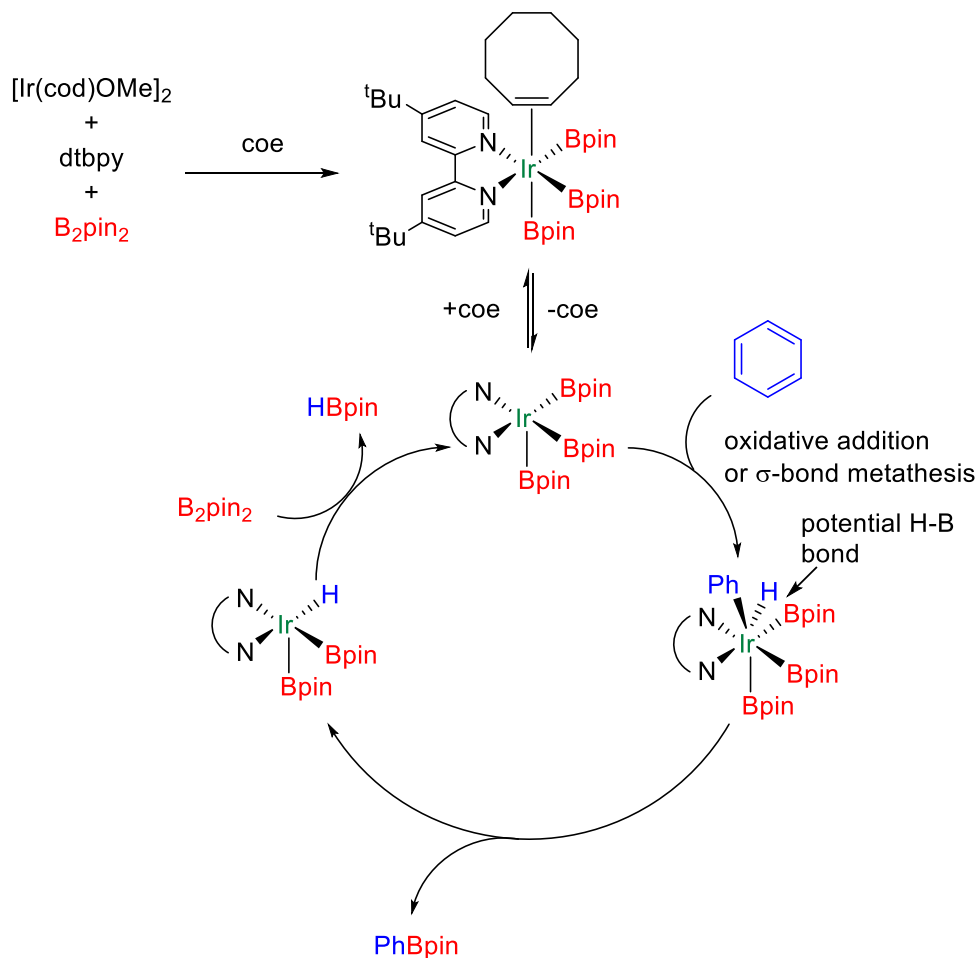
1.3.2 Catalytic C–H Borylation

1.3.2.1 Iridium-Catalyzed C–H Borylation of Fluoroarenes

The first study that showed that iridium complexes had the ability to promote the C–H borylation of arenes was reported by Marder *et al.* in 1993.^[27] In this report, the first trisboryl iridium complex, $[(\eta^6\text{-tol})\text{Ir}(\text{Bcat})_3]$, was prepared by a reaction of excess HBcat (cat = catecholato) with $[\eta^5\text{-indenyl}\text{Ir}(\text{cod})]$ (cod = *cis*-1,5-cyclooctadiene) in toluene (tol). The GC/MS total ion chromatogram included in the Supporting Information section showed the formation of small amounts of two isomers of tolyl-Bcat as a byproduct (< 1%) arising from borylation of the toluene solvent.^[27] However, attempts to optimize this remarkable C–H borylation reaction as a catalytic process were not conducted in this study.

Ishiyama, Hartwig, and Miyaura *et al.* reported the iridium-catalyzed C–H borylation of arenes using a combination of $[\text{Ir}(\text{cod})\text{OMe}]_2$ as a precatalyst, 4,4'-di-*tert*-butylbipyridine (dtbpy) as a ligand, and B_2pin_2 (Bpin = 4,4,5,5-tetramethyl-1,3,2-dioxaborolanyl) as the boron source.^[28] This catalyst system is one of the most widely used methods currently employed for the C–H borylation of arenes. Based on NMR data, detection of proposed intermediates, kinetic data and isotopic labelling studies Hartwig *et al.* proposed a mechanistic pathway for this iridium-catalyzed borylation reaction (Scheme 1-3). The trisboryl complex $[\text{Ir}(\text{dtbpy})(\text{coe})(\text{Bpin})_3]$ (coe = cyclooctene), was reported to be the resting state in these borylation reactions. This species could also be prepared in high yields from the independent reaction of $[\text{Ir}(\text{cod})\text{OMe}]_2$ with dtbpy, coe, and HBpin. Interestingly, attempts to generate this trisboryl species using B_2pin_2 gave significantly lower yields. Once this trisboryl species is generated, the reaction is believed to proceed *via* dissociation of the labile coe ligand to give an unsaturated catalytically-active trisboryl iridium(III) complex. Sakaki *et al.* carried out DFT calculations which also indicated that this type of trisboryl iridium(III) complex is the active species in the catalytic process. This is followed by a rate-limiting C–H bond cleavage of the arene to give an hydridotrisboryl iridium(V) intermediate which is stabilized by the electron-rich dtbpy ligand and by strong σ -donation by the boryl ligand. Reductive elimination

would proceed to give the borylated arene product along with a hydridobisboryl iridium(III) species. Oxidative addition of B_2pin_2 with loss of $HBpin$ would then regenerate the active catalytic species.^[29,30]



Scheme 1-3. A plausible mechanism for the iridium-catalyzed C–H borylation of arenes.^[29,30]

The selectivity of this iridium-catalyzed borylation method was found to be influenced more by the steric effects of the substituent groups on the arene ring rather than by directing or electronic effects. Thus, borylation occurred predominantly at less sterically-hindered C–H bonds (Figure 1-5).^[30]

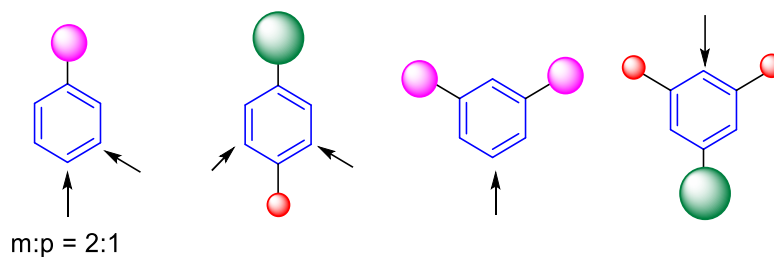
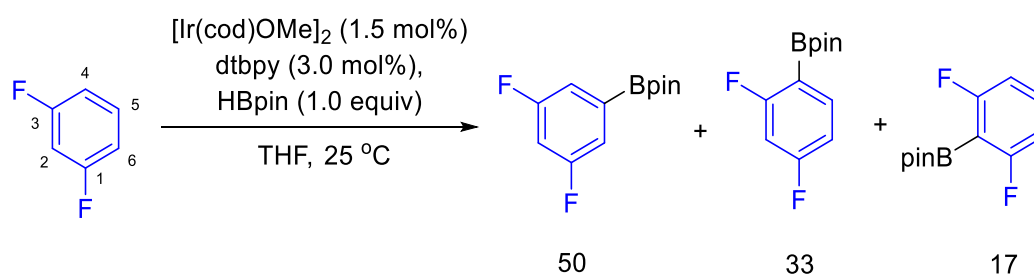


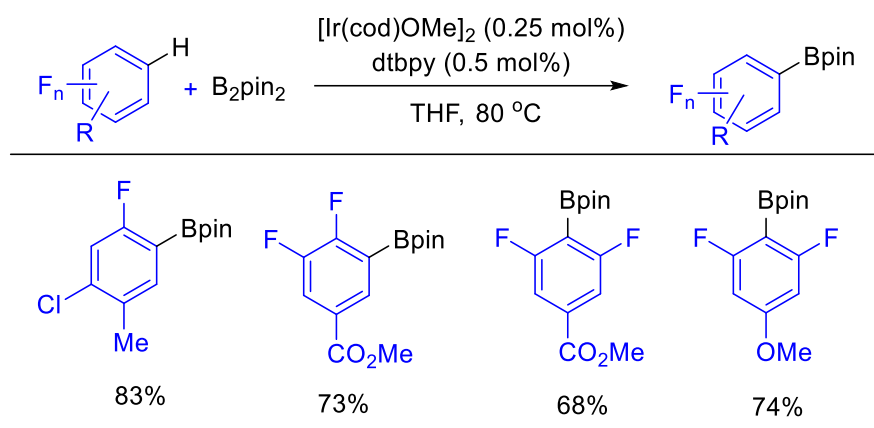
Figure 1-5. Regioselectivity of iridium-catalyzed C–H borylations.^[30]

Hartwig's borylation method was used by Smith *et al.* employing fluorinated arene substrates such as 1,3-difluorobenzene using HBpin.^[31] As shown in Scheme 1-4, the regioselectivity of the borylation follows the order $5 > 4 > 2$, due to the steric effect of the fluorine substituents.



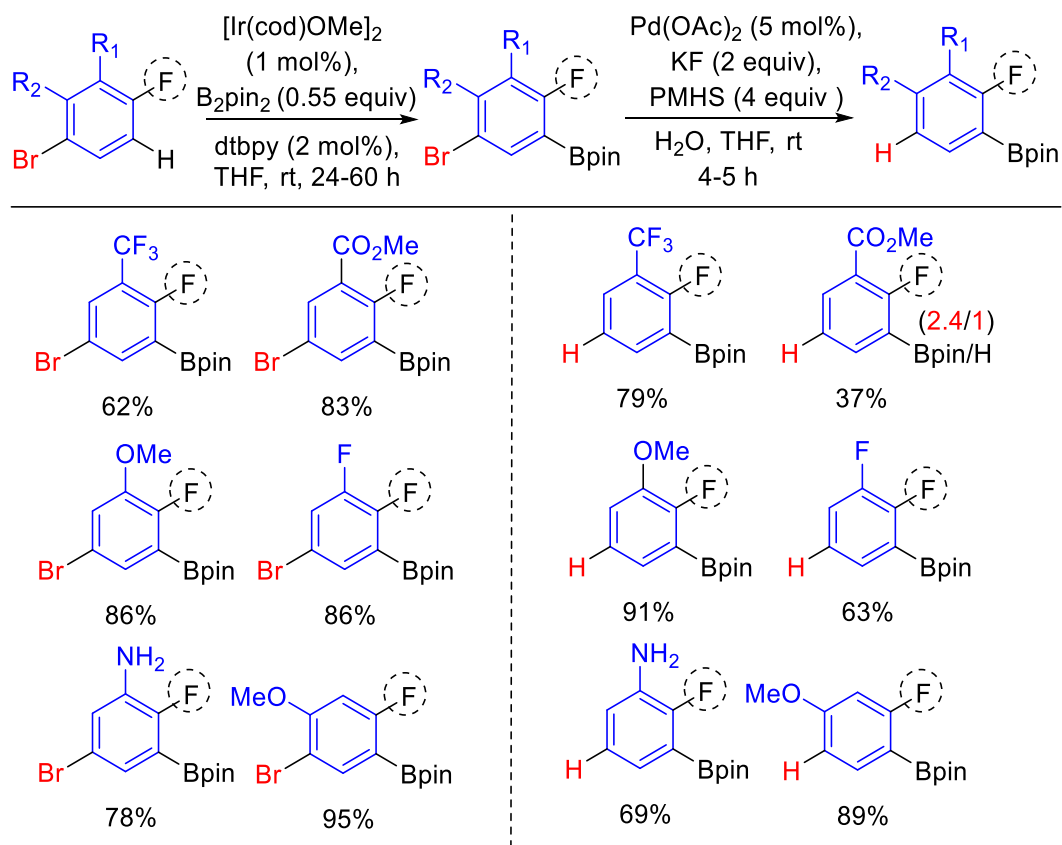
Scheme 1-4. The iridium-catalyzed C–H borylation of 1,3-difluorobenzene.^[31]

A subsequent study by Hartwig *et al.* expanded the scope of the iridium-catalyzed C–H borylation reaction to include disubstituted fluoroarenes bearing ancillary substituents with various steric parameters.^[32] As shown in Scheme 1-5, this borylation method utilized B₂pin₂ and was effective in targeting the least sterically-encumbered C–H bond. As a result, reactions with substituted 1,3-difluoroarene derivatives gave the corresponding borylated products in which the Bpin groups have been incorporated at the 2-position.



Scheme 1-5. Iridium-catalyzed C–H borylation of fluoroarenes.^[32]

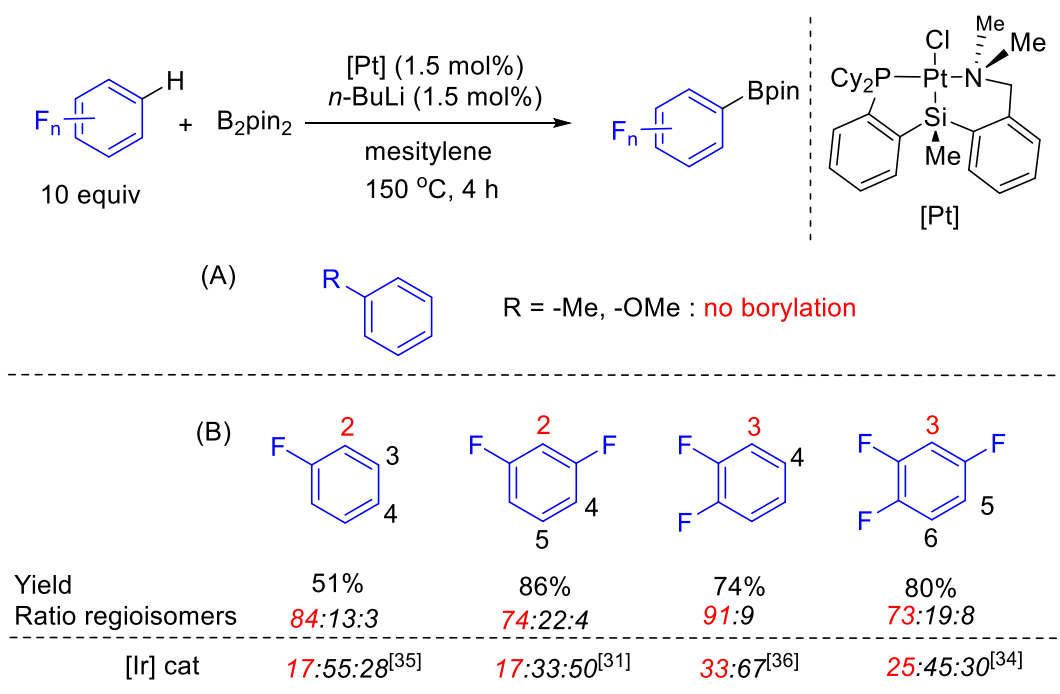
In 2014, Maleczka Jr. *et al.*^[33] introduced a two step catalytic iridium-catalyzed C–H borylation and palladium-catalyzed dehalogenation process as a way of selectively generating *ortho*-fluoro aryl boronates. The arene substrates originally contain bromide as the leaving group *para* to the fluorine substituent (Scheme 1-6). The key to this selectivity is blocking borylation at the position *meta* to the fluorine substituent due to steric repulsion from the bulkier bromide group. A subsequent palladium-catalyzed hydrodehalogenation of the bromide substituent in the presence of the reducing agent polymethylhydrosiloxane (PMHS), which is activated by potassium fluoride, leads to the final product. Notably, it was also observed that electron poor arenes led to dehalogenation at a greater rate than electron rich arenes. It is important to note that protodeboration was not observed to any significant degree during the dehalogenation step (see Section 1.4), except in the case of the methylbenzoate derivative which gave the the desired product in only 37% yield in a 2.4:1 ratio.



Scheme 1-6. A two-step iridium-catalyzed borylation / palladium-catalyzed dehalogenation.^[33]

1.3.2.2 Platinum-Catalyzed C–H Borylation of Fluoroarenes

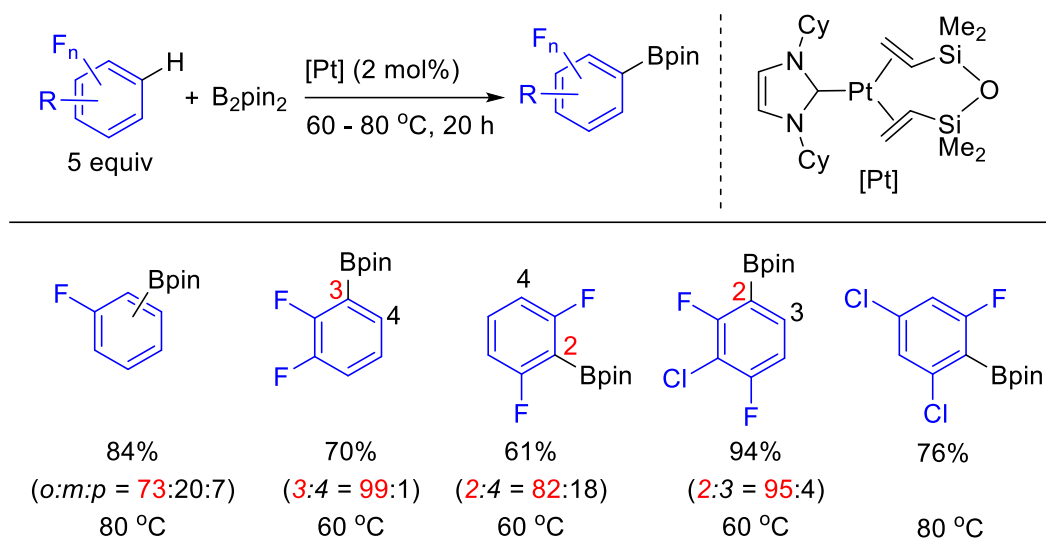
The iridium-catalyzed C–H borylation that targets a C–H bond *ortho* to a fluorine substituent requires steric repulsion from other substituents. In 2015, however, Iwasawa *et al.*^[34] reported a platinum complex bearing a PSiN-pincer type ligand in the presence of *n*-butyllithium that catalyzed the C–H borylation of fluoroarenes with B_2pin_2 . Interestingly, this method is selective for the borylation of C–H bonds *ortho* to the fluorine substituent in good yield without the presence of steric protecting ancillary substituents. Notably, under these conditions C–H borylation did not work for unactivated arenes such as anisole and toluene (Scheme 1-7A). Interestingly, this method represents a useful alternative to the iridium-catalyzed systems for the borylation of C–H bonds that are *ortho* to fluorine substituents without the need of sterically-protecting substituents (Scheme 1-7B).^[31,34-36]



Scheme 1-7. Platinum-catalyzed C–H borylation of fluoroarenes: (A) electron rich arene substrates; (B) fluorinated arene substrates.^[34]

In the same year, Tobisu and Chatani *et al.* reported a series of [Pt(NHC)(dvtms)] complexes (NHC = *N*-heterocyclic carbene; dvtms = divinyltetramethyldisiloxane) as catalyst precursors for the C–H borylation of arenes. These complexes are air stable and easy to prepare in two steps from H₂[PtCl₆].^[37] This study demonstrated that introducing NHC ligands gave turnover numbers (TON) up to 157 in reactions using ICy (1,3-bis(cyclohexyl)imidazolin-2-ylidene) as the ligand. Selected examples from the scope of these borylations revealed that introducing additional fluorine substituents increased the reactivity and selectivity in favor of generating *ortho*-directed borylated products (Scheme 1-8).

Selectivities observed in platinum-catalyzed C–H reactions reported by Iwasawa^[34] and Tobisu and Chatani^[37] were dictated by electronic effects, whereupon the most acidic arene C–H bonds *ortho* to the fluorine groups underwent borylation. This is in contrast with the iridium-catalyzed systems discussed previously which are governed predominantly by steric effects that target less-sterically hindered C–H bonds.^[28]



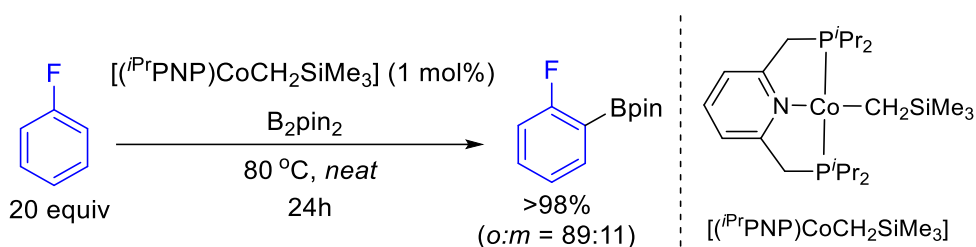
Scheme 1-8. Platinum-catalyzed C–H borylation of fluoroarenes.^[37]

1.3.2.3 Cobalt-Catalyzed C–H Borylation of Fluorobenzenes

In 2014, Chirik *et al.* reported pincer-ligated cobalt alkyl complexes which catalyze the C–H borylation of arenes and heteroarenes.^[38] Electron-rich arenes bearing only one substituent such as toluene and anisole are also viable substrates for C–H borylations but show less regioselectivity than the electron-deficient fluorobenzene, the only example reported employing a fluoroarene substrate.

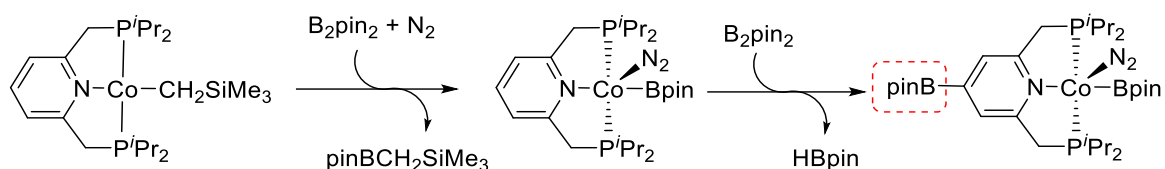
Using the complex $[(i^{\text{Pr}}\text{PNP})\text{CoCH}_2\text{SiMe}_3]$ as a catalyst precursor for arene borylations, electron deficient substrates, including fluorobenzene, afforded products with higher selectivities. Borylation occurred *ortho* to the electron-withdrawing fluorine substituent with an *ortho* : *meta* ratio of 89:11 (Scheme 1-9), whereupon the fluorine substituent was believed to have an *ortho*-directing effect presumably due to the increased C–H acidity of the hydrogen substituents in the *ortho*-position.^[39]

In 2019, Chirik *et al.* reported that the *ortho*-to-fluorine selectivity is due to a lower barrier for the C(sp²)–H oxidative addition of the fluorinated arenes to the Co(I) center compared to unactivated arenes such as toluene or *m*-xylene. Computational studies showed that the cobalt-aryl bond is strengthened with increasing number of *ortho*-fluorine substituents in the relevant intermediates of the $(i^{\text{Pr}}\text{PNP})\text{Co}$ -catalyzed C–H borylation.^[40] This is in accordance with earlier studies by Jones *et al.* and Eisenstein and Perutz *et al.* who showed a large *ortho*-fluorine effect on the strength of metal-aryl bonds.^[41-43]

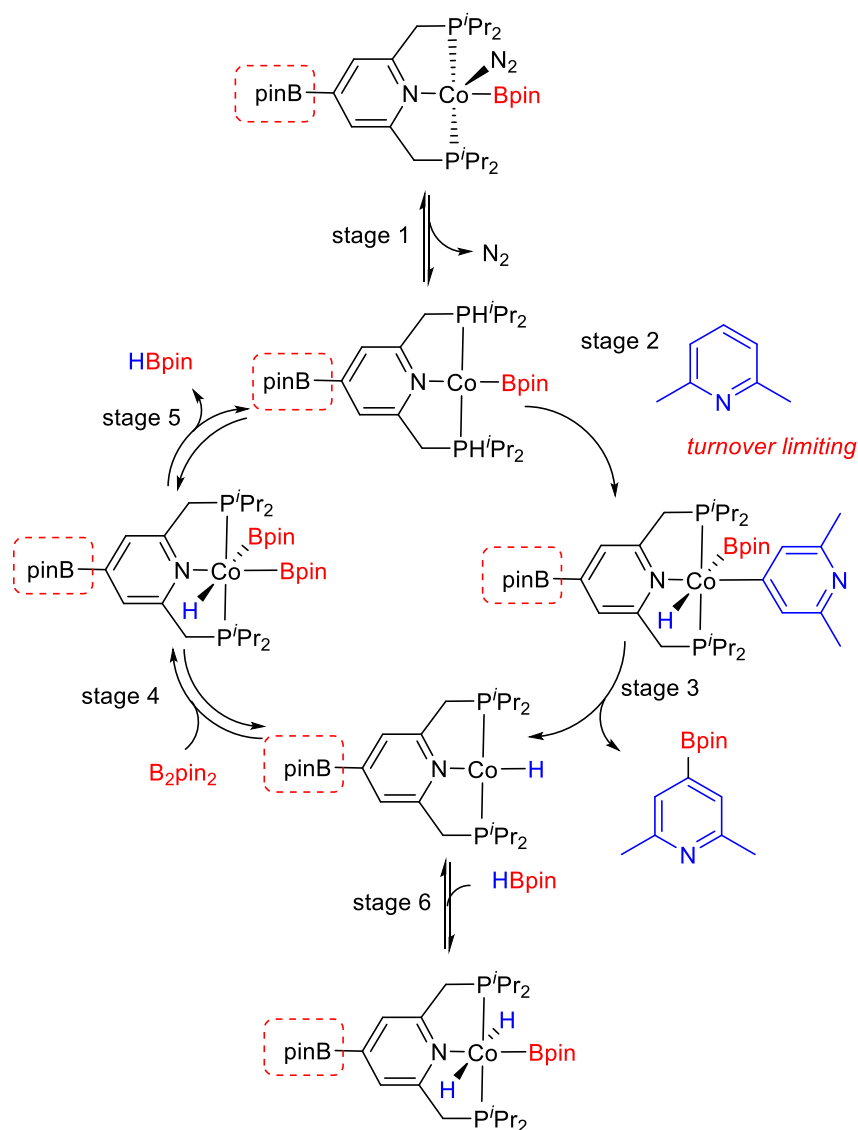


Scheme 1-9. C–H borylation of arenes using Chirik’s first generation cobalt precatalyst.^[38]

In 2016, Chirik *et al.* reported that treatment of the precatalyst $[(i\text{PrPNP})\text{CoCH}_2\text{SiMe}_3]$ with B_2pin_2 , under a N_2 atmosphere afforded $[(i\text{PrPNP})\text{Co}(\text{N}_2)\text{Bpin}]$ along with N_2 coordination and the concomitant formation of $\text{Me}_3\text{SiCH}_2\text{Bpin}$ (Scheme 1-10). Interestingly, excess B_2pin_2 led to C–H borylation at the 4-position of the pyridine moiety of the catalyst to give $[4\text{-Bpin-}(i\text{PrPNP})\text{Co}(\text{N}_2)\text{Bpin}]$ as the resting state.^[44] Using 2,6-lutidine as a substrate, Chirik proposed that the catalytic cycle involves a Co(I)/Co(III) pathway. Following N_2 dissociation from $[4\text{-Bpin-}(i\text{PrPNP})\text{Co}(\text{N}_2)\text{Bpin}]$, C(sp^2)–H oxidative addition of the arene to cobalt(I) boryl intermediate occurs to give a cobalt(III) hydrido boryl aryl intermediate (Scheme 1-11, stages 1 and 2). A subsequent B–C reductive elimination step releases the borylated product and the cobalt(I) hydride complex (Scheme 1-11, stage 3). Oxidative addition of B_2pin_2 and reductive elimination of HBpin closes the catalytic cycle (Scheme 1-11, stages 4 and 5). At higher conversions, when a substantial amount of HBpin is generated, oxidative addition of HBpin to the cobalt(I) hydride species occurs to generate the resting state $[4\text{-Bpin-}(i\text{PrPNP})\text{Co}(\text{H})_2\text{Bpin}]$ (Scheme 1-11, stage 6). Notably, with benzene or *N*-heteroarene substrates, Chirik *et al.* found that C(sp^2)–H oxidative addition of the arene ligand to the cobalt(I) boryl intermediate is the turnover-limiting step and that the process is irreversible. Interestingly, in 2019, they also reported that fluorination of the arene substrate activates the C(sp^2)–H bonds as the barrier for the oxidative addition is decreased and the process becomes reversible, hence this step was predicted unlikely to be turnover-limiting.^[40]



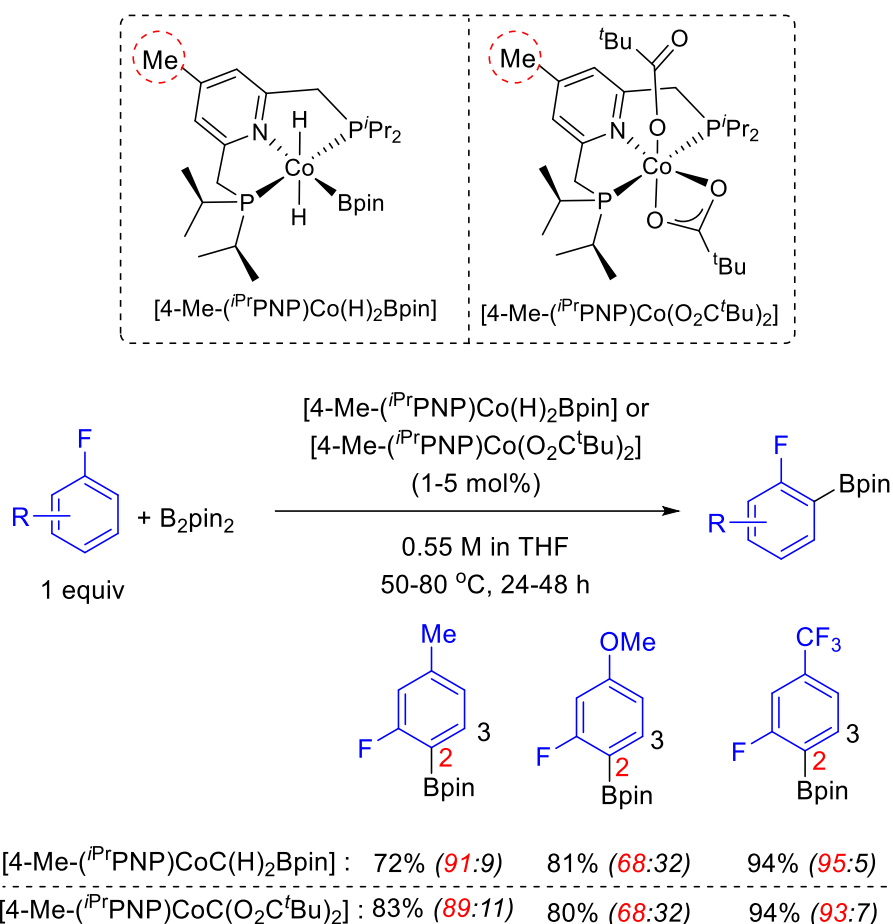
Scheme 1-10. Borylation occurred at the 4-position of the pyridine moiety of the cobalt catalyst that causes catalyst deactivation.^[44]



Scheme 1-11. Proposed mechanism for the cobalt-catalyzed borylation of arenes with B_2pin_2 .^[44]

Catalyst C–H borylation occurred at the 4-position of the pyridine ligand (Scheme 1-10) and is disadvantageous for the catalytic performance, as the metal center becomes less electron-rich and oxidative addition is inhibited upon borylation. This observation led to the development of a second

generation of the Chirik cobalt precatalysts [4-Me-(*i*PrPNP)Co(H)₂Bpin] and [4-Me-(*i*PrPNP)Co(O₂C^tBu)₂] in which methyl substituents were located at the 4-position of the pyridine ligand to prevent ligand C–H borylation.^[39] As shown in Scheme 1-12, the precatalysts [4-Me-(*i*PrPNP)Co(H)₂Bpin] and [4-Me-(*i*PrPNP)Co(O₂C^tBu)₂] are effective for the catalytic *ortho*-to-fluorine C–H borylation of substituted fluoroarenes using B₂pin₂ as the boron source and THF as the solvent (Scheme 1-12). Notably, this method is not viable for fluoroarene substrates containing bromo and chloro substituents (not shown).

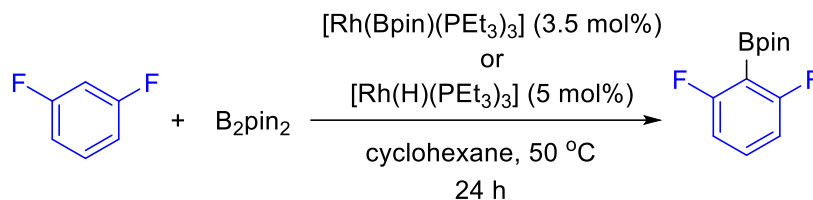


Scheme 1-12. Catalytic C–H borylation of fluoroarenes using Chirik’s second generation cobalt precatalysts.^[39]

1.3.2.4 Rhodium-Catalyzed C–H Borylation of Fluorinated Benzene

In 2015, Braun *et al.*^[45] developed a rhodium-catalyzed C–H borylation of arenes to generate boron-containing products *ortho* to two fluorine substituents using either B₂pin₂ or HBpin. For example, treatment of 1,3,5-trifluorobenzene or 1,3-difluorobenzene with excess B₂pin₂ in the presence of

catalytic amounts of either $[\text{Rh}(\text{Bpin})(\text{PEt}_3)_3]$ or $[\text{Rh}(\text{H})(\text{PEt}_3)_3]$ in cyclohexane at 50 °C for 24 hours generated the corresponding C–H borylation products in good yield (Scheme 1-13). However, it should be noted that the C–H borylation performance was poor for heteroarene substrates. For example, reactions employing 2,3,5,6-tetrafluoropyridine as the borylation substrate and 5 mol% $[\text{Rh}(\text{H})(\text{PEt}_3)_3]$ as the catalyst precursor gave 2,3,5,6- $\text{C}_5\text{NF}_4\text{Bpin}$ in only 44% yield even after longer reaction times (7 days).

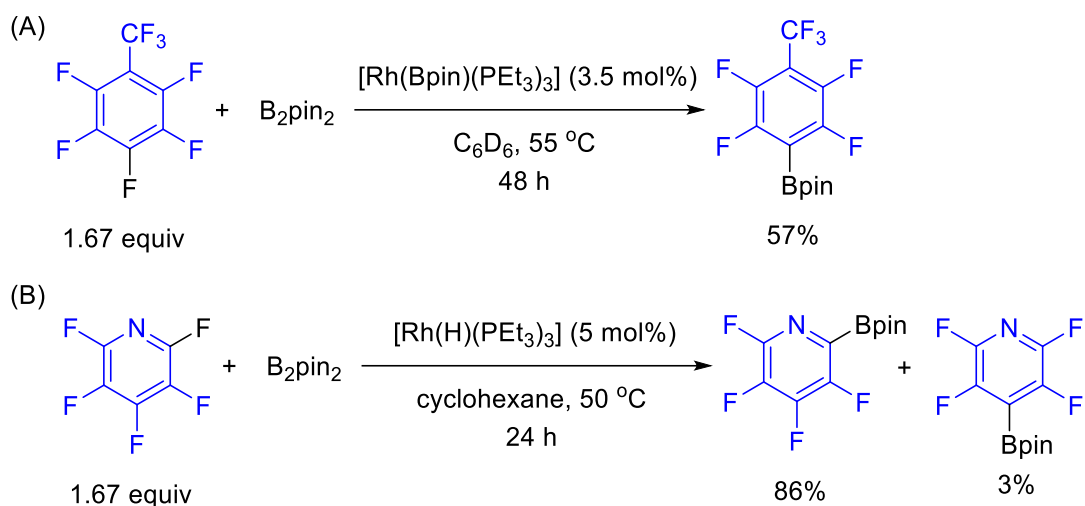


Scheme 1-13. Rhodium-catalyzed C–H borylation of 1,3-fluorobenzene.^[45]

1.3.3 Catalytic C–F Borylation

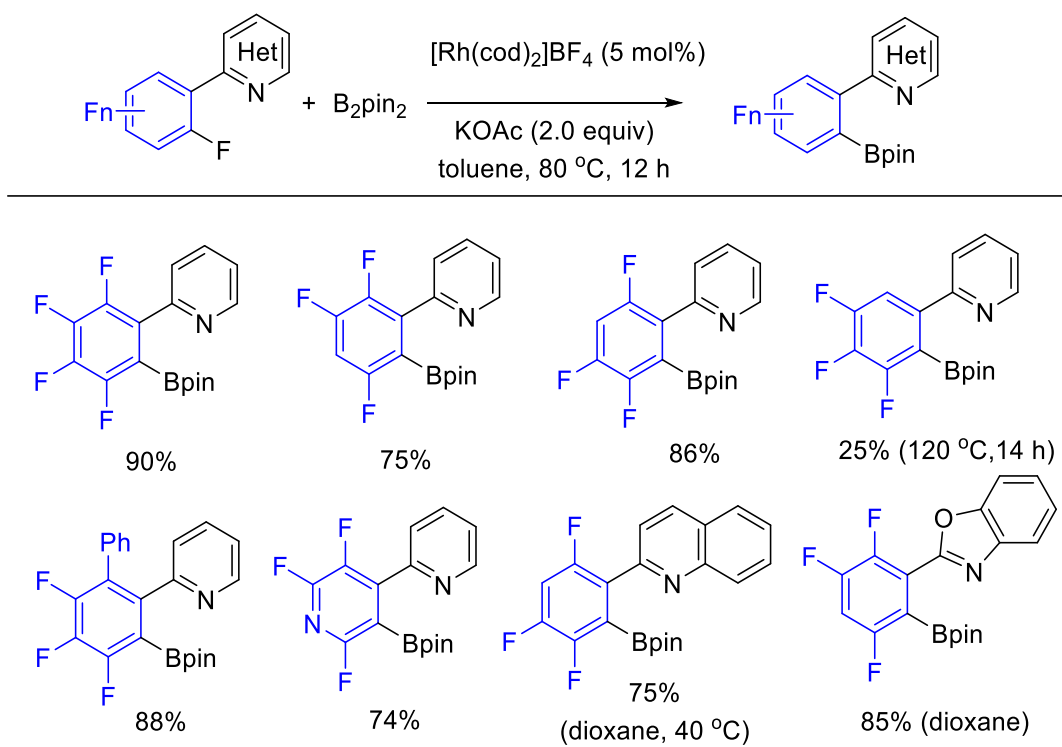
1.3.3.1 Rhodium-Catalyzed C–F Borylation of Fluoroarenes

Conversion of partially fluorinated arene compounds *via* C–F bond borylation is another option to generate fluoride-containing aryl boronate esters. In 2007, Marder and Perutz *et al.* reported the stoichiometric reaction of C–F borylation of fluoropyridines promoted by $[\text{Rh}(\text{SiPh}_3)(\text{PMe}_3)_3]$.^[46] Inspired by these stoichiometric processes, Braun *et al.* demonstrated that Rh(I) complexes could be used for the catalytic C–F borylation of fluoroarenes,^[45] pentafluoropyridine,^[47] and hexafluoropropene.^[48] The authors showed that adding 3.5 mol% of $[\text{Rh}(\text{Bpin})(\text{PEt}_3)_3]$ into a mixture that contained 1,2,3,4,5-pentafluoro-6-(trifluoromethyl)benzene and B_2Pin_2 in benzene at 55 °C for 2 days gave the C–F borylation product 4-Bpin- $\text{C}_6\text{F}_4(\text{CF}_3)$ in a yield of 57% (based on B_2Pin_2) (Scheme 1-14A).^[45] Under similar conditions, using 5 mol% $[\text{Rh}(\text{Bpin})(\text{PEt}_3)_3]$ in cyclohexane, catalytic C–F borylation of pentafluoropyridine occurred at the 2-position to give $\text{C}_5\text{NF}_4\text{Bpin}$ as the main product (86%) (Scheme 1-14B). Interestingly, when other fluoroarene substrates such as 1,3,5-trifluorobenzene or 1,3-difluorobenzene were employed, the authors observed that C–H borylation occurred instead of C–F borylation.

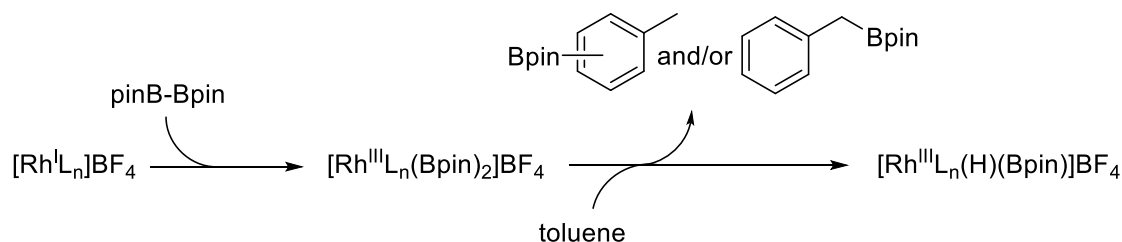


Scheme 1-14. Rhodium-catalyzed C–F borylation of perfluorotoluene and perfluoropyridine.^[45]

In 2015, Zhang *et al.* reported that the commercially available complex $[\text{Rh}(\text{cod})_2]\text{BF}_4$ could be used as a precatalyst for the *ortho*-selective C–F borylation of 2-(fluorophenyl)pyridine with B_2pin_2 . The reaction was conducted in the presence of potassium acetate as a base in toluene at 80 °C.^[49] Notably, *ortho*-selective C–F borylation was directed by the *N*-heterocyclic substituent. As shown in Scheme 1-15, C–F borylation only occurred *ortho* to the pyridyl group in good to excellent yields. However, if the substrate has a hydrogen substituent *ortho* to the pyridyl group, such as 2-(2,3,4,5-tetrafluorophenyl)pyridine, C–H and C–F borylation both occurred, with products generated in 45% and 25% yields, respectively (Scheme 1-15). Preliminary mechanistic studies suggest that the toluene solvent acts as a hydrogen source for the formation of the rhodium hydride complex $[\text{Rh}^{\text{III}}\text{L}_n(\text{H})(\text{Bpin})]\text{BF}_4$ as a key intermediate to initiate the catalytic process (Scheme 1-16).



Scheme 1-15. Rhodium-catalyzed *ortho*-selective C–F borylation of polyfluoroarenes.^[49]

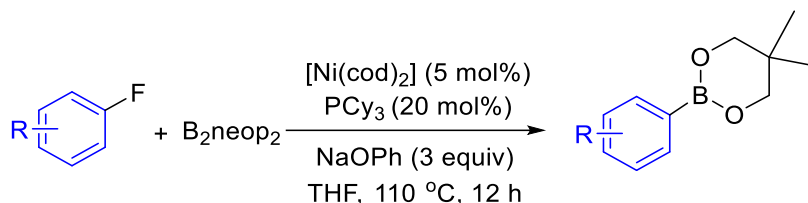


Scheme 1-16. Generation of $[\text{Rh}^{\text{III}}\text{L}_n(\text{H})(\text{Bpin})]\text{BF}_4$ as a key intermediate in the catalytic process.^[49]

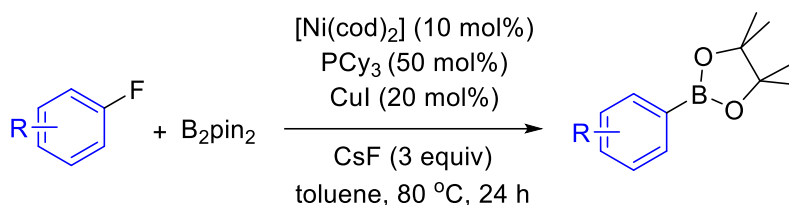
1.3.3.2 Nickel-Catalyzed C–F Borylation of Fluoroarenes

Several studies have been reported regarding the development of nickel-mediated C–F activation of arenes in stoichiometric processes.^[1,2,50–53] However, effective catalytic borylations of these substrates using nickel catalysts were reported only recently by Martin *et al.* (Scheme 1-17).^[54] In this initial study, a combination of $[\text{Ni}(\text{cod})_2]$ and PCy_3 (tricyclohexylphosphine) as a precatalyst system was effective to promote the C–F borylation of fluorinated aryls with B_2neop_2 (neop = neopentyl glycolato) to give products in up to 81% yield. However, employing B_2pin_2 , instead of B_2neop_2 , resulted in no borylation products. Soon after, Niwa and Hosoya *et al.* used B_2pin_2 as the

boron source and employed nickel and copper cocatalyst systems to borylate the C–F bond of fluoroarenes in up to 99% yield (Scheme 1-18).^[55] However, they did not examine polyfluorinated substrates. As a result, this reaction furnished non-fluorinated aryl boronate esters.



Scheme 1-17. Nickel-catalyzed C–F borylation of aryl fluorides with B_2neop_2 .^[54]



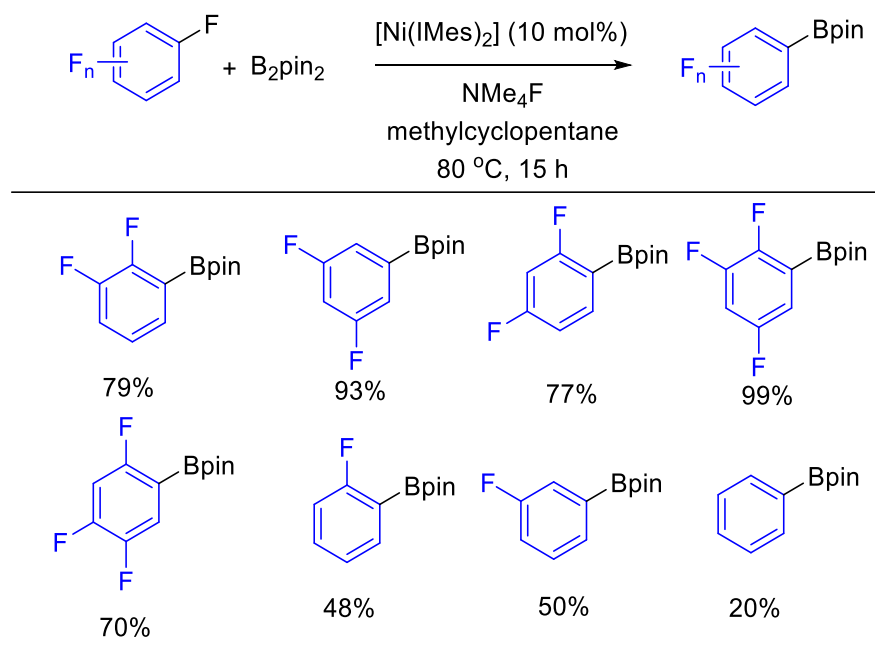
Scheme 1-18. Nickel/copper-catalyzed defluoroborylation of fluoroarenes with B_2pin_2 .^[55]

In 2016, Radius and Marder *et al.* employed an NHC-nickel complex as a precatalyst for the C–F borylation of partially fluorinated arenes using B_2pin_2 . Optimal conversions were achieved using $\text{Ni}(\text{IMes})_2$ (IMes = 1,3-dimesitylimidazol-2-ylidene) in the presence of tetramethylammonium fluoride (NMe_4F) in methylcyclopentane at 80–100 °C (Scheme 1-19).^[56] A mechanistic pathway was proposed based on experimental studies (Scheme 1-20), whereupon the initial reaction of $\text{Ni}(\text{IMes})_2$ with fluoroarene proceeds *via* oxidative addition of the C–F bond to give $[\text{Ni}(\text{IMes})_2(\text{F})(\text{Ar}_\text{F})]$. Then, the presence of NMe_4F (or CsF) led to a fluoride adduct with B_2pin_2 which promoted boryl transfer to the Ni(II) complex to give *trans*- $[\text{Ni}(\text{IMes})_2(\text{Bpin})(\text{Ar}_\text{F})]$ along with $[\text{F}_2\text{Bpin}]^-$. Finally, rapid reductive elimination occurred to provide $\text{Ar}_\text{F}\text{-Bpin}$ and regenerate $[\text{Ni}(\text{IMes})_2]$.

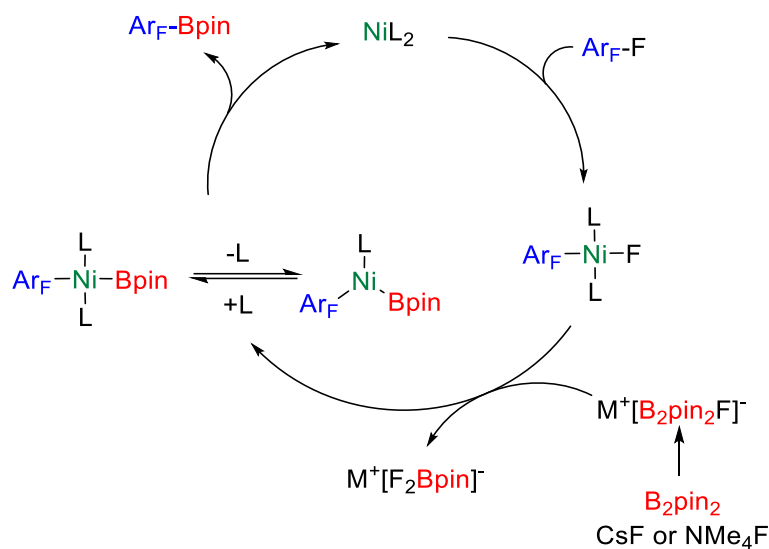
Noteworthy is that these nickel-catalyzed C–F borylations require high temperatures to facilitate the rate-determining transmetalation step, although C–F oxidative addition to $[\text{Ni}(\text{IME})_2]$ proved facile at room temperature. It is interesting to note that a rhodium biphenyl complex could be used as a triplet sensitizer to enhance the transmetalation with B_2pin_2 to the nickel(II) complex. The reaction was conducted in the presence of visible light (400 nm) using CsF as a base, and proved

effective for the C–F borylation of polyfluoroarenes at room temperature (Scheme 1-21).^[57] In the absence of the rhodium complex, the intermediate complex $[\text{NiF}(\text{Ar}_\text{F})(\text{IMes})_2]$ decomposed quickly under irradiation in the presence of B_2pin_2 . Interestingly, this decomposition pathway could be circumvented by indirect excitation of the triplet states of the nickel(II) complex *via* the photoexcited rhodium biphenyl complex. The triplet energy transfer accelerated the transmetalation step and thus the whole borylation process. The proposed mechanism suggested that the long-lived triplet excited state of the rhodium complex functions as the photosensitizer that provides facile triplet energy transfer (TET) to *trans*- $[\text{NiF}(\text{Ar}_\text{F})(\text{IMes})_2]$, facilitating dissociation of one of the NHC ligands (Scheme 1-22). The resulting 3-coordinate nickel complex reacts with B_2pin_2 , or its anionic adduct $\text{Cs}[\text{FB}_2\text{pin}_2]$, to give $[\text{Ni}(\text{IMes})(\text{Ar}_\text{F})(\text{Bpin})]$ which was proposed to be followed by rapid reductive elimination releasing the borylated arene products and $[\text{Ni}(\text{IMes})]$.

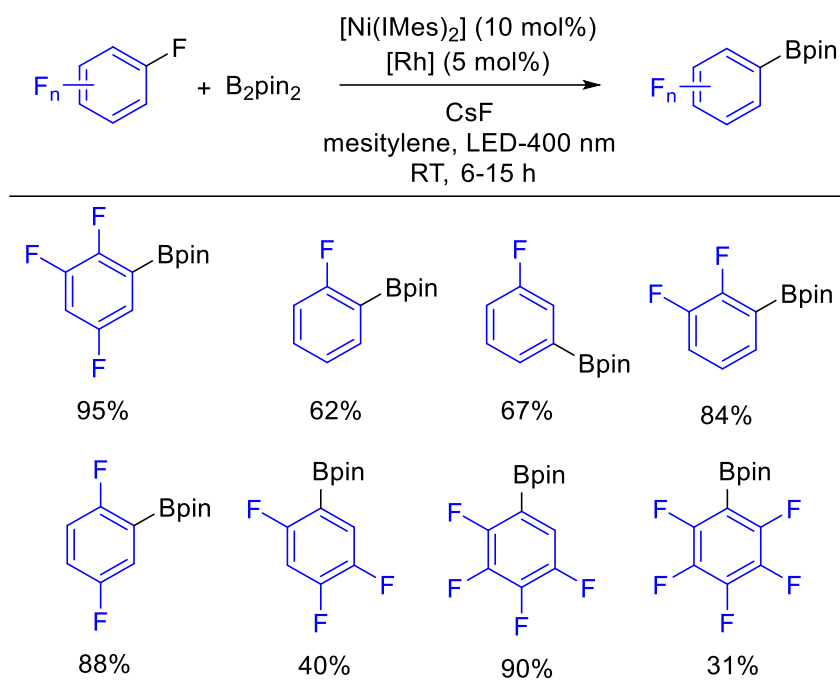
Thermal^[56] and photocatalytic^[57] C–F borylation procedures have subsequently been developed that are selective and efficient in generating fluorinated aryl pinacol boronate products. However, those C–F borylation methods were not able to generate $\text{C}_6\text{F}_5\text{Bpin}$ from C_6F_6 in any appreciable yields. As these methods require the use of a strong base, protodeboration may be responsible for the low yields.



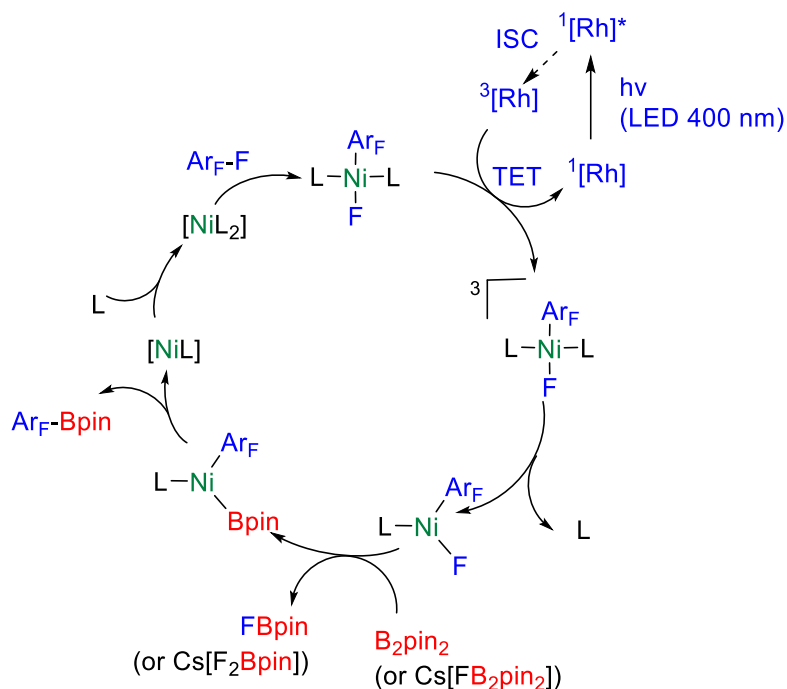
Scheme 1-19. Thermal-catalytic C–F borylation of fluoroarenes using a Ni precatalyst.^[56]



Scheme 1-20. Proposed mechanism for the thermal-catalytic C–F borylation of fluoroarenes using an NHC-Ni catalyst.^[56]



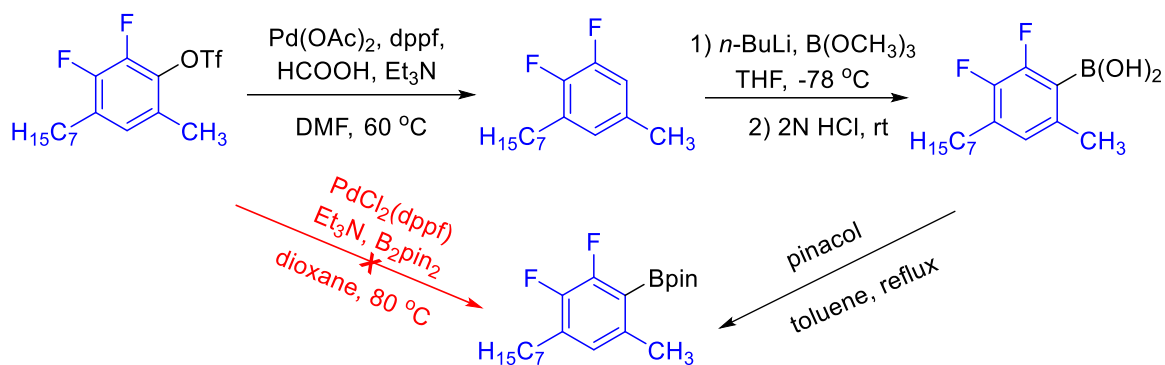
Scheme 1-21. Photocatalytic C–F borylation of fluoroarenes using a dual Ni/Rh catalyst.^[57]



Scheme 1-22. Proposed mechanism for the photocatalytic C–F borylation of fluoroarenes using $[\text{Rh}]/[\text{Ni}(\text{IMes})_2]$ via triplet energy transfer (TET).^[57]

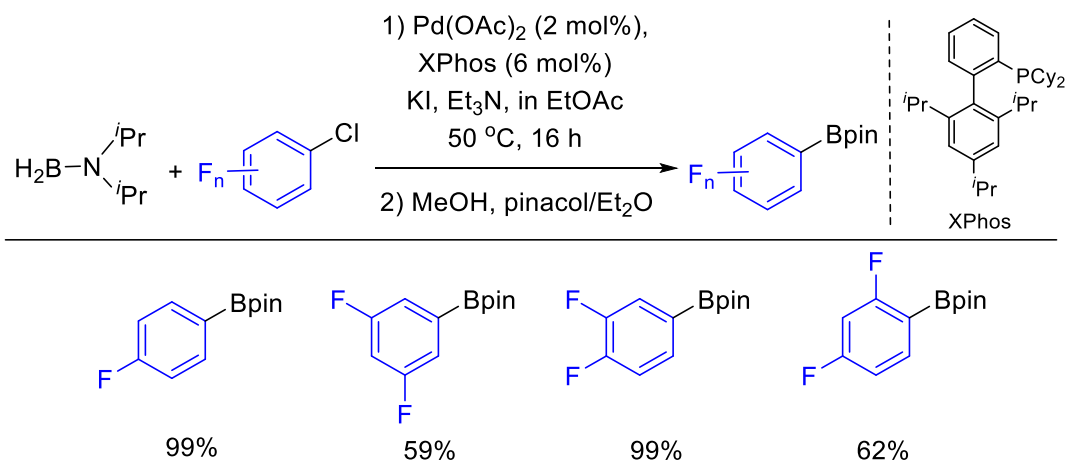
1.3.4 Catalytic C–X Activation (X = Cl, Br, I, OTf)

The transition metal-catalyzed C–X (X = Cl, Br, I, OTf) borylation reaction provides another option for introducing boronate ester groups selectively into fluorinated aryl halides or triflates.^[58-68] Masuda *et al.* reported that $[\text{PdCl}_2(\text{dppf})]$ (dppf = 1,1'-bis(diphenylphosphino)ferrocene) acts as an active catalyst precursor for the C–X borylation of aryl halides and triflates with B_2pin_2 in the presence of excess of Et_3N .^[66] Masuda's methodology was attempted by Cammidge *et al.* for the borylation of aryl triflates in which the C–OTf bond was *ortho* to a C–F and a C– CH_3 bond; however, no reaction was observed under these conditions (Scheme 1-23). To generate the desired boronate ester, Cammidge *et al.* resorted to using an *ortho* lithiation method, demonstrating the challenges associated with some transition metal-catalyzed C–OTf borylation reactions.^[67]

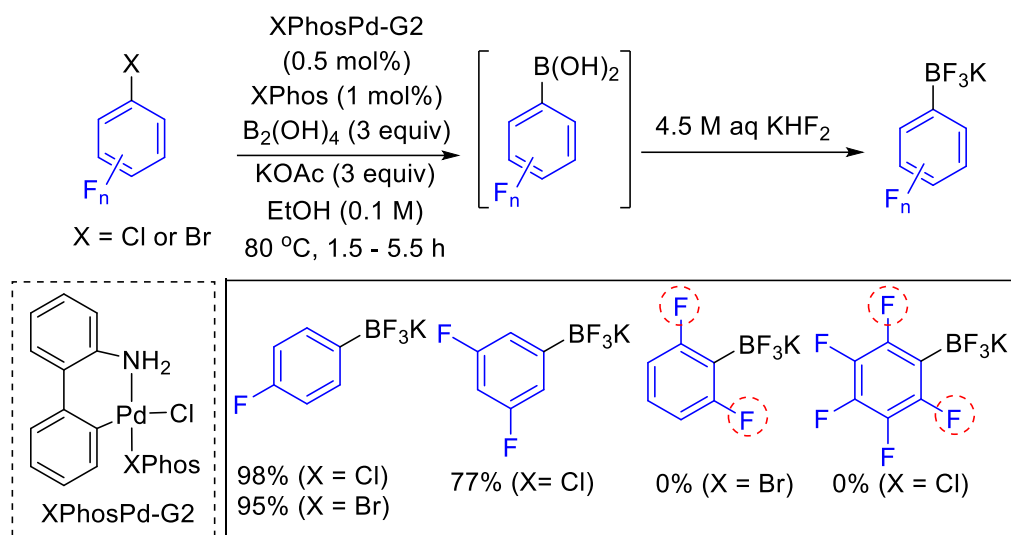


Scheme 1-23. Transition metal-catalyzed C–OTf borylation vs. lithiation to synthesize *ortho*-fluorinated aryl boronates.^[67]

Several examples of transition metal-catalyzed C–X borylation reactions generating products with the C–B moiety located *ortho*, *meta*, and *para* to the fluorine substituents have been reported.^[56,61-65,67] For example, in 2014, Pucheault *et al.* reported a palladium-catalyzed C–Cl borylation in the synthesis of aryl boronate ester derivatives using aryl(amino)boranes in good to excellent yields (Scheme 1-24). However, attempts to generate di *ortho*-fluorinated aryl boronates were not examined.^[64]

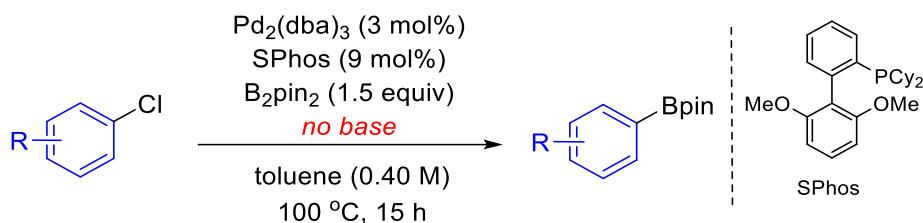


Scheme 1-24. Palladium-catalyzed C–Cl borylation to construct fluorinated aryl boronate esters.^[64]



Scheme 1-25. C–X borylation to construct fluorinated aryl-boronates using the precatalyst XphosPd-G2.^[68]

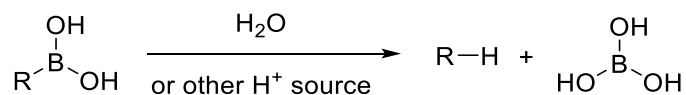
Earlier attempts to use transition metal-catalyzed C–X (X = Cl, Br, I) borylations to generate aryl-Bpin products containing two *ortho*-fluorine substituents all proved unsuccessful. For example, in 2012, Molander *et al.* reported the borylation of aryl-X (X = Br, Cl, I, OTf) with B₂(OH)₄ using second generation of Buchwald precatalyst XPhosPd-G2, followed by the conversion of the borylated aryl boronic acid product into potassium trifluoroborate analogues. This method is effective to generate borylated products in good to excellent yields; however, notably, the reaction failed to employ aryl-X substrates, in which the C–X bond is flanked by two C–F bonds, *e.g.*, 2-bromo-1,3-difluorobenzene and 1-chloro-2,3,4,5,6-pentafluorobenzene (Scheme 1-25).^[68] These reactions were typically conducted in the presence of stoichiometric amounts of base, but the resulting products are unstable under these conditions resulting in considerable amounts of protodeboronated fluoroarene species. Although Matsubara and Yorimitsu *et al.* developed a base-free palladium-catalyzed C–Cl borylation of aryl chlorides with diboron compounds, generating di-*ortho*-fluorinated aryl-Bpin derivatives was not examined (Scheme 1-26).^[69]



Scheme 1-26. Base-free borylation of aryl chlorides with B_2pin_2 .^[69]

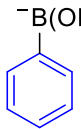
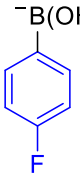
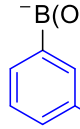
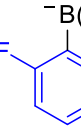
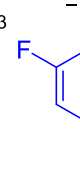
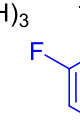
1.4 Protodeboronation of Fluorinated Aryl Boronates

Before going into detail about the catalytic applications of fluorinated aryl boronates, it is important to discuss the stability issue associated with these compounds. One major problem involves the protodeboronation of fluorinated aryl boronic acids, which is accelerated in compounds containing *ortho*-fluorine substituents. As mentioned previously, protodeboronation involves protonolysis of the boron group to give a new aryl C–H bond (Scheme 1-27). The influence of *ortho*-fluorine substituents on the protodeboronation of aryl boronic acids was initially reported by Kuivila *et al.* in 1963, who studied the rate of protodeboronation of fluorinated aryl boronates at pH 6.5 at 90 °C in aqueous malonate buffer (Table 1-1).^[70] It was concluded that: (i) in the case of mono fluoride substrates the rates of protodeboronation decreased in the order of *ortho* > *para* > *meta*; (ii) for difluoro-substituted aryl boronic acids, protodeboronation rates were faster for *ortho-meta*-substituted substrates as opposed to those in the *ortho-para*-positions; and (iii) that $\text{C}_6\text{F}_5\text{B}(\text{OH})_2$, which involved all *ortho*-, *meta*-, and *para*-fluorine positions, had the highest rates of protodeboronation.

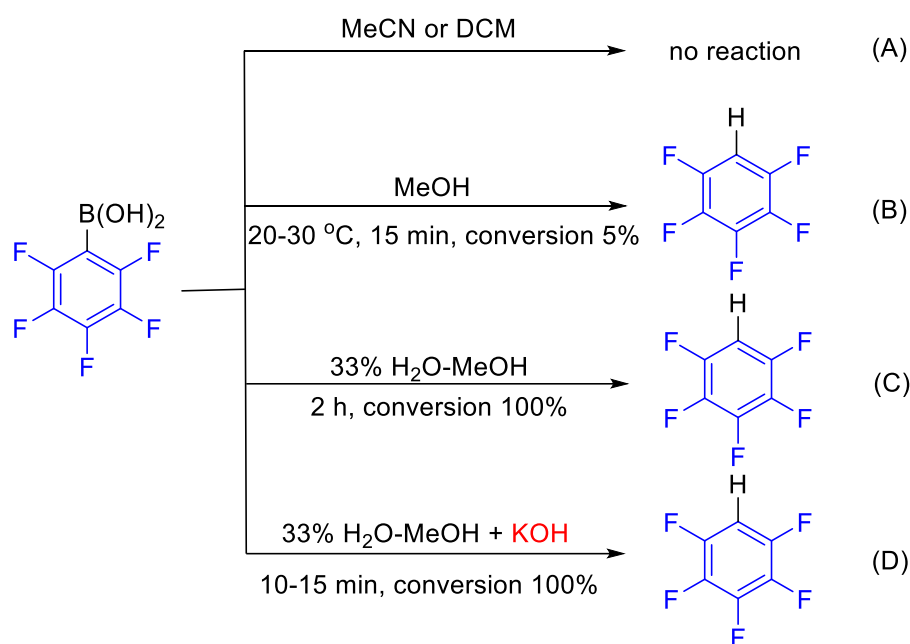


Scheme 1-27. A general protodeboronation reaction.

Table 1-1. Effect of fluorine substituents on the relative rates of protodeboronation of aryl boronic acids.^[25,70]

							
k_{rel}	1.0	1.4	0.3	11	--	--	Kuivila, 1963
k_{rel}	1.0	1.4	0.98	243	616	1548	Lloyd-Jones, 2017

In 2002, Frohn and Adonin *et al.* also reported the protodeboronation of fluorinated aryl boronic acids.^[71] In this study, they found that $C_6F_5B(OH)_2$ was stable in MeCN and dichloromethane, but was less stable in methanol at 20–30 °C with about 5% conversion to the decomposition product per 15 minutes (Scheme 1-28). Moreover, the protodeboronation rate of $C_6F_5B(OH)_2$ was faster in a 33% H_2O -MeOH solvent mixture and the process was complete within 2 hours to give C_6F_5H . The addition of KOH increased the rate of protodeboronation so that the reaction was complete within 10–15 minutes.

**Scheme 1-28.** Protodeboronation of $C_6F_5B(OH)_2$: (A) in acetonitrile or dichloromethane; (B) in methanol; (C) in 33% H_2O -methanol; (D) in 33% H_2O -methanol + KOH.^[71]

Protodeboronation of $C_6F_5B(OH)_2$ was immediate and occurred exothermically in a mixture of D_2O -pyridine at room temperature within 3–5 minutes (Table 1-2, entry 1). Not surprisingly, when the aryl boronic acid contained only one *ortho*-fluorine group, protodeboronation occurred considerably more slowly than with substrates containing two *ortho*-fluorine groups (Table 1-2, entries 2, 4 and entries 8, 9). Notably, with no *ortho*-fluorine substituent, protodeboronation did not occur for electron deficient compounds such as 3,4,5- $C_6F_3H_2B(OH)_2$ even after 180 minutes at high temperatures (Table 1-2, entry 7).

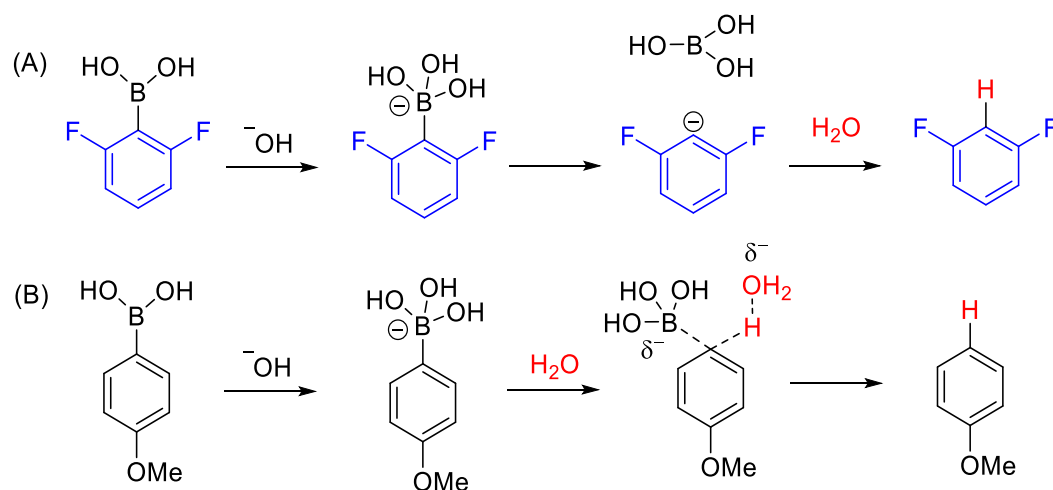
Table 1-2. Total conversion of polyfluorophenyl- $B(OH)_2$ into deuteropolyfluorobenzenes (ArD) in 9% D_2O -pyridine (v/v).^[71]

Entry	Compound	T (°C)	Time of conversion (min)
1	$C_6F_5B(OH)_2$	25	< 3 – 5
2	2,3,4,5- $C_6F_4HB(OH)_2$	100	50
3	2,3,4,6- $C_6F_4HB(OH)_2$	32	210 ^[a]
4	2,3,4,6- $C_6F_4HB(OH)_2$	100	15
5	2,3,5,6- $C_6F_4HB(OH)_2$	32	60
6	2,4,6- $C_6F_3H_2B(OH)_2$	100	90
7	3,4,5- $C_6F_3H_2B(OH)_2$	100	180, no reaction
8	2,4- $C_6F_2H_3B(OH)_2$	100	1140 (19 hours) ^[b]
9	2,6- $C_6F_2H_3B(OH)_2$	100	150

^[a] Conversion 82 %. ^[b] Conversion 53 %.

Lloyd-Jones *et al.*^[25] studied the mechanism, supported by experimental and computational evidence, for the protodeboronation of aryl boronic acid containing *ortho*-fluorine substituents. They disclosed that protodeboronation occurs *via* a C–B heterolysis of a trihydroxy organoboronate intermediate ($[M]^+[ArB(OH)_3]^-$), which notably does not require water in this step. This is followed by a proton transfer from water to generate the hydrolyzed product (Scheme 1-29A). Protodeboronation of 2,6-difluorophenyl boronic acid is rapid due to the *ortho*-fluorine substituents stabilizing an *ipso*-aryl carbanion with delocalization of the negative charge ($n \rightarrow \sigma^*_{C(2)-C(3)}$ and $n \rightarrow \sigma^*_{C(6)-C(5)}$) into the C(2)–F and C(6)–F bonds and, hence, the accompanying rehybridization increases the s-character at the carbanion (C1) (Figure 1-6). Furthermore, their kinetic studies showed that unimolecular heterolysis of the aryl boronate ester to give boric acid is the rate-limiting

step (Scheme 1-29A). However, unlike di-*ortho*-fluoro substituted aryl boronic acids, the rate limiting step of protodeboronation in electron-rich aryl boronic acids was observed to be proton transfer from a molecule of water followed by cleavage of the C–B bond to generate boric acid (Scheme 1-29B). Twenty isomers of $C_6F_{5-n}H_nB(OH)_2$ were studied with half-lives ($t_{1/2}$) that measured spanning 9 orders of magnitude, from < 3 minutes to 6.5 months, showing that *ortho*-fluorinated aryl boronic acids accelerated protodeboronation, with $C_6F_5B(OH)_2$ displaying the fastest rate.



Scheme 1-29. Mechanism of the base-catalyzed protodeboronation of (A) 2,6-difluorinated aryl boronic acid vs. (B) 4-anisyl boronic acid.^[25]

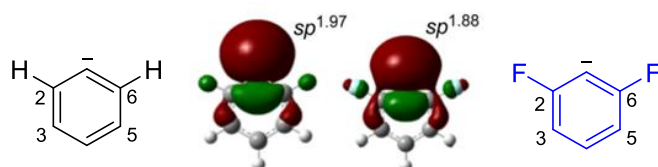
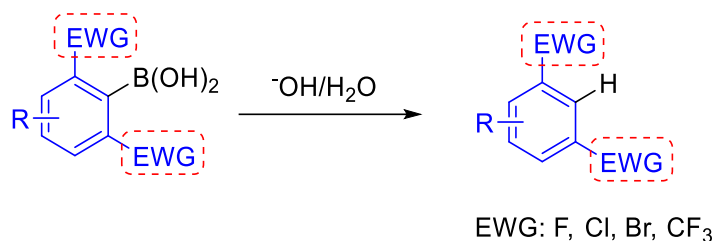


Figure 1-6. NLMO analyses of non-fluorinated and 2,6-difluorinated aryl anions which will be generated by C–B heterolysis of their corresponding trihydroxy aryl boronates. Adapted with permission.^[25] Copyright 2017, American Chemical Society.

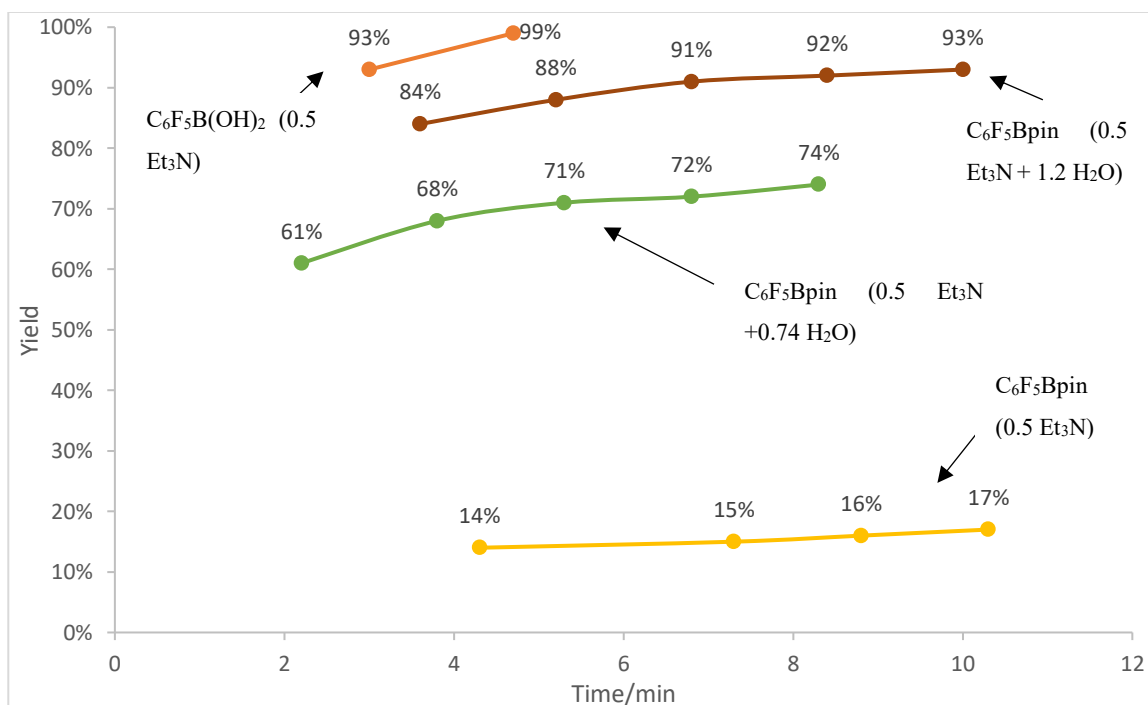
Interestingly, Perrin *et al.* reported that many typical electron-deficient aryl boronic acids, including fluorinated derivatives, are stable in acidic solutions of 0.1 M HCl.^[72] Under aqueous basic conditions (200 mM hydroxide), aryl boronic acids that contain di-*ortho*-substituted electron withdrawing groups such as fluoride, chloride, bromide, and trifluoromethyl groups, are unstable towards protodeboronation (Scheme 1-30).



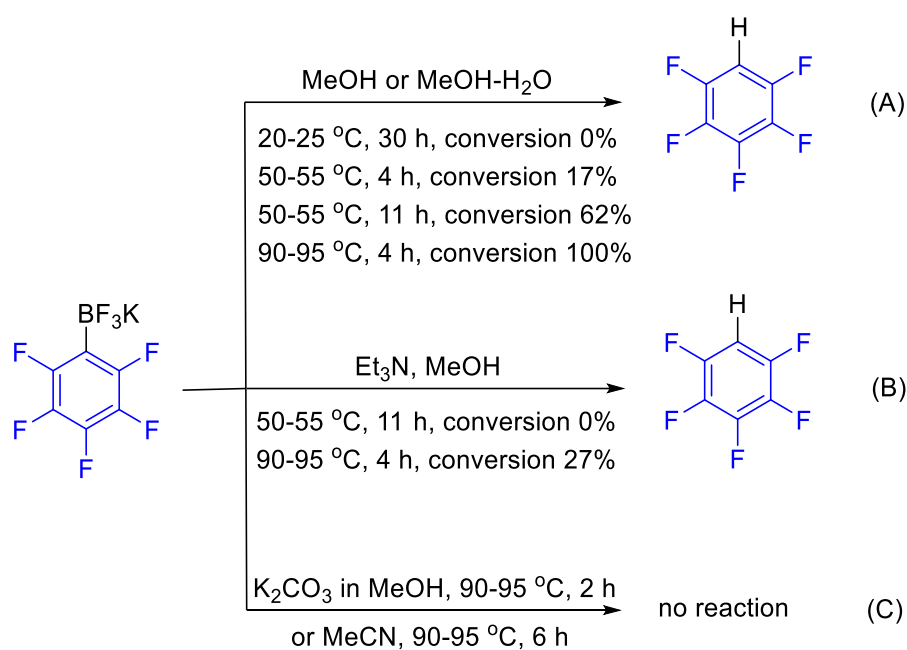
Scheme 1-30. Base-promoted protodeboronation of electron-poor 2,6-disubstituted aryl boronic acids.^[72]

Carrow *et al.* studied the influence of triethylamine and/or water with respect to the stability of C₆F₅Bpin and C₆F₅B(OH)₂ towards protodeboronation.^[73] Notably, triethylamine was used as received and contains trace amounts of water. In this study, they measured the yield of C₆F₅H that was generated from the protodeboronation of C₆F₅B(OH)₂ and C₆F₅Bpin solutions in THF-triethylamine and treated with various numbers of equivalents of water. As shown in Chart 1-1, in the presence of triethylamine (0.5 equivalent), C₆F₅Bpin is much more stable than C₆F₅B(OH)₂. Thus, it can be concluded that C₆F₅Bpin is more stable than its boronic acid analogue in anhydrous basic solution.

Chart 1-1. Yield of C₆F₅H that resulted from protodeboronation of C₆F₅B(OH)₂ or C₆F₅Bpin determined by ¹⁹F NMR spectroscopy.^[73]



Adonin *et al.* investigated the protodeboronation of potassium polyfluoroaryltrifluoroborate salts ($\text{Ar}_F\text{-BF}_3\text{K}$).^[74] Unlike $\text{C}_6\text{F}_5\text{B}(\text{OH})_2$, which is prone towards protodeboronation at 20–30 °C (ca. 5% conversion within 15 minutes), $\text{C}_6\text{F}_5\text{BF}_3\text{K}$ was stable over 30 hours upon treatment with methanol or aqueous methanol at 20–25 °C (Scheme 1-29A). However, this salt slowly protodeboronated at elevated temperatures such as 50–55 °C (17% and 62% after 4 and 11 hours, respectively) or 90–95 °C (conversion was complete after 4 hours) (Scheme 1-31A). Interestingly, protodeboronation could be reduced by addition of base, such as Et_3N or K_2CO_3 (Scheme 1-31B). It should be noted that protodeboronation did not occur when $\text{C}_6\text{F}_5\text{BF}_3\text{K}$ was treated with K_2CO_3 in methanol or in weakly basic solvents such as MeCN (Scheme 1-31C). In addition, opposite results were found under acidic conditions. Frohn *et al.* had previously reported that $\text{C}_6\text{F}_5\text{BF}_3\text{K}$ was readily protodeboronated within 6 hours in 40% HF_{aq} at elevated temperatures (85–95 °C).^[75]



Scheme 1-31. Protodeboronation of $\text{C}_6\text{F}_5\text{BF}_3\text{K}$ in methanol: (A) without base; (B) with Et_3N ; and (C) with K_2CO_3 or MeCN.^[74]

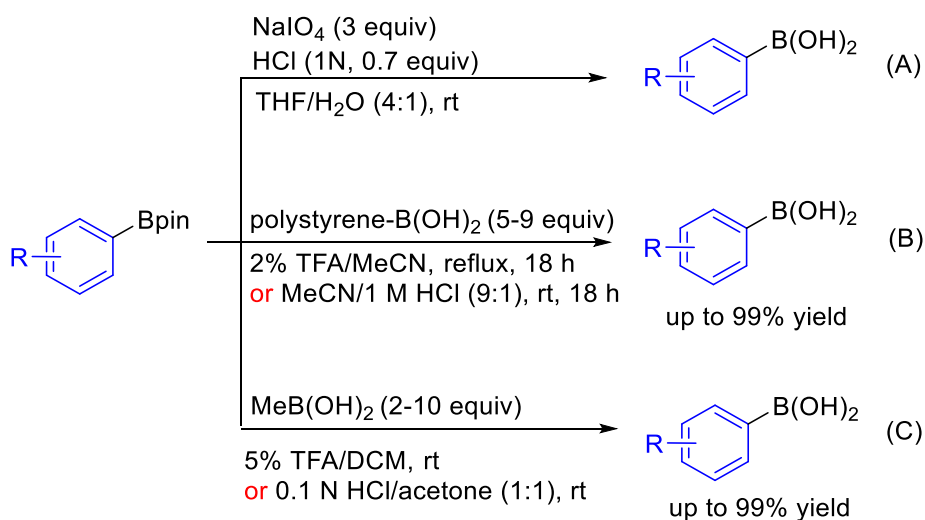
In summary, under aqueous basic conditions *ortho*-fluorine groups are known to promote the protodeboronation of aryl boronates (except for trifluoroborate salts). Furthermore, $\text{C}_6\text{F}_5\text{B}(\text{OH})_2$, which contains fluorine substituents at all positions, is remarkably unstable with respect to this decomposition pathway and remains a challenging substrate for use in organic synthesis.

1.5 Applications of Fluorinated Aryl Boronates in Organic Synthesis

1.5.1 Intermediates for the Introduction of Functional Groups

1.5.1.1 Conversion of Fluorinated Aryl Boronate Esters to Boronic Acids or Trifluoroborate Salts

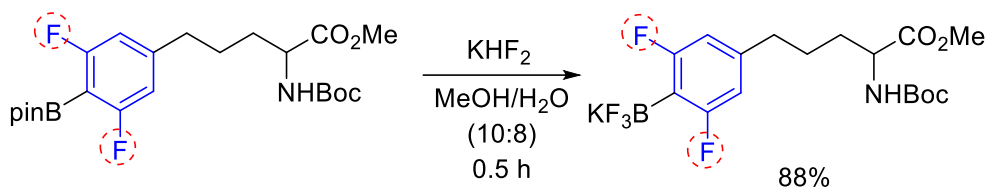
The reactivity of organoboron compounds is dictated by the substituents bound to the boron atom and, hence, the resulting Lewis acidity of the compound. For example, aryl pinacol boronate esters are less reactive than aryl boronic acids or trifluoroborate analogues as substrates for the copper-catalyzed C–N cross-coupling of aryl amines^[76,77] or C–O coupling with phenols.^[77] The conversion of aryl pinacol boronate esters to their boronic acid analogues has been reported *via* oxidative hydrolysis^[77,78] or transesterification with excess polystyrene boronic acid^[79] or methyl boronic acid.^[80] In general, these methods are conducted under acidic conditions in the presence of trifluoroacetic acid (TFA) or HCl (Scheme 1-32). However, these methodologies have not yet examined for aryl boronate ester substrates containing *ortho*-fluorine substituents.



Scheme 1-32. Conversion of aryl pinacol boronates to their boronic acid analogues *via* oxidative hydrolysis (A) or transesterification with polystyrene boronic acid (B) or methyl boronic acid (C).^[77-80]

Organotrifluoroborates are reportedly more stable to air and moisture than their boronic acid or ester counterparts.^[81-84] The conversion of aryl boronate esters to the corresponding trifluoroborate

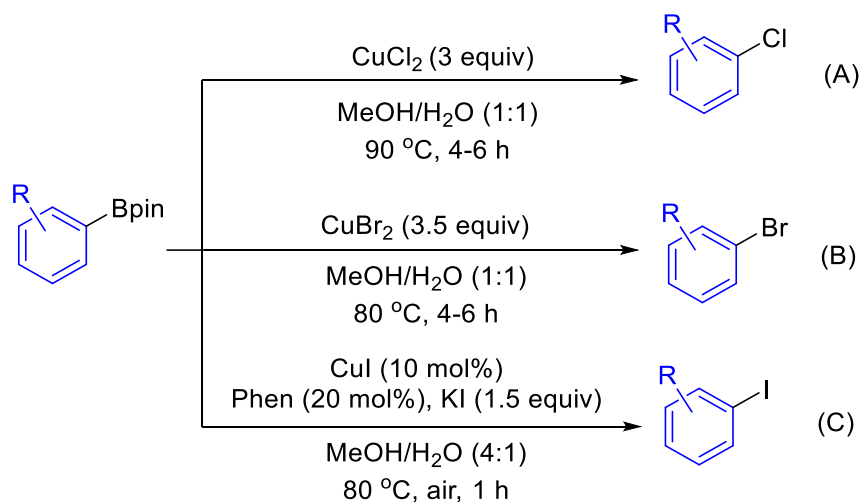
analogues is readily accomplished with the addition of potassium hydrogen difluoride (KHF₂).^[78,85] As shown in Scheme 1-33, the method is viable for the conversion of aryl pinacol boronates containing two *ortho*-fluorines in high yields.



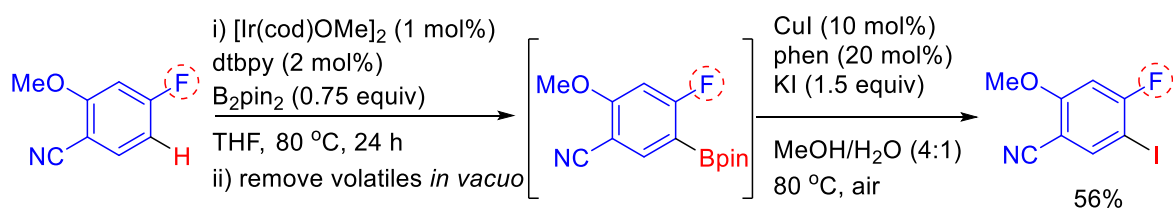
Scheme 1-33. Conversion of a 2,6-fluorinated aryl pinacol boronate to its trifluoroborate analogue.^[85]

1.5.1.2 Conversion of Fluorinated Aryl Boronate Esters to Aryl Halides

Aryl halides are among the most important intermediates in organic synthesis. Reliable methods to convert aryl boronate esters to aryl chlorides or bromides *via* addition of stoichiometric amounts of CuCl₂ or CuBr₂ (Scheme 1-34A and B) have been reported.^[86] However, addition of CuI to aryl boronate esters under these conditions did not afford the corresponding aryl iodides. Subsequent research found that a reliable method to generate these aryl iodides is the addition of stoichiometric amounts of potassium iodide (KI) as the source of iodide along with a combination of 10 mol% CuI and 20 mol% of phenanthroline at 80 °C (Scheme 1-34C).^[87] Hartwig, *et al.* were able to carry out a tandem iridium-catalyzed borylation/copper-catalyzed iodination of aryl pinacol boronates with substrates involving only one *ortho*-fluorine substituent (Scheme 1-35).^[87]



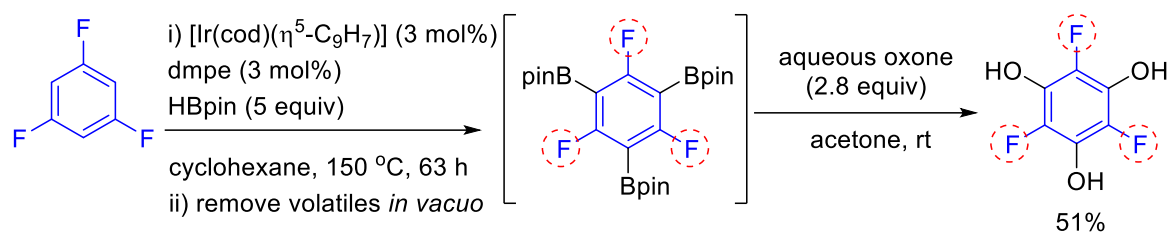
Scheme 1-34. Conversion of aryl pinacol boronate esters to aryl halides.^[86,87]



Scheme 1-35. One pot C–H borylation and iodination of an *ortho*-fluorinated aryl pinacol boronate ester.^[87]

1.5.1.3 Conversion of Fluorinated Aryl Boronate Esters to Phenols

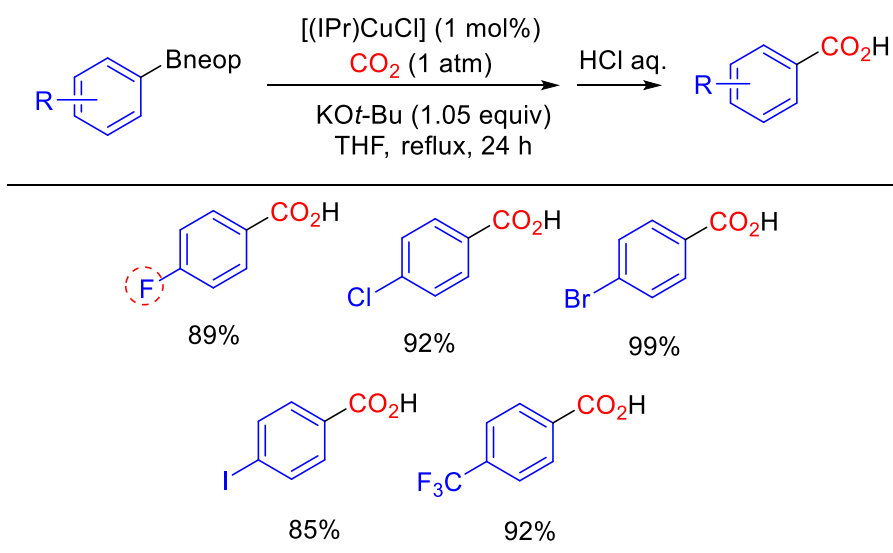
Phenols are important building blocks in organic synthesis, having diverse applications in areas such as polymer and pharmaceutical chemistry.^[88] A reliable method to generate aryl hydroxyl compounds is *via* oxidation of aryl boronate esters using aqueous oxone. Indeed, Maleczka, *et al.* combined the oxidation of aryl pinacol boronate esters as a second step after an initial iridium-catalyzed borylation. Notably, this method is efficient for the generation of phenols in which the C–OH bond is flanked by two C–F bonds (Scheme 1-36).^[89]



Scheme 1-36. Iridium-catalyzed borylation/oxidation of fluorinated arenes.^[89]

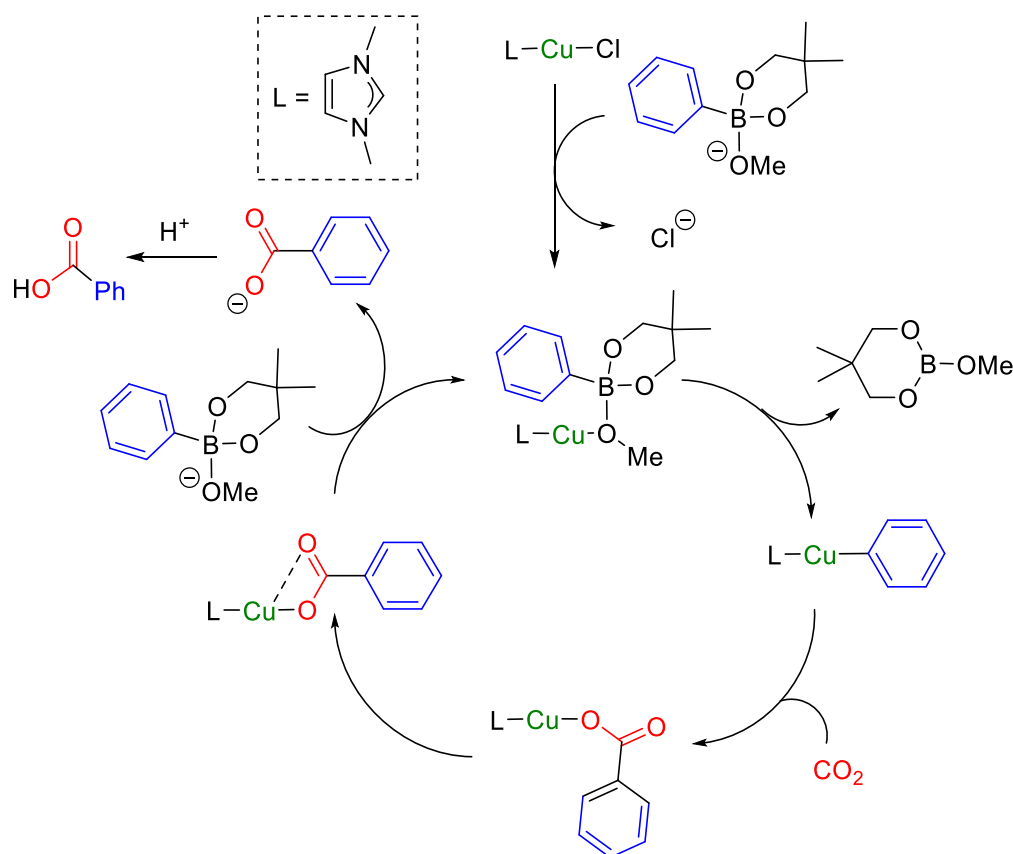
1.5.1.4 Conversion of Fluorinated Aryl Boronate Esters to Corresponding Carboxylic Acids

Carbon dioxide is an important feedstock in the chemical industry and is used in the construction of medicinal, agricultural, and specialty chemicals.^[90] In 2008, Hou *et al.* reported the carboxylation of aryl-Bneop (neop = neopentylglycolato) derivatives, using an NHC-copper complex as the catalyst.^[91] Thus, $[(\text{IPr})\text{CuCl}]$ (IPr = 1,3-bis(2,6-diisopropylphenyl)-imidazol-2-ylidene) is efficient to catalyze the carboxylation of aryl-Bneop, in the presence of CO_2 (balloon), $\text{KO}t\text{-Bu}$ as the base, in THF solution, under reflux for 24 hours, followed by addition of 1M hydrochloric acid solution. Appreciable yields can also be obtained using a catalyst system formed *in situ* from a combination of Cu(I) or Cu(II) salts such as CuCl , CuBr , CuCl_2 or $\text{Cu}(\text{OAc})_2$ with protonated NHC ligands such as $\text{IPr}\cdot\text{HCl}$ or $\text{IMes}\cdot\text{HCl}$. As shown in Scheme 1-37, these conditions are efficient for aryl-Bneop derivatives bearing electron-withdrawing substituents such as fluorine, chlorine, bromine, iodine, and CF_3 at the *para*-position to generate the corresponding carboxylation products in good to excellent yields. However, challenging *ortho*-fluorinated aryl-Bneop substrates were not examined.



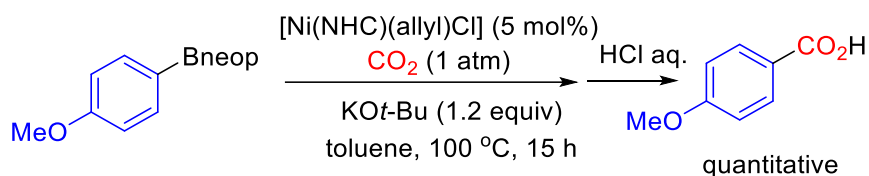
Scheme 1-37. Scope of the copper-catalyzed carboxylation of electron-deficient aryl-Bneop compounds.^[91]

In 2010, Lin, Marder, *et al.* reported DFT calculations on the mechanism of the above reaction using $[(NHC)Cu(OMe)]$ as a model complex and phenyl-Bneop as the substrate.^[92] They proposed that the catalytic carboxylation occurs *via* three major steps (Scheme 1-38): (i) base-assisted transmetalation of phenyl-Bneop with $(NHC)CuCl$ to give $[(NHC)Cu(Ph)]$; (ii) rate determining insertion of CO_2 into the Cu-Ph bond to give $[(NHC)Cu-OC(O)Ph]$; and, finally (iii) this intermediate reacts with the alkoxy adduct of phenyl-Bneop to release the benzoate product and regenerate the catalyst.

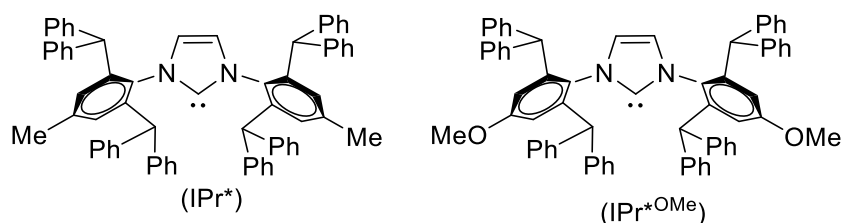


Scheme 1-38. Proposed mechanism of the copper-catalyzed carboxylation of phenyl-Bneop.^[92]

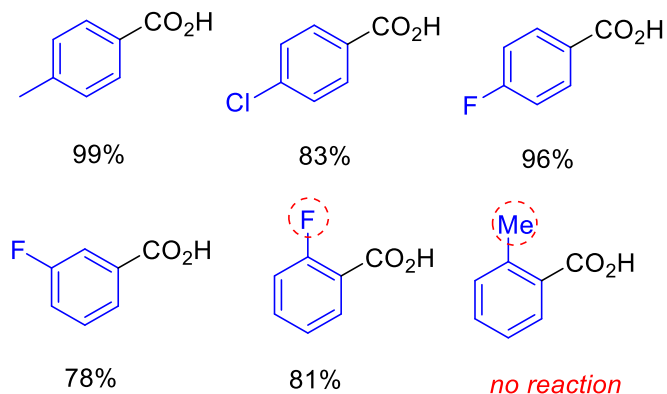
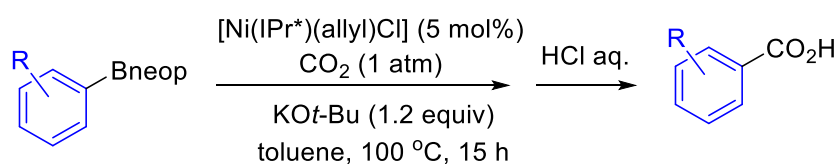
The carboxylation of fluorinated aryl-Bneop derivatives was also reported by Nolan *et al.* in 2014 using a NHC-nickel complex as the catalyst.^[93] Among the nickel complexes examined for this reaction, $[Ni(IPr^*)(allyl)Cl]$ and $[Ni(IPr^{*OMe})(allyl)Cl]$ were found to give carboxylation products in near quantitative yields (Scheme 1-39). It should be noted that the reaction can be conducted using a catalyst system formed *in situ* from $[Ni(cod)_2]$ and IPr^* . Reactions are viable for aryl-Bneop bearing electron-rich or electron-poor substituents to give the corresponding carboxylation products in good to excellent yields (Scheme 1-40). However, this method was not effective for aryl-Bneop derivatives bearing sterically bulky substituents at the *ortho*-position. Interestingly, no reaction was observed using other aryl boron reagents such as boronic acids, pinacolates, or potassium trifluoroborates. It was suggested that the addition of a strong base, such as $KOt-Bu$, accelerated the transmetalation step and the overall reaction of 4-fluorophenyl-Bneop (Scheme 1-41). Further carboxylation of the aryltrialkoxo borate gave the corresponding carboxylic acid in good yield even without the addition of base.



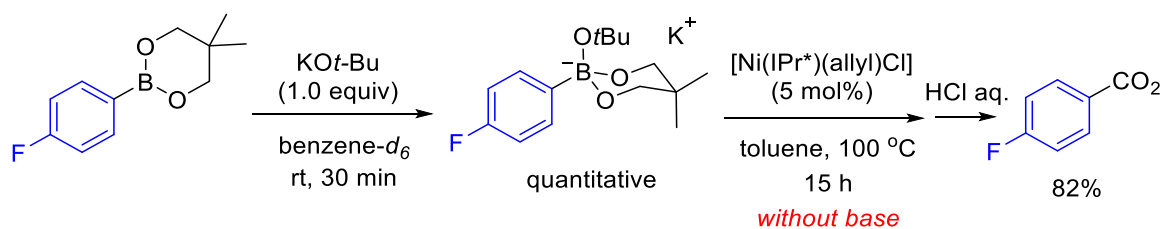
Yield is near quantitative if Ni precatalyst = $[\text{Ni}(\text{IPr}^*)(\text{allyl})\text{Cl}]$, or
 $[\text{Ni}(\text{IPr}^*\text{OMe})(\text{allyl})\text{Cl}]$, or
 $[\text{Ni}(\text{cod})_2] / \text{IPr}^*$



Scheme 1-39. Optimized conditions for nickel-catalyzed carboxylations.^[93]



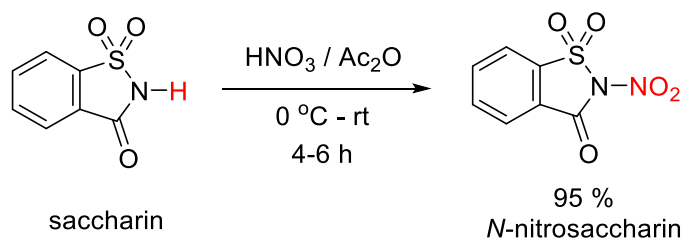
Scheme 1-40. The scope of nickel-catalyzed carboxylations.^[93]



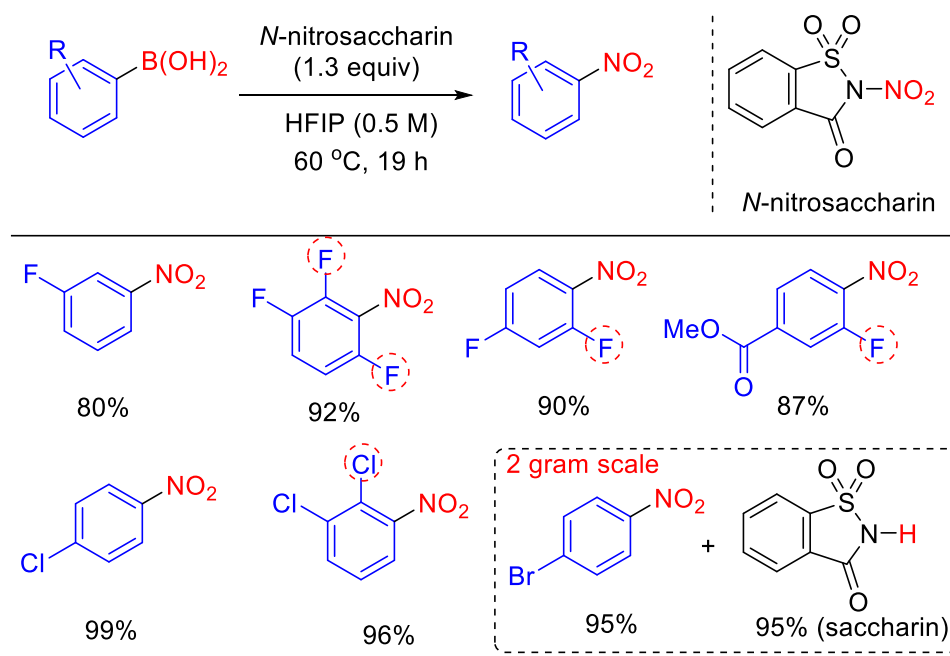
Scheme 1-41. The role of KOt-Bu in transmetalation reactions of aryl-Bneop compounds.^[93]

1.5.1.5 Conversion of Fluorinated Aryl Boronates to Nitro Arenes

Nitroaromatic compounds are highly useful synthons in pharmaceutical chemistry.^[94] Although no examples of the conversion of aryl boronate esters into their nitroaromatic counterparts have been reported, these useful compounds can be prepared using aryl boronic acids^[95] or trifluoroborate salts.^[96] Recently, Katayev *et al.* reported the conversion of aryl boronic acids into their nitro analogues using non-metal, recyclable, and bench-stable nitrating reagents, such as *N*-nitrosaccharin.^[95] *N*-Nitrosaccharin was readily synthesized from the reaction of a saccharin solution in acetic anhydride with nitric acid (Scheme 1-42). The reaction of electron-deficient aryl boronic acids with 1.3 equivalents of *N*-nitrosaccharin in 0.6 M hexafluoroisopropanol at 60 °C for 19 hours gave the corresponding aromatic nitro compounds in good to excellent yield (Scheme 1-43). Notably, high conversion was also observed for unstable and challenging substrates such as aryl boronic acids containing two *ortho*-fluorine groups and could be scaled up to the gram level.



Scheme 1-42. Synthesis of *N*-nitrosaccharin.^[95]

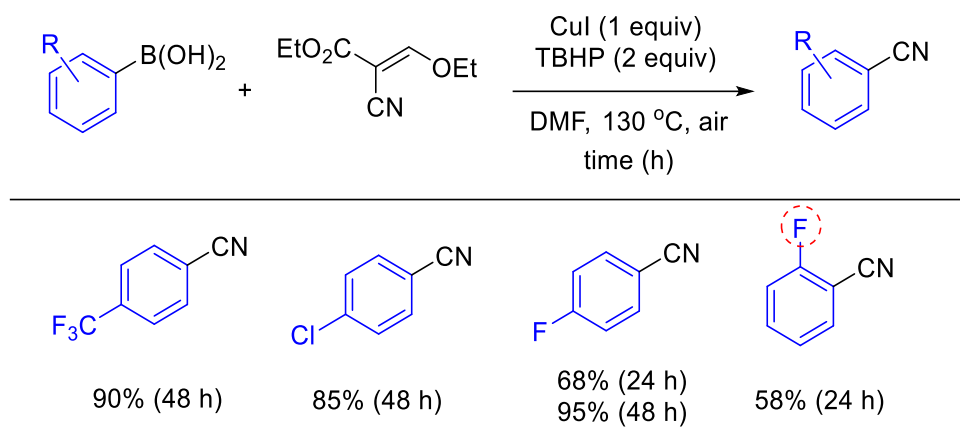


Scheme 1-43. *Ipsso*-Nitration of aryl boronic acids using *N*-nitrosaccharin as the nitrating reagent.^[95]

1.5.1.6 Conversion of Fluorinated Aryl Boronates to Cyanoarenes

Introducing cyano groups into drug candidates frequently improves the pharmacodynamics and pharmacokinetics of the molecules.^[97] In 2012, Hartwig *et al.* reported that a $[\text{Ir}(\text{cod})\text{OMe}]_2$ catalyzed arene C–H borylation, followed by a copper-mediated cyanation using $\text{Zn}(\text{CN})_2$ and a stoichiometric amount of a base, such as CsF , afforded the corresponding desired cyano products.^[98] In 2013, Han *et al.* showed a combination of $\text{Cu}_2\text{O}/N,N'$ -dimethylethylenediamine (DMEDA) catalyzed the cyanation of aryl pinacol boronate esters in the presence of trimethylsilyl cyanide (TMS-CN).^[99] In 2006, Liebeskind *et al.* reported the palladium-catalyzed/copper-mediated cyanation of aryl boronic acids with benzylthiocyanate as a CN source.^[100] In 2016, Senanayake *et al.* reported a low loading $[\{\text{RhCl}(\text{cod})\}_2]$ -catalyzed cyanation of aryl boronic acids with dimethylmalononitrile (DMMN) in the presence of stoichiometric amount of base, such as Cs_2CO_3 .^[101] The cyanation of *ortho*-fluorinated aryl boronic acids was reported by Qi *et al.* in 2016.^[102] In this study, the cyanation of aryl boronic acids was achieved using 2 equivalents of ethyl (ethoxymethylene)cynoacetate as the CN source in the presence of 1 equivalent of copper iodide and 2 equivalents of *tert*-butyl hydroperoxide (TBHP) as the oxidant. As shown in Scheme 1-44,

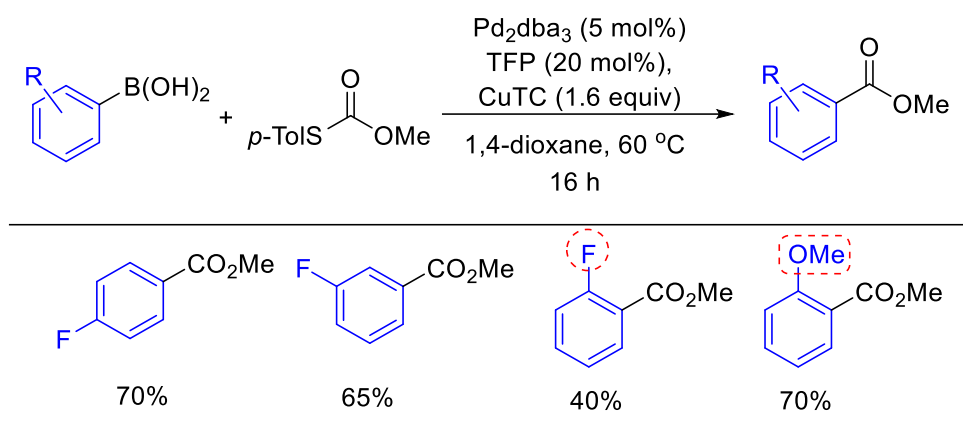
these reactions tolerated aryl boronic acid substrates bearing electron-withdrawing substituents such as trifluoromethyl, chlorine, and fluorine at the *ortho*- or *para*-positions to give cyanoarenes in excellent yields after 48 hours. However, attempts to promote the cyanation of aryl boronic acids bearing two *ortho*-fluorine groups were not examined.



Scheme 1-44. Copper-promoted cyanation of aryl boronic acids with ethyl (ethoxymethylene)cynoacetate as the cyanating agent.^[102]

1.5.1.7 Methyl Esterification of Fluorinated Aryl Boronates

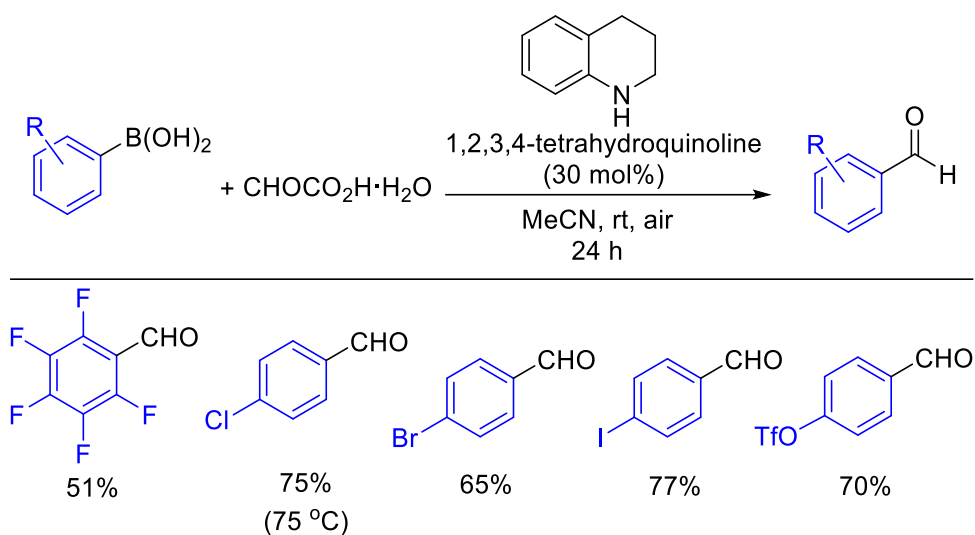
Aryl carboxylate esters are another important class of compounds in organic synthesis and pharmaceutical chemistry.^[103] The esterification of fluorinated aryl boronates was initially reported by Xu and Dai *et al.*^[104] In this study, *O*-methyl *S*-*p*-toluenyl thiocarbonate was used as the methoxy carbonylation reagent. A catalytic amount of Pd₂(dba)₃/TFP (tri(2-furyl)phosphine) was used as the catalyst system, in the presence of stoichiometric amounts of copper(I) thiophene-2-carboxylate (CuTC). Previously, CuTC salts were proposed in the Liebeskind-Srogl cross-coupling reaction to have a role in forming a strong Cu–S bond with the thioester, thus accelerating the transmetalation step with the palladium catalyst.^[105] As shown in Scheme 1-45, the reaction is viable for employing aryl boronic acids bearing a fluorine substituent in either the *para*- or *meta*-position. In general, reactions using *ortho*-electron-donating substituents gave higher yields than those containing electron-withdrawing substituents.



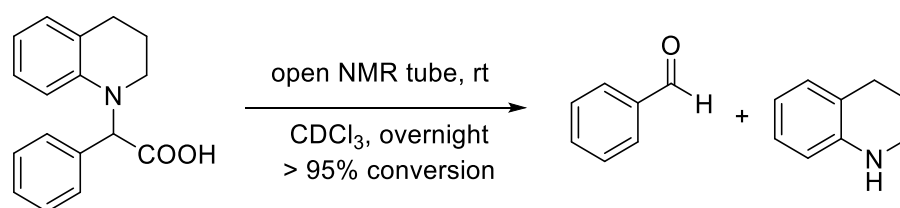
Scheme 1-45. Palladium-catalyzed esterification of aryl boronic acids.^[104]

1.5.1.8 Conversion of Fluorinated Aryl Boronates to Aldehydes

Compounds containing an aldehyde group are important synthons in organic synthesis as they can readily be transformed into a plethora of functional groups. For example, Vemuravenib, which is used for treatment of late-stage melanoma, and Sitagliptin, which is a promising antidiabetic candidate, are synthesized from fluorinated benzaldehyde derivatives (Figure 1-1).^[3] In 2017, Wang *et al.* reported a method to convert aryl boronic acids to aldehydes in the presence of glyoxylic acid monohydrate and 1,2,3,4-tetrahydroquinoline acting as an organocatalyst.^[106] This method was successful using the challenging substrate, $\text{C}_6\text{F}_5\text{B(OH)}_2$, to give 2,3,4,5,6-pentafluorobenzaldehyde in a fair yield (51%). Interestingly, this reaction was tolerant of aryl boronic acids bearing reactive groups such as *para*-chlorine, bromine, iodine, and triflate (Scheme 1-46). The reaction was proposed to involve a Petasis intermediate, whereupon independent synthesis of this species followed by treatment with CDCl_3 in air afforded benzaldehyde quantitatively (Scheme 1-47).



Scheme 1-46. Amine-catalyzed formylation of aryl boronic acids with glyoxylic acid.^[106]



Scheme 1-47. Conversion of a Petasis intermediate to give benzaldehyde.^[106]

1.5.2 Homocoupling Reaction

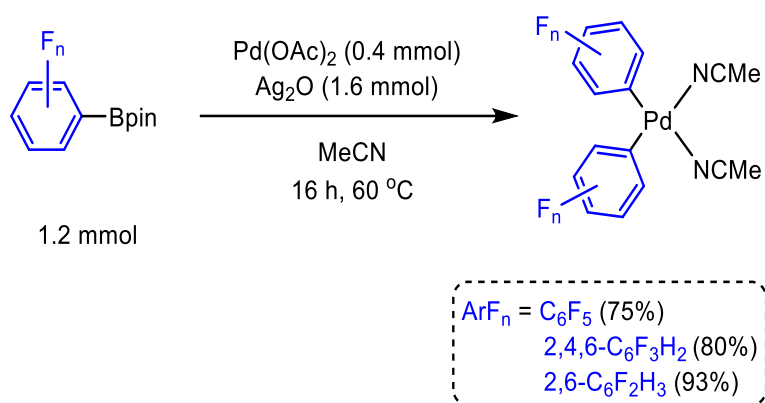
1.5.2.1 Palladium-catalyzed Homocoupling of Polyfluorophenyl Boronate

Esters

In transition metal catalysis, reductive elimination is an important step to release the coupled products.^[107,108] Indeed, two electronic effects play an important role in the reductive elimination of $[\text{ML}_2(\text{Ar})(\text{Ar}')]$ complexes containing group-10 metals to form biaryl compounds $\text{Ar}-\text{Ar}'$. Reductive elimination is favorable if the ancillary ligands are weak electron donors or strong π -acceptors.^[109] Furthermore, the rate of reductive elimination of $\text{Ar}-\text{Ar}'$ from these complexes decreases in the order $\text{Ar}_{\text{rich}}-\text{Ar}'_{\text{poor}} > \text{Ar}_{\text{rich}}-\text{Ar}'_{\text{rich}} > \text{Ar}_{\text{poor}}-\text{Ar}'_{\text{poor}}$ (Ar_{rich} = electron rich aryl; Ar_{poor} = electron poor aryl). Moreover, reductive elimination of very electron poor diaryls, such as $\text{C}_6\text{F}_5-\text{C}_6\text{F}_5$, is challenging owing to the strong metal- C_{aryl} bonds.^[110-112]

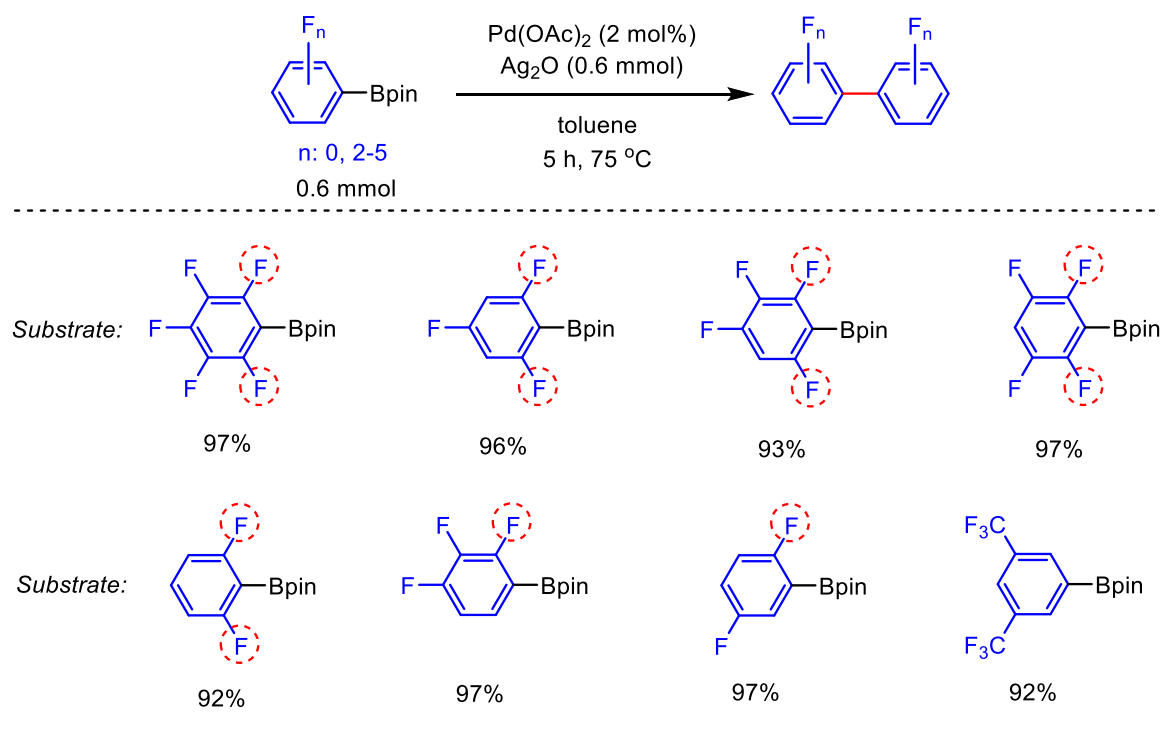
In 2011, Menezes and Oliveira *et al.* reported optimized conditions for the homocoupling of potassium aryl trifluoroborates salts in aqueous media.^[113] However, if the aryl groups contain two *ortho*-fluorine substituents, homocoupling products were not observed. In 2020, Radius and Marder *et al.*^[114] reported an efficient palladium-catalyzed homocoupling reaction of aryl pinacol boronates containing two *ortho*-fluorine groups. Reactions conducted in noncoordinating solvents such as toluene, benzene, or *m*-xylene were found to promote reductive elimination in the absence of ancillary ligands or coordinating solvents. Indeed, reactions conducted in weakly coordinating solvents were impeded by the formation of stable complexes of the type *cis*-[PdL₂(Ar_F)₂].

In this same investigation, the palladium-catalyzed homocoupling of fluorinated aryl-Bpin compounds was conducted in the presence of stoichiometric amounts of silver oxide, which acted not only as an oxidant but also had a role in facilitation of the transmetalation step (see Section 1.5.3.3 for the role of Ag₂O in transmetalation). Only reactions of aryl-Bpin compounds containing one *ortho*-fluorine group proved successful. Further investigation showed that stoichiometric reactions of C₆F₅Bpin, 2,4,6-trifluorophenyl-Bpin, and 2,6-difluorophenyl-Bpin with palladium acetate in MeCN once again resulted in the formation of the stable complexes *cis*-[Pd(NCMe)₂(C₆F₅)₂], *cis*-[Pd(NCMe)₂(2,4,6-C₆F₃H₂)₂], and *cis*-[Pd(NCMe)₂(2,6-C₆F₂H₃)₂], respectively (Scheme 1-48). Thus, it was concluded that: (i) reductive elimination from [PdL₂(Ar)₂] is problematic if the aryl ring contains two *ortho*-fluorines; and (ii) the use of weakly coordinating solvents, such as MeCN, generate stable complexes that shut down the homocoupling reaction. Therefore, the use of ‘noncoordinating’ arene solvents such as toluene, benzene, or *m*-xylene was required for the homocoupling of 2,6-C₆F_{2+n}H_{3-n}Bpin in excellent yields as long as no stronger coordinating solvents or ligands are present (Scheme 1-49).



Scheme 1-48. Synthesis of *cis*-[Pd(NCMe)(ArF_n)₂].^[114]

DFT calculations at the B3LYP-D3/def2-TZVP/6-311+g(2d,p)/IEFPCM // B3LYP-D3/SDD/6-31g**/IEFPCM level of theory were performed, which indicated an exergonic process and lower barrier (< 21 kcal/mol) for the reductive elimination of Pd(C₆F₅)₂ complexes bearing arene ligands, compared to stronger coordinating solvents or ancillary ligands (acetonitrile, THF, SMe₂, and PMe₃), which showed not only an endergonic process, but also required high energy barriers (> 34 kcal/mol). The reductive elimination from [Pd(η^n -Ar)(C₆F₅)₂] has a low barrier due to: (i) ring slippage of the arene ligand as the hapticity changes from η^6 in the reactant to η^n ($n \leq 3$) in the transition state and the product, which led to less σ -repulsion; and (ii) more favorable π -back-bonding from Pd(Ar_F)₂ to the arene fragment in the transition state. These findings support the experimental results, which showed that the palladium-catalyzed homocoupling of 2,6-difluoro-aryl-Bpin derivatives is efficient in aromatic solvents.

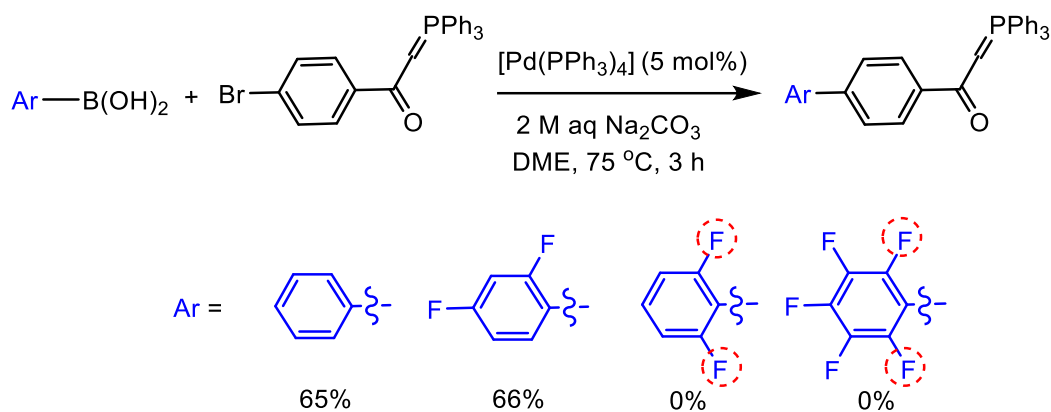


Scheme 1-49. Palladium-catalyzed homocoupling of fluorinated aryl pinacol boronates in toluene.^[114]

1.5.3 Suzuki-Miyaura Cross-Coupling

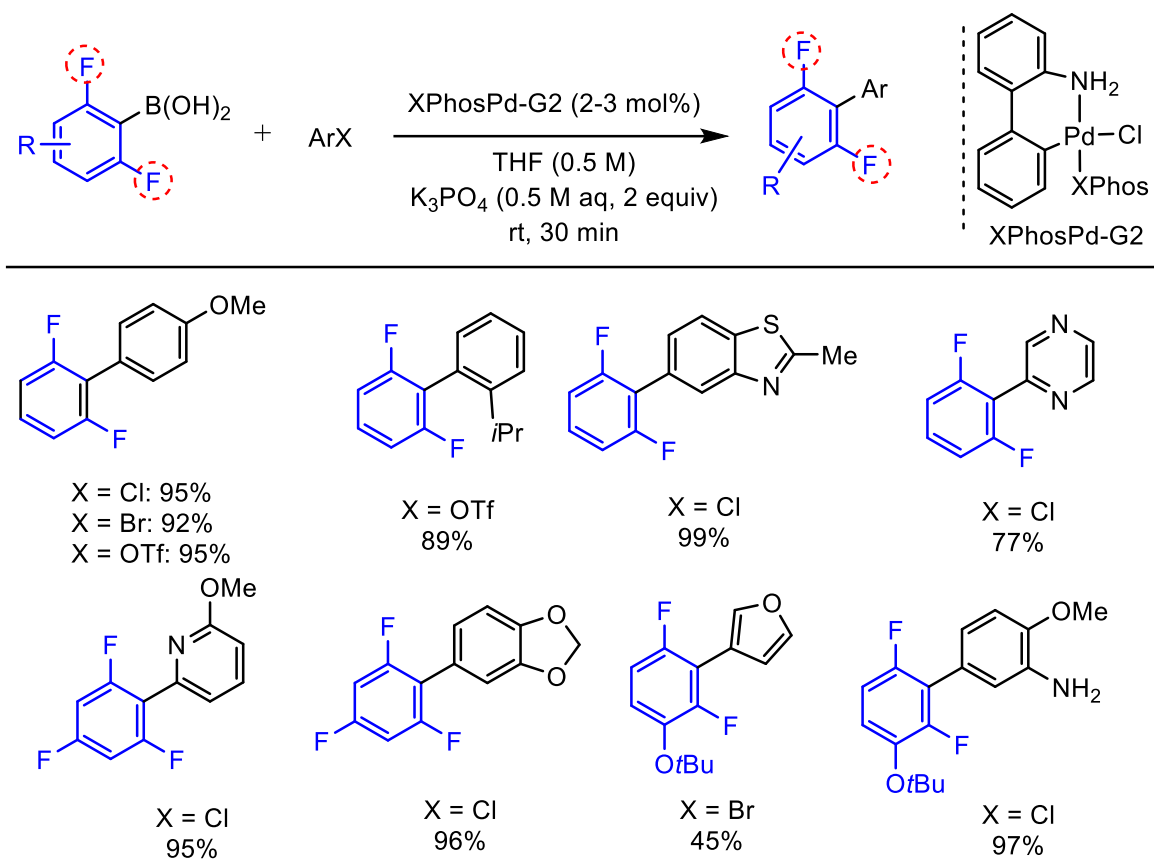
1.5.3.1 Palladium-Catalyzed Suzuki-Miyaura Cross-Coupling to Polyfluorophenyl Boronic Acids and Esters

The Suzuki-Miyaura cross-coupling reaction is well known as one of the most important methodologies for generating a C–C bond and has been widely utilized in the synthesis of natural products and in materials chemistry, including large-scale production.^[115-117] However, employing fluorinated aryl boronates that contain two *ortho*-fluorines in this reaction has been challenging.^[118-122] For example, Thiemann *et al.* reported optimized conditions for the palladium-catalyzed Suzuki-Miyaura cross-coupling of 4-bromobenzoylmethylidetriphenylphosphoran with fluorine-containing aryl boronic acids in good yields in some cases (Scheme 1-50).^[120] However, under these conditions, if the aryl boronic acids had two *ortho*-fluorines, *e.g.*, 2,6-difluorophenylboronic acid and pentafluorophenylboronic acid, the corresponding cross-coupled products were not observed. The reaction was only efficient for aryl boronic acid compounds bearing one *ortho*-fluorine.



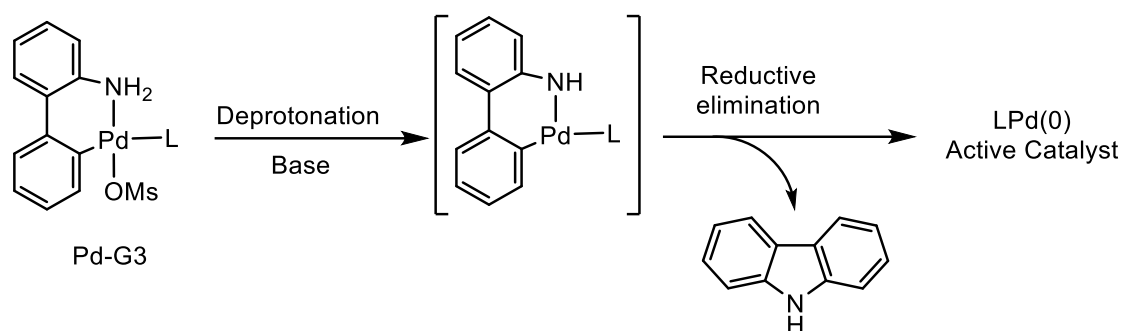
Scheme 1-50. Palladium-catalyzed cross-coupling of phosphoranes with aryl boronic acids.^[120]

In 2010, Buchwald *et al.* showed that the rate of transmetalation was accelerated by an increased number of fluorine substituents and that compounds containing *ortho*-fluorine groups displayed the highest activities.^[123] The precatalyst XPhosPd-G2 (Scheme 1-51) provided an active XPhosPd(0) species which underwent oxidative addition *in situ* and enhanced the cross-coupling rate. The rate of protodeboronation of polyfluorophenyl boronic acids was impeded by employing 0.5 M K₃PO₄ in THF at room temperature. These reactions were efficient for the Suzuki-Miyaura cross-coupling of 2,6-difluorophenylboronic acids derivatives with aryl bromides, chlorides, and triflates, but poor yields were observed using aryl iodides. The protodeboronation of 2,3,6-trifluorophenylboronic acid was rapid and poor yields were observed. This observation was supported by Lloyd-Jones *et al.* who showed that aryl boronic acids containing fluorine substituents at both the *ortho*- and *meta*-positions were susceptible to rapid protodeboronation.^[25]



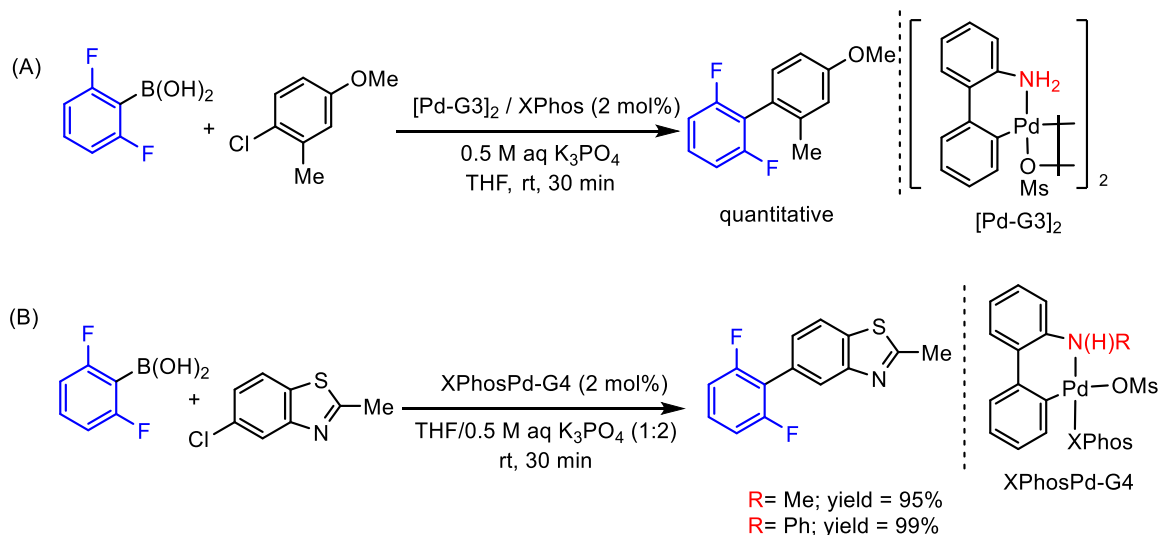
Scheme 1-51. Buchwald Pd-G2 precatalyst for Suzuki-Miyaura cross-coupling of polyfluorophenylboronic acids with aryl halides.^[123]

Later, Buchwald *et al.* replaced the precatalyst Pd-G2 with Pd-G3, by exchanging the chloride ligand at Pd-G2 with a noncoordinating methanesulfonate ligand (MS).^[124] However, activation of the precatalyst LPd-G3 to generate LPd(0) often resulted in a carbazole byproduct that reacted with the starting materials and made the isolation of products challenging (Scheme 1-52). It is important to note that there is a significant health risk associated with NH₂-aminobiphenyl impurities in pharmaceuticals.^[125]



Scheme 1-52. Activation of the Buchwald Pd-G3 precatalyst.^[124]

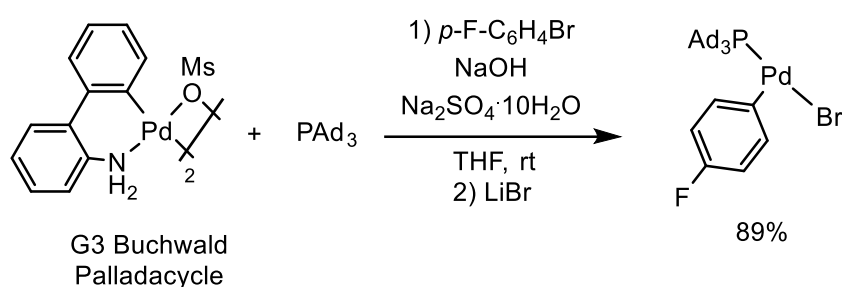
Further development generated precatalysts *via* the replacement of the NH₂-aminobiphenyl ligand of Pd-G3 with *N*-methyl or *N*-phenyl analogues to generate Pd-G4.^[126] Similar to Pd-G2, XPhos was also reported to be the optimal ligand in reactions with the dimer of Pd-G3 or the monomer of Pd-G4 for the Suzuki-Miyaura cross-coupling of 2,6-difluorophenyl boronic acid with aryl halides. Under these conditions, cross-coupled products were afforded in excellent yields (Scheme 1-53).^[124,126]



Scheme 1-53. Buchwald (A) Pd-G3 or (B) Pd-G4 precatalysts for the cross-coupling of 2,6-difluorophenyl boronic acids with aryl chlorides.^[124,126]

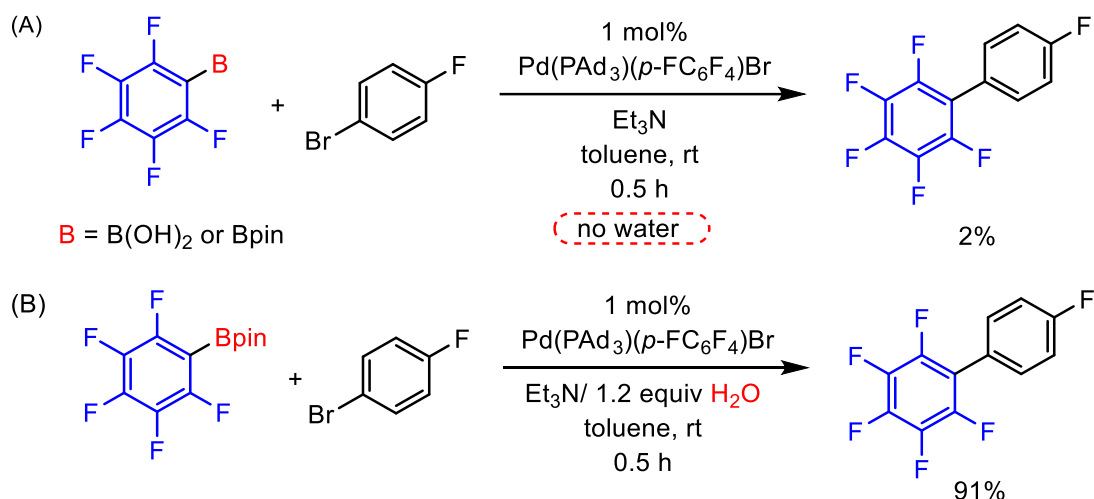
In 2018, Carrow *et al.* synthesized a series of unsaturated complexes of the type Pd(L)(Ar)X, including Pd(PAD₃)(*p*-FC₆H₄)Br (PAD₃ = tri(1-adamantyl)phosphine), which was found to be an efficient ‘on-cycle’ precatalyst.^[73] This system allowed for the Suzuki-Miyaura cross-couplings of highly fluorinated aryl boronic acids with aryl or heteroaryl bromides and proved to be faster than

the competing protodeboronation degradation pathway. The synthesis of the precatalyst proceeded *via* a room temperature reaction of G3 Buchwald palladacycle with 1-bromo-4-fluorobenzene (Scheme 1-54). The catalytic process initially occurred *via* deprotonation of the PAd₃-palladacycle G3 using sodium hydroxide, which led to the C–N reductive elimination of carbazole and the generation of an active species (PAd₃)Pd(0). The Pd(0) species generated is then believed to be trapped by 1-bromo-4-fluorobenzene, undergoing oxidative addition to give Pd(PAd₃)(*p*-FC₆H₄)Br. It is important to note that this T-shaped precatalyst is stable in air, under moisture, and on silica gel, which allows its easy purification *via* flash chromatography.



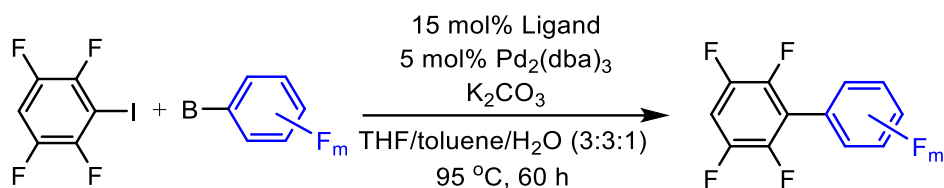
Scheme 1-54. Synthesis of Pd(PAd₃)(*p*-FC₆H₄)Br/Carrow precatalyst.^[73]

Treating a mixture containing C₆F₅B(OH)₂ with 1-bromo-4-fluorobenzene, 1 mol% of Pd(PAd₃)(*p*-FC₆H₄)Br with 1.1 equivalent of Et₃N at room temperature, afforded the corresponding cross-coupled product in only 2% yield (Scheme 1-55A). However, for reactions employing C₆F₅Bpin, an increased yield of 91% was obtained upon addition of 1.2 equivalents of water to the mixture (Scheme 1-55B). Notably, using insoluble salts such as Na₂SO₄·10H₂O as a source of water which can be released slowly in the reaction gave the highest yield in 93%. On the other hand, reactions with C₆F₅B(OH)₂ were still ineffective. These optimized conditions are appropriate for coupling various fluorinated aryl boronic acids or esters with aryl bromides and hetero aryl bromides in good yields. Unlike C₆F₅Bpin, which is more stable to wet triethylamine, C₆F₅B(OH)₂ decomposes within minutes to give C₆F₅H in 99% yield (see Section 1.4, Chart 1-1).



Scheme 1-55. Precatalyst Pd(PAd₃)(*p*-FC₆H₄)Br for cross-coupling of C₆F₅B(OH)₂ or its -Bpin analogue with (*p*-FC₆H₄)Br: (A) without water; or (B) with addition of water.^[73]

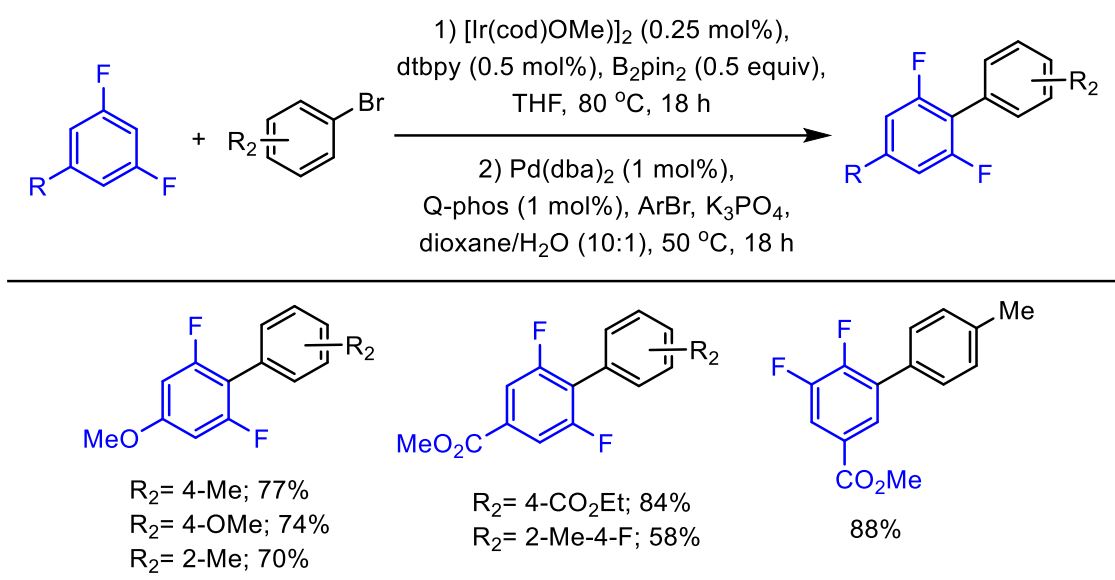
In 2017, Bulfield and Huber reported methods for the synthesis of polyfluorinated biphenyls, with fluorine substituents being present in both coupling partners.^[121] They employed a combination of 5 mol% of Pd₂(dba)₃ and 15 mol% of a phosphine ligand to couple fluorinated aryl boronates with fluorinated aryl halides. The reactions required K₂CO₃ as a base and long reaction times of 60 hours at 95 °C. They also selected different phosphine ligands to optimize each cross-coupling reaction that employed different fluorine substituents on aryl boronates and aryl halides. Selected examples are shown in Table 1-3 for the cross-coupling of 1,2,4,5-tetrafluoro-3-iodobenzene with different aryl boronates and ligands. Overall, aryl boronic acids that contain one *ortho*-fluorine group such as 2,3,4-trifluorophenyl boronic acid are still more difficult to undergo cross-coupling reactions than analogues with no *ortho*-fluorine groups, such as 3,4,5-trifluorophenyl boronic acid (Table 1-3, entries 1 and 2). However, better yields were obtained when neopentyl glycol boronic esters (Bneop) and (*N*-methyliminodiacetic acid) boronate (BMIDA) analogues were used (Table 1-3, entry 2). Employing the most electron deficient substrate, however, pentafluorophenyl boronic acid or its trifluoroborate salt analogue were not viable substrates under these conditions. (Table 1-3, entry 4).

Table 1-3. Palladium-catalyzed Suzuki-Miyaura cross-coupling to achieve polyfluorinated biaryls.^[121]

Entry	[B]-Ar _F	Product	Optimized yield (Ligand)
1			98% (CyJohnPhos)
2			28%, B: B(OH) ₂ (XPhos); 84%, B: Bneop (DavePhos); 80%, B: BMIDA (CyJohnPhos)
3			62% (DavePhos)
4			0%, B: B(OH) ₂ ; < 5%, B: BF ₃ ⁻ salt

In 2012, Hartwig *et al.* reported a method to synthesize fluorinated biaryls *via* a one-pot, two-step process, *i.e.*, iridium-catalyzed C–H borylation of fluoroarenes followed by Suzuki-Miyaura cross-coupling using a simple palladium catalyst (*vide supra*).^[32] Using this method, borylation occurred selectively *ortho* to the fluorine substituent due to its small size and the steric repulsion of other bulkier substituents such as methoxy, carboxylate, and chloride groups, etc. Buchwald *et al.*^[123,124,126] and Carrow *et al.*^[73] showed that highly reactive palladium precatalysts were needed to employ unstable substrates such as 2,6-difluoroaryl boronic acid. Interestingly, in a

further report, Hartwig *et al.* demonstrated that a combination of 1 mol% of Pd(dba)₂ and equimolar Q-Phos (1,2,3,4,5-pentaphenyl-1'-(di-*tert*-butylphosphino)ferrocene) was sufficient to catalyze effectively the Suzuki-Miyaura cross-coupling of *in situ* generated 2,3-difluoroaryl and 2,6-difluoroaryl pinacol boronate esters with aryl bromides. The Suzuki-Miyaura cross-coupling reaction was conducted in the presence of K₃PO₄ as a base in a mixture of dioxane and water (10:1), at 50 °C for 18 h. As shown in Scheme 1-56, the cross-coupled products were generated in good yields.

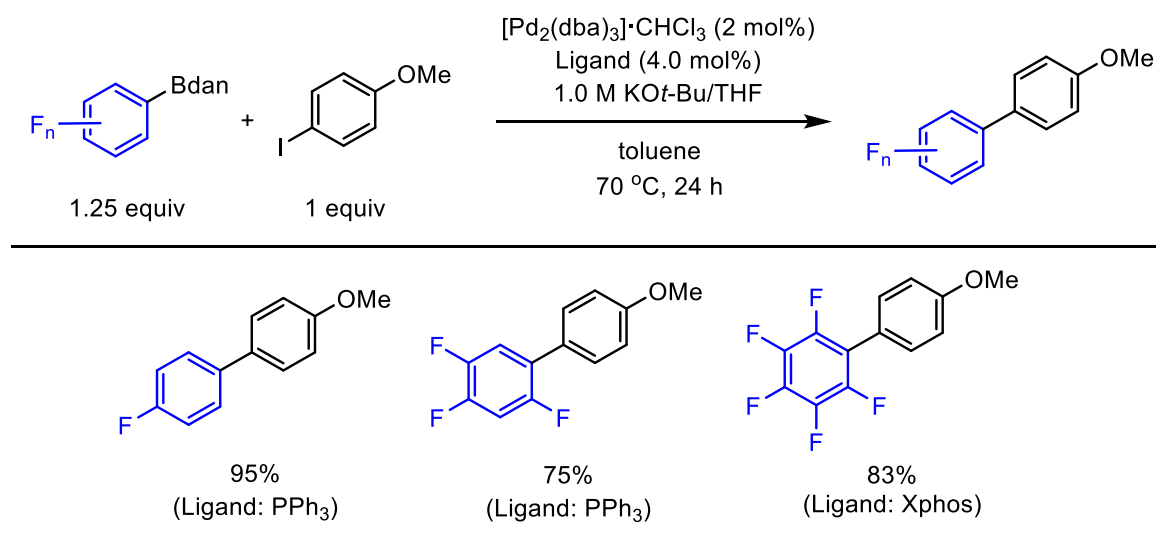


Scheme 1-56. Iridium-catalyzed C–H borylation / palladium-catalyzed cross-coupling of fluoroarenes with aryl bromides.^[32]

The Lewis acidity of the boron atom is important for the reactivity of organoboron compounds in cross-coupling reactions. In 2007, Suginome *et al.* introduced protected analogues of aryl boronates, namely aryl-Bdan (dan = naphthalene-1,8-diaminato) derivatives, for which the C–B bond is less reactive due to the reduced Lewis acidity of the boron atom.^[127] In 2020, Saito *et al.*^[128] and Tsuchimoto *et al.*^[129] reported a method to apply aryl-Bdan compounds in Suzuki-Miyaura cross-coupling reactions. Indeed, Saito *et al.*^[128] reported examples of different polyfluorophenyl-Bdan derivatives, especially C₆F₅Bdan, that were coupled without difficulty with aryl iodides using a combination of common palladium catalyst precursors such as [Pd₂(dba)₃]·CHCl₃ and ligands such as XPhos. The reactions were conducted in the presence of a 1

M solution of KO*t*-Bu/THF, in toluene, at 70 °C for 24 hours to give cross-coupled products in good yields (Scheme 1-57). Under these conditions, the addition of water inhibits the palladium-catalyzed cross-coupling process of aryl-Bdan with the aryl iodide. In contrast, Carrow *et al.*^[73] previously reported that the addition of water was required to improve the performance of the palladium-catalyzed cross-coupling of aryl pinacol boronates with aryl bromides (Scheme 1-55).

It should be mentioned that Cammers-Goodwin *et al.* showed that C₆F₅B(OH)₂ is susceptible to nucleophilic attack at its *para*-carbon atom to replace the *para*-fluoro-substituent with potassium *tert*-butoxide (KO*t*-Bu).^[130] However, the method described by Saito *et al.*^[128] above used excess strong base, such as a 1 M solution of KO*t*-Bu in THF, but, interestingly, attack at the *para*-carbon was not mentioned.

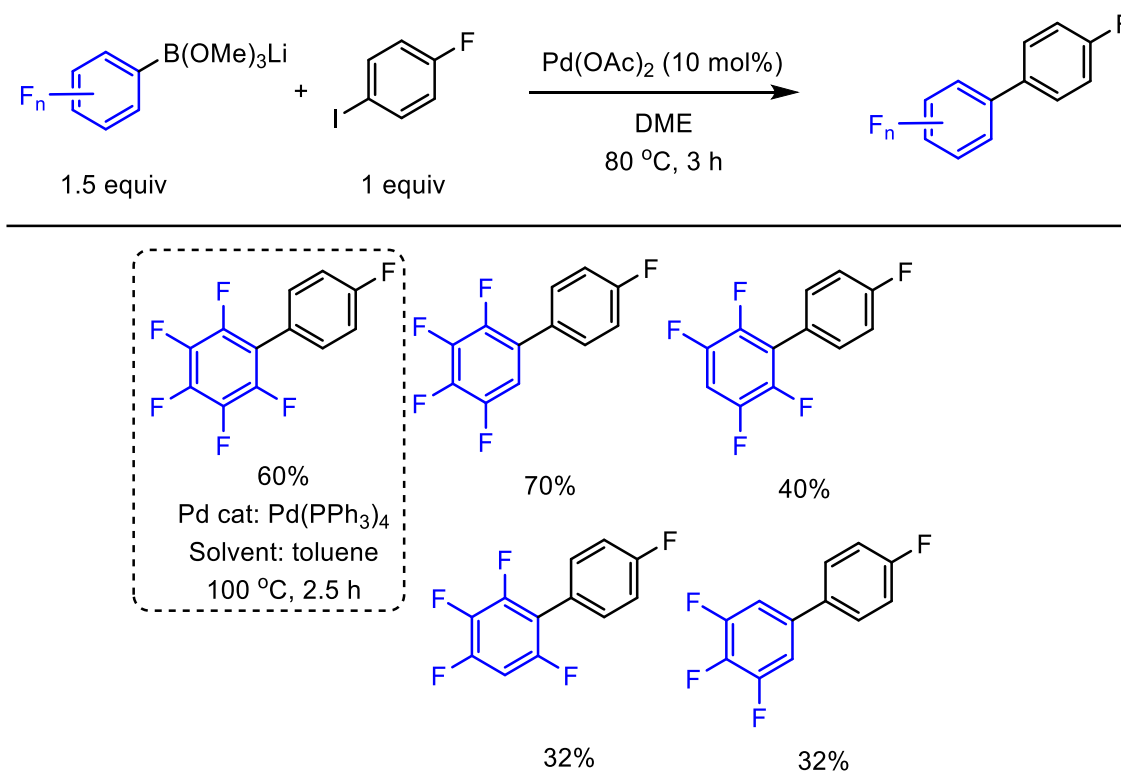


Scheme 1-57. Palladium-catalyzed Suzuki-Miyaura cross-coupling of polyfluoroaryl-Bdan and aryl iodide.^[128]

1.5.3.2 Palladium-Catalyzed Suzuki-Miyaura Cross-Coupling of Polyfluorophenyl Borate Salts

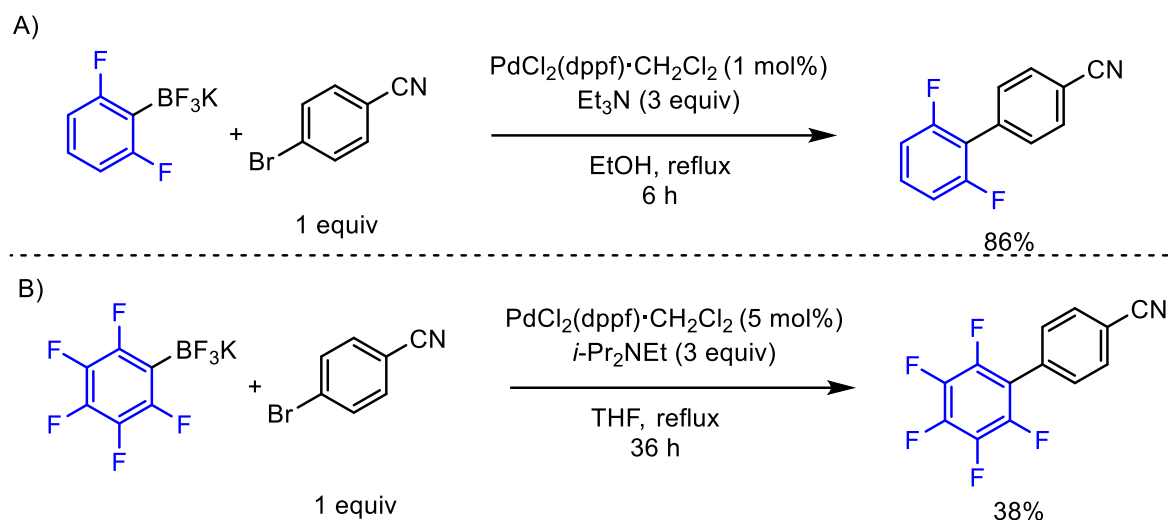
In 2003, Frohn and Adonin *et al.*^[131] reported the application of lithium polyfluorophenyltrimethoxyborates Ar_F-B(OMe)₃Li in Suzuki Miyaura cross-coupling reactions under base-free conditions. They observed optimal yields using C₆F₅B(OMe)₃Li and

4-fluoriodobenzene along with 10 mol% of $\text{Pd}(\text{PPh}_3)_4$ as a catalyst. (Scheme 1-58). However, the same conditions were not effective for other $\text{Ar}_F\text{-B}(\text{OMe})_3\text{Li}$ substrates containing hydrogen substituents, but the yields could be improved using 10 mol% of $\text{Pd}(\text{OAc})_2$ as the catalyst precursor and DME as the solvent. The authors showed that fluorinated aryl- $\text{B}(\text{OMe})_3\text{Li}$ compounds were more reactive and gave better yields than their potassium trifluoroborate salt analogues.^[132] Notably, the yield of the cross-coupled product from the reaction of $\text{C}_6\text{F}_5\text{B}(\text{OMe})_3\text{Li}$ with 4-fluoriodobenzene was improved by the addition of stoichiometric amounts of silver oxide.



Scheme 1-58. Palladium-catalyzed cross-coupling of fluorinated aryl- $\text{B}(\text{OMe})_3\text{Li}$ with 4-fluoriodobenzene.^[131]

In 2003, Molander *et al.*^[133] reported an effective method using a low loading of $\text{PdCl}_2(\text{dppf})\cdot\text{CH}_2\text{Cl}_2$ to catalyze the Suzuki-Miyaura cross-coupling of aryl halides with potassium heteroaryltrifluoroborate salts. These authors demonstrated that 2,6-difluorophenyl- BF_3K was a viable substrate in the reaction (Scheme 1-59A), but also that this method was less effective in reactions employing $\text{C}_6\text{F}_5\text{BF}_3\text{K}$ (Scheme 1-59B).



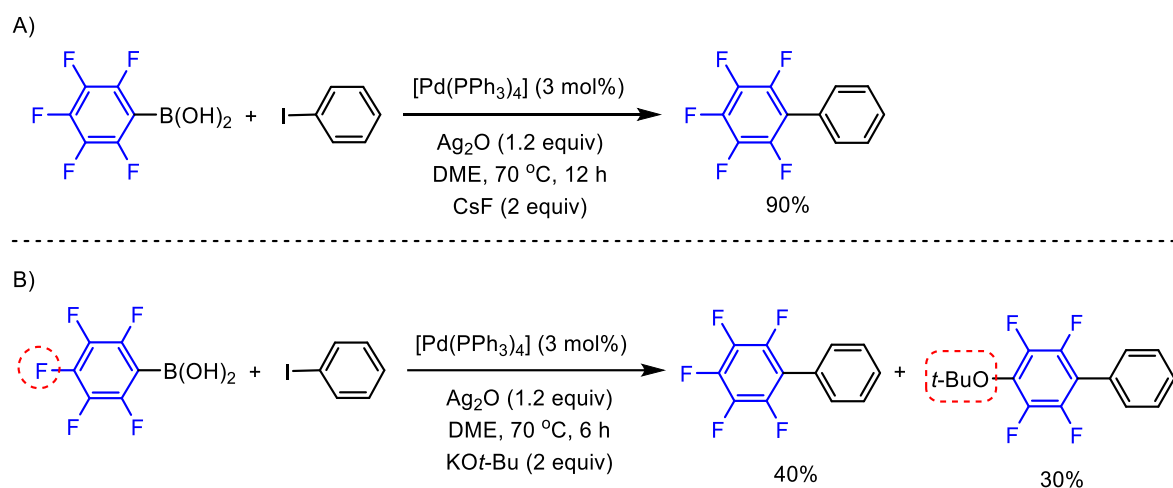
Scheme 1-59. Palladium-catalyzed cross-coupling of potassium fluorinated-aryltrifluoroborates with 4-bromobenzonitrile.^[133]

1.5.3.3 Silver Oxide-Assisted Palladium-Catalyzed Suzuki-Miyaura Cross-Coupling Reaction of Fluorinated Aryl Boronic Acids or Borate Salts

In 1987, Kishi *et al.*^[134] reported that rates of the palladium-catalyzed Suzuki-Miyaura cross-coupling reaction are 30 times faster in the presence of silver oxide (Ag_2O) compared to those reactions using common bases such as potassium hydroxide. In 2003, Osakada *et al.*^[135] showed that the reaction of $[\text{Pd}(\text{PEt}_3)_2(\text{C}_6\text{F}_5)\text{I}]$ with Ag_2O in toluene-water gave the stable complex $[\text{Pd}(\text{PEt}_3)_2(\text{C}_6\text{F}_5)\text{OH}]$ with concomitant formation of silver iodide (AgI). Furthermore, $[\text{Pd}(\text{PEt}_3)_2(\text{C}_6\text{F}_5)\text{OH}]$ underwent transmetalation with 4-methoxyphenylboronic acid followed by reductive elimination to give the corresponding fluorinated biphenyl product. Thus, it was suggested that Ag_2O replaces the halide ligand (X) in $[\text{PdL}_2(\text{Ar})\text{X}]$ with an OH ligand, to give an hydroxy-palladium species that has a higher affinity for transmetalation.

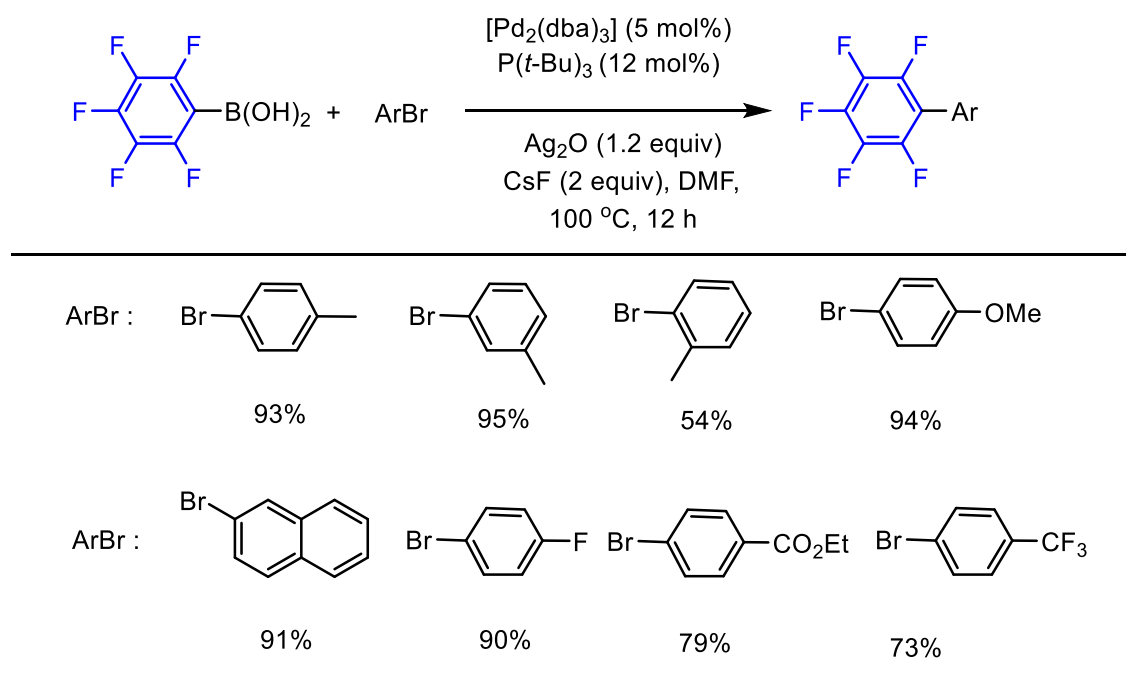
As Ag_2O is known to accelerate the transmetalation of aryl boronates (*vide supra*), this phenomenon was exploited to accelerate the Suzuki-Miyaura cross-coupling with, *e.g.*, 2,6-difluoro-substituted aryl boronate substrates. In 2005, Korenaga *et al.* employed 3 mol% of $[\text{Pd}(\text{PPh}_3)_4]$ as a

catalyst precursor, and CsF as a base, to achieve the cross-coupling of $C_6F_5B(OH)_2$ with iodobenzene in DME at 70 °C (Scheme 1-60A).^[136] It should be noted that using $KOt\text{-}Bu$ as a base also accelerated this reaction, but it gave the byproduct $p\text{-}(t\text{-}BuO)\text{-}C_6F_4\text{-}C_6H_5$ in 30% yield (Scheme 1-60B). It is known that the *para*-position of pentafluorophenyl is susceptible to nucleophilic attack to replace the *para*-fluoro-substituent at $C_6F_5B(OH)_2$ with an alkoxide base.^[130]



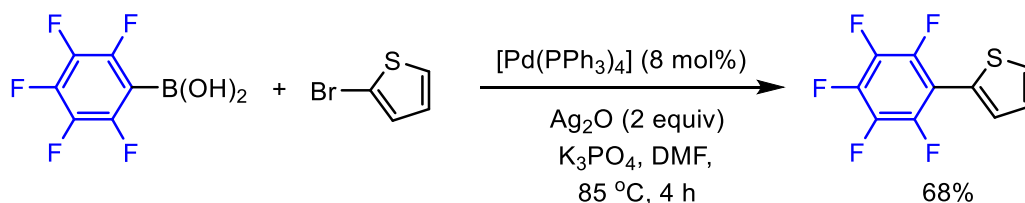
Scheme 1-60. Ag_2O -assisted palladium-catalyzed cross-coupling of $C_6F_5B(OH)_2$ with iodobenzene.^[136]

Furthermore, Korenaga *et al.*^[136] reported optimized conditions for the use of aryl bromide instead of aryl iodide substrates and demonstrated that a combination of 2.5 mol% of $Pd_2(dba)_3$ and 6 mol% of $PtBu_3$ in DMF, at 100 °C, for 12 hours, gave the cross-coupled products in fair to good yields (Scheme 1-61). Overall, electron-rich aryl bromides afforded the cross-coupled products in more than 90% yield and were consequently more favorable compared to electron-poor aryl bromides. However, sterically hindered electron-rich aryl bromides, such as 2-methyl-phenylboronic acid, gave the cross-coupled product in only 54%. Less efficient cross-coupling was found employing phenyl chloride or triflate instead of the analogous bromide to give the corresponding products in 39% and 4% yield, respectively.



Scheme 1-61. Ag_2O -assisted palladium-catalyzed cross-coupling of $\text{C}_6\text{F}_5\text{B}(\text{OH})_2$ with aryl bromides.^[136]

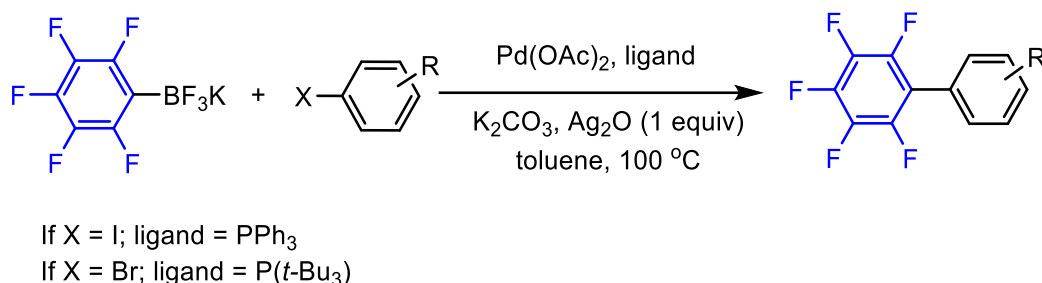
In 2005, Takimiya *et al.* reported the Suzuki-Miyaura cross-coupling reaction employing heteroarenes, such as 2-bromothiophene derivatives with $\text{C}_6\text{F}_5\text{B}(\text{OH})_2$.^[137] For example, using pentafluorophenyl boronic acid with 2-bromothiophene with 8 mol% $[\text{Pd}(\text{PPh}_3)_4]$ along with an excess of K_3PO_4 and Ag_2O , led to the cross-coupled product in moderate yield (Scheme 1-62).



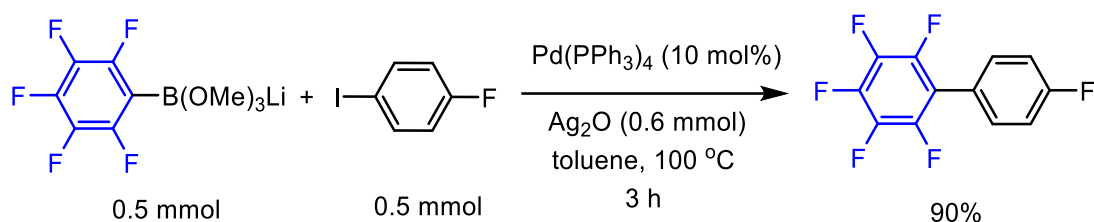
Scheme 1-62. Palladium-catalyzed cross-coupling of pentafluorophenyl boronic acid with 2-bromothiophene.^[137]

In 2002, Frohn and Adonin *et al.*^[138] reported optimized conditions for the Suzuki-Miyaura cross-coupling of potassium pentafluorophenyltrifluoroborate ($\text{C}_6\text{F}_5\text{BF}_3\text{K}$), which was chosen as it is more stable in the presence of base compared to its boronic acid analogue. Thus, a combination of 10 mol% of $\text{Pd}(\text{OAc})_2$, 20 mol% of PPh_3 , and 2 equivalents of K_2CO_3 catalyzed the Suzuki-Miyaura cross-coupling of $\text{C}_6\text{F}_5\text{BF}_3\text{K}$ with aryl iodides in toluene at $100\text{ }^\circ\text{C}$ within 3 hours. However, this reaction only gave the corresponding products in good yields in the presence of stoichiometric

amounts of Ag_2O (Scheme 1-63). In 2015, Adonin *et al.* extended his method to cross-couple $\text{C}_6\text{F}_5\text{BF}_3\text{K}$ with aryl bromides.^[139] In 2003, Frohn and Adonin *et al.* employed $\text{C}_6\text{F}_5\text{B}(\text{OMe})_3\text{Li}$ instead of its $-\text{BF}_3\text{K}$ analogue and, interestingly, in this case sufficient yields were obtained without the presence of base, but stoichiometric amounts of Ag_2O were necessary (Scheme 1-64).^[131]

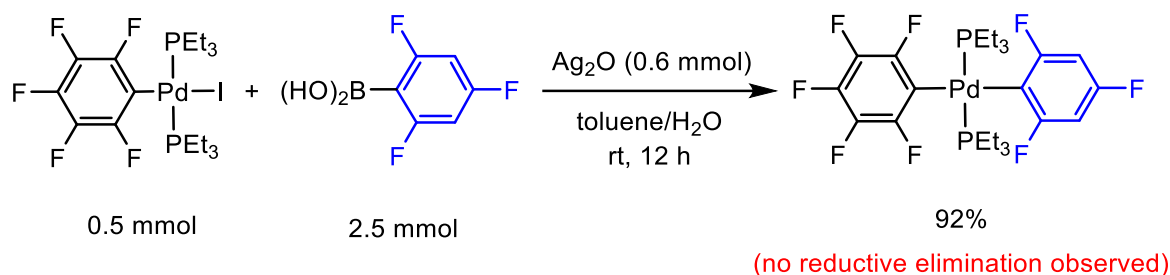


Scheme 1-63. Palladium-catalyzed cross-coupling of $\text{C}_6\text{F}_5\text{BF}_3\text{K}$ with aryl iodides and bromides.^[138,139]



Scheme 1-64. Palladium-catalyzed cross-coupling of $\text{C}_6\text{F}_5\text{B}(\text{OMe})_3\text{Li}$ with 1-fluoro-4-iodobenzene.^[131]

As mentioned in section 1.5.2, the palladium-catalyzed homocoupling of aryl pinacol boronates to generate symmetrical fluorinated biaryls with two *ortho*-fluorines in each ring must be conducted in arene solvents to reduce the energy barrier of the reductive elimination step.^[114] It was previously mentioned in section 1.5.3.1 and Table 1-3 that Bulfield and Huber reported optimized conditions for constructing polyfluorobiphenyls *via* Suzuki-Miyaura cross-coupling of fluorinated aryl-boronic acid derivatives and fluorinated aryl halides, using a combination of $\text{Pd}_2(\text{dba})_3$ and phosphine ligands in good to excellent yields;^[121] however, the reaction failed to couple pentafluorophenyl boronic acid derivatives with 1,2,4,5-tetrafluoro-3-iodobenzene (Table 1-3, entry 4). Moreover, Osakada *et al.* reported the reaction of $[\text{Pd}(\text{PEt}_3)_2(\text{C}_6\text{F}_5)\text{I}]$ with $2,4,6\text{-C}_6\text{F}_3\text{H}_2\text{B}(\text{OH})_2$ in the presence of an excess of Ag_2O to give *trans*- $[\text{Pd}(\text{PEt}_3)_2(\text{C}_6\text{F}_5)(2,4,6\text{-C}_6\text{F}_3\text{H}_2)]$ in 92% yield, but no reductive elimination product was observed (Scheme 1-65).^[135]



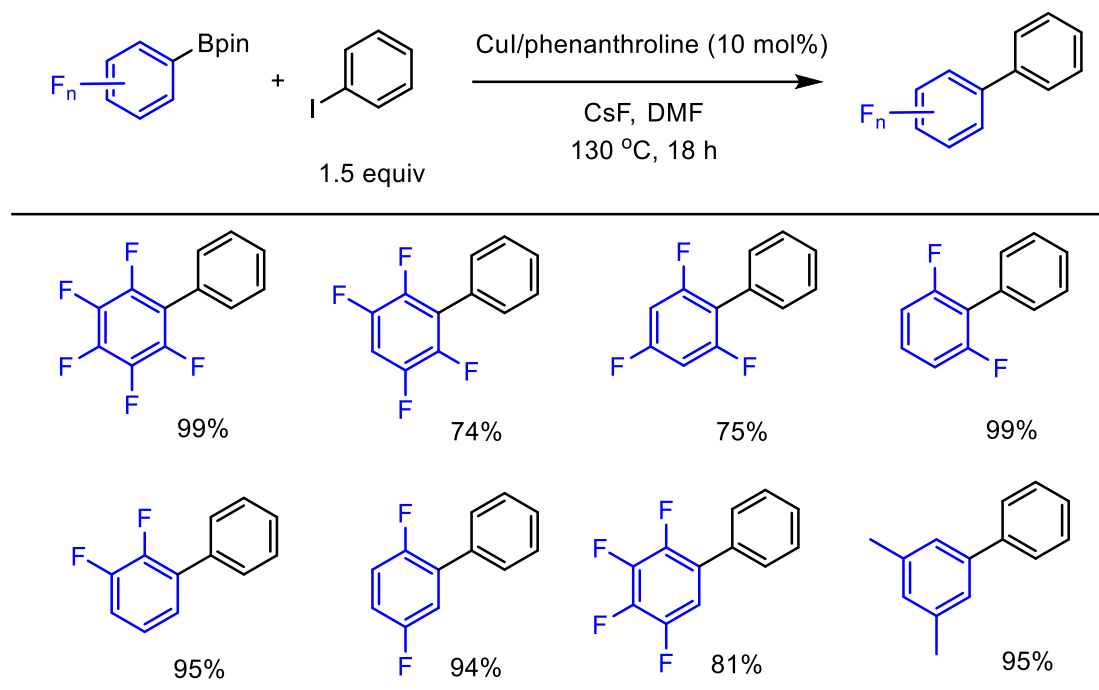
Scheme 1-65. Synthesis of *trans*-[Pd(PEt₃)₂(C₆F₅)(2,4,6-C₆F₃H₂)].^[135]

1.5.3.4 Copper-Catalyzed Suzuki-Miyaura Cross-Coupling of Fluorinated Aryl Boronic Esters

As described in sections 1.5.3.1 – 1.5.3.3, the palladium-catalyzed Suzuki-Miyaura cross-coupling of fluorinated aryl boronic acids requires one of the following methods to achieve acceptable to good yield: (i) a stoichiometric amount of silver oxide; (ii) a highly reactive palladium precatalysts such as second, third, and fourth generation Buchwald precatalysts or Carrow precatalysts; (iii) a one pot-two step iridium-catalyzed C–H borylation of fluoroarenes with B₂pin₂ followed by a palladium-catalyzed Suzuki-Miyaura cross-coupling reaction; or (iv) *via* protection of the boron using more stable moieties such as Bdan (*vide supra*). Several reports employing economically-viable and earth-abundant low toxicity metals, such as copper, as catalyst systems have been of recent significant interest for Suzuki-Miyaura cross-coupling reactions.^[140-147] Thus, Radius and Marder reported the copper-catalyzed Suzuki-Miyaura cross-coupling of highly fluorinated aryl boronic esters with aryl halides.^[17] A combination of 10 mol% copper iodide and 10 mol% phenanthroline with CsF as a base proved effective in the cross-coupling of fluorinated aryl pinacol boronates with aryl iodides to generate cross-coupled products in good to excellent yields (Scheme 1-66).

This method was also applicable to polyfluorophenyl borate salts such as pentafluorophenyl-BF₃K. Notably, slightly lower yields were obtained when employing 2,4,6-trifluorophenyl-Bpin and 2,3,5,6-tetrafluorophenyl-Bpin due to the formation of C–H arylation byproducts. It is known that C–H bonds that are flanked by two C–F bonds have a high acidity and can be directly arylated.^[148-150] However, these results showed that C–Bpin groups are more reactive than C–H bonds within the

arylation target. Cross-coupling of aryl bromides instead of aryl iodides with polyfluoroaryl–Bpin is also possible if an increased amount of the CuI/phenanthroline catalyst in a mixture of DMF and toluene (1:1) is used.



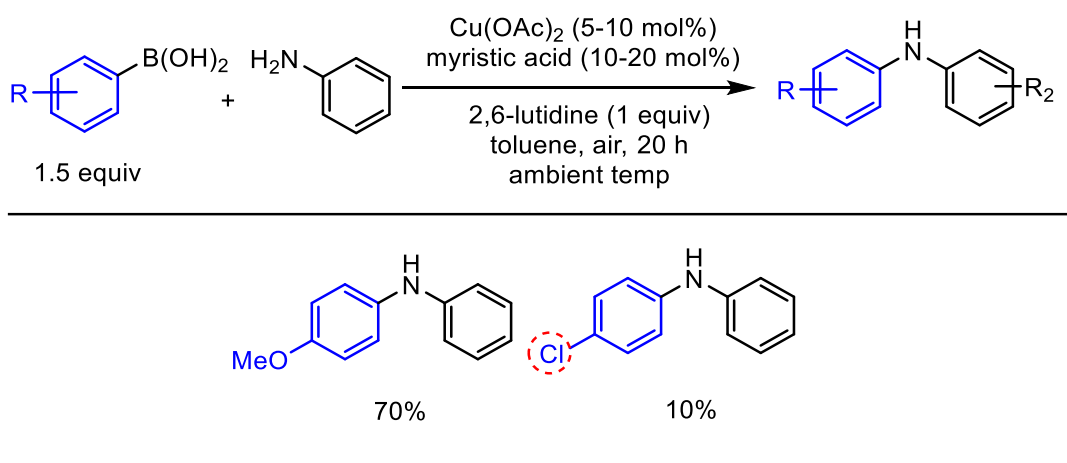
Scheme 1-66. Copper-catalyzed cross-coupling of polyfluorophenyl–Bpin with phenyl iodide.^[17]

1.5.4 C–N Cross-Coupling

1.5.4.1 Copper-Catalyzed Chan-Evans-Lam C–N Cross-Coupling of Fluorinated Aryl Boronic Acids with Amines

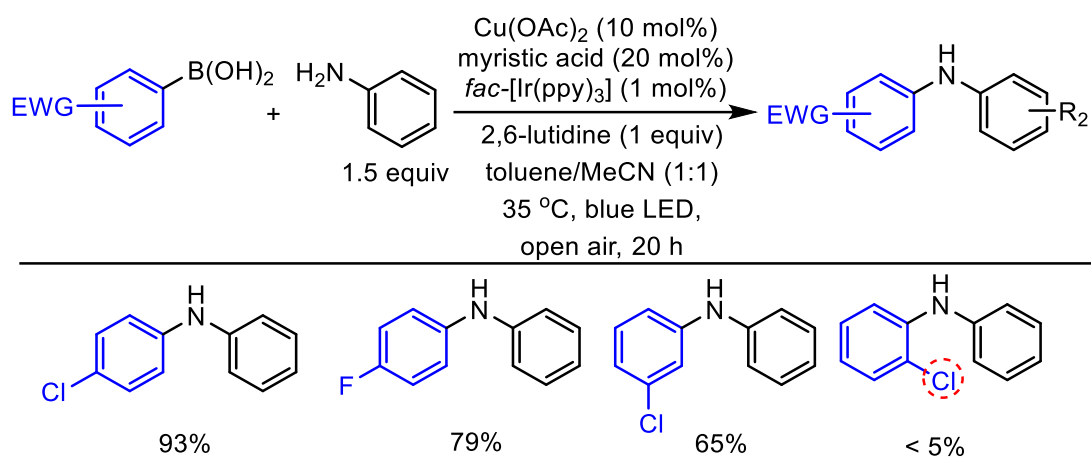
Aromatic amines are widely utilized as important compounds in agrochemical^[151] and pharmaceutical science.^[152] A C–N cross-coupling reaction of aryl amines with aryl boronic acids or esters is a powerful way to approach the corresponding diarylamines, known as Chan-Evans-Lam cross-coupling reactions.^[153-155] It should be mentioned that Chan-Evans-Lam cross-couplings to form C–N bonds are conveniently conducted using a copper catalyst system at room temperature, providing an advantageous route compared with cross-couplings of aryl halides using commonly employed yet commercially expensive, palladium precatalysts that required high temperatures for

the reaction to go to completion.^[156,157] In 2001, it was reported that the optimal conditions for the copper-catalyzed Chan-Evans-Lam cross-coupling of aryl amines with aryl boronic acids could be achieved in the presence of a low-loading of added myristic acid along with stoichiometric amounts of 2,6-lutidine.^[158] However, the reaction was not effective for aryl boronic acids bearing electron-withdrawing substituents such as chloride (Scheme 1-67).



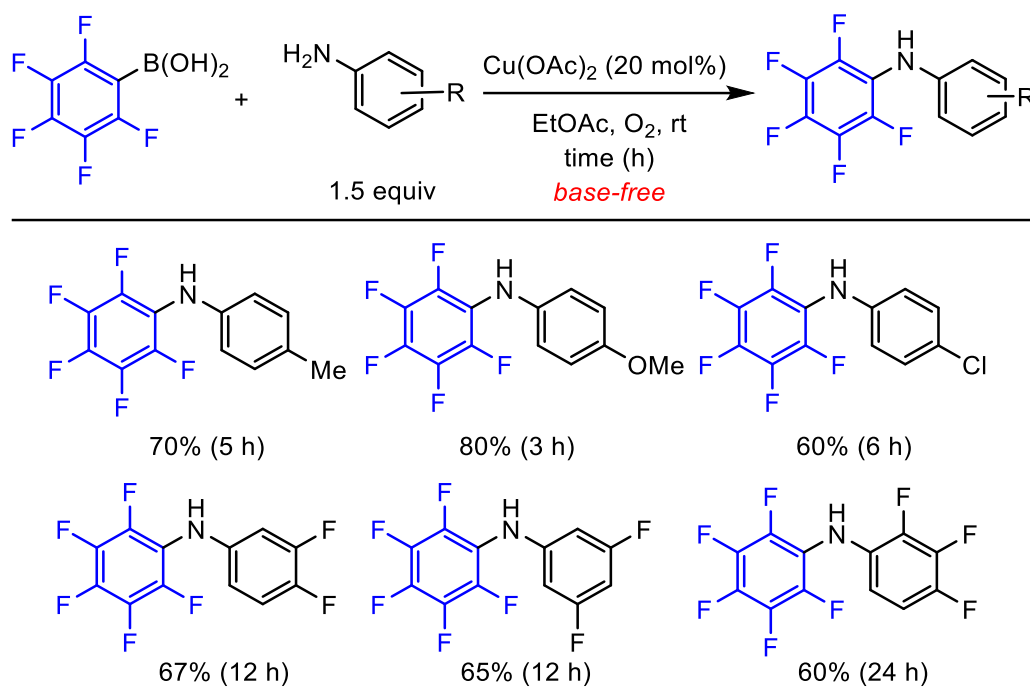
Scheme 1-67. Copper(II)-catalyzed N-arylation of aryl boronic acids with anilines.^[158]

In 2015, Kobayashi *et al.* optimized these conditions using copper(II) acetate as a catalyst and a *fac*-[Ir(ppy)₃] complex as a photocatalyst in the presence of blue LEDs and 2,6-lutidine as a base.^[159] As shown in Scheme 1-68, this method is viable for the C–N cross-coupling employing aryl boronic acids bearing electron-withdrawing substituents such as chlorine or fluorine at the *para*-position, and not unexpectedly, was better than those with electron-withdrawing halides at the *meta*- or *ortho*-positions. Thus, solving this problem in C–N cross-coupling of anilines with aryl boronic acids bearing *ortho*-chlorine or *ortho*-fluorine might require conducting the reactions under base-free condition to slow down the protodeboronation.



Scheme 1-68. Visible light-mediated C–N coupling of electron-deficient aryl boronic acids and aniline.^[159]

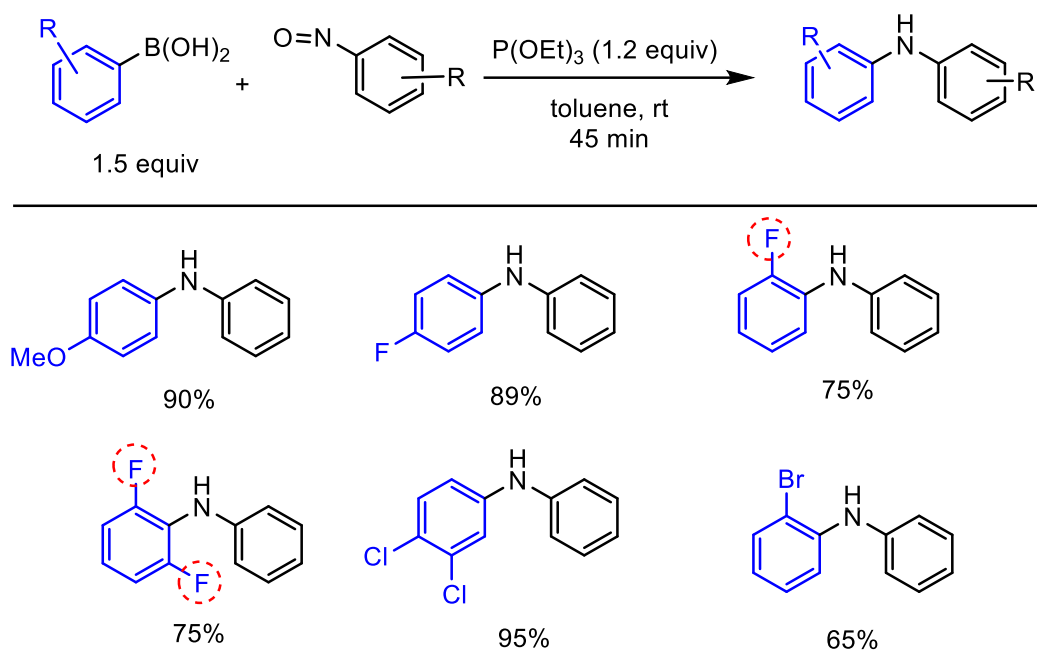
However, prior to Kobayashi's report, in 2008, Su *et al.* reported the copper-catalyzed *N*-arylation reaction of pentafluorophenyl boronic acid with aniline.^[160] The optimized reaction was conducted using copper(II) acetate as a precatalyst under an oxygen atmosphere and notably base-free conditions. As shown in Scheme 1-69, the cross-coupling reaction was tolerant of anilines containing aryl rings bearing electron-rich or electron-poor moieties, and the cross-coupled products were generated in moderate to good yields. It is important to note that the reaction failed in the presence of bases such as Et₃N or pyridine, due to the problematic protodeboronation issue. The reaction also failed when using a copper(I) precatalyst, such as copper iodide instead of a copper(II) catalyst, or in the absence of oxygen. It should be mentioned here that aside from the desired cross-coupling products, the reactions were contaminated by minor byproducts of protodeboronation and homocoupling of pentafluorophenyl boronic acid. Interestingly, employing alkyl amines instead of anilines generated *N*-alkyl-2,2',3,3',4',5,5',6,6'-nona-fluorobiphenyl-4-amines in moderate yields (not shown).



Scheme 1-69. Cu(II)-catalyzed *N*-arylation of $C_6F_5B(OH)_2$ with anilines.^[160]

1.5.4.2 Phosphine-Mediated Chan-Evans-Lam C–N Cross-Coupling of Fluorinated Aryl Boronic Acids with Nitrosoarenes

Another option to synthesize unsymmetrical diarylamines can be approached *via* C–N cross-coupling of aryl boronic acids with nitrosoarenes. In 2018, Csáký *et al.* reported the coupling of aryl boronic acids with nitrosoarenes under transition metal-free and neutral (base-free) conditions.^[161] Reactions were mediated by triethoxyphosphine in toluene to generate unsymmetrical diarylamines in fair to excellent yields at room temperature (Scheme 1-70). However, the desired coupling product was not observed when aryl pinacol boronates or potassium trifluoroborates were used in place of the boronic acid analogues. The reaction tolerated sensitive substrates such as aryl boronic acids containing two *ortho*-fluorines, as base-free conditions slowed the decomposition protodeboronation pathways.

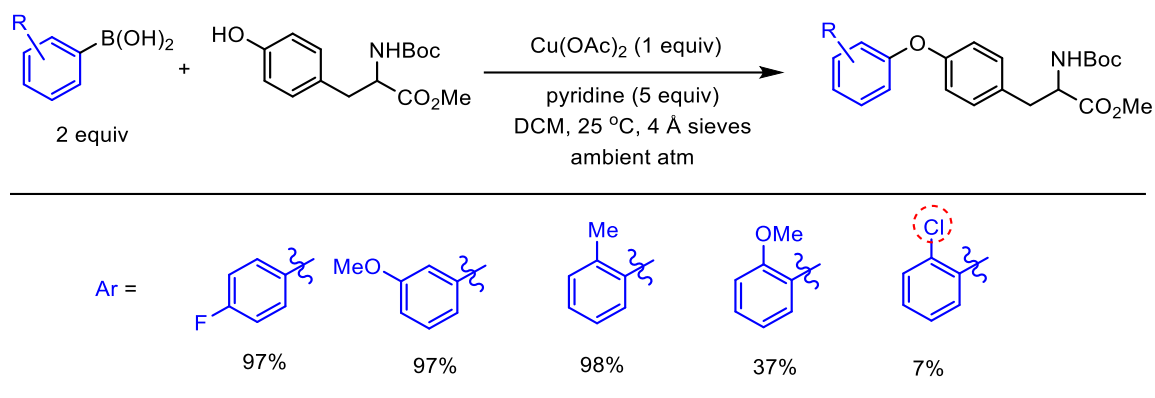


Scheme 1-70. Phosphine-mediated C–N cross-coupling of aryl boronic acids with nitrosoarenes.^[161]

1.5.5 C–O Cross-Coupling

1.5.5.1 Challenges in the Chan-Evans-Lam C–O Cross-Coupling of *ortho*-Electron-Withdrawing-Substituted Aryl Boronic Acids and Phenols to Form Diaryl Ethers

In 1998, Evans *et al.* reported the synthesis of diaryl ethers *via* copper-promoted C–O cross-coupling of aryl boronic acids with phenols.^[162] Reactions were conducted in the presence of 1 equivalent of Cu(OAc)_2 , 5 equivalents of pyridine using 4 Å molecular sieves in dichloromethane in air at 25 °C. Products were generated in good to excellent yields for aryl boronic acids bearing electron-donating groups at the *ortho*-, *meta*-, or *para*-positions (Scheme 1-71). Reactions were also viable for aryl boronic acids bearing electron-deficient substituents, such as fluorine, at the *para*- or *meta*-positions. However, the reaction was not effective if the electron-deficient substituent was at the *ortho*-position (7% yield) and the predominant pathway was, once again, derived from protodeborylation.

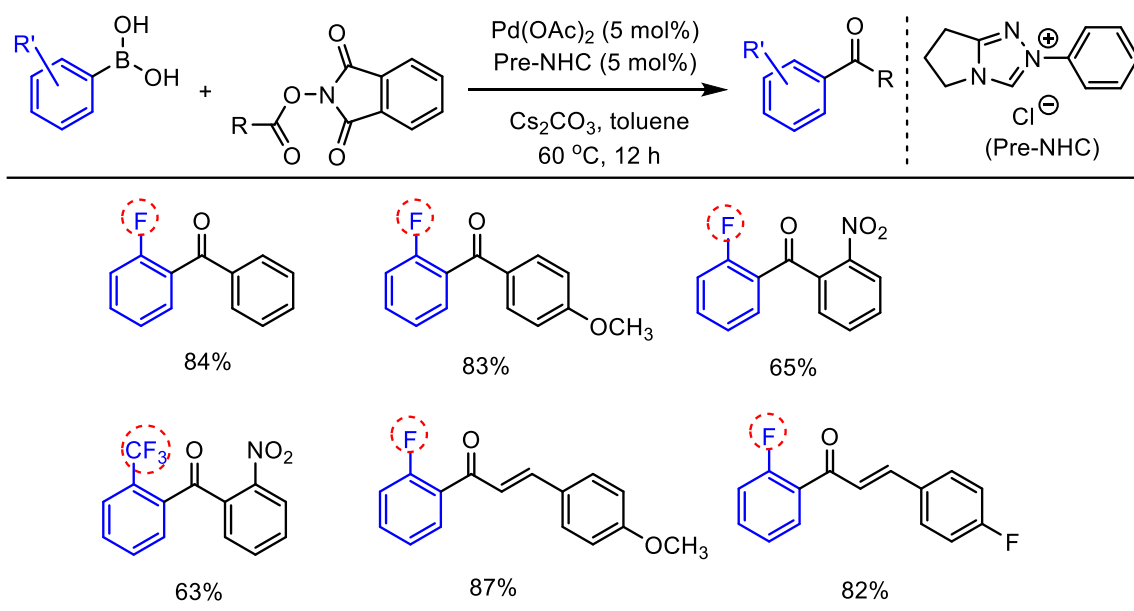


Scheme 1-71. Cu-promoted C–O cross-coupling of aryl boronic acids with phenol derivatives.^[162]

1.5.6 C–C(O) Cross-Coupling

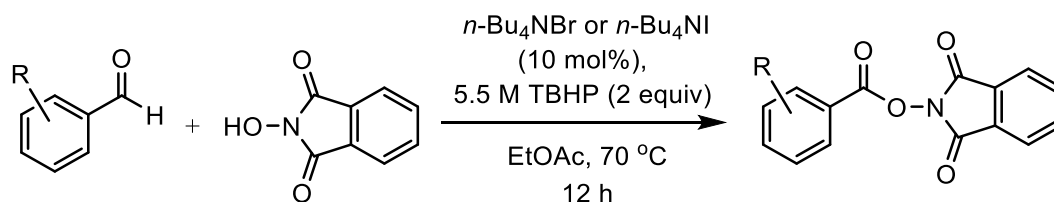
1.5.6.1 Palladium-catalyzed C–C(O) Cross-Coupling of Fluorinated Aryl Boronic Acids and N-(Aryl-carboxyloxy)phthalamides

Aryl ketones are important aromatic compounds that have found many applications in medicinal chemistry.^[3] In 2014, Sun *et al.* reported the C–C(O) cross-coupling of *N*-(aryl-carboxyloxy)phthalamides with aryl boronic acids.^[163] These reactions were catalyzed by a low loading of Pd(OAc)₂ and an NHC ligand that was formed *in situ* from a triazole-based NHC precursor. As shown in Scheme 1-72, the reaction was viable for unstable substrates such as *ortho*-fluorinated aryl boronic acids giving moderate to good yields. Aryl boronic acids bearing other electron-withdrawing substituents, such as trifluoromethyl groups, were also effective in this reaction. The chemistry was extended to *N*-(alkenylcarboxyloxy)phthalamides, which coupled with *ortho*-fluorinated aryl boronic acids in good yield. The authors proposed a mechanism which involves the oxidative addition of *N*-(aryl-carboxyloxy)phthalamides, followed by transmetalation with the boronic acid, and subsequent reductive elimination to release the cross-coupled products.



Scheme 1-72. Pd-NHC-catalyzed C–C(carbonyl) cross-coupling to synthesize diaryl ketones.^[163]

In 2012, Barbas III *et al.* reported a convenient way to synthesize *N*-(aryl-carbonyloxy)phthalamides *via* the cross-coupling amidation and esterification of aryl carboxylic acids and *N*-(hydroxy)phthalamides.^[164] Reactions were conducted in ethyl acetate in the presence of a catalytic amount of tetrabutylammonium bromide, ($n\text{Bu}_4\text{NBr}$), or iodide ($n\text{Bu}_4\text{NI}$), as the precatalyst using 5.5 M *tert*-butyl hydrogen peroxide (TBHP) as the co-oxidant (Scheme 1-73). The reaction proved unsuccessful using alkyl aldehydes in place of aryl aldehydes, indicating that the aromatic group had a significant function in stabilizing the active species.

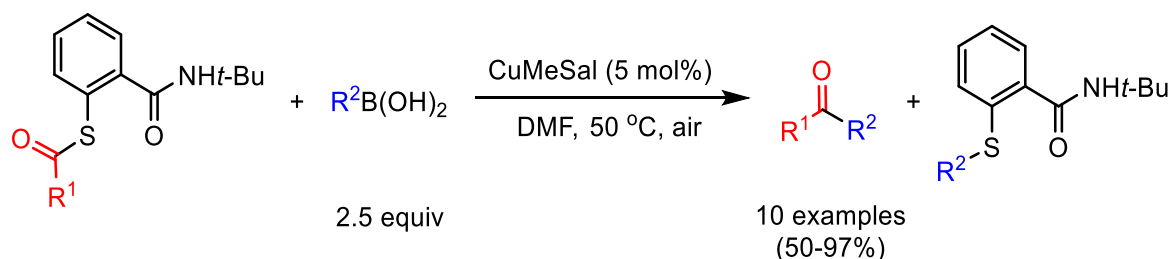


Scheme 1-73. Esterification/amidation of aldehydes with *N*-hydroxyphthalimide catalyzed by $n\text{-Bu}_4\text{NBr}$ or $n\text{-Bu}_4\text{NI}$.^[164]

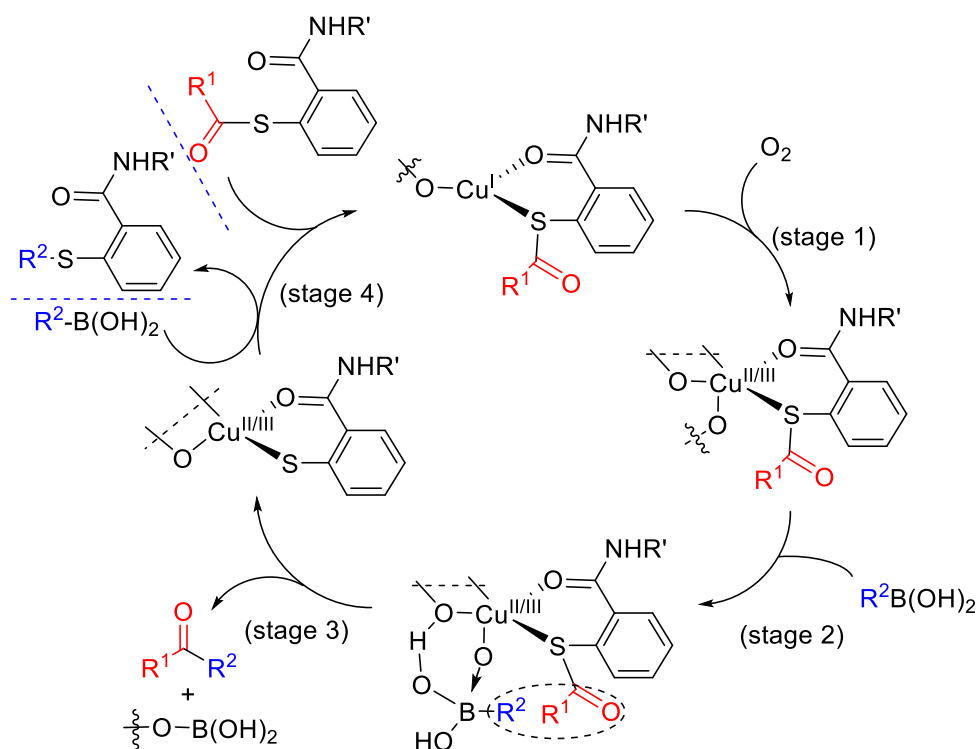
1.5.6.2 Copper-Catalyzed C–C(O) Cross-Coupling of Fluorinated Aryl Boronic Acids and Thiol Esters (Liebskind-Srogl Cross-Coupling)

In 2007, Liebskind *et al.* reported the copper-catalyzed cross-coupling of organoboronic acids with thiol esters in air using 5 mol% of Cu(I)-3-methylsalicylate (CuMeSal) under base-free condition, to generate ketones as cross-coupled products in moderate to excellent yields (Scheme 1-74).^[165] It should be mentioned that previous Liebskind-Srogl cross-coupling reactions required palladium precatalysts along with stoichiometric amounts of copper(I) carboxylate as a mediator, whereupon the copper(I) salt was thought necessary to facilitate the transmetalation step from boron to palladium.^[105] Further investigation suggested that the copper(I) ion generates a thermodynamically stable Cu–SR species. Liebskind intuitively realized that this Cu–SR bond could be activated in the presence of the second equivalent of the organoboronic acid, thus generating a catalytically-active Cu(I) species.

The catalytic mechanism was proposed based on the presence of O₂, which initially led to oxidation of Cu(I) to Cu(II)/(III) (Scheme 1-75, stage 1), followed by coordination of the organoboronic acid and the release of the cross-coupled product (Scheme 1-75, stages 2 and 3). Finally, the Cu–SR bond is activated in the presence of an excess of the organoboronic acid, thus regenerating the Cu(I) intermediate and continuing the catalytic process (Scheme 1-75, stage 4).

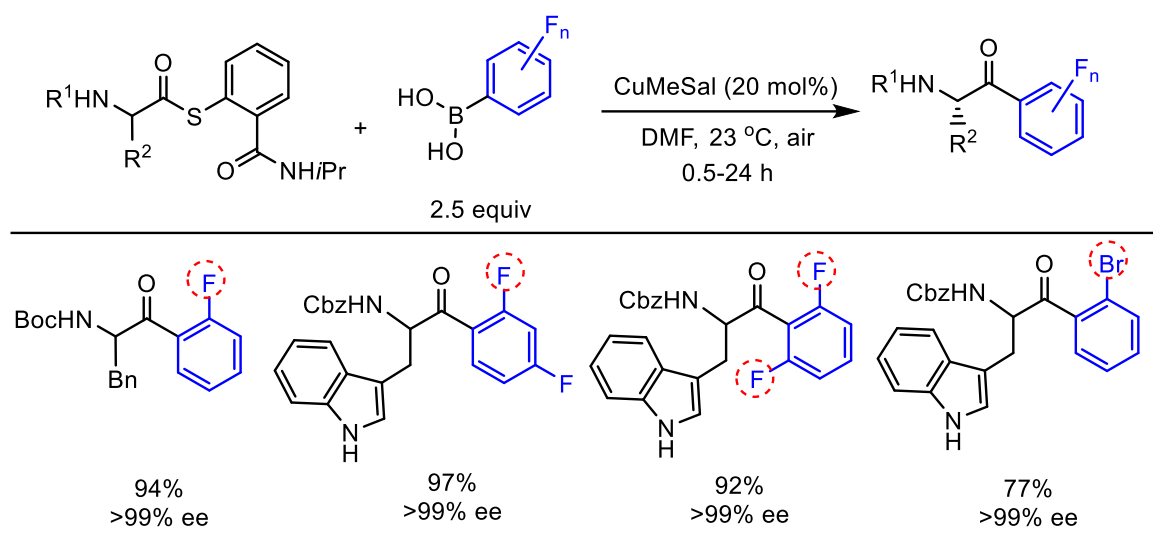


Scheme 1-74. Copper-catalyzed cross-coupling of thiol esters and boronic acids.^[165]



Scheme 1-75. Proposed mechanistic pathway for the copper-catalyzed cross-coupling of thiol esters and boronic acids in aerobic conditions.^[165]

This reaction was effective for a wide range of aryl boronic acids that are not stable to basic conditions, including those containing *ortho*-fluorine substituents.^[166] The scope of this study was expanded to include the synthesis of peptidyl ketones, which are important compounds in the development of molecular therapeutics (Scheme 1-76). This reaction also proved successful using *ortho*-brominated aryl boronic acids without effecting the bromide substituent. Notably, the authors mentioned that neither the formation of oxidative homocoupling products of the aryl boronic acids nor the racemization of the mono-peptidyl ketones was detected.

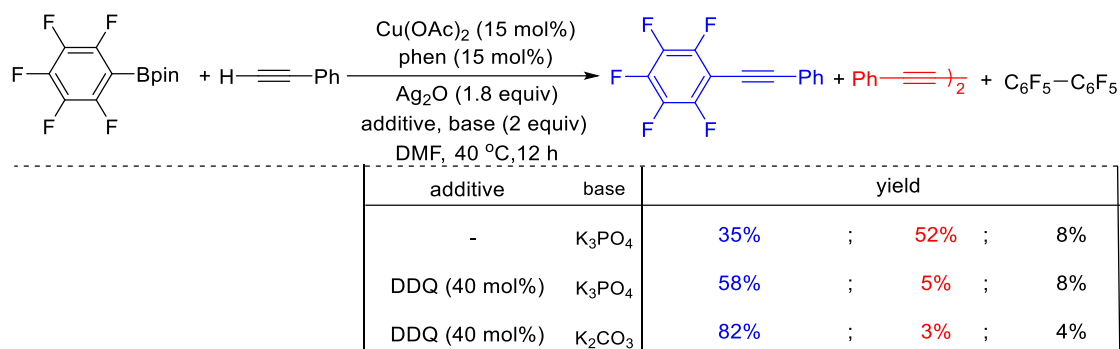


Scheme 1-76. Copper-catalyzed cross-coupling of peptidyl thiol esters and boronic acids, where Sal = 3-methylsalicylate.^[166]

1.5.7 C–C(alkyne) Cross-Coupling

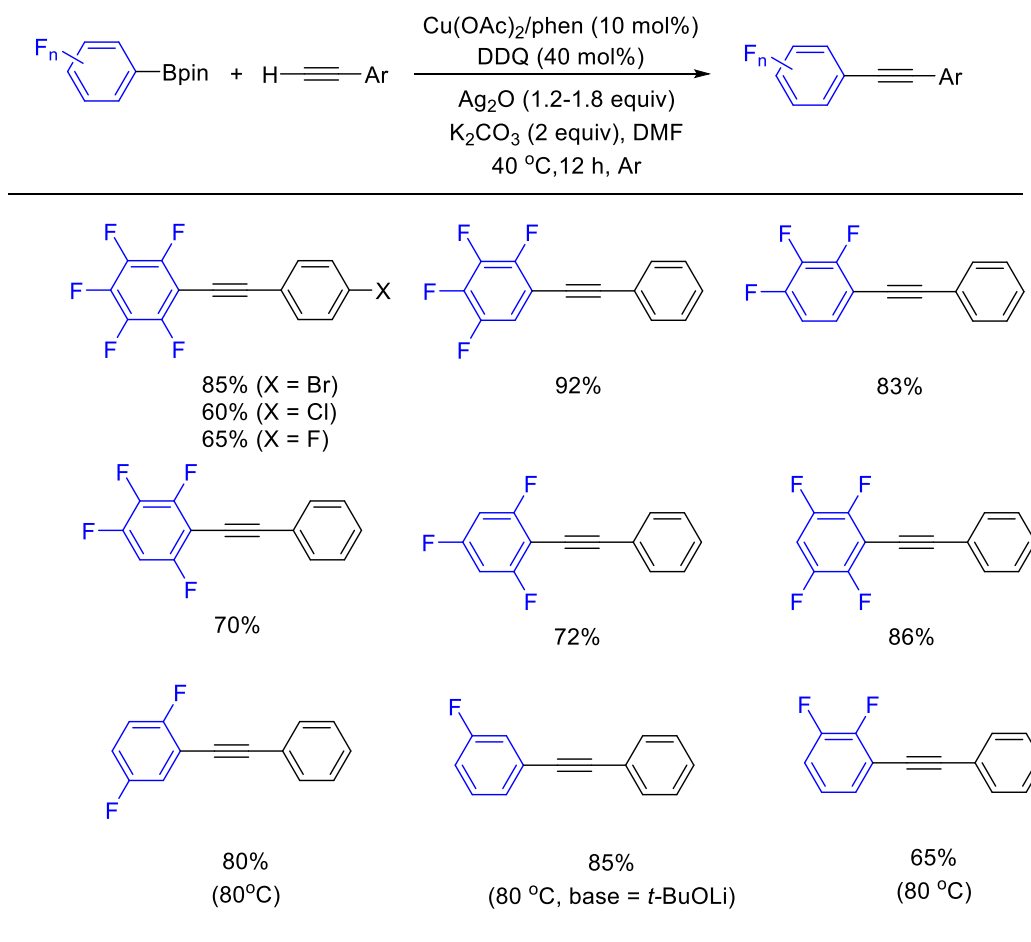
1.5.7.1 Copper-Catalyzed Oxidative Cross-Coupling of Fluorinated Aryl Boronates with Terminal Alkynes

Marder and Radius *et al.* reported that a combination of $\text{Cu}(\text{OAc})_2$ with phenanthroline effectively catalyzed the oxidative cross-coupling of highly fluorinated aryl-Bpin compounds with terminal alkynes under mild conditions.^[167] The reaction of pentafluorophenyl-Bpin with ethynylbenzene using 1.8 equivalents of Ag_2O as the oxidant and 2 equivalents of K_3PO_4 gave the homocoupled alkyne compound as the major product (Scheme 1-77). Interestingly, the use of 2,3-dichloro-5,6-dicyano-1,4-benzoquinone (DDQ) reduced the amount of alkyne homocoupling and increased the desired cross-coupled product. The authors proposed that DDQ functions as an electron-transfer mediator. Using K_2CO_3 as the base proved the most efficient and gave cross-coupling products in good yield.



Scheme 1-77. Optimization reaction of copper-catalyzed oxidative cross-coupling of fluorinated aryl-Bpin with terminal alkynes.^[167]

A number of polyfluorinated aryl-Bpin compounds containing *ortho*-fluorine substituents proved to be viable substrates under these reaction conditions and gave rise to the corresponding cross-coupled products in moderate to good yields. This reaction was also successful using electron-deficient ethynylbenzenes bearing bromine, chlorine, and fluorine groups at the *para*-position (Scheme 1-78). Unfortunately, no desired products were observed for reactions with 4-nitro-phenyl and 4-cyano-phenylalkyne (not shown).



Scheme 1-78. Scope of the copper-catalyzed oxidative coupling of polyfluorophenyl with terminal alkynes.^[167]

1.6 Conclusion and Perspective

As naturally occurring sources of aryl fluorides have not yet been identified, this class of molecules must be generated through chemical synthesis. Fluorinated aryl boronates, important synthons for the generation of these important fluoroarenes, can be synthesized in stoichiometric or catalytic processes using different methods, such as C–H, C–F, and C–X (X = Cl, Br, I, OTf) borylations. Under aqueous basic conditions, protodeboronation of fluorinated aryl boronic acids can be problematic only if the aromatic group contains *ortho*-fluorine substituents. Pentafluorophenyl boronic acid combines di-*ortho*-, di-*meta*-, and *para*-fluorine substituent groups that promote the protodeboronation and it is by far the most challenging substrate to be applied in the organic synthesis. This protodeboronation issue has now been solved in many cases, and thus

polyfluorinated aryl boronates, especially those containing *ortho*-fluorine substituents, can be converted to chlorides, bromides, iodides, phenols, carboxylic acids, nitro groups, cyanides, methylesters and aldehyde analogues. Boron-containing substrates can be implemented in many cross-coupling reactions, such as in the Suzuki-Miyaura cross-coupling with aryl halides, the Chan Evans-Lam C–N cross-coupling with aryl amines or nitrosoarenes, C–C(O) cross-coupling reactions with *N*-(aryl-carbonyloxy)phthalamides or thiol esters (Liebskind-Srogl cross-coupling), and the oxidative cross-coupling with terminal alkynes. The difficult reductive elimination step from highly stable complexes of the type $[\text{PdL}_2(2,6\text{-C}_6\text{F}_{2+n}\text{H}_{3-n})_2]$ frequently impedes these reactions and is the next challenge to be addressed in the homocoupling of 2,6-di-fluorinated aryl pinacol boronates. Progress has been made in this area by employing arene solvents and non-coordinating ligands. Future work will certainly focus on using economically and less toxic methodologies to generate this remarkably useful family of compounds.

1.7 References

- [1] J. Wang, M. S. Rosello, J. L. Aceña, C. Pozo, A. E. Sorochinsky, S. Fustero, V. A. Soloshonok, H. Liu, *Chem. Rev.* **2014**, *114*, 2432–2506.
- [2] H.-J. Bohm, D. Banner, S. Bendels, M. Kansy, B. Kuhn, K. Müller, U. Obst-Sander, M. Stahl, *ChemBioChem* **2004**, *5*, 637–643.
- [3] C. D. Isanbor, D. O'Hagan, *J. Fluorine Chem.* **2006**, *127*, 303–319.
- [4] J.-P. Begue, D. Bonnet-Delpon, *J. Fluorine Chem.* **2006**, *127*, 992–1012.
- [5] K. L. Kirk, *J. Fluorine Chem.* **2006**, *127*, 1013–1029.
- [6] K. Müller, C. Faeh, F. Diederich, *Science* **2007**, *317*, 1881–1886.
- [7] W. K. Hagmann, *J. Med. Chem.* **2008**, *51*, 4359–4369.
- [8] D. O'Hagan, *J. Fluorine Chem.* **2010**, *131*, 1071–1081.
- [9] C. Cullinane, G. B. Deacon, P. R. Drago, A. P. Erven, P. C. Junk, J. Luu, G. Meyer, S. Schmitz, I. Ott, J. Schur, L. K. Webster, A. Klein, *Dalton Trans.* **2018**, *47*, 1918–1932.
- [10] V. A. Montes, G. Li, R. Pohl, J. Shinar, *Adv. Mater.* **2004**, *16*, 2001–2003.
- [11] T. Tsuzuki, N. Shirasawa, T. Suzuki, S. Tokito, *Adv. Mater.* **2003**, *15*, 1455–1458.
- [12] M. S. Jang, S. Y. Song, H. K. Shim, *Polymer* **2000**, *41*, 5675–5679.
- [13] R. Ragni, A. Punzi, F. Babudri, G. M. Farinola, *Eur. J. Org. Chem.* **2018**, 3500–3519.
- [14] Y. Sakamoto, T. Suzuki, A. Miura, H. Fujikawa, S. Tokito, Y. Taga, *J. Am. Chem. Soc.* **2000**, *122*, 1832–1833.
- [15] J. Lieffrig, A. G. Niassy, O. Jeannin, M. Fourmigue, *Cryst. Eng. Comm.* **2015**, *17*, 50–57.
- [16] G. M. Espallargas, A. Recuenco, F. M. Romero, L. Brammer, S. Libri, *Cryst. Eng. Comm.* **2012**, *14*, 6381–6383.
- [17] Y. P. Budiman, A. Friedrich, U. Radius, T. B. Marder, *ChemCatChem* **2019**, *11*, 5387–5396.
- [18] T. Chen, I. Popov, O. Zenasni, O. Daugulis, O. S. Miljanic, *Chem. Commun.* **2013**, *49*, 6846–6848.
- [19] H. Yi, M. Albrecht, A. Valkonen, K. Rissanen, *New J. Chem.* **2015**, *39*, 746–749.

- [20] B. Maiti, K. Wang, S. Bhandari, S. D. Bunge, R. J. Twieg, B. D. Dunietz, *J. Mater. Chem. C* **2019**, *7*, 3881–3888.
- [21] M.-H. Yoon, A. Facchetti, C. E. Stern, T. J. Marks, *J. Am. Chem. Soc.* **2006**, *128*, 5792–5801.
- [22] L. Keyes, K. A. Love, J. A. Aromatic C–F Activation: Converting Fluoroarenes to Useful Building Blocks. In *C–H and C–X Bond Functionalization*, (Eds.: X. Ribas), Royal Society of Chemistry, Cambridge, U.K, **2013**.
- [23] T. Ahrens, J. Kohlmann, M. Ahrens, T. Braun, *Chem. Rev.* **2015**, *115*, 931–941.
- [24] H. J. Frohn, H. Franke, P. Fritzen, V. V. Bardin, *J. Organomet. Chem.* **2000**, *598*, 127–135.
- [25] P. A. Cox, M. Reid, A. G. Leach, A. D. Campbell, E. J. King, G. C. Lloyd-Jones, *J. Am. Chem. Soc.* **2017**, *139*, 13156–13165.
- [26] H.-J. Frohn, N. Y. Adonin, V. V. Bardin, V. F. Starichenko, *Z. Anorg. Allg. Chem.* **2002**, *628*, 2827–2833.
- [27] P. Nguyen, H. P. Blom, S. A. Westcott, N. J. Taylor, T. B. Marder, *J. Am. Chem. Soc.* **1993**, *115*, 9329–9330.
- [28] T. Ishiyama, J. Takagi, J. F. Hartwig, *Angew. Chem. Int. Ed.* **2002**, *41*, 3056–3058.
- [29] H. Tamura, H. Yamazaki, H. Sato, S. Sakaki, *J. Am. Chem. Soc.* **2003**, *125*, 16114–16126.
- [30] I. A. I. Mkhaliid, J. H. Barnard, T. B. Marder, J. M. Murphy, J. F. Hartwig, *Chem. Rev.* **2010**, *110*, 890–931.
- [31] G. A. Chotana, M. A. Rak, M. R. Smith, *J. Am. Chem. Soc.* **2005**, *127*, 10539–10544.
- [32] D. W. Robbins, J. F. Hartwig, *Org. Lett.* **2012**, *14*, 4266–4269.
- [33] C. R. K. Jayasundara, J. M. Unold, J. Oppenheimer, M. R. Smith, III, R. E. Maleczka, Jr., *Org. Lett.* **2014**, *16*, 6072–6075.
- [34] J. Takaya, S. Ito, H. Nomomoto, N. Saito, N. Kirai, N. Iwasawa, *Chem. Commun.* **2015**, *51*, 17662–17665.
- [35] C. F. Rentzsch, E. Tosh, W. A. Herrmann, F. E. Kühn, *Green Chem.* **2009**, *11*, 1610–1617.
- [36] M. I. Gonzalez, E. D. Bloch, J. A. Mason, S. J. Teat, J. R. Long, *Inorg. Chem.* **2015**, *5*, 2995–3005.
- [37] T. Furukawa, M. Tobisu, N. Chatani, *J. Am. Chem. Soc.* **2015**, *137*, 12211–12214.

- [38] J. V. Obligacion, S. P. Semproni, P. J. Chirik, *J. Am. Chem. Soc.* **2014**, *136*, 4133–4136.
- [39] J. V. Obligacion, M. J. Bezdek, P. J. Chirik, *J. Am. Chem. Soc.* **2017**, *139*, 2825–2832.
- [40] T. P. Pabst, J. V. Obligacion, E. Rochette, I. Pappas, P. J. Chirik, *J. Am. Chem. Soc.* **2019**, *141*, 15378–15389.
- [41] M. E. Evans, C. L. Burke, S. Yaibuathes, E. Clot, O. Eisenstein, W. D. Jones, *J. Am. Chem. Soc.* **2009**, *131*, 13464–13473.
- [42] E. Clot, M. Besora, F. Maseras, C. Mègret, O. Eisenstein, B. Oelckers, R. N. Perutz, *Chem. Commun.* **2003**, 490–491.
- [43] E. Clot, C. Mègret, O. Eisenstein, R. N. Perutz, *J. Am. Chem. Soc.* **2009**, *131*, 7817–7827.
- [44] J. V. Obligacion, S. P. Semproni, I. Pappas, P. J. Chirik, *J. Am. Chem. Soc.* **2016**, *138*, 10645–10653.
- [45] S. I. Kallane, M. Teltewskoi, T. Braun, B. Braun, *Organometallics* **2015**, *34*, 1156–1169.
- [46] R. J. Lindup, T. B. Marder, R. N. Perutz, A. C. Whitwood, *Chem. Commun.* **2007**, 3664–3666.
- [47] T. Braun, M. Ahijado Salomon, K. Altenhöner, M. Teltewskoi, S. Hinze, *Angew. Chem. Int. Ed.* **2009**, *48*, 1818–1822.
- [48] M. Teltewskoi, J. A. Panetier, S. A. Macgregor, T. Braun, *Angew. Chem. Int. Ed.* **2010**, *49*, 3947–3951.
- [49] W.-H. Guo, Q.-Q. Min, J.-W. Gu, X. Zhang, *Angew. Chem. Int. Ed.* **2015**, *54*, 9075–9078.
- [50] E. Clot, O. Eisenstein, N. Jasim, S. A. Macgregor, J. E. McGrady, R. N. Perutz, *Acc. Chem. Res.* **2011**, *44*, 333–348.
- [51] T. Schaub, U. Radius, *Chem. Eur. J.* **2005**, *11*, 5024–5030.
- [52] T. Schaub, M. Backes, U. Radius, *J. Am. Chem. Soc.* **2006**, *128*, 15964–15965.
- [53] M. W. Kuntze-Fechner, H. Verplancke, L. Tendra, M. Diefenbach, I. Krummenacher, H. Braunschweig, T. B. Marder, M. C. Holthausen, U. Radius, *Chem. Sci.* **2020**, DOI. 10.1039/D0SC04237D.
- [54] X.-W. Liu, J. Echavarren, C. Zarate, R. Martin, *J. Am. Chem. Soc.* **2015**, *137*, 12470–12473.
- [55] T. Niwa, H. Ochiai, Y. Watanabe, T. Hosoya, *J. Am. Chem. Soc.* **2015**, *137*, 14313–14318.

- [56] J. Zhou, M. W. Kuntze-Fechner, R. Bertermann, U. S. D. Paul, J. H. J. Berthel, A. Friedrich, Z. Du, T. B. Marder, U. Radius, *J. Am. Chem. Soc.* **2016**, *138*, 5250–5253.
- [57] Y.-M. Tian, X.-N. Guo, M. W. Kuntze-Fechner, I. Krummenacher, H. Braunschweig, U. Radius, A. Steffen, T. B. Marder, *J. Am. Chem. Soc.* **2018**, *140*, 17612–17623.
- [58] W. K. Chow, O. Y. Yuen, P. Y. Choy, C. M. So, C. P. Lau, W. T. Wong, F. Y. A. Kwong, *RSC Adv.* **2013**, *3*, 12518–12539.
- [59] S. K. Bose, A. Deißberger, A. Eichhorn, P. G. Steel, Z. Lin, T. B. Marder, *Angew. Chem. Int. Ed.* **2015**, *54*, 11843–11847.
- [60] C. Kleeber, L. Dang, Z. Lin, T. B. Marder, *Angew. Chem. Int. Ed.* **2009**, *48*, 5350–5354.
- [61] W. Zhu, D. Ma, *Org. Lett.* **2006**, *8*, 261–263.
- [62] L. Kuehn, M. Huang, U. Radius, T. B. Marder, *Org. Biomol. Chem.* **2019**, *17*, 6601–6606.
- [63] T. Yoshida, L. Ilies, E. Nakamura, *ACS Catal.* **2017**, *7*, 3199–3203.
- [64] H. D. S. Guerrand, L. D. Marciasini, M. Jousseau, M. Vaultier, M. Pucheault, *Chem. Eur. J.* **2014**, *20*, 5573–5579.
- [65] J. Dong, H. Guo, W. Peng, Q.-S. Hu, *Tetrahedron Lett.* **2019**, *60*, 760–763.
- [66] M. Murata, T. Oyama, S. Watanabe, Y. Masuda, *J. Org. Chem.* **2000**, *65*, 164–168.
- [67] A. N. Cammidge, K. V. L. Crépy, *J. Org. Chem.* **2003**, *68*, 6832–6835.
- [68] G. A. Molander, S. L. J. Trice, S. M. Kennedy, S. D. Dreher, M. T. Tudge, *J. Am. Chem. Soc.* **2012**, *134*, 11667–11673.
- [69] Y. Yamamoto, H. Matsubara, H. Yorimitsu, A. Osuka, *ChemCatChem* **2016**, *8*, 2317–2320.
- [70] H. G. Kuivila, J. F. Reuwer, Jr., J. A. Mangravite, *Can. J. Chem.* **1963**, *41*, 3081–3090.
- [71] H. J. Frohn, N. Y. Adonin, V. V. Bardin, *Z. Anorg. Allg. Chem.* **2002**, *628*, 2834–2838.
- [72] J. Lozada, Z. Liu, D. M. Perrin, *J. Org. Chem.* **2014**, *79*, 5365–5368.
- [73] L. Chen, H. Francis, B. P. Carrow, *ACS Catal.* **2018**, *8*, 2989–2994.
- [74] N. Y. Adonin, A. Y. Shabalin, V. V. Bardin, *J. Fluorine Chem.* **2014**, *168*, 111–120.
- [75] V. V. Bardin, S. G. Idemskaya, H.-J. Frohn, *Z. Anorg. Allg. Chem.* **2002**, *628*, 883–890.
- [76] T. D. Quach, R. A. Batey, *Org. Lett.* **2003**, *5*, 4397–4400.
- [77] C. C. Tzschucke, J. M. Murphy, J. F. Hartwig, *Org. Lett.* **2007**, *9*, 761–764.

- [78] J. M. Murphy, C. Tzschuche, J. F. Hartwig, *Org. Lett.* **2007**, *9*, 757–760.
- [79] T. E. Pennington, C. Kardiman, C. A. Hutton, *Tetrahedron Lett.* **2004**, *45*, 6657–6660.
- [80] S. P. A. Hinkes, C. D. P. Klein, *Org. Lett.* **2019**, *21*, 3048–3052.
- [81] N. Ellis, G. A. Molander, *Acc. Chem. Res.* **2007**, *40*, 275–286.
- [82] R. Figueroa, G. A. Molander, *Aldrichimica Acta* **2005**, *38*, 49–56.
- [83] H. S. Stegani, R. Cella, A. S. Vieira, *Tetrahedron* **2007**, *63*, 3623–3658.
- [84] S. Darses, J.-P. Gener, *Eur. J. Org. Chem.* **2003**, *22*, 4313–4327.
- [85] H. Audi, E. Rémond, M.-J. Eymin, A. Tessier, R. Malacea-Kabbara, S. Jugé, *Eur. J. Org. Chem.* **2013**, 7960–7972.
- [86] J. M. Murphy, X. Liao, J. F. Hartwig, *J. Am. Chem. Soc.* **2007**, *129*, 15434–15435.
- [87] B. M. Partridge, J. F. Hartwig, *Org. Lett.* **2013**, *15*, 140–143.
- [88] J. H. P. Tyman, *Synthetic and Natural Phenols*, Elsevier, New York, 1996.
- [89] R. E. Maleczka, Jr., F. Shi, D. Holmes, M. R. Smith, III, *J. Am. Chem. Soc.* **2003**, *125*, 7792–7793.
- [90] T. Sakakura, J.-C. Choi, H. Yasuda, *Chem. Rev.* **2007**, *107*, 2365–2387.
- [91] T. Ohishi, M. Nishiura, Z. Hou, *Angew. Chem. Int. Ed.* **2008**, *47*, 5792–5795; *Angew. Chem.* **2008**, *120*, 5876–5879.
- [92] L. Dang, Z. Lin, T. B. Marder, *Organometallics* **2010**, *29*, 917–927.
- [93] Y. Makida, E. Marelli, A. M. Z. Slawin, S. P. Nolan, *Chem. Commun.* **2014**, *50*, 8010–8013.
- [94] K. Nepali, H.-Y. Lee, J.-P. Liou, *J. Med. Chem.* **2019**, *62*, 2851–2893.
- [95] K. Zhang, A. Budinska, A. Passera, D. Katayev, *Org. Lett.* **2020**, *22*, 2714–2719.
- [96] M. Al-Masum, R. L. Welch, *Tetrahedron Lett.* **2014**, *55*, 1726–1728.
- [97] F. F. Fleming, L. Yao, P. C. Ravikumar, L. Funk, B. C. Shook, *J. Med. Chem.* **2010**, *53*, 7902–7917.
- [98] C. W. Liskey, X. Liao, J. F. Hartwig, *J. Am. Chem. Soc.* **2010**, *132*, 11389–11391.
- [99] Y. Ye, Y. Wang, P. Liu, F. Han, *Chin. J. Chem.* **2013**, *31*, 27–30.
- [100] Z. Zhang, L. S. Liebeskind, *Org. Lett.* **2006**, *8*, 4331–4333.
- [101] C. A. Malapit, J. T. Reeves, C. A. Busacca, A. R. Howell, C. H. Senanayake, *Angew. Chem.*

- Int. Ed.* **2016**, *55*, 326–330.
- [102] C. Qi, X. Hu, H. He, *Synlett* **2016**, *27*, 1979–1982.
- [103] J. Otera, *Esterification: Methods, Reactions, and Applications*; Wiley-VCH, Weinheim, **2010**.
- [104] Y.-F. Cao, L.-J. Li, M. Liu, H. Xu, H.-X. Dai, *J. Org. Chem.* **2020**, *85*, 4475–4481.
- [105] H.-G. Cheng, H. Chen, Y. Liu, Q. Zhou, *Asian J. Org. Chem.* **2008**, *7*, 490–508.
- [106] H. Huang, C. Yu, X. Li, Y. Zhang, Y. Zhang, X. Chen, P. S. Mariano, H. Xie, W. Wang, *Angew. Chem. Int. Ed.* **2017**, *56*, 8201–8205.
- [107] Crabtree, R.H. *The Organometallic Chemistry of the Transition Metals*, 6th ed.; Wiley-VCH: New York, **2014**.
- [108] J. F. Hartwig, *Organotransition Metal Chemistry: From Bonding to Catalysis*, University Science Books, Sausalito, CA, **2010**.
- [109] J. F. Hartwig, *Inorg. Chem.* **2007**, *46*, 1936–1947.
- [110] T. Koizumi, A. Yamazaki, T. Yamamoto, *Dalton Trans.* **2008**, 3949–3952.
- [111] L. Gu, L. M. Wolf, W. Thiel, C. W. Lehmann, M. Alcarazo, *Organometallics* **2018**, *37*, 665–672.
- [112] E. Gioria, J. del Pozo, J. M. Martínez-Ilarduya, P. Espinet, *Angew. Chem. Int. Ed.* **2016**, *55*, 13276–13280.
- [113] E. F. Santos-Filho, J. C. Sousa, N. M. M. Bezerra, P. H. Menezes, R. A. Oliveira, *Tetrahedron Lett.* **2011**, *52*, 5288–5291.
- [114] Y. P. Budiman, A. Jayaraman, A. Friedrich, F. Kerner, U. Radius, T. B. Marder, *J. Am. Chem. Soc.* **2020**, *142*, 6036–6050.
- [115] N. Miyaura, A. Suzuki, *Chem. Rev.* **1995**, *95*, 2457–2483.
- [116] A. Suzuki, *Angew. Chem. Int. Ed.* **2011**, *50*, 6722–6737.
- [117] N. Miyaura, *Cross-Coupling Reactions: A Practical Guide*, Springer, New York, **2002**.
- [118] M. Havelková, D. Dvůrák, M. Hocek, *Synthesis* **2001**, *11*, 1704–1710.
- [119] M. Havelková, M. Hocek, M. Česnek, D. Dvůrák, *Synlett* **1999**, *7*, 1145–1147.

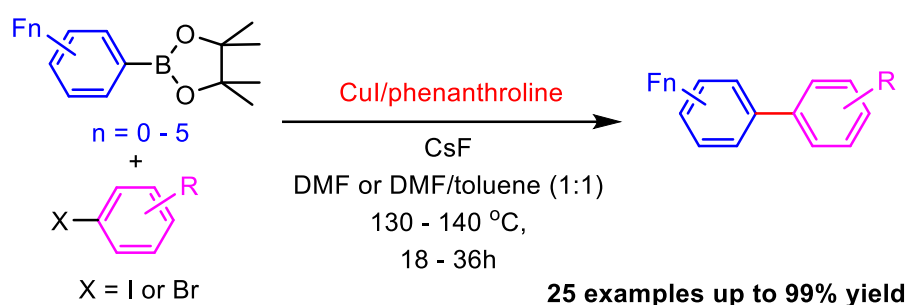
- [120] T. Thiemann, K. Umeno, D. Ohira, E. Inohae, T. Sawada, S. Mataka, *New J. Chem.* **1999**, *23*, 1067–1070.
- [121] D. Bulfield, S. M. Huber, *J. Org. Chem.* **2017**, *82*, 13188–13203.
- [122] J. Kohlmann, T. Braun, R. Laubenstein, R. Herrmann, *Chem. Eur. J.* **2017**, *23*, 12218–12232.
- [123] T. Kinzel, Y. Zhang, S. L. Buchwald, *J. Am. Chem. Soc.* **2010**, *132*, 14073–14075.
- [124] N. C. Bruno, M. T. Tudge, S. L. Buchwald, *Chem. Sci.* **2013**, *4*, 916–920.
- [125] Z. Feng, W. Hu, W. N. Rom, F. A. Beland, M.-S. Tang, *Carcinogenesis* **2002**, *23*, 1721–1727
- [126] N. C. Bruno, N. Niljianskul, S. L. Buchwald, *J. Org. Chem.* **2014**, *79*, 4161–4166.
- [127] H. Nogushi, K. Hojo, M. Suginome, *J. Am. Chem. Soc.* **2007**, *129*, 758–759.
- [128] Y. Mutoh, K. Yamamoto, S. Saito, *ACS Catal.* **2020**, *10*, 352–357.
- [129] H. Yoshida, M. Seki, S. Kamio, H. Tanaka, Y. Izumi, J. Li, I. Osaka, M. Abe, H. Andoh, T. Yajima, T. Tani, T. Tsuchimoto, *ACS Catal.* **2020**, *10*, 346–351.
- [130] J. Chen, A. Cammers-Goodwin, *Tetrahedron Lett.* **2003**, *44*, 1503–1506.
- [131] H.-J. Frohn, N. Y. Adonin, V. V. Bardin, V. F. Starichenko, *J. Fluorine Chem.* **2003**, *122*, 195–199.
- [132] H.-J. Frohn, N. Y. Adonin, V. V. Bardin, V. F. Starichenko, *J. Fluorine Chem.* **2002**, *117*, 115–120.
- [133] G. A. Molander, B. Biolatto, *J. Org. Chem.* **2003**, *68*, 4302–4314.
- [134] J. Uenishi, J. M. Beau, R. W. Armstrong, Y. Kishi, *J. Am. Chem. Soc.* **1987**, *109*, 4756–4758.
- [135] Y. Nishihara, H. Onodera, K. Osakada, *Chem. Commun.* **2004**, 192–193.
- [136] T. Korenaga, T. Kosaki, R. Fukumura, T. Ema, T. Sakai, *Org. Lett.* **2005**, *7*, 4915–4917.
- [137] K. Takimiya, N. Niihara, T. Otsubo, *Synthesis* **2005**, *10*, 1589–1592.
- [138] H.-J. Frohn, N. Y. Adonin, V. V. Bardin, V. F. Starichenko, *Tetrahedron Lett.* **2002**, *43*, 8111–8114.
- [139] V. V. Bardin, A. Y. Shabalin, N. Y. Adonin, *Beilstein J. Org. Chem.* **2015**, *11*, 608–616.
- [140] Y. Zhou, W. You, K. B. Smith, M. K. Brown, *Angew. Chem. Int. Ed.* **2014**, *53*, 3475–3479.

- [141] S. K. Gurung, S. Thapa, A. Kae, D. A. Dickie, R. Giri, *Org. Lett.* **2014**, *16*, 1264–1267.
- [142] J. H. Li, D. P. Wang, *Eur. J. Org. Chem.* **2006**, *72*, 2063–2056.
- [143] J.-H. Li, J.-L. Li, D.-P. Wang, S.-F. Pi, Y.-X. Xie, M.-B. Zhang, X.-C. Hu, *J. Org. Chem.* **2007**, *72*, 2053–2057.
- [144] M. B. Thathagar, J. Beckers, G. Rothenberg, *J. Am. Chem. Soc.* **2002**, *124*, 11858–11859.
- [145] J. Mao, J. Guo, F. Fang, S.-J. Ji, *Tetrahedron* **2008**, *64*, 3905–3911.
- [146] S. K. Gurung, S. Thapa, B. Shrestha, R. Giri, *Org. Chem. Front.* **2015**, *2*, 649–653.
- [147] A. M. Bergmann, A. M. Oldham, W. You, M. K. Brown, *Chem. Commun.* **2018**, *54*, 5381–5384.
- [148] H. Q. Do, O. Daugulis, *J. Am. Chem. Soc.* **2008**, *130*, 1128–1129.
- [149] H. Q. Do, R. M. Khan, O. A. Daugulis, *J. Am. Chem. Soc.* **2008**, *130*, 15185–15192.
- [150] A. Dahiya, C. Fricke, F. Schoenebeck, *J. Am. Chem. Soc.* **2020**, *142*, 7754–7759.
- [151] J. H. Montgomery, *In Agrochemicals Desk Reference: Environmental Data*; Lewis Publishers, Chelsea, MI, **1993**.
- [152] M. Negwer, *In Organic-Chemical Drugs and their Synonyms: (An International Survey)*, 7th ed., Akademie Verlag GmbH, Berlin, **1994**.
- [153] D. M. T. Chan, K. L. Monaco, R.-P. Wang, M. P. Winters, *Tetrahedron Lett.* **1998**, *39*, 2933–2936.
- [154] P. Y. S. Lam, C. G. Clark, S. Saubern, J. Adams, M. P. Winters, D. M. T. Chan, A. Combs, *Tetrahedron Lett.* **1998**, *39*, 2941–2944.
- [155] J. C. Vantourout, R. P. Law, A. Isidro-Llobet, S. J. Atkinson, *J. Org. Chem.* **2016**, *81*, 3941–3950.
- [156] B. P. Fors, S. L. Buchwald, *J. Am. Chem. Soc.* **2018**, *132*, 15914–15917.
- [157] Q. Sheng, J. F. Hartwig, *Org. Lett.* **2008**, *10*, 4109–4112.
- [158] J. C. Antilla, S. L. Buchwald, *Org. Lett.* **2001**, *3*, 2077–2079.
- [159] W.-J. Yoo, T. Tsukamoto, S. Kobayashi, *Angew. Chem. Int. Ed.* **2015**, *54*, 6587–6590.
- [160] W. Zhong, Z. Liu, C. Yu, W. Su, *Synlett.* **2008**, *18*, 2888–2982.
- [161] S. Roscales, A. G. Csáký, *Org. Lett.* **2018**, *20*, 1667–1671.

- [162] D. A. Evans, J. L. Katz, T. R. West, *Tetrahedron Lett.* **1998**, *39*, 2937–2940.
- [163] F. Gao, H. Feng, Z. Sun, *Tetrahedron Lett.* **2014**, *55*, 6541–6454.
- [164] B. Tan, N. Toda, C. F. Barbas III, *Angew. Chem. Int. Ed.* **2012**, *51*, 12538–12541.
- [165] J. M. Villalobos, J. Srogi, L. S. Liebeskind, *J. Am. Chem. Soc.* **2007**, *129*, 15734–15735.
- [166] L. S. Liebeskind, H. Yang, H. Li, *Angew. Chem. Int. Ed.* **2009**, *48*, 1417–1421.
- [167] Z. Liu, Y. P. Budiman, Y.-M. Tian, A. F. Friedrich, M. Huang, S. A. Westcott, U. Radius, T. B. Marder, *Chem. Eur. J.* **2020**, DOI: 10.1002/chem.202002888.

Chapter 2

Copper-Catalyzed Suzuki-Miyaura Cross-Coupling of Highly Fluorinated Aryl Boronate Esters with Aryl Iodides and Bromides and Fluoroarene-Arene π -Stacking Interactions in the Products



2 Copper-Catalyzed Suzuki-Miyaura Cross-Coupling of Highly Fluorinated Aryl Boronate Esters with Aryl Iodides and Bromides and Fluoroarene-Arene π -Stacking Interactions in the Products

Adapted with permission from Y. P. Budiman, A. Friedrich, U. Radius, T. B. Marder, *ChemCatChem* **2019**, *11*, 5387–5396. Copyright (2019) Wiley-VCH.

2.1 Abstract

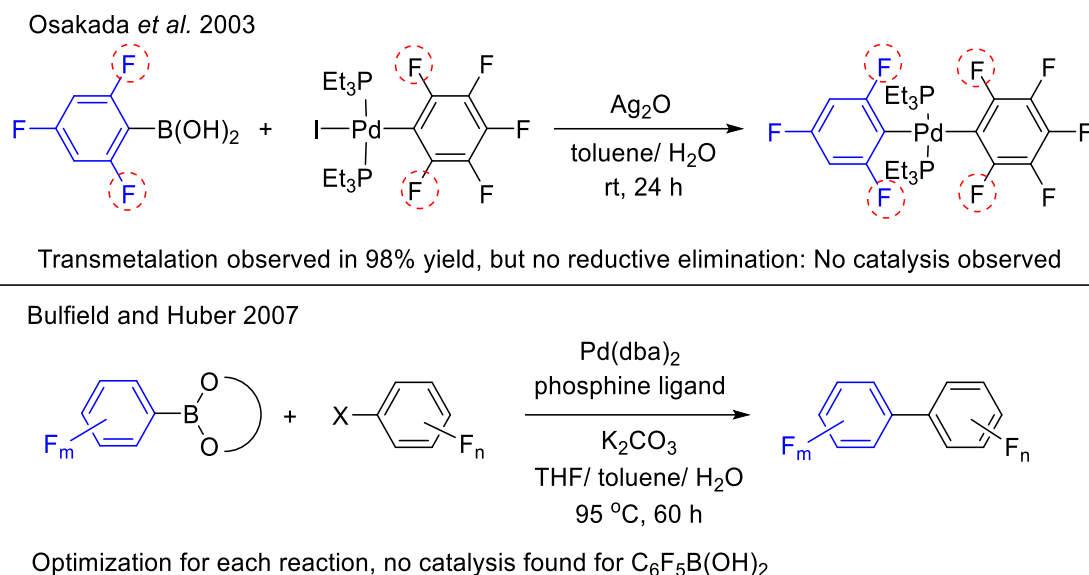
A combination of copper iodide and phenanthroline as the ligand is an efficient catalyst for Suzuki-Miyaura cross-coupling of highly fluorinated boronate esters (aryl-Bpin) with aryl iodides and bromides to generate fluorinated biaryls in good to excellent yields. This method represents a nice alternative to traditional cross-coupling methods which require palladium catalysts and stoichiometric amounts of silver oxide. We note that $\pi \cdots \pi$ stacking interactions dominate the molecular packing in the partly fluorinated biaryl crystals investigated herein. They are present either between the arene and perfluoroarene, or solely between arenes or perfluoroarenes, respectively.

2.2 Introduction

The conversion of highly fluorinated aromatics into fluorinated aryl boronate esters is desirable as aryl boronate esters are useful building blocks for organic synthesis.^[1] We recently reported the successful defluoroborylation of polyfluorinated aromatics using an NHC nickel complex (NHC = *N*-Heterocyclic Carbene) as a catalyst and the diboron(4) compound B₂pin₂ (pin = pinacolato) as the boron source.^[2] Having a good source of fluorinated aryl boronates in hand, we were interested to explore the chemistry of these electron withdrawing molecules, especially in Suzuki-Miyaura cross-coupling reactions which are employed in various fields, from the synthesis of natural products to materials chemistry, including large-scale production.^[3] Applications of polyfluorobiphenyls, are quite numerous including medicinal chemistry,^[4] organic light emitting diodes,^[5] electron-transport

materials,^[6] crystal engineering,^[7] metal-organic frameworks (MOFs),^[8] and supramolecular chemistry.^[9]

However, Suzuki-Miyaura cross-coupling of highly fluorinated aryl boronate esters, especially pentafluorophenyl boronates is highly challenging under typical Suzuki-Miyaura conditions,^[10] as the transfer of C₆F₅ to the palladium centre in the transmetalation step is usually inefficient.^[11c] In many cases, stoichiometric amounts of costly silver oxide (Ag₂O) were added in addition to the palladium catalyst to enhance the transmetalation step and thus to obtain the desired coupling product in fair to good yield.^[11] In 1987, it was initially reported by Kishi *et al.* that Ag₂O can accelerate the rate of palladium-catalyzed Suzuki-Miyaura cross-coupling of alkenylboronic acids with alkenyl iodides with the relative rate being 30 times faster than that using common bases such as KOH.^[12] Inspired by that, in 2002, Frohn and Adonin *et al.* used 1.2 equivalents of Ag₂O to enhance the efficiency of Pd(OAc)₂/PPh₃/K₂CO₃ to catalyze the Suzuki-Miyaura cross-coupling of C₆F₅B(OMe)₃Li^[11f] or C₆F₅BF₃K^[11g] with aryl iodides in toluene. In 2005, Korenaga *et al.*^[11c] reported an effective method for coupling of C₆F₅B(OH)₂ with aryl iodides using Pd(PPh₃)₄/CsF in DMF and for coupling with aryl bromides using Pd₂(dba)₃/PtBu₃/CsF in DMF, in both cases requiring 1.2 equivalents of Ag₂O. In 2015, Adonin *et al.* extended their previous studies^[11g] to the coupling of C₆F₅BF₃K with aryl bromides instead of iodides employing Pd(OAc)₂/PtBu₃/K₂CO₃ in toluene, but this was still only effective in the presence of 1.2 equivalents of Ag₂O.^[11b] Osakada *et al.* reported that Ag₂O has the ability to replace the halide ligand of the catalyst to generate an hydroxy-palladium species, which shows higher reactivity in the transmetalation step with aryl boronates. The reaction of *trans*-[Pd(PEt₃)₂(C₆F₅)I] with Ag₂O in toluene-water, for example, generates the complex *trans*-[Pd(PEt₃)₂(C₆F₅)(OH)], which undergoes transmetalation with the boronic acid 4-MeOC₆H₄B(OH)₂.^[13] In 2010, Buchwald *et al.* reported the precatalyst XPhos-Pd-G2 to solve the problem, and this works without additional Ag₂O to catalyze the coupling of 2,6-difluorophenyl-B(OH)₂ with aryl chlorides, bromides, and triflates but, interestingly, did not work for aryl iodides.^[11h] However, this palladium catalyst is quite expensive or at least requires a multistep synthesis.



Scheme 2-1. Recent challenges for Pd-catalyzed Suzuki-Miyaura cross-coupling to achieve polyfluorinated biaryls.

Previously, Osakada *et al.*^[13] showed that 2,4,6-trifluorophenyl-B(OH)₂ reacts with *trans*-[Pd(C₆F₅)(PEt₃)₂I] in the presence of Ag₂O in toluene and H₂O, but the reaction stops with generation of the stable intermediate *trans*-[Pd(C₆F₅)(2,4,6-C₆F₃H₂)(PEt₃)₂] as reductive elimination was not observed for this complex. Thus, for palladium complexes [L₂Pd(Ar)(Ar')], if both Ar and Ar' are highly electron deficient, the reductive elimination step becomes much more difficult, as the Pd–Ar bonds are strong.^[14] Those reports show the current challenge for the palladium catalyzed Suzuki-Miyaura cross-coupling of C₆F₅-boronates with fluorinated aryl halides (Ar_F–X), especially if the C–X bond flanked by two C–F bonds.

Polyfluorinated biaryls can be synthesized *via* Suzuki-Miyaura cross-coupling of polyfluorinated aryl boronic acids or esters and polyfluorinated aryl iodides, as reported by Bulfield and Huber^[10d] using palladium catalysts. They employed both fluoroaryl boronate and fluoroaryl halide substrates as coupling partners using a combination of palladium sources and various phosphine ligands. Although this reaction works in some cases, they had to optimise each reaction separately for the corresponding aryl boronate and aryl halide, using different types of expensive phosphine ligands. These reactions all required long reaction times (over 60 hours) and a procedure that would work for C₆F₅B(OH)₂ was not developed.

Recently, research to replace precious metal catalysts with cheaper and Earth-abundant metals^[15] as well as metals of lower toxicity^[16] has attracted much attention. Several groups have developed Cu(I) catalysts for Suzuki-Miyaura cross-coupling reactions.^[17] For example, Li *et al.* have developed a copper/DABCO ligand catalyst system, but the reaction, however, does not work for sterically hindered and electron-deficient aryl boronic acids.^[17c,d] Brown *et al.* reported that a combination of CuCl with XantPhos can effectively catalyze Suzuki-Miyaura cross-coupling of aryl iodides with aryl boronic acid neopentylglycol esters (Bneop)^[17a] and later using Cy₃PCuCl catalyst for a cross-coupling of aryl-Bpin with heteroaryl bromides.^[17h] Other systems involve the use of copper nanoclusters^[17e] or copper powder in polyethylene glycol solvents.^[17f] Giri *et al.* reported an efficient system employing CuI and *o*-(di-*tert*-butylphosphino)-*N,N*-dimethylaniline (PN) as the ligand for efficient Suzuki-Miyaura cross-coupling of aryl-Bneop with aryl iodides^[17b] and extended with electron deficient aryl bromides.^[17h] However, to the best of our knowledge, there are no reports of copper-catalyzed Suzuki-Miyaura cross-coupling reaction of electron deficient, highly fluorinated aryl boronate esters, and only a few examples of the use of aryl bromides in Cu-catalyzed Suzuki-Miyaura reactions.^[17f,g,h] On the other hand, the optimized conditions for Cu-catalyzed Suzuki-Miyaura cross-coupling employing aryl-Bpin and aryl iodide as coupling partners is still challenging, as Brown, *et al.*^[17a] and Giri, *et al.*^[17b] reported that their optimized methods to employ aryl-Bpin instead of aryl-Bneop only affording fair yields.

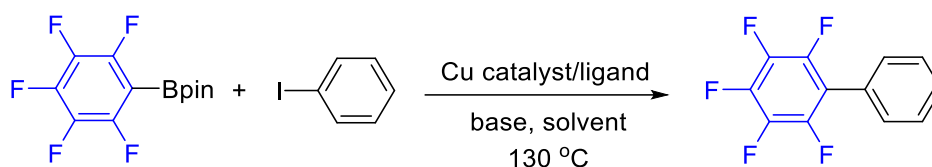
Herein, we report Suzuki-Miyaura cross-coupling of aryl iodides and bromides with highly fluorinated aryl boronate esters (Ar_F-Bpin), catalyzed by phenanthroline-ligated copper complexes. Notably, Cu(I)-catalyzed Suzuki-Miyaura cross-coupling of C₆F₅Bpin does not require the addition of silver oxide to achieve quantitative yields.

2.3 Result and Discussion

2.3.1 Optimization of Reaction Conditions

We began our investigation using the most electron deficient compound, C₆F₅Bpin (**2_1a**), which was synthesized *via* an Ir-catalyzed C–H borylation reaction.^[18] Coupling of C₆F₅Bpin with phenyl iodide (**2_2a**) to give 2,3,4,5,6-pentafluoro biphenyl (**2_3a**) was chosen as a model reaction. Giri *et al.*^[17g] studied the mechanism of Cu(I)-catalyzed Suzuki-Miyaura cross-coupling and showed that, after the formation of [(PN)CuI]₂, the addition of CsF led to the formation of [(PN)CuF]₂, which then yielded [(PN)CuPh] after transmetalation with an aryl-Bneop reagent. Inspired by that work, we screened Cu(I) salts with different ligands, bases and solvents.

As Giri *et al.* demonstrated that the combination of CuI and *o*-(di-*tert*-butylphosphino)-*N,N*-dimethylaniline (PN), CsF, in DMF/dioxane solvent at 130 °C was efficient for the Suzuki-Miyaura cross-coupling of aryl-Bneop with aryl iodide,^[17b,g] we initially tried to employ these conditions to cross-couple C₆F₅Bpin with phenyl iodide, but obtained only a 5% isolated yield of the biaryl product after 18 h (Table 2-1, entry 1). Changing the PN-ligand to *N*-only-based chelating ligands such as 2,2'-bipyridine (bpy) and 4,4'-di-*tert*-butyl-2,2'-bipyridyl (dtbpy) (Table 2-1, entries 2 and 3) led to better yields (42% and 57%, respectively), while phenanthroline emerged as the best ligand for our purpose. The reaction of C₆F₅Bpin with 1.5 equivalents of iodobenzene in DMF at 130 °C in the presence of 10 mol% CuI, 10 mol% phenanthroline, and 2 equivalents of CsF afforded the cross-coupling product in an excellent yield of 99% after workup (Table 2-1, entry 4). The use of monodentate 4-(dimethylamino)pyridine (DMAP) instead of phenanthroline led to much poorer activity (21% yield, Table 2-1, entry 5).

Table 2-1. Suzuki-Miyaura cross-coupling of C₆F₅Bpin with PhI.^[a]

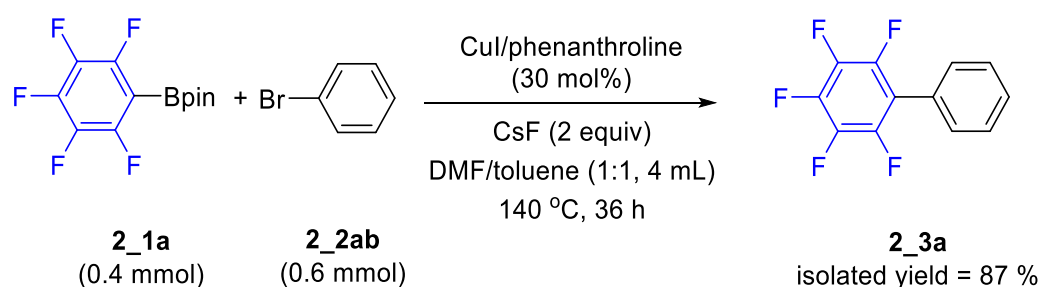
Entry	Cu catalyst	Ligand	Base	Solvent	Time	Yield (%) ^[b]
1	CuI	PN	CsF	DMF/dioxane	18	5
2	CuI	bpy	CsF	DMF	24	42
3	CuI	dtbpy	CsF	DMF	24	57
4	CuI	phenanthroline	CsF	DMF	18	99 ^[c] 48 ^[d]
5	CuI	DMAP	CsF	DMF	24	21
6	CuCl	phenanthroline	CsF	DMF	24	55
7	CuBr	phenanthroline	CsF	DMF	24	36
8	CuI	phenanthroline	KF	DMF	24	68
9	CuI	phenanthroline	NMe ₄ F	DMF	24	29
10	CuI	phenanthroline	K ₃ PO ₄	DMF	24	3
11	CuI	phenanthroline	CsF	Toluene	24	0 ^[e]
12	CuI	phenanthroline	CsF	THF	24	0 ^[f]
13	CuI	-	CsF	DMF	24	26
14	CuI	phenanthroline	-	DMF	24	0
15	-	phenanthroline	CsF	DMF	24	0
16	(Phen)CuI	-	CsF	DMF	18	94

^[a] General conditions: **2_1a** (0.4 mmol), **2_2a** (0.6 mmol), Cu catalyst (10 mol%), ligand (10 mol%), base (2 equiv), solvent (3 mL), under argon. ^[b] Isolated yield after flash chromatography.

^[c] C₆F₅BF₃K instead of C₆F₅Bpin. ^[d] T = 100 °C. ^[e] T = 110 °C. ^[f] T = 60 °C.

CuCl and CuBr, in place of CuI, were also tested but led to a decrease of the isolated yields to 55% and 36%, respectively (Table 2-1, entries 6 and 7). It is important to note that hydroxide and alkoxide bases must be avoided as the *para*-carbon atom of C₆F₅Bpin is susceptible to nucleophilic attack by these bases and they can replace the *para*-fluoro-substituent on the perfluorinated boronate substrate.^[11c] Thus, we examined fluorides and phosphates as bases and found that CsF gave the best results. Similarly, Korenaga *et al.*^[11c] observed that CsF gave the highest yield for the Suzuki-Miyaura cross-coupling of C₆F₅B(OH)₂ with aryl halides using a Pd-catalyst. Using KF instead of CsF also gave a good yield of 68% (Table 2-1, entry 7), whereas NMe₄F afforded the product in only 29% yield (Table 2-1, entry 8). Non-fluoride bases such as K₃PO₄ resulted in a poor yield of 3% (Table 2-1, entry 10).

Toluene and THF were ineffective solvents at temperatures close to their boiling points (Table 2-1, entries 11 and 12). It is interesting to note that without any additional ligand, the copper catalyst still gave a 26% yield (Table 2-1, entry 13) and was more active than the system employing PN as the ligand (Table 2-1, entry 1). The absence of either CsF or CuI resulted in no product formation, indicating that both base and catalyst are required. A combination of CuI and phenanthroline generates [(Phen)CuI]^[20] as using preformed [(Phen)CuI] gave an excellent yield (Table 2-1, entry 16). CsF reacts as a nucleophile and exchanges the halide ligand at Cu(I) to generate a CuF complex,^[17b] which reacts more readily with the aryl boronate ester in the transmetalation step and thus accelerates the transfer of the aryl group to the metal. CuI gave better results than CuBr or CuCl probably because the low bond energy^[19] led to a more efficient anion exchange with CsF. It is also known that the reaction of [(phen)CuI] and CsF in DMF gives [(phen)CuF].^[20] Thus a combination of 10 mol% of CuI/phenanthroline, and 2 equivalents of CsF, in DMF at 130 °C emerged as the ideal conditions for the Suzuki-Miyaura cross-coupling of C₆F₅Bpin with aryl iodide. The use of organotrifluoroborates is attractive as these are inexpensive and more stable towards air and moisture than organoboronate substrates.^[21] Thus, we also employed C₆F₅BF₃K^[11b,f] for the Suzuki-Miyaura cross-coupling and found that this also produced C₆F₅-C₆H₅ in an almost quantitative yield of 99% (Table 2-1, entry 4).



Scheme 2-2. Cross-coupling reaction of C₆F₅BPin with PhBr.

While the use of aryl bromides and aryl boronate substrates for Cu-catalyzed Suzuki-Miyaura cross-coupling has been reported,^[17g] the reaction of aryl bromides with electron-deficient aryl boronate substrates was found to be difficult.^[17g] We found that phenyl bromide was effective in reactions with C₆F₅BPin in a mixed solvent system such as DMF : toluene (1:1) by increasing the

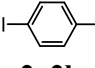
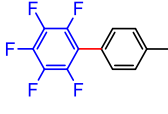
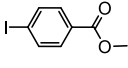
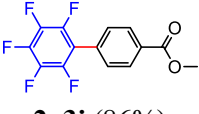
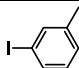
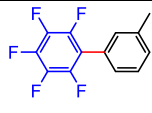
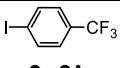
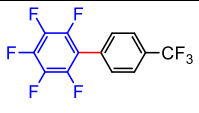
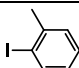
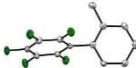
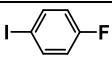
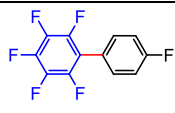
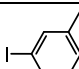
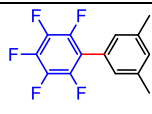
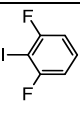
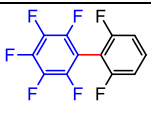
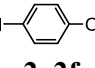
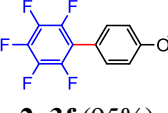
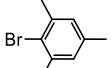
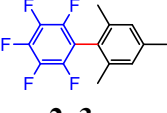
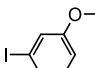
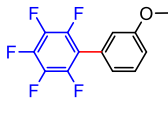
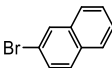
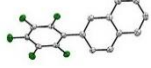
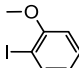
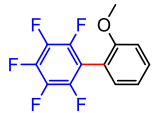
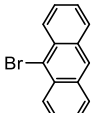
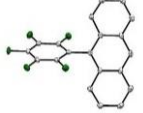
loading of CuI/phenanthroline to 30 mol%, generating the cross-coupling product in 87% yield (Scheme 2-2).

2.3.2 Investigation of Reaction Scope

Having determined the optimal conditions for both phenyl iodides and bromides, we next investigated the scope of the reaction of C₆F₅Bpin with different aryl iodides and bromides (Table 2-2). Aryl iodides bearing electron donating groups (**2_2b**, **2_2c**, **2_2e**, **2_2f**, **2_2g**) at *meta* or *para* positions gave good to excellent yields (88-95%), whereas sterically more hindered substrates such as 2-methylphenyl iodide (**2_2d**), 2-methoxyphenyl iodide (**2_2h**), and mesityl bromide (**2_2m**) gave fair to moderate yields (57-71%). Aryl iodides bearing electron withdrawing substituents, such as methyl 4-iodobenzoate (**2_2i**), 4-iodotrifluorotoluene (**2_2j**), and 4-fluorophenyl iodide (**2_2k**), gave very good to excellent yield (86-93%). In palladium catalysis, if both Ar_F-Bpin and Ar_F-X have two *ortho*-fluoro substituents, reductive elimination has been reported to be difficult^[13] (Scheme 2-1), but in our case, 1,3-difluoro-2-iodobenzene (**2_2l**) also provided a good yield (77%). Naphthalene and anthracene derivatives are interesting for application in blue organic light-emitting diodes (OLED).^[22] Thus, we employed 2-bromonaphthalene (**2_2n**) and 9-bromoanthracene (**2_2o**) in our reaction, and these substrates generated 75% and 78% isolated yields of the corresponding perfluoro phenyl naphthalene and anthracene products, respectively.

Furthermore, we varied the number of fluoro substituents on the aryl-Bpin reagent in coupling reactions with phenyl iodide or bromide. Thus, reaction of other fluorinated aryl-Bpin such as 2,6-difluorophenyl-Bpin (**2_4a**), 2,3- or 2,5-difluorophenyl-Bpin (**2_4b**, **2_4c**), 2,3,4-trifluorophenyl-Bpin (**2_4d**), 2,3,4,5-tetrafluorophenyl-Bpin (**2_4e**), can be coupled with an aryl iodide affording good to excellent yields (Table 2-3, entries 1–5).

Table 2-2. Cu-catalyzed cross-coupling of C₆F₅Bpin with Ar-X (X = I or Br).^[a]

Entry	Ar-X	Product (Yield) ^[b]	Entry	Ar-X	Product (Yield) ^[b]
1	 2_2b	 2_3b (90%)	8	 2_2i	 2_3i (86%)
2	 2_2c	 2_3c (88%)	9	 2_2j	 2_3j (91%)
3	 2_2d	 2_3d (67%)	10	 2_2k	 2_3k (93%)
4	 2_2e	 2_3e (88%)	11	 2_2l	 2_3l (77%)
5	 2_2f	 2_3f (95%)	12	 2_2m	 2_3m (57%)(80%) ^[c]
6	 2_2g	 2_3g (91%)	13	 2_2n	 2_3n (75%)
7	 2_2h	 2_3h (71%)	14	 2_2o	 2_3o (78%)

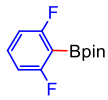
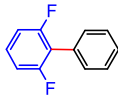
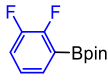
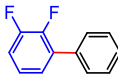
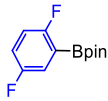
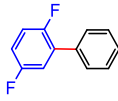
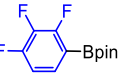
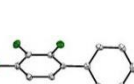
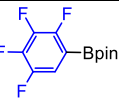
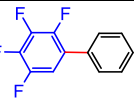
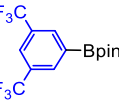
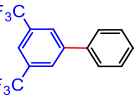
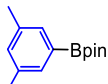
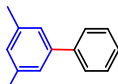
^[a] Standard conditions: C₆F₅Bpin (0.4 mmol), Ar-X (0.6 mmol), CuI/phenanthroline (10 mol% if X = I; 30 mol% if for X = Br), CsF (0.8 mmol), DMF (3 mL, if X = I) or DMF/toluene (1:1, 4 mL, if X = Br), T (130 °C if X = I; 140 °C if X = Br), t (18 h if X = I; 36 h if X = Br), under argon.

^[b] Isolated yield after flash chromatography. ^[c] CuI/phenanthroline (50 mol%).

In term of coupling with an aryl bromide, 2,6-difluorophenyl-Bpin (**2_4a**) proceeded nicely to give the coupling product in 85% yield (Table 2-3. entry 1). However, if the aryl-Bpin has one *ortho*-fluoro substituent, 50 mol% of CuI/phenanthroline is required to couple nicely with aryl bromide (Table 2-3, entries 2-5). Another type of electron deficient aryl boronate ester, namely 3,5-bis(trifluoromethyl)phenyl-Bpin (**2_4f**), also coupled nicely with phenyl iodide,

but its coupling with phenyl bromide proved difficult (Table 2-3, entry 6). On the other hand, electron-rich 3,5-dimethylphenyl-Bpin (**2_4g**) coupled well with phenyl iodide, but was not viable for phenyl bromide (Table 2-3, entry 7), indicating that in this system, aryl bromides only couple efficiently with electronic deficient aryl-Bpin compounds. However, our results show that aryl iodides can be coupled not only with electron deficient aryl-Bpin compounds but also with electron rich ones.

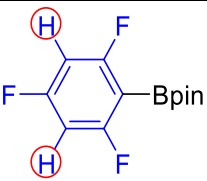
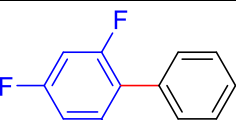
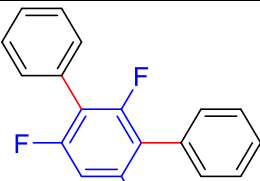
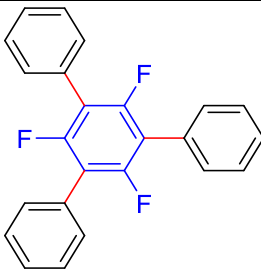
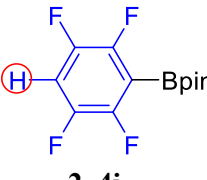
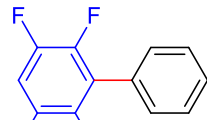
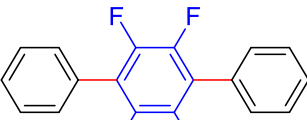
Table 2-3. Cu-catalyzed cross-coupling of various fluorinated and nonfluorinated aryl-Bpin with PhX (X= I or Br).^[a]

Entry	Ar-Bpin	Product	Yield (%) ^[b]	
			X= I	X= Br
1	 2_4a	 2_5a	99	85
2	 2_4b	 2_5b	95	59 (80) ^[c]
3	 2_4c	 2_5c	94	73 ^[c]
4	 2_4d	 2_5d	93	54 (70) ^[c]
5	 2_4e	 2_5e	81	42 ^[c]
6	 2_4f	 2_5f	92	35
7	 2_4g	 2_5g	95	trace

^[a] Standard conditions: Ar-Bpin (0.4 mmol), PhX (0.6 mmol), CuI/phenanthroline (10 mol% if X = I; 30 mol% if X = Br), CsF (0.8 mmol), DMF (3 mL, if X = I) or DMF/toluene (1:1, 4 mL, if X = Br), T (130 °C if X = I; 140 °C if X = Br), t (18 h if X = I; 36 h if X = Br), under argon. ^[b] Isolated yield after flash chromatography. ^[c] CuI/phenanthroline (50 mol%).

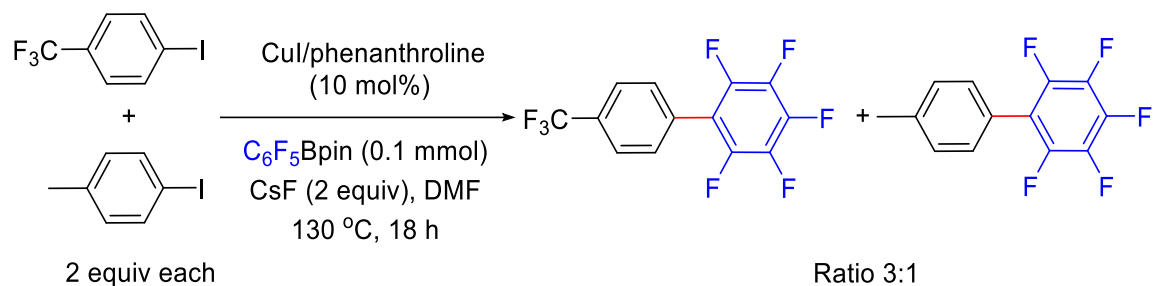
Notably, when 2,4,6-trifluorophenyl-Bpin (**2_4h**) and 2,3,5,6-tetrafluorophenyl-Bpin (**2_4i**) were employed, besides good yields of the expected coupling products, we also observed C–H arylation byproducts generated in small (<10%) amounts after C–Bpin arylation occurred (Table 2-4, entries 1 and 2). It is known that the high acidity of the C–H bonds flanked by two C–F groups can be used in direct arylation.^[23] However, our results show that even though both carbons are electron deficient, the C–Bpin group is more reactive than the C–H moiety as an arylation target.

Table 2-4. Cross-coupling of 2,4,6-F₃C₆H₂Bpin and 2,3,5,6-F₄C₆HBpin with PhX (X = I or Br).^[a]

Entry	Ar _F -Bpin	Product and Yield (%) ^[b]
1	 2_4h	 2_5h X: I (75%), Br (70%)  2_5h' X: I (8%), Br (5%)  2_5h'' X: I or Br (trace)
2	 2_4i	 2_5i X: I (74%), Br (69%)  2_5i' X: I (10%), Br (9%)

^[a] Standard conditions: 0.4 mmol of Ar_F-Bpin, 0.4 mmol of PhX, CuI/phenanthroline (10 mol% if X = I or 30 mol% if X = Br), CsF (0.8 mmol), DMF (3 mL, if X = I) or DMF/toluene (1:1, 4 mL, if X = Br), T (130 °C if X = I; 140 °C if X = Br), t (18 h if X = I; 36 h if X = Br), under argon. ^[b] Isolated yield after flash chromatography.

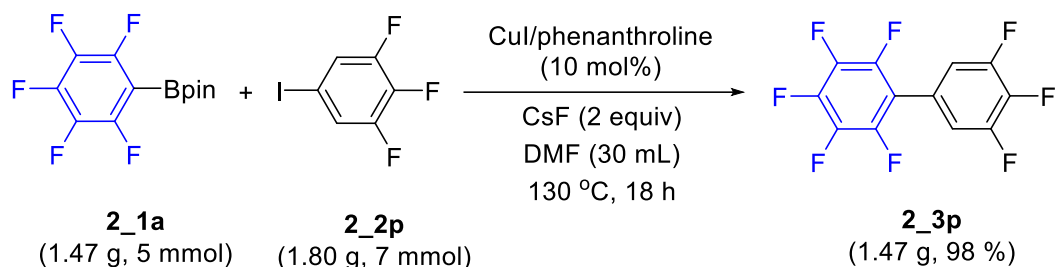
Generally, aryl halides bearing electron-withdrawing groups are more reactive and give better yields compared to aryl halides bearing electron-donating groups. We compared the reactivities of electron-poor and electron-rich aryl halides by reacting a 1:1 mixture of 4-trifluoromethyliodobenzene and 4-iodotoluene with C₆F₅Bpin (Scheme 2-3). Trifluoromethylphenyl iodide was more reactive, resulting in a 3:1 ratio of the trifluoromethyl to methyl-substrated pentafluorobiphenyl compounds.



Scheme 2-3. Comparison of the reactivities of an electron poor and an electron rich aryl iodide.

2.3.3 Gram Scale Reaction

These conditions can be used to prepare polyfluorinated biaryl products on a gram scale. Thus, the coupling of C₆F₅Bpin with 1,2,3-trifluoro-5-iodobenzene (**2_3o**) was conducted without any difficulty using the standard conditions to provide a 98% yield of the unsymmetrical octafluoro biphenyl product (Scheme 2-4).



Scheme 2-4. Gram scale reaction.

2.3.4 Molecular and Crystal Structures: Intermolecular $\pi\cdots\pi$ Stacking Interactions

The crystal structures of the polyfluorinated biaryls **2_3d**, **2_3n**, **2_3o**, and **2_5d** were analyzed using single-crystal X-ray diffraction. A comparison of the molecular geometries of these compounds in their crystal structures (Figure 2-1) shows a small influence of the steric demand of the hydrogenated aryl group in the vicinity of the C–C bonds joining the rings and, hence, of the repulsion between both groups of the biaryl units on their geometries. The central C–C bond is in the range 1.483(4) – 1.495(2) Å (Table 2-5) which is typical of biphenyl compounds.^[24] It is slightly

longer in compounds **2_3d** and **2_3o** than in **2_3n** and **2_5d**, although only within 1–2 esds. The twist between the aryl moieties of the biaryl is slightly stronger in compounds **2_3d** and **2_3o** ($61.66(5)$ and $64.28(5)^\circ$) than in **2_3n** and **2_5d** ($51.23(15)$ and $49.76(7)^\circ$) (Table 2-5). These small differences are likely due to the substitution at the *ortho* position of the non-fluorinated phenyl ring. In **2_3d**, a methyl group is bonded at the *ortho* position and in **2_3o**, the central phenyl ring of the anthracene moiety is bonded to the fluorinated phenyl ring. This increases the bulkiness of these aryl moieties in close vicinity to the central C–C bond and, hence, to the respective fluorinated phenyl rings. Large twist angles are also reported in the bulky biaryl compounds with a pentafluorophenyl group bonded to benzo[*h*]quinoline (67°),^[25a] in 9,10-bis(pentafluorophenyl)anthracene (68°),^[25b] and in 5-perfluorophenyl-11-phenyltetracene (72°).^[25c]

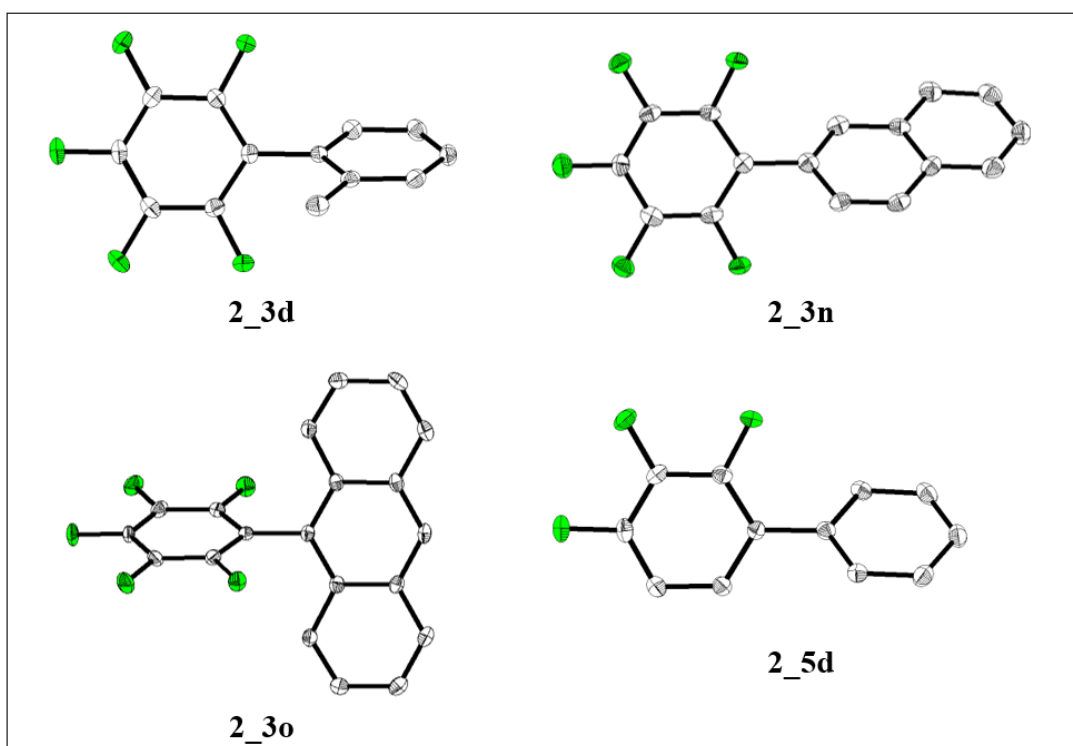


Figure 2-1. The solid-state molecular structures of **2_3d**, **2_3n**, **2_3o**, and **2_5d** determined by single-crystal X-ray diffraction at 100 K. All ellipsoids are drawn at the 50% probability level, and H atoms are omitted for clarity. Colours: white (carbon), green (fluorine).

Table 2-5. Selected bond lengths (Å) and angles (°) of **2_3d**, **2_3n**, **2_3o**, and **2_5d**.

	2_3d	2_3n	2_3o	2_5d
C _{Aryl(H)} –C _{Aryl(F)}	1.495(2)	1.484(7)	1.490(2)	1.483(4)
∠ Aryl(H)-Aryl(F)	61.66(5)	51.23(15)	64.28(5)	49.76(7)

Particularly interesting in the crystal structure analyses are the intermolecular interactions and, hence, molecular packing in these compounds. The presence of both fluorinated and nonfluorinated aryl groups leads to the formation of opposite multipoles of these moieties due to the differences in electronegativity of hydrogen and fluorine atoms with respect to the carbon atoms. This often results in attractive multipole forces between the aromatic and perfluoroaromatic groups, also called the arene-perfluoroarene interaction, and, hence, in face-to-face π -stacking with mean interplanar distances between 3.3 and 3.6 Å.^[26] This type of interaction is mostly found in co-crystals of arenes and perfluoroarenes, which form highly oriented, π -stacked systems.^[26c,27] However, also self-complementary compounds that contain both perfluorinated and nonfluorinated aryl groups, such as 2,3,4,5,6-pentafluorobiphenyl and 1-pentafluorophenyl-2-phenylacetylene, form arene-perfluoroarene interactions.^[27d,28a] This is also the case in the polyfluorinated biaryl compounds **2_3n** and **2_5d** in which the arene-perfluoroarene interaction determines the packing of the molecules (Table 2-6).

Table 2-6. Aryl⋯aryl (π ⋯ π) distances (Å) in crystals of **2_3d**, **2_3n**, **2_3o**, and **2_5d** at 100 K: centroid-centroid distance, interplanar separation, and offset shift.

Compound	Aryl⋯Aryl	Centroid-centroid distance	Interplanar separation	Offset shift ^[a]
2_3d	Aryl(F)⋯Aryl(F)	3.9121(15)	3.4489(16)	1.846(2)
2_3n	Aryl(F)⋯Aryl(H)	3.823(3)	3.398(5) / 3.473(4)	1.753(7) / 1.599(6)
		3.767(3)	3.408(4) / 3.354(5)	1.605(6) / 1.714(7)
2_3o	Aryl(H)⋯Aryl(H)	3.9397(18)	3.4625(18)	1.879(2)
		4.2171(19)	3.4043(18)	2.489(2)
2_5d	Aryl(F/H)⋯Aryl(H)	3.696(2)	3.380(2) / 3.336(2)	1.494(4) / 1.591(4)

^[a] The offset shift, also called inter-centroid shift, is the distance within a plane of an aryl ring between the centroid of the respective aryl ring and the intersection point with the normal to the plane through the centroid of the other aryl ring.

In compound **2_3n** the biaryls form columns of offset face-to-face π -stacked naphthalene and perfluorophenyl moieties along the *b* axis. Due to the large twist angle of ca. 51° of the biaryl, the columnar stacks are cross-like formed (Figure 2-2). Similar cross-like columnar stacks are observed in 2,3,4,5,6-pentafluorobiphenyl, 1,2,4,5-tetrafluoro-3-phenyl-6(trifluoromethyl)benzene, and 4'-bromo-2,3,5,6-tetrafluorobiphenyl-4-carbonitrile, which show biphenyl twist angles of 52° , 50° , and 41° , respectively.^[28] In compound **2_5d** only part of one phenyl ring is fluorinated. Still, the arene-perfluoroarene interaction leads to π -stacking between phenyl and 2,3,4-trifluoro phenyl rings. However, the phenyl and partly fluorinated phenyl rings are π -stacked with different neighboring molecules. Hence, they do not form a columnar arrangement but instead, zig-zag like chains along the *c* axis (Figure 2-3). The packing of the molecules in compound **2_3d** follows a similar pattern as in **2_5d** (Figure 2-4). However, the type of $\pi\cdots\pi$ interactions is different as there is no arene-perfluoroarene interaction present. Instead, neighboring perfluorophenyl moieties are π -stacked *via* perfluoroarene-perfluoroarene interactions and neighboring tolyl moieties are offset-stacked forming zig-zag chains along the *a* axis.

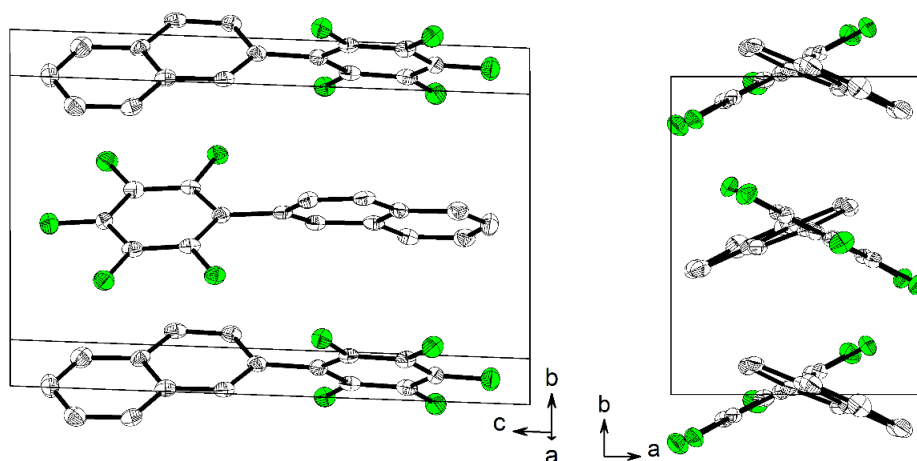


Figure 2-2. Crystal structure of **2_3n** projected along (left) an axis close to the *a* axis and (right) along the *b* axis, at 100 K. Perfluorophenyl and naphthalene moieties are π -stacked along the *b* axis *via* arene-perfluoroarene interactions. The intramolecular angle between the planes of the perfluorophenyl and naphthalene moieties is 51° leading to the formation of cross-like stacks (right). All ellipsoids are drawn at the 50% probability level, and H atoms are omitted for clarity. Colours: white (carbon), green (fluorine).

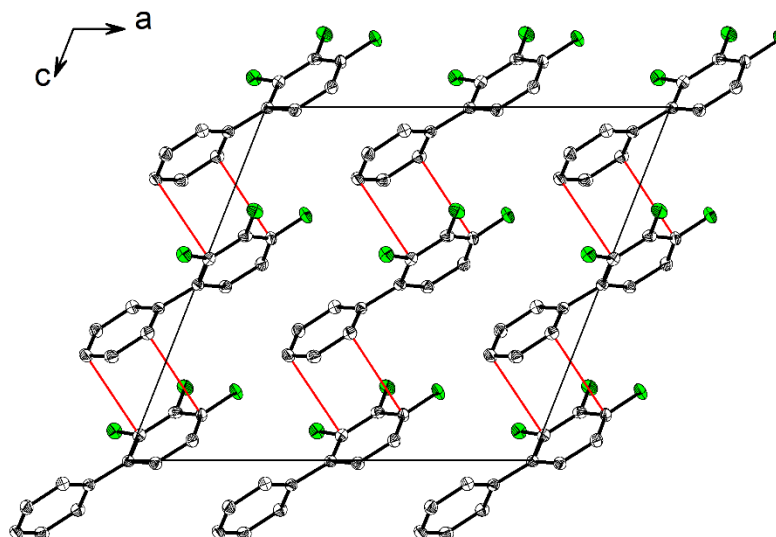


Figure 2-3. Crystal structure of **2_5d** projected along the *b* axis, at 100 K. Phenyl and partly fluorinated phenyl rings are π -stacked with different neighboring molecules *via* the arene-perfluoroarene interaction. All ellipsoids are drawn at the 50% probability level, and H atoms are omitted for clarity. Colours: white (carbon), green (fluorine). Close C...C contacts are shown in red.

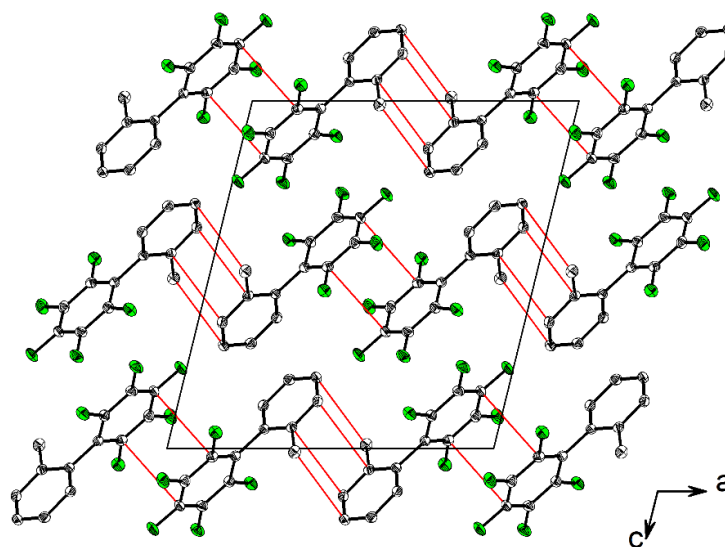


Figure 2-4. Crystal structure of **2_3d** projected along the *b* axis, at 100 K. Neighboring perfluorophenyl moieties are π -stacked, while tolyl moieties are offset-stacked. All ellipsoids are drawn at the 50% probability level, and H atoms are omitted for clarity. Colours: white (carbon), green (fluorine). Close C...C contacts are shown in red.

Finally, in compound **2_30** the intermolecular packing is dominated by π -stacking arene-arene interactions between the anthracene moieties, which form stacks along the *a* axis (Table 2-6, Figure 2-5). Similarly, offset $\pi\cdots\pi$ stacking is observed between the tetracene moieties of the compound 5-perfluorophenyl-11-phenyltetracene.^[25c] 9,10-bis(pentafluorophenyl)anthracene was reported as a host system with benzene or 1,4-dioxane guest molecules.^[25b] In these structures, no $\pi\cdots\pi$ interactions are observed, but C–F $\cdots\pi$ interactions are dominant for the molecular arrangement in the crystal structures. In contrast, the bulky 5-pentafluorophenyl-benzo[*h*]quinoline exhibits both arene-perfluoroarene and arene-arene π -stacking interactions in the crystal structure.^[25a]

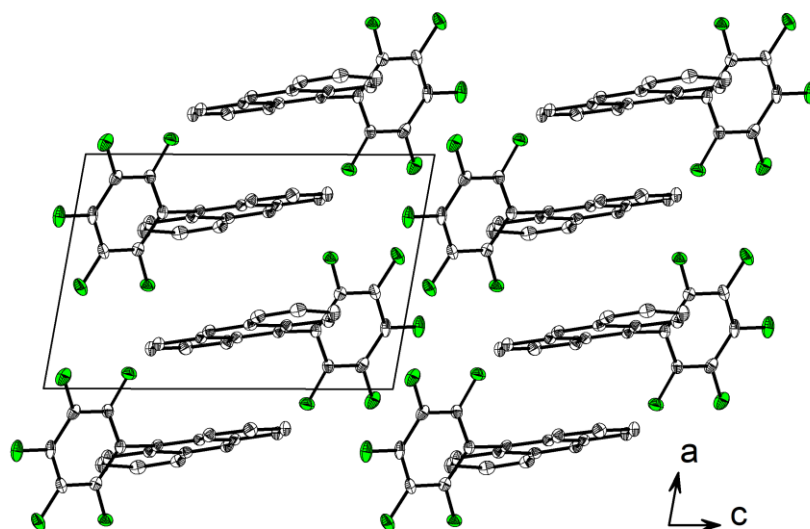


Figure 2-5. Crystal structure of **2_30** projected along the *b* axis, at 100 K. Anthracene moieties are π -stacked along the *a* axis. All ellipsoids are drawn at the 50% probability level, and H atoms are omitted for clarity. Colours: white (carbon), green (fluorine).

2.4 Conclusions

In summary, a combination of copper (I) iodide with phenanthroline as the ligand is an efficient catalyst for Suzuki-Miyaura cross-coupling reactions of electron deficient C₆F₅Bpin with aryl iodides and bromides in up to quantitative yield. Thus, the reaction proceeds using a non-toxic and inexpensive Earth-abundant metal catalyst, replacing the traditional palladium catalysts which require large amounts of silver oxide as an additive. This reaction is also viable for cross-coupling a

wide range of fluorinated phenyl boronic acid pinacol esters with aryl iodides or bromides. Notably, for aryl iodides, it can be used not only for coupling with electron deficient fluoroaryl boronates, but also for electron rich aryl boronates giving excellent yields.

A diverse range of $\pi\cdots\pi$ stacking interactions is observed in the partly perfluorinated biaryl compounds investigated herein, ranging from arene-perfluoroarene interactions (**2_3n**, **2_5d**) to arene-arene (**2_3o**) and perfluoroarene-perfluoroarene (**2_3d**) interactions. Other applications of highly fluorinated aryl boronate substrates are under investigation in our laboratory.

2.5 Detailed Experiments and Characterization Data

2.5.1 General Information

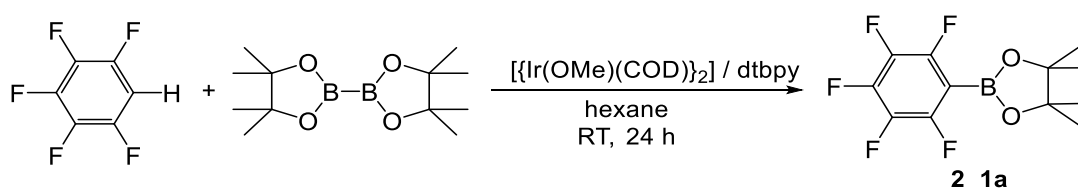
All reagents were purchased from Alfa-Aesar, Aldrich, ABCR or VWR, and were checked for purity by GC-MS and/or ^1H NMR spectroscopy and used as received. B_2pin_2 was kindly provided by AllyChem Co. Ltd. (Dalian, China). Dimethylformamide (DMF) was dried over calcium hydride and distilled before use, and stored in a Schlenk flask with 3Å molecular sieve under argon atmosphere. Tetrahydrofuran (THF) and toluene were argon saturated, dried using an Innovative Technology Inc. Pure-Solv Solvent Purification System.

Automated flash chromatography was performed on silica gel (Biotage SNAP cartridge KP-Sil 10 g and KP-Sil 25 g) using a Biotage® Isolera Four system. Commercially available, precoated TLC plates (Polygram® Sil G/UV254) were purchased from Machery-Nagel. The removal of solvent was performed on a rotary evaporator *in vacuo* at a maximum temperature of 40 °C. GC-MS analyses were performed using an Agilent 7890A gas chromatograph (column: HP-5MS 5% phenylmethylsiloxane, 10 m, Ø 0.25 mm, film 0.25 μm ; injector: 250 °C; oven: 40 °C (2 min), 40 °C to 280 °C (20 °Cmin⁻¹); carrier gas: He (1.2 mL min⁻¹) equipped with an Agilent 5975C inert MSD with triple-axis detector operating in EI mode and an Agilent 7693A series auto sampler/injector. HRMS analyses were performed using a Thermo Fischer Scientific Exactive Plus Orbitrap MS system (ASAP probe). Elemental analyses were performed on a Leco CHNS-932 Elemental Analyzer in our Institute.

All NMR spectra were recorded at 298 K using a Bruker Avance I 500 (^1H NMR, 500 MHz; $^{13}\text{C}\{^1\text{H}\}$ NMR, 125 MHz; $^{13}\text{C}\{^{19}\text{F}\}$ NMR, 125 MHz; ^{19}F NMR, 470 MHz), a Bruker DRX-300 (^1H , 300 MHz; $^{13}\text{C}\{^1\text{H}\}$, 75 MHz; $^{11}\text{B}\{^1\text{H}\}$, 96 MHz); a Bruker Avance Neo ($^{19}\text{F}\{^1\text{H}\}$, 376 MHz); and a Bruker Avance I 200 ($^{19}\text{F}\{^1\text{H}\}$ NMR, 188 MHz). ^1H NMR chemical shifts are reported relative to TMS and were referenced *via* residual proton resonances of the corresponding deuterated solvent (CDCl_3 : 7.26 ppm; C_6D_6 : 7.16 ppm), $^{13}\text{C}\{^1\text{H}\}$ NMR and $^{13}\text{C}\{^{19}\text{F}\}$ NMR spectra are reported relative to TMS *via* the carbon signals of the deuterated solvent (CDCl_3 : 77.16 ppm; C_6D_6 : 128.06 ppm), ^{19}F NMR and $^{19}\text{F}\{^1\text{H}\}$ spectra are reported relative to external CFCl_3 , and $^{11}\text{B}\{^1\text{H}\}$ NMR chemical shifts are quoted relative to $\text{BF}_3\cdot\text{Et}_2\text{O}$ as external standard.

2.5.2 Synthesis and Characterization of Pentafluorophenyl Boronic Acid

Pinacol Ester



$\text{C}_6\text{F}_5\text{Bpin}$ (**2_1a**)^[29] was synthesized *via* C-H borylation according to a literature procedure.^[30] In a glove box, bis(pinacolato)diboron (9.06 g / 35.70 mmol), $[\text{Ir}(\text{COD})(\text{OMe})]_2$ (0.47 g / 0.71 mmol), 4-4'-di-*tert*-butyl-2,2'-bipyridine (0.19 g / 0.71 mmol), degassed pentafluorobenzene (6.00 g / 35.70 mmol), and 50 mL of hexane was added into a 250 mL two neck round bottom flask. The flask was capped and the solution was stirred at room temperature. After 24 h, the solution was concentrated *in vacuo*. The residue was purified *via* column chromatography on silica gel (hexane). After concentrating the fractions containing the product, the residue was dried under reduced pressure to yield the pure corresponding product as a white solid (9.95 g, 95%).

^1H NMR (300 MHz, CDCl_3) δ = 1.38 (*s*, 12H; CH_3); $^{13}\text{C}\{^1\text{H}\}$ NMR (125 MHz, CDCl_3) δ = 149.4 (*dm*, $^1J_{\text{F,C}}$ = 251 Hz), 143.1 (*dm*, $^1J_{\text{F,C}}$ = 257 Hz), 137.4 (*dm*, $^1J_{\text{F,C}}$ = 252 Hz), 85.2, 24.8; ^{19}F NMR (470 MHz, CDCl_3) δ = -162.0 – -161.9 (*m*, 2F), -149.8 (*tt*, $^3J_{\text{F,F}}$ = 20 Hz, $^4J_{\text{F,F}}$ = 4 Hz, 1F), -129.6 –

-129.5 (*m*, 2F). $^{11}\text{B}\{^1\text{H}\}$ NMR (96 MHz, CDCl_3) $\delta = 29.0$. **GC-MS**: [*t* = 8.058 min] *m/z*: 294 [*M*] $^+$. **HRMS (ASAP)** calcd. for $\text{C}_{12}\text{H}_{12}\text{BF}_5\text{O}_2+\text{H}^+$: 295.0923 [*M*+*H*] $^+$; found: 295.0912.

2.5.3 General Procedure for Suzuki-Miyaura Cross-Coupling Reactions

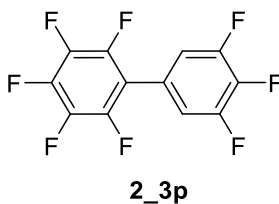
Unless otherwise noted, perfluorinated phenyl boronic acid pinacol ester (0.4 mmol), the arylhalide (Ar-X) (0.6 mmol), CuI (10 mol% if X = iodide; 30–50 mol% if X = bromide), phenanthroline (10 mol% if X = iodide; 30–50 mol% if X = bromide), and CsF (0.8 mmol, 2 equiv), were added inside a glovebox to a Schlenk flask that is equipped with a stirring bar. The flask was capped and taken out of the glovebox. Solvent (DMF 3 mL if X = iodide; 1/1 mixture of DMF and toluene, 4 mL if X = bromide) were added under an argon atmosphere using a Schlenk vacuum line. The reaction was heated and stirred at 130 °C for 18 h if X = iodide or at 140 °C for 36 h if X = bromide. After cooling to room temperature, the resulting mixture was extracted with ethyl acetate (3 x 20 mL). The organic phase was dried over MgSO_4 , filtered, and concentrated *in vacuo*. The residue was finally purified by flash column chromatography on silica gel (hexane). After evaporation to dryness, the residue was dried under reduced pressure to yield the pure product.

2.5.4 Competition Reaction of 4-Iodotoluene and 4-Iodobenzotrifluoride

Copper (I) iodide (2 mg, 0.01 mmol), 1,10-phenanthroline (2 mg, 0.01 mmol), 4-iodotoluene (43 mg, 0.2 mmol), 4-iodobenzotrifluoride (54 mg, 0.2 mmol), pentafluorobenzene (29 mg, 0.1 mmol), CsF (30 mg, 0.2 mmol), were added inside a glovebox to a Schlenk flask that was equipped with a stirring bar. The flask was capped and taken out of the glovebox. DMF (1.0 mL) was added under argon atmosphere *via* Schlenk vacuum line. The reaction was heated and stirred at 130 °C for 18 h. The molar ratio of the fluoro products 2,3,4,5,6-pentafluoro-4'-(trifluoromethyl)-biphenyl and 2,3,4,5,6-pentafluoro-4'-methylbiphenyl was determined to be 3 to 1 by GC-MS analysis of the crude reaction mixture.

2.5.5 Gram Scale Reaction Procedure: Synthesis and Characterization

Data of 2,3,3',4,4',5,5',6-Octafluoro Biphenyl (**2_3p**)^[31]

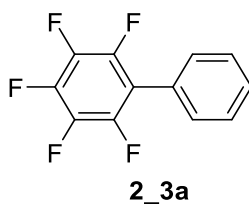


In a glovebox under argon, pentafluorophenylboronic acid pinacol ester (1.47 g, 5.00 mmol), methyl 4-iodobenzoate 1,2,3-trifluoro-5-iodobenzene (1.80 g, 7.00 mmol), CuI (95 mg, 0.50 mmol, 10 mol%), phenanthroline (90 mg, 0.50 mmol, 10 mol%), and CsF (1.52 g, 10.0 mmol, 2 equiv) were added to a 100 mL Schlenk flask that was equipped with a stirring bar. The flask was capped and taken out of the glovebox. Then DMF (30 mL) that was deoxygenated *via* freeze-pump-thaw method was added to the Schlenk flask under argon. The solution was stirred and heated at 130 °C for 18 h. After cooling to room temperature, the resulting mixture was diluted with ethyl acetate (60 mL) and washed with brine (3 x 60 mL). The organic phase was dried over MgSO₄, filtered, and concentrated *in vacuo*. The residue was finally purified by flash column chromatography over silica gel (hexane). After concentrating the fractions containing the product, the residue was dried under reduced pressure. Product **2_3p** was obtained as a clear oil (1.47 g, 98%).

¹H NMR (300 MHz, CDCl₃) δ = 7.15 – 7.04 (*m*, 2H, Ar-H); ¹³C{¹H} NMR (125 MHz, CDCl₃) δ = 151.5 (*ddd*, ¹J_{F,C} = 252 Hz, ²J_{F,C} = 10 Hz, ³J_{F,C} = 4 Hz), 144.2 (*dm*, ¹J_{F,C} = 250 Hz), 113.2 (*t*, ³J_{F,C} = 16 Hz), 141 (*dm*, ¹J_{F,C} = 256 Hz), 140.6 (*dt*, ²J_{F,C} = 15 Hz, ¹J_{F,C} = 256 Hz), 138.0 (*dm*, ¹J_{F,C} = 252 Hz), 122.3 – 122.0 (*m*), 115.0 (*dm*, ³J_{C,F} = 17 Hz); ¹⁹F{¹H} NMR (188 MHz, CDCl₃) δ = -161.0 – -160.8 (*m*, 2F), -158.9 (*t*, ³J_{F,F} = 21 Hz, 1F), -152.9 (*t*, ³J_{F,F} = 21 Hz, 1F), -142.7 (*dd*, ³J_{F,F} = 21 Hz, ⁴J_{F,F} = 8 Hz, 2F), -133.1 (*d*, ³J_{F,F} = 21 Hz, 2F); **GC-MS**: [t = 7.577 min] m/z: 298 [M]⁺; **HRMS (ASAP)** calcd. for C₁₂H₂F₈⁺: 298.0023 [M]⁺; found: 298.0011.

2.5.6 Experimental Procedures and Characterization of Products

Synthesis of 2,3,4,5,6-pentafluorobiphenyl (**2_3a**)^[32]



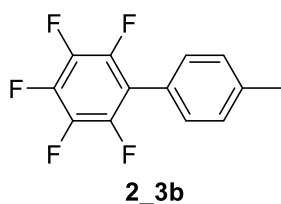
From the cross-coupling reaction of C₆F₅Bpin with C₆H₅I

Compound **2_3a** was synthesized following the general procedure and using the following chemicals and conditions: C₆F₅Bpin (118 mg, 0.40 mmol), C₆H₅I (122 mg, 0.60 mmol, 1.5 equiv), CuI (8 mg, 0.04 mmol, 10 mol%), phenanthroline (7 mg, 0.04 mmol, 10 mol%), CsF (122 mg, 0.80 mmol, 2 equiv), and DMF (3 mL), 130 °C, 18 h. After flash column chromatography (hexane), **2_3a** was obtained as a white solid (97 mg, 99%).

From the cross-coupling reaction of C₆F₅Bpin with C₆H₅Br

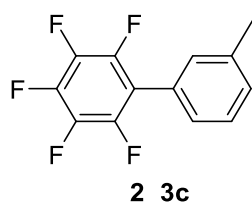
Compound **2_3a** was synthesized following the general procedure and using the following chemicals and conditions: C₆F₅Bpin (118 mg, 0.40 mmol), C₆H₅Br (94 mg, 0.60 mmol, 1.5 equiv), CuI (23 mg, 0.12 mmol, 30 mol%), phenanthroline (22, 0.12 mmol, 30 mol%), CsF (122 mg, 0.80 mmol, 2 equiv), DMF/toluene (1:1, 4 mL), 140 °C, 36 h. After flash column chromatography (hexane) **2_3a** was obtained as a white solid (85 mg, 87%).

¹H NMR (500 MHz, CDCl₃) δ = 7.52 – 7.45 (m, 3H; Ar-H), 7.41 – 7.44 (m, 2H),. **¹³C{¹H} NMR** (126MHz, CDCl₃) δ = 144.3 (*dm*, ¹J_{F,C} = 248 Hz), 140.5 (*dm*, ¹J_{F,C} = 254 Hz), 138.0 (*dm*, ¹J_{F,C} = 251 Hz), 130.3, 129.4, 128.9, 126.6, 116.0 (*td*, ³J_{F,C} = 17 Hz, ³J_{F,C} = 4 Hz); **¹⁹F NMR** (470 MHz, CDCl₃) δ = -162.4 – -162.2 (*m*, 2F), -155.7 (*t*, ²J_{F,F} = 21 Hz, 1F), -143.2 (*dd*, ³J_{F,F} = 21 Hz, ⁴J_{F,F} = 8 Hz, 2F); **GC-MS**: [t = 5.479 min] m/z: 244 [M]⁺; **HRMS (ASAP)** calcd. for C₁₂H₅F₅⁺: 244.0306 [M]⁺; found: 244.0298.

Synthesis of 2,3,4,5,6-pentafluoro-4'-methylbiphenyl (2_3b)^[32]


Compound **2_3b** was synthesized following the general procedure and using the following chemicals and conditions: C₆F₅Bpin (118 mg, 0.40 mmol), 1-iodo-4-methylbenzene (131 mg, 0.60 mmol, 1.5 equiv), CuI (8 mg, 0.04 mmol, 10 mol%), phenanthroline (7 mg, 0.04 mmol, 10 mol%), CsF (122 mg, 0.80 mmol, 2 equiv), DMF (3 mL), 130 °C, 18 h. After flash column chromatography (hexane), **2_3b** was obtained as a white solid (93 mg, 90%).

¹H NMR (500 MHz, CDCl₃) δ = 7.32 (s, 4H; Ar-H), 2.44 (s, 3H; CH₃); ¹³C{¹H} NMR (126 MHz, CDCl₃) δ = 144.3 (*dm*, ¹J_{F,C} = 247 Hz), 140.3 (*dm*, ¹J_{F,C} = 253 Hz), 139.6, 138.0 (*dm*, ¹J_{F,C} = 250 Hz), 130.1, 129.6, 123.5, 116.2 (*td*, ²J_{F,C} = 17 Hz, ³J_{F,C} = 4 Hz), 21.5; ¹⁹F NMR (470 MHz, CDCl₃) δ = -162.5 – -162.3 (*m*, 2F), -156.1 (*t*, ³J_{F,F} = 21 Hz, 1F), -143.4 (*dd*, ³J_{F,F} = 23 Hz, ⁴J_{F,F} = 8 Hz, 2F); **GC-MS**: [t = 8.518 min] m/z: 258 [M]⁺; **HRMS (ASAP)** calcd. for C₁₃H₇F₅⁺: 258.0462 [M]⁺; found: 258.0455.

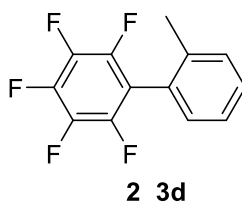
Synthesis of 2,3,4,5,6-pentafluoro-3'-methylbiphenyl (2_3c)^[32]


Compound **2_3c** was synthesized following the general procedure and using the following chemicals and conditions: C₆F₅Bpin (118 mg, 0.40 mmol), 1-iodo-3-methylbenzene (131 mg, 0.60 mmol, 1.5 equiv), CuI (8 mg, 0.04 mmol, 10 mol%), phenanthroline (7 mg, 0.04 mmol, 10 mol%), CsF (122 mg, 0.80 mmol, 2 equiv), DMF (3 mL), 130 °C, 18 h. After flash column chromatography (hexane), **2_3c** was obtained as a white solid (90 mg, 88%).

¹H NMR (500 MHz, CDCl₃) δ = 7.38 (*t*, ⁴J_{H,H} = 8 Hz, 1H; Ar-H), 7.28 (*m*, 1H; Ar-H), 7.22 (*m*, 2H;

Ar-H), 2.42 (s, 3H; CH₃); ¹³C{¹H} NMR (126 MHz, CDCl₃) δ = 144.3 (*dm*, ¹J_{F,C} = 247 Hz), 139.4 (*dm*, ¹J_{F,C} = 250 Hz), 130.9 (*dm*, ¹J_{F,C} = 251 Hz), 138.6, 130.9, 130.2, 128.7, 127.3, 126.4, 116.2 (*td*, ²J_{F,C} = 17 Hz, ³J_{F,C} = 4 Hz), 21.6; ¹⁹F NMR (470 MHz, CDCl₃) δ = -162.5 – -162.3 (*m*, 2F), -155.9 (*t*, ³J_{F,F} = 21 Hz, 1F), -143.1 (*dd*, ³J_{F,F} = 23 Hz, ⁴J_{F,F} = 8 Hz, 2F); **GC-MS**: [t = 6.108 min] m/z: 258 [M]⁺; **HRMS (ASAP)** calcd. for C₁₃H₇F₅⁺: 258.0462 [M]⁺; found: 258.0458.

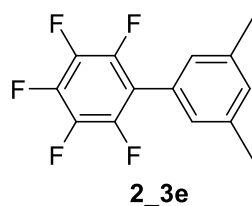
Synthesis of 2,3,4,5,6-pentafluoro-2'-methylbiphenyl (**2_3d**)^[32]



Compound **2_3d** was synthesized following the general procedure and using the following chemicals and conditions: C₆F₅Bpin (118 mg, 0.40 mmol), 1-iodo-2-methylbenzene (131 mg, 0.60 mmol, 1.5 equiv), CuI (8 mg, 0.04 mmol, 10 mol%), phenanthroline (7 mg, 0.04 mmol, 10 mol%), CsF (122 mg, 0.80 mmol, 2 equiv), DMF (3 mL), 130 °C, 18 h. After flash column chromatography (hexane), **2_3d** was obtained as a white solid (69 mg, 67%). Crystals suitable for X-ray diffraction were obtained by slow evaporation of a hexane solution of **2_3d** at room temperature.

¹H NMR (500 MHz, CDCl₃) δ = 7.41 – 7.35 (*m*, 2H; Ar-H), 7.30 (*td*, ³J_{H,H} = 7 Hz, ⁴J_{H,H} = 1 Hz; 1H; Ar-H); 7.20 (*d*, ³J_{H,H} = 7 Hz, 1H; Ar-H), 2.19 (s, 3H; CH₃); ¹³C {¹H} NMR (126 MHz, CDCl₃) δ = 144.2 (*dm*, ¹J_{F,C} = 246 Hz), 140.8 (*dm*, ¹J_{F,C} = 253 Hz), 137.8 (*dm*, ¹J_{F,C} = 251 Hz), 137.5, 130.7, 130.6, 129.8, 126.2, 126.0 (*m*), 115.7 (*td*, ²J_{F,C} = 20 Hz, ³J_{F,C} = 4 Hz), 19.8; ¹⁹F NMR (470 MHz, CDCl₃) δ = -162.3 – -162.2 (*m*, 2F), -155.3 (*t*, ³J_{F,F} = 21 Hz, 1F), -140.53 (*dd*, ³J_{F,F} = 23 Hz, ⁴J_{F,F} = 8 Hz, 2F); **GC-MS**: [t = 5.584 min] m/z: 258 [M]⁺; **HRMS (ASAP)** calcd for C₁₂H₅F₅⁺: 258.0462 [M]⁺; found: 258.0459.

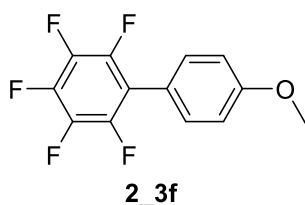
Synthesis of 2,3,4,5,6-pentafluoro-3',5'-dimethylbiphenyl (**2_3e**)^[33]



Compound **2_3e** was synthesized following the general procedure and using the following chemicals and conditions: C₆F₅Bpin (118 mg, 0.40 mmol), 1-iodo-3,5-dimethylbenzene (139 mg, 0.60 mmol, 1.5 equiv), CuI (8 mg, 0.04 mmol, 10 mol%), phenanthroline (7 mg, 0.04 mmol, 10 mol%), CsF (122 mg, 0.80 mmol, 2 equiv), DMF (3 mL), 130 °C, 18 h. After flash column chromatography (hexane), **2_3e** was obtained as a white solid (86 mg, 88%).

¹H NMR (500 MHz, CDCl₃) δ = 7.11 (*s*, 2H; Ar-H), 7.04 (*s*, 1H; Ar-H), 2.39 (*s*, 6H; CH₃); ¹³C{¹H} NMR (126 MHz, CDCl₃) δ = 144.3 (*dm*, ¹J_{F,C} = 247 Hz), 140.4 (*dm*, ¹J_{F,C} = 253 Hz), 138.5, 137.9 (*dm*, ¹J_{F,C} = 250 Hz), 131.1, 127.9, 126.3, 116.4 (*td*, ²J_{F,C} = 18 Hz, ³J_{F,C} = 4 Hz), 21.4; ¹⁹F NMR (470 MHz, CDCl₃) δ = -162.6 – -162.5 (*m*, 2F), -156.2 (*t*, ³J_{F,F} = 21 Hz, 1F), -143.0 (*dd*, ³J_{F,F} = 23 Hz, ⁴J_{F,F} = 8 Hz, 2F); GC-MS: [t = 8.999 min] m/z: 272 [M]⁺; HRMS (ASAP) calcd. for C₁₄H₉F₅+H⁺: 273.0697 [M+H]⁺; found: 273.0683.

Synthesis of 2,3,4,5,6-pentafluoro-4'-methoxybiphenyl (**2_3f**)^[32]

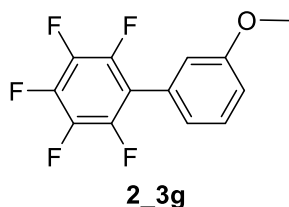


Compound **2_3f** was synthesized following the general procedure and using the following chemicals and conditions: C₆F₅Bpin (118 mg, 0.40 mmol), 1-iodo-4-methoxybenzene (140 mg, 0.60 mmol, 1.5 equiv), CuI (8 mg, 0.04 mmol, 10 mol%), phenanthroline (7 mg, 0.04 mmol, 10 mol%), CsF (122 mg, 0.80 mmol, 2 equiv), DMF (3 mL), 130 °C, 18 hours. After flash column chromatography (hexane), **2_3f** was obtained as a white solid (105 mg, 95%).

¹H NMR (500 MHz, CDCl₃) δ = 7.38 – 7.34 (*m*, 2H; Ar-H), 7.03 – 7.00 (*m*, 2H; Ar-H), 3.87 (*s*, 3H;

CH₃); ¹³C{¹H} NMR (126 MHz, CDCl₃) δ = 160.4, 144.3 (*dm*, ¹J_{F,C} = 243 Hz), 140.1 (*dm*, ¹J_{F,C} = 246 Hz), 137.0 (*dm*, ¹J_{F,C} = 257 Hz), 131.6, 118.5, 115.9 (*td*, ²J_{F,C} = 17 Hz, ³J_{F,C} = 4 Hz), 114.4, 55.5; ¹⁹F NMR (470 MHz, CDCl₃) δ = -162.6 – -162.5 (*m*, 2F), -156.5 (*t*, ³J_{F,F} = 21 Hz, 1F), -143.6 (*dd*, ³J_{F,F} = 23 Hz, ⁴J_{F,F} = 8 Hz, 2F); GC-MS: [t = 9.508 min] m/z: 274 [M]⁺; HRMS (ASAP) calcd. for C₁₃H₇F₅+H⁺: 275.0490 [M+H]⁺; found: 275.0479.

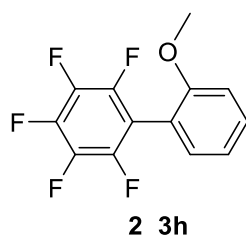
Synthesis of 2,3,4,5,6-pentafluoro-3'-methoxybiphenyl (2_3g)^[32]



Compound **2_3g** was synthesized following the general procedure and using the following chemicals and conditions: C₆F₅Bpin (118 mg, 0.40 mmol), 1-iodo-3-methoxybenzene (140 mg, 0.60 mmol, 1.5 equiv), CuI (8 mg, 0.04 mmol, 10 mol%), phenanthroline (7 mg, 0.04 mmol, 10 mol%), CsF (122 mg, 0.80 mmol, 2 equiv), DMF (3 mL), 130 °C, 18 h. After flash column chromatography (hexane), **2_3g** was obtained as a white solid (100 mg, 91%).

¹H NMR (500 MHz, CDCl₃) δ = 7.41 (*tm*, ³J_{H,H} = 8 Hz, 1H; Ar-H), 7.02 – 6.98 (*m*, 2 H, Ar-H), 6.94 (*sex*, ³J_{H,H} = 1 Hz, 1H; Ar-H), 3.85 (*s*, 3H; CH₃); ¹³C{¹H} NMR (126 MHz, CDCl₃) δ = 159.7, 144.2 (*dm*, ¹J_{F,C} = 248 Hz), 140.4 (*dm*, ¹J_{F,C} = 257 Hz), 136.8 (*dm*, ¹J_{F,C} = 251 Hz), 129.7, 127.5, 122.5, 115.8, 115.8 (*td*, ²J_{F,C} = 19 Hz, ³J_{F,C} = 4 Hz), 114.9, 55.4; ¹⁹F NMR (470 MHz, CDCl₃) δ = -162.3 – -162.2 (*m*, 2F), -155.6 (*t*, ³J_{F,F} = 21 Hz, 1F), -142.8 (*dd*, ³J_{F,F} = 23 Hz, ⁴J_{F,F} = 8 Hz, ⁵J_{F,F} = 1 Hz, 2F); GC-MS: [t = 9.310 min] m/z: 274 [M]⁺; HRMS (ASAP) calcd for C₁₃H₇F₅O+H⁺: 275.0490 [M+H]⁺; found: 275.0478.

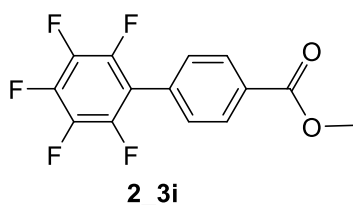
Synthesis of 2,3,4,5,6-pentafluoro-2'-methoxybiphenyl (**2_3h**)^[33]



Product **2_3h** was synthesized following the general procedure and using the following chemicals and conditions: C₆F₅Bpin (118 mg, 0.40 mmol), 1-iodo-2-methoxybenzene (140 mg, 0.60 mmol, 1.5 equiv), CuI (8 mg, 0.04 mmol, 10 mol%), phenanthroline (7 mg, 0.04 mmol, 10 mol%), CsF (122 mg, 0.80 mmol, 2 equiv), DMF (3 mL), 130 °C, 18 hours. After flash column chromatography (hexane), **2_3h** was obtained as a white solid (78 mg, 71%).

¹H NMR (500 MHz, CDCl₃) δ = 7.48 – 7.44 (*m*, 1H; Ar-H), 7.23 (*d*, ³J_{H,H} = 7 Hz, 1H; Ar-H), 7.06 (*td*, ³J_{H,H} = 7 Hz, ⁴J_{H,H} = 1 Hz, 1H; Ar-H), 7.03 (*d*, ³J_{H,H} = 8 Hz, 1H; Ar-H), 3.81 (*s*, 3H; CH₃); ¹³C{¹H} NMR (126 MHz, CDCl₃) δ = 157.2, 145.6 (*dm*, ¹J_{F,C} = 246 Hz), 140.7 (*dm*, ¹J_{F,C} = 253 Hz), 136.7 (*dm*, ¹J_{F,C} = 250 Hz), 131.9, 131.4, 120.8, 115.4, 112.9 (*td*, ²J_{F,C} = 19 Hz, ³J_{F,C} = 4 Hz), 111.4, 55.8; ¹⁹F NMR (470 MHz, CDCl₃) δ = -163.3 – -163.1 (*m*, 2F), -156.2 (*t*, ³J_{F,F} = 21 Hz, ⁴J_{F,F} = 1 Hz, 1F), -140.2 (*m*, 2F); GC-MS: [t = 8.949 min] m/z: 274 [M]⁺; HRMS (ASAP) calcd. for C₁₃H₇F₅O+H⁺: 275.0490 [M+H]⁺; found: 275.0480.

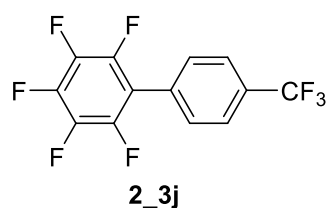
Synthesis of methyl 2',3',4',5',6'-pentafluoro-biphenyl-4-carboxylate (**2_3i**)^[34]



Compound **2_3i** was synthesized following the general procedure and using the following chemicals and conditions: C₆F₅Bpin (118 mg, 0.40 mmol), 4-iodobenzoate (157 mg, 0.60 mmol, 1.5 equiv), CuI (8 mg, 0.04 mmol, 10 mol%), phenanthroline (7 mg, 0.04 mmol, 10 mol%), CsF (122 mg, 0.80 mmol, 2 equiv), DMF (3 mL), 130 °C, 18 h. After flash column chromatography (hexane), **2_3i** was obtained as a white solid (104 mg, 86%).

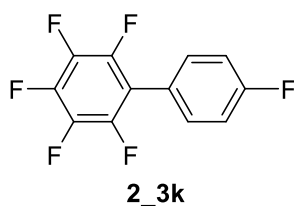
^1H NMR (500 MHz, CDCl_3) δ = 8.17 – 8.15 (*m*, 2H; Ar-H), 7.53 – 7.50 (*m*, 2H; Ar-H), 3.96 (*s*, 3H; CH_3); **$^{13}\text{C}\{^1\text{H}\}$ NMR** (126 MHz, CDCl_3) δ = 166.5, 142.0, 131.1, 130.4, 130.0, 52.5; **$^{13}\text{C}\{^{19}\text{F}\}$ NMR** (126 MHz, CDCl_3 , (for C_6F_5)) δ = 144.2, 141.0, 138.1, 131.1 (*t*, $^2J_{\text{H,C}} = 8$ Hz), 130.4 (*dd*, $^1J_{\text{H,C}} = 163$ Hz, $^2J_{\text{H,C}} = 6$ Hz), 130.0 (*dd*, $^1J_{\text{H,C}} = 165$ Hz, $^2J_{\text{H,C}} = 6$ Hz), 115.1, 52.5 (*q*, $^1J_{\text{H,C}} = 147$ Hz); **^{19}F NMR** (470 MHz, CDCl_3) δ = -161.6 – -161.5 (*m*, 2F), -154.1 (*t*, $^3J_{\text{F,F}} = 21$ Hz, 1F), -142.8 – -142.7 (*m*, 2F); **GC-MS**: [t = 7.908 min] m/z: 302 [M]⁺; **HRMS (ASAP)** calcd. for $\text{C}_{13}\text{H}_7\text{F}_5\text{O}+\text{H}^+$: 303.0439 [$M+\text{H}$]⁺; found: 303.0430.

Synthesis of 2,3,4,5,6-pentafluoro-4'-(trifluoromethyl)biphenyl (**2_3j**)^[32]



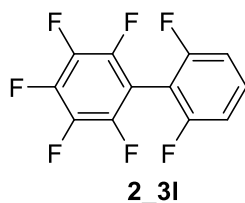
Compound **2_3j** was synthesized following the general procedure and using the following chemicals and conditions: $\text{C}_6\text{F}_5\text{Bpin}$ (118 mg, 0.40 mmol), 1-iodo-4-(trifluoromethyl)benzene (163 mg, 0.60 mmol, 1.5 equiv), CuI (8 mg, 0.04 mmol, 10 mol%), phenanthroline (7 mg, 0.04 mmol, 10 mol%), CsF (122 mg, 0.80 mmol, 2 equiv), DMF (3 mL), 130 °C, 18 h. After flash column chromatography (hexane), **2_3j** was obtained as a clear oil (114 mg, 91%).

^1H NMR (500 MHz, CDCl_3) δ = 7.77 (*dm*, $^3J_{\text{H,H}} = 8$ Hz, 2H; Ar-H), 7.57 (*dm*, $^3J_{\text{H,H}} = 8$ Hz, 2H; Ar-H); **$^{13}\text{C}\{^1\text{H}\}$ NMR** (126 MHz, CDCl_3) δ = 144.3 (*dm*, $^1J_{\text{F,C}} = 249$ Hz), 141.1 (*dm*, $^1J_{\text{F,C}} = 253$ Hz), 138.1 (*dm*, $^1J_{\text{F,C}} = 253$ Hz), 131.6 (*q*, $^3J_{\text{F,C}} = 33$ Hz), 130.8 (*t*, $^2J_{\text{F,C}} = 2$ Hz), 130.3, 125.9 (*q*, $^4J_{\text{F,C}} = 4$ Hz), 123.9 (*q*, $^1J_{\text{F,C}} = 272$ Hz), 114.7 (*td*, $^2J_{\text{F,C}} = 17$ Hz, $^3J_{\text{F,C}} = 4$ Hz); **^{19}F NMR** (470 MHz, CDCl_3) δ = -161.5 – -161.3 (*m*, 2F), -153.8 (*tm*, $^3J_{\text{F,F}} = 21$ Hz, 1F), -143.0 – -142.9 (*m*, 2F), -62.97 (*s*, 3F); **GC-MS**: [t = 5.506 min] m/z: 312 [M]⁺. **HRMS (ASAP)** calcd. for $\text{C}_{13}\text{H}_7\text{F}_5\text{O}+\text{H}^+$: 312.0180 [M]⁺; found: 312.0174.

Synthesis of 2,3,4,4',5,6-hexafluorobiphenyl (2_3k)^[32]

Compound **2_3k** was synthesized following the general procedure and using the following chemicals and conditions: C₆F₅Bpin (118 mg, 0.40 mmol), 1-iodo-4-fluorobenzene (133 mg, 0.60 mmol, 1.5 equiv), CuI (8 mg, 0.04 mmol, 10 mol%), phenanthroline (7 mg, 0.04 mmol, 10 mol%), CsF (122 mg, 0.80 mmol, 2 equiv), DMF (3 mL), 130 °C, 18 h. After flash column chromatography (hexane), **2_3k** was obtained as a white solid (98 mg, 93%).

¹H NMR (500 MHz, CDCl₃) δ = 7.42 – 7.39 (*m*, 2H), 7.22 – 7.12 (*m*, 2H); ¹³C{¹H} NMR (126 MHz, CDCl₃) δ = 163.2 (*d*, ¹J_{F,C} = 250 Hz), 144.1 (*dm*, ¹J_{F,C} = 248.0 Hz), 140.5 (*dm*, ¹J_{F,C} = 254 Hz), 137.9 (*dm*, ¹J_{F,C} = 251 Hz), 132.1 (*dt*, ³J_{F,C} = 8 Hz, ⁴J_{F,C} = 2 Hz), 122.3, 116.0 (*d*, ²J_{F,C} = 22 Hz), 114.9 (*td*, ²J_{F,C} = 17 Hz, ³J_{F,C} = 4 Hz); ¹⁹F NMR (470 MHz, CDCl₃) δ = -162.1 – -162.0 (*m*, 2F), -155.2 (*t*, ³J_{F,F} = 21 Hz, 1F), -143.4 – -143.3 (*m*, 2F), -111.3 (*tt*, ³J_{F,H} = 8 Hz, ⁴J_{F,H} = 5 Hz, 1F); **GC-MS**: [t = 7.910 min] m/z: 262 [*M*]⁺; **HRMS (ASAP)** calcd for C₁₂H₄F₆⁺: 262.0212 [*M*]⁺; found: 262.0203.

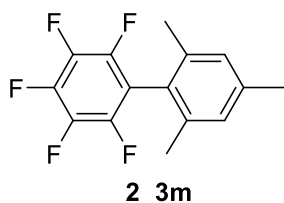
Synthesis of 2,2',3,4,5,6,6'-heptafluorobiphenyl (2_3l)^[35]

Compound **2_3l** was synthesized following the general procedure and using the following chemicals and conditions: C₆F₅Bpin (118 mg, 0.40 mmol), 2,6-difluoro-1-iodobenzene (144 mg, 0.60 mmol, 1.5 equiv), CuI (8 mg, 0.04 mmol, 10 mol%), phenanthroline (7 mg, 0.04 mmol, 10 mol%), CsF (122 mg, 0.80 mmol, 2 equiv), DMF (3 mL), 130 °C, 18 h. After flash column chromatography (hexane), **2_3l** was obtained as a clear oil (86 mg, 77 %). Due to its volatility, it is difficult to remove the solvent without significant loss of **2_3l**, and it was difficult to obtain an ¹H NMR free of solvent.

¹H NMR (500 MHz, CDCl₃) δ = 7.48 (*tt*, ³J_{H,H} = 9 Hz, ⁴J_{H,F} = 6 Hz, 1H), 7.09 – 7.04 (*m*, 2H); ¹³C{¹H}

NMR (126 MHz, CDCl₃) δ = 160.5 (*dd*, $^1J_{F,C}$ = 253 Hz, $^3J_{F,C}$ = 6 Hz), 144.7 (*dm*, $^1J_{F,C}$ = 247 Hz), 141.9 (*dm*, $^1J_{F,C}$ = 256 Hz), 138.9 (*dm*, $^1J_{F,C}$ = 229 Hz), 132.3 (*t*, $^3J_{F,C}$ = 10 Hz), 111.9 (*dd*, $^2J_{F,C}$ = 21 Hz, $^4J_{F,C}$ = 5 Hz), 104.4 (*td*, $^2J_{F,C}$ = 19 Hz, $^3J_{F,C}$ = 4 Hz), 104.1 (*t*, $^2J_{F,C}$ = 19 Hz); **¹⁹F{¹H} NMR** (376 MHz, CDCl₃) δ = -161.9 – -161.7 (*m*, 2F), -152.6 (*tt*, $^3J_{F,F}$ = 21 Hz, $^4J_{F,F}$ = 2 Hz, 1F), -138.0 – -137.9 (*m*, 2F), -110.2 (*t*, $^4J_{F,F}$ = 8 Hz, 2F); **GC-MS**: [t = 7.334 min] m/z: 280 [M]⁺; **HRMS (ASAP)** calcd. for C₁₂H₃F₇⁺: 280.0117 [M]⁺; found: 280.0106.

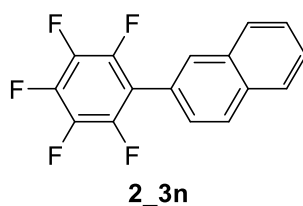
Synthesis of 2,3,4,5,6-pentafluoro-2',4',6'-trimethylbiphenyl (**2_3m**)^[36]



Compound **2_3m** was synthesized following the general procedure and using the following chemicals and conditions: C₆F₅Bpin (118 mg, 0.40 mmol), 1-bromo-2,4,6-trimethylbenzene (144 mg, 0.60 mmol, 1.5 equiv), CuI (23 mg, 0.12 mmol, 30 mol%), phenanthroline (22 mg, 0.12 mmol, 30 mol%), CsF (122 mg, 0.80 mmol, 2 equiv), DMF/toluene (1:1, 4 mL), 140 °C, 36 h. After flash column chromatography (hexane), **2_3m** was obtained as a clear oil (65 mg, 57 %). Due to its volatility, it is difficult to remove the solvent without significant loss of **2_3m**, and it was difficult to obtain an ¹H NMR free of solvent.

¹H NMR (500 MHz, CDCl₃) δ = 6.99 (*s*, 4H; Ar-H), 2.34 (*s*, 3H; CH₃), 2.05 (*s*, 6H; CH₃); **¹³C{¹H} NMR** (126 MHz, CDCl₃) δ = 143.1 (*dm*, $^1J_{F,C}$ = 243 Hz), 139.6 (*dm*, $^1J_{F,C}$ = 257 Hz), 139.4, 136.8 (*dm*, $^1J_{F,C}$ = 252 Hz), 137.3, 128.7, 122.7 (*q*, $^3J_{F,C}$ = 2 Hz), 114.5 (*td*, $^2J_{F,C}$ = 20 Hz, $^3J_{F,C}$ = 4 Hz), 21.3, 20.2; **¹⁹F NMR** (470 MHz, CDCl₃) δ = -162.1 – -162.0 (*m*, 2F), -155.4 (*t*, $^3J_{F,F}$ = 21 Hz, 1F), -140.1 (*dd*, $^4J_{F,F}$ = 8 Hz, $^3J_{F,F}$ = 24 Hz, 2F); **GC-MS**: [t = 8.874 min] m/z: 286 [M]⁺; **HRMS (ASAP)** calcd for C₁₅H₁₁F₅+H⁺: 287.0854 [M+H]⁺; found: 287.0840.

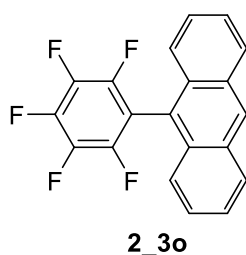
Synthesis of 2-(perfluorophenyl)naphthalene (**2_3n**)^[37]



Compound **2_3n** was synthesised following the general procedure and using the following chemicals and conditions: C₆F₅Bpin (118 mg, 0.40 mmol), 2-bromonaphthalene (124 mg, 0.60 mmol, 1.5 equiv), CuI (23 mg, 0.12 mmol, 30 mol%), phenanthroline (22 mg, 0.12 mmol, 30 mol%), CsF (122 mg, 0.80 mmol, 2 equiv), DMF/toluene (1:1, 4 mL), 140 °C, 36 h. After flash column chromatography (hexane), **2_3n** was obtained as a white solid (88 mg, 75%). Crystals suitable for X-ray diffraction were obtained by slow evaporation of a hexane solution of **2_3n** at room temperature.

¹H NMR (500 MHz, CDCl₃) δ = 7.97 – 7.95 (*d*, ³J_{H,H} = 9 Hz, 1H, Ar-H), 7.94 (*s*, 1H, Ar-H), 7.92 – 7.89 (*m*, 2H, Ar-H), 7.60 – 7.54 (*m*, 2H, Ar-H), 7.50 (*dq*, ³J_{H,H} = 8 Hz, ⁴J_{H,H} = 2 Hz, Ar-H, 1H); ¹³C{¹H} NMR (126 MHz, CDCl₃) δ = 143.5 (*dm*, ¹J_{F,C} = 246 Hz), 139.6 (*dm*, ¹J_{F,C} = 256 Hz), 137.1 (*dm*, ¹J_{F,C} = 245 Hz), 133.4, 133.2, 130.3, 128.6, 128.4, 127.9, 127.4, 127.2, 126.9, 123.9, 116.2 (*td*, ²J_{F,C} = 17 Hz, ³J_{F,C} = 4); ¹⁹F NMR (470 MHz, CDCl₃) δ = -162.12 (*m*, 2F), -155.40 (*t*, ³J_{F,F} = 21 Hz, 1F), -143.0 (*dd*, ³J_{F,F} = 23 Hz, ⁴J_{F,F} = 8 Hz, 2F); GC-MS: [t = 11.108 min] m/z: 294 [*M*]⁺; HRMS (ASAP) calcd. for C₁₆H₇F₅+H⁺: 295.0541 [*M*+H]⁺; found: 295.0528.

9-(perfluorophenyl)anthracene (**2_3o**)

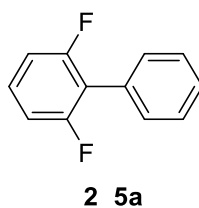


Compound **2_3o** was synthesized following the general procedure and using the following chemicals and conditions: C₆F₅Bpin (118 mg, 0.40 mmol), 9-bromoanthracene (153 mg, 0.60 mmol, 1.5 equiv), CuI (23 mg, 0.12 mmol, 30 mol%), phenanthroline (22 mg, 0.12 mmol, 30 mol%), CsF (122 mg,

0.80 mmol, 2 equiv), DMF/toluene (1:1, 4 mL), 140 °C, 36 h. After flash chromatography (hexane), **2_3o** was obtained as a white solid (107 mg, 78%). Crystals suitable for X-ray diffraction were obtained by slow evaporation of a hexane solution of **2_3o** at room temperature. This compound is new.

¹H NMR (500 MHz, CDCl₃) δ = 7.46 – 7.55 (*m*, 6H, Ar-H), 8.09 (*s*, 1H, Ar-H), 8.10-8.11 (*m*, 1H, Ar-H), 8.64 (*s*, 1H, Ar-H); **¹³C{¹H} NMR** (126 MHz, CDCl₃) δ = 145.1 (*dm*, ¹J_{F,C} = 248 Hz), 141.4 (*dm*, ¹J_{F,C} = 254 Hz), 138.1 (*dm*, ¹J_{F,C} = 250 Hz), 131.4, 130.7, 129.6, 129.1, 127.2, 125.6, 124.8, 119.8 (*m*), 112.7 (*td*, ²J_{F,C} = 20 Hz, ³J_{F,C} = 4 Hz); **¹³C{¹⁹F} NMR** (126 MHz, CDCl₃) δ = 145.1, 141.4, 138.1, 131.4 (*m*), 130.7 (*m*), 129.6 (*dt*, ¹J_{H,C} = 159 Hz, ³J_{H,C} = 5 Hz), 129.1 (*dt*, ¹J_{H,C} = 160 Hz, ²J_{H,C} = 6 Hz), 127.2 (*dd*, ¹J_{H,C} = 161 Hz, ²J_{H,C} = 9 Hz), 125.6 (*dd*, ¹J_{H,C} = 161 Hz, ²J_{H,C} = 8 Hz), 124.8 (*dd*, ¹J_{H,C} = 160 Hz, ²J_{H,C} = 7 Hz), 119.7 (*m*), 112.7; **¹⁹F NMR** (470 MHz, CDCl₃) δ = -161.4 (*m*, 2F), -153.6 (*t*, ³J_{F,F} = 21 Hz, 1F), -138.0 (*dm*, ³J_{F,F} = 25 Hz, 2F); **GC-MS**: [t = 13.139 min] m/z: 344 [*M*]⁺; **HRMS (ASAP)** calcd. for C₂₀H₉F₅+H⁺: 345.0697 [*M*+H]⁺; found: 345.0682; **elemental analysis** calcd (%) for C₂₀H₉F₅: C, 69.77; H, 2.64; found: C, 69.86; H, 2.81.

2,6-difluorobiphenyl (**2_5a**)^[38]



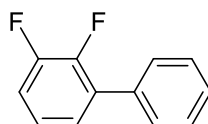
From the cross-coupling reaction of 2,6-F₂C₆H₃Bpin with C₆H₅I

Compound **2_5a** was synthesized following the general procedure and using the following chemicals and conditions: 2,6-difluorophenylboronic acid pinacol ester (96 mg, 0.40 mmol), iodobenzene (122 mg, 0.60 mmol, 1.5 equiv), CuI (8 mg, 0.04 mmol, 10 mol%), phenanthroline (7 mg, 0.04 mmol, 10 mol%), CsF (122 mg, 0.80 mmol, 2 equiv), and DMF (3 mL), 130 °C, 18 h. After flash chromatography (hexane), **2_5a** was obtained as a white solid (76 mg, 99%).

From the cross-coupling reaction of 2,6-F₂C₆H₃Bpin with C₆H₅Br

Compound **2_5a** was synthesized following the general procedure and using the following chemicals and conditions: 2,6-difluorophenylboronic acid pinacol ester (96 mg, 0.40 mmol), bromobenzene (94 mg, 0.60 mmol, 1.5 equiv), CuI (23 mg, 0.12 mmol, 30 mol%), phenanthroline (22 mg, 0.12 mmol, 30 mol%), CsF (122 mg, 0.80 mmol, 2 equiv), DMF/toluene (1:1, 4 mL), 140 °C, 36 h. After flash column chromatography (hexane), **2_5a** was obtained as a white solid (64 mg, 85%).

¹H NMR (500 MHz, CDCl₃) δ = 7.50 – 7.45 (*m*, 4 H; Ar-H), 7.44 – 7.39 (*m*, 1 H, Ar-H), 7.31 – 7.25 (*m*, 1H; Ar-H), 7.02 – 6.96 (*m*, 2H; Ar-H); ¹³C{¹H} NMR (126 MHz, CDCl₃) δ = 160.3 (*dd*, ¹J_{F,C} = 248 Hz, ³J_{F,C} = 7 Hz), 130.4 (*t*, ³J_{F,C} = 2 Hz), 129.3, 129.0 (*t*, ³J_{F,C} = 10 Hz), 128.4, 128.4, 118.6 (*t*, ²J_{F,C} = 19 Hz), 111.8 (*dd*, ²J_{F,C} = 20 Hz, ⁴J_{F,C} = 7 Hz); ¹⁹F{¹H} NMR (376 MHz, CDCl₃) δ = -114.6 (*s*, 2F); GC-MS: [t = 8.429 min] m/z: 190 [M]⁺; HRMS (ASAP) calcd. for C₁₂H₈F₂+H⁺: 191.0667 [M+H]⁺; found: 191.0658.

Synthesis of 2,3-difluorobiphenyl (2_5b)^[39]**2_5b****From the cross-coupling reaction of 2,3-F₂C₆H₃Bpin with C₆H₅I**

Compound **2_5b** was synthesized following the general procedure and using the following chemicals and conditions: 2,3-difluorophenylboronic acid pinacol ester (96 mg, 0.40 mmol), iodobenzene (122 mg, 0.60 mmol, 1.5 equiv), CuI (8 mg, 0.04 mmol, 10 mol%), phenanthroline (7 mg, 0.04 mmol, 10 mol%), CsF (122 mg, 0.80 mmol, 2 equiv), and DMF (3 mL), 130 °C, 18 h. After flash column chromatography (hexane) product **2_5b** was obtained as a clear oil (72 mg, 95%).

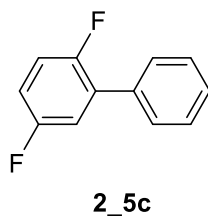
From the cross-coupling reaction of 2,3-F₂C₆H₃Bpin with C₆H₅Br

Compound **2_5b** was synthesized following the general procedure and using the following chemicals and conditions: 2,3-difluorophenylboronic acid pinacol ester (96 mg, 0.40 mmol), bromobenzene (94 mg, 0.60 mmol, 1.5 equiv), CuI (38 mg, 0.20 mmol, 50 mol%), phenanthroline

(36 mg, 0.20 mmol, 50 mol%), CsF (122 mg, 0.80 mmol, 2 equiv), DMF/toluene (1:1, 4 mL), 140 °C, 36 h. After flash column chromatography (hexane), **2_5b** was obtained as a clear oil (61 mg, 80%).

¹H NMR (500 MHz, CDCl₃) δ = 7.56 – 7.52 (*m*, 2H; Ar-H), 7.48 – 7.45 (*m*, 2H), 7.42 – 7.37 (*m*, 1H; Ar-H), 7.22 – 7.18 (*m*, 1H; Ar-H), 7.16 – 7.11 (*m*, 2H; Ar-H); ¹³C{¹H} NMR (126 MHz, CDCl₃) δ = 151.3 (*dd*, ¹J_{F,C} = 248 Hz, ²J_{F,C} = 13 Hz), 148.1 (*dd*, ¹J_{F,C} = 250 Hz, ²J_{F,C} = 13 Hz), 134.9 (*dd*, ³J_{F,C} = 3 Hz, ⁴J_{F,C} = 1 Hz), 131.5 (*d*, ²J_{F,C} = 10 Hz), 129.1 (*d*, ⁴J_{F,C} = 3 Hz), 128.7, 128.3, 125.5 (*dd*, ³J_{F,C} = 3 Hz, ⁴J_{F,C} = 2 Hz), 124.2 (*dd*, ³J_{F,C} = 7 Hz, ⁴J_{F,C} = 5 Hz), 116.2 (*d*, ²J_{F,C} = 17 Hz); ¹⁹F{¹H} NMR (376 MHz, C₆D₆) δ = -143.7 (*d*, ³J_{F,F} = 21 Hz, 1F), -137.9 (*d*, ³J_{F,F} = 21 Hz, 1F); GC-MS: [t = 8.529 min] m/z: 190 [M]⁺. HRMS (ASAP) calcd. for C₁₂H₈F₂+H⁺: 190.0589 [M]⁺; found: 190.0585.

Synthesis of 2,5-difluorobiphenyl (**2_5c**)^[40]



From the cross-coupling reaction of 2,5-F₂C₆H₃Bpin with C₆H₅I

Compound **2_5c** was synthesized following the general procedure and chemicals and conditions: 2,5-difluorophenylboronic acid pinacol ester (96 mg, 0.40 mmol), iodobenzene (122 mg, 0.60 mmol, 1.5 equiv), CuI (8 mg, 0.04 mmol, 10 mol%), phenanthroline (7 mg, 0.04 mmol, 10 mol%), CsF (122 mg, 0.80 mmol, 2 equiv), and DMF (3 mL), 130 °C, 18 h. After flash column chromatography (hexane), **2_5c** was obtained as a clear oil (72 mg, 94%).

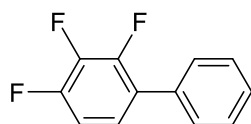
From the cross-coupling reaction of 2,5-F₂C₆H₃Bpin with C₆H₅Br

Compound **2_5c** was synthesized following the general procedure and using the following chemicals and conditions: 2,5-difluorophenylboronic acid pinacol ester (96 mg, 0.40 mmol), bromobenzene (94 mg, 0.60 mmol, 1.5 equiv), CuI (38 mg, 0.20 mmol, 50 mol%), phenanthroline (36 mg, 0.20 mmol, 50 mol%), CsF (122 mg, 0.80 mmol, 2 equiv), DMF/toluene (1:1, 4 mL), 140 °C, 36 h. After

flash column chromatography (hexane), **2_5c** was obtained as a clear oil (56 mg, 73%).

¹H NMR (500 MHz, CDCl₃) δ = 7.56 – 7.53 (*m*, 2H; Ar-H), 7.47 (*tt*, ³*J*_{H,H} = 3 Hz, ³*J*_{H,H} = 7 Hz, 2H; Ar-H), 7.42 – 7.39 (*m*, 1H), 7.18 – 7.09 (*m*, 2H), 7.00 (*ddt*, ³*J*_{H,F} = 9 Hz, ³*J*_{H,H} = 7 Hz, ⁴*J*_{H,F} = 4 Hz, 1H; Ar-H); **¹³C{¹H} NMR** (126 MHz, CDCl₃) δ = 159.0 (*dd*, ⁴*J*_{F,C} = ¹*J*_{F,C} = 242 Hz, ⁴*J*_{F,C} = 2 Hz), 156.0 (*dd*, ¹*J*_{F,C} = 244 Hz, ⁴*J*_{F,C} = 2 Hz), 135.0 (*t*, ³*J*_{F,C} = 2 Hz), 130.6 (*dd*, ²*J*_{F,C} = 16 Hz, ³*J*_{F,C} = 8 Hz), 129.1 (*d*, ⁴*J*_{F,C} = 3 Hz), 128.8, 128.4, 117.4 (*dd*, ²*J*_{F,C} = 26 Hz, ³*J*_{F,C} = 9 Hz), 117.1 (*dd*, ²*J*_{F,C} = 24 Hz, ³*J*_{F,C} = 4 Hz), 115.4 (*dd*, ²*J*_{F,C} = 24 Hz, ³*J*_{F,C} = 9 Hz); **¹⁹F{¹H} NMR** (376 MHz, CDCl₃) δ = -124.2 (*d*, ⁵*J*_{F,F} = 18 Hz, 1F), -119.1 (*d*, ⁵*J*_{F,F} = 18 Hz, 1F); **GC-MS**: [t = 8.333 min] m/z: 190 [*M*]⁺; **HRMS (ASAP)** calcd.. for C₁₂H₈F₂⁺: 190.0589 [*M*]⁺; found: 190.0582.

Synthesis of 2,3,4-trifluorobiphenyl (**2_5d**)^[41]



2_5d

From the cross-coupling reaction of 2,3,4-F₃C₆H₂Bpin with C₆H₅I

Compound **2_5d** was synthesized following the general procedure and using the following chemicals and conditions: 2,3,4-trifluorophenylboronic acid pinacol ester (103.22 mg, 0.40 mmol), iodobenzene (122 mg, 0.60 mmol, 1.5 equiv), CuI (8 mg, 0.04 mmol, 10 mol%), phenanthroline (7 mg, 0.04 mmol, 10 mol%), CsF (122 mg, 0.80 mmol, 2 equiv), and DMF (3 mL), 130 °C, 18 h. After flash column chromatography (hexane), **2_5d** was obtained as a white solid (77 mg, 93%).

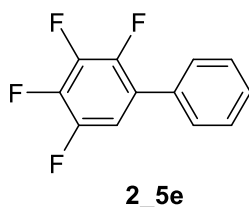
From the cross-coupling reaction of 2,3,4-F₃C₆H₂Bpin with C₆H₅Br

Compound **2_5d** was synthesized following the general procedure and using the following chemicals and conditions: 2,3,4-trifluorophenylboronic acid pinacol ester (103.22 mg, 0.40 mmol), bromobenzene (94 mg, 0.60 mmol, 1.5 equiv), CuI (38 mg, 0.20 mmol, 50 mol%), phenanthroline (36 mg, 0.20 mmol, 50 mol%), CsF (122 mg, 0.80 mmol, 2 equiv), DMF/toluene (1:1, 4 mL), 140 °C, 36 hours. After flash column chromatography (hexane), **2_5d** was obtained as a white solid (58

mg, 70%). Crystals suitable for X-ray diffraction were obtained by slow evaporation of a hexane solution of **2_5d** at room temperature.

¹H NMR (500 MHz, CDCl₃) δ = 7.52 – 7.45 (*m*, 4H), 7.43 – 7.40 (*m*, 1H), 7.18 – 7.13 (*m*, 1H), 7.07 – 7.01 (*m*, 1H); **¹³C NMR** (126 MHz, CDCl₃) δ = 150.63, (*ddd*, ¹J_{F,C} = 250 Hz, ²J_{F,C} = 10 Hz, ³J_{F,C} = 3 Hz), 148.93 (*ddd*, ¹J_{F,C} = 251 Hz, ²J_{F,C} = 10 Hz, ³J_{F,C} = 3 Hz), 140.5 (*ddd*, ¹J_{F,C} = 251 Hz, ²J_{F,C} = 16 Hz, ³J_{F,C} = 15 Hz), 134.2 (*quin*, ³J_{F,C} = 1 Hz), 129.0 (*dd*, ⁴J_{F,C} = 3 Hz, ⁵J_{F,C} = 1 Hz), 128.8, 128.4, 126.9 (*ddd*, ²J_{F,C} = 11 Hz, ³J_{F,C} = 4 Hz, ⁴J_{F,C} = 1 Hz), 124.0 (*quin*, ³J_{F,C} = 4 Hz), 112.2 (*dd*, ²J_{F,C} = 17 Hz, ³J_{F,C} = 4 Hz); **¹⁹F{¹H} NMR** (376 MHz, C₆D₆) δ = -160.1 (*t*, ³J_{F,F} = 21 Hz, 1F), -139.0 (*dd*, ³J_{F,F} = 21 Hz, ⁴J_{F,F} = 7 Hz, 1F), -136.1 (*dd*, ³J_{F,F} = 21 Hz, ⁴J_{F,F} = 7 Hz, 1F); **GC-MS**: [t = 8.388 min] m/z: 208 [M]⁺; **HRMS (ASAP)** calcd. for C₁₂H₇F₃⁺: 208.0494 [M]⁺; found: 208.0487.

Synthesis of 2,3,4,5-tetrafluorobiphenyl (**2_5e**)^[42]



From the cross-coupling reaction of 2,3,4,5-F₄C₆HBpin with C₆H₅I

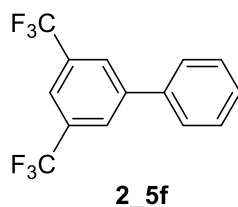
Compound **2_5e** was synthesized following the general procedure and using the following chemicals and conditions: 2,3,4,5-tetrafluorophenylboronic acid pinacol ester (110 mg, 0.40 mmol), iodobenzene (122 mg, 0.60 mmol, 1.5 equiv), CuI (8 mg, 0.04 mmol, 10 mol%), phenanthroline (7 mg, 0.04 mmol, 10 mol%), CsF (122 mg, 0.80 mmol, 2 equiv), and DMF (3 mL), 130 °C, 18 h. After flash column chromatography (hexane), **2_5e** was obtained as a white solid (73 mg, 81%).

From the cross-coupling reaction of 2,3,4,5-F₄C₆HBpin with C₆H₅Br

Compound **2_5e** was synthesized following the general procedure and using the following chemicals and conditions: 2,3,4,5-tetrafluorophenylboronic acid pinacol ester (110 mg, 0.40 mmol), bromobenzene (94 mg, 0.60 mmol, 1.5 equiv), CuI (38 mg, 0.20 mmol, 50 mol%), phenanthroline (36 mg, 0.20 mmol, 50 mol%), CsF (122 mg, 0.80 mmol, 2 equiv), DMF/toluene (1:1, 4 mL), 140 °C, 36 h. After flash column chromatography (hexane), **2_5e** was obtained as a white solid (38 mg, 42%).

¹H NMR (500 MHz, CDCl₃) δ = 7.50 – 7.42 (*m*, 5H; Ar-H), 7.06 (*m*, 1H; Ar-H); **¹³C{¹H}** NMR (126 MHz, CDCl₃) δ = 147.2 (*dddd*, ¹J_{F,C} = 247 Hz, ²J_{F,C} = 10 Hz, ³J_{F,C} = 4 Hz, ⁴J_{F,C} = 3 Hz), 145.0 (*dddd*, ¹J_{F,C} = 248 Hz, ²J_{F,C} = 11 Hz, ³J_{F,C} = 4 Hz, ⁴J_{F,C} = 1 Hz), 141.4 (*dddd*, ¹J_{F,C} = 253 Hz, ²J_{F,C} = 17 Hz, ²J_{F,C} = 12 Hz, ³J_{F,C} = 4 Hz), 139.9 (*dddd*, ¹J_{F,C} = 254 Hz, ²J_{F,C} = 17 Hz, ²J_{F,C} = 13 Hz, ³J_{F,C} = 3 Hz), 133.2 (*sex*, ³J_{F,C} = 1 Hz), 129.0, 128.9 (*dd*, ⁴J_{F,C} = 3 Hz, ⁵J_{F,C} = 1 Hz), 128.9, 125.6 (*ddd*, ²J_{F,C} = 12 Hz, ³J_{F,C} = 7 Hz, ³J_{F,C} = 4 Hz), 111.5 (*dt*, ²J_{F,C} = 20 Hz, ³J_{F,C} = 3 Hz); **¹⁹F{¹H}** NMR (376 MHz, CDCl₃) δ = -157.1 (*ddd*, ³J_{F,F} = 21 Hz, ³J_{F,F} = 20 Hz, ⁴J_{F,F} = 3 Hz, 1F), -155.2 (*ddd*, ³J_{F,F} = 21 Hz, ³J_{F,F} = 20 Hz, ⁴J_{F,F} = 2 Hz, 1F), -143.8 (*ddd*, ³J_{F,F} = 21 Hz, ⁴J_{F,F} = 13 Hz, ⁵J_{F,F} = 3 Hz, 1F), -139.6 (*ddd*, ³J_{F,F} = 21 Hz, ⁴J_{F,F} = 13 Hz, ⁵J_{F,F} = 2 Hz, 1F); **GC-MS**: [t = 8.131 min] m/z: 226 [M]⁺; **HRMS (ASAP)** calcd. for C₁₂H₆F₄⁺: 226.0400 [M]⁺; found: 226.0392.

Synthesis of 3,5-bis(trifluoromethyl)biphenyl (**2_5f**)^[43]



From the cross-coupling reaction of 3,5-(CF₃)₂-C₆H₃Bpin with C₆H₅I

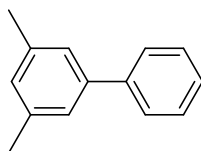
Compound **2_5f** was synthesized following the general procedure and using the following chemicals and conditions: 3,5-bis(trifluoromethyl)phenylboronic acid pinacol ester (136.03 mg, 0.40 mmol), iodobenzene (122 mg, 0.60 mmol, 1.5 equiv), CuI (8 mg, 0.04 mmol, 10 mol%), phenanthroline (7 mg, 0.04 mmol, 10 mol%), CsF (122 mg, 0.80 mmol, 2 equiv), and DMF (3 mL), 130 °C, 18 h. After flash column chromatography (hexane), **2_5f** was obtained as a clear oil (107 mg, 92%).

From the cross-coupling reaction of 3,5-(CF₃)₂-C₆H₃Bpin with C₆H₅Br

Compound **2_5f** was synthesized following the general procedure and using the following chemicals and conditions: 3,5-bis(trifluoromethyl)phenylboronic acid pinacol ester (136.03 mg, 0.40 mmol), bromobenzene (94 mg, 0.60 mmol, 1.5 equiv), CuI (23 mg, 0.12 mmol, 30 mol%), phenanthroline (22 mg, 0.12 mmol, 30 mol%), CsF (122 mg, 0.80 mmol, 2 equiv), DMF/toluene (1:1, 4 mL), 140 °C, 36 hours. After flash column chromatography (hexane), **2_5f** was obtained as a clear oil (41 mg, 35 %).

$^1\text{H NMR}$ (500 MHz, CDCl_3) δ = 8.02 (*s*, 2H; Ar-H), 7.86 (*s*, 1H; Ar-H), 7.62 – 7.60 (*m*, 2H; Ar-H), 7.53 – 7.50 (*m*, 2H; Ar-H), 7.48 – 7.44 (*m*, 1H; Ar-H); $^{13}\text{C}\{^1\text{H}\}$ NMR (126 MHz, CDCl_3) δ = 143.5, 138.4, 132.3 (*q*, $^2J_{\text{F,C}}$ = 33 Hz), 129.4, 129.0, 127.39, 127.37, 123.5 (*q*, $^3J_{\text{F,C}}$ = 273 Hz), 121.0 (*sept*, $^3J_{\text{F,C}}$ = 4 Hz); $^{19}\text{F NMR}$ (470 MHz, CDCl_3) δ = -62.8 (*s*, 6F); **GC-MS**: [t = 5.394 min] m/z: 290 [*M*] $^+$; **HRMS (ASAP)** calcd. for $\text{C}_{14}\text{H}_8\text{F}_6^+$: 290.0525 [*M*] $^+$; found: 290.0513.

Synthesis of 3,5-dimethylbiphenyl (**2_5g**)^[44]



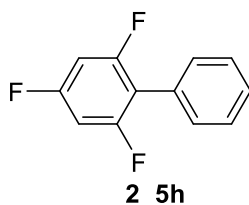
2_5g

From the cross-coupling reaction of 3,5-Me₂C₆H₃Bpin with C₆H₅I

Compound **2_5g** was synthesized following the general procedure and using the following chemicals and conditions: 3,5-dimethylphenylboronic acid pinacol ester (93 mg, 0.40 mmol), iodobenzene (122 mg, 0.60 mmol, 1.5 equiv), CuI (8 mg, 0.04 mmol, 10 mol%), phenanthroline (7 mg, 0.04 mmol, 10 mol%), CsF (122 mg, 0.80 mmol, 2 equiv), and DMF (3 mL), 130 °C, 18 h. After flash column chromatography (hexane), **2_5g** was obtained as a clear oil (69 mg, 95 %).

$^1\text{H NMR}$ (500 MHz, C_6D_6) δ = 7.64 (*m*, 2H; Ar-H), 7.48 (*m*, 2H; Ar-H), 7.39 (*m*, 1H; Ar-H), 7.28 (*m*, 2H; Ar-H), 7.06 (*m*, 1H; Ar-H), 2.45 (*s*, 6H; CH₃); $^{13}\text{C}\{^1\text{H}\}$ NMR (75 MHz, CDCl_3) δ = 141.6, 141.4, 138.4, 129.0, 128.8, 127.3, 127.2, 125.2, 21.5; **GC-MS**: [t = 9.764 min] m/z: 182 [*M*] $^+$; **HRMS (ASAP)** calcd. for $\text{C}_{14}\text{H}_{14}+\text{H}^+$: 183.1168 [*M+H*] $^+$; found: 183.1160.

Synthesis of 2,4,6-trifluorobiphenyl (**2_5h**)^[45]



2_5h

From the cross-coupling reaction of 2,4,6-F₃C₆H₂Bpin with C₆H₅I

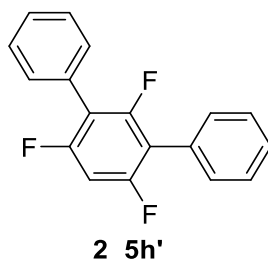
Compound **2_5h** was synthesized following the general procedure and using the following

chemicals and conditions: 2,4,6-trifluorophenylboronic acid pinacol ester (103 mg, 0.40 mmol), iodobenzene (82 mg, 0.40 mmol, 1 equiv), CuI (8 mg, 0.04 mmol, 10 mol%), phenanthroline (7 mg, 0.04 mmol, 10 mol%), CsF (122 mg, 0.80 mmol, 2 equiv), and DMF (3 mL), 130 °C, 18 h. After flash column chromatography (hexane), **2_5h** was obtained as a white solid (63 mg, 75 %).

From the cross-coupling reaction of 2,4,6-F₃C₆H₂Bpin with C₆H₅Br

Compound **2_5h** was synthesized following the general procedure and using the following chemicals and conditions: 2,4,6-trifluorophenylboronic acid pinacol ester (103 mg, 0.40 mmol), bromobenzene (63 mg, 0.40 mmol, 1 equiv), CuI (23 mg, 0.12 mmol, 30 mol%), phenanthroline (22 mg, 0.12 mmol, 30 mol%), CsF (122 mg, 0.80 mmol, 2 equiv), DMF/toluene (1:1, 4 mL), 140 °C, 36 h. After flash column chromatography (hexane), **2_5h** was obtained as a white solid (58 mg, 70 %).

¹H NMR (500 MHz, CDCl₃) δ = 6.80 – 6.74 (*m*, 2H), 7.49 – 7.40 (*m*, 5H); ¹³C{¹H} NMR (126 MHz, CDCl₃) δ = 162.0 (*dt*, ¹J_{F,C} = 249 Hz, ³J_{F,C} = 16 Hz), 160.4 (*ddd*, ¹J_{F,C} = 249 Hz, ³J_{F,C} = 15 Hz, ³J_{F,C} = 10 Hz), 130.5 (*q*, ³J_{F,C} = 1 Hz), 130.4 (*td*, J_{F,C} = 2 Hz, J_{F,C} = 1 Hz), 128.5, 128.5, 115.1 (*td*, ²J_{F,C} = 19 Hz, ⁴J_{F,C} = 5 Hz), 100.8 – 100.4 (*m*); ¹⁹F{¹H} NMR (376 MHz, C₆D₆) δ = -114.9 (*t*, ³J_{F,F} = 6 Hz, 1F), -112.9 (*d*, ³J_{F,F} = 6 Hz, 2F); **GC-MS**: [t = 7.816 min] m/z: 208 [M]⁺; **HRMS (ASAP)** calcd for C₁₂H₇F₃⁺: 208.0494 [M]⁺; found: 208.0489.

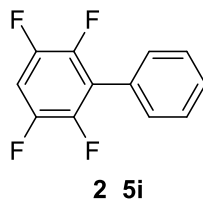


2',4',6'-trifluoro-1,1':3',1''-terphenyl (2_5h')^[45] was also isolated as a white solid from either iodobenzene or bromobenzene as a minor byproduct (9 mg, 8% and 6 mg, 5% yields, respectively).

¹H NMR (500 MHz, CDCl₃) δ = 7.49 – 7.39 (*m*, 10H; Ar-H), 6.88 (*td*, ³J_{H,F} = 10 Hz, ⁵J_{H,F} = 2 Hz, 1H; Ar-H); ¹³C{¹H} NMR (126 MHz, CDCl₃) δ = 159.0 (*ddd*, ¹J_{F,C} = 249 Hz, ³J_{F,C} = 15 Hz, ³J_{F,C} =

10 Hz), 157.3 (*dt*, $^1J_{F,C} = 249$ Hz, $^4J_{F,C} = 9$ Hz), 130.5 (*q*, $^3J_{F,C} = 1$ Hz), 128.7, 128.5 (2C), 115.5 – 115.1 (*m*), 100.7 (*td*, $^2J_{F,C} = 27$ Hz, $^4J_{F,C} = 4$ Hz); ^{19}F NMR (470 MHz, CDCl_3) $\delta = -115.0$ (*t*, $^3J_{F,F} = 6$ Hz, 1F), -112.9 (*dd*, $^4J_{F,F} = 6$ Hz, $^3J_{F,H} = 10$ Hz, 2F); **HRMS (ASAP)** calcd. for $\text{C}_{18}\text{H}_{11}\text{F}_3 + \text{H}^+$: 285.0886 [$M + \text{H}$] $^+$; found: 285.0866.

Synthesis of 2,3,5,6-tetrafluorobiphenyl (**2_5i**)^[46]



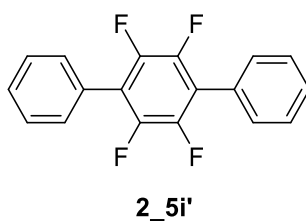
From the cross-coupling reaction of 2,3,5,6-F₄C₆HBpin with C₆H₅I

Compound **2_5i** was synthesized following the general procedure and using the following chemicals and conditions: 2,3,5,6-tetrafluorophenylboronic acid pinacol ester (110 mg, 0.40 mmol), iodobenzene (82 mg, 0.40 mmol, 1 equiv), CuI (8 mg, 0.04 mmol, 10 mol%), phenanthroline (7 mg, 0.04 mmol, 10 mol%), CsF (122 mg, 0.80 mmol, 2 equiv), and DMF (3 mL), 130 °C, 18 h. After flash column chromatography (hexane), **2_5i** was obtained as a white solid (67 mg, 74%).

From the cross-coupling reaction of 2,4,6-F₃C₆H₂Bpin with C₆H₅Br

Compound **2_5i** was synthesized following the general procedure and using the following chemicals and conditions: 2,3,5,6-tetrafluorophenylboronic acid pinacol ester (110 mg, 0.40 mmol), bromobenzene (63 mg, 0.40 mmol, 1 equiv), CuI (23 mg, 0.12 mmol, 30 mol%), phenanthroline (22 mg, 0.12 mmol, 30 mol%), CsF (122 mg, 0.80 mmol, 2 equiv), DMF/toluene (1:1, 4 mL), 140 °C, 36 h. After flash column chromatography (hexane), **2_5i** was obtained as a white solid (62 mg, 69%).

^1H NMR (500 MHz, CDCl_3) $\delta = 7.52$ - 7.44 (*m*, 5H), 7.07 (*tt*, $^3J_{H,F} = 10$ Hz, $^4J_{H,F} = 7$ Hz, 1H); $^{13}\text{C}\{^1\text{H}\}$ NMR (126 MHz, CDCl_3) $\delta = 146.4$ (*dm*, $^1J_{F,C} = 248$ Hz), 143.9 (*dddd*, $^1J_{F,C} = 247$ Hz, $^2J_{F,C} = 14$ Hz, $^3J_{F,C} = 5$ Hz, $^4J_{F,C} = 4$ Hz), 130.2 (*t*, $^4J_{F,C} = 2$ Hz), 129.3, 128.7, 127.6 (*t*, $^3J_{F,C} = 2$ Hz), 121.6 (*t*, $^2J_{F,C} = 17$ Hz), 105.0 (*t*, $^2J_{F,C} = 23$ Hz); $^{19}\text{F}\{^1\text{H}\}$ NMR (376 MHz, C_6D_6) $\delta = -144.2$ (*dd*, $^3J_{F,F} = 23$ Hz, $^4J_{F,F} = 13$ Hz, 2F), -139.3 (*dd*, $^3J_{F,F} = 23$ Hz, $^4J_{F,F} = 13$ Hz, 2F); **GC-MS**: [t = 8.115 min] m/z: 226 [M] $^+$; **HRMS (ASAP)** calcd. for $\text{C}_{12}\text{H}_6\text{F}_4 + \text{H}^+$: 226.0400 [M] $^+$; found: 226.0394.



1,4-diphenyl tetrafluoro benzene (2_5i')^[47] was also isolated as a white solid from either iodobenzene or bromobenzene as a minor byproduct (12 mg / 10% and 11 mg / 9%, yields respectively). This compound has low solubility in deuterated solvents.

¹H NMR (500 MHz, CDCl₃) δ = 7.36 (*m*, 4H), 7.19 (*m*, 4H), 7.12 (*tm*, ³*J*_{H,H} = 7 Hz, 2H); **¹³C{¹H} NMR** (126 MHz, CDCl₃) δ = 130.3, 129.3, 128.8, 127.7; **¹³C{¹⁹F} NMR** (126 MHz, CDCl₃, (for C₆F₄)) δ = 144.2, 119.8; **¹⁹F NMR** (470 MHz, CDCl₃) δ = 144.38 (*s*, 4F); **GC-MS**: [t = 12.248 min] m/z: 302 [*M*]⁺; **HRMS (ASAP)** calcd. for C₁₈H₁₀F₄⁺: 302.0713 [*M*]⁺; found: 302.0700.

2.5.7 Single-Crystal X-ray Diffraction Data

Crystal structure determination. Crystals suitable for single-crystal X-ray diffraction were selected, coated in perfluoropolyether oil, and mounted on MiTeGen sample holders. Diffraction data were collected on Bruker X8 Apex II 4-circle diffractometers with CCD area detectors using Mo-K α radiation monochromated by graphite (**2_3n**, **2_3o**, **2_5d**) or multi-layer focusing mirrors (**2_3d**). The crystals were cooled using an Oxford Cryostream low-temperature device. Data were collected at 100 K. The images were processed and corrected for Lorentz-polarisation effects and absorption as implemented in the Bruker software packages. The structures were solved using the intrinsic phasing method (SHELXT)^[48] and Fourier expansion technique. All non-hydrogen atoms were refined in anisotropic approximation, with hydrogen atoms ‘riding’ in idealized positions, by full-matrix least squares against F² of all data, using SHELXL^[49] software and the SHELXLE graphical user interface.^[50] The crystal structure of **2_3n** was refined as a two-component twin, with the twin matrix (1 0 0, 0 -1 0, -1 0 -1). The twin fraction parameter was refined to 1%. Diamond^[51] software was used for graphical representation. Crystal data and experimental details are listed in Table 2-S1; full structural information has been deposited with Cambridge Crystallographic Data Centre. CCDC-1917134 (**2_3d**), 1917135 (**2_3n**), 1917136 (**2_3o**), and 1917137 (**2_5d**).

Table 2-S1: Single-crystal X-ray diffraction data and structure refinements of **2_3d**, **2_3n**, **2_3o**, and **2_5d**.

Data	2_3d	2_3n	2_3o	2_5d
CCDC number	1917134	1917135	1917136	1917137
Empirical formula	C ₁₃ H ₇ F ₅	C ₁₆ H ₇ F ₅	C ₂₀ H ₉ F ₅	C ₁₂ H ₇ F ₃
Formula weight / g·mol ⁻¹	258.19	294.22	344.27	208.18
<i>T</i> / K	100 (2)	100(2)	100(2)	100(2)
Radiation, λ / Å	MoK α 0.71073	MoK α 0.71073	MoK α 0.71073	MoK α 0.71073
Crystal size / mm ³	0.566×0.44× 0.292	0.545×0.125× 0.064	0.267×0.201× 0.116	0.608×0.208× 0.157
Crystal color, habit	colorless block	colorless plate	colorless plate	colorless needle
μ / mm ⁻¹	0.156	0.152	0.137	0.133
Crystal system	monoclinic	monoclinic	triclinic	monoclinic
Space group	<i>P</i> 2 ₁ / <i>n</i>	<i>P</i> 2 ₁	<i>P</i> $\bar{1}$	<i>C</i> <i>c</i>
<i>a</i> / Å	12.325(4)	6.195(3)	7.549(3)	13.044(7)
<i>b</i> / Å	6.518(3)	7.578(4)	9.167(2)	6.004(3)
<i>c</i> / Å	13.482(5)	12.748(6)	11.479(3)	12.238(7)
α / °	90	90	70.599(9)	90
β / °	103.785(14)	101.596(19)	76.724(11)	111.529(13)
γ / °	90	90	78.18(2)	90
Volume / Å ³	1051.9(7)	586.3(5)	722.1(4)	891.6(8)
<i>Z</i>	4	2	2	4
ρ_{calc} / g·cm ⁻³	1.630	1.667	1.583	1.551
<i>F</i> (000)	520	296	348	424
θ range / °	2.013 – 26.791	2.688 – 25.975	1.910 – 28.413	3.358 – 30.689
Reflections collected	11724	6767	15092	13310
Unique reflections	2240	2094	3625	2772
Parameters / restraints	164 / 0	191 / 1	226 / 0	136 / 2
Goof on <i>F</i> ²	1.071	1.049	1.043	1.071
R ₁ [<i>I</i> >2 σ (<i>I</i>)]	0.0342	0.0575	0.0492	0.0380
wR ² (all data)	0.0880	0.1483	0.1320	0.0968
Max. / min. residual electron density / e·Å ⁻³	0.290 / -0.176	0.483 / -0.249	0.294 / -0.297	0.273 / -0.243

2.6 References

- [1] a) Synthesis and Application of Organoboron Compounds (Eds.: E. Fernandez, A. Whiting), Springer, Berlin, **2015**; b) Boronic Acids: Preparation and Applications in Organic Synthesis and Medicine (Eds.: D. G. Hall), Wiley-VCH, Weinheim, **2006**; c) I. A. I. Mkhaliid, J. H. Barnard, T. B. Marder, J. M. Murphy, J. F. Hartwig, *Chem. Rev.* **2010**, *110*, 890–931.
- [2] a) J. Zhou, M. W. Kuntze-Fechner, R. Bertermann, U. S. D. Paul, J. H. J. Berthel, A. Friedrich, Z. Du, T. B. Marder, U. Radius, *J. Am. Chem. Soc.* **2016**, *138*, 5250–5253; b) Y.-M. Tian, X.-N. Guo, M. W. Kuntze-Fechner, I. Krummenacher, H. Braunschweig, U. Radius, A. Steffen, T. B. Marder, *J. Am. Chem. Soc.* **2018**, *140*, 17612–17623.
- [3] a) N. Miyaura, A. Suzuki, *Chem. Rev.* **1995**, *95*, 2457–2483; b) A. Suzuki, *Angew. Chem. Int. Ed.* **2011**, *50*, 6722–6737; c) N. Miyaura, *Cross-Coupling Reactions: A Practical Guide*, Springer, New York, **2002**.
- [4] a) A. Zahn, C. Brotschi, C. Leumann, *Chem. Eur. J.* **2005**, *11*, 2125–2129; b) M. G. N. Russell, R. W. Carling, J. R. Atack, F. A. Bromidge, S. M. Cook, P. Hunt, C. Isted, M. Lucas, R. M. McKernan, A. Mitchinson, K. W. Moore, R. Narquizian, A. J. Macaulay, D. Thomas, S. A. Thompson, K. A. Wafford, J. L. Castro, *J. Med. Chem.* **2005**, *48*, 1367–1383; c) J. Wang, M. S. Rosello, J. L. Aceña, C. Pozo, A. E. Sorochinsky, S. Fustero, V. A. Soloshonok, H. Liu, *Chem. Rev.* **2014**, *114*, 2432–2506.
- [5] a) V. A. Montes, G. Li, R. Pohl, J. Shinar, P. Anzenbacher, *Adv. Mater.* **2004**, *16*, 2001–2003; b) T. Tsuzuki, N. Shirasawa, T. Suzuki, S. Tokito, *Adv. Mater.* **2003**, *15*, 1455–1458; c) M. S. Jang, S. Y. Song, H. K. Shim, *Polymer* **2000**, *41*, 5675–5679.
- [6] Y. Sakamoto, T. Suzuki, A. Miura, H. Fujikawa, S. Tokito, Y. Taga, *J. Am. Chem. Soc.* **2000**, *122*, 1832–1833.
- [7] a) J. Lieffrig, A. G. Niassy, O. Jeannin, M. Fourmigue, *Cryst. Eng. Comm.* **2015**, *17*, 50–57; b) G. M. Espallargas, A. Recuenco, F. M. Romero, L. Brammer, S. Libri, *Cryst. Eng. Comm.* **2012**, *14*, 6381–6383.

- [8] T. Chen, I. Popov, O. Zenasni, O. Daugulis, O. S. Miljanic, *Chem. Commun.* **2013**, *49*, 6846–6848.
- [9] H. Yi, M. Albrecht, A. Valkonen, K. Rissanen, *New J. Chem.* **2015**, *39*, 746–749;
- [10] a) M. Havelková, D. Dvůrák, M. Hocek, *Synthesis* **2001**, *11*, 1704–1710; b) M. Havelková, M. Hocek, M. Česnek, D. Dvůrák, *Synlett* **1999**, *7*, 1145–1147; c) T. Thiemann, K. Umeno, D. Ohira, E. Inohae, T. Sawada, S. Mataka, *New J. Chem.* **1999**, *23*, 1067–1070; d) D. Bulfield, S. M. Huber, *J. Org. Chem.* **2017**, *82*, 13188–13203; e) For stoichiometric model reactions for the transmetalation step see: J. Kohlmann, T. Braun, R. Laubenstein, R. Herrmann, *Chem. Eur. J.* **2017**, *23*, 12218–12232.
- [11] a) N. Y. Adonin, V. V. Bardin. *Russ. Chem. Rev.* **2010**, *79*, 757–785; b) V. V. Bardin, A. Y. Shabalin, N. Y. Adonin, *Beilstein J. Org. Chem.* **2015**, *11*, 608–616; c) T. Korenaga, T. Kosaki, R. Fukumura, T. Ema, T. Sakai, *Org. Lett.* **2005**, *7*, 4915–4917; d) K. Takimiya, N. Niihara, T. Otsubo, *Synthesis* **2005**, 1589–1592; e) J. Chen, A. Cammers-Goodwin, *Tetrahedron Lett.* **2003**, *44*, 1503–1506; f) H. J. Frohn, N. Y. Adonin, V. V. Bardin, V. F. Starichenko, *J. Fluorine Chem.* **2003**, *122*, 195–199; g) H. J. Frohn, N. Y. Adonin, V. V. Bardin, V. F. Starichenko, *Tetrahedron Lett.* **2002**, *43*, 8111–8114; h) for reaction without silver oxide see: T. Kinzel, Y. Zhang, S. L. Buchwald, *J. Am. Chem. Soc.* **2010**, *132*, 14073–14075.
- [12] J. Uenishi, J. M. Beau, R. W. Armstrong, Y. J. Kishi, *Am. Chem. Soc.* **1987**, *109*, 4756–4758.
- [13] Y. Nishihara, H. Onodera, K. Osakada, *Chem. Commun.* **2004**, 192–193.
- [14] T. Koizumi, A. Yamazaki, T. Yamamoto, *Dalton Trans.* **2008**, 3949–3952.
- [15] a) F. Chen, T. Wang, *Chem. Rev.* **2014**, *114*, 8613–8661; b) I. Bauer, H. J. Knölker, *Chem. Rev.* **2015**, *115*, 3170–3387; c) S. Z. Tasker, E. A. Standley, T. F. Jamison, *Nature* **2014**, *509*, 299–309; d) L. Mao, R. Bertermann, R. Emmert, K. J. Szabó, T. B. Marder, *Org. Lett.* **2017**, *19*, 6586–6589; e) S. K. Bose, S. Brand, H. O. Omoregie, M. Haehnel, J. Maier, G. Bringmann, T. B. Marder, *ACS Catal.* **2016**, *6*, 8332–8335.
- [16] The European Medicines Agency set a limit of daily oral exposure to various metals: palladium, 100 µg/day; N nickel, 300 µg /day; copper, 2500 µg/day.

- [17] a) Y. Zhou, W. You, K. B. Smith, M. K. Brown, *Angew. Chem., Int. Ed.*, **2014**, *53*, 3475–3479; b) S. K. Gurung, S. Thapa, A. Kae, D. A. Dickie, R. Giri, R. *Org. Lett.* **2014**, *16*, 1264–1267; c) J. H. Li, D. P. Wang, *Eur. J. Org. Chem.* **2006**, 2063–2066; d) J. Li, J. L. Li, D. P. Wang, S. F. Pi, Y. X. Xie, M. B. Zhang, X. C. Hu, *J. Org. Chem.* **2007**, *72*, 2053–2057; e) M. B. Thathagar, J. Beckers, G. Rothenberg, *J. Am. Chem. Soc.* **2002**, *124*, 11858–11859; f) J. Mao, J. Guo, F. Fang, S. J. Ji, *Tetrahedron* **2008**, *64*, 3905–3911; g) S. K. Gurung, S. Thapa, B. Shrestha, R. Giri, *Org. Chem. Front.* **2015**, *2*, 649–653; h) A. M. Bergmann, A. M. Oldham, W. You, M. K. Brown, *Chem. Commun.* **2018**, *54*, 5381–5384.
- [18] T. Ishiyama, J. Takagi, J. F. Hartwig, *Angew. Chem. Int. Ed.* **2002**, *41*, 3056–3058.
- [19] J. E. Mayer, R. B. Levy, *J. Chem. Phys.* **1933**, *1*, 647–648.
- [20] M. Ohashi, N. Ishida, K. Ando, Y. Hashimoto, A. Shigaki, K. Kikushima, S. Ogoshi, *Chem. Eur. J.* **2018**, *24*, 9794–9798.
- [21] a) G.A. Molander, N. Ellis, *Acc. Chem. Res.* **2007**, *40*, 275–286; b) G. A. Molander, R. Figueroa, *Aldrichimica Acta* **2005**, *38*, 49–56; c) H. A. Stefani, R. Cella, A. S. Vieira, *Tetrahedron* **2007**, *63*, 3623–3658; d) S. Darses, J. P. Genet, *Eur. J. Org. Chem.* **2003**, *22*, 4313–4327.
- [22] a) M. S. Gong, H. S. Lee, Y. M. Jeon, *J. Mater. Chem.* **2010**, *20*, 10735–10746; b) S. S. Choi, M. H. Jeong, S. H. Lee, M. H. Park, Y. Chung, *Bull. Korean Chem. Soc.* **2016**, *37*, 136–141.
- [23] a) H. Q. Do, O. Daugulis, *J. Am. Chem. Soc.* **2007**, *129*, 12404–12405; b) M. Lafrance, C. N. Rowley, T. K. Woo, K. Fagnou, *J. Am. Chem. Soc.* **2006**, *128*, 8754–8756; c) M. Lafrance, D. Shore, K. Fagnou, *Org. Lett.* **2006**, *8*, 5097–5100; d) Y. Y. Song, Z. J. Fu, Q. H. Xiong, Z. J. Li, J. Li, H. Cai, *J. Iran. Chem. Soc.* **2016**, *13*, 1931–1936.
- [24] F. H. Allen, O. Kennard, D. G. Watson, L. Brammer, A. G. Orpen, R. Taylor, *J. Chem. Soc., Perkin Trans. 2*, **1987**, S1-S19.
- [25] a) B. Orwat, M.-j. O. Oh, M. Kubicki, I. Kownacki, *Adv. Synth. Catal.* **2018**, *360*, 3331–3344; b) I. Yoshitane, K. Kensaku, K. Kakuhiro, T. Nobuo, S. Tomohiro, K. Reiko, M. Yoshio, *Lett. Org. Chem.* **2009**, *6*, 588–592; c) T. Okamoto, K. Nakahara, A. Saeki, S. Seki, J. H. Oh, H. B. Akkerman, Z. N. Bao, Y. Matsuo, *Chem. Mater.* **2011**, *23*, 1646–1649.

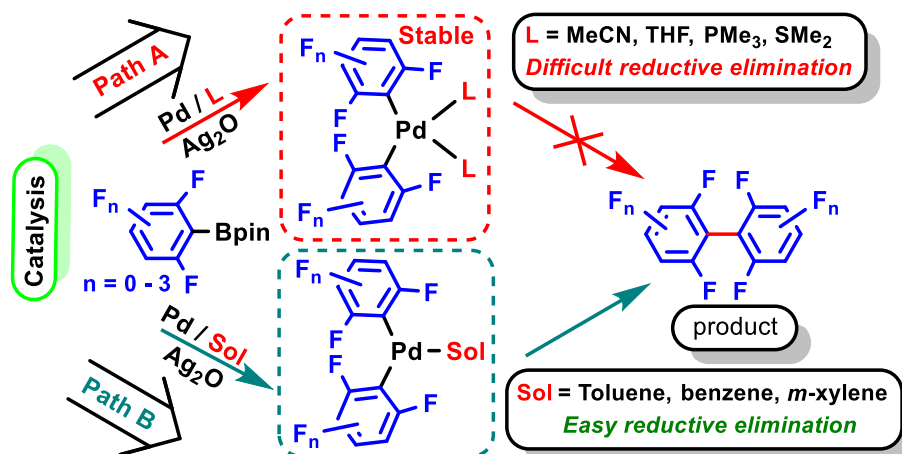
- [26] a) A. Hori, Arene-Perfluoroarene Interactions in Coordination Architectures. In *The Importance of Pi-Interactions in Crystal Engineering: Frontiers in Crystal Engineering*, John Wiley & Sons: Chichester, UK, **2012**; 163–185; b) T. Dahl, *Acta Chem. Scand.* **1988**, *42*, 1–7; c) J. C. Collings, K. P. Roscoe, R. L. Thomas, A. S. Batsanov, L. M. Stimson, J. A. K. Howard, T. B. Marder, *New J. Chem.* **2001**, *25*, 1410–1417.
- [27] a) A. S. Batsanov, J. A. K. Howard, T. B. Marder, E. G. Robins, *Acta Crystallogr.* **2001**, *C57*, 1303–1305; b) J. C. Collings, K. P. Roscoe, E. G. Robins, A. S. Batsanov, L. M. Stimson, J. A. K. Howard, S. J. Clark, T. B. Marder, *New J. Chem.* **2002**, *26*, 1740–1746; c) J. C. Collings, A. S. Batsanov, J. A. K. Howard, T. B. Marder, *Cryst. Eng.* **2002**, *5*, 37–46; d) C. E. Smith, P. S. Smith, R. L. Thomas, E. G. Robins, J. C. Collings, C. Y. Dai, A. J. Scott, S. Borwick, A. S. Batsanov, S. W. Watt, S. J. Clark, C. Viney, J. A. K. Howard, W. Clegg, T. B. Marder, *J. Mater. Chem.* **2004**, *14*, 413–420; e) J. C. Collings, P. S. Smith, D. S. Yufit, A. S. Batsanov, J. A. K. Howard, T. B. Marder, *CrystEngComm*, **2004**, *6*, 25–28; f) S. W. Watt, C. Dai, A. J. Scott, J. M. Burke, R. L. Thomas, J. C. Collings, C. Viney, W. Clegg, *Angew. Chem. Int. Ed.* **2004**, *43*, 3061–3063; g) J. C. Collings, A. S. Batsanov, J. A. K. Howard, D. A. Dickie, J. A. C. Clyburne, H. A. Jenkins, T. B. Marder, *J. Fluorine Chem.* **2005**, *126*, 515–519; h) A. S. Batsanov, J. C. Collings, T. B. Marder, *Acta Crystallogr.* **2006**, *C62*, m229–m231; i) J. C. Collings, J. M. Burke, P. S. Smith, A. S. Batsanov, J. A. K. Howard, T. B. Marder, *Org. Biomol. Chem.* **2004**, *2*, 3172–3178; j) A. S. Batsanov, J. C. Collings, J. A. K. Howard, T. B. Marder, D. F. Perepichka, *Acta Crystallogr.* **2001**, *C57*, 1306–1307; k) A. S. Batsanov, J. C. Collings, J. A. K. Howard, T. B. Marder, *Acta Crystallogr.* **2001**, *E57*, o950–o952; l) J. C. Collings, A. S. Batsanov, J. A. K. Howard, T. B. Marder, *Acta Crystallogr.* **2001**, *C57*, 870–872; m) A. S. Batsanov, J. A. K. Howard, D. Albesa-Jove, J. C. Collings, Z. Q. Liu, I. A. I. Mkhalid, M. H. Thibault, T. B. Marder, *Cryst. Growth Des.* **2012**, *12*, 2794–2802; n) A. S. Batsanov, I. A. I. Mkhalid, T. B. Marder, *Acta Crystallogr.* **2007**, *E63*, o1196–o1198; o) J. C. Collings, A. S. Batsanov, J. A. K. Howard, T. B. Marder, *Can. J. Chem.* **2006**, *84*, 238–242; p) C. Dai, P. Nguyen, T. B. Marder, T. B. Marder, A. J. Scott, W. Clegg, C. Viney, C. Viney, *Chem. Commun.* **1999**, 2493–2494.

- [28] a) C. P. Brock, D. G. Naeae, N. Goodhand, T. A. Hamor, *Acta Crystallogr.* **1978**, *B34*, 3691–3696; b) A. U. Meyer, T. Slanina, C.-J. Yao, B. König, *Acs. Catal.* **2016**, *6*, 369–375; c) R. Heckel, J. Hulliger, A. Schwarzer, E. Weber, *Acta Crystallogr.* **2015**, *E71*, o347–o348.
- [29] Y. T. Tsoi, Z. Zhou, W. Y. Yu, *Org. Lett.* **2011**, *13*, 5370–5373;
- [30] T. Ishiyama, J. Takagi, K. Ishida, N. Miyaoura, N. R. Anastasi, J. F. Hartwig, *J. Am. Chem. Soc.* **2002**, *124*, 390;
- [31] D. Bulfield, S. M. Huber, *J. Org. Chem.* **2017**, *82*, 13188–13203;
- [32] T. Korenaga, T. Kosaki, R. Fukumura, T. Ema, T. Sakai, *Org. Lett.* **2005**, *7*, 4915–4918;
- [33] Y. Lin, M. Cai, Z. Fanga, H. Zhao, *RSC Adv.* **2017**, *7*, 34722–34729;
- [34] O. René, K. Fagnou, *Org. Lett.* **2010**, *12*, 2116–2119;
- [35] G. J. P. Perry, J. M. Quibell, A. Panigrahi, I. Larrosa, *J. Am. Chem. Soc.* **2017**, *139*, 11527–11536;
- [36] Q. Zhao, C. Li, C. H. Senanayake, W. Tang, *Chem. Eur. J.* **2013**, *19*, 2261–2265;
- [37] L. W. Sardzinski, W. C. Wertjes, A. M. Schnaith, D. Kalyani, *Org. Lett.* **2015**, *17*, 1256–1259;
- [38] A. Nagaki, N. Takabayashi, Y. Moriwaki, J. Yoshida, *Chem. Eur. J.* **2012**, *18*, 11871–11875;
- [39] T. Chen, J. T. Guan, Z. Y. Zhang, J. J. Chen, F. Liu, X. Liu, *J. Heterocycl. Chem.* **2018**, *55*, 551–555;
- [40] T. Noël, S. Kuhn, A. J. Musacchio, K. F. Jensen, S. L. Buchwald, *Angew. Chem. Int. Ed.* **2011**, *50*, 5943–5946;
- [41] K. J. Allen, R. Bolton, G. H. Williams, *J. Chem. Soc. Perkin. Trans. 2*, **1983**, *0*, 691–695;
- [42] H. Li, J. Liu, C. L. Sun, B. J. Li, Z. J. Shi, *Org. Lett.* **2011**, *13*, 276–279;
- [43] I. A. Mkhalid, H. F. Al-Shaikh, *Asian J. Chem.* **2014**, *26*, 2077–2082;
- [44] C. M. So, C. P. Lau, A. S. C. Chan, F. Y. Kwong, *J. Org. Chem.* **2008**, *73*, 7731–7734;
- [45] H. H. Zhang, J. Dong, Q. S. Hu, *Eur. J. Org. Chem.* **2014**, 1327–1332;
- [46] L. Davin, R. McLellan, A. R. Kennedy, E. Hevia, *Chem. Commun.* **2017**, *53*, 11650–11653;
- [47] P. K. Mandali, D. K. Chand, *Catal. Commun.* **2013**, *31*, 16–20;
- [48] G. Sheldrick, *Acta Crystallogr.* **2015**, *A71*, 3–8;

- [49] G. Sheldrick, *Acta Crystallogr.* **2008**, *A64*, 112–122;
- [50] C. B. Hübschle, G. M. Sheldrick, B. Dittrich, *J. Appl. Cryst.* **2011**, *44*, 1281–1284;
- [51] K. Brandenburg, Diamond (version 4.4.0), Crystal and Molecular Structure Visualization, Crystal Impact H. Putz & K. Brandenburg GbR, Bonn (Germany), **2017**.

Chapter 3

Palladium-Catalyzed Homocoupling of Highly Fluorinated Aryl Boronates: Studies of the Influence of Strongly vs. Weakly Coordinating Solvents on the Reductive Elimination Process



3 Palladium-Catalyzed Homocoupling of Highly Fluorinated Aryl Boronates: Studies of the Influence of Strongly vs. Weakly Coordinating Solvents on the Reductive Elimination Process

Adapted with permission from Y. P. Budiman, A. Jayaraman, A. Friedrich, F. Kerner, U. Radius, T. B. Marder, *J. Am. Chem. Soc.*, **2020**, *142*, 6036–6050. Copyright (2020) American Chemical Society.

3.1 Abstract

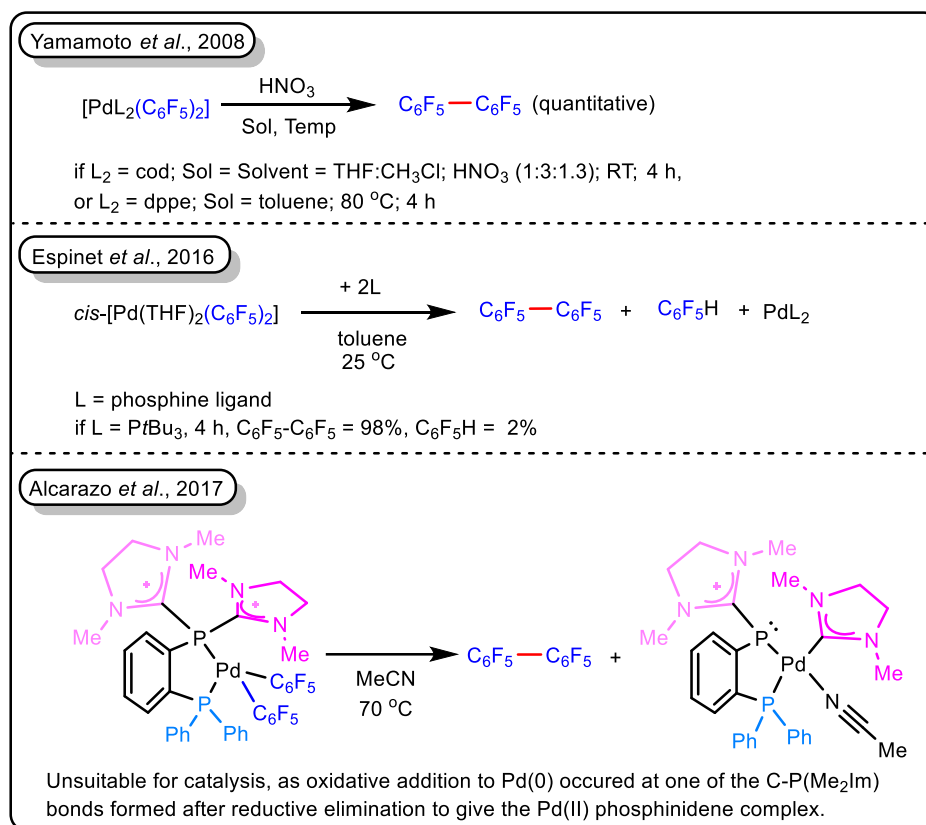
C–C reductive elimination from $[\text{PdL}_2(\text{C}_6\text{F}_5)_2]$ to form polyfluorinated biaryls has been a challenge for over 50 years. Thus, palladium-catalyzed homocoupling of aryl boronates ($\text{Ar}_\text{F}\text{--Bpin}$) containing two *ortho*-fluorine substituents is very difficult as the reaction typically stops at the $[\text{PdL}_2(\text{Ar}_\text{F})_2]$ stage after two transmetalation steps. The transmetalated complexes *cis*- $[\text{Pd}(\text{MeCN})_2(\text{C}_6\text{F}_5)_2]$ (**3_3a**), *cis*- $[\text{Pd}(\text{MeCN})_2(2,4,6\text{-C}_6\text{F}_3\text{H}_2)_2]$ (**3_3b**), and *cis*- $[\text{Pd}(\text{MeCN})_2(2,6\text{-C}_6\text{F}_2\text{H}_3)_2]$ (**3_3e**) have been isolated from the reaction of $\text{Ar}_\text{F}\text{--Bpin}$ with $\text{Pd}(\text{OAc})_2$ in acetonitrile solvent, with no homocoupling observed. However, catalytic homocoupling proceeds smoothly in a “weakly-coordinating” arene solvent as long as no ancillary ligands or coordinating solvents are present. DFT computations performed reveal that the active catalyst formed by arene solvent coordination leads to an overall reduced barrier for the reductive elimination step compared to the formation of stable $[\text{PdL}_2(\text{Ar}_\text{F})_2]$ complexes in the presence of a donor ligand or solvent L.

3.2 Introduction

Many transition metal-catalyzed processes consist of steps such as oxidative addition, reductive elimination, migratory insertion, transmetalation, and β -hydride elimination.^[1] Reductive elimination is often important for the final product-releasing step. Generally, two electronic effects have been observed for the reductive elimination from the $[\text{ML}_2(\text{Ar})(\text{Ar}')]$ complexes containing

group-10 metals. As the metal is formally reduced in the process, reductive elimination of Ar–Ar' from these complexes is usually faster if the ancillary ligand L is only weakly electron donating or strongly π -accepting.^[2] Furthermore, the rates of reductive elimination from these complexes are higher when an electron-rich and an electron-poor aryl group are involved in the reaction compared to two electron-rich aryl groups. The slowest reductive elimination rate steps are typically found when both aryl groups are electron-poor.^[2] In particular, $[\text{PdL}_2(\text{C}_6\text{F}_5)_2]$ complexes are well known for their high stability and, thus, reluctantly undergo reductive elimination,^[3] due to their strong Pd–Ar bonds.^[3g,h] Consequently, palladium-catalyzed homocoupling of $\text{C}_6\text{F}_5\text{B}(\text{OR})_2$,^[4] and Suzuki-Miyaura cross-coupling of $\text{C}_6\text{F}_5\text{B}(\text{OR})_2$ with 2,6- $\text{C}_6\text{F}_{2+n}\text{H}_{3-n}\text{X}$ are found to be difficult.^[5] For example, Oliveira *et al.* reported optimized conditions for the Pd-catalyzed homocoupling of Ar– BF_3K in an aqueous solvent which leads to coupled products in good to very good yields.^[4] Notably, if the substrates have two *ortho*-fluorine substituents, *e.g.*, $\text{C}_6\text{F}_5\text{BF}_3\text{K}$ or 2,6- $\text{C}_6\text{F}_2\text{H}_3\text{BF}_3\text{K}$, the corresponding homocoupling products were not observed.^[4] Regarding Suzuki-Miyaura cross-coupling, Osakada *et al.*^[5b] reported the reaction of 2,4,6-trifluorophenylboronic acid with *trans*- $[\text{Pd}(\text{PET}_3)_2(\text{C}_6\text{F}_5)\text{I}]$ in the presence of Ag_2O in toluene/ H_2O which led to the formation of a stable intermediate *trans*- $[\text{Pd}(\text{PET}_3)_2(\text{C}_6\text{F}_5)(2,4,6\text{-C}_6\text{F}_3\text{H}_2)]$ and no reductive elimination was observed.

As early as in 1970, Rausch and Tibbets reported the synthesis of $[\text{PdL}_2(\text{C}_6\text{F}_5)_2]$ ($\text{L} = \text{PPh}_2\text{Me}$; $\text{L}_2 = \text{bpy}$)^[3f] and, in 1964 and 1965, Rosevear and Stone reported that $[\text{NiL}_2(\text{C}_6\text{F}_5)_2]$ ($\text{L} = \text{PET}_3, \text{PPh}_3$; $\text{L}_2 = \text{bpy}$)^[6] and $[\text{PtL}_2(\text{C}_6\text{F}_5)_2]$ ($\text{L} = \text{PET}_3, \text{PPh}_3$; $\text{L}_2 = \text{dppe}$)^[7] are stable complexes. Jones *et al.*^[8a] and Perutz *et al.*^[8b,c] reported that a high M–Ar bond energy can be achieved when two *ortho*-fluorine substituents are present on the aryl group. Thus, as long as the two aryl groups contain two *ortho*-fluorine substituents, $[\text{PdL}_2(\text{Ar}_\text{F})_2]$ complexes are stable, *e.g.*, $[\text{PdL}_2(\text{C}_6\text{F}_4(4\text{-C}_5\text{H}_{10}\text{N}))_2]$ ($\text{L}_2 = \text{dppe}, \text{cod}$)^[9] and $[\text{PdL}_2(2,4,6\text{-C}_6\text{F}_3\text{H}_2)_2]$ ($\text{L} = \text{PhCN}, \text{PET}_3, \text{AsPh}_3, \text{P}(\text{OMe})_3, \text{P}(\text{OEt})_3, \text{P}(\text{OPh})_3$; $\text{L}_2 = \text{cod}, \text{tmen}$).^[10]



Scheme 3-1. Previous efforts to enhance reductive elimination from $[\text{PdL}_2(\text{C}_6\text{F}_5)_2]$.

Due to the high stability of $[\text{PdL}_2(\text{C}_6\text{F}_5)_2]$ complexes, researchers were encouraged to develop efficient methods to enhance the rate of the reductive elimination step (Scheme 3-1). In 2008, Yamamoto *et al.* demonstrated that addition of a Brønsted acid, HNO₃, promotes the reductive elimination of C₆F₅-C₆F₅ from *cis*- $[\text{PdL}_2(\text{C}_6\text{F}_5)_2]$ ($\text{L}_2 = \text{cod}$, bpy, and dppb).^[3g] Although this strategy is successful under stoichiometric conditions, it is not compatible with the catalytic homocoupling of aryl boronates, as basic reagents are required to activate Ar-B(OR)₂ for transmetalation to the Pd center.^[11]

In 2016, Espinet *et al.*^[12] reported that reductive elimination of C₆F₅-C₆F₅ from *cis*- $[\text{Pd}(\text{THF})_2(\text{C}_6\text{F}_5)_2]$ could be promoted by introduction of phosphine ligands, (*PtBu*₃, *o*-TolPEWO-F, *tBuXPhos*, P(C₆F₅)₃, PhPEWO-F, P(*o*-Tol)₃, *tBuBrettPhos*, Xantphos, and PhPEWO-H), in toluene solvent. They suggested that immediate reductive elimination to form C₆F₅-C₆F₅ occurred after rapid ligand substitution. Among different phosphines examined for efficient stoichiometric reductive elimination, *PtBu*₃ was ranked as the best ligand according to initial coupling rates.

In 2017, Alcarazo *et al.*^[3h] attempted to solve the problem by synthesizing $[\text{PdL}_2(\text{C}_6\text{F}_5)_2]$ and employing two different α -dicationic chelating ancillary ligands, both containing a PPh_2 moiety and a strong π -acceptor $[\text{P}(\text{Me}_2\text{Im})_2]^{+2}$ unit ($\text{Me}_2\text{Im} = 1,3$ -dimethylimidazolidine-2-ylidene) connected *via o*-phenylene or 2,2'-biphenylene linkers, respectively. Both complexes were calculated to have a low energy barrier (~ 23 kcal/mol) for reductive elimination due to the strong acceptor character of the ancillary ligands which enhances electron deficiency at the Pd center. However, they found these complexes unsuitable for catalysis as, after reductive elimination, the resulting Pd(0) complex inserted into one of the P–C bonds of the dicationic ligands to form Pd(II) phosphinidene complexes.

We recently reported the thermal^[13a] and photocatalytic^[13b] defluoroborylation of fluoroarenes using an NHC-nickel complex as catalyst (NHC = *N*-Heterocyclic Carbene) and B_2pin_2 (pin = pinacolato) as the boron source. Subsequently, we focused on applications of the resulting $\text{Ar}_\text{F}\text{-Bpin}$ products in organic synthesis. Very recently, we reported optimized conditions for Suzuki-Miyaura cross-coupling of $\text{Ar}_\text{F}\text{-Bpin}$ with aryl-iodide / bromide as a coupling partner, using a combination of CuI and phenanthroline as the catalyst precursor,^[14] and the Ni-catalyzed Suzuki-Miyaura cross-coupling of aryl boronates with polyfluorinated arenes *via C–F* activation.^[13c] Herein we expand the applications of $\text{Ar}_\text{F}\text{-Bpin}$ species to the homocoupling reaction using a palladium catalyst, as the reductive elimination from $\text{Pd}(\text{II})(2,6\text{-C}_6\text{F}_{2+n}\text{H}_{3-n})_2$ complexes to generate symmetrical fluorinated biphenyls is still very challenging. Symmetrical polyfluorinated biphenyls have been receiving considerable attention as they have potential applications in organic semiconductors,^[15] electron-transport materials,^[16] crystal-engineering,^[17] and supramolecular chemistry.^[18] Fluorinated organic compounds, as well as some metal complexes with a fluorinated aryl ligand, are prospective antiproliferative agents against HT-29 (colon carcinoma) and MCF-7 (breast adenocarcinoma).^[9]

Thus, we report a strategy to enhance the reductive elimination rate of $\text{Pd}(\text{II})(2,6\text{-C}_6\text{F}_{2+n}\text{H}_{3-n})_2$ complexes in the Pd-catalyzed homocoupling of $\text{Ar}_\text{F}\text{-Bpin}$ compounds. Using acetonitrile as the reaction solvent, we also isolated the complexes *cis*- $[\text{Pd}(\text{MeCN})_2(\text{C}_6\text{F}_5)_2]$ (**3_3a**), *cis*- $[\text{Pd}(\text{MeCN})_2(2,4,6\text{-C}_6\text{F}_3\text{H}_2)_2]$ (**3_3b**), and *cis*- $[\text{Pd}(\text{MeCN})_2(2,6\text{-C}_6\text{F}_2\text{H}_3)_2]$ (**3_3e**) after double

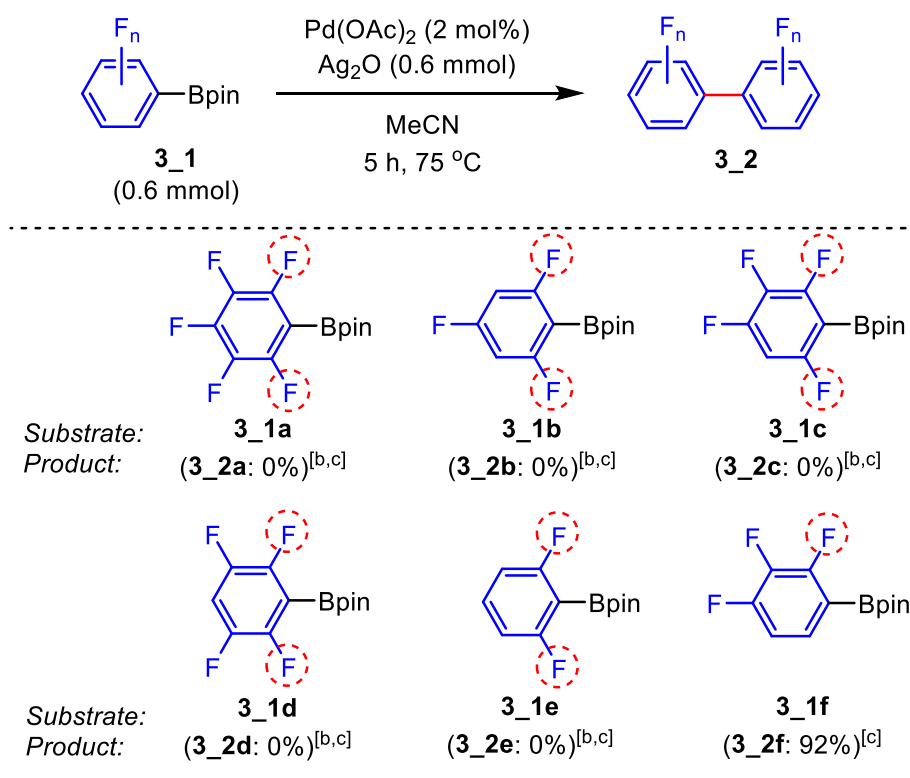
transmetalation, as these proved resistant to reductive elimination. However, the Pd-catalyzed homocoupling of 2,6-C₆F_{2+n}H_{3-n}Bpin substrates proceeds smoothly if no ancillary ligand or strongly coordinating solvent is used. DFT computations were performed to gain additional insight into the reductive elimination step and to understand why the catalytic homocoupling reactions conducted in arene solvents is efficient, whereas it is difficult in the presence of ancillary ligands or coordinating solvents.

3.3 Results and Discussion

3.3.1 Experimental Studies

We began by examining the homocoupling reaction of 0.6 mmol of C₆F₅Bpin (**3_1a**) catalyzed by 2 mol% of Pd(OAc)₂ in the presence of stoichiometric Ag₂O, which not only acts as an oxidizer for *in situ* formed Pd(0), but is also suggested to act as an accelerator for the transmetalation process.^[5b,19,20] For example, Osakada *et al.* reported that *trans*-[Pd(PEt₃)₂(C₆F₅)I] reacts with Ag₂O in toluene/H₂O to generate *trans*-[Pd(PEt₃)₂(C₆F₅)(OH)], which undergoes facile transmetalation with the boronic acid 4-MeOC₆H₄B(OH)₂.^[5b] As it is well documented that employing strong Lewis basic ligands, such as mono- or bidentate phosphorus or nitrogen based ligands, stops the coupling reaction by formation of stable [PdL₂(C₆F₅)₂] complexes,^[3] to facilitate the reductive elimination of C₆F₅-C₆F₅ we planned to conduct the coupling reaction in weakly coordinating solvents without adding any ancillary ligands. It was anticipated that these solvents, upon coordination to the Pd center, would provide a less electron-rich environment at the metal center, thereby facilitating reductive elimination from the presumably four-coordinate *cis*-[Pd(solvent)₂(C₆F₅)₂] complex or three-coordinate *cis*-[Pd(solvent)(C₆F₅)₂] complex. It was previously proposed that acetonitrile can act as a labile ligand in *cis*-[Pd(MeCN)(PMe₃)(R)₂] (R = Me, Ph, vinyl).^[21] This lability enables facile generation of the three-coordinate complex [Pd(PMe₃)(R)₂] and the ensuing reductive elimination of R₂. Conducting the reaction in acetonitrile solvent, which was neither anhydrous nor dried or distilled, however, did not lead to homocoupling (Scheme 3-2). Using dry acetonitrile did not help. Likewise, no homocoupling product was formed with the aryl boronates 2,4,6-C₆F₃H₂Bpin (**3_1b**),

2,3,4,6-C₆F₄HBpin (**3_1c**), 2,3,5,6-C₆F₄HBpin (**3_1d**), or 2,6-C₆F₂H₃Bpin (**3_1e**) in this solvent (Scheme 3-2). However, with 2,3,4-C₆F₃H₂Bpin (**3_1f**), which has only one *ortho*-fluorine substituent, a quantitative formation of the homocoupled product **3_2f** was observed. From these data, it is clear that the reductive elimination is difficult only if the Ar_F-Bpin contains two *ortho*-fluorine substituents.^[4,5b,9,10] This phenomena is in accordance with the theoretical research by Jones *et al.*^[8a] and Perutz *et al.*^[8b,c] who showed that the strength of the M–aryl bond strongly depends on the number of *ortho*-fluorine substituents on the aryl ring. Thus, it can be suggested that diaryl complexes containing two *ortho*-fluorines on each aryl ring have a high Pd–Ar bond energy and, in turn, a higher energy barrier for the reductive elimination step than those containing only one or no *ortho*-fluorine substituent.

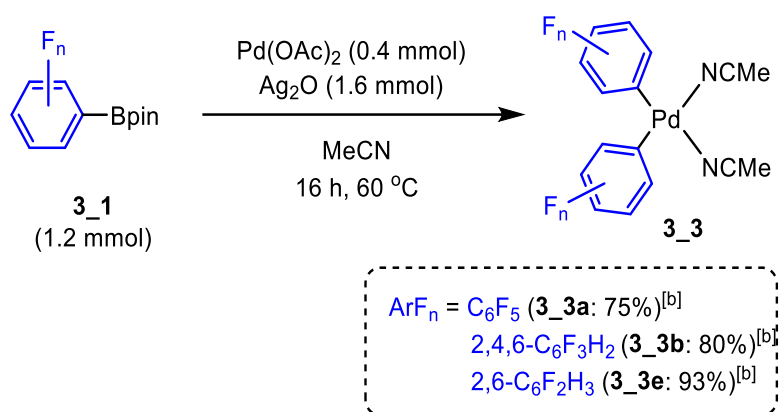


^[a] General condition: 0.6 mmol of Ar_{F_n}-Bpin (**3_1**), 2 mol% of Pd(OAc)₂, 0.6 mmol of Ag₂O, in 1.5 ml of MeCN, 5 h, at 75 °C, air. ^[b] No product was observed. ^[c] Isolated yield.

Scheme 3-2. Pd-catalyzed homocoupling of Ar_{F_n}-Bpin in MeCN.^[a]

The reaction of 1.2 mmol of C₆F₅Bpin (**3_1a**), 2,4,6-C₆F₃H₂Bpin (**3_1b**), or 2,6-C₆F₂H₃Bpin (**3_1e**) with 0.4 mmol of Pd(OAc)₂ and 1.6 mmol of Ag₂O in 4 mL of MeCN for 16 h at 60 °C

stopped after the double transmetalation step (Scheme 3-3), and the resulting complexes *cis*-[Pd(MeCN)₂(C₆F₅)₂] (**3_3a**), *cis*-[Pd(MeCN)₂(2,4,6-C₆F₃H₂)₂] (**3_3b**), and *cis*-[Pd(MeCN)₂(2,6-C₆F₂H₃)₂] (**3_3e**) were isolated in good yields. All these products were characterized by NMR and IR spectroscopy, elemental analysis and single-crystal X-ray diffraction (Figure 1 and see Section 3.5 Detailed Experiments and Characterization Data).



^[a] General conditions: 1.20 mmol of Ar_F-Bpin, 0.40 mmol of Pd(OAc)₂, 1.60 mmol of Ag₂O, in 4 mL of MeCN, 16 h, 60 °C, in air. ^[b] Isolated yield.

Scheme 3-3. Synthesis of *cis*-[Pd(MeCN)₂(ArF_n)₂].^[a]

Single crystals of *cis*-[Pd(MeCN)₂(C₆F₅)₂] (**3_3a**), *cis*-[Pd(MeCN)₂(2,4,6-C₆F₃H₂)₂] (**3_3b**), and *cis*-[Pd(MeCN)₂(2,6-C₆F₂H₃)₂] (**3_3e**) were grown by vapor diffusion of CD₃CN/Et₂O solutions placed in a larger vessel containing toluene (**3_3a**, **3_3e**) and by vapor diffusion of an Et₂O solution with hexane (**3_3b**). The crystal structures, as shown in Figure 1, reveal that the complexes have *cis*-conformations, as reported for other complexes such as *cis*-[PdL₂(C₆F₅)₂], (L = THF,^[22a] CO,^[22a] NH₃,^[22b] NH=CMe₂,^[22b] NH=C(OMe)Me,^[22c] 7-azaindoly^[22d] and PPh₃^[3i]).

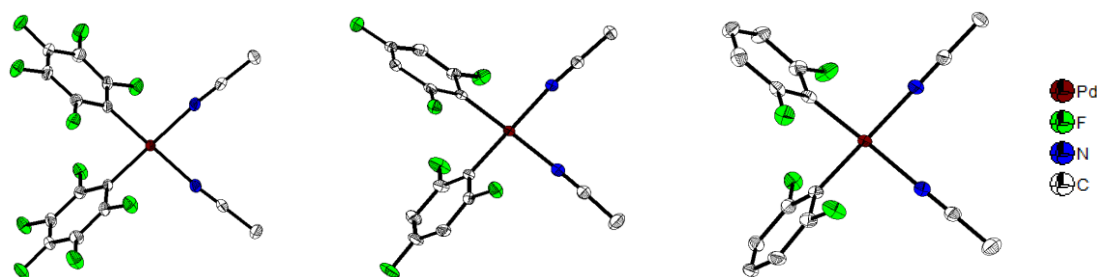


Figure 3-1. Molecular structures of **3_3a** (left), **3_3b** (middle), and **3_3e** (right) determined by single-crystal X-ray diffraction at 100 or 103 K. Ellipsoids are drawn at the 50% probability level, and H atoms as well as the disordered diethyl ether solvent molecule are omitted for clarity. Only one of two symmetry independent molecules of **3_3b** is shown. Colors: red (palladium), green (fluorine), blue (nitrogen), white (carbon).

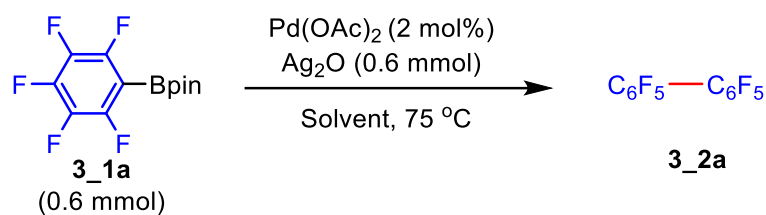
The isolation of complexes **3_3a**, **3_3b**, and **3_3e** shows that even a weakly donating ligand such as MeCN is sufficient to stabilize the $[\text{Pd}(\text{C}_6\text{F}_5)_2]$, $[\text{Pd}(2,4,6\text{-C}_6\text{F}_3\text{H}_2)_2]$, and $[\text{Pd}(2,6\text{-C}_6\text{F}_2\text{H}_3)_2]$ complexes, formed after double transmetalation, and thus to inhibit reductive elimination. Yamamoto *et al.*^[3g] suggested that effective reductive elimination from $[\text{PdL}_n(\text{C}_6\text{F}_5)_2]$ depends on weak Pd–C_{ipso}(C₆F₅) bonds and shorter C_{ipso}(C₆F₅)–C_{ipso}(C₆F₅) distances. Jones *et al.*^[8a] and Perutz *et al.*^[8b,c] reported that the maximum increase in M–aryl bond strength is achieved with two *ortho*-fluorine substituents, while the total number of fluorines only has a minor effect on the M–aryl bond strength. As shown in Table 3-1, the Pd–C_{ipso}(Ar_F) lengths, as well as C_{ipso}(Ar_F)–C_{ipso}(Ar_F) distances and C_{ipso}(Ar_F)–Pd–C_{ipso}(Ar_F) angles are almost the same for *cis*- $[\text{Pd}(\text{MeCN})_2(\text{C}_6\text{F}_5)_2]$ (**3_3a**), *cis*- $[\text{Pd}(\text{MeCN})_2(2,4,6\text{-C}_6\text{F}_3\text{H}_2)_2]$ (**3_3b**), and *cis*- $[\text{Pd}(\text{MeCN})_2(2,6\text{-C}_6\text{F}_2\text{H}_3)_2]$ (**3_3e**).

Table 3-1. Selected bond lengths (Å) and angles (°) of **3_3a**, **3_3b**, and **3_3e**.

	3_3a	3_3b		3_3e
		Molecule 1	Molecule 2	
Pd–C _{ipso} (Ar _F)	1.998(3)	1.988(2)	1.997(2)	1.996 (4)
		2.002(2)	1.997(2)	1.998 (4)
C _{ipso} (Ar _F)···C _{ipso} (Ar _F)	2.774(5)	2.773(3)	2.755(3)	2.752 (5)
C _{ipso} –Pd–C _{ipso}	87.94(15)	88.06(9)	87.23(9)	87.09 (15)
∠ Ar–Ar	72.75(13)	98.77(8)	73.38(8)	86.76(11)

We then continued to screen conditions for the homocoupling of C_6F_5Bpin (**3_1a**) (Table 3-2). Intriguingly, shifting from coordinating solvents to non-coordinating ones^[23] such as toluene, benzene, or *m*-xylene generated the homocoupling product $C_6F_5-C_6F_5$ (**3_2a**) in nearly quantitative yield (entry 1). The reaction is found to be slow in perfluorobenzene solvent, as it required 3 days to afford good yield (entry 2). It should be noted that the arene solvents used were neither anhydrous nor dried or distilled. In contrast to the outcomes obtained using arene solvents, no product was observed when coordinating solvents such as THF or Et_3N were used (entry 3); presumably, stable $[PdL_2(C_6F_5)_2]$ ($L = THF, Et_3N$) complexes were formed. In fact, the stable *cis*- $[Pd(THF)_2(C_6F_5)_2]$ ^[22a] and *cis*- $[Pd(NH_3)_2(C_6F_5)_2]$ ^[22b] complexes are well known. Using other coordinating solvents such as DMF or DMSO also failed to afford homocoupling product. In contrast to $Pd(OAc)_2$, heterogenous Pd(0), namely Pd/C, did not catalyze the homocoupling reaction (entry 4), indicating that our catalytic process is not promoted by clusters, nanoparticles, etc. No homocoupling product was formed when using $PdCl_2$ instead of $Pd(OAc)_2$ (entry 5). This unsuccessful outcome is likely due to the poor solubility of $PdCl_2$ in toluene.

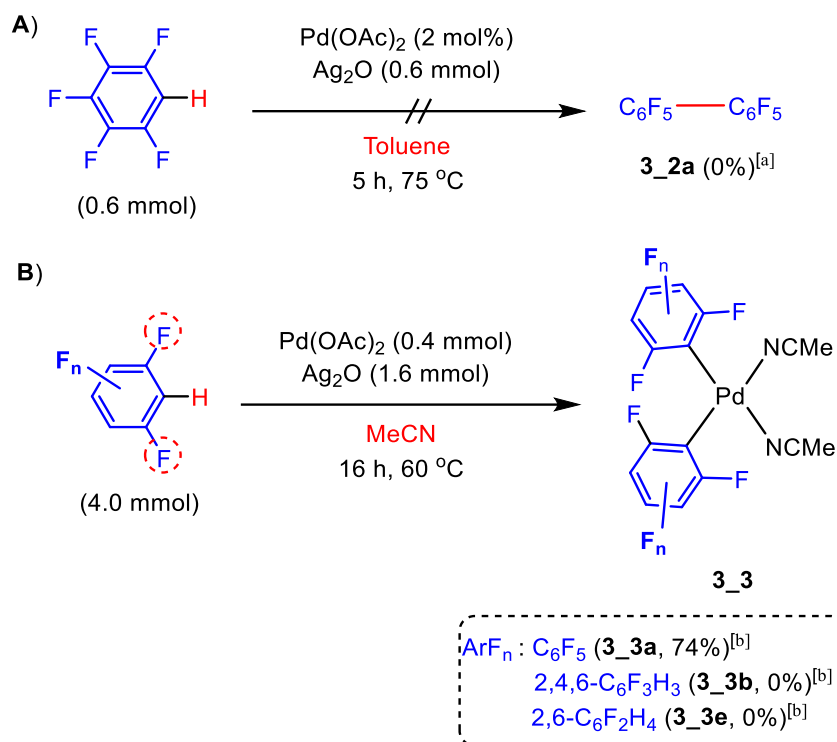
Espinet *et al.* reported that addition of 2 equivalents of $PtBu_3$ to *cis*- $[Pd(THF)_2(C_6F_5)_2]$ in toluene enhances the reductive elimination of $C_6F_5-C_6F_5$ under much milder conditions (Scheme 3-1).^[12] The authors suggested that fast ligand substitution with the bulky, strongly σ -donating $PtBu_3$ ligand leads to a three-coordinate Pd complex,^[24] *cis*- $[Pd(PtBu_3)(C_6F_5)_2]$, and enhances the elimination of $C_6F_5-C_6F_5$. Inspired by that, we added 4 mol% of $PtBu_3$ as a ligand to the reaction mixture to examine for the possibility of achieving efficient catalytic reaction under ambient conditions but, unfortunately, it failed to generate any homocoupling product, even at a high temperature (Table 3-2, entry 6). We did not screen any other phosphine ligands, as many complexes of the form $[Pd(PR_3)_2(C_6F_5)_2]$ are known and are stable with respect to reductive elimination.^[3,5b]

Table 2. Reaction conditions screened for Pd-catalyzed homocoupling of Ar_F-Bpin.^[a]

Entry	Solvent	Time (h)	Yield (%) ^[b]
1	toluene, benzene, or <i>m</i> -xylene	5	> 94
2	C ₆ F ₆	5	36
		24	54
		72	75
3	THF, Et ₃ N, DMF, or DMSO	5	0 ^[c]
4	toluene	24	trace ^[d]
5	toluene	5	trace ^[e]
6	toluene + 4 mol% of P <i>t</i> Bu ₃	24	0 ^[e] (0) ^[c,f]

^[a] General conditions: 0.60 mmol of **3_1a**, 2 mol% of Pd(OAc)₂, 0.60 mmol of Ag₂O, in 1.5 mL of solvent, 5-72 h, 75 °C, in air. ^[b] Isolated yield. ^[c] Product was not observed. ^[d] Using Pd/C (0.5, 5 or 10 mol%) in place of Pd(OAc)₂. ^[e] Using PdCl₂ (2 mol%) in place of Pd(OAc)₂. ^[f] Under argon and using dried toluene.

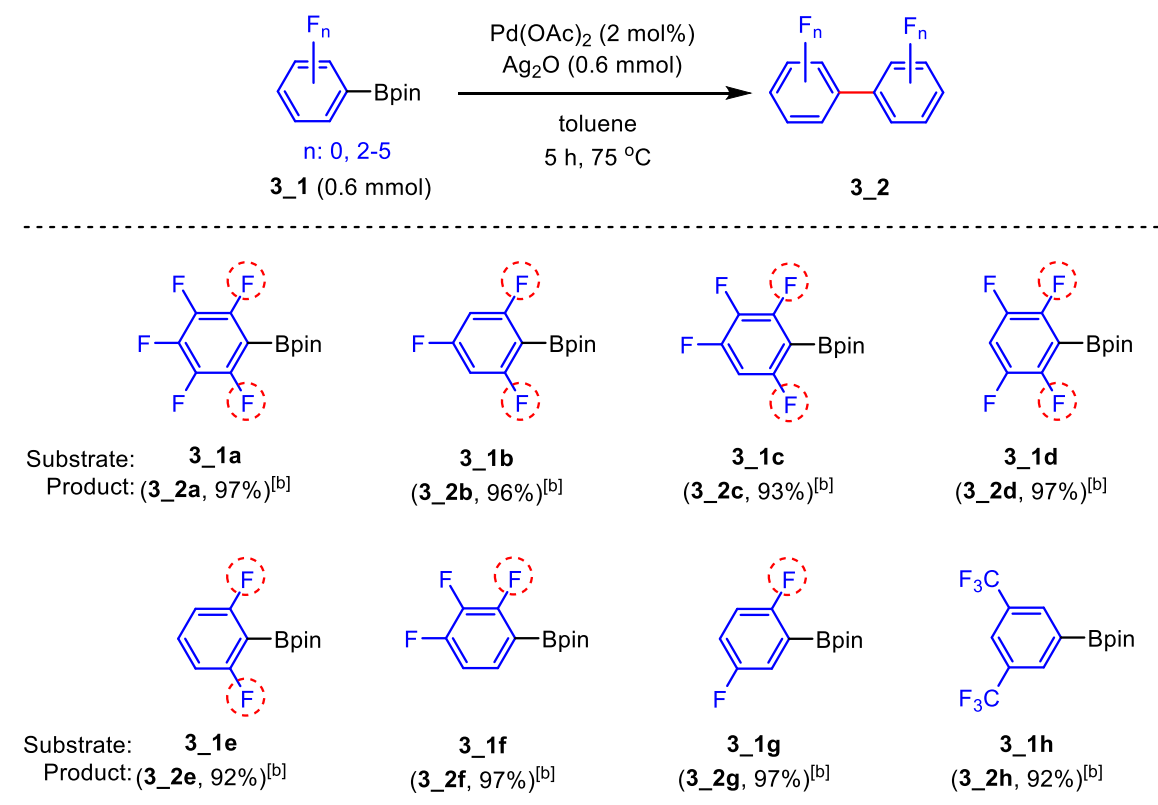
We attempted to employ C₆F₅H instead of C₆F₅Bpin as a substrate in toluene under the above optimized conditions, but no homocoupling product was generated (Scheme 3-4A),^[25] consistent with a process in which the C-Bpin moiety is important for transmetalation, and that C-H oxidative addition did not occur in toluene solvent. Interestingly, however, conducting the same reaction in MeCN solvent afforded a 74% isolated yield of complex **3_3a** (Scheme 3-4B), indicating that MeCN could function as a base and/or a sufficiently strong donor ligand on Pd to activate the C-H bond of C₆F₅H,^[25d] but MeCN solvent has to be avoided if the reductive elimination product **3_2a** is desired. Notably, no conversion was observed when employing 1,3,5-trifluorobenzene and 1,5-difluorobenzene as substrates, even in MeCN solvent (Scheme 3-4B).



^[a] Condition: C₆F₅H (0.6 mmol), Pd(OAc)₂ (2 mol%), Ag₂O (0.6 mmol), toluene (1.5 ml), 75 °C, 5 h, in air. ^[b] Conditions: ArF_n (4 mmol), Pd(OAc)₂ (0.4 mmol), Ag₂O (1.6 mmol), MeCN (4 ml), 60 °C, 16 h, in air.

Scheme 3-4. Attempted homocoupling reaction using C₆F₅H, 1,3,5-C₆F₃H₂, and 1,5-C₆F₂H₃ substrates.

Using toluene as the solvent under the above optimized conditions, we expanded the scope to other fluorinated aryl-Bpin derivatives (Scheme 3-5). Compounds in which the C–Bpin bond is flanked by two C–F bonds (**3_1a**, **3_1b**, **3_1c**, **3_1d**, **3_1e**), only one C–F bond (**3_1f**, **3_1g**) or no *ortho*-fluorines (**3_1h**), all proved to be suitable substrates, and the respective homocoupled products **3_2a**, **3_2b**, **3_2c**, **3_2d**, **3_2e**, **3_2f**, **3_2g**, **3_2h** were formed in excellent yields.



^[a] General conditions: Ar_F-Bpin (0.6 mmol), Pd(OAc)₂ (2 mol%), Ag₂O (0.6 mmol), toluene (1.5 mL), 75 °C, 5 h, in air. ^[b] Isolated yield.

Scheme 3-5. Reaction scope for the homocoupling of ArF_n-Bpin in toluene.^[a]

3.3.2 Crystal and Molecular Structures of the Fluorinated Biaryl Products: Intermolecular $\pi \cdots \pi$ Stacking Interactions.

Crystal structures of the products 2,2',3,3',5,5',6,6'-octafluorobiphenyl (**3_2d**) and 2,2',3,3',4,4'-hexafluorobiphenyl (**3_2f**) were obtained *via* single-crystal X-ray diffraction. The molecular geometries of these compounds in their crystal structures are shown in Figure 3-2. The central C–C bonds are equal within one standard deviation and are in the range 1.485(2) – 1.487(4) Å (Table 3-3) which is typical of biphenyl compounds.^[26] The twist between the aryl moieties of the biaryl compounds is slightly stronger in **3_2d** (58.06(4)°) than in **3_2f** (47.02(6)°) (Table 3-3). This difference is likely due to the larger steric demand of fluorine in close vicinity to the central C–C bond joining the rings and, hence, to the stronger repulsion between the fluorine atoms of both aryl units in **3_2d**. A similar twist angle to that of **3_2f** was also reported for 2,3,4-trifluorobiphenyl (49.76(7)°).^[14]

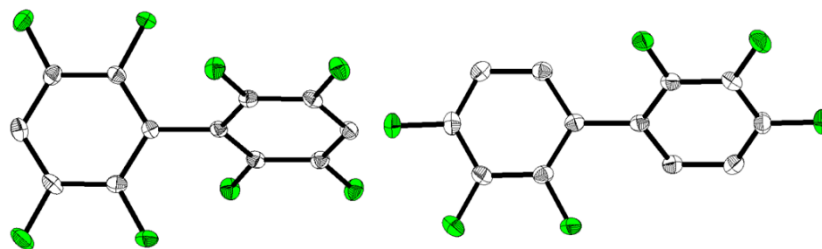


Figure 3-2. Solid-state molecular structures of **3_2d** (left) and **3_2f** (right) determined by single-crystal X-ray diffraction at 100 K. Ellipsoids are drawn at the 50% probability level, and H atoms are omitted for clarity. Compound **3_2f** shows a two-fold rotational symmetry. Colors: white (carbon), green (fluorine).

Table 3-3. Selected bond lengths (Å) and angles (°) of **3_2d** and **3_2f**, and $\pi\cdots\pi$ stacking distances in **3_2f**.

	3_2d	3_2f
conjunction bond C _{Aryl} –C _{Aryl}	1.4852(16)	1.487(4)
∠ Aryl–Aryl	58.06(4)	47.02(6)
centroid-centroid distance	-	3.6980(1)
interplanar separation	-	3.3911(16)
offset shift ^[a]	-	1.475(4)

^[a] The offset shift, also called inter-centroid shift, is the distance within a plane of an aryl ring between the centroid of the respective aryl ring and the intersection point with the normal to the plane through the centroid of the other aryl ring.

Particularly interesting in the crystal structure analysis are the intermolecular interactions and, hence, molecular packing in these compounds. In compound **3_2d** there are no π - π stacking interactions present. A weak C–H \cdots F interaction with an angle of 124.62(8)° and a few weak F \cdots F interactions with distances of 2.7078(12)–2.9169(15) Å are observed between the molecules (Table 3-6 in Section 3.5.7 Single Crystal X-ray Diffraction Data). However, in compound **3_2f**, the biaryls form columns of offset face-to-face π -stacked 2,3,4-trifluoro phenyl rings along the *c* axis. The interplanar separation between the trifluorophenyl rings is typical for π - π stacking interactions (3.3911(16) Å, Table 3-3). Due to the large twist angle of ca. 47° of the biaryl, the columnar stacks

are cross-like (Figure 3-3). Similar cross-like columnar stacks are observed in 2,3,4,5,6-pentafluorobiphenyl,^[27a] 1,2,4,5-tetrafluoro-3-phenyl-6(trifluoromethyl)benzene,^[27a] 4'-bromo-2,3,5,6-tetrafluorobiphenyl-4-carbonitrile,^[27a] and 2-(perfluorophenyl)naphthalene^[14] which show biphenyl twist angles of 52, 50, 41, and 51°, respectively. Weak intermolecular C–H···F and F···F interactions are formed between the stacks (Table 3-6 in Section 3.5.7 Single Crystal X-ray Diffraction Data).

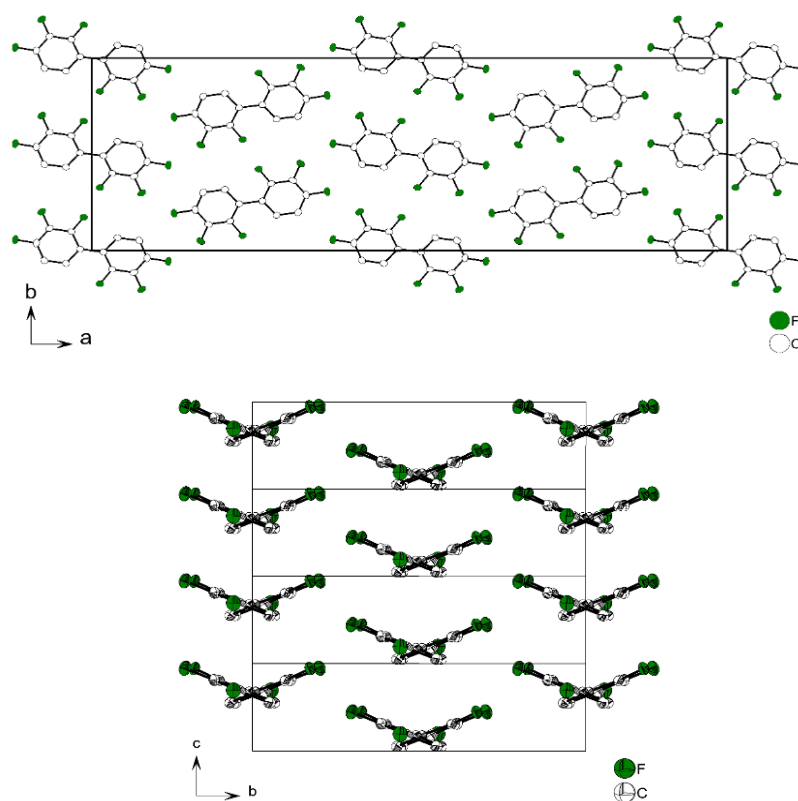


Figure 3. Crystal structure of **3_2f** projected along the *c* axis (top), which is the stacking direction of the molecules, and the *a* axis (bottom), at 100 K. Trifluorophenyl rings are π -stacked along the *c* axis. The intramolecular angle between the aryl rings of the biaryl is 47° leading to the formation of cross-like stacks (bottom). Only a section of the crystal structure, *i.e.*, one fourth along the *a* direction, is plotted in the bottom projection, while four unit cells are shown along the *c* axis. Ellipsoids are drawn at the 50% probability level, and H atoms are omitted for clarity. Colors: white (carbon), green (fluorine).

3.3.3 Computational Studies

The observation that stable highly fluorinated diaryl palladium(II) complex ligated with two acetonitriles, *cis*-[Pd(MeCN)₂(C₆F₅)₂] (**3_3a**), can be isolated from our attempted catalytic homocoupling reactions conducted in acetonitrile suggests that the transmetalation process is facile under the reaction conditions employed. It is also apparent that the transmetalation step is facile for the reactions performed in other solvents, including THF, benzene, toluene, *m*-xylene and probably perfluorobenzene. Thus, it can be proposed that the rate determining step in these homocoupling reactions is reductive elimination. To understand why the catalytic homocoupling reactions conducted in acetonitrile and THF failed, while they are successful in arene solvents, computations on the reductive elimination step were performed using DFT at the B3LYP-D3/Def2TZVP/6-311+g(2d,p)/IEFPCM // B3LYP-D3/SDD/6-31g**/IEFPCM level (see Section 3.6 Detailed Description of Computational Details).

3.3.3.1 Brief Overview of Previous Theoretical Studies on Reductive Elimination from *cis*-[PdL₂RR']

Several theoretical studies on C-H, C-C, C-E, and C-X reductive elimination from palladium complexes of type *cis*-[PdL₂R₂] have been reported. However, in comparison to the oxidative addition step, reductive elimination has been less well studied theoretically.^[28] For a long time, the reductive elimination step was generally assumed to be fast and irreversible. However, recent experimental studies have shown that there are systems in which reductive elimination is a slow step for the formation of C-C bonds.^[29] Based on previous theoretical studies, reductive elimination from *cis*-[PdL₂R₂] is generally accepted to be a concerted step occurring from a *cis*-complex. The earliest detailed theoretical study on reductive elimination from d⁸-metal complexes of group 10 metals was the 1981 report by Tatsumi *et al.*^[30] In this study, the authors employed extended Hückel calculations with a weighted *Hij* approximation and analyzed how switching the transition metal within the same group, as well as the ligands on the square planar complexes influences the activation barrier for the

reductive elimination of two *cis*-positioned alkyl groups. This study disclosed that, in comparison to Pd(II) and Pt(II) complexes, Ni(II) complexes can readily facilitate the reductive elimination of ethane from two *cis*-positioned methyl ligands. Moreover, this study also suggested that, upon dissociation of one of the neutral ligands from *cis*-[ML₂R₂] complexes, the resulting three-coordinate complexes (*cis*-[MLR₂]) can adopt either a T- or Y-shape geometry. Complexes with a T-shape geometry, that have the two eliminating groups positioned *cis* to each other, tend to undergo reductive elimination readily, whereas complexes with a Y-shape geometry tend to facilitate the *cis/trans* isomerization of the two alkyl groups.

Goddard *et al.* have explored theoretically, using the Hartree-Fock and generalized valence bond approximations, the factors which facilitate the reductive coupling of H–H, C–H and C–C bonds to produce molecular hydrogen and alkanes from the four-coordinate d⁸-complexes *cis*-[M(PH₃)₂RR'] (M = Pd, Pt; R, R' = H, Me), and reported that the reductive elimination barrier increases in the order H-H < C–H < C–C.^[31] For this trend, the authors noted that the faster reductive elimination of H₂ results from the better orbital overlap between the two eliminating hydride ligands, whereas the extent of such overlap is reduced as we move towards more carbon-based eliminating ligands for which the orbitals are more directed. For the C–C reductive elimination, Espinet *et al.* conducted a combined theoretical and experimental study on C_{sp³}–C_{sp³} and C_{sp²}–C_{sp²} reductive elimination from *cis*-[Pd(PMe₃)₂R₂], and *cis*-[Pd(PMe₃)LR₂] complexes possibly formed *in situ* from addition of coupling promoters (L = acetonitrile, ethene, maleic anhydride) to *cis*-[Pd(PMe₃)₂R₂].^[21] Their computational study at the B3LYP/SDD/6-31g* level of theory predicted a reductive elimination barrier of ~29 kcal/mol for the C_{sp³}–C_{sp³} coupling from *cis*-[Pd(PMe₃)₂(Me)₂], and a barrier of ~12 kcal/mol for C_{sp²}–C_{sp²} coupling from complexes of the type *cis*-[Pd(PMe₃)₂R₂] (R = vinyl and Ph). Morukuma *et al.* carried out a similar theoretical study, using the ONIOM(B3LYP/SDD/6-311g*:B3LYP/LANL2DZ) level of theory, on the reductive elimination from Pd(II) and Pt(II) complexes by employing the simplest phosphine ligand PH₃ as a model.^[24b] Their computations predicted a lower barrier for the model complexes of the type *cis*-[Pd(PH₃)₂R₂] (R = Me, vinyl, Ph, ethynyl) compared to their PMe₃ analogues. For example, the reductive

elimination barrier for $C_{sp^3}-C_{sp^3}$ coupling was reduced from ~ 29 kcal/mol to ~ 24 kcal/mol upon switching the phosphine ligand from PMe_3 to PH_3 . Likewise, for the vinyl case, the barrier was reduced from 12 kcal/mol to 6 kcal/mol when PMe_3 is replaced with PH_3 . However, for the bis-phenyl complex, the reductive elimination barrier was predicted to be similar in both cases. While the reductive elimination barrier for $C_{sp}-C_{sp}$ coupling from the PMe_3 complex was not computed, it was calculated for the PH_3 complex $cis-[Pd(PH_3)_2(CCH)_2]$ which was found to have a barrier of ~ 11 kcal/mol, *i.e.*, in between the barriers of its vinyl and methyl analogues, with the vinyl complex having the lower barrier.

Ariafard and Yates reported details of both electronic and steric effects of phosphine ligands on the reductive elimination of ethane and butadiene from $cis-[Pd(PR_3)_2R_2]$ ($R = Me, vinyl$) at the B3LYP/LANL2DZ/6-31g* level of theory.^[24a] The authors concluded that both factors play a role in the reductive elimination process for the parent four-coordinate complex, whereas only the electronics dominated in the three-coordinate complex $cis-[Pd(PR_3)R_2]$, formed from the parent complex *via* dissociation of a PR_3 ligand. Notably, steric factors in the starting four-coordinate complex $cis-[Pd(PR_3)_2R_2]$ destabilize it, while both factors stabilized the reductive elimination transition state. These factors led to a reduced reductive elimination barrier for this step. However, this reduced barrier is still high relative to that of the respective three-coordinate complex. Overall, from all these computational studies, the reductive elimination barrier for C–C coupling from the four- and three-coordinate Pd(II) complexes generally increases in the order $C_{sp}-C_{sp} < C_{sp^2}-C_{sp^2} < C_{sp^3}-C_{sp^3}$. In 2010, Korenaga *et al.* reported a combined experimental and theoretical study (theory level: B3LYP/LANL2DZ/6-31g*) of the electronic and steric effects of various diphosphine ligands on reductive elimination of biphenyl from the Pt(II) complex $cis-[Pt(diphosphine)(Ph)_2]$.^[32] The authors suggested that the electronic effects of diphosphine ligands contribute mainly to the reductive elimination rates. In particular, electron-poor diphosphine ligands that have the ability to act as a weak σ -donor significantly reduced the reductive elimination barrier in comparison to the ones which are strongly σ donating.^[32] It was reasoned that electron-poor diphosphine ligands decrease the d-orbital energy gap between the important high-lying molecular orbital of the starting

four-coordinate complex and its reductive elimination transition state, and thereby reduce the reductive elimination barrier. Thus far, much theoretical focus was placed on the reductive elimination of different C-C single bonds and, to the best of our knowledge, there was only one report on a computational study of $C_{sp^2}-C_{sp^2}$ reductive elimination from $[PdL_2(Ar)_2]$ complexes containing fluorinated aryl ligands.^[3h] Alcarazo *et al.* reported a combined experimental and computational study of the reductive elimination from symmetrical and dicationic unsymmetrical diphosphine ligand-containing Pd(II) complexes of type *cis*- $[Pd(\text{diphosphine})(C_6F_5)_2]$. Their computations at the BP86-D3/def2-SVP level of theory revealed that the dicationic unsymmetrical diphosphine ligand makes the coupling process not only exergonic but also, remarkably, reduces the reductive elimination barrier to ~ 23 kcal/mol, whereas employing a symmetrical ligand makes the process highly endergonic with a barrier of ~ 32 kcal/mol. By virtue of its strong π -accepting character, the cationic phosphine component of the unsymmetrical diphosphine ligand was reasoned to be responsible for the reduced reductive elimination barrier in the former case, as the cationic phosphine unit readily accepts the electron density that is accumulated on the metal during the transition state for the reductive elimination process.

3.3.3.2 Computational Results and Discussion

It was previously demonstrated that the Pd-catalyzed Suzuki-Miyaura cross-coupling of C_6F_5 -boronates with aryl iodides or bromides requires a stoichiometric amount of silver oxide (Ag_2O) to accelerate the transmetalation between C_6F_5 -boronates and Pd(II) complexes. Ag_2O has not been considered to play a role in the reductive elimination from a diaryl palladium complex.^[5b,20] Other previous studies have indicated that the acceleration of transmetalation with Ag_2O in the presence of H_2O led to the generation of an hydroxy complex that shows a higher reactivity for transmetalation with aryl boronates.^[5b,20c] In our case, the formation of a stoichiometric amount of the stable diaryl palladium(II) intermediates *cis*- $[Pd(MeCN)_2(C_6F_5)_2]$ (**3_3a**), *cis*- $[Pd(MeCN)_2(2,4,6-C_6F_3H_2)_2]$ (**3_3b**), and *cis*- $[Pd(MeCN)_2(2,6-C_6F_2H_3)_2]$ (**3_3e**) from the homocoupling reactions conducted in acetonitrile solvent with excess Ag_2O present implies that Ag_2O is ineffective in accelerating the

reductive elimination process. Moreover, treatment of **3_3e** in the non-polar solvent toluene without addition of Ag_2O led to decomposition and gave the reductive elimination product **3_2e** quantitatively (see Section 3.5.7 for details), implying again that Ag_2O does not accelerate reductive elimination. Hence, our computational emphasis was placed exclusively on the reductive elimination step without the engagement of Ag_2O .

As the reaction conducted in acetonitrile led to intermediate **3_3a**, two possible mechanistic routes from this intermediate, as shown in Figure 3-4, were conceived for the coupling step. The first route involves a concerted reductive elimination pathway whereby reductive elimination takes place directly from complex **3_3a**, and the second route, a dissociative pathway, involves an initial dissociation of an MeCN ligand,¹⁹ leading to the three-coordinate Pd(II) complex *cis*-[Pd(MeCN)(C₆F₅)₂], followed by reductive elimination. Computations at the B3LYP-D3/TZVP level of theory show that this is a slightly endergonic reaction and the barrier for reductive elimination directly from *cis*-[Pd(MeCN)₂(C₆F₅)₂] (**3_3a**) is 34.3 kcal/mol (pathway A, Figure 3-4). The second route (pathway B, Figure 3-4) did not bring down the overall reductive elimination barrier significantly with respect to that of pathway A, although the barrier of the actual reductive elimination step itself *via* this route was reduced by 7.0 kcal/mol. As this coupling reaction is already slightly endergonic and possess a high barrier achieving this reaction catalytically is unlikely. Like acetonitrile, THF can also form the bis(solvent) complex *cis*-[Pd(THF)₂(C₆F₅)₂] (**7**).

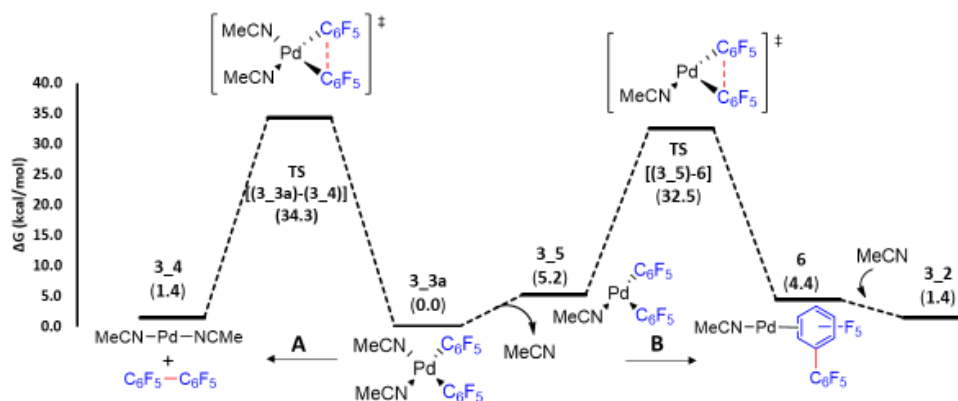


Figure 3-4. Computed mechanistic pathways (DFT, B3LYP-D3/TZVP) for the C–C reductive elimination step from the bis-perfluoroaryl complex ligated with acetonitrile. Gibbs free energy values (kcal/mol) relative to reactant (**3_3a**) are given in parentheses.

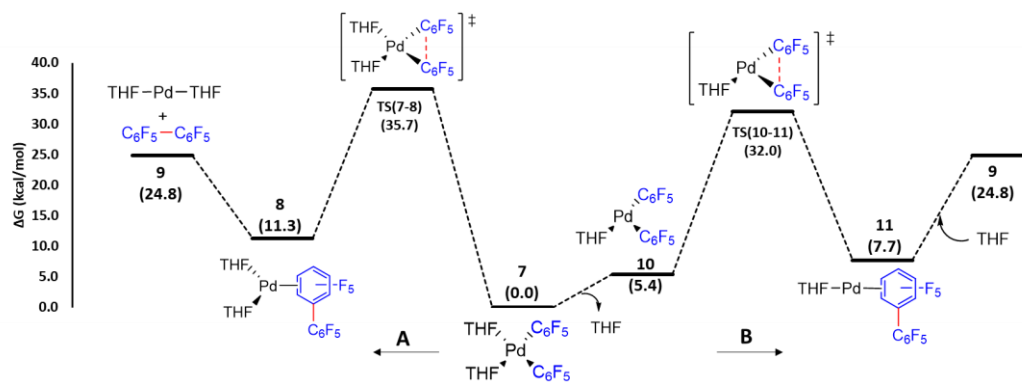


Figure 3-5. Computed mechanistic pathways (DFT, B3LYP-D3/TZVP) for the C–C reductive elimination step from the bis-perfluoroaryl complex ligated with THF. Gibbs free energy values (kcal/mol) relative to reactant (**7**) are given in parentheses.

While the THF complex **7** was not isolated or observed in our reactions, it is a known compound which was structurally characterized by X-ray crystallography.^[22a] Therefore, for reactions conducted in THF, the involvement of two routes resembling that of acetonitrile can be envisioned. For the first route (Pathway A, Figure 3-5), computations predict a high barrier comparable to that of the acetonitrile complex *cis*-[Pd(MeCN)₂(C₆F₅)₂] (**3_3a**). Even *via* the second route, *i.e.*, the dissociative pathway, no reduction in the overall barrier was obtained (pathway B, Figure 3-5). Furthermore, this homocoupling reaction is highly endergonic. Overall, such catalytic homocoupling reactions attempted in THF will likely not be rewarding. While this was the exact outcome we obtained from the experiments conducted in THF, the recent demonstration by Espinet *et al.*^[12] of successful reductive coupling of perfluorobiphenyl using the synthesized THF complex *cis*-[Pd(THF)₂(C₆F₅)₂] (**7**) in toluene suggests that either a THF ligand dissociates or both THF ligands were displaced by a toluene solvent prior to the reductive elimination step. Only under one of these conditions could their reported experimental barrier of 23.1 kcal/mol be obtained. Though not experimentally explored in the current work, we have computationally explored the possibilities of reductive elimination from the bis(perfluorophenyl)palladium complexes containing two other simple ligands, namely dimethylsulfide and trimethylphosphine. Two mechanistic pathways, as discussed above for complex *cis*-[Pd(MeCN)₂(C₆F₅)₂] (**3_3a**), are also possible with these ligands. Calculations show that, with these two ligands, the reductive elimination barriers remain high for the first route (pathway A, Figures 3-6 and 3-7), and the overall barrier is even higher for the second

route (pathway B, Figures 3-6 and 3-7). Overall, our computations on reductive elimination from fluorinated bis-phenyl square planar complexes of the type cis -[PdL₂(C₆F₅)₂] suggest that the barrier for reductive elimination from the four-coordinate complex is too high to overcome under the reaction conditions we employed, and the T-shaped tricoordinate complexes of type [PdL(C₆F₅)₂] that result from the dissociation of L in cis -[PdL₂(C₆F₅)₂], while possessing a lower barrier for the actual reductive elimination step, still place the overall reductive elimination barrier at similar or higher energies than those of cis -[PdL₂(C₆F₅)₂].

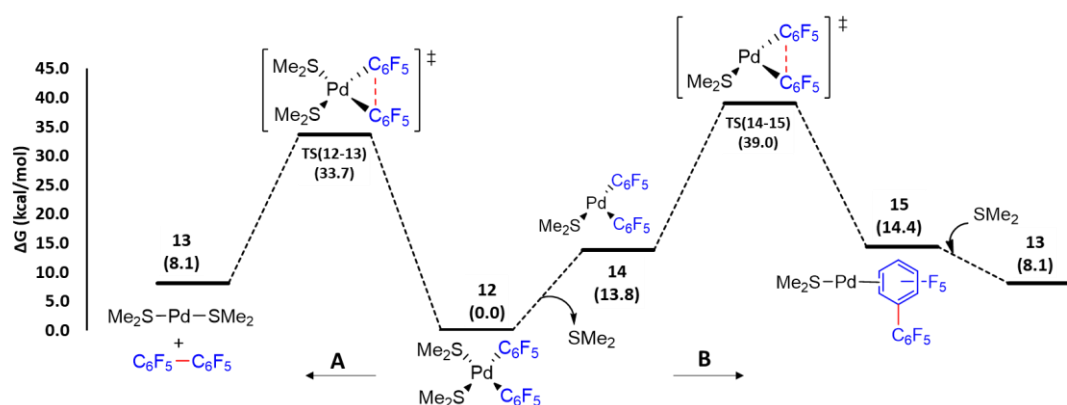


Figure 3-6. Computed mechanistic pathways (DFT, B3LYP-D3/TZVP) for the C–C reductive elimination step from the bis-perfluoroaryl complex ligated with dimethylsulfide. Gibbs free energy values (kcal/mol) relative to reactant (**12**) are given in parentheses.

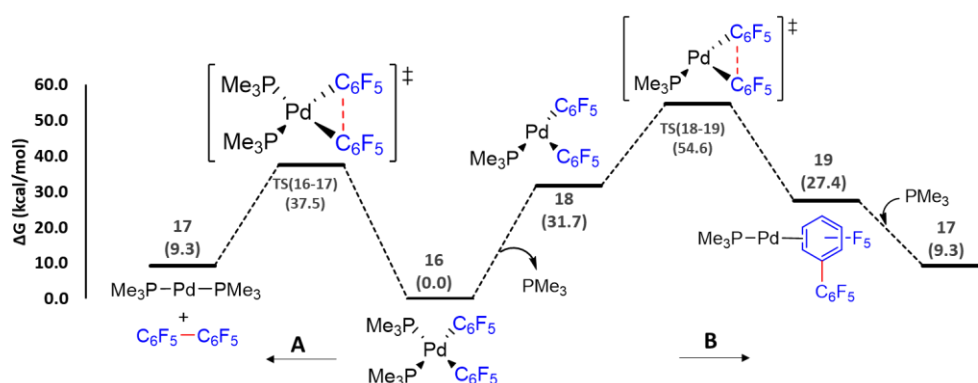


Figure 3-7. Computed mechanistic pathways (DFT, B3LYP-D3/TZVP) for the C–C reductive elimination step from the bis-perfluoroaryl complex ligated with PMe₃. Gibbs free energy values (kcal/mol) relative to reactant (**16**) are given in parentheses.

To understand the feasibility of the catalytic reactions in aromatic solvents, computations were performed on two mechanistic pathways for reductive elimination: (i) with an aromatic solvent coordinated to the metal; and (ii) without any arene coordination to the metal. Benzene, toluene, *m*-

xylylene, and perfluorobenzene were explored as solvents. For the metal complexed with an aromatic solvent, a slightly distorted η^6 -interaction was calculated for the ground state structure of $[\text{Pd}(\eta^6\text{-arene})(\text{C}_6\text{F}_5)_2]$. Ring slippage of the arene ligand along the reaction coordinate was calculated to occur and the hapticity change may best be described as going from η^6 in the reactant to η^n ($n \leq 3$) in the transition state and the products. The optimized structures of the benzene complex $[\text{Pd}(\eta^6\text{-C}_6\text{H}_6)(\text{C}_6\text{F}_5)_2]$ **20**, the primary elimination product **21** and of the transition state **TS(20-21)** (see also Figure 3-9) are shown in Figure 3-8.

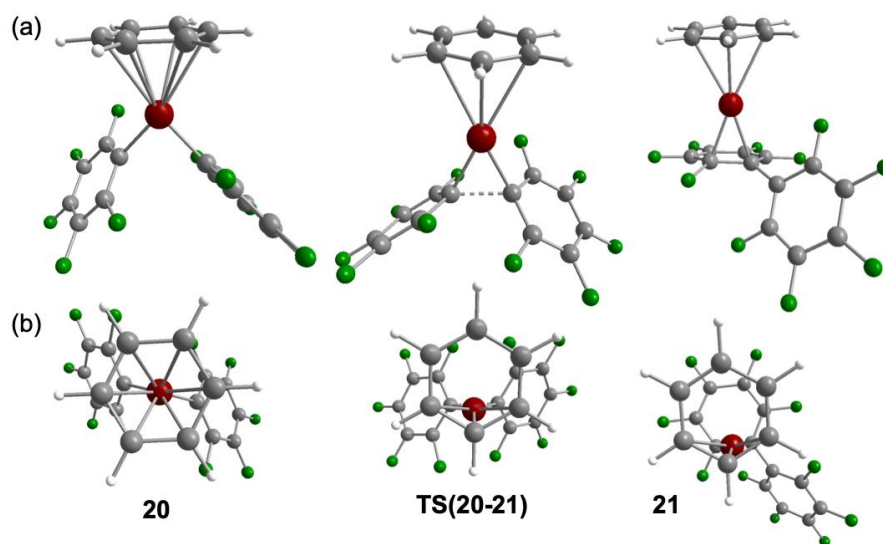


Figure 3-8. Side-view (a) and view along the arene-Pd vector (b) of the DFT-optimized structures (B3LYP-D3/TZVP) of the benzene complexes $[\text{Pd}(\eta^6\text{-C}_6\text{H}_6)(\text{C}_6\text{F}_5)_2]$ **20**, the primary elimination product **21** and the transition state **TS(20-21)**. Calculated Pd-C_{arene} distances [Å]: **20**: 2.61735, 2.61795, 2.64026, 2.64086, 2.66559, 2.66676, **TS(20-21)**: 2.27466, 2.60792, 2.60934, 3.20505, 3.20613, 3.47771, **21**: 2.23648, 2.56489, 2.63107, 3.20371, 3.25464, 3.51379.

For $[\text{Pd}(\eta^n\text{-arene})(\text{C}_6\text{F}_5)_2]$ complexes **20**, **25**, **30** and **35** the overall reductive elimination process in all of the aromatic solvents is exergonic. In benzene, a reductive elimination barrier of only 20.4 kcal/mol (ΔG^\ddagger) was found for the first route (pathway A, Figure 3-9). This overall barrier, in comparison with that of the two routes for complexes that involve MeCN or THF solvent, is exceptionally low and can be readily overcome under the reaction conditions employed experimentally. The examination of a second route for reductive elimination led only to the observation of an elevated overall barrier of 29.8 kcal/mol (pathway B, Figure 3-9). Thus, due to the

disparity in the barriers, it can be suggested that reductive elimination *via* the first route is predominant for this reductive elimination process. The computed results for reductive elimination of the two mechanistic routes involving the solvents toluene, *m*-xylene, and perfluorobenzene are displayed in Figures 3-10, 3-11, and 3-12, respectively. The computed free energy profiles in toluene

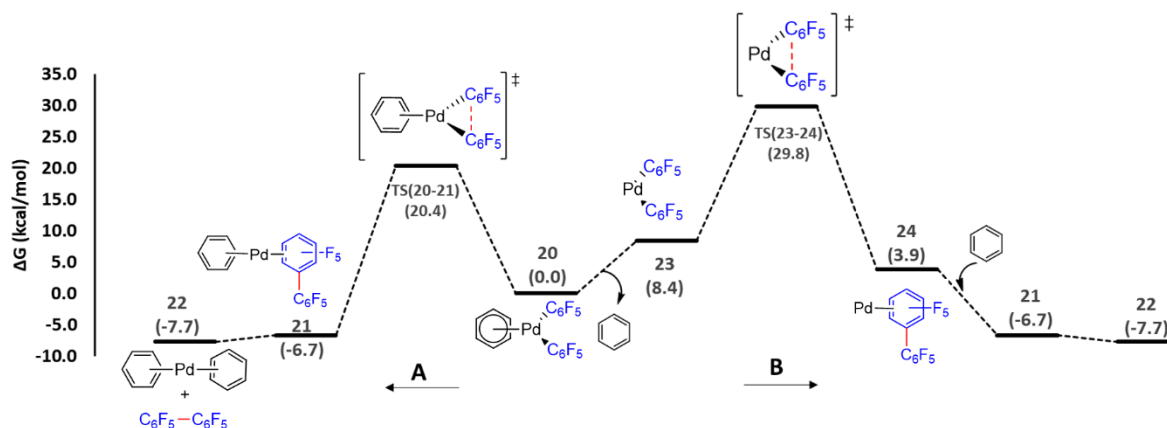


Figure 3-9. Computed mechanistic pathways (DFT, B3LYP-D3/TZVP) for the C–C reductive elimination step from the bis-perfluoroaryl complex ligated with benzene. Gibbs free energy values (kcal/mol) relative to reactant (**20**) are given in parentheses.

and *m*-xylene follow a similar trend to that in benzene. However, unlike in benzene, toluene and *m*-xylene, in perfluorobenzene the dissociation of the perfluorobenzene from the postulated reactant **35** was found to be exergonic. Therefore, the overall barriers for both mechanistic routes which were found to be similar to each other come from the dissociated $\text{Pd}(\text{C}_6\text{F}_5)_2$ complex **38**. As a result, both pathways might be possible. Despite the lowest reductive elimination barrier predicted in this solvent, catalytic experiments provided lower conversions in comparison with the outcomes of catalytic experiments carried out in other aromatic solvents in the same reaction times (Table 3-2, entry 2). Prolonging the reaction time did improve the desired outcome of this reaction and afforded the product in a good yield (75%). One reason for such a slow conversion may be the deactivation of the catalyst, possibly *via* oxidative addition of a C–F bond of the coordinated perfluorobenzene solvent after the reductive elimination step, or the poor ability of the oxidizing reagent Ag_2O to oxidize the electron-poor $\text{Pd}(0)$ complex **36** that has formed after the reductive elimination step. The computed barrier for a C–F oxidative addition process was found to be only 24.8 kcal/mol (TS(**36-40**), Figure 12), which is accessible under our reaction conditions. However, treating the *cis*-

[Pd(MeCN)₂(2,6-C₆F₂H₃)₂] complex (**3_3e**) in toluene with 3 equivalents of perfluorobenzene at 75 °C for a day did not show any indication of C-F oxidative addition to Pd(0) even though we obtained the coupled product **3_2e** in > 99% yield (see a test for the possibility of C-F oxidative addition in Scheme 3-6, section 3.3.4).

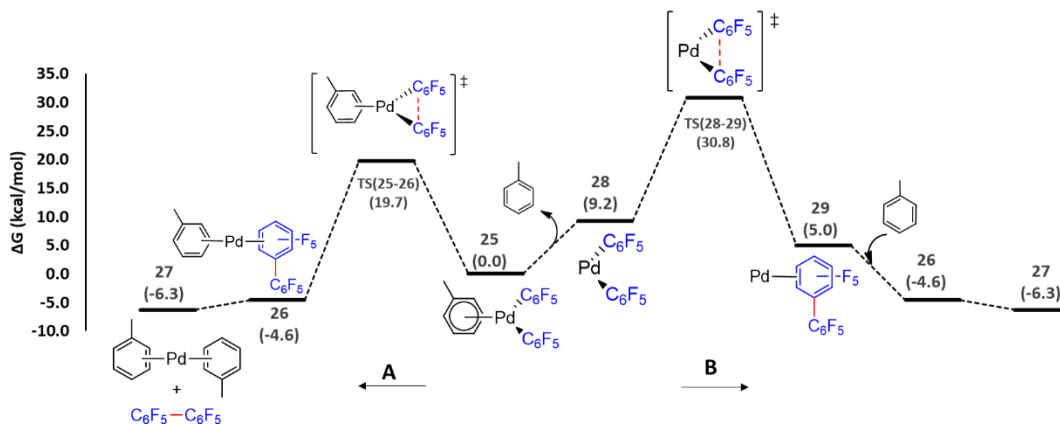


Figure 3-10. Computed mechanistic pathways (DFT, B3LYP-D3/TZVP) for the C–C reductive elimination step from the bis-perfluoroaryl complex ligated with toluene. Gibbs free energy values (kcal/mol) relative to reactant (**25**) are given in parentheses.

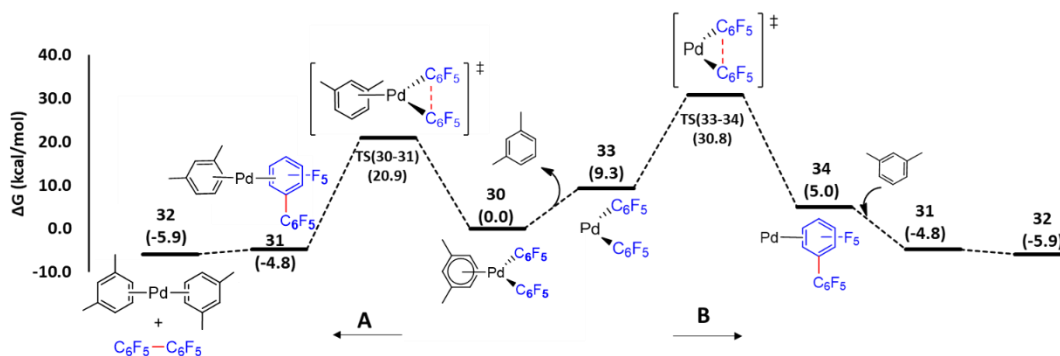


Figure 3-11. Computed mechanistic pathways (DFT, B3LYP-D3/TZVP) for the C–C reductive elimination step from the bis-perfluoroaryl complex ligated with *m*-xylene. Gibbs free energies (kcal/mol) relative to reactant (**30**) are given in parentheses.

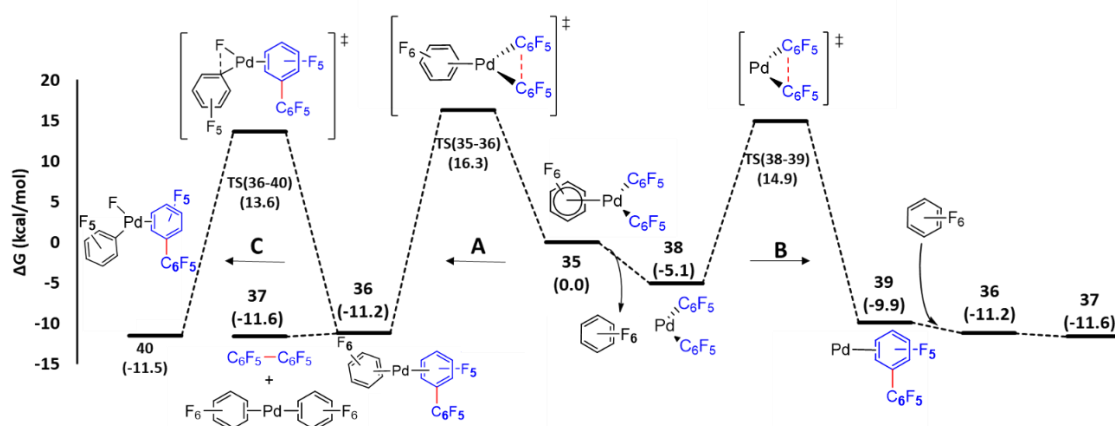


Figure 3-12. Computed mechanistic pathways (DFT, B3LYP-D3/TZVP) for the C–C reductive elimination step from the bis-perfluoroaryl complex ligated with perfluorobenzene and a possible mode of deactivation of the catalyst. Gibbs free energy values (kcal/mol) relative to reactant (**35**) are given in parentheses.

As the reductive elimination process generates a lone pair on the transition metal, the level of stabilization of this lone pair ($d_{x^2-y^2}$) was examined by analyzing the interactions between the ligands L_2 and η^n -Ar and the bent (C_{2v}) fragment $[Pd(C_6F_5)_2]$ of cis - $[PdL_2(C_6F_5)_2]$ ($L = MeCN, THF, SMe_2, PMe_3$) and $[Pd(\eta^6-Ar)(C_6F_5)_2]$ ($Ar = C_6H_6, C_7H_8, C_8H_{10}, C_6F_6$) and their corresponding reductive elimination transition states. Thus, EDA-NOCV calculations,^[33] performed at the B3LYP-D3/TZVP level of theory, offer detailed information on the interactions in terms of Pauli repulsion (ΔE_{Pauli}), attractive electrostatic interaction (ΔE_{elstat}) and orbital interaction (ΔE_{orb}) and also the attractive dispersion interaction (ΔE_{disp}) (Tables 3-7 and 3-8 in Section 3.6.2.1 Numerical results from EDA-NOCV analysis). More explanations of these terms are provided in the EDA-NOCV analysis section in Section 3.6.2 EDA-NOCV Analysis Results. Table 3-4 summarizes the results of our calculations. The contribution to the overall barrier by distortion energy ($\Delta\Delta E_{dist}$), which is the difference in energy penalty linked with the distortion of the interacting fragments from their equilibrium geometries to the frozen geometries of the reactant and transition state, was found to be similar in all cases with calculated $\Delta\Delta E_{dist}$ values between +12.9 and +19.4 kcal/mol (Table 3-4, column a). Therefore, the differences observed for the barriers of the reductive elimination step for different ligands can be explained by contributions from the intrinsic interaction energies ($\Delta E_{int} = \Delta E_{Pauli} + \Delta E_{elstat} + \Delta E_{orb} + \Delta E_{disp}$). The interaction energy ΔE_{int} (Table 3-4, column b) of the reactants

decreases in the order $[\text{Pd}(\text{PMe}_3)_2(\text{C}_6\text{F}_5)_2]$ **16** (-102.0 kcal/mol) > $[\text{Pd}(\text{SMe}_2)_2(\text{C}_6\text{F}_5)_2]$ **12** (-70.8 kcal/mol) > $[\text{Pd}(\text{THF})_2(\text{C}_6\text{F}_5)_2]$ **7** (-58.1 kcal/mol) > $[\text{Pd}(\text{MeCN})_2(\text{C}_6\text{F}_5)_2]$ **3_3a** (-55.3 kcal/mol) > $[\text{Pd}(\eta^n\text{-C}_8\text{H}_{10})(\text{C}_6\text{F}_5)_2]$ **30** (-32.6 kcal/mol) \approx $[\text{Pd}(\eta^n\text{-C}_7\text{H}_8)(\text{C}_6\text{F}_5)_2]$ **25** (-30.3 kcal/mol) \approx $[\text{Pd}(\eta^n\text{-C}_6\text{H}_6)(\text{C}_6\text{F}_5)_2]$ **20** (-27.4 kcal/mol) > $[\text{Pd}(\eta^n\text{-C}_6\text{F}_6)(\text{C}_6\text{F}_5)_2]$ **35** (-12.2 kcal/mol), which reflects the different behavior of the ligands.

ΔE_{int} was reduced significantly for *cis*- $[\text{PdL}_2(\text{C}_6\text{F}_5)_2]$ when moving from the reactant to the reductive elimination transition state as indicated by the differences $\Delta\Delta E_{\text{int}}$. The interaction energy term between the ligands L_2 and $[\text{Pd}(\text{C}_6\text{F}_5)_2]$ decreases for $\text{L} = \text{MeCN}$ (**3_3a**, $\Delta\Delta E_{\text{int}} = +19.9$ kcal/mol), THF (**7**, $\Delta\Delta E_{\text{int}} = +21.3$ kcal/mol), SMe_2 (**12**, $\Delta\Delta E_{\text{int}} = +18.7$ kcal/mol) and PMe_3 (**16**, $\Delta\Delta E_{\text{int}} = +25.0$ kcal/mol) (Table 3-4, column b), whereas $\Delta\Delta E_{\text{int}}$ remains almost constant for $[\text{Pd}(\eta^n\text{-Ar})(\text{C}_6\text{F}_5)_2]$ (+1.2 to +4.3 kcal/mol) and even increases for $[\text{Pd}(\eta^n\text{-C}_6\text{F}_6)(\text{C}_6\text{F}_5)_2]$ (-4.7 kcal/mol). A closer inspection of the sum of the electrostatic contributions $\Delta\Delta E_{\text{Pauli}}$ and $\Delta\Delta E_{\text{elstat}}$ reveals that it varies little and remains almost constant going from the ground state to the transition state. The sum of $\Delta\Delta E_{\text{Pauli}}$ and $\Delta\Delta E_{\text{elstat}}$ is +3.2 kcal/mol for $[\text{Pd}(\text{MeCN})_2(\text{C}_6\text{F}_5)_2]$, +4.8 kcal/mol for $[\text{Pd}(\text{THF})_2(\text{C}_6\text{F}_5)_2]$, +1.5 kcal/mol for $[\text{Pd}(\text{SMe}_2)_2(\text{C}_6\text{F}_5)_2]$, -1.4 kcal/mol for $[\text{Pd}(\text{C}_6\text{F}_5)_2(\text{PMe}_3)_2]$, -5.3 kcal/mol for $[\text{Pd}(\eta^n\text{-C}_6\text{H}_6)(\text{C}_6\text{F}_5)_2]$, -5.8 kcal/mol for $[\text{Pd}(\eta^n\text{-C}_7\text{H}_8)(\text{C}_6\text{F}_5)_2]$, -5.5 kcal/mol for $[\text{Pd}(\eta^n\text{-C}_8\text{H}_{10})(\text{C}_6\text{F}_5)_2]$, and -1.0 kcal/mol for $[\text{Pd}(\eta^n\text{-C}_6\text{F}_6)(\text{C}_6\text{F}_5)_2]$ (Table 3-4, columns d and e). The change in $\Delta\Delta E_{\text{int}}$ is mainly attributable to a change in the orbital interaction energies $\Delta\Delta E_{\text{orb}}$ on going from the ground state to the transition state (Table 3-4, column e).

Table 3-4. Results of EDA-NOCV analysis (B3LYP-D3/TZVP level of theory) on the interaction between the ligands L_2 and η^n -Ar and the bent fragment (C_{2v}) $[Pd(C_6F_5)_2]$ of various reactants $[Pd L_2(C_6F_5)_2]$ ($L = MeCN, THF, SMe_2, PMe_3$) and $[Pd(\eta^n-Ar)(C_6F_5)_2]$ ($Ar = C_6H_6, C_7H_8, C_8H_{10}, C_6F_6$) and their corresponding transition states of the reductive elimination of perfluorobiphenyl from these complexes.^[a]

L/Ar	(a) ΔE_{dist}	(b) ΔE_{int}	(c) ΔE_{Pauli}	(d) ΔE_{elstat}	(e) ΔE_{orb}	(f) ΔE_{σ}	(g) ΔE_{π}	(h) $\Delta E_{orb(rest)}$	(i) ΔE_{disp}
MeCN (3_3a)	1.2	-55.3	130.6	-117.1	-60.6	-41.7	-8.6	-10.3	-8.2
TS[(3_3a)-4]	17.5	-35.4	106.5	-89.8	-45.1	-21.1	-14.2	-9.9	-7.0
TS[(3_3a)-4]-(3_3a) ($\Delta\Delta E$)	16.3	19.9	-24.1	27.3	15.5	20.6	-5.6	0.4	1.2
THF (7)	1.8	-58.1	102.5	-95.6	-44.2	-29.1	– ^[b]	-15.3	-20.8
TS(7-8)	17.9	-36.8	80.0	-68.3	-27.8	-18.1	– ^[b]	-9.7	-20.7
TS(7-8)- 7 ($\Delta\Delta E$)	16.1	21.3	-22.5	27.3	16.4	11.0	–	5.6	0.1
SMe ₂ (12)	2.7	-70.8	162.7	-141.2	-70.6	-47.4	-3.9	-19.3	-21.7
TS(12-13)	17.8	-52.1	163.9	-141.0	-54.5	-37.7	-4.0	-12.8	-20.6
TS(12-13)- 12 ($\Delta\Delta E$)	15.1	18.7	1.2	0.3	16.1	9.7	-0.1	6.5	1.1
PMe ₃ (16)	5.6	-102.0	280.0	-250.1	-104.7	-79.2	-10.5	-15.0	-27.2
TS(16-17)	18.5	-77.0	281.1	-252.6	-81.4	-57.6	-11.9	-11.9	-24.1
TS(16-17)- 16 ($\Delta\Delta E$)	12.9	25.0	1.1	-2.5	23.2	21.6	-1.4	3.1	3.1
C ₆ H ₆ (20)	1.6	-27.4	64.5	-45.5	-35.0	-22.8	-3.0	-9.2	-11.3
TS(20-21)	19.2	-26.2	66.8	-53.1	-31.3	-14.2	-12.4	-4.7	-8.6
TS(20-21)- 20 ($\Delta\Delta E$)	17.6	1.2	2.3	-7.6	3.7	8.6	-9.4	4.5	2.7
C ₇ H ₈ (25)	1.8	-30.3	67.8	-48.5	-36.6	-23.4	-3.2	-10.0	-12.9
TS(25-26)	19.2	-27.5	68.0	-54.6	-31.8	-14.4	-12.5	-4.8	-9.2
TS(25-26)- 25 ($\Delta\Delta E$)	17.4	2.8	0.2	-6.0	4.8	9.0	-9.3	5.2	3.8
C ₈ H ₁₀ (30)	1.9	-32.6	69.1	-50.5	-37.6	-20.8	-3.3	-13.5	-13.6
TS(30-31)	19.1	-28.4	68.3	-55.2	-30.7	-14.1	-11.5	-5.0	-10.7
TS(30-31)- 30 ($\Delta\Delta E$)	17.2	4.3	-0.8	-4.7	6.9	6.7	-8.2	8.5	2.9
C ₆ F ₆ (35)	1.3	-12.2	53.6	-25.4	-28.9	-18.4	-2.1	-8.4	-11.6
TS(35-36)	20.7	-16.9	68.9	-41.5	-30.1	-9.7	-15.5	-4.8	-14.2
TS(35-36)- 35 ($\Delta\Delta E$)	19.4	-4.7	15.2	-16.2	-1.1	8.7	-13.4	3.6	-2.6

^[a] Energies are given in kcal/mol. ^[b] No π back-donation interaction was found. Details regarding the derivation of different orbital interaction components (ΔE_{σ} , ΔE_{π} and $\Delta E_{orb(rest)}$) from the EDA-NOCV analysis are provided in Section 3.6.

The orbital interactions (ΔE_{orb}) in our systems are comprised of three different components: (i) σ donation interaction (ΔE_{σ}) from neutral ligand(s) to the $Pd(Ar_F)_2$ fragment (Table 3-4, column f); (ii) π back-donation interaction (ΔE_{π}) from the $Pd(Ar_F)_2$ fragment to neutral ligand(s) (Table 3-4, column g); and (iii) the rest of the orbital interactions ($\Delta E_{orb(rest)}$), which mostly entails the electronic polarization within each fragment. The difference in the orbital interactions $\Delta\Delta E_{orb}$ of *cis*-

[PdL₂(C₆F₅)₂] is +15.5 kcal/mol for L = MeCN, +16.4 kcal/mol for L = THF, +16.1 kcal/mol for L = SMe₂ and +23.2 kcal/mol for L = PMe₃ (Table 4, column e). This significant reduction in ΔE_{orb} in the transition states is mainly attributable to a decreased σ -interaction (Table 4, column f): MeCN (**3_3a**, $\Delta\Delta E_{\sigma} = +20.6$ kcal/mol), THF (**7**, $\Delta\Delta E_{\sigma} = +11.0$ kcal/mol), SMe₂ (**12**, $\Delta\Delta E_{\sigma} = +9.7$ kcal/mol) and PMe₃ (**16**, $\Delta\Delta E_{\sigma} = +21.6$ kcal/mol). $\Delta\Delta E_{\text{orb}}$ increases by only a small amount (-1.1 – +6.9 kcal/mol) for [Pd(η^n -Ar)(C₆F₅)₂], as a result of the ring slippage and an increase in π -acceptance in the transition state, as the π -contribution becomes favorable by -9.4 kcal/mol for [Pd(η^n -C₆H₆)(C₆F₅)₂], -9.3 kcal/mol for [Pd(η^n -C₇H₈)(C₆F₅)₂], -8.2 kcal/mol for [Pd(η^n -C₈H₁₀)(C₆F₅)₂], and -13.4 kcal/mol for [Pd(η^n -C₆F₆)(C₆F₅)₂] (Table 3-4, columns e and g). Although the difference in orbital contributions $\Delta\Delta E_{\text{orb}}$ in all cases can be explained using mainly the contributions from σ donation ($\Delta\Delta E_{\sigma}$) and π back-donation ($\Delta\Delta E_{\pi}$) interactions, impact from the rest of the orbital interactions ($\Delta\Delta E_{\text{orb}(\text{rest})}$) is also sizable (Table 3-4, column h), suggesting that there exist considerable polarization effects. The attractive energy contribution due to dispersion interactions, which arises from the attractive forces between the induced dipoles of the interacting fragments, in both reactant and transition state of all cases was found to be substantial albeit slightly less pronounced in the transition states (Table 3-4, column i). This contribution to the overall barrier is contained in ΔE_{int} . Changes in the dispersion interaction $\Delta\Delta E_{\text{disp}}$ play only a minor role in the increase in the reductive elimination barrier, as the maximum difference between reactant and transition state is only +3.8 kcal/mol (Table 3-4, column i).

According to our calculations, the lower barrier for the complexes [Pd(η^n -Ar)(C₆F₅)₂] is due to: (i) ring slippage of the arene ligand and the adjustment of the arene ring to the electronic situation at the metal, which leads to less σ -repulsion in the reductive elimination transition state; and (ii) more favorable π back-bonding from Pd(Ar)₂ to the arene fragment in the transition state. These factors lead to a lower lying transition state for [Pd(η^n -Ar)(C₆F₅)₂]. Furthermore, the 2e⁻ donor ligands of [PdL₂(C₆F₅)₂] stabilize the ground state much better than η^n -Ar ligand in [Pd(η^n -Ar)(C₆F₅)₂] and both factors, destabilization of the ground state of Pd(C₆F₅)₂ and stabilization of the

reductive elimination transition state of $\text{Pd}(\text{C}_6\text{F}_5)_2$ for $\eta^1\text{-Ar}$ in comparison to L, lead to a significantly reduced barrier for reductive elimination.

Overall, insights gained into the bonding interactions between various ligands and the $\text{Pd}(\text{Ar}_F)_2$ fragment using the EDA-NOCV method suggest that it is the weakly donating and strongly accepting characters of arene ligands that minimize the reductive elimination barrier compared to stronger donor and weaker acceptor ligands L. Ligands such as MeCN, THF, SMe_2 and PMe_3 stabilize the (electron poor) Pd(II) ground state more efficiently than an arene ligand, whereas the arenes stabilize the developing charge in the transition state better than L. Both destabilization of the ground state and stabilization of the transition state by arene ligands lead to lower barriers for the reductive elimination process.

3.3.4 Catalytic Cycle of the Homocoupling Reaction

A plausible mechanism for the homocoupling reaction of fluorinated aryl boronates conducted in arene solvent is depicted in Figure 3-13. Ag_2O likely plays two roles. First, in the presence of trace moisture, it assists in the transmetalation process,^[5b,20c] generating species C and two equivalents of HOBpin. The latter can condense yielding pinBOBpin, regenerating water. Second, following reductive elimination of the product biaryl from C, Ag_2O oxidizes Pd(0) to Pd(II) to restart the cycle. Indeed, a silver mirror forms during the reaction.

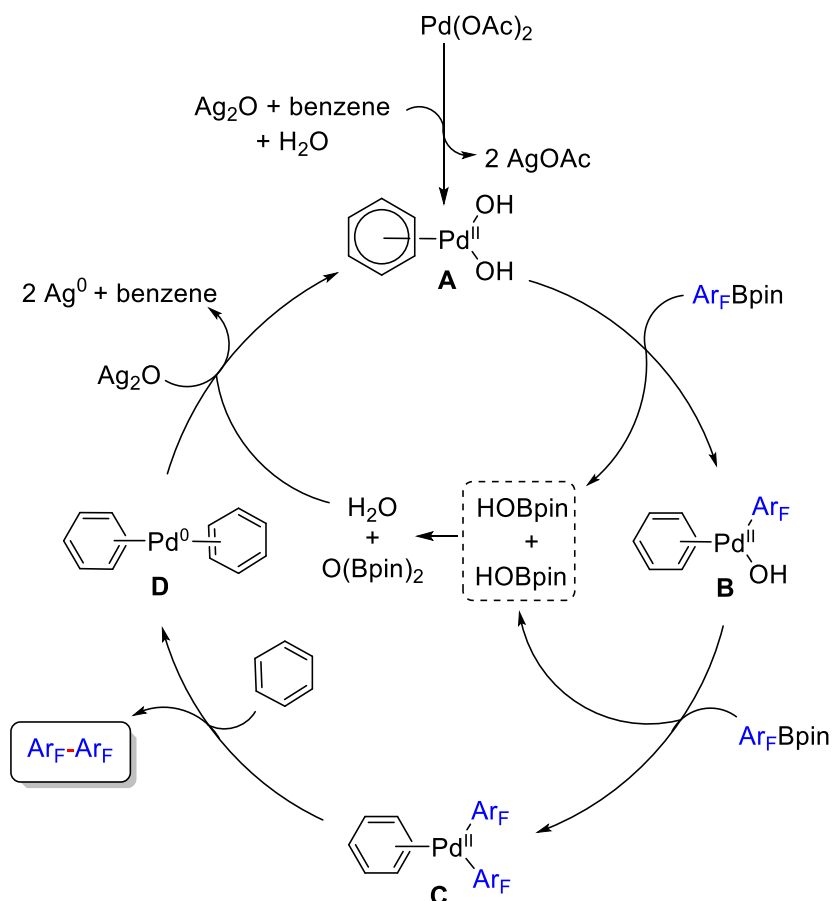


Figure 3-13. Proposed mechanism for the palladium-catalyzed homocoupling of fluorinated aryl boronates.

3.4 Conclusions

In summary, we demonstrated that the palladium-catalyzed homocoupling of highly fluorinated aryl-boronate esters containing two *ortho*-fluorine substituents does not proceed in coordinating solvents because the reaction stalls at the *cis*- $[\text{PdL}_2(\text{Ar}_F)_2]$ stage, as demonstrated by the isolation of the stable complexes *cis*- $[\text{Pd}(\text{MeCN})_2(\text{C}_6\text{F}_5)_2]$ (**3_3a**), *cis*- $[\text{Pd}(\text{MeCN})_2(2,4,6\text{-C}_6\text{F}_3\text{H}_2)_2]$ (**3_3b**), and *cis*- $[\text{Pd}(\text{MeCN})_2(2,6\text{-C}_6\text{F}_2\text{H}_3)_2]$ (**3_3e**). This investigation also introduces the use of aryl boronates instead of aryl Grignard or lithium substrates^[3,9] to synthesize $[\text{PdL}_2(\text{Ar}_F)_2]$ complexes. Avoiding ligands and employing very weakly coordinating solvents (“non-coordinating”) such as toluene, benzene or *m*-xylene allows the catalytic homocoupling reaction to proceed smoothly, providing fluorinated biphenyl products.

DFT computations predict that catalytic homocoupling reactions of highly fluorinated aryl boronate esters conducted in acetonitrile, THF, SMe_2 and PMe_3 are unfeasible, as the overall reductive elimination process is endergonic, and the reductive elimination step has a high barrier. While this is the case with strong σ donating solvents and ligands, computations indicate that coupling reactions carried out in aromatic solvents, which are, in general, weak σ donors and π acceptors, should be highly feasible, as the reductive elimination process is not only sufficiently exergonic, but also the overall barrier for reductive elimination was found to be < 21 kcal/mol. The lower barrier for the reductive elimination from $[(\eta^{\text{Ar}}\text{-Ar})\text{Pd}(\text{C}_6\text{F}_5)_2]$ is due to: (i) ring slippage of the arene ligand and the adjustment of the arene ring to the electronic situation at the metal which leads to less σ -repulsion in the reductive elimination transition state; and (ii) more favorable π back-bonding from $\text{Pd}(\text{Ar}_F)_2$ to the arene fragment in the transition state. Inspection of the reaction coordinates of the homocoupling process conducted in different solvents nicely explains our experimental results which showed that no catalysis takes place in acetonitrile and THF solvents, whereas catalytic homocoupling is efficient in aromatic solvents.

3.5 Detailed Experiments and Characterization Data

3.5.1 General Information

Unless otherwise noted, all reagents were purchased from Alfa-Aesar, Sigma-Aldrich, ABCR, VWR, Fluorochem or Acros, and were checked for purity by GC-MS and/or ^1H NMR spectroscopy and used as received. B_2pin_2 was kindly provided by AllyChem Co. Ltd. (Dalian, China). Acetonitrile (Honeywell, HPLC grade), triethylamine (Aldrich, $\geq 99.5\%$), tetrahydrofuran (Carl Roth, HPLC grade), dimethyl sulfoxide (Acros, $\geq 99.8\%$), dimethylformamide (VWR, HPLC grade), benzene (Honeywell, ACS Reagent grade), hexafluorobenzene (Fluorochem, $\geq 97\%$), *m*-xylene (Acros, $\geq 99\%$), and toluene (VWR, ACS Reagent grade) were used as received and were not dried.

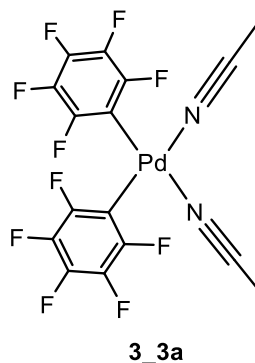
Automated flash chromatography was performed using silica gel (Biotage SNAP cartridge KP-Sil 10 g and KP-Sil 25 g) using a Biotage® Isolera Four system. Commercially available,

precoated TLC plates (Polygram® Sil G/UV254) were purchased from Machery-Nagel. The removal of solvent was performed on a rotary evaporator *in vacuo* at a maximum temperature of 30 °C.

GC-MS analyses were performed using an Agilent 7890A gas chromatograph (column: HP-5MS 5% phenylmethylsiloxane, 10 m, Ø 0.25 mm, film 0.25 µm; injector: 250 °C; oven: 40 °C (2 min), 40 °C to 280 °C (20 °C·min⁻¹); carrier gas: He (1.2 mL min⁻¹) equipped with an Agilent 5975C inert MSD with triple-axis detector operating in EI mode and an Agilent 7693A series auto sampler/injector. HRMS analyses were performed using a Thermo Fischer Scientific Exactive Plus Orbitrap MS system (APCI and ASAP probe). Infrared spectra were recorded on a Nicolet 380 FT-IR spectrometer as solids, using an ATR unit, and are reported in cm⁻¹. Elemental analyses were performed on a LECO CHNS-932 Elemental Analyzer.

All NMR spectra were recorded at 298 K using a Bruker Avance I 500 (¹H NMR, 500 MHz; ¹³C{¹H} NMR, 125 MHz; ¹³C{¹⁹F} NMR, 125 MHz; ¹⁹F NMR, 470 MHz), a Bruker DRX-300 (¹H, 300 MHz; ¹¹B{¹H}, 96 MHz), or a Bruker Avance Neo (¹³C{¹H} NMR, 101 MHz; ¹⁹F{¹H} NMR, 376 MHz) spectrometer. ¹H NMR chemical shifts are reported relative to TMS and were referenced *via* residual proton resonances of the corresponding deuterated solvent (CDCl₃: 7.26 ppm; C₆D₆: 7.16 ppm; CD₃CN: 1.94; DMSO-*d*₆: 2.50 ppm), ¹³C{¹H} NMR and ¹³C{¹⁹F} NMR spectra are reported relative to TMS *via* the carbon signals of the deuterated solvent (CDCl₃: 77.16 ppm; C₆D₆: 128.06 ppm; CD₃CN: 1.32 ppm, 118.26 ppm; DMSO-*d*₆: 39.52 ppm), ¹⁹F NMR and ¹⁹F{¹H} spectra are reported relative to external CFCl₃, and ¹¹B{¹H} NMR chemical shifts are quoted relative to BF₃·Et₂O as external standard.

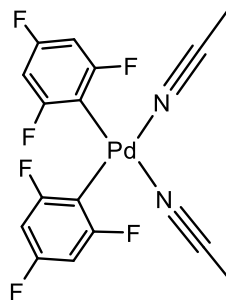
3.5.2 Synthesis of *cis*-[Pd(MeCN)₂(C₆F₅)₂] (**3_3a**)



In air, into a dried vial containing 4 mL of MeCN solvent and equipped with a stirring bar was added Pd(OAc)₂ (90 mg, 0.40 mmol) and the mixture was stirred until homogenous. Then, C₆F₅Bpin (**3_1a**) (353 mg, 1.2 mmol) or C₆F₅H (672 mg, 4 mmol) and Ag₂O (371 mg, 1.60 mmol) were added to the solution and the vial was sealed. The suspension was then stirred at 60 °C for 16 h. After cooling to room temperature, the resulting mixture was filtered through a pad of Celite. The solution was evaporated to dryness under reduced pressure at 30 °C and the residue was diluted with Et₂O:DCM (1:1). The resulting precipitate was collected by filtration and washed with Et₂O:DCM (1:1), hexane, and air-dried to give the product as a brownish-white solid (157 mg, 75%, *via* C₆F₅Bpin), (157 mg, 74%, *via* C₆F₅H). Colorless single crystals suitable for X-ray diffraction were grown *via* vapor diffusion of CD₃CN/Et₂O solutions placed in a larger vessel containing toluene at room temperature.

¹H NMR (500 MHz, DMSO-*d*₆) δ = 2.07 (*s*, 6H, CH₃CN); ¹³C{¹H} NMR (125 MHz, DMSO-*d*₆) δ = 146.9 (*dm*, ¹J_{H-C} = 226 Hz, C_{arom}-F_o), 136.8 (*dm*, ¹J_{H-C} = 212 Hz, C_{arom}-F_p), 135.0 (*dm*, ¹J_{H-C} = 240 Hz, C_{arom}-F_m), 118.1 (CH₃CN), 1.2 (CH₃CN); ¹³C{¹⁹F} NMR (125 MHz, DMSO-*d*₆, for C₆F₅) δ = 146.9 (C_{arom}-F_o), 136.8 (C_{arom}-F_p), 135.0 (C_{arom}-F_m) 118.1 (*m*, CH₃CN), 1.2 (*q*, ¹J_{H-C} = 136 Hz, CH₃CN); the chemical shift of C_{arom}-Pd can be seen clearly in CD₃CN; ¹³C{¹⁹F} NMR (125 MHz, CD₃CN, for C₆F₅) δ = 148.4 (C_{arom}-F_o), 138.3 (C_{arom}-F_p), 136.6 (C_{arom}-F_m), 109.4 (C_{arom}-Pd), the chemical shifts of CH₃CN overlapped with those of CD₃CN; ¹⁹F{¹H} NMR (376 MHz, CD₃CN) δ = -166.1 – -165.9 (*m*, 4F_m), -162.9 (*t*, ³J_{F-F} = 19 Hz, 2F_p), -117.7 – -117.6 (*m*, 4F_o); **Mp**: 163 °C dec.; **Anal. Calcd** for C₁₆H₆F₁₀N₂Pd: C, 36.77; H, 1.16; N, 5.36. Found: C, 36.93; H, 1.44; N, 5.59; **IR** (ATR [cm⁻¹]) = 2331 (ν_{CN}), 2304 (ν_{CN}).

3.5.3 Synthesis of *cis*-[Pd(MeCN)₂(2,4,6-C₆F₃H₂)₂] (**3_3b**)

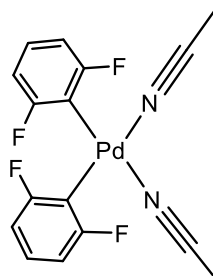
**3_3b**

In air, into a dried vial containing 4 mL of MeCN solvent and equipped with a stirring bar was added Pd(OAc)₂ (90 mg, 0.40 mmol) and the mixture was stirred until homogeneous. Then, 2,4,6-trifluorophenyl-Bpin (**3_1b**) (310 mg, 1.20 mmol) and Ag₂O (371 mg, 1.60 mmol) were added to the solution and the vial was sealed. The suspension was then stirred at 60 °C for 16 h. After cooling to room temperature, the resulting mixture was filtered through a pad of Celite. The solution was evaporated to dryness under reduced pressure at 30 °C and the residue was diluted with Et₂O:DCM (1:1) and the resulting precipitate was collected *via* filtration to give a pale yellow solution. This was concentrated, and addition of hexane precipitated a yellow solid, which was collected by filtration, washed with hexane, and air-dried to give a pale yellow solid (144 mg, 80%). Colorless single crystals suitable for X-ray diffraction were grown *via* vapor diffusion of Et₂O solutions placed in a larger vessel containing hexane at room temperature.

¹H NMR (300 MHz, CDCl₃) δ = 6.31 (*q*, ³J_{H-F} = 5 Hz, 2H, C_{arom}-H), 2.14 (*s*, 6H, CH₃CN); ¹³C{¹H} NMR (125 MHz, DMSO-*d*₆) δ = 165.2 (*dm*, ¹J_{F-C} = 230.8 Hz, C_{arom}-F_o), 160.6 (*dm*, ¹J_{F-C} = 237.8 Hz, C_{arom}-F_p) 118.1 (*m*, CH₃CN), 98.4 (*dd*, ²J_{F-C} = 38 Hz, ²J_{F-C} = 24 Hz, C_{arom}-H), 1.2 (CH₃CN); ¹³C{¹⁹F} NMR (125 MHz, DMSO-*d*₆) δ = 165.2 (*m*, C_{arom}-F_o), 160.5 (*t*, ²J_{H-C} = 6 Hz, C_{arom}-F_p), 118.1 (*m*, CH₃CN), 98.4 (*d*, ¹J_{H-C} = 166 Hz, ³J_{H-C} = 4 Hz, C_{arom}-H), 1.1 (*q*, ¹J_{H-C} = 136 Hz, CH₃CN); the chemical shift of C_{arom}-Pd can be seen clearly in CDCl₃; ¹³C{¹⁹F} NMR (125 MHz, CDCl₃) δ = 165.9 (*m*, C_{arom}-F_o), 161.1 (*t*, ²J_{H-C} = 6 Hz, C_{arom}-F_p), 117.4 (*m*, CH₃CN), 106.3 (C_{arom}-Pd), 98.2 (*dd*, ¹J_{H-C} = 165 Hz, ³J_{H-C} = 4 Hz, C_{arom}-H), 2.9 (*q*, ¹J_{H-C} = 146 Hz, CH₃CN); ¹⁹F{¹H} NMR (376 MHz, CD₃CN) δ = -119.8 – -119.7 (*m*, 2F_p), -86.3 – -86.2 (*m*, ⁴J_{F-F} = 3 Hz, 4F_o); **Mp**: 133 °C dec.; **Anal. Calcd** for

$C_{16}H_{10}F_6N_2Pd$: C, 42.64; H, 2.24; N, 6.22. Found: C, 42.25; H, 2.22; N, 6.22; **IR** (ATR [cm^{-1}]): 2324 (ν_{CN}), 2230 (ν_{CN}).

3.5.4 Synthesis of *cis*-[Pd(MeCN)₂(2,6-C₆F₂H₃)₂] (**3_3e**)



3_3e

In air, into a dried vial containing 4 mL of MeCN solvent and equipped with a stirring bar was added Pd(OAc)₂ (90 mg, 0.40 mmol) and the mixture was stirred until homogenous. Then, 2,6-difluorophenylboronic acid pinacol ester (**3_1e**) (288 mg, 1.20 mmol), and Ag₂O (371 mg, 1.60 mmol) were added to the solution and the vial was sealed. The suspension was then stirred at 60 °C for 16 h. After cooling to room temperature, the resulting mixture was filtered through a pad of Celite. The solution was evaporated to dryness under reduced pressure at 30 °C and the residue was diluted with Et₂O:DCM (1:1). The resulting precipitate was collected by filtration and washed with Et₂O:DCM (1:1), hexane, and air-dried to give the product as a yellowish-white solid (155 mg, 93%). Colorless single crystals suitable for X-ray diffraction were grown *via* vapor diffusion of CD₃CN/Et₂O solutions placed in a larger vessel containing toluene at room temperature.

¹H NMR (300 MHz, DMSO-*d*₆) δ = 6.96 – 6.86 (*m*, 2H, C_{arom}-H_p), 6.57 – 6.53 (*dd*, ³*J*_{H-H} = 8 Hz, ³*J*_{H-F} = 6 Hz, 4H, C_{arom}-H_m), 2.07 (*s*, 6H, CH₃CN); **¹³C{¹H} NMR** (101 MHz, DMSO-*d*₆) δ = 126.2 (C_{arom}-H_p), 118.1 (CH₃CN), 1.1 (CH₃CN); due to low solubility in DMSO-*d*₆, the chemical shifts of C_{arom}-F and C_{arom}-Pd bonds were not detected, but it can be seen clearly in CD₃CN; **¹³C{¹H} NMR** (101 MHz, CD₃CN) δ = 167.8 (*dm*, ¹*J*_{F-C} = 231 Hz, C_{arom}-F), 126.5 (*m*, C_{arom}-H_p), 114.6 (C_{arom}-Pd), 110.0 (*d*, ²*J*_{F-C} = 33 Hz, C_{arom}-H_m), the chemical shifts of CH₃CN overlapped with those of CD₃CN; **¹³C{¹⁹F} NMR** (126 MHz, CD₃CN) δ = 167.7 (*dm*, ²*J*_{H-C} = 13 Hz, C_{arom}-F), 126.5 (*d*, ¹*J*_{H-C} = 162 Hz, C_{arom}-H_p), 114.6 (C_{arom}-Pd), 110.0 (*dd*, ¹*J*_{H-C} = 161 Hz, ²*J*_{H-C} = 9 Hz, C_{arom}-H_m), the chemical shifts

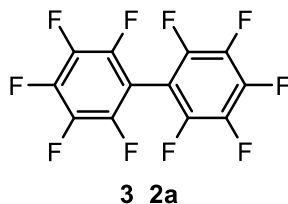
of CH₃CN overlapped with those of CD₃CN; ¹⁹F{¹H} NMR (376 MHz, CD₃CN) δ = -88.5 (*s*, 4F_o); **Mp**: 129 °C dec.; **Anal. Calcd** for C₁₆H₁₂F₄N₂Pd: C, 46.34; H, 2.92; N, 6.76. Found: C, 46.02; H, 2.89; N, 6.62. **IR** (ATR [cm⁻¹]): 2322 (ν_{CN}), 2294 (ν_{CN}).

3.5.5 General Procedure for Homocoupling of Fluorinated Aryl Boronic Acid Pinacol Esters (ArF_n-Bpin)

In air, into a dried vial that was equipped with a stirring bar contained 1.5 mL of toluene, was added the corresponding ArF_n-Bpin (0.6 mmol), Pd(OAc)₂ (3 mg, 0.012 mmol, 2 mol%), and Ag₂O (139 mg, 0.60 mmol, 1 equiv). After sealing the vial, the suspension was stirred for 5 h at 75 °C. After cooling to room temperature, the solvent was evaporated *in vacuo* and the residue was purified by flash column chromatography on silica gel (hexane) to obtain the corresponding product.

3.5.6 Experimental Procedures and Characterization of Products

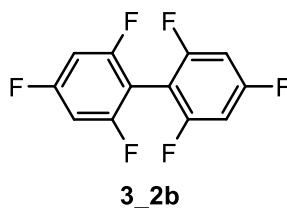
Synthesis of perfluorobiphenyl (3_2a)



Compound **3_2a** was synthesized following the general procedure and using the following chemicals and conditions: C₆F₅Bpin (**3_1a**) (176 mg, 0.60 mmol), Pd(OAc)₂ (3 mg, 0.012 mmol, 2 mol%), Ag₂O (139 mg, 0.60 mmol, 1 equiv), and toluene (1.5 mL), 75 °C, 5 h. After flash column chromatography (hexane), product **3_2a** was obtained as a white solid (97 mg, 97%).

¹³C{¹⁹F} NMR (125 MHz, CDCl₃) δ = 144.8 (C_{arom}-F_o), 142.8 (C_{arom}-F_p), 138.1 (C_{arom}-F_m), 101.7 (C_{arom}-C_{arom}); ¹⁹F{¹H} NMR (376 MHz, CDCl₃) δ = -160.3 – -160.2 (*m*, 4F_m), -149.7 (*tm*, ³J_{F-F} = 21 Hz, 2F_p), -137.4 – -137.3 (*m*, 4F_o); **GC-MS**: [t = 6.492 min] m/z: 334 [M]⁺; **HRMS (APCI)** calcd for C₁₂F₁₀ [M]⁺: 333.9835; found: 333.9825. Spectroscopic data matched those in the literature.^[35]

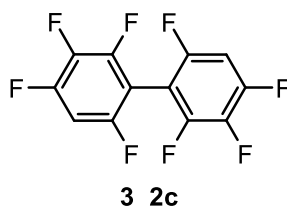
Synthesis of 2,2',4,4',6,6'-hexafluorobiphenyl (**3_2b**)



Compound **3_2b** was synthesized following the general procedure and using the following chemicals and conditions: 2,4,6-trifluorophenylboronic acid pinacol ester (**3_1b**) (155 mg, 0.60 mmol), Pd(OAc)₂ (3 mg, 0.012 mmol, 2 mol%), Ag₂O (139 mg, 0.6 mmol, 1 equiv), and toluene (1.5 mL), 75 °C, 5 h. After flash column chromatography (hexane), product **3_2b** was obtained as a white solid (75 mg, 96%).

¹H NMR (300 MHz, C₆D₆) δ = 6.32 – 6.22 (*m*, 4H, C_{arom}-H_m); ¹³C{¹H} NMR (125 MHz, CDCl₃) δ = 163.6 (*dt*, ¹J_{F-C} = 251 Hz, ³J_{F-C} = 15 Hz, C_{arom}-F_p), 160.9 (*dm*, ¹J_{F-C} = 251 Hz, C_{arom}-F_o), 102.4 (*m*, C_{arom}-C_{arom}), 100.7 (*m*, C_{arom}-H_m); ³C{¹⁹F} NMR (125 MHz, CDCl₃) δ = 163.6 (*t*, ²J_{H-C} = 6 Hz, C_{arom}-F_p), 160.9 (*t*, ²J_{H-C} = 3 Hz, C_{arom}-F_o), 102.4 (*tt*, ³J_{H-C} = 5 Hz, ⁴J_{H-C} = 1 Hz, C_{arom}-C_{arom}), 100.7 (*dd*, ¹J_{H-C} = 169 Hz, ³J_{H-C} = 4 Hz, C_{arom}-H_m); ¹⁹F{¹H} NMR (376 MHz, CDCl₃) δ = -107.4 – -107.3 (*m*, 4F_o), -106.1 – -106.0 (*m*, 2F_p); **GC-MS**: [t = 4.520 min] m/z: 262 [M]⁺; **HRMS (APCI)** calcd for C₁₂H₃F₆ [M-H]⁻: 261.0144; found: 261.0146. Spectroscopic data matched those in the literature.^[35]

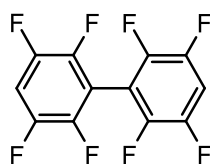
Synthesis of 2,2',3,3',4,4',6,6'-octafluorobiphenyl (**3_2c**)



Compound **3_2c** was synthesized following general procedure and using following chemicals and conditions: 2,3,4,6-tetrafluorophenylboronic acid pinacol ester (**3_1c**) (179 mg, 0.60 mmol), Pd(OAc)₂ (3 mg, 0.012 mmol, 2 mol%), Ag₂O (139 mg, 0.6 mmol, 1 equiv), and toluene (1.5 mL), 75 °C, 5 h. After column chromatography (hexane) product **3_2c** was obtained as colorless oil (83 mg, 93%).

$^1\text{H NMR}$ (500 MHz, CDCl_3) $\delta = 6.96 - 6.91$ (*m*, 2H, $\text{C}_{\text{arom-H}_m}$); $^{13}\text{C}\{^1\text{H}\}$ NMR (125 MHz, CDCl_3) $\delta = 101.4$ (*m*, $\text{C}_{\text{arom-H}_m}$), chemical shifts of C-F bonds were not detected (but see $^{13}\text{C}\{^{19}\text{F}\}$ NMR spectra below); $^{13}\text{C}\{^{19}\text{F}\}$ NMR (125 MHz, CDCl_3) $\delta = 154.9$ (*d*, $^2J_{\text{H-C}} = 7$ Hz, $\text{C}_{\text{arom-F}_o}$ '), 151.9 (*d*, $^2J_{\text{H-C}} = 7$ Hz, $\text{C}_{\text{arom-F}_p}$), 149.5 ($\text{C}_{\text{arom-F}_o}$), 137.6 (*d*, $^3J_{\text{H-C}} = 7$ Hz, $\text{C}_{\text{arom-F}_m}$), 102.7 (*d*, $^3J_{\text{H-C}} = 6$ Hz, $\text{C}_{\text{arom-C}_{\text{arom}}}$), 101.4 (*d*, $^1J_{\text{H-C}} = 170$ Hz, $\text{C}_{\text{arom-H}_m}$); $^{19}\text{F}\{^1\text{H}\}$ NMR (376 MHz, CDCl_3) $\delta = -163.9 - -163.7$ (*m*, 2F_m), $-130.4 - -130.3$ (*m*, 2F_o), -128.9 (*dm*, $^3J_{\text{F-F}} = 23$ Hz, 2F_p), $-113.7 - -113.6$ (*m*, $2\text{F}_o'$); **GC-MS**: [t = 6.860 min] m/z: 298 [M] $^+$; **HRMS (APCI)** calcd for $\text{C}_{12}\text{H}_1\text{F}_8$ [$M\text{-H}$] $^-$: 296.9956; found: 296.9956. Spectroscopic data matched those in the literature.^[36]

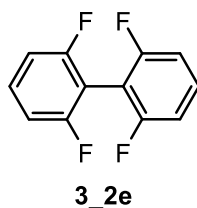
Synthesis of 2,2',3,3',5,5',6,6'-octafluorobiphenyl (**3_2d**)



3_2d

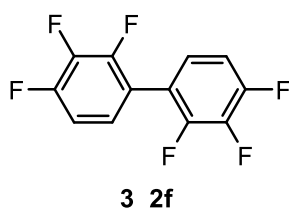
Compound **3_2d** was synthesized following general procedure and using following chemicals and conditions: 2,3,5,6-tetrafluorophenylboronic acid pinacol ester (**3_1d**) (179 mg, 0.6 mmol), $\text{Pd}(\text{OAc})_2$ (3 mg, 0.012 mmol, 2 mol%), Ag_2O (139 mg, 0.6 mmol, 1 equiv), and toluene (1.5 mL), 75 °C, 5 h. After flash column chromatography (hexane) product **3_2d** was obtained as white solid (86 mg, 97%). White colorless single crystals suitable for X-ray diffraction were obtained by slow evaporation of a hexane solution at ambient temperature.

$^1\text{H NMR}$ (500 MHz, C_6D_6) $\delta = 6.10 - 6.16$ (*m*, 2H, $\text{C}_{\text{arom-H}_p}$); $^{13}\text{C}\{^1\text{H}\}$ NMR (125 MHz, C_6D_6) $\delta = 146.1$ (*dm*, $^1J_{\text{F-C}} = 240$ MHz, $\text{C}_{\text{arom-F}_o}$), 144.2 (*dm*, $^1J_{\text{F-C}} = 245$ MHz, $\text{C}_{\text{arom-F}_p}$), 108.0 (*t*, $^1J_{\text{F-C}} = 23$ Hz, $\text{C}_{\text{arom-H}_p}$); $^{13}\text{C}\{^{19}\text{F}\}$ NMR (125 MHz, C_6D_6) $\delta = 146.1$ (*d*, $^3J_{\text{H-C}} = 7$ Hz, $\text{C}_{\text{arom-F}_o}$), 144.2 (*d*, $^2J_{\text{H-C}} = 9$ Hz, $\text{C}_{\text{arom-F}_m}$), 108.0 (*d*, $^1J_{\text{H-C}} = 108$ Hz, $\text{C}_{\text{arom-H}_p}$), 107.9 (*d*, $^4J_{\text{H-C}} = 1$ Hz); $^{19}\text{F}\{^1\text{H}\}$ NMR (376 MHz, C_6D_6) $\delta = -139.2 - -139.1$ (*m*, 4F_o), $-137.8 - -137.7$ (*m*, 4F_m); **GC-MS**: [t = 7.157 min] m/z: 298 [M] $^+$; **HRMS (APCI)** calcd for $\text{C}_{12}\text{H}_2\text{F}_8$ [M] $^+$: 298.0023; found: 298.0015. Spectroscopic data matched those in the literature.^[37]

Synthesis of 2,2',6,6'-tetrafluorobiphenyl (3_2e)

Compound **3-2e** was synthesized following general procedure and using following chemicals and conditions: 2,6-difluorophenylboronic acid pinacol ester (**3_1e**) (136 mg, 0.60 mmol), Pd(OAc)₂ (3 mg, 0.012 mmol, 2 mol%), Ag₂O (139.04 mg, 0.6 mmol), and toluene (1.5 mL), 75 °C, 5 h. After flash column chromatography (hexane) product **3_2e** was obtained as colorless oil (61 mg, 90%).

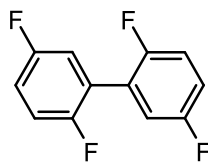
¹H NMR (500 MHz, CDCl₃) δ = 7.43 – 7.38 (*m*, 2H, C_{arom}-H_p), 7.04 – 7.01 (*m*, 4H, C_{arom}-H_m); ¹³C{¹H} NMR (125 MHz, CDCl₃) δ = 160.7 (*dm*, ¹J_{F-C} = 252 Hz, C_{arom}-F_o), 131.0 – 130.9 (*m*, C_{arom}-H_p), 111.7 – 111.4 (*m*, C_{arom}-H_m), 106.8 (*t*, ²J_{F-C} = 21 Hz, C_{arom}-C_{arom}); ¹³C{¹⁹F} NMR (125 MHz, CDCl₃) δ = 160.7 (*dm*, ²J_{H-C} = 13 Hz, C_{arom}-F_o), 131.0 (*d*, ¹J_{H-C} = 164 Hz, C_{arom}-H_p), 111.5 (*ddd*, ¹J_{H-C} = 166 Hz, ²J_{H-C} = 8 Hz, ³J_{H-C} = 1 Hz, C_{arom}-H_m), 106.8 – 106.7 (*m*, C_{arom}-C_{arom}); ¹⁹F{¹H} NMR (376 MHz, CDCl₃) δ = -110.6 (*s*, 4F_o); **GC-MS**: [t = 7.797 min] m/z: 226 [*M*]⁺; **HRMS (APCI)** calcd for C₁₂H₆F₄ [*M*⁺]: 226.0400; found: 226.0397. Spectroscopic data matched those in the literature.^[38]

2,2',3,3',4,4'-hexafluorobiphenyl (3_2f)

Compound **3_2f** was synthesized following general procedure and using following chemicals and conditions: 2,3,4-trifluorophenylboronic acid pinacol ester (**3_1f**) (157 mg, 0.6 mmol), Pd(OAc)₂ (3 mg, 0.012 mmol, 2 mol%), Ag₂O (139 mg, 0.6 mmol, 1 equiv), and toluene (1.5 mL), 75 °C, 5 h. After flash column chromatography (hexane), product **3_2f** was obtained as white solid (76 mg, 97%). White colorless single crystals suitable for X-ray diffraction were obtained by slow evaporation of a hexane solution at ambient temperature.

^1H NMR (300 MHz, C_6D_6) δ = 6.36 – 6.23 (*m*, 4H, $\text{C}_{\text{arom}}\text{-H}_{\text{o,m}}$); **$^{13}\text{C}\{^1\text{H}\}$ NMR** (125 MHz, C_6D_6) δ = 151.5 (*ddd*, $^1J_{\text{F-C}} = 251$ Hz, $^2J_{\text{F-C}} = 10$ Hz, $^3J_{\text{F-C}} = 3$ Hz, $\text{C}_{\text{arom}}\text{-F}_{\text{p}}$), 149.2 (*dm*, $^1J_{\text{F-C}} = 254$ Hz, $\text{C}_{\text{arom}}\text{-F}_{\text{o}}$), 140.6 (*dt*, $^1J_{\text{F-C}} = 252$ Hz, $^2J_{\text{F-C}} = 16$ Hz, $\text{C}_{\text{arom}}\text{-F}_{\text{m}}$), 124.9 (*oct*, $^2J_{\text{F-C}} = 2$ Hz, $\text{C}_{\text{arom}}\text{-H}_{\text{m}}$), 119.4 (*m*, $\text{C}_{\text{arom}}\text{-C}_{\text{arom}}$), 112.3 (*dd*, $^3J_{\text{F-C}} = 18$ Hz, $^4J_{\text{F-C}} = 4$ Hz, $\text{C}_{\text{arom}}\text{-H}_{\text{o}}$); **$^{13}\text{C}\{^{19}\text{F}\}$ NMR** (125 MHz, C_6D_6) δ = 151.5 (*dd*, $^2J_{\text{H-C}} = 12$ Hz, $^3J_{\text{H-C}} = 4$ Hz, $\text{C}_{\text{arom}}\text{-F}_{\text{p}}$), 149.2 (*d*, $^3J_{\text{H-C}} = 11$ Hz, $\text{C}_{\text{arom}}\text{-F}_{\text{o}}$), 140.6 (*d*, $^3J_{\text{H-C}} = 8$ Hz, $\text{C}_{\text{arom}}\text{-F}_{\text{m}}$), 124.9 (*d*, $^1J_{\text{H-C}} = 167$ Hz, $\text{C}_{\text{arom}}\text{-H}_{\text{m}}$), 119.4 (*dd*, $^2J_{\text{H-C}} = 9$ Hz, $^3J_{\text{H-C}} = 4$ Hz, $\text{C}_{\text{arom}}\text{-C}_{\text{arom}}$), 112.3 (*d*, $^1J_{\text{H-C}} = 168$ Hz, $\text{C}_{\text{arom}}\text{-H}_{\text{o}}$); **$^{19}\text{F}\{^1\text{H}\}$ NMR** (376 MHz, C_6D_6) δ = -159.4 – -159.3 (*m*, 2F_{m}), -135.1 – -135.0 (*m*, 2F_{o}), -133.4 (*dm*, $^3J_{\text{F-F}} = 21$ Hz, 2F_{p}); **GC-MS**: [t = 8.119 min] m/z: 262 [M]⁺; **HRMS (APCI)** calcd for $\text{C}_{12}\text{H}_4\text{F}_6$ [M]⁺: 262.0212; found: 262.0207. Spectroscopic data matched those in the literature.^[39]

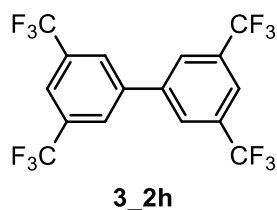
Synthesis of 2,2',5,5'-tetrafluorobiphenyl (**3_2g**)



3_2g

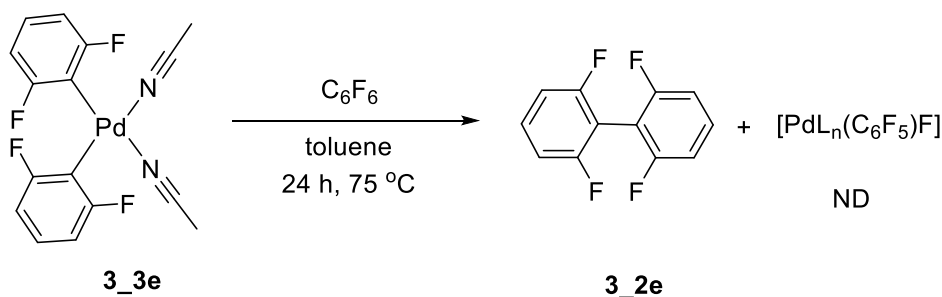
Compound **3_2g** was synthesized following general procedure and using following chemicals and conditions: 2,5-difluorophenylboronic acid pinacol ester (**3_1g**) (136 mg, 0.60 mmol), $\text{Pd}(\text{OAc})_2$ (3 mg, 0.012 mmol, 2 mol%), Ag_2O (139.04 mg, 0.6 mmol), and toluene (1.5 mL), 75 °C, 5 h. After flash column chromatography (hexane) product **3_2g** was obtained as white solid (66 mg, 98%).

^1H NMR (300 MHz, CDCl_3) δ = 7.18 – 7.04 (*m*, 6H, $\text{C}_{\text{arom}}\text{-H}_{\text{o,m,p}}$); **$^{13}\text{C}\{^1\text{H}\}$ NMR** (125 MHz, CDCl_3) δ = 158.6 (*dd*, $^1J_{\text{F-C}} = 243$ Hz, $^4J_{\text{F-C}} = 2$ Hz, $\text{C}_{\text{arom}}\text{-F}_{\text{m}}$), 155.9 (*ddd*, $^1J_{\text{F-C}} = 247$ Hz, $^4J_{\text{F-C}} = 2$ Hz, $^4J_{\text{F-C}} = 2$ Hz, $\text{C}_{\text{arom}}\text{-F}_{\text{o}}$), 123.9 – 123.7 (*m*, $\text{C}_{\text{arom}}\text{-C}_{\text{arom}}$), 117.9 (*dt*, $^2J_{\text{F-C}} = 25$ Hz, $^3J_{\text{F-C}} = 3$ Hz, $\text{C}_{\text{arom}}\text{-H}_{\text{o}}$), 117.4 – 117.0 (*m*, $\text{C}_{\text{arom}}\text{-H}_{\text{p}}$), 116.8 (*dm*, $^2J_{\text{F-C}} = 24$ Hz, $\text{C}_{\text{arom}}\text{-H}_{\text{m}}$); **$^{19}\text{F}\{^1\text{H}\}$ NMR** (376 MHz, CDCl_3) δ = -120.9 – -120.8 (*m*, 2F_{m}), -118.9 – -118.8 (*m*, 2F_{o}); **GC-MS**: [t = 5.530 min] m/z: 226 [M]⁺; **HRMS (APCI)** calcd. for $\text{C}_{12}\text{H}_6\text{F}_4$ [M]⁺: 226.0400; found: 226.0399. Spectroscopic data matched those in the literature.^[40]

3,3',5,5'-tetrakis(trifluoromethyl)biphenyl (3_2h)

Compound **3_2h** was synthesized following general procedure and using following chemicals and conditions: 3,5-di(trifluoromethyl)phenylboronic acid pinacol ester (**3_1h**) (204 mg, 0.60 mmol), Pd(OAc)₂ (3 mg, 0.012 mmol, 2 mol%), Ag₂O (139.04 mg, 0.6 mmol), and toluene (1.5 mL), 75 °C, 5 h. After flash column chromatography (hexane) product **3_2h** was obtained as white solid (118 mg, 92%).

¹H NMR (500 MHz, CDCl₃) δ = 8.03 (*s*, 4H, C_{arom}-H_o), 7.99 (*s*, 2H, C_{arom}-H_p); ¹³C{¹H} NMR (125 MHz, CDCl₃) δ = 140.6 (C_{arom}-C_{arom}), 133.07 (*q*, ²J_{F-C} = 34 Hz, C_{arom}-CF₃), 127.7 (*m*, C_{arom}-H_o), 123.2 (*q*, ¹J_{F-C} = 273 Hz, CF₃), 122.8 (*quin*, ³J_{F-C} = 4 Hz, C_{arom}-H_p); ¹⁹F NMR (470 MHz, CDCl₃) δ = -62.9 (*s*, 12F, CF₃); GC-MS: [t = 6.985 min] m/z: 426 [M]⁺; HRMS (APCI) calcd for C₁₆H₆F₁₂ [M]⁺: 426.0283; found: 426.0275. Spectroscopic data matched those in the literature.^[41]

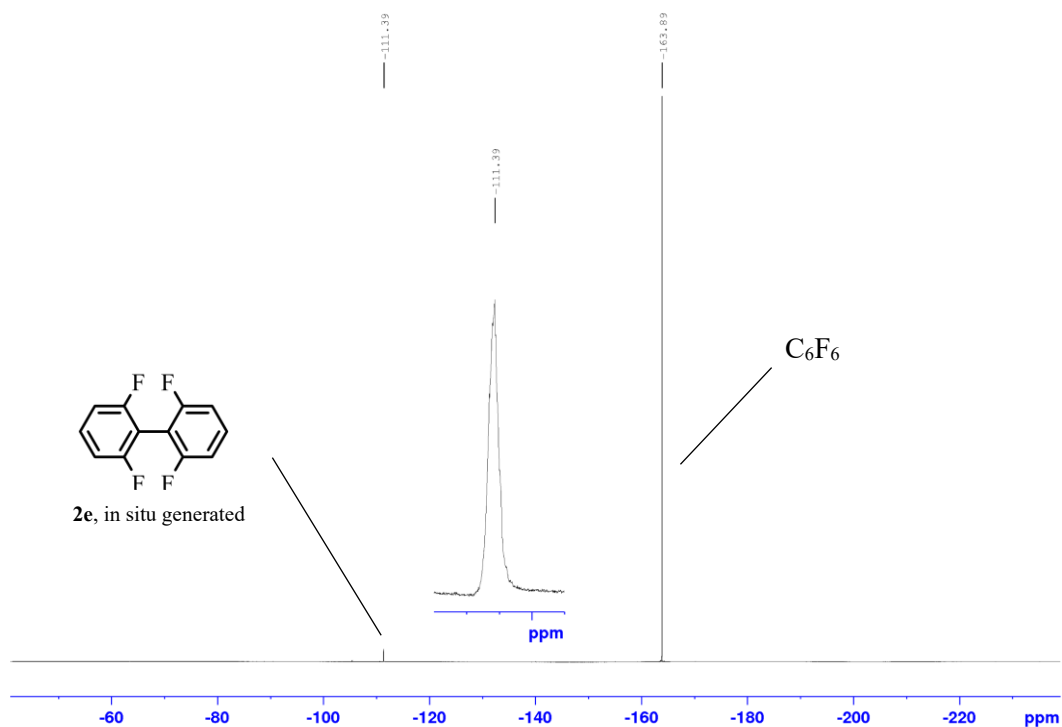
3.5.7 A Test for the Possibility of C–F Oxidative Addition

Scheme 3-6. Reductive elimination of **3_2e** from **3_3e** in the presence of C₆F₆ in toluene.

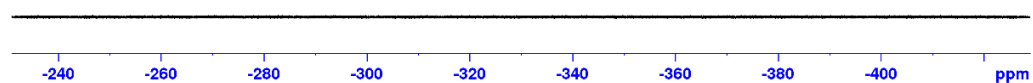
Experimental procedure. Inside the glove box, under argon, into a J. Young NMR tube, were added compound **3_3e** (8 mg, 0.02 mmol), C₆F₆ (11 mg, 0.06 mmol) and toluene (0.4 mL). After sealing, the NMR tube was taken out of the glove box, heated at 75 °C for 24 h, and monitored by ¹⁹F NMR spectroscopy. The conversion to give **3_2e** is complete after 10 minutes. However, after 24 h, we

did not detect any Pd complex arising from C-F activation of C_6F_6 . The ^{19}F NMR spectrum of our reaction mixture is shown below. According to the literature,^[34] the ^{19}F NMR chemical shifts for a typical $[PdL_2(C_6F_5)F]$ complex such as *trans*- $[Pd(Cy_3P)_2(C_6F_5)F]$ is $\delta = -110.1$ (*m*, 2F, C_6F_5), -164.8 (*m*, 1F, C_6F_5), -165.8 (*m*, 2F, C_6F_5), -325.0 (*br s*, 1F, Pd-F).

^{19}F NMR spectrum of the reaction mixture in Scheme S2 (-40 – -240 ppm region)



^{19}F NMR spectrum of the reaction mixture in Scheme S2 (-230 – -430 ppm region)



3.5.8 Single Crystal X-ray Diffraction Data

Crystal structure determination. Crystals suitable for single-crystal X-ray diffraction were selected, coated in perfluoropolyether oil, and mounted on MiTeGen sample holders. Diffraction data of **3_2d**, **3_3a**, and **3_3b** were collected on Bruker X8 Apex II 4-circle diffractometers with CCD area detectors using Mo-K α radiation monochromated by multi-layer focusing mirrors. Diffraction data of **3_2f** and **3_3e** were collected on a Rigaku Oxford Diffraction XtaLAB Synergy diffractometer with a semiconductor HPA-detector (HyPix-6000) and multi-layer mirror monochromated Cu-K α radiation for the **3_2f** and Mo-K α for the **3_3e**. The crystals were cooled using an Oxford Cryostreams low-temperature device. Data were collected at 100 or 103 K. The images were processed and corrected for Lorentz-polarization effects and absorption as implemented in the Bruker software packages (**3_2d**, **3_3a**, **3_3b**) or using the CrysAlis^{Pro} software from Rigaku Oxford Diffraction (**3_2f**, **3_3e**). The structures were solved using the intrinsic phasing method (SHELXT)^[42] and Fourier expansion technique. All non-hydrogen atoms were refined in anisotropic approximation, with hydrogen atoms ‘riding’ in idealized positions, by full-matrix least squares against F² of all data, using SHELXL^[43] software and the SHELXLE graphical user interface.^[44] Diamond^[45] software was used for graphical representation. Crystal data and experimental details are listed in Table 3-5; full structural information has been deposited with the Cambridge Crystallographic Data Centre. CCDC-1939238 (**3_2d**), 1951276 (**3_2f**), 1939239 (**3_3a**), 1939240 (**3_3b**), 1953484 (**3_3e**).

Table 3-5. Single-crystal X-ray diffraction data and structure refinements of **3_2d**, **3_2f**, **3_3a**, **3_3b** and **3_3e**.

Data	3_2d ^[a]	3_2f	3_3a ^[a]	3_3b ^[a]	3_3e
CCDC number	1939238	1951276	1939239	1939240	1953484
Empirical formula	C ₁₂ H ₂ F ₈	C ₁₂ H ₄ F ₆	C ₁₆ H ₆ F ₁₀ N ₂ Pd · 0.5(C ₄ H ₁₀ O)	C ₁₆ H ₁₀ F ₆ N ₂ Pd	C ₁₆ H ₁₂ F ₄ N ₂ Pd
Formula weight / g·mol ⁻¹	298.14	262.15	559.69	450.66	414.68
<i>T</i> / K	103(2)	100(2)	103(2)	100(2)	100(2)
Radiation, λ / Å	MoKα 0.71073	CuKα 1.54184	MoKα 0.71073	MoKα 0.71073	MoKα 0.71073
Crystal size / mm ³	0.20 × 0.25 × 0.26	0.76 × 0.08 × 0.04	0.17 × 0.18 × 0.32	0.09 × 0.19 × 0.28	0.15 × 0.11 × 0.09
Crystal color, habit	colorless block	colorless needle	colorless block	colorless block	colorless plate
μ / mm ⁻¹	0.215	1.677	1.080	1.208	1.211
Crystal system	orthorhombic	orthorhombic	orthorhombic	monoclinic	monoclinic
Space group	<i>Pbca</i>	<i>Fdd2</i>	<i>Pnna</i>	<i>P2₁/n</i>	<i>P2₁</i>
<i>a</i> / Å	10.994(3)	40.0791(8)	8.612(3)	9.5500(15)	9.1923(3)
<i>b</i> / Å	8.897(4)	13.0995(3)	14.566(6)	17.778(5)	8.9775(2)
<i>c</i> / Å	20.967(3)	3.69800(10)	15.189(5)	19.108(3)	9.5988(3)
α / °	90	90	90	90	90
β / °	90	90	90	90.415(7)	90.225(3)
γ / °	90	90	90	90	90
Volume / Å ³	2050.9(11)	1941.51(8)	1905.4(13)	3244.2(12)	792.13(4)
<i>Z</i>	8	8	4	8	2
ρ _{calc} / g·cm ⁻³	1.931	1.794	1.951	1.845	1.739
<i>F</i> (000)	1168	1040	1092	1760	408
θ range / °	1.943 – 28.376	4.413 – 74.263	1.937 – 28.360	1.565 – 29.130	4.244 – 61.014
Reflections collected	37562	8216	18707	69798	24242
Unique reflections	2565	850	2386	8733	4817
Parameters / restraints	181 / 0	82 / 1	180 / 82	455 / 0	210 / 0
GooF on <i>F</i> ²	1.041	1.056	1.074	1.063	1.044
R ₁ [<i>I</i> > 2σ(<i>I</i>)]	0.0319	0.0317	0.0310	0.0294	0.0266
wR ² (all data)	0.0900	0.0813	0.0794	0.0770	0.0588
Max. / min. residual electron density / e·Å ⁻³	0.498 / -0.236	0.193 / -0.221	0.907 / -0.494	0.706 / -0.868	1.06 / -0.53

^[a] For compounds **3_2d**, **3_3a**, and **3_3b**, the unit-cell parameters and their standard deviations were obtained from a combination of the random-error standard deviations from the original least-squares refinement with the systematic-error component estimated from 32 Monte-Carlo simulations using the Bruker software package. For this reason, the standard deviations of the unit-cell parameters are significantly larger for these compounds than for **3_2f** and **3_3e**, and they represent a better overall estimation of the realistic standard deviations.

Table 3-6. Intermolecular C–H···F–C, H···F, C···F, and F···F interaction distances (Å) and angles (°) in compounds **3_2d** and **3_2f** at 100 K.

Compound	C–H···F / F···F	H···F	C/F···F	∠(CHF)
3_2d	C10–H10···F1	2.3949(9)	3.0376(15)	124.62(8)
	F2···F5		2.7078(12)	
	F3···F8		2.8717(12)	
	F6···F7		2.9169(15)	
3_2f	C4–H4···F2	2.6021(13)	3.261(3)	126.77(14)
	F1···F1		2.923(2)	

3.6 Detailed Description of Computational Details

3.6.1 Computational Details

All computations were performed using the Gaussian 09 (Revision E.01) package.^[46] Geometry optimizations, without any symmetry constraints, and frequency calculations were performed using the hybrid DFT functional B3LYP^[47] augmented with Tomasi's polarizable continuum model (PCM),^[48] Grimme's dispersion correction (GD3) and Becke-Johnson damping (BJ).^[49] For these calculations, the SDD basis set for palladium was used and the 6-31G** basis set for all other atoms was used. Transition state geometries were obtained using `opt = (ts, noeigentest, calcfc)` algorithms.^[50] All optimized transition state structures were verified as maxima with only one imaginary frequency, and the magnitudes of all frequencies were greater than the residual frequencies due to rotations and translations. In addition, each transition state established was ensured to be on the preferred reaction path by performing “plus-and-minus-displacement” minimization calculations in which the transition state structure was displaced ca. 0.05 Å or 5° along the imaginary frequency normal mode in both directions.^[51] The displaced geometries were subsequently optimized to the nearest minimum. Zero-point vibrational energies, and thermal corrections were computed from frequency calculations with a standard state of 298 K and 1 atm. Single point energy calculations were performed at the same level of theory with the triple-zeta basis sets Def2TZVP (Pd) and 6-311+g(2d,p) (other atoms).

3.6.2 EDA-NOCV Analysis Results

Bonding analyses were performed at the B3LYP-D3/TZVP level of theory using the ADF 2017.207 package.^[52] The intrinsic interactions between the ligand(s) and the metal fragment of various palladium complexes were probed using the combined energy decomposition analysis (EDA)^[53] and natural orbitals for chemical valence (NOCV)^[54] method (EDA-NOCV) as established by Ziegler et al.^[55] The distortion energy (ΔE_{dist}) is the change in energy between the frozen fragments A* and B* of compound A-B and the fragments in their equilibrium geometries. The EDA calculations provide information on the intrinsic interaction energy (ΔE_{int}), which is the energy difference between the compound A-B and its frozen fragments A* and B*. From the EDA calculations, the interaction energy ΔE_{int} can be partitioned into three main components ($\Delta E_{\text{int}} = \Delta E_{\text{elstat}} + \Delta E_{\text{Pauli}} + \Delta E_{\text{orb}}$). The term ΔE_{elstat} is the change in energy due to the quasiclassical electrostatic interaction between the unperturbed charge distributions of the prepared fragments. This ΔE_{elstat} part is energetically attractive. The term ΔE_{Pauli} stands for the change in energy associated with the Pauli repulsion that comprises the destabilizing interactions between the electrons with same spin on either fragment. Energetically, the ΔE_{Pauli} component is repulsive. The term ΔE_{orb} represents the attractive energy contribution from each irreducible representation of the point group of the interacting system. The dispersion interaction that arises from the attractive forces between the induced dipoles of interacting fragments is considered to be an important component of chemical bonding; therefore, the energy contribution due to the dispersion interactions (ΔE_{disp}) was computed explicitly, using Grimme's dispersion correction (GD3),^[49a] and added as an extra component to ΔE_{int} . The ΔE_{disp} is, in general, attractive. The coupled method of EDA-NOCV aids in partitioning the total orbital interactions into pairwise contributions of the orbital interactions; thus, the nature of interaction between fragments can be identified as σ donation (ΔE_{σ}), π back-donation (ΔE_{π}) and intra-fragment polarization ($\Delta E_{\text{orb}(\text{rest})}$) interactions. Furthermore, the EDA-NOCV analysis demonstrates that most chemical systems usually have a very small number of significant contributions of ΔE_{orb} . The deformation density (charge deformation, $\Delta\rho_k$) that arises from mixing the orbital pairs of the interacting fragments yields information on the amount and shape of charge flow due to the orbital interactions

in the compound. The associated energy term ΔE_{orb}^k gives the strength of the orbital interactions. Thus, with the EDA-NOCV analysis, both qualitative ($\Delta\rho_k$) and quantitative (ΔE_{orb}^k) details of the strength of individual pairs of orbital interactions can be obtained. More details on the EDA and EDA-NOCV methods and their applications for bonding analysis can be found in the literature.^[56]

3.6.2.1 Numerical Results from EDA-NOCV Analysis

Table 3-7. EDA-NOCV results of the chemical bonding in **3_3a**, **TS[(3_3a)-4]**, **7**, **TS(7-8)**, **12**, **TS(12-13)**, **16**, and **TS(16-17)** at the B3LYP-D3/TZVP level of theory. Energies are in kcal/mol. The first fragment is Pd(Ar_F)₂ for all, and the other fragment(s) is/are MeCN for **3_3a** and **TS[(3_3a)-4]**, THF for **7** and **TS(7-8)**, SMe₂ for **12** and **TS(12-13)**, and PMe₃ for **16** and **TS(16-17)**.

Structure	3_3a	TS[(3_3a)-4]	7	TS(7-8)	12	TS(12-13)	16	TS(16-17)
ΔE_{int}	-55.3	-35.4	-58.1	-36.8	-70.8	-52.1	-102.0	-77.0
ΔE_{Pauli}	130.6	106.5	102.5	80.0	162.7	163.9	280.0	281.1
ΔE_{disp}	-8.2	-7.0	-20.8	-20.7	-21.7	-20.6	-27.2	-24.1
$\Delta E_{\text{elstat}}^{\text{[a]}}$	-117.1	-89.8	-95.6	-68.3	-141.2	-141.0	-250.1	-252.6
	(65.9%)	(66.6%)	(68.4%)	(71.1%)	(66.7%)	(72.1%)	(70.5%)	(75.6%)
$\Delta E_{\text{orb}}^{\text{[a]}}$	-60.6	-45.1	-44.2	-27.8	-70.6	-54.5	-104.7	-81.4
	(34.1%)	(33.4%)	(31.6%)	(28.9%)	(33.3%)	(27.9%)	(29.5%)	(24.4%)
$\Delta E^1_{\text{orb}}^{\text{[b]}}$	-24.5	-16.2	-19.8	-11.5	-33.0	-17.2	-51.9	-24.9
	(40.4%)	(35.9%)	(44.8%)	(41.4%)	(46.7%)	(31.6%)	(49.6%)	(30.6%)
$\Delta E^2_{\text{orb}}^{\text{[b]}}$	-9.5	-10.4	-9.3	-6.6	-14.4	-14.9	-19.4	-23.9
	(15.7%)	(23.1%)	(21.0%)	(23.7%)	(20.4%)	(27.3%)	(18.5%)	(29.4%)
$\Delta E^3_{\text{orb}}^{\text{[b]}}$	-7.7	-3.8			-5.0	-5.6	-7.9	-8.8
	(12.7%)	(8.4%)	-[c]	-[c]	(7.1%)	(10.3%)	(7.5%)	(10.8%)
$\Delta E^4_{\text{orb}}^{\text{[b]}}$	-4.5	-4.8			-3.9	-4.0	-5.4	-11.9
	(7.4%)	(10.6%)	-[c]	-[c]	(5.5%)	(7.3%)	(5.2%)	(14.6%)
$\Delta E^5_{\text{orb}}^{\text{[b]}}$	-4.1						-5.1	
	(6.8%)	-[c]	-[c]	-[c]	-[c]	-[c]	(4.9%)	-[c]
$\Delta E_{\sigma}^{\text{[b]}}$	-41.7	-21.1	-29.1	-18.1	-47.4	-37.7	-79.2	-57.6
	(68.8%)	(46.8%)	(65.8%)	(65.1%)	(67.1%)	(69.2%)	(75.6%)	(70.8%)
$\Delta E_{\pi}^{\text{[b]}}$	-8.6	-14.2			-3.9	-4.0	-10.5	-11.9
	(14.2%)	(31.5%)	-[c]	-[c]	(5.5%)	(7.3%)	(10.0%)	(14.6%)
$\Delta E_{\text{orb}(\text{rest})}^{\text{[b]}}$	-10.3	-9.9	-15.3	-9.7	-19.3	-12.8	-15.0	-11.9
	(17.0%)	(22.0%)	(34.6%)	(34.9%)	(27.3%)	(23.5%)	(14.3%)	(14.6%)

^[a] The value in parenthesis denote the percentage contribution to the total attractive interaction ($\Delta E_{\text{elstat}} + \Delta E_{\text{orb}}$). ^[b] The value in parenthesis denote the percentage contribution to the total orbital interaction (ΔE_{orb}). ^[c] No or insignificant energy contribution was found.

Table 3-8. EDA-NOCV results of the chemical bonding in **20**, **TS(20-21)**, **25**, **TS(25-26)**, **30**, **TS(30-31)**, **35**, and **TS(35-36)** at the B3LYP-D3/TZVP level of theory. Energies are in kcal/mol. The first fragment is Pd(Ar_F)₂ for all, and the other fragment is benzene for **20** and **TS(20-21)**, toluene for **25** and **TS(25-26)**, *m*-xylene for **30** and **TS(30-31)**, and perfluorobenzene for **35** and **TS(35-36)**.

Structure	20	TS(20-21)	25	TS(25-26)	30	TS(30-31)	35	TS(35-36)
ΔE_{int}	-27.4	-26.2	-30.3	-27.5	-32.6	-28.4	-12.2	-16.9
ΔE_{Pauli}	64.5	66.8	67.8	68.0	69.1	68.3	53.6	68.9
ΔE_{disp}	-11.3	-8.6	-12.9	-9.2	-13.6	-10.7	-11.6	-14.2
$\Delta E_{\text{elstat}}^{[a]}$	-45.5 (56.5%)	-53.1 (62.9%)	-48.5 (57.0%)	-54.6 (63.2%)	-50.5 (57.3%)	-55.2 (64.3%)	-25.4 (46.8%)	-41.5 (58.0%)
$\Delta E_{\text{orb}}^{[a]}$	-35.0 (43.5%)	-31.3 (37.1%)	-36.6 (43.0%)	-31.8 (36.8%)	-37.6 (42.7%)	-30.7 (35.7%)	-28.9 (53.2%)	-30.1 (42.0%)
$\Delta E^1_{\text{orb}}^{[b]}$	-12.0 (34.3%)	-9.8 (31.3%)	-12.8 (35.0%)	-9.6 (30.2%)	-13.4 (35.6%)	-8.6 (28.0%)	-9.1 (31.5%)	-11.6 (37.9%)
$\Delta E^2_{\text{orb}}^{[b]}$	-7.2 (20.6%)	-9.7 (31.0%)	-7.2 (19.7%)	-9.8 (30.8%)	-7.4 (19.7%)	-9.7 (31.6%)	-5.9 (20.4%)	-7.7 (25.6%)
$\Delta E^3_{\text{orb}}^{[b]}$	-3.0 (8.6%)	-4.5 (14.4%)	-3.2 (8.7%)	-4.7 (14.8%)	-3.3 (8.8%)	-4.5 (14.7%)	-3.4 (11.8%)	-4.0 (13.3%)
$\Delta E^4_{\text{orb}}^{[b]}$	-3.6 (10.3%)	-2.6 (8.3%)	-3.4 (9.3%)	-2.9 (9.1%)	- ^[c]	-2.9 (9.4%)	-2.1 (7.3%)	-2.0 (6.6%)
$\Delta E_{\sigma}^{[b]}$	-22.8 (65.1%)	-14.2 (45.4%)	-23.4 (63.9%)	-14.4 (45.3%)	-20.8 (55.3%)	-14.1 (45.9%)	-18.4 (65.4%)	-9.7 (32.2%)
$\Delta E_{\pi}^{[b]}$	-3.0 (8.6%)	-12.4 (39.6%)	-3.2 (8.7%)	-12.5 (39.3%)	-3.3 (8.8%)	-11.5 (37.5%)	-2.1 (7.3%)	-15.5 (51.5%)
$\Delta E_{\text{orb}(\text{rest})}^{[b]}$	-9.2 (26.3%)	-4.7 (15.0%)	-10.0 (27.3%)	-4.8 (15.1%)	-13.5 (35.9%)	-5.0 (16.3%)	-8.4 (29.1%)	-4.8 (15.9%)

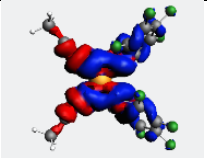
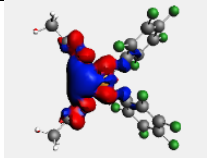
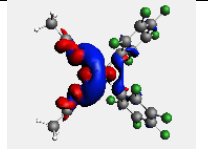
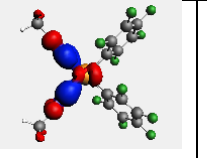
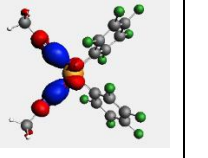
^[a] The value in parenthesis denote the percentage contribution to the total attractive interaction ($\Delta E_{\text{elstat}} + \Delta E_{\text{orb}}$). ^[b] The value in parenthesis denote the percentage contribution to the total orbital interaction (ΔE_{orb}). ^[c] No or insignificant energy contribution was found.

3.6.2.2 Plots of Deformation Density, Associated Energy and the Orbitals Involved in the Interaction

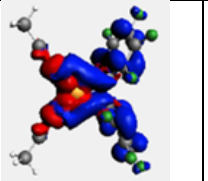
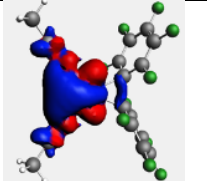
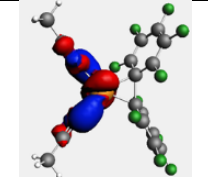
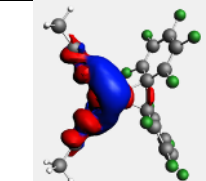
The important deformation densities ($\Delta\rho_k$), which show the change in the electronic structure that arise from the pairwise orbital interactions among the fragments in their closed-shell state, and that are associated with significant orbital interactions in all reactants and selected transition states, are provided below in the first row. The associated energy (ΔE^k_{orb}) gained from each charge deformation upon orbital interaction between the fragments and the respective eigen value (v), representing the size of the charge flow, are also given in the same row. The color code for the direction of charge

flow (charge transfer) in the deformation density plots is red to blue. Information concerning the type of orbital interaction and the orbitals of fragments engaged in that interaction, which are derived from deformation densities and eigenvalues, are given in the second row.

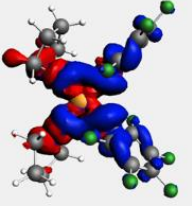
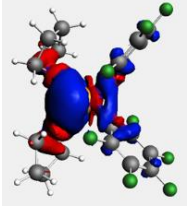
For *cis*-[Pd(MeCN)₂(C₆F₅)₂] (3_3a):

Deformation density	 $\Delta\rho_1$; $\Delta E^1_{\text{orb}} = -24.5$ kcal/mol; $v = \pm 0.46$	 $\Delta\rho_2$; $\Delta E^2_{\text{orb}} = -9.5$ kcal/mol; $v = \pm 0.26$	 $\Delta\rho_3$; $\Delta E^3_{\text{orb}} = -7.7$ kcal/mol; $v = \pm 0.22$	 $\Delta\rho_4$; $\Delta E^4_{\text{orb}} = -4.5$ kcal/mol; $v = \pm 0.21$	 $\Delta\rho_5$; $\Delta E^5_{\text{orb}} = -4.1$ kcal/mol; $v = \pm 0.20$
Type of interaction and the orbitals of fragments involved in the interaction	σ-donation (HOMO-2 of MeCN-1 and MeCN-2 fragments to LUMO of Pd(Ar _F) ₂ fragment)	σ-donation (HOMO-2 of MeCN-1 and MeCN-2 fragments to LUMO+1 of Pd(Ar _F) ₂ fragment)	σ-donation (HOMO-2 of MeCN-1 and MeCN-2 fragments to LUMO+1 of Pd(Ar _F) ₂ fragment)	π back-donation (HOMO-6 of Pd(Ar _F) ₂ fragment to LUMO+2 of MeCN-1 and MeCN-2 fragments)	π back-donation (HOMO-6 of Pd(Ar _F) ₂ fragment to LUMO+2 of MeCN-1 and MeCN-2 fragments)

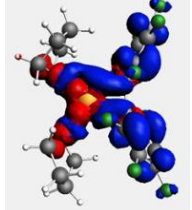
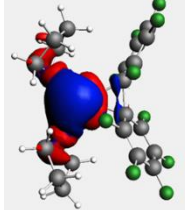
For TS[(3_3a)-4]:

Deformation density	 $\Delta\rho_1$; $\Delta E^1_{\text{orb}} = -16.2$ kcal/mol; $v = \pm 0.38$	 $\Delta\rho_2$; $\Delta E^2_{\text{orb}} = -10.4$ kcal/mol; $v = \pm 0.33$	 $\Delta\rho_3$; $\Delta E^3_{\text{orb}} = -3.8$ kcal/mol; $v = \pm 0.20$	 $\Delta\rho_4$; $\Delta E^4_{\text{orb}} = -4.8$ kcal/mol; $v = \pm 0.19$
Type of interaction and the orbitals of fragments involved in the interaction	σ-donation (HOMO-2 of MeCN-1 and MeCN-2 fragments to LUMO+1 of Pd(Ar _F) ₂ fragment)	π back-donation (HOMO-3 of Pd(Ar _F) ₂ fragment to LUMO+1 of MeCN-1 and MeCN-2 fragments)	π back-donation (HOMO-1 of Pd(Ar _F) ₂ fragment to LUMO+2 of MeCN-1 and MeCN-2 fragments)	σ-donation (HOMO-2 of MeCN-1 and MeCN-2 fragments to LUMO of Pd(Ar _F) ₂ fragment)

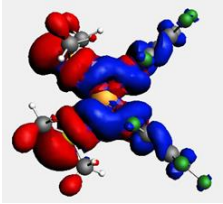
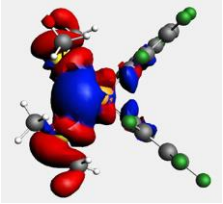
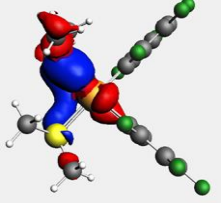
For *cis*-[Pd(THF)₂(C₆F₅)₂] (7):

Deformation density	 <p>$\Delta\rho_1; \Delta E^1_{\text{orb}} = -19.8$ kcal/mol; $v = \pm 0.46$</p>	 <p>$\Delta\rho_2; \Delta E^2_{\text{orb}} = -9.3$ kcal/mol; $v = \pm 0.25$</p>
Type of interaction and the orbitals of fragments involved in the interaction	<p>σ-donation (HOMO-1 of THF-1 and THF-2 fragments to LUMO of Pd(Ar_F)₂ fragment)</p>	<p>σ-donation (HOMO-1 of THF-1 and THF-2 fragments to LUMO+1 of Pd(Ar_F)₂ fragment)</p>

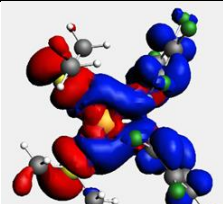
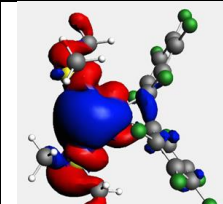
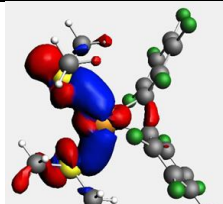
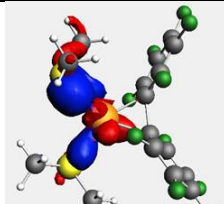
For TS(7-8):

Deformation density	 <p>$\Delta\rho_1; \Delta E^1_{\text{orb}} = -11.5$ kcal/mol; $v = \pm 0.35$</p>	 <p>$\Delta\rho_2; \Delta E^2_{\text{orb}} = -9.3$ kcal/mol; $v = \pm 0.25$</p>
Type of interaction and the orbitals of fragments involved in the interaction	<p>σ-donation (HOMO of THF-1 and THF-2 fragments to LUMO+1 and LUMO+2 of Pd(Ar_F)₂ fragment, respectively)</p>	<p>σ-donation (HOMO-1 and HOMO of THF-1 and THF-2 fragments, respectively, to LUMO of Pd(Ar_F)₂ fragment)</p>

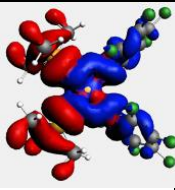
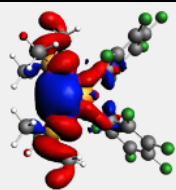
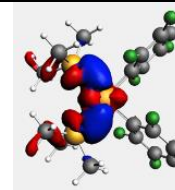
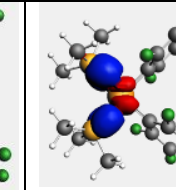
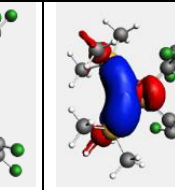
For *cis*-[Pd(SMe₂)₂(C₆F₅)₂] (12):

Deformation density	 $\Delta\rho_1; \Delta E^1_{\text{orb}} = -33.0$ kcal/mol; $v = \pm 0.67$	 $\Delta\rho_2; \Delta E^2_{\text{orb}} = -14.4$ kcal/mol; $v = \pm 0.31$	 $\Delta\rho_3; \Delta E^3_{\text{orb}} = -3.9$ kcal/mol; $v = \pm 0.17$
Type of interaction and the orbitals of fragments involved in the interaction	σ-donation (HOMO of SMe ₂ -1 and SMe ₂ -2 fragments to LUMO of Pd(Ar _F) ₂ fragment)	σ-donation (HOMO of SMe ₂ -1 and SMe ₂ -2 fragments to LUMO+1 of Pd(Ar _F) ₂ fragment)	π back-donation (HOMO-6 of Pd(Ar _F) ₂ fragment to LUMO+1 of SMe ₂ -2 fragment)

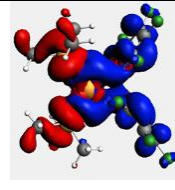
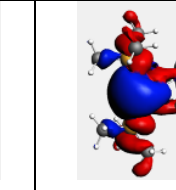
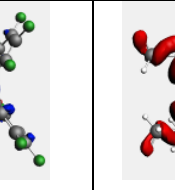
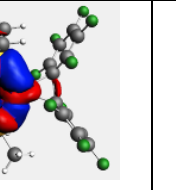
For TS(12-13):

Deformation density	 $\Delta\rho_1; \Delta E^1_{\text{orb}} = -17.2$ kcal/mol; $v = \pm 0.47$	 $\Delta\rho_2; \Delta E^2_{\text{orb}} = -14.9$ kcal/mol; $v = \pm 0.38$	 $\Delta\rho_3; \Delta E^3_{\text{orb}} = -5.6$ kcal/mol; $v = \pm 0.20$	 $\Delta\rho_4; \Delta E^4_{\text{orb}} = -4.0$ kcal/mol; $v = \pm 0.17$
Type of interaction and the orbitals of fragments involved in the interaction	σ-donation (HOMO of SMe ₂ -1 and SMe ₂ -2 fragments to LUMO+1 of Pd(Ar _F) ₂ fragment)	σ-donation (HOMO of SMe ₂ -1 and SMe ₂ -2 fragments to LUMO of Pd(Ar _F) ₂ fragment)	σ-donation (HOMO of SMe ₂ -2 fragment to LUMO of Pd(Ar _F) ₂ fragment)	π back-donation (HOMO-2 of Pd(Ar _F) ₂ fragment to LUMO+1 of SMe ₂ -2 fragment)

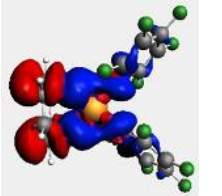
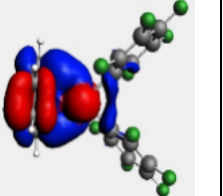
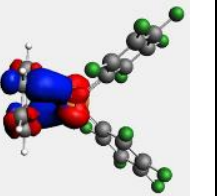
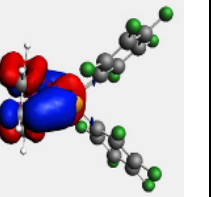
For *cis*-[Pd(PMe₃)₂(C₆F₅)₂] (16):

Deformation density	 $\Delta\rho_1; \Delta E^1_{\text{orb}} = -51.9$ kcal/mol; $\nu = \pm 0.84$	 $\Delta\rho_2; \Delta E^2_{\text{orb}} = -19.4$ kcal/mol; $\nu = \pm 0.38$	 $\Delta\rho_3; \Delta E^3_{\text{orb}} = -7.9$ kcal/mol; $\nu = \pm .23$	 $\Delta\rho_4; \Delta E^4_{\text{orb}} = -5.4$ kcal/mol; $\nu = \pm 0.20$	 $\Delta\rho_5; \Delta E^5_{\text{orb}} = -5.1$ kcal/mol; $\nu = \pm 0.20$
Type of interaction and the orbitals of fragments involved in the interaction	σ-donation (HOMO of PMe ₃ -1 and PMe ₃ -2 fragments to LUMO of Pd(Ar _F) ₂ fragment)	σ-donation (HOMO of PMe ₃ -1 and PMe ₃ -2 fragments to LUMO+1 of Pd(Ar _F) ₂ fragment)	σ-donation (HOMO of PMe ₃ -1 and PMe ₃ -2 fragments to LUMO+1 of Pd(Ar _F) ₂ fragment)	π back-donation (HOMO-5 of Pd(Ar _F) ₂ fragment to LUMO+8 of PMe ₃ -1 and PMe ₃ -2 fragments)	π back-donation (HOMO-6 of Pd(Ar _F) ₂ fragment to LUMO+8 of PMe ₃ -1 and PMe ₃ -2 fragments)

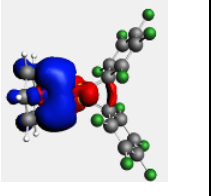
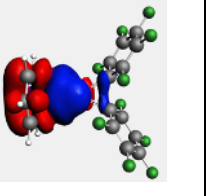
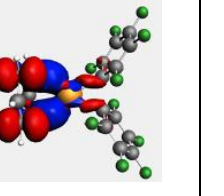
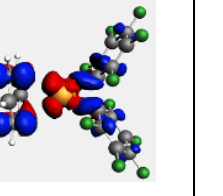
For TS(16-17):

Deformation density	 $\Delta\rho_1; \Delta E^1_{\text{orb}} = -24.9$ kcal/mol; $\nu = \pm 0.60$	 $\Delta\rho_2; \Delta E^2_{\text{orb}} = -23.9$ kcal/mol; $\nu = \pm 0.45$	 $\Delta\rho_3; \Delta E^3_{\text{orb}} = -8.8$ kcal/mol; $\nu = \pm 0.24$	 $\Delta\rho_4; \Delta E^4_{\text{orb}} = -11.9$ kcal/mol; $\nu = \pm 0.29$
Type of interaction and the orbitals of fragments involved in the interaction	σ-donation (HOMO of PMe ₃ -1 and PMe ₃ -2 fragments to LUMO+1 of Pd(Ar _F) ₂ fragment)	σ-donation (HOMO of PMe ₃ -1 and PMe ₃ -2 fragments to LUMO of Pd(Ar _F) ₂ fragment)	σ-donation (HOMO of PMe ₃ -1 and PMe ₃ -2 fragments to LUMO+2 of Pd(Ar _F) ₂ fragment)	π back-donation (HOMO-2 of Pd(Ar _F) ₂ fragment to LUMO+1 of PMe ₃ -1 and PMe ₃ -2 fragments)

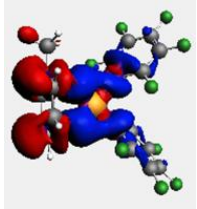
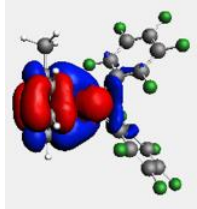
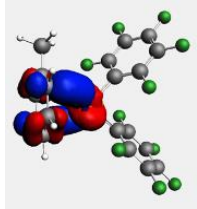
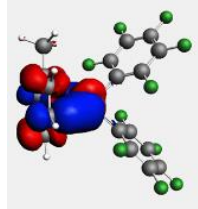
For *cis*-[Pd(C₆H₆)(C₆F₅)₂] (20):

Deformation density	 $\Delta\rho_1$; $\Delta E^1_{\text{orb}} = -12.0$ kcal/mol; $\nu = \pm 0.41$	 $\Delta\rho_2$; $\Delta E^2_{\text{orb}} = -7.0$ kcal/mol; $\nu = \pm 0.26$	 $\Delta\rho_3$; $\Delta E^3_{\text{orb}} = -3.0$ kcal/mol; $\nu = \pm 0.20$	 $\Delta\rho_4$; $\Delta E^4_{\text{orb}} = -3.6$ kcal/mol; $\nu = \pm 0.18$
Type of interaction and the orbitals of fragments involved in the interaction	σ-donation (HOMO of benzene fragment to LUMO of Pd(Ar _F) ₂ fragment)	σ-donation (HOMO-4 of benzene fragment to LUMO+1 of Pd(Ar _F) ₂ fragment)	π back-donation (HOMO-5 of Pd(Ar _F) ₂ fragment to LUMO+1 of benzene fragment)	σ-donation (HOMO-4 of benzene to LUMO+1 of Pd(Ar _F) ₂ fragment)

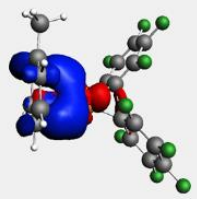
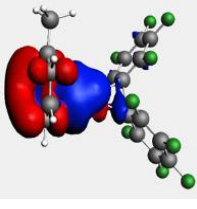
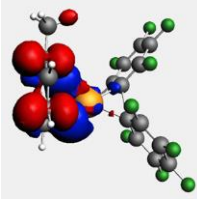
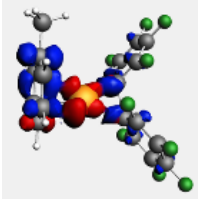
For TS(20-21):

Deformation density	 $\Delta\rho_1$; $\Delta E^1_{\text{orb}} = -9.8$ kcal/mol; $\nu = \pm 0.33$	 $\Delta\rho_2$; $\Delta E^2_{\text{orb}} = -9.7$ kcal/mol; $\nu = \pm 0.28$	 $\Delta\rho_3$; $\Delta E^3_{\text{orb}} = -4.5$ kcal/mol; $\nu = \pm 0.22$	 $\Delta\rho_4$; $\Delta E^4_{\text{orb}} = -2.6$ kcal/mol; $\nu = \pm 0.19$
Type of interaction and the orbitals of fragments involved in the interaction	π back-donation (HOMO-3 and HOMO-6 of Pd(Ar _F) ₂ fragment to LUMO of benzene fragment)	σ-donation (HOMO of benzene fragment to LUMO of Pd(Ar _F) ₂ fragment)	σ-donation (HOMO-1 of benzene fragment to LUMO+1 of Pd(Ar _F) ₂ fragment)	π back-donation (HOMO of Pd(Ar _F) ₂ fragment to LUMO+1 of benzene)

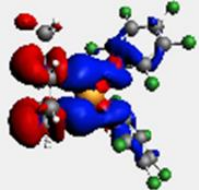
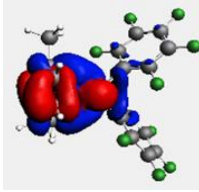
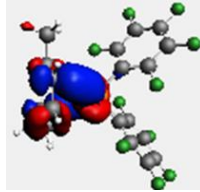
For *cis*-[Pd(C₇H₈)(C₆F₅)₂] (25):

Deformation density	 $\Delta\rho_1; \Delta E^1_{\text{orb}} = -12.8$ kcal/mol; $v = \pm 0.43$	 $\Delta\rho_2; \Delta E^2_{\text{orb}} = -7.2$ kcal/mol; $v = \pm 0.26$	 $\Delta\rho_3; \Delta E^3_{\text{orb}} = -3.2$ kcal/mol; $v = \pm 0.20$	 $\Delta\rho_4; \Delta E^4_{\text{orb}} = -3.4$ kcal/mol; $v = \pm 0.18$
Type of interaction and the orbitals of fragments involved in the interaction	σ-donation (HOMO of toluene fragment to LUMO of Pd(Ar _F) ₂ fragment)	σ-donation (HOMO-4 of toluene fragment to LUMO+1 of Pd(Ar _F) ₂ fragment)	π back-donation (HOMO-5 of Pd(Ar _F) ₂ fragment to LUMO+1 of toluene fragment)	σ-donation (HOMO-4 of toluene to LUMO+1 of Pd(Ar _F) ₂ fragment)

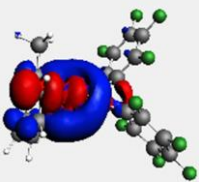
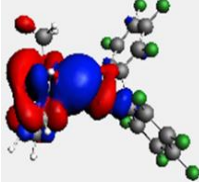
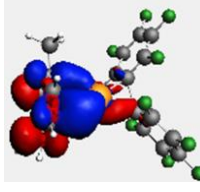
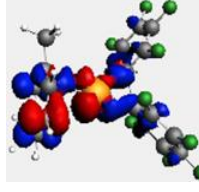
For TS(25-26):

Deformation density	 $\Delta\rho_1; \Delta E^1_{\text{orb}} = -9.6$ kcal/mol; $v = \pm 0.33$	 $\Delta\rho_2; \Delta E^2_{\text{orb}} = -9.8$ kcal/mol; $v = \pm 0.28$	 $\Delta\rho_3; \Delta E^3_{\text{orb}} = -4.6$ kcal/mol; $v = \pm 0.24$	 $\Delta\rho_4; \Delta E^4_{\text{orb}} = -2.9$ kcal/mol; $v = \pm 0.19$
Type of interaction and the orbitals of fragments involved in the interaction	π back-donation (HOMO-3 of Pd(Ar _F) ₂ fragment to LUMO of toluene fragment)	σ-donation (HOMO-1 and HOMO-4 of toluene fragment to LUMO of Pd(Ar _F) ₂ fragment)	σ-donation (HOMO of toluene fragment to LUMO+1 of Pd(Ar _F) ₂ fragment)	π back-donation (HOMO of Pd(Ar _F) ₂ fragment to LUMO+1 of toluene)

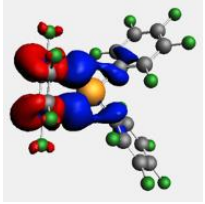
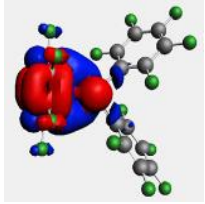
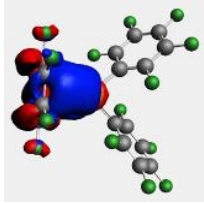
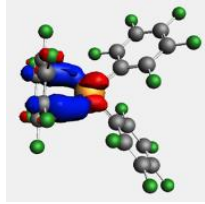
For *cis*-[Pd(C₈H₁₀)(C₆F₅)₂] (30):

Deformation density			
	$\Delta\rho_1; \Delta E^1_{\text{orb}} = -13.4$ kcal/mol; $v = \pm 0.45$	$\Delta\rho_2; \Delta E^2_{\text{orb}} = -7.4$ kcal/mol; $v = \pm 0.26$	$\Delta\rho_3; \Delta E^3_{\text{orb}} = -3.3$ kcal/mol; $v = \pm 0.19$
Type of interaction and the orbitals of fragments involved in the interaction	σ-donation (HOMO of <i>m</i> -xylene fragment to LUMO of Pd(Ar _F) ₂ fragment)	σ-donation (HOMO-4 of <i>m</i> -xylene fragment to LUMO+1 of Pd(Ar _F) ₂ fragment)	π back-donation (HOMO-5 of Pd(Ar _F) ₂ fragment to LUMO+1 of <i>m</i> -xylene fragment)

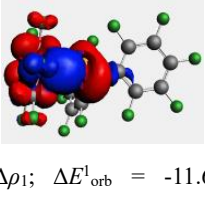
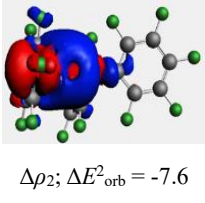
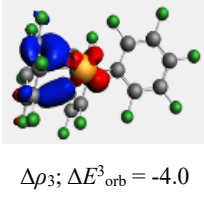
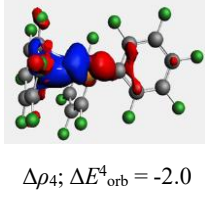
For TS(30-31):

Deformation density				
	$\Delta\rho_1; \Delta E^1_{\text{orb}} = -8.6$ kcal/mol; $v = \pm 0.31$	$\Delta\rho_2; \Delta E^2_{\text{orb}} = -9.7$ kcal/mol; $v = \pm 0.30$	$\Delta\rho_3; \Delta E^3_{\text{orb}} = -4.4$ kcal/mol; $v = \pm 0.22$	$\Delta\rho_4; \Delta E^4_{\text{orb}} = -2.9$ kcal/mol; $v = \pm 0.19$
Type of interaction and the orbitals of fragments involved in the interaction	π back-donation (HOMO-3 of Pd(Ar _F) ₂ fragment to LUMO+1 of <i>m</i> -xylene fragment)	σ-donation (HOMO of <i>m</i> -xylene fragment to LUMO of Pd(Ar _F) ₂ fragment)	σ-donation (HOMO-1 of <i>m</i> -xylene fragment to LUMO+1 of Pd(Ar _F) ₂ fragment)	π back-donation (HOMO of Pd(Ar _F) ₂ fragment to LUMO of <i>m</i> -xylene)

For *cis*-[Pd(C₆F₆)(C₆F₅)₂] (35):

Deformation density	 $\Delta\rho_1; \Delta E^1_{\text{orb}} = -9.1$ kcal/mol; $v = \pm 0.35$	 $\Delta\rho_2; \Delta E^2_{\text{orb}} = -5.9$ kcal/mol; $v = \pm 0.23$	 $\Delta\rho_3; \Delta E^3_{\text{orb}} = -2.1$ kcal/mol; $v = \pm 0.16$	 $\Delta\rho_4; \Delta E^4_{\text{orb}} = -3.4$ kcal/mol; $v = \pm 0.19$
Type of interaction and the orbitals of fragments involved in the interaction	σ-donation (HOMO of perfluorobenzene fragment to LUMO of Pd(Ar _F) ₂ fragment)	σ-donation (HOMO-2 of perfluorobenzene fragment to LUMO+1 of Pd(Ar _F) ₂ fragment)	σ-donation (HOMO-2 of perfluorobenzene to LUMO+1 of Pd(Ar _F) ₂ fragment)	π back-donation (HOMO-5 of Pd(Ar _F) ₂ fragment to LUMO+1 of perfluorobenzene fragment)

For TS(35-36):

Deformation density	 $\Delta\rho_1; \Delta E^1_{\text{orb}} = -11.6$ kcal/mol; $v = \pm 0.35$	 $\Delta\rho_2; \Delta E^2_{\text{orb}} = -7.6$ kcal/mol; $v = \pm 0.29$	 $\Delta\rho_3; \Delta E^3_{\text{orb}} = -4.0$ kcal/mol; $v = \pm 0.21$	 $\Delta\rho_4; \Delta E^4_{\text{orb}} = -2.0$ kcal/mol; $v = \pm 0.12$
Type of interaction and the orbitals of fragments involved in the interaction	π back-donation (HOMO-1 of Pd(Ar _F) ₂ fragment to LUMO of perfluorobenzene fragment)	σ-donation (HOMO of perfluorobenzene fragment to LUMO of Pd(Ar _F) ₂ fragment)	π back-donation (HOMO-6 of Pd(Ar _F) ₂ fragment to LUMO+1 of perfluorobenzene)	σ-donation (HOMO-2 of perfluorobenzene fragment to LUMO+1 of Pd(Ar _F) ₂ fragment)

3.7 References

- [1] a) R. H. Crabtree, *The organometallic chemistry of the transition metals*; 6th Ed.; Wiley-VCH; New York, 2014; b) J. F. Hartwig, *Organotransition metal chemistry: from bonding to catalysis*; University Science Books; Sausalito, CA. **2010**.
- [2] J. F. Hartwig, *Inorg. Chem.* **2007**, *46*, 1936–1947.
- [3] a) P. Espinet, J. M. Martínez-Ilarduya, C. Pérez-Briso, A. L. Casado, M. A. Alonso, *J. Organomet. Chem.* **1998**, *551*, 9–20; b) R. Uson, J. Fornies, J. Gimeno, P. Espinet, R. Navarro, *J. Organomet. Chem.* **1974**, *81*, 115–122; c) G. B. Deacon, I. L. Grayson, *Transition Met. Chem.* **1983**, *8*, 131–139; d) G. Sánchez, J. L. Serrano, F. Momblona, F. Ruiz, J. García, J. Pérez, G. López, P. A. Chaloner, P. Hitchcock, *Polyhedron* **2001**, *20*, 571–578; e) G. García, G. López, *Inorg. Chim. Acta*, **1981**, *52*, 87–90; f) M. D. Rausch, F. E. Tibbetts, *J. Organomet. Chem.* **1970**, *21*, 487–494; g) T. Koizumi, A. Yamazaki, T. Yamamoto, *Dalton Trans.* **2008**, 3949–3952; h) L. Gu, L. M. Wolf, W. Thiel, C. W. Lehmann, M. Alcarazo, *Organometallics* **2018**, *37*, 665–672; i) K. Miki, N. Kasai, H. Kurosawa, *Acta Crystallogr.* **1988**, *C44*, 1131–1134.
- [4] E. F. Santos-Filho, J. C. Sousa, N. M. M. Bezerra, P. H. Menezes, R. A. Oliveira, *Tetrahedron Lett.* **2011**, *52*, 5288–5291.
- [5] a) D. Bulfield, S. M. Huber, *J. Org. Chem.* **2017**, *82*, 13188–13203; b) Y. Nishihara, H. Onodera, K. Osakada, *Chem. Commun.* **2004**, 192–193.
- [6] J. R. Phillips, D. T. Rosevear, F. G. A. Stone, *J. Organomet. Chem.* **1964**, *2*, 455–460.
- [7] D. T. Rosevear, F. G. A. Stone, *J. Chem. Soc.* **1965**, 5275–5279.
- [8] a) M. E. Evans, C. L. Burke, S. Yaibuathes, E. Clot, O. Eisenstein, W. D. Jones, *J. Am. Chem. Soc.* **2009**, *131*, 13464–13473; b) E. Clot, M. Besora, F. Maseras, C. Mégret, O. Eisenstein, B. Oelckers, R. N. Perutz, *Chem. Commun.* **2003**, 490–491; c) E. Clot, C. Mégret, O. Eisenstein, R. N. Perutz, *J. Am. Chem. Soc.* **2009**, *131*, 7817–7827.
- [9] C. Cullinane, G. B. Deacon, P. R. Drago, A. P. Erven, P. C. Junk, J. Luu, G. Meyer, S. Schmitz, I. Ott, J. Schur, L. K. Webstera, A. Klein, *Dalton Trans.* **2018**, *47*, 1918–1932.

- [10] G. López, G. Garcia, M. D. Santana, G. Sánchez, J. Ruiz, J. A. Hermoso, A. Vegas, M. Martínez-Ripoll. *J. Chem. Soc., Dalton Trans.* **1990**, 1621–1626.
- [11] a) H. Yoshida, Y. Yamaryo, J. Ohshita, A. Kunai, *Tetrahedron Lett.* **2003**, *44*, 1541–1544; b) C. Adamo, C. Amatore, I. Ciofini, A. Jutand, H. Lakmini, *J. Am. Chem. Soc.* **2006**, *128*, 6829–6836.
- [12] E. Gioria, J. del Pozo, J. M. Martínez-Ilarduya, P. Espinet, *Angew. Chem., Int. Ed.* **2016**, *55*, 13276–13280.
- [13] a) J. Zhou, M. W. Kuntze-Fechner, R. Bertermann, U. S. D. Paul, J. H. J. Berthel, A. Friedrich, Z. Du, T. B. Marder, U. Radius, *J. Am. Chem. Soc.* **2016**, *138*, 5250–5253; b) Y.-M. Tian, X.-N. Guo, M. W. Kuntze-Fechner, I. Krummenacher, H. Braunschweig, U. Radius, A. Steffen, T. B. Marder, *J. Am. Chem. Soc.* **2018**, *140*, 17612–17623; c) J. Zhou, J. H. J. Berthel, M. W. Kuntze-Fechner, A. Friedrich, T. B. Marder, U. Radius, *J. Org. Chem.* **2016**, *81*, 5789–5794.
- [14] Y. P. Budiman, A. Friedrich, U. Radius, T. B. Marder, *ChemCatChem* **2019**, *11*, 5387–5396..
- [15] a) B. Maiti, K. Wang, S. Bhandari, S. D. Bunge, R. J. Twieg, B. D. Dunietz, *J. Mater. Chem. C*, **2019**, *7*, 3881–3888; b) M.-H. Yoon, A. Facchetti, C. E. Stern, T. J. Marks, *J. Am. Chem. Soc.* **2006**, *128*, 5792–5801.
- [16] Y. Sakamoto, T. Suzuki, A. Miura, H. Fujikawa, S. Tokito, Y. Taga, *J. Am. Chem. Soc.* **2000**, *122*, 1832–1833.
- [17] a) J. Lieffrig, A. G. Niassy, O. Jeannin, M. Fourmigue, *CrystEngComm* **2015**, *17*, 50–57; b) G. M. Espallargas, A. Recuenco, F. M.; Romero, L. Brammer, S. Libri, *CrystEngComm* **2012**, *14*, 6381–6383.
- [18] H. Yi, M. Albrecht, A. Valkonen, K. Rissanen, *New J. Chem.* **2015**, *39*, 746–749.
- [19] J. M. Weibel, A. Blanc, P. Pale, *Chem. Rev.* **2008**, *108*, 3149–3173.
- [20] Ag₂O-promoted Suzuki–Miyaura reactions of C₆F₅B(OR)₂ have been reported. See: a) N. Y. Adonin, V. B. Vadim, *Russ. Chem. Rev.* **2010**, *79*, 757–785; b) V. V. Bardin, A. Y. Shabalina, N. Y. Adonin, *Beilstein J. Org. Chem.* **2015**, *11*, 608–616; c) T. Korenaga, T. Kosaki, R. Fukumura, T. Ema, T. Sakai, *Org. Lett.* **2005**, *7*, 4915–4917; d) K. Takimiya, N.

- Niihara, T. Otsubo, *Synthesis* **2005**, *10*, 1589–1592; e) J. Chen, A. Cammers-Goodwin, *Tetrahedron Lett.* **2003**, *44*, 1503–1506; f) H.-J. Frohn, N. Y. Adonin, V. V. Bardin, V. F. Starichenko, *J. Fluorine Chem.* **2003**, *122*, 195–199; g) H.-J. Frohn, N. Y. Adonin, V. V. Bardin, V. F. Starichenko, *Tetrahedron Lett.* **2002**, *43*, 8111–8114.
- [21] M. Pérez-Rodríguez, A. A. C. Braga, M. Garcia-Melchor, M. H. Pérez-Temprano, J. A. Casares, G. Ujaque, A. R. de Lera, R. Álvarez, F. Maseras, P. Espinet, *J. Am. Chem. Soc.* **2009**, *131*, 3650–3657.
- [22] a) I. Ara, J. Forniés, A. Martín, L. F. Martín, B. Menjón, H. Miedes, *Dalton Trans.* **2010**, *39*, 7301–7309; b) J. Ruiz, V. Rodríguez, N. Cutillas, G. López, *Organometallics* **2002**, *21*, 4912–4918; c) J. Ruiz, C. Natalia, R. Venancio, J. Sampedro, G. López, P. A. Chaloner, P. B. Hitchcock, *J. Chem. Soc., Dalton Trans.* **1999**, 2939–2946; d) J. Ruiz, V. Rodríguez, C. de Haro, A. Espinosa, J. Pérez, *Dalton Trans.* **2010**, *39*, 3290–3301.
- [23] R. Díaz-Torres, S. Alvarez, *Dalton Trans.* **2011**, *40*, 10742–10750.
- [24] a) A. Ariaifard, B. F. Yates, *J. Organomet. Chem.* **2009**, *694*, 2075–2084; b) V. P. Ananikov, D. G. Musaev, K. Morokuma, *Eur. J. Inorg. Chem.* **2007**, 5390–5399.
- [25] a) Y. Wei, J. Kan, M. Wang, W. Su, M. Hong, *Org. Lett.* **2009**, *11*, 3346–3349; b) Y. Wei, W. Su, *J. Am. Chem. Soc.* **2010**, *132*, 16377–16379; c) H. Li, J. Liu, C.-L. Sun, B.-J. Li, Z.-J. Shi, *Org. Lett.* **2010**, *13*, 276–279; d) X. Fang, Y. Huang, X. Chen, X. Lin, Z. Bai, K. W. Huang, Y. Yuan, Z. Weng, *J. Fluorine Chem.* **2013**, *151*, 50–57.
- [26] F. H. Allen, O. Kennard, D. G. Watson, L. Brammer, A. G. Orpen, R. Taylor, *J. Chem. Soc., Perkin Trans. 2*, **1987**, S1-S19.
- [27] a) C. P. Brock, D. G. Nae, N. Goodhand, T. A. Hamor, *Acta Crystallogr.* **1978**, *B34*, 3691–3696; b) A. U. Meyer, T. Slanina, C.-J. Yao, B. König, *ACS Catal.* **2016**, *6*, 369–375; c) R. Heckel, J. Hulliger, A. Schwarzer, E. Weber, *Acta Crystallogr.* **2015**, *E71*, o347-o348.
- [28] a) L. Xue, Z. Lin, *Chem. Soc. Rev.* **2010**, *39*, 1692–1705; b) M. García-Melchor, A. A. C. Braga, A. Lledós, G. Ujaque, F. Maseras, *Acc. Chem. Res.* **2013**, *46*, 2626–2634.
- [29] a) H. Zhang, X. Luo, K. Wongkhan, H. Duan, Q. Li, L. Zhu, J. Wang, A. S. Batsanov, J. A. K. Howard, T. B. Marder, A. Lei, *Chem. Eur. J.* **2009**, *15*, 3823–3829; b) L. Jin, H. Zhang,

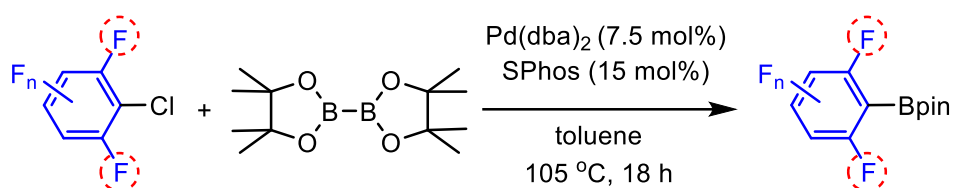
- P. Li, J. R. Sowa, A. Lei, *J. Am. Chem. Soc.* **2009**, *131*, 9892–9893; c) J. S. Mathew, M. Klussmann, H. Iwamura, F. Valera, A. Futran, E. A. C. Emanuelsson, D. G. Blackmond, *J. Org. Chem.* **2006**, *71*, 4711–4722; d) M. Ohashi, R. Doi, S. Ogoshi, *Chem. Eur. J.* **2014**, *20*, 2040–2048; e) T. Kinzel, Y. Zhang, S. L. Buchwald, *J. Am. Chem. Soc.* **2010**, *132*, 14073–14075; f) H.-H. Zhang, J. Dong, Q.-S. Hu, *Eur. J. Org. Chem.* **2014**, *2014*, 1327–1332; g) E. J. Cho, T. D. Senecal, T. Kinzel, Y. Zhang, D. A. Watson, S. L. Buchwald, *Science* **2010**, *328*, 1679–1681; h) M. C. Nielsen, K. J. Bonney, F. Schoenebeck, *Angew. Chem., Int. Ed.* **2014**, *53*, 5903–5906.
- [30] K. Tatsumi, R. Hoffmann, A. Yamamoto, J. K. Stille, *Bull. Chem. Soc. Jpn*, **1981**, *54*, 1857–1867.
- [31] a) J. J. Low, W. A. Goddard, *J. Am. Chem. Soc.* **1984**, *106*, 6928–6937; b) J. J. Low, W. A. Goddard, *Organometallics* **1986**, *5*, 609–622; c) J. J. Low, W. A. Goddard, *J. Am. Chem. Soc.* **1986**, *108*, 6115–6128.
- [32] T. Korenaga, K. Abe, A. Ko, R. Maenishi, T. Sakai, *Organometallics* **2010**, *29*, 4025–4035.
- [33] a) M. P. Mitoraj, A. Michalak, T. A. Ziegler, *J. Chem. Theory Comput.* **2009**, *5*, 962–975; b) L. Zhao, M. von Hopffgarten, D. M. Andrada, G. Frenking, *Wiley Interdiscip. Rev. Comput. Mol. Sci.* **2018**, *8*, e1345.
- [34] S. A. Macgregor, D. Christopher Roe, W. J. Marshall, K. M. Bloch, V. I. Bakmutov, V. V. Grushin, *J. Am. Chem. Soc.* **2005**, *127*, 15304–15321.
- [35] M. Hofer, E. Gomez-Bengo, C. A. Nevado, *Organometallics* **2014**, *33*, 1328–1332.
- [36] G. B. Deacon, R. J. Phillips, *Aust. J. Chem.* **1978**, *31*, 1729–1724.
- [37] K. Kikushima, M. Grellier, M. Ohashi, M. Ogoshi, *Angew. Chem., Int. Ed.* **2017**, *56*, 16191–16196.
- [38] T. Truong, J. Alvarado, L. D. Tran, O. Daugulis, *Org. Lett.* **2010**, *2*, 1200–1203.
- [39] G. B. Deacon, A. J. Koplick, W. D. Ravertyand, D. G. Vince, *J. Org. Chem.* **1979**, *182*, 121–141.
- [40] B. Maiti, K. Wang, S. Bhandari, S. D. Bunge, R. J. Twieg, B. D. Dunietz, *J. Mater. Chem. C*, **2019**, *7*, 3881–3888.

- [41] S. A. R. Mulla, S. S. Chavan, M. Y. Pathan, S. M. Inamdar, T. M. Y. Shaikh, *RSC Adv.* **2015**, *5*, 24675–24680.
- [42] G. Sheldrick, *Acta Crystallogr.* **2015**, *A71*, 3–8.
- [43] Sheldrick, *Acta Crystallogr.* **2008**, *A64*, 112–122.
- [44] C. B. Hübschle, G. M. Sheldrick, B. Dittrich, *J. Appl. Crystallogr.* **2011**, *44*, 1281–1284.
- [45] K. Brandenburg, Diamond (version 4.4.0), Crystal and Molecular Structure Visualization, Crystal Impact H. Putz & K. Brandenburg GbR, Bonn (Germany), **2017**.
- [46] M. J. Frisch, G. W. Trucks, H. B. Schlegel, G. E. Scuseria, M. A. Robb, J. R. Cheeseman, G. Scalmani, V. Barone, B. Mennucci, G. A. Petersson, H. Nakatsuji, M. Caricato, X. Li, H. P. Hratchian, A. F. Izmaylov, J. Bloino, G. Zheng, J. L. Sonnenberg, M. Hada, M. Ehara, K. Toyota, R. Fukuda, J. Hasegawa, M. Ishida, T. Nakajima, Y. Honda, O. Kitao, H. Nakai, T. Vreven, J. A. Montgomery, Jr., J. E. Peralta, F. Ogliaro, M. Bearpark, J. J. Heyd, E. Brothers, K. N. Kudin, V. N. Staroverov, T. Keith, R. Kobayashi, J. Normand, K. Raghavachari, A. Rendell, J. C. Burant, S. S. Iyengar, J. Tomasi, M. Cossi, N. Rega, J. M. Millam, M. Klene, J. E. Knox, J. B. Cross, V. Bakken, C. Adamo, J. Jaramillo, R. Gomperts, R. E. Stratmann, O. Yazyev, A. J. Austin, R. Cammi, C. Pomelli, J. W. Ochterski, R. L. Martin, K. Morokuma, V. G. Zakrzewski, G. A. Voth, P. Salvador, J. J. Dannenberg, S. Dapprich, A. D. Daniels, O. Farkas, J. B. Foresman, J. V. Ortiz, J. Cioslowski, D. J. Fox, *Gaussian 09 (Rev. E.01)*, Gaussian, Inc.: Wallingford CT, **2010**.
- [47] a) A. D. Becke, *Phys. Rev. A*, **1988**, *38*, 3098–3100; b) A. D. Becke, *J. Chem. Phys.* **1993**, *98*, 5648–5652; c) C. Lee, W. Yang, R. G. Parr, *Phys. Rev. B*, **1988**, *37*, 785–789.
- [48] J. Tomasi, B. Mennucci, R. Cammi, *Chem. Rev.* **2005**, *105*, 2999–3094.
- [49] a) S. Grimme, S. Antony, S. Ehrlich, H. Krieg, *J. Chem. Phys.*, **2010**, *132*, 15414; b) S. Grimme, S. Ehrlich, L. Goerigk, *J. Comp. Chem.* **2011**, *32*, 1456–1465.
- [50] J. Baker, *J. Comp. Chem.* **1986**, *7*, 385–395.
- [51] a) A. L. L. East, G. M. Berner, A. D. Morcom, L. Mihichuk, *J. Chem. Theory Comput.*, **2008**, *4*, 1274–1282; b) A. Jayaraman, L. L. East, *J. Org. Chem.* **2012**, *77*, 351–356; c) S. Nilewar, A. Jayaraman, B. T. Sterenberg, *Organometallics* **2018**, *37*, 4699–4710; d) A.

- Jayaraman, G. M. Berner, L. M. Mihichuk, A. L. L. East, *J. Mol. Catal. A.* **2011**, *351*, 143–153;
- e) A. Jayaraman, H. Powell-Davies, F. G. Fontaine, *Tetrahedron* **2019**, *75*, 2118–2127.
- [52] ADF 2017.207, SCM, Theoretical chemistry, Vrije Universiteit, Amsterdam, The Netherlands, <http://www.scm.com>.
- [53] a) K. J. Morokuma, *Chem. Phys.* **1971**, *55*, 1236; b) T. Ziegler, A. Rauk, *Inorg. Chem.* **1979**, *18*, 1755–1759.
- [54] a) M. Mitoraj, A. Michalak, *Organometallics* **2007**, *26*, 6576–6580; b) M. Mitoraj, A. Michalak, *J. Mol. Model* **2008**, *14*, 681–687.
- [55] M. P. Mitoraj, A. Michalak, T. A. Ziegler, *J. Chem. Theory Comput.* **2009**, *5*, 962–975.
- [56] L. Zhao, *Wiley Interdiscip. Rev. Comput. Mol. Sci.* **2018**, *8*, e1345.

Chapter 4

Base-Free Pd-Catalyzed C–Cl Borylation of Fluorinated Aryl Chlorides



base-free-helps to stabilize the products

4 Base-Free Pd-Catalyzed C–Cl Borylation of Fluorinated Aryl Chlorides

4.1 Abstract

Catalytic C–X borylation of aryl halides containing two *ortho*-fluorines has been found to be challenging, as most previous methods require stoichiometric amounts of base and the polyfluorinated aryl boronates suffer from protodeboronation, which is accelerated by *ortho*-fluorine substituents. Herein, we report that a combination of Pd(dba)₂ (dba = dibenzylideneacetone) with SPhos (2-dicyclohexylphosphino-2',6'-dimethoxybiphenyl) as a ligand is efficient to catalyze the C–Cl borylation of aryl chlorides containing two *ortho*-fluorine substituents. This method, conducted under base-free conditions, is compatible with the resulting di-*ortho*-fluorinated aryl boronate products which are sensitive to base.

4.2 Introduction

Fluorine-containing organic molecules have found many applications in pharmaceuticals,^[1] agrochemicals,^[2] and organic materials.^[3] Currently, one-third of the top performing drugs on the market possess fluorine in their structures,^[1–8] and some contain two *ortho*-fluorine substituents (Figures 4-1 and 4-2). As a source of naturally occurring aryl fluorides has not been identified, this class of molecules must be produced through chemical synthesis.

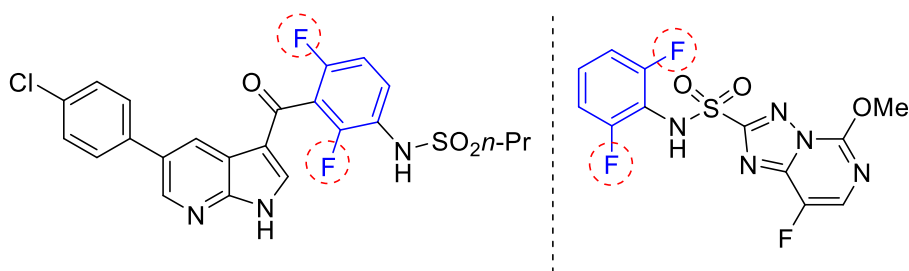


Figure 4-1. Di-*ortho*-fluorinated arene-containing drugs and agrochemicals: Vemuravenib (left) used for treatment of late-stage of melanoma. Florasulam (right) is used as herbicide.^[1a,2c]

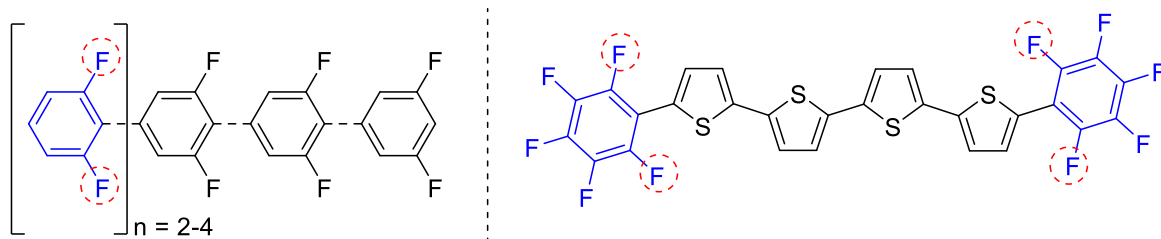
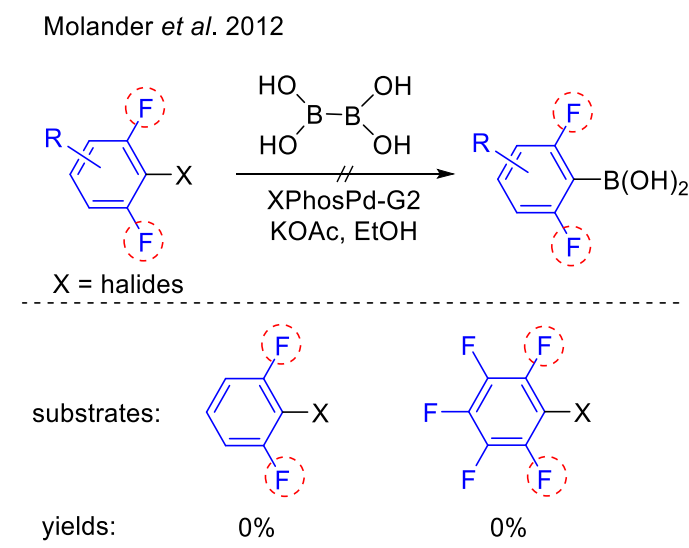


Figure 4-2. Fluoroarenes in materials science: 2,6-difluorinated oligophenyls (left) and fluoroarene-thiophene oligomer (right) for semi conductors.^[3c,d]

Currently, one promising methodology to produce functionalized fluorine-containing organic compounds utilizes borylation chemistry, and the resulting boryl group can be converted into diverse functional groups. Recently, transition metal-catalyzed C–H borylation of arenes with *ortho*-to-fluorine selectivity has been reported.^[4-6] However, contamination by side products occurring from borylation *meta*- or *para*-to-fluorine positions led to difficulty in purification. Thus, C–X borylation reactions ($X = \text{halide}$) provide an option for introducing boronate ester groups selectively into fluorinated aryl halides.^[7]

Catalytic processes to convert di-*ortho*-fluorinated aryl halides into boronate analogues are difficult as most such methodologies require use of stoichiometric amounts of base,^[7] and the resulting di-*ortho*-fluorinated aryl boronate derivatives are not stable under such conditions due to protodeboration^[8] which is accelerated by *ortho*-fluorine substituents. The mechanism of protodeboration of aryl boronic acids containing two *ortho*-fluorine substituents was examined by Lloyd-Jones *et al.*^[8a] via experimental and computational studies. They reported that rapid protodeboration of di-*ortho*-fluorinated aryl boronic acids occurs via C–B heterolysis of a trihydroxy organoboronate intermediate ($[M]^+[ArB(OH)_3]^-$), which notably does not need water at this step. Subsequently, proton transfer from water led to the hydrolyzed product. Twenty isomers of $C_6F_{5-n}H_nB(OH)_2$ were studied with half-lives ($t_{1/2}$) spanning 9 orders of magnitude, from < 3 minutes to 6.5 months, and it was observed that *ortho*-fluorinated aryl boronic acids accelerated protodeboration, with $C_6F_5B(OH)_2$ showing the fastest rate.^[8a] Protodeboration also occurred with di-*ortho*-fluorinated aryl-Bpin (Bpin = 4,4,5,5-tetramethyl-1,3,2-dioxaborolanyl) compounds although the rate is slower than that for $-B(OH)_2$ analogues.^[4a,8c]

In 2012, Molander *et al.* reported borylation of aryl-X (X = Br, Cl, I, OTf) with $B_2(OH)_4$ using the second-generation Buchwald precatalyst XPhosPd-G2, followed by the conversion of the aryl boronic acids into potassium trifluoroborate analogues. This method is effective to generate borylated products in good to excellent yields. However, if the C–X bond is flanked by two C–F bonds, *e.g.*, 2-bromo-1,3-difluorobenzene and 1-chloro-2,3,4,5,6-pentafluorobenzene, the borylations were difficult (Scheme 4-1).^[7k] Thus, effective catalytic C–X borylation methods to convert 2,6-di-*ortho*-fluorinated aryl halides into boronate analogues remain challenging.



Scheme 4-1. Previous efforts to borylate di-*ortho*-fluorinated aryl-halides.

Previously, the only reliable aryl halide C–X borylation methods to generate aryl boronates containing two *ortho*-fluorines were stoichiometric processes *via* conversion of fluorinated aryl halides into aryl lithium or aryl Grignard reagents followed by addition of trialkoxyborates to generate fluorinated aryl trialkoxyborates.^[8a,9] Subsequent addition of HCl led to the generation of the corresponding boronic acid. Unfortunately, these traditional methodologies suffered from low yields and harsh reaction conditions as both aryl lithium and Grignard reagents react violently with oxygen and moisture and decompose readily, and the formation of stoichiometric metal salts made isolation of the desired products difficult.

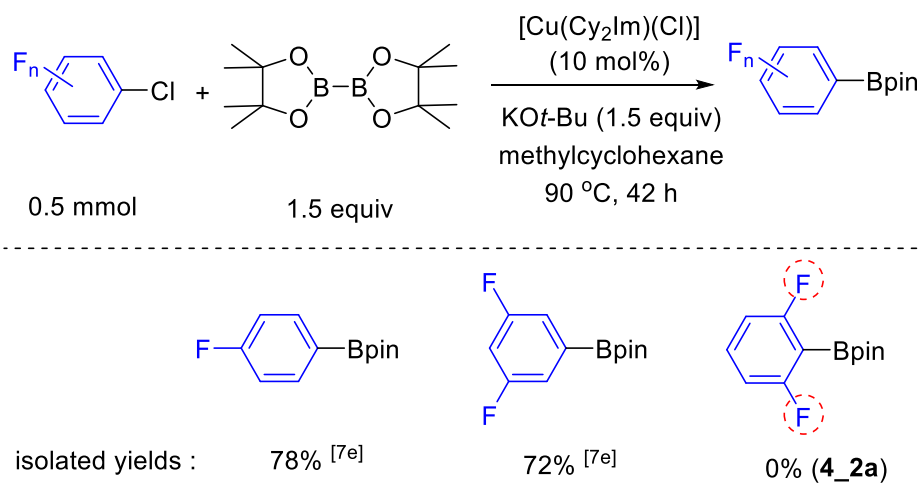
Recently, we have reported thermal^[10a] and photocatalytic^[10b] C–F borylation of partially fluorinated arenes using NHC nickel complexes (NHC = *N*-Heterocyclic Carbene) to generate

fluorinated aryl-Bpin in fair to excellent yields. The reactions are effective and selective to give the fluorinated aryl boronates containing one or no *ortho*-fluorines, but not selective to generate aryl boronates containing two *ortho*-fluorines. Notably, the borylation of C₆F₆ to generate C₆F₅Bpin gave a low yield.

Very recently, we have reported applications of fluorinated aryl boronate substrates, including those containing two *ortho*-fluorines, in Suzuki-Miyaura cross-couplings^[11a] and oxidative cross-couplings with terminal alkynes^[11b] using copper catalysts, and homocoupling reactions using palladium catalysts.^[12] Compared to aryl bromides and iodides, aryl chlorides are less expensive and more readily available. Herein we reported a method to provide di-*ortho*-fluorinated aryl boronates, *via* the palladium-catalyzed C–Cl borylation of di-*ortho*-fluorinated aryl chlorides using B₂pin₂ in good to excellent yields. This method is conducted under base-free conditions, thus, stabilizing the di-*ortho*-fluorinated boronate products from decomposition.

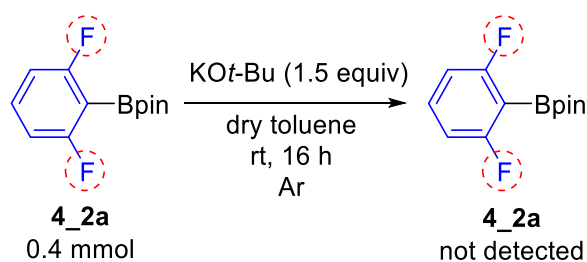
4.3 Results and Discussion

We previously reported that copper NHC complexes are efficient catalysts for C–Cl borylation in the presence of stoichiometric amounts of a strong base such as potassium *tert*-butoxide (KO*t*-Bu), in methylcyclohexane, at 90 °C. These conditions were efficient to generate fluorinated aryl-Bpin compounds such as 4-fluorophenyl-Bpin, and 3,5-difluorophenyl-Bpin, in which the fluorines are present in *para*- or di-*meta*-positions (Scheme 4-2).^[7e] We tested this set of conditions employing the challenging substrate 2-chloro-1,3-difluorobenzene, in which fluorines are present in both *ortho*-positions. However, this method failed as no borylated products were detected (Scheme 4-2). It should be noted that Frohn and Adonin *et al.* examined the treatment of fluorinated aryl boronic acids with wet pyridine.^[8c] Unlike *ortho*-fluorinated aryl boronic acid derivatives which are protodeboronated rapidly, interestingly, electron-deficient aryl boronic acids with no *ortho*-fluorines, such as 3,4,5-trifluorophenyl boronic acid, are stable towards protodeboronation even at 100 °C after 3 hours.



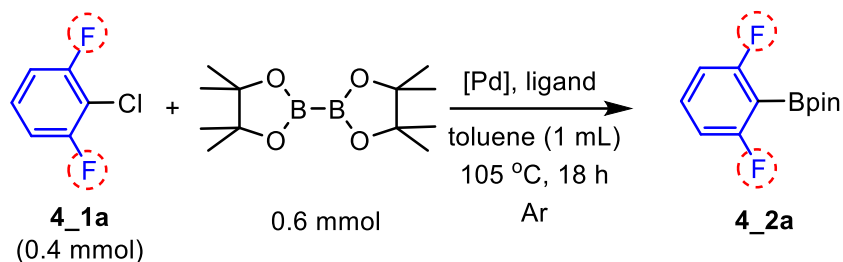
Scheme 4-2. Cu-catalyzed C–Cl borylation of fluorinated aryl chlorides.

We believed that such a low yield of **4_2a** (Scheme 4-2) is due to the decomposition of the borylated product 2,6-fluorophenyl-Bpin in the presence of the strong base KO*t*-Bu. Thus, we reacted 0.4 mmol of 2,6-fluorophenyl-Bpin, with 0.6 mmol of KO*t*-Bu in a vial containing 4 mL of dry toluene with stirring at room temperature for 16 hours under argon (Scheme 4-3). Afterward, the reaction mixture was examined by ¹⁹F {¹H} NMR spectroscopy (under argon) and GC-MS (in air). We found that 2,6-difluorophenyl-Bpin was no longer present. In addition, in 2012 Hartwig *et al.* reported that 2,6-difluorophenyl-Bpin decomposed within 30 minutes in a THF solution containing a weak base such as 2 M aqueous Na₂CO₃, at 50 °C.^[4a] In 2018, Carrow *et al.* treated C₆F₅Bpin and C₆F₅B(OH)₂ with wet triethylamine (weak base), and found that C₆F₅Bpin underwent protodeboronation, but the rate was slower than that for C₆F₅B(OH)₂.^[8e] Hence, it can be suggested that the best conditions to synthesize 2,6-difluorophenyl-Bpin derivatives are base-free methods. Previously, we tried to use our optimized conditions with the NHC-copper complex to catalyze the C–Cl borylation of aryl chlorides, without base, but it did not work.^[7e]

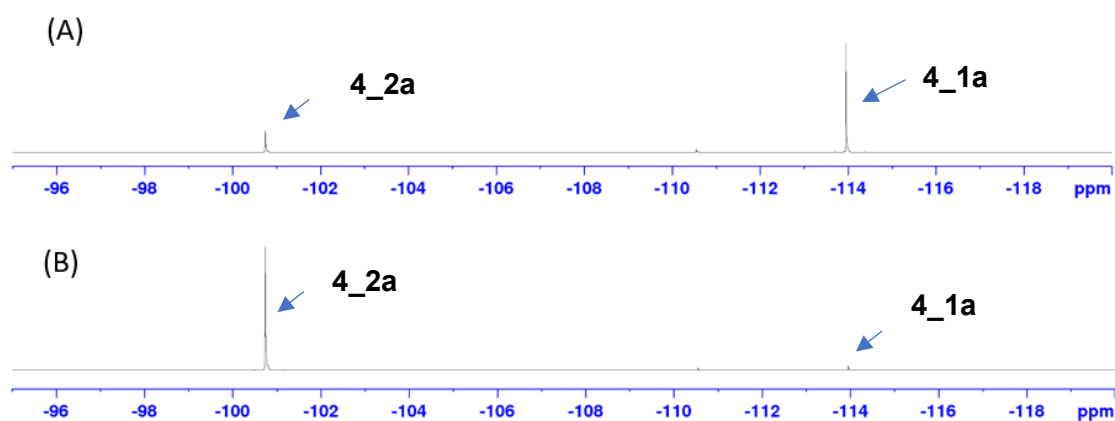


Scheme 4-3. KO*t*-Bu promoted decomposition of 2,6-di-fluorophenyl-Bpin.

Recently, Matsubara and Yorimitsu *et al.* reported that a combination of catalytic amounts of Pd₂(dba)₃ (tris(dibenzylideneacetone)dipalladium(0)) and SPhos (2-dicyclohexylphosphino-2',6'-dimethoxybiphenyl) in toluene under base-free conditions, is effective to catalyze C–Cl borylation of aryl chlorides, using B₂pin₂ as the boron source. However, aryl chloride substrates containing two *ortho*-fluorine substituents were not examined.^[13] Hence, we used the Matsubara and Yorimitsu conditions, for the borylation of 1,5-difluoro-6-chloro-benzene, with stirring for 18 h at 105 °C. Surprisingly, it is not efficient as only a 17% yield of product was isolated (Table 4-1, entry 1). Interestingly, using Pd(dba)₂ instead of Pd₂(dba)₃ increased the efficiency to 92% yield. We repeated the reactions under the conditions in Table 4-1, entries 1 and 2, and *in situ* ¹⁹F{¹H} NMR spectroscopy confirmed that a combination Pd(dba)₂ as a precatalyst and SPhos as a ligand gave 99% conversion (Figure 4-3). We also utilized both commercial and freshly prepared samples of Pd₂(dba)₃ with similar results. The lower activity of Pd₂(dba)₃ compared with that of Pd(dba)₂ is likely a result of the lower solubility of the former in toluene. Using the Pd(II) salt Pd(OAc)₂ proved inefficient (Table 4-1, entry 3). Other ligands such as *Pt*Bu₃ (tri-*tert*-butylphosphine) and JohnPhos (2-(di-*tert*-butylphosphino)biphenyl) in combination with Pd(dba)₂ decreased the efficiency (Table 4-1, entries 4 and 5). No reactions were observed using bidentate phosphine or nitrogen-based ligands such as XantPhos (4,5-bis(diphenylphosphino)-9,9-dimethylxanthene), dppp (1,3-bis(diphenylphosphino)propane), or phenanthroline (Table 4-1, entries 6-8).

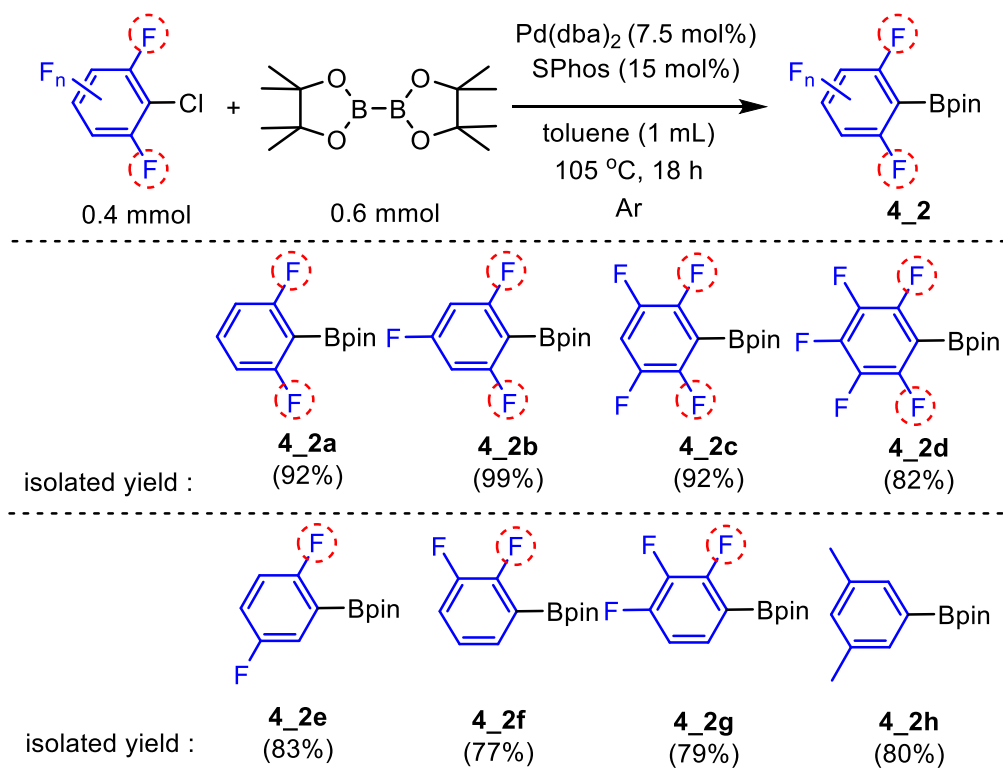
Table 4-1. Reaction conditions screened for the Pd-catalyzed borylation of 1,5-difluoro-6-chlorobenzene.

Entry	[Pd]	Ligand	Isolated yield
1	Pd ₂ (dba) ₃ (4 mol%)	SPhos (16 mol%)	17%
2	Pd(dba)₂ (7.5 mol%)	SPhos (15 mol%)	92%
3	Pd(OAc) ₂ (8 mol%)	SPhos (16 mol%)	11%
4	Pd(dba) ₂ (8 mol%)	PtBu ₃ (16 mol%)	61%
5	Pd(dba) ₂ (8 mol%)	JohnPhos (16 mol%)	35%
6	Pd(dba) ₂ (8 mol%)	XantPhos (8 mol%)	0%
7	Pd(dba) ₂ (8 mol%)	DPPP (8 mol%)	0%
8	Pd(dba) ₂ (8 mol%)	phenanthroline (8 mol%)	0%

**Figure 4-3.** ¹⁹F {¹H} NMR spectra of reaction mixtures: (A) conditions stated in Table 4-1, entry 1; (B) conditions stated in Table 4-1, entry 2.

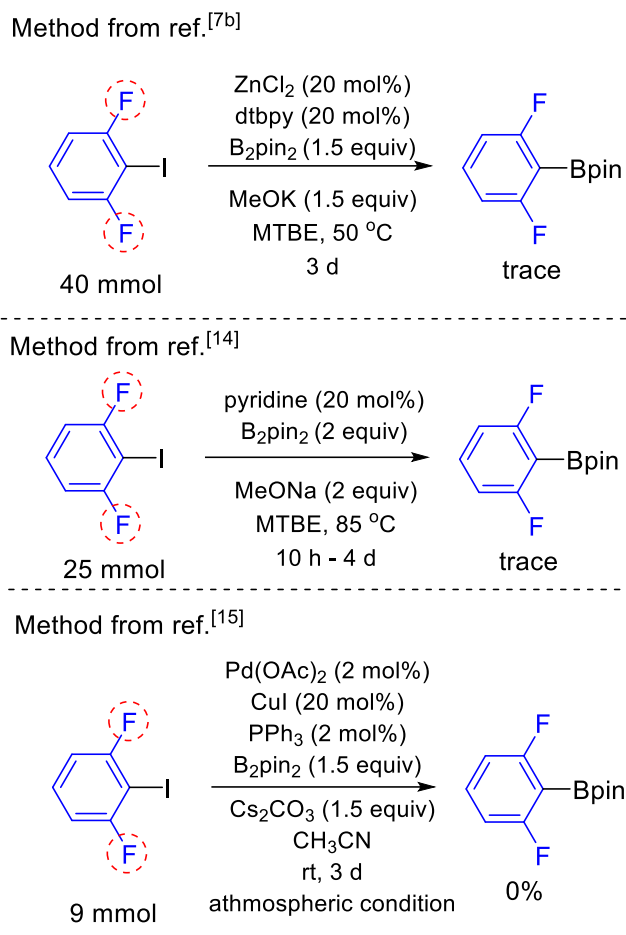
Having optimal conditions in hand, we expanded the scope reactions for other fluorinated aryl chloride substrates (Scheme 4-4), thus generating di-*ortho*-fluorinated aryl-Bpin derivatives

(**4_2a** – **4_2d**) via catalytic C–Cl borylation in excellent yields. The substrate scope was expanded to include aryl chlorides containing one or no *ortho*-fluorines and the products (**4_2e** – **4_2h**) were isolated in good to very good yields.



Scheme 4-4. Reaction scope for the borylation of fluorinated aryl chloride derivatives.

We also attempted to use other established methods for the C–X borylation of aryl halides containing two *ortho*-fluorine substituents. Notably, those methods require stoichiometric amounts of base, and proved efficient to generate aryl boronates in good to excellent yields.^[7b,14,15] However, employing aryl halides containing two *ortho*-fluorines were not examined in the previous studies. Thus, we attempted to use those methods to employ aryl halides containing two *ortho*-fluorine substituents. Not surprisingly, they proved inefficient (Scheme 4-5).



Scheme 4-5. Attempted borylation of di-*ortho*-fluorinated aryl halides using established methods that require stoichiometric amounts of base.

4.4 Conclusions

In summary, we report a base-free catalytic method for C–Cl borylation of aryl chlorides containing two *ortho*-fluorines using a combination of Pd(dba)₂ and SPhos as a ligand, to generate previously challenging di-*ortho*-fluorinated aryl-Bpin products. Our base-free conditions prevent the decomposition of the di-*ortho*-fluorinated aryl boronate products. This method provides a nice alternative to traditional approaches using lithium or Grignard reagents.^[8a,9] The fluorinated aryl boronate products are useful substrates for Suzuki-Miyaura cross-coupling with aryl halides,^[11a] oxidative cross-coupling with terminal alkynes,^[11b] homocoupling reactions,^[12] etc.

4.5 Detailed Experiments and Characterization Data

4.5.1 General Information

Unless otherwise noted, all reagents were purchased from Alfa-Aesar, Sigma-Aldrich, Fluorochem, Apollo Chemicals, Acros, OxChem and were checked for purity by GC-MS and/or ^1H NMR spectroscopy and used as received. B_2pin_2 was kindly provided by AllyChem Co. Ltd. (Dalian, China). HPLC grade solvents were argon saturated, dried using an Innovative Technology Inc. Pure-Solv Solvent Purification System, and further deoxygenated using the freeze-pump-thaw method.

Automated flash chromatography was performed using silica gel (Biotage SNAP cartridge KP-Sil 10 g and KP-Sil 25 g) using a Biotage® Isolera Four system. Commercially available, precoated TLC plates (Polygram® Sil G/UV254) were purchased from Machery-Nagel. The removal of solvent was performed on a rotary evaporator *in vacuo* at a maximum temperature of 40 °C.

GC-MS analyses were performed using an Agilent 7890A gas chromatograph (column: HP-5MS 5% phenylmethylsiloxane, 10 m, Ø 0.25 mm, film 0.25 µm; injector: 250 °C; oven: 40 °C (2 min), 40 °C to 280 °C (20 °C·min⁻¹); carrier gas: He (1.2 mL min⁻¹) equipped with an Agilent 5975C inert MSD with triple-axis detector operating in EI mode and an Agilent 7693A series auto sampler/injector. HRMS analyses were performed using a Thermo Fischer Scientific Exactive Plus Orbitrap MS system (APCI and ASAP probe).

All NMR spectra were recorded at 298 K using Bruker Avance I 500 (^1H NMR, 500 MHz; $^{13}\text{C}\{^1\text{H}\}$ NMR, 126 MHz; ^{19}F NMR, 471 MHz), Bruker DRX-300 ($^{13}\text{C}\{^1\text{H}\}$ 75 MHz; $^{11}\text{B}\{^1\text{H}\}$, 96 MHz), or Bruker Avance Neo (^1H NMR, 400 MHz; $^{13}\text{C}\{^1\text{H}\}$ NMR, 101 MHz; $^{19}\text{F}\{^1\text{H}\}$ NMR, 377 MHz) spectrometers. ^1H NMR chemical shifts are reported relative to TMS and were referenced *via* residual proton resonances of the corresponding deuterated solvent (CDCl_3 : 7.26 ppm), $^{13}\text{C}\{^1\text{H}\}$ NMR spectra are reported relative to TMS *via* the carbon signals of the deuterated solvent (CDCl_3 : 77.16 ppm), ^{19}F NMR and $^{19}\text{F}\{^1\text{H}\}$ spectra are reported relative to external CFCl_3 , and $^{11}\text{B}\{^1\text{H}\}$

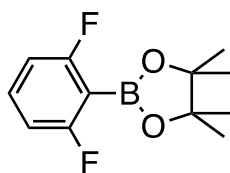
NMR chemical shifts are quoted relative to $\text{BF}_3 \cdot \text{Et}_2\text{O}$ as external standard. In the $^{19}\text{F}\{^1\text{H}\}$ and ^{19}F NMR spectra of some of the products containing fluorine atoms *ortho* to the boryl group, a smaller set of signals can be observed slightly downfield from the larger signals, with an integration ratio of ca. 20:80, which is the result of the natural abundance of the ^{10}B and ^{11}B isotopes. As the isotope effect is relatively small, it is only observed for most downfield shifted resonances assigned to the *ortho* fluorines, as these F atoms are closest to the boron atom.

4.5.2 General Procedure for Pd-Catalyzed C–Cl Borylation

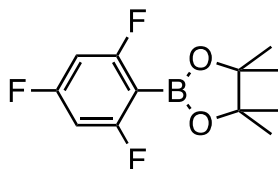
In a glove box, under an argon atmosphere, into a dried vial equipped with a stirring bar and containing 1 mL of toluene, were added $\text{Pd}(\text{dba})_2$ (17 mg, 0.03 mmol), and SPhos (25 mg, 0.06 mmol), and the mixture was stirred until homogeneous. Then, B_2pin_2 (152 mg, 0.6 mmol) and the corresponding fluorinated aryl chlorides (0.4 mmol) were added. After sealing the vial and removal from the glove box, the suspension was stirred for 18 h at 105 °C. After cooling to room temperature, the solvent was evaporated *in vacuo* and the residue was purified by flash column chromatography on silica gel (ethyl acetate : hexane = 2 : 98) and the product was crystallized in a freezer (-30 °C).

4.5.3 Characterization (GC-MS, NMR and HRMS data) of Products

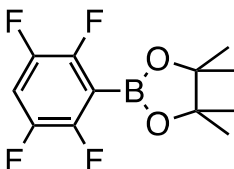
2-(2,6-difluorophenyl)-4,4,5,5-tetramethyl-1,3,2-dioxaborolane (4_2a)



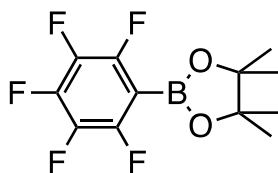
Isolated yield: 92% (88 mg, pale yellow solid). ^1H NMR (400 MHz, CDCl_3) δ = 7.35 (*tt*, J = 8, 7 Hz, 1H), 6.87–6.81 (*m*, 2H), 1.38 (*s*, 12H); $^{19}\text{C}\{^1\text{H}\}$ NMR (100 MHz, CDCl_3) δ = 166.8 (*dd*, $^1J_{\text{C-F}}$ = 250 Hz, $^3J_{\text{C-F}}$ = 13 Hz), 133.2 (*t*, $^3J_{\text{C-F}}$ = 11 Hz), 111.2 (*m*), 84.4, 24.9; $^{19}\text{F}\{^1\text{H}\}$ NMR (377 MHz, CDCl_3) δ = 100.7 (*s*, 2F); $^{11}\text{B}\{^1\text{H}\}$ NMR (160 MHz, CDCl_3) δ = 29.8; GC-MS: [t = 9.196 min] m/z: 240 [M] $^+$; **HRMS (APCI)** calcd for [$\text{C}_{12}\text{H}_{16}\text{BF}_2\text{O}_2$] $^+$ [M +H] $^+$: 241.1206; found 241.1195. Spectroscopic data matched those in the literature.^[16]

4,4,5,5-tetramethyl-2-(2,4,6-trifluorophenyl)-1,3,2-dioxaborolane (4_2b)

Isolated yield: 99% (102 mg, pale yellow solid). $^1\text{H NMR}$ (500 MHz, CDCl_3) $\delta = 6.62\text{--}6.57$ (*m*, 2H), 1.36 (*s*, 12H); $^{13}\text{C}\{^1\text{H}\}$ NMR (126 MHz, CDCl_3) $\delta = 167.4$ (*dm*, $^1J_{\text{C-F}} = 252$ Hz), 165 (*dt*, $^1J_{\text{C-F}} = 252$ Hz, $^3J_{\text{C-F}} = 16$ Hz), 100.2 (*m*), 84.4, 24.8; $^{19}\text{F}\{^1\text{H}\}$ NMR (377 MHz, CDCl_3) $\delta = -97.2$ (*d*, $^3J_{\text{F-F}} = 9$ Hz, 2F), -103.1 (*t*, $^3J_{\text{F-F}} = 9$ Hz, 1F); $^{11}\text{B}\{^1\text{H}\}$ NMR (128 MHz, CDCl_3) $\delta = 29.4$; GC-MS: [t = 8.763 min] m/z: 258 [*M*] $^+$; HRMS (ASAP) Calcd for $[\text{C}_{12}\text{H}_{15}\text{BO}_2\text{F}_3]^+$ [*M*+H] $^+$: 259.1112; found 259.1104. Spectroscopic data matched those in the literature.^[16]

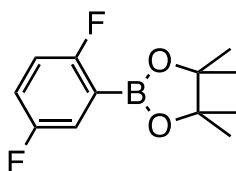
4,4,5,5-tetramethyl-2-(2,3,5,6-tetrafluorophenyl)-1,3,2-dioxaborolane (4_2c)

Isolated yield: 92% (101 mg, pale yellow solid). $^1\text{H NMR}$ (400 MHz, CDCl_3) $\delta = 7.10$ (*tt*, $^3J_{\text{H-F}} = 9$ Hz, $^4J_{\text{H-F}} = 7$ Hz, 1H), 1.38 (*s*, 12H); $^{13}\text{C}\{^1\text{H}\}$ NMR (101 MHz, CDCl_3) $\delta = 148.8$ (*dm*, $^1J_{\text{C-F}} = 251$ Hz), 144.6 (*dm*, $^1J_{\text{C-F}} = 253$ Hz), 108.7 (*tt*, $^2J_{\text{C-F}} = 22$ Hz, $^3J_{\text{C-F}} = 2$ Hz), 85.1, 24.8; $^{19}\text{F}\{^1\text{H}\}$ NMR (377 MHz, CDCl_3) $\delta = -131.0$ (*dd*, $J_{\text{F-F}} = 22$ Hz, $J_{\text{F-F}} = 15$ Hz), -139.3 (*dd*, $J_{\text{F-F}} = 22$ Hz, $J_{\text{F-F}} = 15$ Hz, 2F); $^{11}\text{B}\{^1\text{H}\}$ NMR (128 MHz, CDCl_3) $\delta = 29.3$ Hz; GC-MS: [t = 8.039 min] m/z: 276 [*M*] $^+$; HRMS (ASAP) Calcd for $[\text{C}_{12}\text{H}_{14}\text{BO}_2\text{F}_4]^+$ [*M*+H] $^+$: 277.1017; found 277.1006. Spectroscopic data matched those in the literature.^[16]

4,4,5,5-tetramethyl-2-(perfluorophenyl)-1,3,2-dioxaborolane (4_2d)

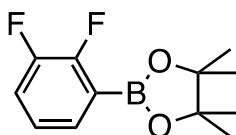
Isolated yield: 82% (96 mg, pale yellow solid). ^1H NMR (500 MHz, CDCl_3) $\delta = 1.38$ (s, 12H); $^{13}\text{C}\{^1\text{H}\}$ NMR (126 MHz, CDCl_3) $\delta = 149.4$ (dm, $^1J_{\text{C-F}} = 251$ Hz), 143.1 (dm, $^1J_{\text{C-F}} = 251$ Hz), 137.4 (dm, $^1J_{\text{C-F}} = 252$ Hz), 85.2, 24.8; ^{19}F NMR (471 MHz, CDCl_3) $\delta = -129.6$ (m, 2F), -149.8 (m, 1F), -261.0 (m, 2F); $^{11}\text{B}\{^1\text{H}\}$ NMR (96 MHz, CDCl_3) $\delta = 29.0$; GC-MS: [t = 8.668 min] m/z: 294 [M] $^+$; HRMS (ASAP) calcd. for $[\text{C}_{12}\text{H}_{13}\text{BF}_5\text{O}_2]^+$: 295.0923 [$M+\text{H}$] $^+$; found: 295.0912. Spectroscopic data matched those in the literature.^[16]

2-(2,5-difluorophenyl)-4,4,5,5-tetramethyl-1,3,2-dioxaborolane (4_2e)



Isolated yield: 83% (80 mg, pale yellow solid) ^1H NMR (500 MHz, CDCl_3) $\delta = 7.40$ –7.36 (m, 1H), 7.10–7.06 (m, 1H), 6.99–6.95 (m, 1H), 1.35 (s, 12H); $^{13}\text{C}\{^1\text{H}\}$ (126 MHz, CDCl_3) $\delta = 163.1$ (dd, $^1J_{\text{C-F}} = 247$ Hz, $^4J_{\text{C-F}} = 2$ Hz), 158.5 (dd, $^1J_{\text{C-F}} = 242$ Hz, $^4J_{\text{C-F}} = 2$ Hz), 122.4 (dd, $^2J_{\text{C-F}} = 22$ Hz, $^3J_{\text{C-F}} = 9$ Hz), 119.8 (dd, $^2J_{\text{C-F}} = 24$ Hz, $^3J_{\text{C-F}} = 9$ Hz), 116.7 (dd, $^2J_{\text{C-F}} = 27$ Hz, $^3J_{\text{C-F}} = 8$ Hz), 84.3, 24.9; $^{19}\text{F}\{^1\text{H}\}$ (377 MHz, CDCl_3) $\delta = -109.4$ (d, $^5J_{\text{F-F}} = 19$ Hz, 1F), -120.6 (d, $^5J_{\text{F-F}} = 19$ Hz, 1F); $^{11}\text{B}\{^1\text{H}\}$ NMR (160 MHz, CDCl_3) $\delta = 30.2$; GC-MS: [t = 8.248 min] m/z: 240 [M] $^+$; HRMS (ASAP) Calcd for $[\text{C}_{12}\text{H}_{16}\text{BO}_2\text{F}_2]^+$ [$M+\text{H}$] $^+$: 241.1206; found 241.1201. Spectroscopic data matched those in the literature.^[17]

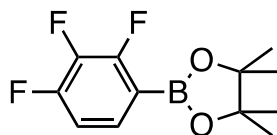
2-(2,3-difluorophenyl)-4,4,5,5-tetramethyl-1,3,2-dioxaborolane (4_2f)



Isolated yield: 77% (74 mg, pale yellow solid). ^1H NMR (500 MHz, CDCl_3) $\delta = 7.47$ –7.44 (m, 1H), 7.26–7.21 (m, 1H), 7.09–7.05 (m, 1H), 1.36 (s, 12H); $^{13}\text{C}\{^1\text{H}\}$ (126 MHz, CDCl_3) $\delta = 154.7$ (dd, $^1J_{\text{C-F}} = 253$ Hz, $^2J_{\text{C-F}} = 12$ Hz), 150.6 (dd, $^1J_{\text{C-F}} = 248$ Hz, $^2J_{\text{C-F}} = 14$ Hz), 131.2 (dd, $^3J_{\text{C-F}} = 7$ Hz, $^4J_{\text{C-F}} = 4$ Hz), 124.2 (dd, $^3J_{\text{C-F}} = 6$ Hz, $^4J_{\text{C-F}} = 4$ Hz), 120.3 (dd, $^2J_{\text{C-F}} = 17$ Hz, $^3J_{\text{C-F}} = 1$ Hz), 84.3, 25.0;

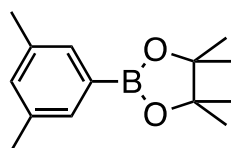
$^{19}\text{F}\{^1\text{H}\}$ (377 MHz, CDCl_3) $\delta = -129.0$ (*d*, $^3J_{\text{F-F}} = 22$ Hz, 1F), -139.1 (*d*, $^3J_{\text{F-F}} = 22$ Hz, 1F); $^{11}\text{B}\{^1\text{H}\}$ NMR (160 MHz, CDCl_3) $\delta = 30.0$; GC-MS: [t = 9.324 min] m/z: 240 [*M*] $^+$; HRMS (ASAP) Calcd for $[\text{C}_{12}\text{H}_{16}\text{BO}_2\text{F}_2]^+$ [*M*+H] $^+$: 241.1206; found 241.1198. Spectroscopic data matched those in the literature.^[18]

4,4,5,5-tetramethyl-2-(2,3,4-trifluorophenyl)-1,3,2-dioxaborolane (4_2g)



Isolated yield: 79% (82 mg, pale yellow solid). ^1H NMR (500 MHz, CDCl_3) $\delta = 7.45$ – 7.40 (*m*, 1H), 6.96 – 6.91 (*m*, 1H), 1.34 (*s*, 12H); $^{13}\text{C}\{^1\text{H}\}$ (126 MHz, CDCl_3) $\delta = 155.8$ (*ddd*, $^1J_{\text{C-F}} = 255$ Hz, $^2J_{\text{C-F}} = 9$ Hz, $^3J_{\text{C-F}} = 4$ Hz), 153.6 (*ddd*, $^1J_{\text{C-F}} = 254$ Hz, $^2J_{\text{C-F}} = 10$ Hz, $^3J_{\text{C-F}} = 4$ Hz), 140.0 ($^1J_{\text{C-F}} = 252$ Hz, $^2J_{\text{C-F}} = 17$ Hz, $^2J_{\text{C-F}} = 15$ Hz), 130.5 (*m*), 112.4 (*dd*, $^2J_{\text{C-F}} = 17$ Hz, $^3J_{\text{C-F}} = 4$ Hz), 84.4 , 24.9 ; $^{19}\text{F}\{^1\text{H}\}$ (377 MHz, CDCl_3) $\delta = -124.8$ (*dd*, $^3J_{\text{F-F}} = 20$ Hz, $^4J_{\text{F-F}} = 11$ Hz, 1F), -130.1 (*dd*, $^3J_{\text{F-F}} = 20$ Hz, $^4J_{\text{F-F}} = 11$ Hz, 1F), -162.1 (*t*, $^3J_{\text{F-F}} = 20$ Hz); $^{11}\text{B}\{^1\text{H}\}$ NMR (128 MHz, CDCl_3) $\delta = 29.8$; GC-MS: [t = 8.249 min] m/z: 258 [*M*] $^+$; HRMS (ASAP) Calcd for $[\text{C}_{12}\text{H}_{15}\text{BO}_2\text{F}_3]^+$ [*M*+H] $^+$: 259.1112; found 259.1106. Spectroscopic data matched those in the literature.^[19]

2-(3,5-dimethylphenyl)-4,4,5,5-tetramethyl-1,3,2-dioxaborolane (4_2h)



Isolated yield: 80 % (74 mg, yellow pale solid). ^1H NMR (500 MHz, CDCl_3) $\delta = 7.46$ – 7.45 (*m*, 2H), 7.12 – 7.11 (*m*, 1H); $^{13}\text{C}\{^1\text{H}\}$ (75 MHz, CDCl_3) $\delta = 137.3$, 133.1 , 132.5 , 83.8 , 25.0 , 21.3 ; $^{11}\text{B}\{^1\text{H}\}$ NMR (96 MHz, CDCl_3) $\delta = 30.9$; GC-MS: [t = 10.374 min] m/z: 232 [*M*] $^+$; HRMS (APCI) Calcd for $[\text{C}_{14}\text{H}_{22}\text{BO}_2]^+$ [*M*+H] $^+$: 233.1707 found 233.1703. Spectroscopic data matched those in the literature.^[20]

4.6 References

- [1] a) J. Wang, M. S. Rosello, J. L. Aceña, C. Pozo, A. E. Sorochinsky, S. Fustero, V. A. Soloshonok, H. Liu, *Chem. Rev.* **2014**, *114*, 2432–2506; b) H.-J. Bohm, D. Banner, S. Bendels, M. Kansy, B. Kuhn, K. Müller, U. Obst-Sander, M. Stahl, *ChemBioChem* **2004**, *5*, 637–643; c) C. D. Isanbor, D. O'Hagan, *J. Fluorine Chem.* **2006**, *127*, 303–319; d) J.-P. Begue, D. Bonnet-Delpon, *J. Fluorine Chem.* **2006**, *127*, 992–1012; e) K. L. Kirk, *J. Fluorine Chem.* **2006**, *127*, 1013–1029; f) K. Müller, C. Faeh, F. Diederich, *Science* **2007**, *317*, 1881–1886; g) W. K. Hagmann, *J. Med. Chem.* **2008**, *51*, 4359–4369; h) D. O'Hagan, *J. Fluorine Chem.* **2010**, *131*, 1071–1081.
- [2] a) P. Jeschke, *ChemBioChem* **2004**, *5*, 570–589; b) P. Jeschke, *Pest Manage. Sci.* **2010**, *66*, 10–27; c) T. Fujiwara, D. O'Hagan, *J. Fluorine Chem.* **2014**, *167*, 16–29.
- [3] a) R. Babudri, G. M. Farinola, F. Naso, R. Ragni, *Chem. Commun.* **2007**, 1003–1022; b) R. Berger, G. Resnati, P. Metrangolo, E. Weber, J. Hulliger, *Chem. Soc. Rev.* **2011**, *40*, 3496–3508; c) B. Maiti, K. Wang, S. Bhandari, S. D. Bunge, R. J. Twieg, B. D. Dunietz, *J. Mater. Chem. C* **2019**, *7*, 3881–3888; d) M.-H. Yoon, A. Facchetti, C. E. Stern, T. J. Marks, *J. Am. Chem. Soc.* **2006**, *128*, 5792–5801.
- [4] For iridium catalyst systems, see: a) D. W. Robbins, J. F. Hartwig, *Org. Lett.* **2012**, *14*, 4266–4269; b) C. R. K. Jayasundara, J. M. Unold, J. Oppenheimer, M. R. Smith, III, R. E. Maleczka, Jr., *Org. Lett.* **2014**, *16*, 6072–6075.
- [5] For platinum catalyst systems, see: a) J. Takaya, S. Ito, H. Nomomoto, N. Saito, N. Kirai, N. Iwasawa, *Chem. Commun.* **2015**, *51*, 17662–17665; b) T. Furukawa, M. Tobisu, N. Chatani, *J. Am. Chem. Soc.* **2015**, *137*, 12211–12214.
- [6] For a cobalt catalyst system, see: J. V. Obligacion, M. J. Bezdek, P. J. Chirik, *J. Am. Chem. Soc.* **2017**, *139*, 2825–2832.
- [7] a) W. K. Chow, O. Y. Yuen, P. Y. Choy, C. M. So, C. P. Lau, W. T. Wong, F. Y. A. Kwong, *RSC Adv.* **2013**, *3*, 12518–12539; b) S. K. Bose, A. Deißberger, A. Eichhorn, P. G. Steel, Z. Lin, T. B. Marder, *Angew. Chem. Int. Ed.* **2015**, *54*, 11843–11847; *Angew. Chem.* **2015**,

- 127, 12009–12014; c) C. Kleeberg, L. Dang, Z. Lin, T. B. Marder, *Angew. Chem. Int. Ed.* **2009**, *48*, 5350–5354; *Angew. Chem.* **121**, 5454–5458; d) W. Zhu, D. Ma, *Org. Lett.* **2006**, *8*, 261–263; e) L. Kuehn, M. Huang, U. Radius, T. B. Marder, *Org. Biomol. Chem.* **2019**, *17*, 6601–6606; f) T. Yoshida, L. Ilies, E. Nakamura, *ACS Catal.* **2017**, *7*, 3199–3203; g) H. D. S. Guerrand, L. D. Marciasini, M. Jousseau, M. Vaultier, M. Pucheault, *Chem. Eur. J.* **2014**, *20*, 5573–5579; h) J. Dong, H. Guo, W. Peng, Q.-S. Hu, *Tetrahedron Lett.* **2019**, *60*, 760–763; i) M. Murata, T. Oyama, S. Watanabe, Y. Masuda, *J. Org. Chem.* **2000**, *65*, 164–168; j) A. N. Cammidge, K. V. L. Crépy, *J. Org. Chem.* **2003**, *68*, 6832–6835; k) G. A. Molander, S. L. J. Trice, S. M. Kennedy, S. D. Dreher, M. T. Tudge, *J. Am. Chem. Soc.* **2012**, *134*, 11667–11673.
- [8] a) P. A. Cox, M. Reid, A. G. Leach, A. D. Campbell, E. J. King, G. C. Lloyd-Jones, *J. Am. Chem. Soc.* **2017**, *139*, 13156–13165; b) H. G. Kuivila, J. F. Reuwer, Jr., J. A. Mangravite, *Can. J. Chem.* **1963**, *41*, 3081–3090; c) H. J. Frohn, N. Y. Adonin, V. V. Bardin, *Z. Anorg. Allg. Chem.* **2002**, *628*, 2834–2838; d) J. Lozada, Z. Liu, D. M. Perrin, *J. Org. Chem.* **2014**, *79*, 5365–5368; e) L. Chen, H. Francis, B. P. Carrow, *ACS Catal.* **2018**, *8*, 2989–2994.
- [9] a) H. J. Frohn, H. Franke, P. Fritzen, V. V. Bardin, *J. Organomet. Chem.* **2000**, *598*, 127–135; b) H.-J. Frohn, N. Y. Adonin, V. V. Bardin, V. F. Starichenko, *Z. Anorg. Allg. Chem.* **2002**, *628*, 2827–2833.
- [10] a) J. Zhou, M. W. Kuntze-Fechner, R. Bertermann, U. S. D. Paul, J. H. J. Berthel, A. Friedrich, Z. Du, T. B. Marder, U. Radius, *J. Am. Chem. Soc.* **2016**, *138*, 5250–5253; b) Y.-M. Tian, X.-N. Guo, M. W. Kuntze-Fechner, I. Krummenacher, H. Braunschweig, U. Radius, A. Steffen, T. B. Marder, *J. Am. Chem. Soc.* **2018**, *140*, 17612–17623.
- [11] a) Y. P. Budiman, A. Friedrich, U. Radius, T. B. Marder, *ChemCatChem* **2019**, *11*, 5387–5396; b) Z. Liu, Y. P. Budiman, Y.-M. Tian, A. F. Friedrich, M. Huang, S. A. Westcott, U. Radius, T. B. Marder, *Chem. Eur. J.* **2020**, DOI: 10.1002/chem.202002888.
- [12] Y. P. Budiman, A. Jayaraman, A. Friedrich, F. Kerner, U. Radius, T. B. Marder, *J. Am. Chem. Soc.* **2020**, *142*, 6036–6050.
- [13] Y. Yamamoto, H. Matsubara, H. Yorimitsu, A. Osuka, *ChemCatChem* **2016**, *8*, 2317–2320.

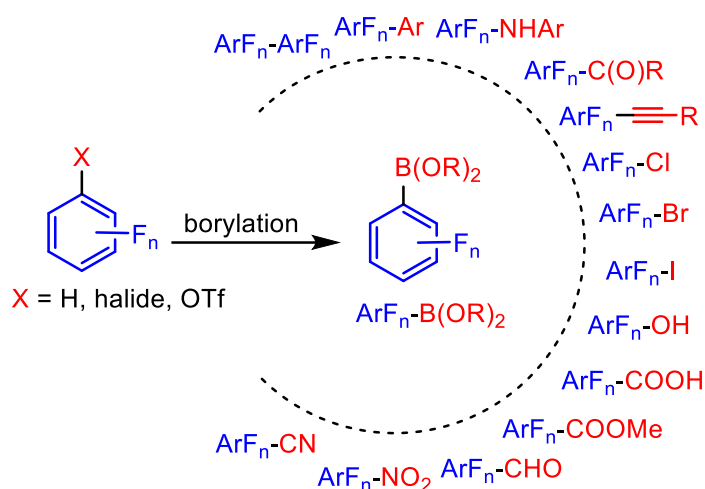
- [14] L. Zhang, L. Jiao, *J. Am. Chem. Soc.* **2017**, *139*, 607–610.
- [15] J. Ratniyom, N. Dechnarong, S. Yotphan, S. Kiatisevi, *Eur. J. Org. Chem.* **2014**, 1381–1385.
- [16] J. Takaya, S. Ito, H. Nomomoto, N. Saito, N. Kirai, N. Iwasawa, *Chem. Commun.* **2015**, *51*, 17662–17665.
- [17] G. A. Chotana, M. A. Rak and M. R. Smith, *J. Am. Chem. Soc.* **2005**, *127*, 10539–10544.
- [18] T. Furukawa, M. Tobisu, N. Chatani, *J. Am. Chem. Soc.* **2015**, *137*, 12211–12214.
- [19] H. Ren, Y.-P. Zhou, Y. Bai, C. Cui, M. Driess, *Chem. Eur. J.* **2017**, *23*, 5663–5667.
- [20] P. Harrisson, J. Morris, T. B. Marder, P. Steel, *Org. Lett.* **2009**, *11*, 3586–3589.

5 Summary

Fluorinated compounds are an important motif, particularly in pharmaceuticals, as one-third of the top performing drugs have fluorine in their structures. Fluorinated biaryls also have numerous applications in areas such as material science, agriculture, crystal engineering, supramolecular chemistry, etc. Thus, the development of new synthetic routes to fluorinated chemical compounds is an important area of current research. One promising method is the borylation of suitable precursors to generate fluorinated aryl boronates as versatile building blocks for organic synthesis.

Chapter 1

In this chapter, the latest developments in the synthesis, stability issues, and applications of fluorinated aryl boronates in organic synthesis are reviewed. The catalytic synthesis of fluorinated aryl boronates using different methods, such as C–H, C–F, and C–X (X = Cl, Br, I, OTf) borylations are discussed. Further studies covering instability issues of the fluorinated boronate derivatives, which are accelerated by *ortho*-fluorine, have been reported, and the applications of these substrates, therefore, need special treatment.



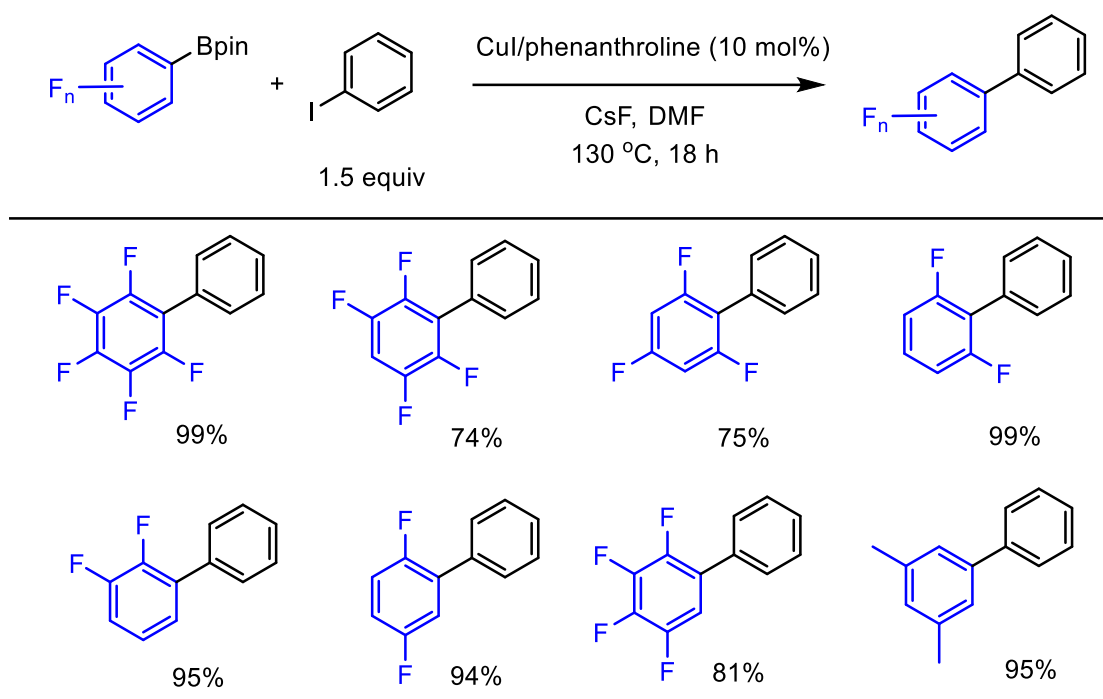
Scheme S-1. Fluorinated aryl boronates as building blocks in organic reactions.

Numerous groups have reported methods to employ highly fluorinated aryl boronates that anticipate the protodeboronation issue; thus, polyfluorinated aryl boronates, especially those containing *ortho*-fluorine substituents, can be converted into chloride, bromide, iodide, phenol, carboxylic acid, nitro, cyano, methyl esters, and aldehyde analogues. These substrates can be applied in many cross-coupling reactions, such as the Suzuki-Miyaura reaction with aryl halides, the Chan-Evans-Lam C–N reaction with aryl amines or nitrosoarenes, C–C(O) reactions with *N*-(aryl-carbonyloxy)phthalamides or thiol esters (Liebskind-Srogl cross-coupling), and oxidative coupling reactions with terminal alkynes. Furthermore, the difficult reductive elimination from the highly stable complex $[\text{PdL}_2(2,6\text{-C}_6\text{F}_{2+n}\text{H}_{3-n})_2]$ was the next challenge to be targeted in the homocoupling of 2,6-di-fluoro aryl pinacol boronates, and it has been solved by conducting the reaction in arene solvents that reduce the energy barrier in this step as long as no coordinating solvent or ancillary ligand is employed.

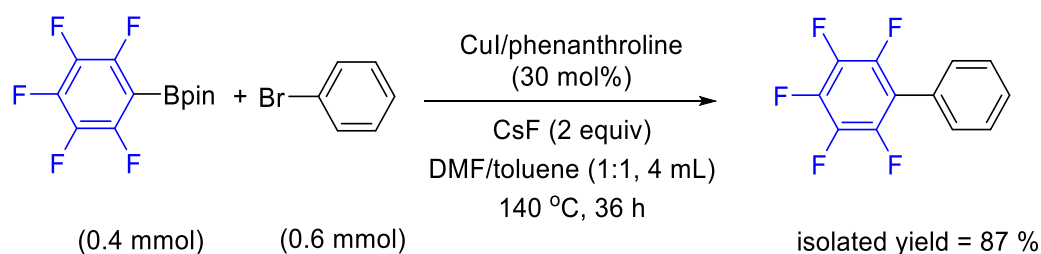
Chapter 2

In this chapter, phenanthroline-ligated copper complexes proved to be efficient catalysts for the Suzuki-Miyaura cross-coupling of highly fluorinated aryl boronate esters ($\text{Ar}_F\text{-Bpin}$) with aryl iodides or bromides. This newly developed method is an attractive alternative to the traditional methods as copper is an Earth-abundant metal, less toxic, and cheaper compared to the traditional methods which commonly required palladium catalysts, and silver oxide that is also often required in stoichiometric amounts. A combination of 10 mol% copper iodide and 10 mol% phenanthroline, with CsF as a base, in DMF, at 130 °C, for 18 hours is efficient to cross-couple fluorinated aryl pinacol boronates with aryl iodides to generate cross-coupled products in good to excellent yields (Scheme S-2). This method is also viable for polyfluorophenyl borate salts such as pentafluorophenyl- BF_3K . Notably, employing aryl bromides instead of aryl iodides for the coupling with fluorinated aryl-Bpin compounds is also possible; however, increased amounts of CuI/phenanthroline catalyst is necessary, in a mixture of DMF and toluene (1:1) (Scheme S-3).

A diverse range of $\pi \cdots \pi$ stacking interactions is observed in the cross-coupling products partly perfluorinated biaryl crystals. They range from arene–perfluoroarene interactions (2-(perfluorophenyl)naphthalene and 2,3,4-trifluorobiphenyl) to arene–arene (9-(perfluorophenyl)anthracene) and perfluoroarene–perfluoroarene (2,3,4,5,6-pentafluoro-2'-methylbiphenyl) interactions.



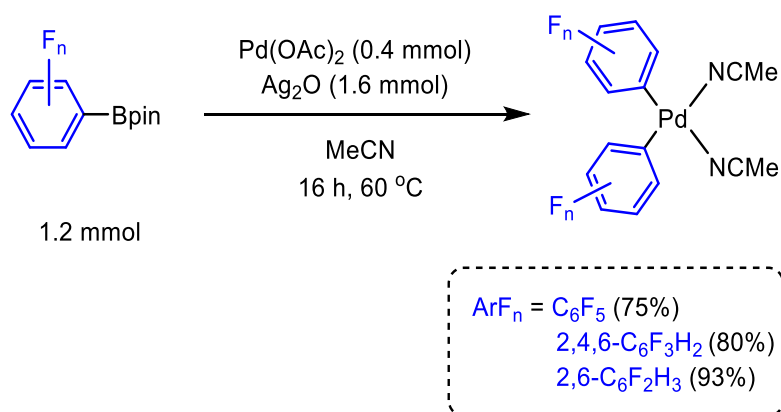
Scheme S-2. Cu-catalyzed cross-coupling of polyfluorophenyl-Bpin compounds with phenyl iodide.



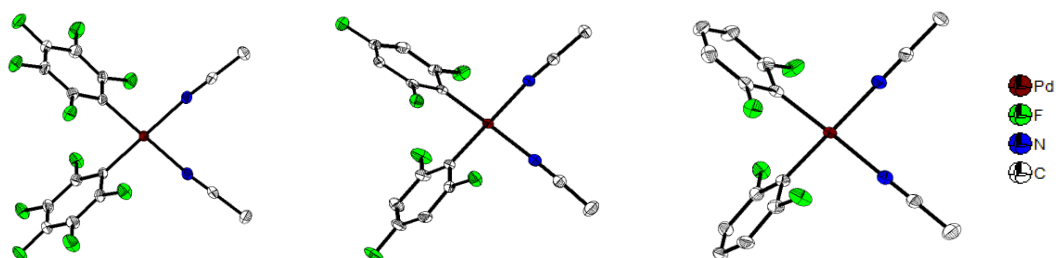
Scheme S-3. Cross-coupling reaction of C₆F₅BPIn with phenyl bromide.

Chapter 3

In this chapter, the efficient Pd-catalyzed homocoupling reaction of aryl pinacol boronates ($\text{Ar}_F\text{-Bpin}$) that contain two *ortho*-fluorines is presented. The reaction must be conducted in a “noncoordinating” solvent such as toluene, benzene, or *m*-xylene and, notably, stronger coordinating solvents or ancillary ligands have to be avoided. Thus, the Pd center becomes more electron deficient and the reductive elimination becomes more favorable. The Pd-catalyzed homocoupling reaction of di-*ortho*-fluorinated aryl boronate derivatives is difficult in strongly coordinating solvents or in the presence of strong ancillary ligands, as the reaction stops at the $[\text{PdL}_2(2,6\text{-C}_6\text{F}_{2+n}\text{H}_{3-n})_2]$ stage after the transmetalations without the reductive elimination taking place. It is known that the rate of reductive elimination of $\text{Ar-Ar}'$ from $[\text{ML}_2(\text{Ar})(\text{Ar}')]$ complexes containing group-10 metals decreases in the order $\text{Ar}_{\text{rich}}\text{-Ar}'_{\text{poor}} > \text{Ar}_{\text{rich}}\text{-Ar}'_{\text{rich}} > \text{Ar}_{\text{poor}}\text{-Ar}'_{\text{poor}}$. Furthermore, reductive elimination of the most electron-poor diaryls, such as $\text{C}_6\text{F}_5\text{-C}_6\text{F}_5$, from $[\text{PdL}_2(\text{C}_6\text{F}_5)_2]$ complexes is difficult and has been a challenge for 50 years, due to their high stability as the $\text{Pd-C}_{\text{aryl}}$ bond is strong. Thus, the Pd-catalyzed homocoupling of perfluoro phenyl boronates is found to be rather difficult.

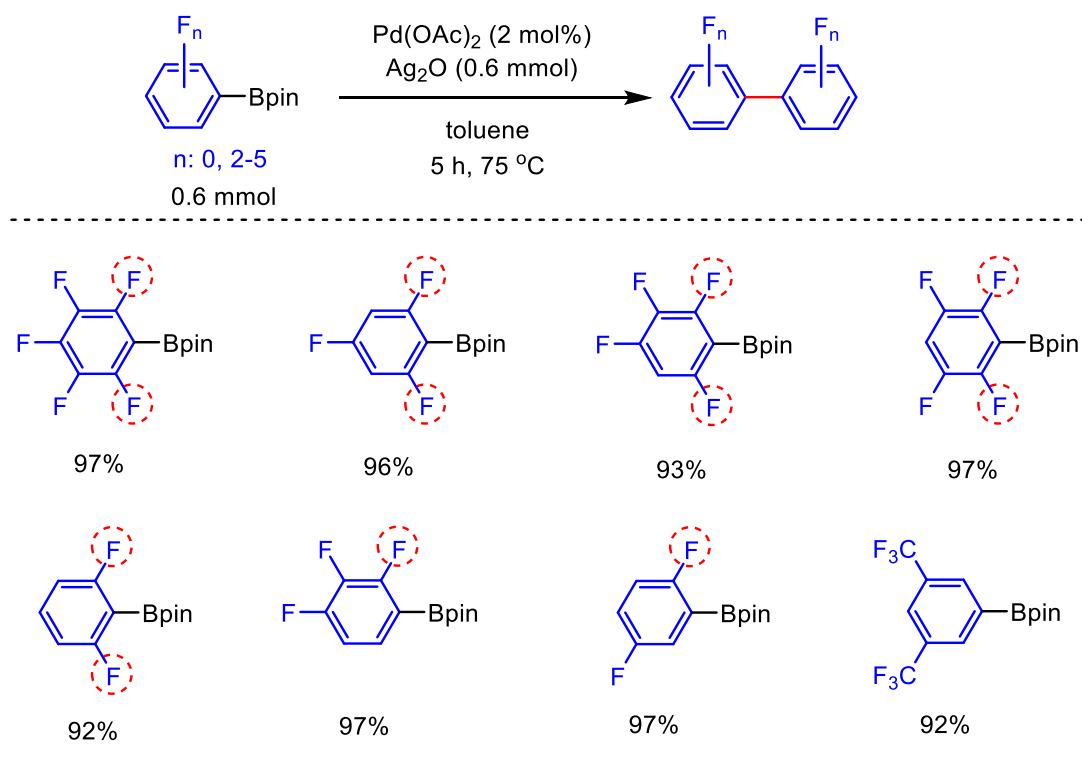


Scheme S-4. Synthesis of *cis*- $[\text{Pd}(\text{MeCN})_2(\text{C}_6\text{F}_5)_2]$, *cis*- $[\text{Pd}(\text{MeCN})_2(2,4,6\text{-C}_6\text{F}_3\text{H}_2)_2]$, and *cis*- $[\text{Pd}(\text{MeCN})_2(2,6\text{-C}_6\text{F}_2\text{H}_3)_2]$.

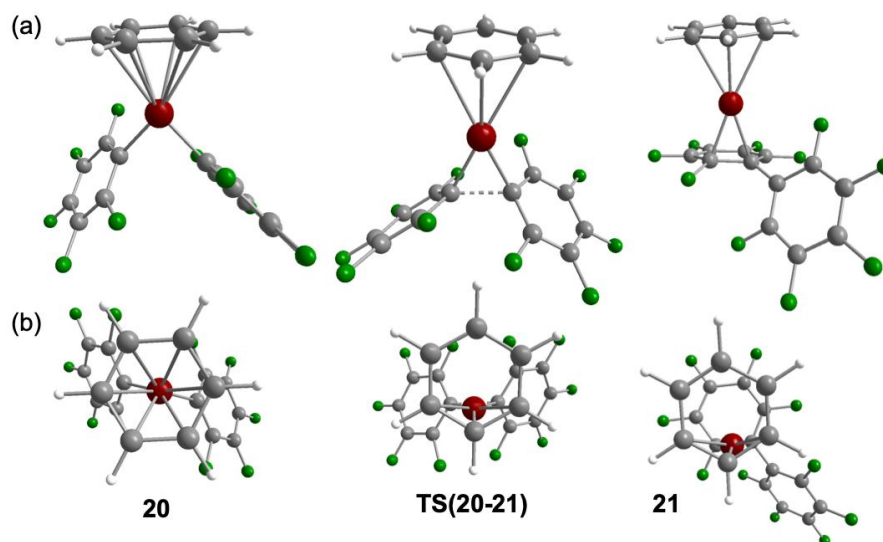


Scheme S-5. Molecular structures of *cis*-[Pd(MeCN)₂(C₆F₅)₂] (left), *cis*-[Pd(MeCN)₂(2,4,6-C₆F₃H₂)₂] (middle), and *cis*-[Pd(MeCN)₂(2,6-C₆F₂H₃)₂] (right) determined by single-crystal X-ray diffraction at 100 or 103 K.

Further investigation showed that stoichiometric reactions of C₆F₅Bpin, 2,4,6-trifluorophenyl-Bpin, or 2,6-difluorophenyl-Bpin with palladium acetate in MeCN stops at the double transmetalation step, as demonstrated by the isolation of *cis*-[Pd(MeCN)₂(C₆F₅)₂], *cis*-[Pd(MeCN)₂(2,4,6-C₆F₃H₂)₂], and *cis*-[Pd(MeCN)₂(2,6-C₆F₂H₃)₂] in quantitative yields (Schemes S-4 and S-5). Thus, it can be concluded that the reductive elimination from diaryl-palladium complexes containing two *ortho*-fluorines in both aryl rings, is difficult even in a weakly coordinating solvent such as MeCN. Therefore, even less coordinating solvents are needed to make the Pd center more electron deficient. Reactions using “noncoordinating” arene solvents such as toluene, benzene, or *m*-xylene were conducted and found to be effective for the catalytic homocoupling of 2,6-C₆F_{2+n}H_{3-n}Bpin. The scope of the reactions was expanded. Using toluene as the solvent, the palladium-catalyzed homocoupling of Ar_F-Bpin derivatives containing one, two or no *ortho*-fluorines gave the coupled products in excellent yields without any difficulties (Scheme S-6).



Scheme S-6. Pd-catalyzed homocoupling of fluorinated aryl pinacol boronates in toluene.



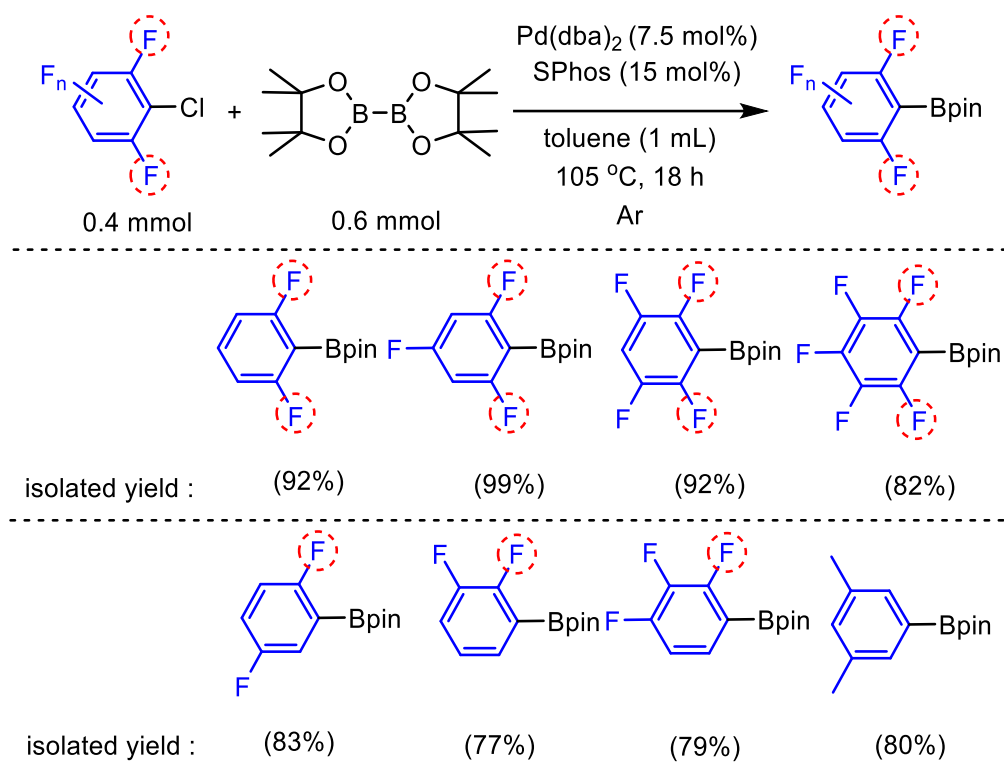
Scheme S-7. Side-view (a) and view along the arene-Pd vector (b) of the DFT-optimized structures (B3LYP-D3/TZVP) of the benzene complexes $[\text{Pd}(\eta^6\text{-C}_6\text{H}_6)(\text{C}_6\text{F}_5)_2]$ **20**, the transition state **TS(20-21)**, and primary elimination product **21**. Calculated Pd-C_{arene} distances [Å]: **20**: 2.617, 2.618, 2.640, 2.641, 2.666, 2.667, **TS(20-21)**: 2.275, 2.608, 2.609, 3.205, 3.206, 3.478, **21**: 2.236, 2.565, 2.631, 3.204, 3.255, 3.514.

DFT calculations at the B3LYP-D3/def2-TZVP/6-311+g(2d,p)/IEFPCM // B3LYP-D3/SDD/6-31g**/IEFPCM level of theory predicted an exergonic process and lower barrier (< 21 kcal/mol) for the reductive elimination of Pd(C₆F₅)₂ complexes bearing arene ligands, compared to stronger coordinating solvents (acetonitrile, THF, SMe₂, and PMe₃), which have high barriers (> 33.7 kcal/mol). Reductive elimination from [Pd(η^n -Ar)(C₆F₅)₂] complexes have low barriers due to: (i) ring slippage of the arene ligand as a hapticity change from η^6 in the reactant to η^n ($n \leq 3$) in the transition state and the product (Scheme S-7), which led to less σ -repulsion; and (ii) more favorable π -back-bonding from Pd(Ar_F)₂ to the arene fragment in the transition state.

Chapter 4

In this chapter, the efficient Pd-catalyzed C–Cl borylation of aryl chlorides containing two *ortho*-fluorines is presented. The reactions are conducted under base-free conditions to prevent the decomposition of the di-*ortho*-fluorinated aryl boronates, which are unstable in the presence of base. As shown in Scheme S-4, a combination of Pd(dba)₂ (dba = dibenzylideneacetone) with SPhos (2-dicyclohexylphosphino-2',6'-dimethoxybiphenyl) as a ligand is efficient to catalyze the C–Cl borylation of aryl chlorides containing two *ortho*-fluorine substituents without base, and the products were isolated in excellent yields. The substrate scope can be expanded to aryl chloride containing one or no *ortho*-fluorines and the borylated products were isolated in good to very good yield. This method provides a nice alternative to traditional methodologies using lithium or Grignard reagents.

Summary



Scheme S-8. Pd-catalyzed C–Cl borylation of fluorinated aryl chlorides.

6 Zusammenfassung

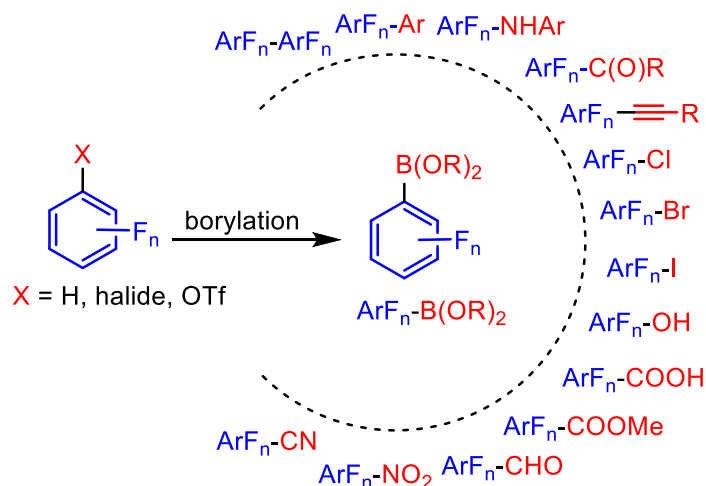
Fluorierte Verbindungen sind insbesondere in der Pharmazie wichtige Bausteine, da ein Drittel der wirksamen Medikamente Fluorsubstituenten beinhalten. Fluorierte Biaryle haben auch zahlreiche Anwendungen in Bereichen wie der Materialwissenschaft, der Landwirtschaft, dem Design molekularer Festkörperstrukturen, der supramolekularen Chemie etc. Daher ist die Entwicklung neuer synthetischer Wege zu fluorierten chemischen Verbindungen sehr gefragt. Eine der vielversprechenden Methoden ist die Borylierung geeigneter Vorstufen zur Erzeugung fluoriertes Arylboronate, die als vielseitige Bausteine für die organische Synthese dienen können.

Kapitel 1

In diesem Kapitel werden die neuesten Entwicklungen in der Synthese, Stabilität und Anwendungen fluoriertes Arylboronate vorgestellt. Die katalytische Synthese fluoriertes Arylboronate mit verschiedenen Methoden, wie der Borylierungen von C–H-, C–F- und C–X-Bindungen (X = Cl, Br, I, OTf) wird diskutiert. Ferner wird auf Instabilitätsprobleme fluoriertes Boronatderivate eingegangen, die durch *ortho*-Fluoratome forciert werden.

Zahlreiche Gruppen haben über Methoden zur Anwendung hochfluoriertes Arylboronate berichtet, die das Problem der Protodeboronierung einbeziehen. So können polyfluoriertes Arylboronate, insbesondere solche, die *ortho*-Fluorsubstituenten enthalten, in Chloride, Bromide, Iodide, Phenole, Carbonsäuren, Nitrosyle, Cyanide, Methylester und Aldehyd-Analoga umgewandelt werden. Diese Substrate können in vielen Kreuzkupplungsreaktionen eingesetzt werden, wie z.B. der Suzuki-Miyaura-Kreuzkupplung mit Arylhalogeniden, der Chan Evans-Lam-Reaktion mit Arylaminen oder Nitrosoarylen, C–C(O)-Reaktionen mit N-(Arylcarbonyloxy)phthalamiden oder Thioestern (Liebskind-Srogl-Kreuzkupplung), sowie oxidative Kupplungsreaktion mit terminalen Alkinen. Darüber hinaus ist die reduktive Eliminierung aus dem hochstabilen Komplex $[\text{PdL}_2(2,6\text{-C}_6\text{F}_{2+n}\text{H}_{3-n})_2]$ eine weitere Herausforderung, die bei der Homokupplung von 2,6-Difluorarylpinakolboronaten angegangen werden sollte. Diese wurde gelöst, indem die Reaktion in aromatischen, nicht koordinierenden Lösungsmitteln durchgeführt

wurde, welche die Energiebarriere in diesem Schritt reduzieren, solange keine Koordination erfolgt.

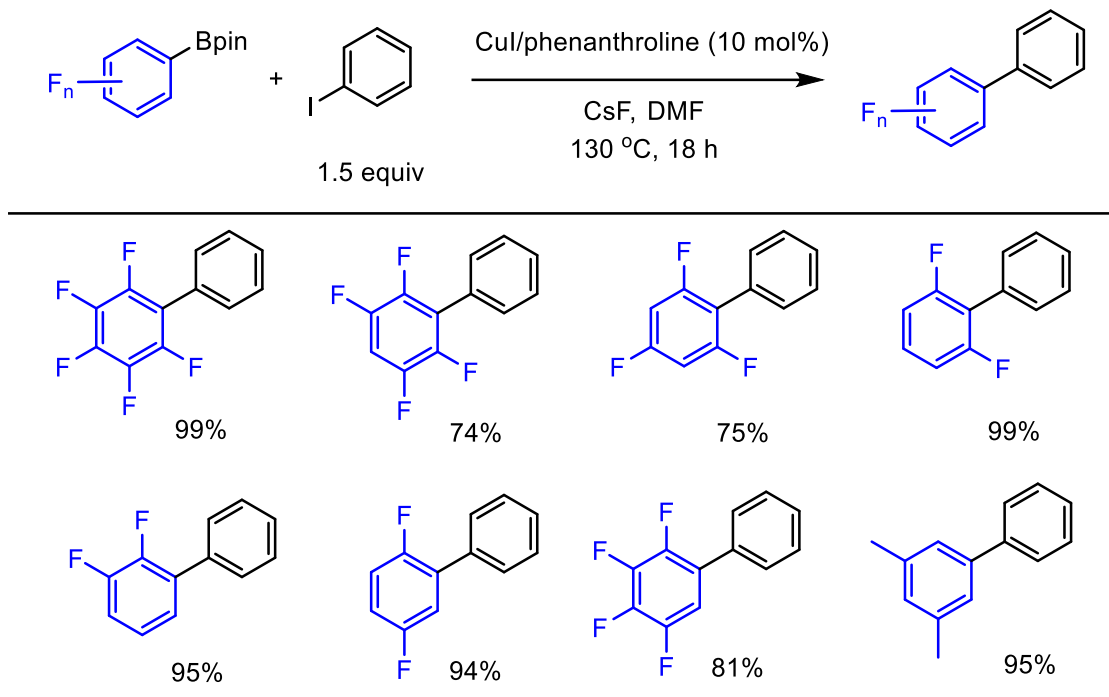


Schema S-1. Fluorierte Arylboronate als Bausteine in organischen Reaktionen.

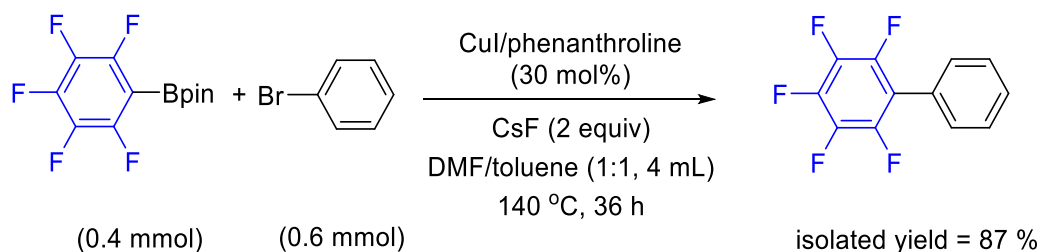
Kapitel 2

In diesem Kapitel werden Kupferkomplexe mit dem Liganden Phenanthrolin als effiziente Katalysatoren für die Suzuki-Miyaura-Kreuzkupplung hochfluorierter Arylboronatester (Ar_F-Bpin) mit Aryliodiden oder -bromiden vorgestellt. Dieses neu entwickelte Katalysatorsystem ist eine attraktive Alternative zu den traditionellen Methoden, da Kupfer ein auf der Erde reichlich vorhandenes Metall ist. Ferner ist es weniger toxisch und billiger im Vergleich zu den traditionellen Methoden, die üblicherweise Palladiumkatalysatoren und Silberoxid, das oft auch in stöchiometrischen Mengen benötigt wird, benötigen. Eine Kombination von 10 mol% Kupferiodid und 10 mol% Phenanthrolin mit CsF als Base, in DMF, bei 130 °C, für 18 Stunden ist effektiv, um fluorierte Arylpinacolboronate mit Aryliodiden zu koppeln. Diese Methode liefert die Kreuzkupplungsprodukte in guter bis ausgezeichneter Ausbeute (Schema S-2) und eignet sich auch für die Darstellung von Polyfluorphenylboratsalze wie Pentafluorphenyl-BF₃K. Nennenswert ist auch der Einsatz von Arylbromiden anstelle von Aryliodiden für die Kopplung mit fluorierten Aryl-Bpin-Verbindungen; allerdings sind erhöhte Mengen an CuI/Phenanthrolin-Katalysator in einer Mischung aus DMF und Toluol (1:1) erforderlich (Schema S-3).

Eine vielfältige Palette von $\pi \cdots \pi$ Wechselwirkungen wird innerhalb von Schichten der Kreuzkupplungs-Produkte partiell fluorierter Biaryle beobachtet. Sie reichen von Aryl-Perfluorarylen Wechselwirkungen (für das 2-(Perfluorphenyl)naphthalin und 2,3,4-Trifluorbiphenyl) bis hin zu Aryl-Aryl (für das 9-Perfluorphenyl)anthracen) und Perfluoraryl-Perfluoraryl-Wechselwirkungen (für das 2,3,4,5,6-Pentafluor-2'-methylbiphenyl).



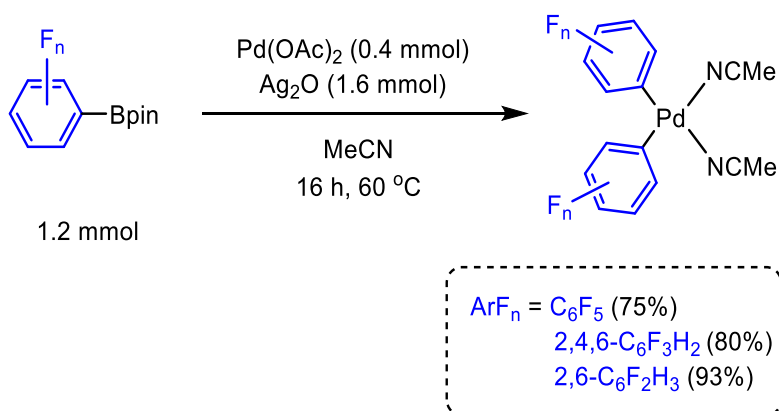
Schema S-2. Die Cu-katalysierte Kreuzkupplung von Polyfluorphenyl-Bpin-Verbindungen mit Phenyljodid.



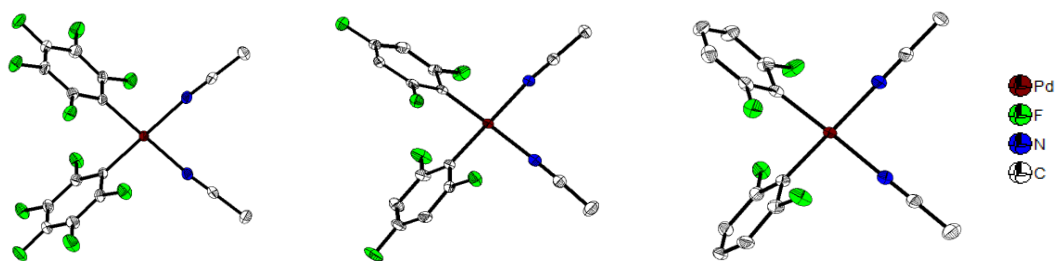
Schema S-3. Kreuzkupplungsreaktion von C_6F_5 -BPin mit Phenylbromid.

Kapitel 3

In diesem Kapitel wird eine effiziente Pd-katalysierte Homokupplungsreaktion von Aryl-Pinacolboronaten ($\text{Ar}_F\text{-Bpin}$), welche zwei *ortho*-Fluoratome enthalten, vorgestellt. Die Reaktion muss in einem "nicht-koordinierenden" Lösungsmittel wie Toluol, Benzol oder *m*-Xylol durchgeführt werden, wobei insbesondere stärker koordinierende Lösungsmittel oder Hilfsliganden vermieden werden müssen. Hierdurch wird das Pd-Zentrum elektronenärmer und die reduktive Eliminierung begünstigt. Bemerkenswert ist, dass die Pd-katalysierte Homokupplung von di-*ortho*-fluorierten Arylboronat-Derivaten in stark koordinierenden Lösungsmitteln oder in Gegenwart von starken Hilfsliganden schwierig ist, da die Reaktion im Stadium des Komplexes $[\text{PdL}_2(2,6\text{-C}_6\text{F}_{2+n}\text{H}_{3-n})_2]$ nach dem Transmetallisierung-Schritt abbricht, ohne dass die reduktive Eliminierung stattfindet. Es ist bekannt, dass die Geschwindigkeit der reduktiven Eliminierung von Ar-Ar aus $[\text{ML}_2(\text{Ar})(\text{Ar})]$ -Komplexen, die Metalle der Gruppe 10 enthalten, in der Reihenfolge $\text{Ar}_{\text{reich}}\text{-Ar}_{\text{arm}} > \text{Ar}_{\text{reich}}\text{-Ar}_{\text{reich}} > \text{Ar}_{\text{arm}}\text{-Ar}_{\text{arm}}$ abnimmt. Darüber hinaus ist die reduktive Eliminierung der meisten elektronenarmen Diaryle wie $\text{C}_6\text{F}_5\text{-C}_6\text{F}_5$ aus $[\text{PdL}_2(\text{C}_6\text{F}_5)_2]$ -Komplexen schwierig und stellt aufgrund ihrer hohen Stabilität seit 50 Jahren eine Herausforderung dar, da hier eine starke Pd- C_{aryl} -Bindung vorliegt. Daher erweist sich die Pd-katalysierte Homokupplung von Perfluorphenylboronaten als ziemlich schwierig.

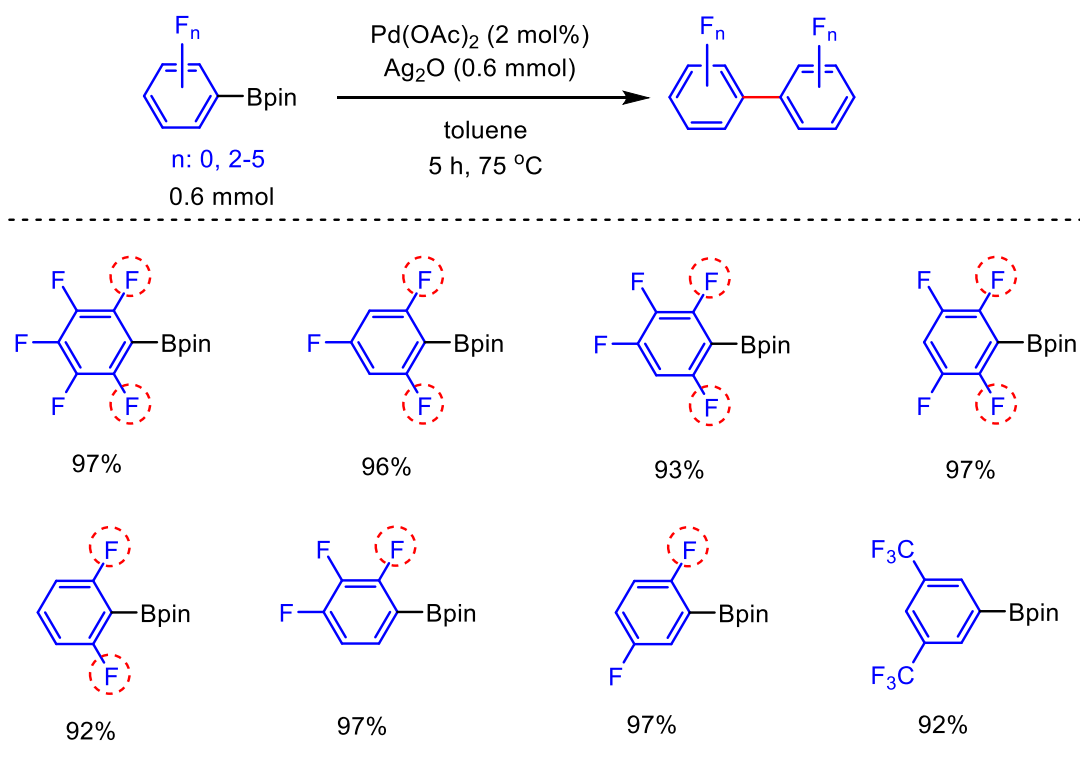


Schema S-4. Synthese von *cis*- $[\text{Pd}(\text{MeCN})_2(\text{C}_6\text{F}_5)_2]$, *cis*- $[\text{Pd}(\text{MeCN})_2(2,4,6\text{-C}_6\text{F}_3\text{H}_2)_2]$, und *cis*- $[\text{Pd}(\text{MeCN})_2(2,6\text{-C}_6\text{F}_2\text{H}_3)_2]$.

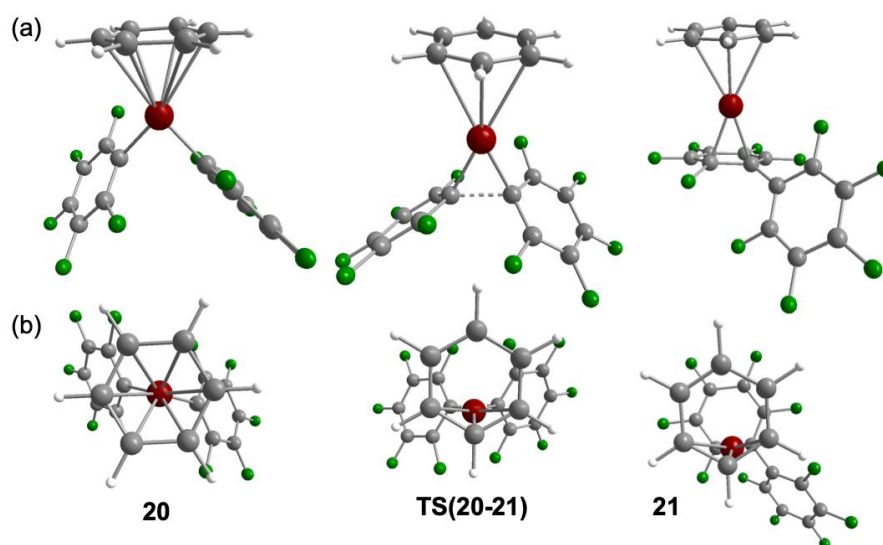


Schema S-5. Molekülstrukturen von *cis*-[Pd(MeCN)₂(C₆F₅)₂] (links), *cis*-[Pd(MeCN)₂(2,4,6-C₆F₃H₂)₂] (mitte), und *cis*-[Pd(MeCN)₂(2,6-C₆F₂H₃)₂] (rechts) bestimmt durch Einkristall-Röntgendiffraktometrie bei 100 oder 103 K.

Weitere Untersuchungen zeigten, dass stöchiometrische Reaktionen von C₆F₅Bpin, 2,4,6-Trifluorphenyl-Bpin oder 2,6-Difluorphenyl-Bpin mit Palladiumacetat in MeCN beim Schritt der doppelten Transmetallierung anhalten, was durch die Isolierung von *cis*-[Pd(MeCN)₂(C₆F₅)₂], *cis*-[Pd(MeCN)₂(2,4,6-C₆F₃H₂)₂] und *cis*-[Pd(MeCN)₂(2,6-C₆F₂H₃)₂] in quantitativen Ausbeuten (Schemata S-4 und S-5) nachgewiesen wurde. Daraus kann geschlossen werden, dass die reduktive Eliminierung aus Diaryl-Palladium-Komplexen, welche zwei *ortho*-Fluoratome an beiden Arylringen enthalten, selbst in einem schwach koordinierenden Lösungsmittel wie MeCN schwierig ist. Deshalb werden noch weniger koordinierende Lösungsmittel benötigt, um das Pd-Zentrum elektronenärmer zu machen. Es wurden Reaktionen mit "nicht-koordinierenden" aromatischen Lösungsmitteln wie Toluol, Benzol oder *m*-Xylol durchgeführt, die sich als wirksam erwiesen haben, um die Homokupplung von 2,6-C₆F_{2+n}H_{3-n}Bpin zu katalysieren. Unter Verwendung von Toluol als Lösungsmittel lieferte die palladiumkatalysierte Homokupplung von Ar_F-Bpin Kopplungsprodukte, die ein, zwei oder keine *ortho*-Fluoratome enthalten in ausgezeichneten Ausbeuten (Schema S-6).



Schema S-6. Pd-katalysierte Homokupplung von fluorierten Aryl-Pinacolboronaten in Toluol.

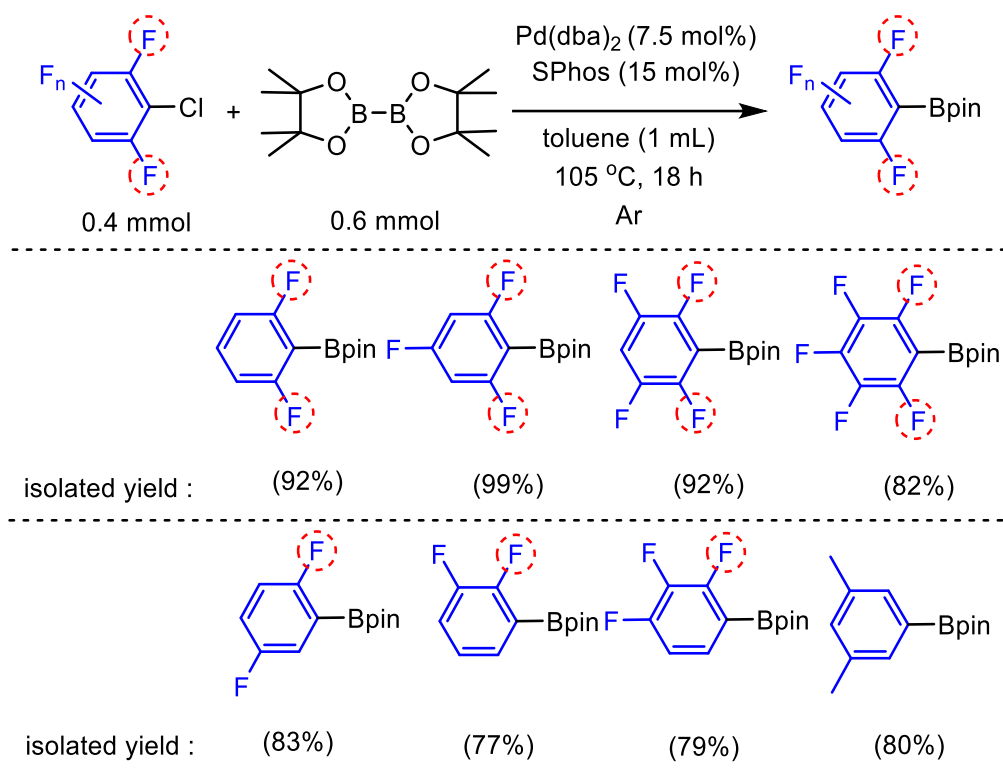


Schema S-7. Seitenansicht (a) und Sicht entlang des Aryl-Pd-Vektors (b) der DFT-optimierten Strukturen (B3LYP-D3/TZVP) der Benzolkomplexe $[\text{Pd}(\eta^6\text{-C}_6\text{H}_6)(\text{C}_6\text{F}_5)_2]$ **20**, der Übergangszustand **TS(20-21)**, und das primäre Eliminierungsprodukt **21**. Berechnete Pd-C_{aryl} Abstände [Å]: **20**: 2.617, 2.618, 2.640, 2.641, 2.666, 2.667, **TS(20-21)**: 2.275, 2.608, 2.609, 3.205, 3.206, 3.478, **21**: 2.236, 2.565, 2.631, 3.204, 3.255, 3.514.

DFT-Berechnungen (B3LYP-D3/def2-TZVP/6-311+g(2d,p)/IEFPCM // B3LYP-D3/SDD/6-31g**/IEFPCM) sagten einen exergonischen Prozess und eine niedrigere Barriere (<21 kcal/mol) für die reduktive Eliminierung von Pd(C₆F₅)₂-Komplexen mit Arylliganden voraus. Dagegen sind Prozesse in stärker koordinierenden Lösungsmitteln (MeCN, THF, SMe₂ und PMe₃) mit einer höheren Barriere ausgewiesen (> 33.7 kcal/mol). Die reduktive Eliminierung von Komplexen [Pd(ηⁿ-Ar)(C₆F₅)₂] haben niedrige Barrieren aufgrund (i) der Haptizitätsänderung des Aryl-Liganden von η⁶ im Reaktanten zu ηⁿ (n ≤ 3) im Übergangszustand und dem Produkt (Schema S-7), was zu einer geringeren Abstoßung führt; und (ii) einer günstigeren π-Rückbindung von Pd(ArF)₂ an das Aryl-Fragment im Übergangszustand.

Kapitel 4

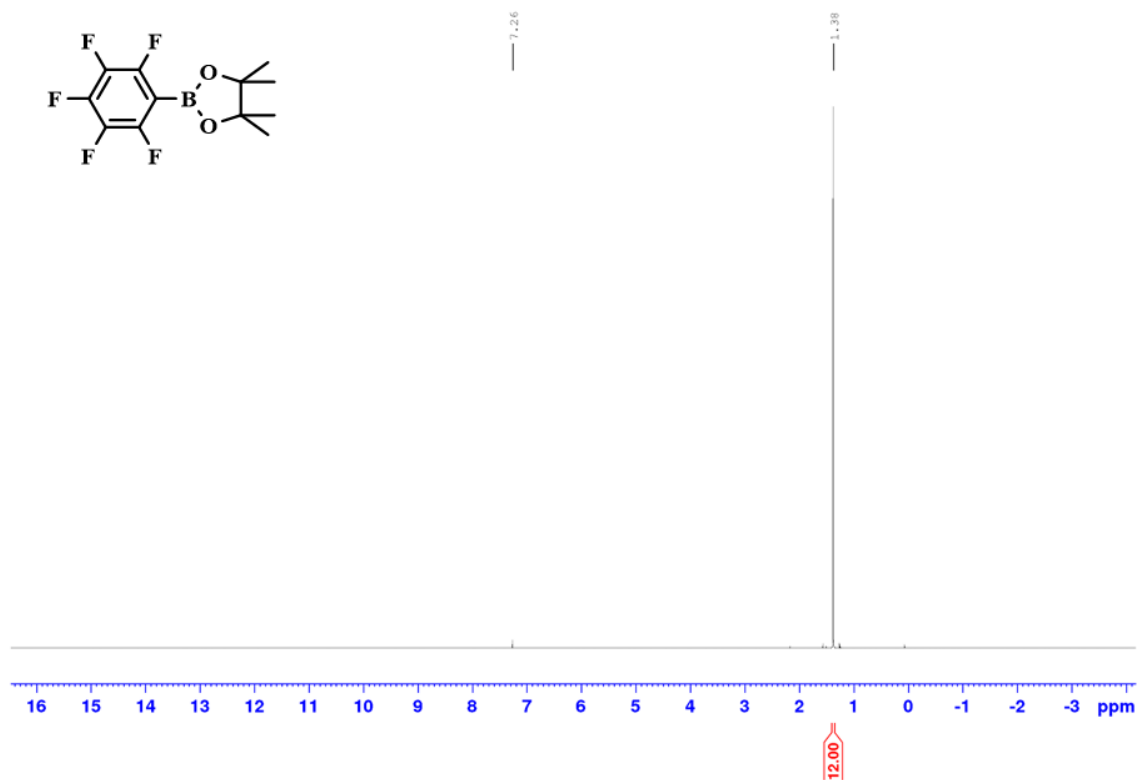
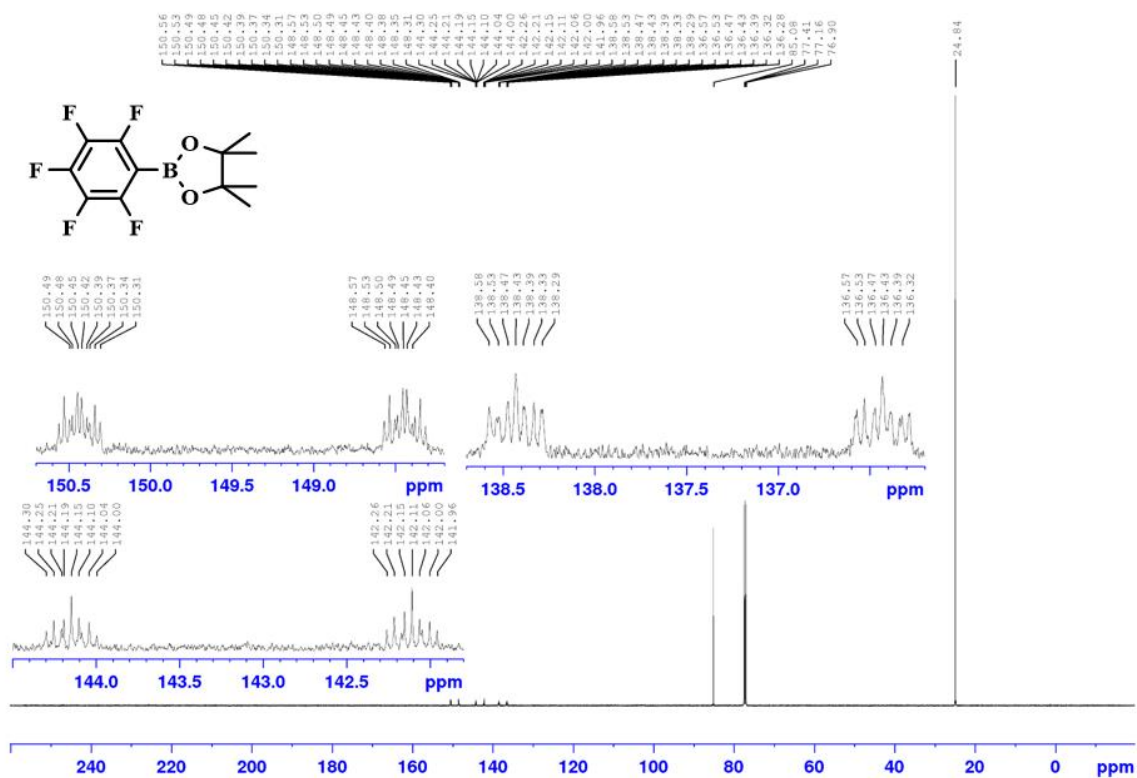
In diesem Kapitel wird eine effiziente Pd-katalysierte C-Cl-Borylierung von Arylchloriden, welche zwei *ortho*-Fluorsubstituenten enthalten, vorgestellt. Um eine Zersetzung der gebildeten *ortho*-fluorierten Arylboronate, die in Gegenwart einer Base instabil sind, zu verhindern, wurde die Reaktionen unter basenfreien Bedingungen durchgeführt. Wie in Schema S-4 gezeigt wird, ist eine Kombination des Komplexes Pd(dba)₂ (dba = dibenzylidenaceton) mit dem Liganden SPhos (2-Dicyclohexylphosphino-2',6'-dimethoxybiphenyl) ein effizienter Katalysator für die basenfreie C-Cl-Borylierung von Arylchloriden mit *ortho*-Fluorsubstituenten. Die Produkte konnten alle in ausgezeichneter Ausbeute isoliert werden. Der Anwendungsbereich dieser Reaktion kann auf Substrate wie Arylchloride mit einem oder keinem *ortho*-Fluorsubstituenten erweitert werden, und die borylierten Produkte wurden in guter bis sehr guter Ausbeute isoliert. Zusammenfassend, stellt diese Methode eine gute Alternative zu den traditionellen Methoden der Synthese über Lithium- oder Grignard-Reagenzien dar.

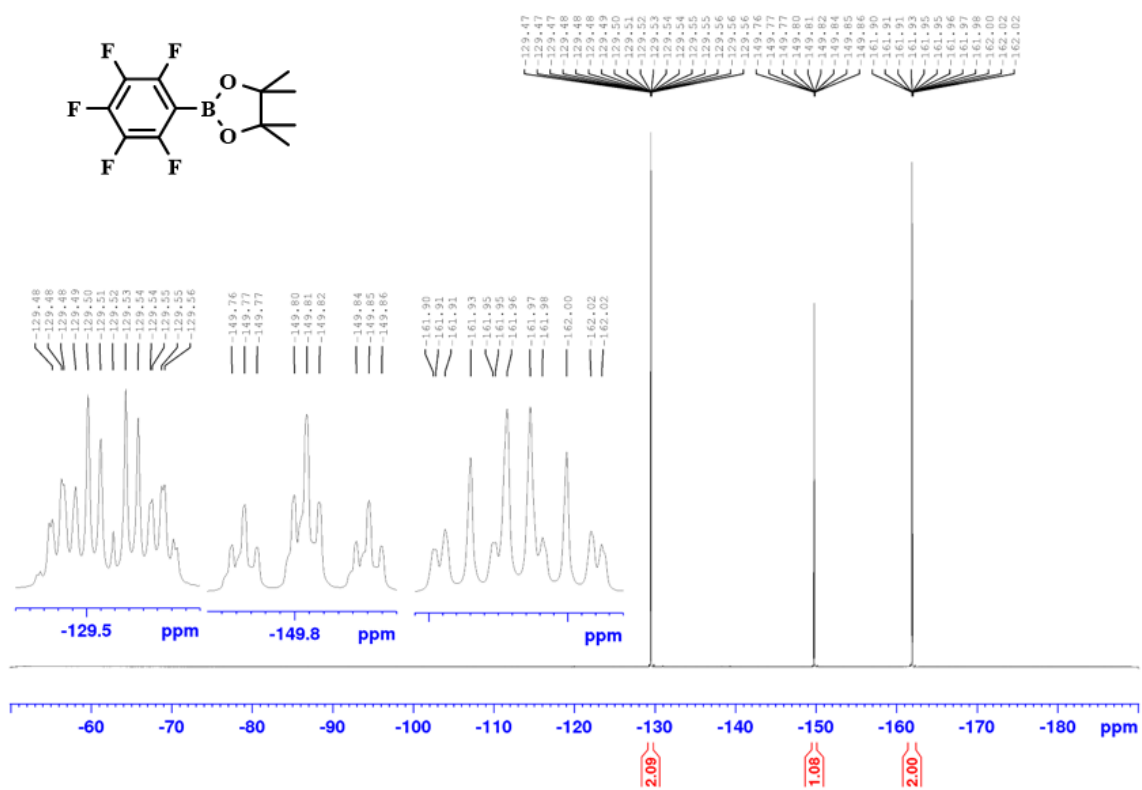
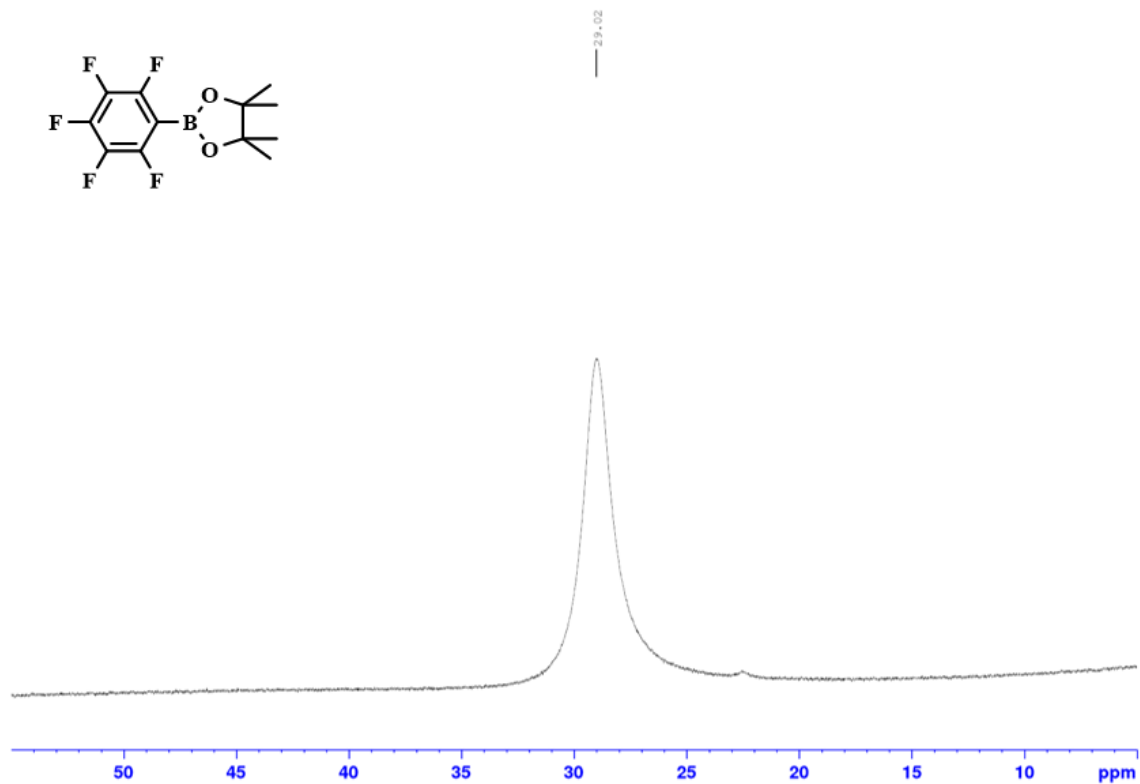


Schema S-8. Pd-katalysierte C–Cl Borylierung von fluorierten Arylchloriden.

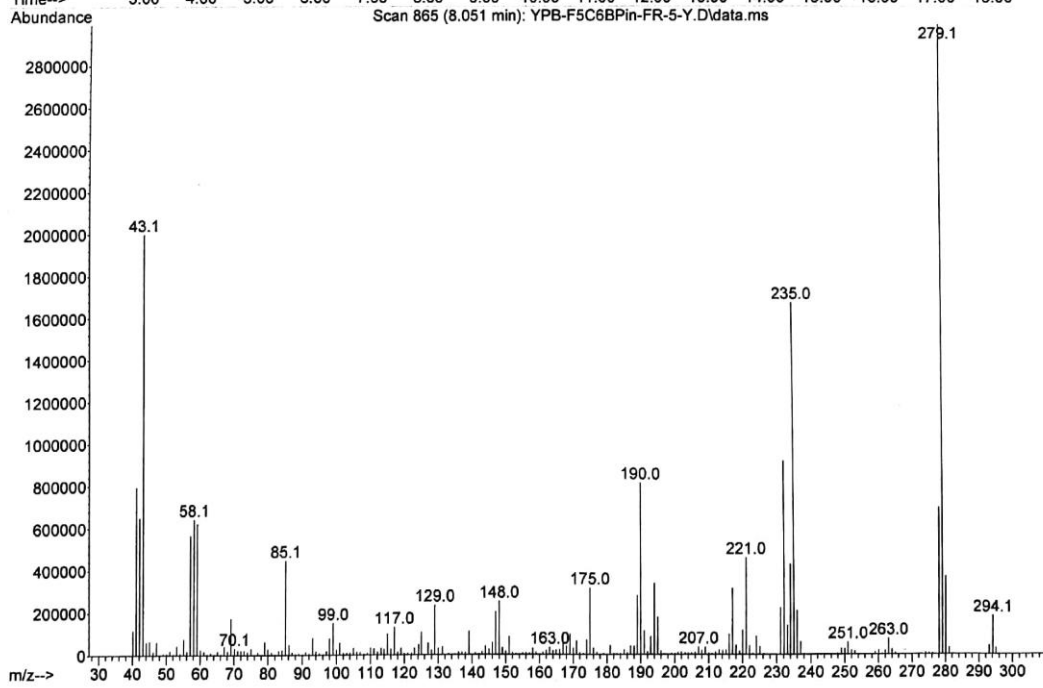
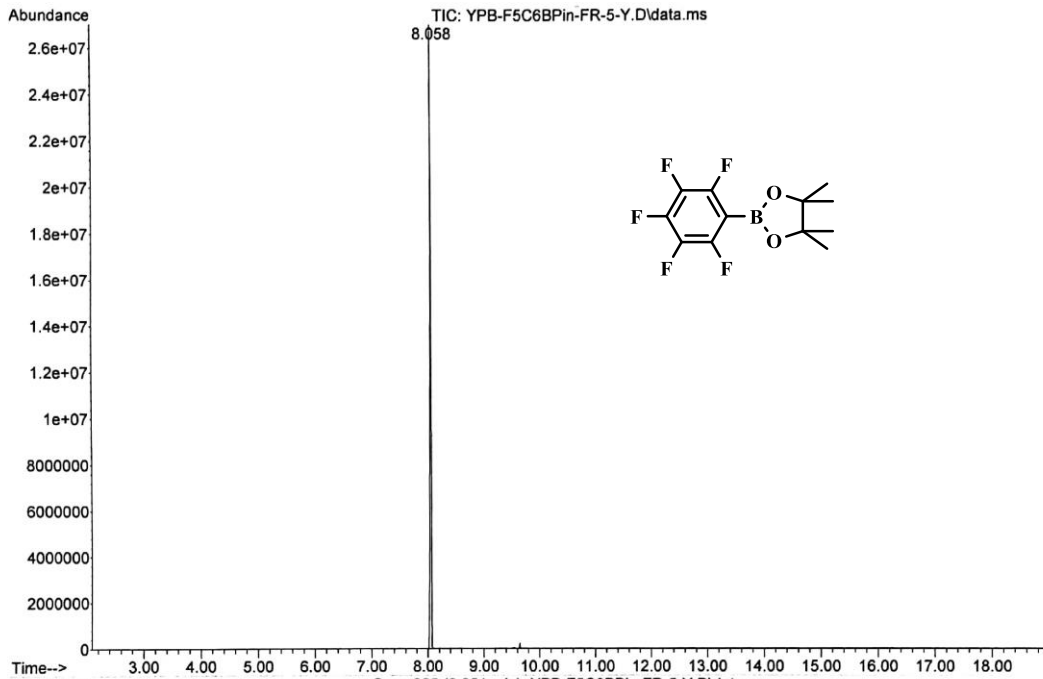
7. Appendix

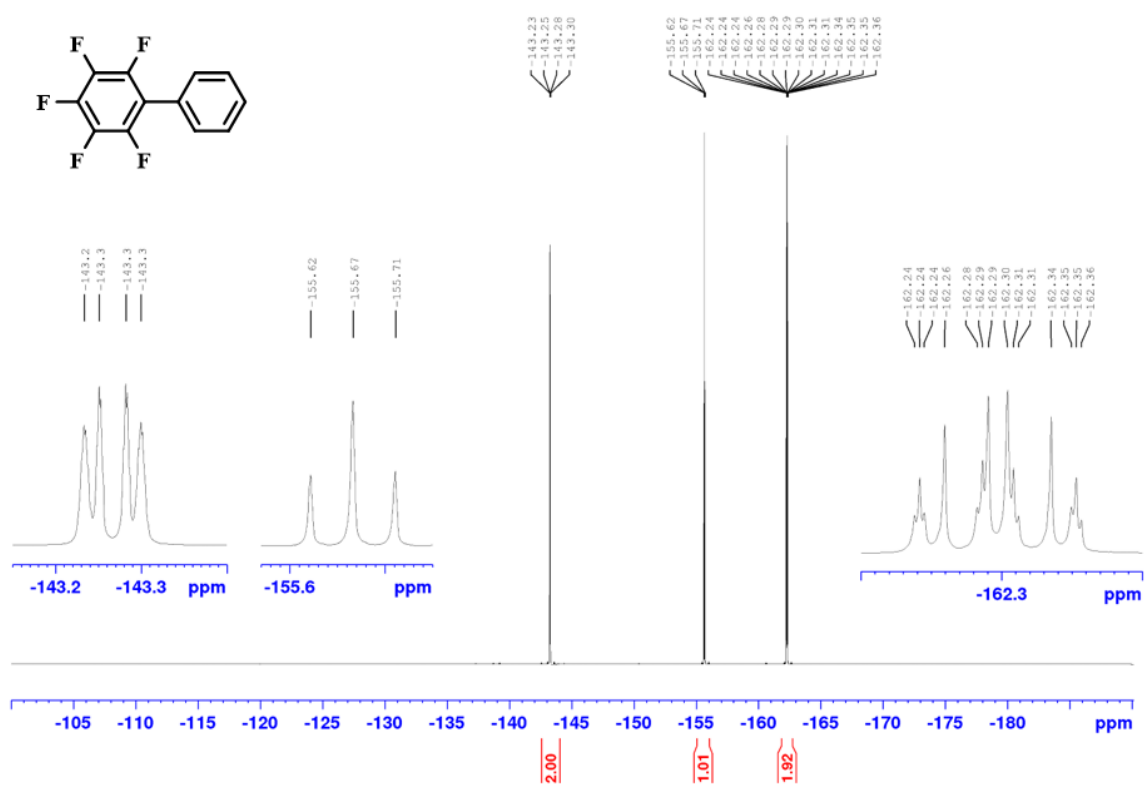
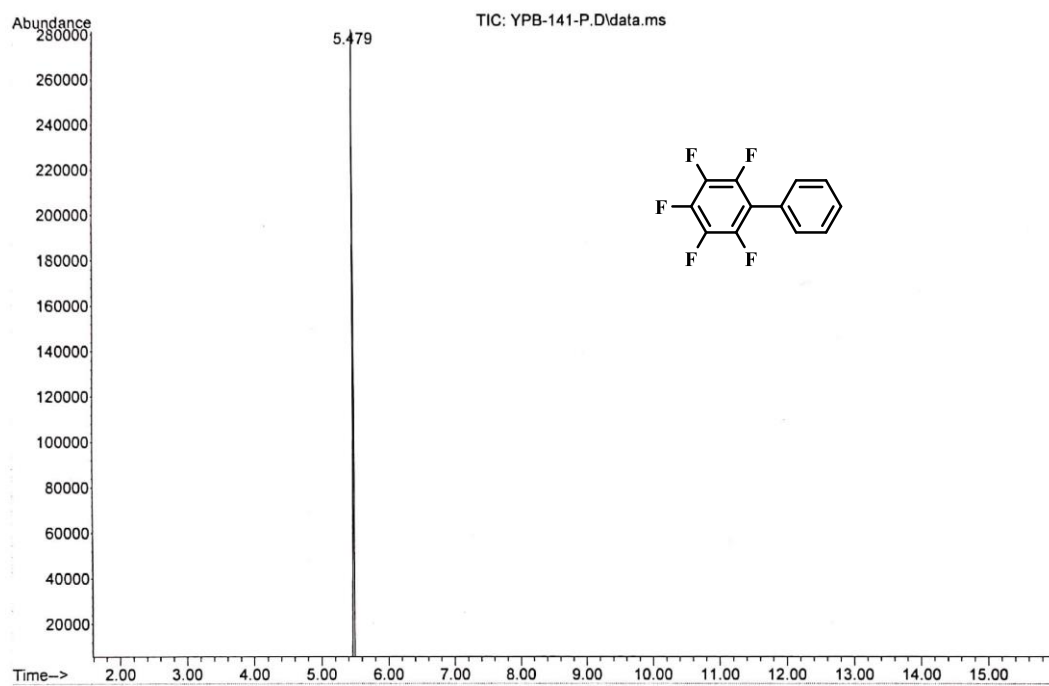
7.1 NMR Spectra for Chapter 2

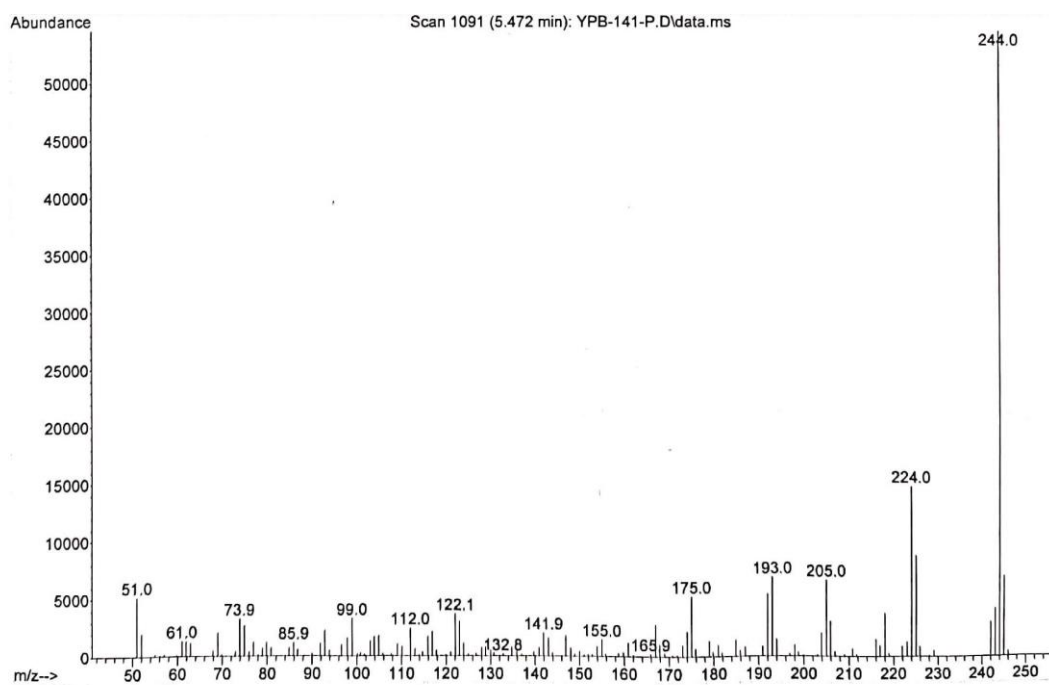
 ^1H NMR Spectrum of 2_1a (300 MHz, CDCl_3) $^{13}\text{C}\{^1\text{H}\}$ NMR Spectrum of 2_1a (125 MHz, CDCl_3)

^{19}F NMR Spectrum of 2_1a (470 MHz, CDCl_3) $^{11}\text{B}\{^1\text{H}\}$ NMR Spectrum of 2_1a (96 MHz, CDCl_3)

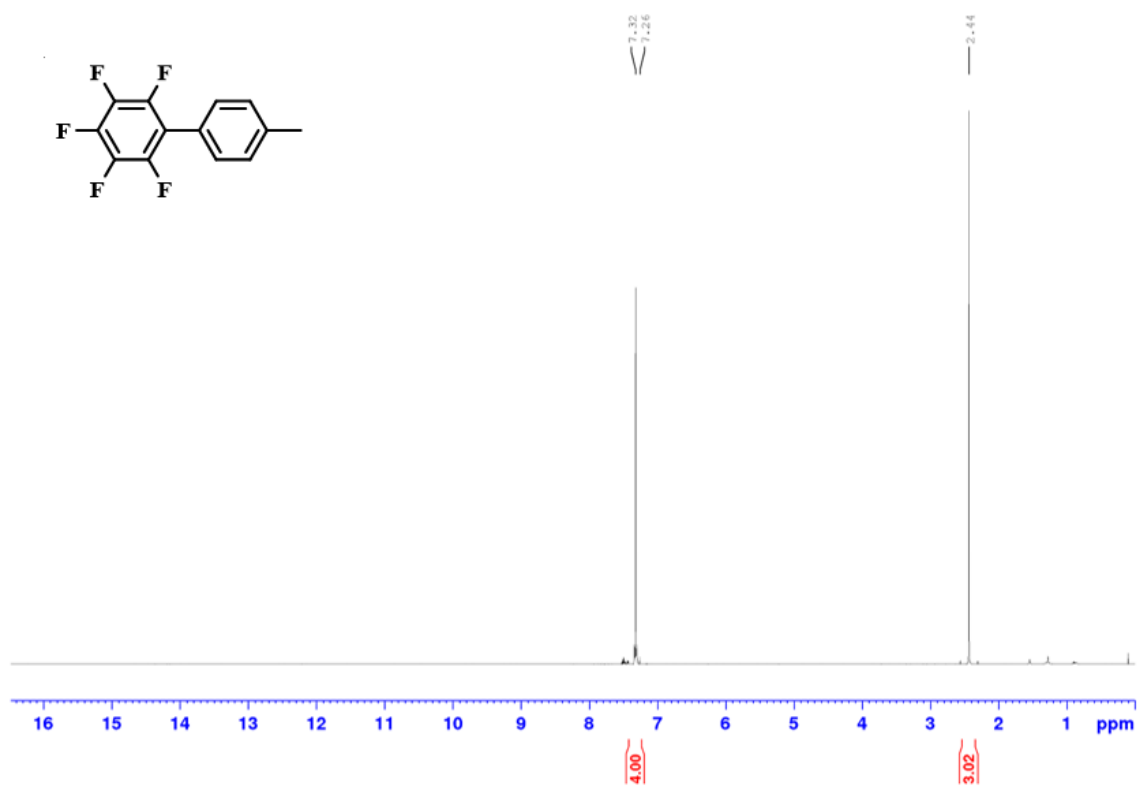
GC-MS of 2_1a



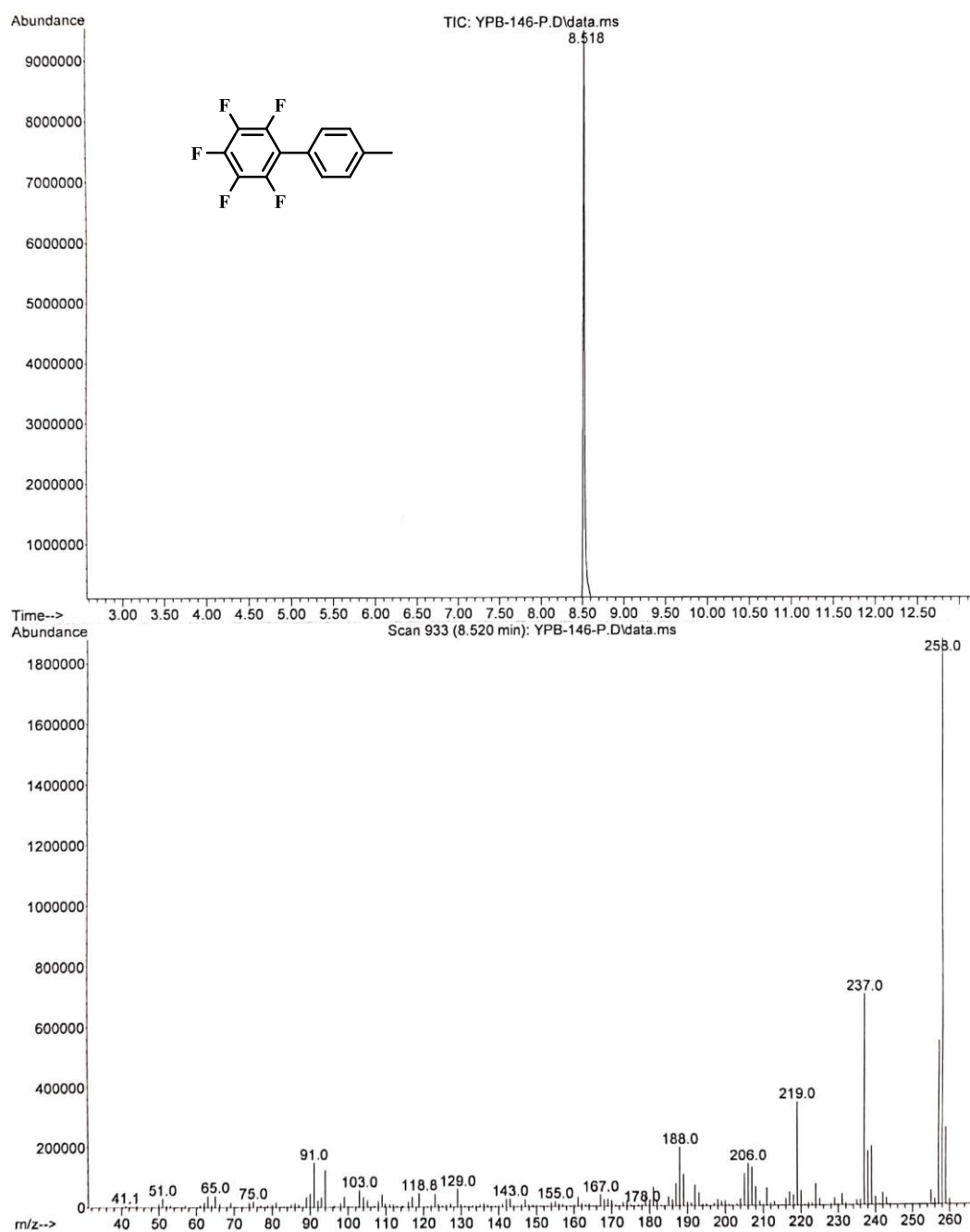
^{19}F NMR Spectrum of 2_3a (470 MHz, CDCl_3)**GC-MS of 2_3a**

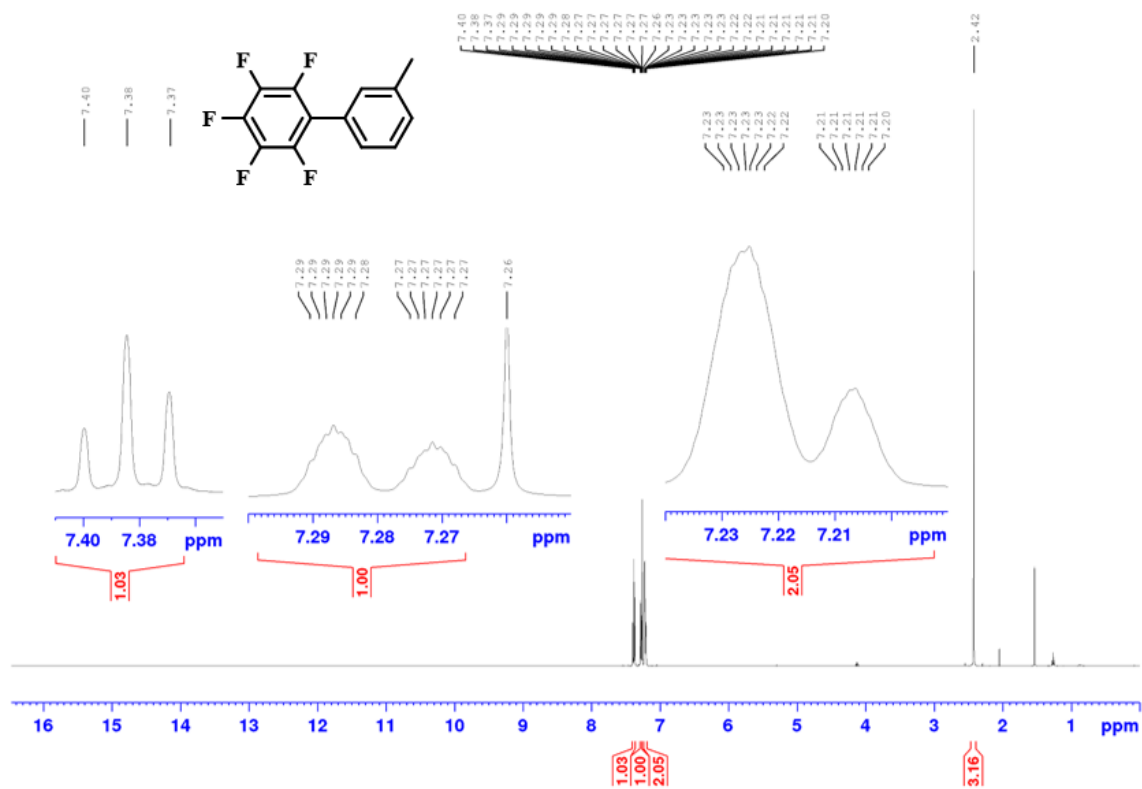
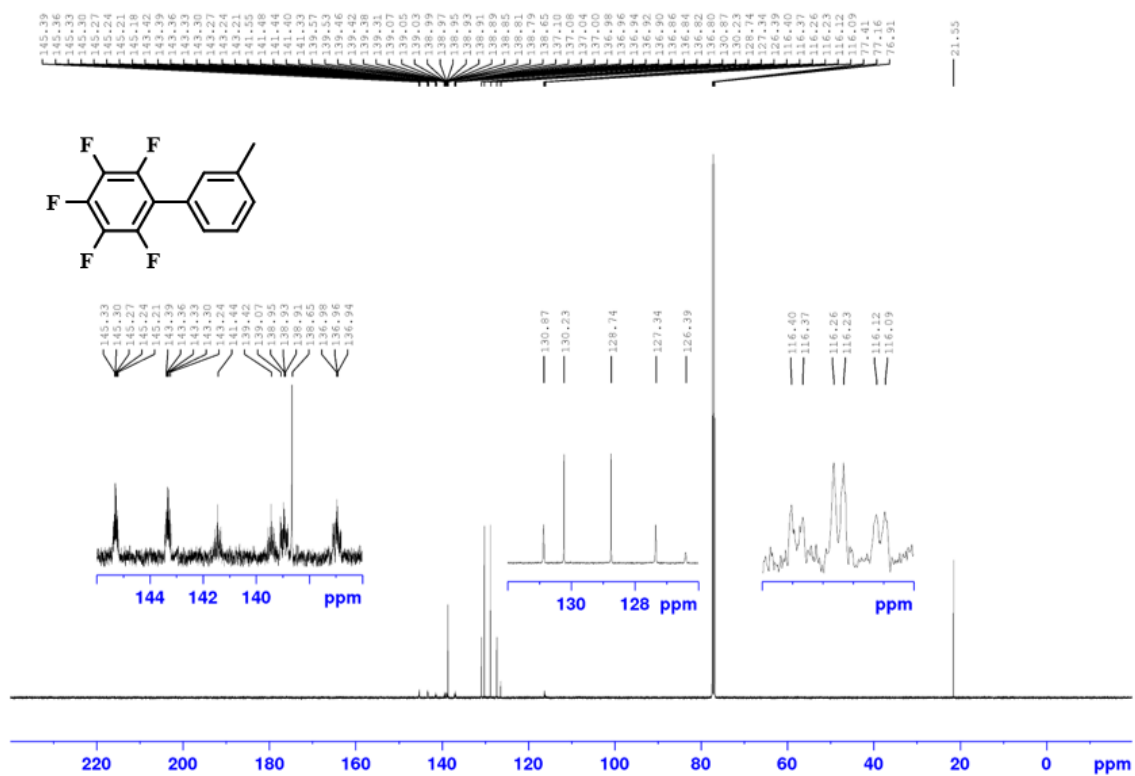


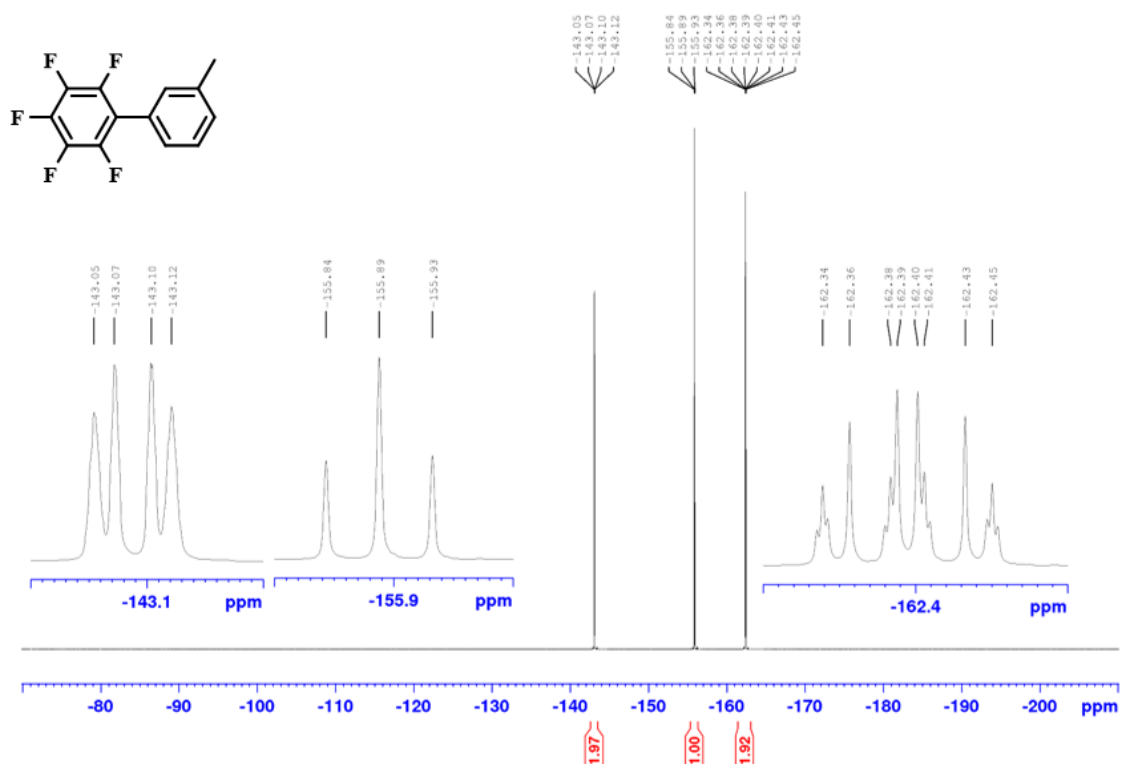
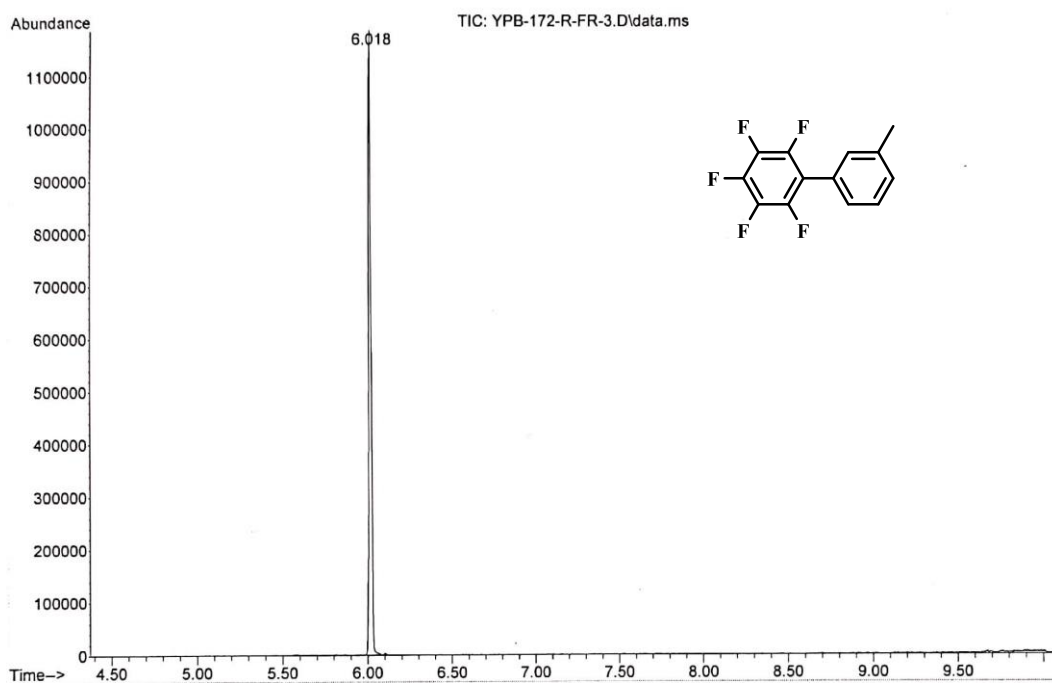
^1H NMR Spectrum of 2_3b (500 MHz, CDCl_3)



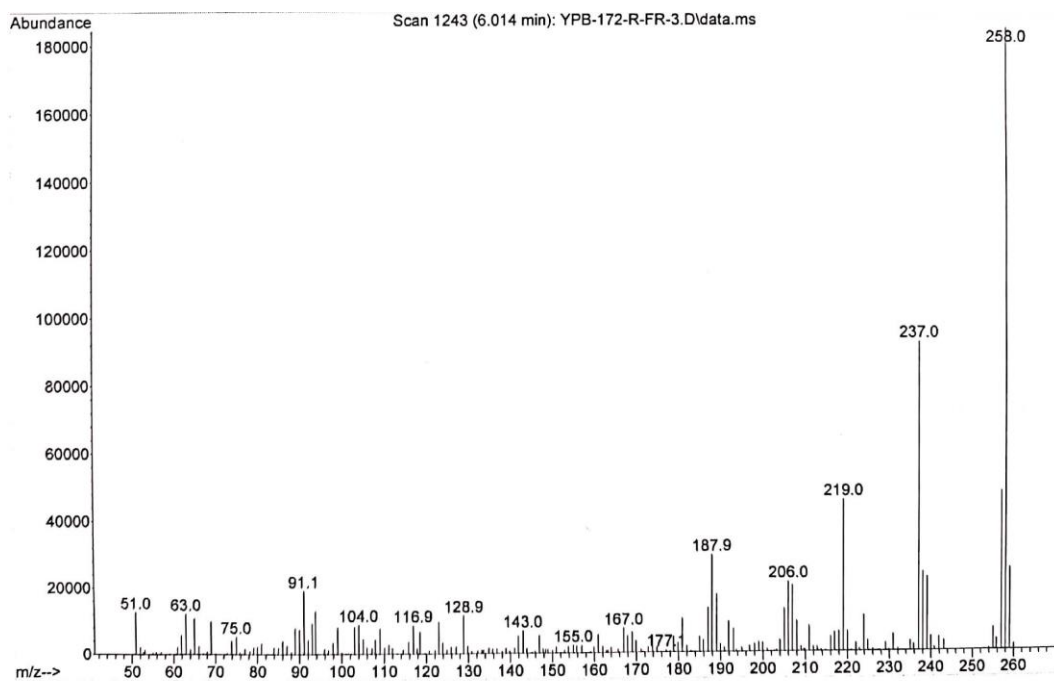
GC-MS of 2_3b



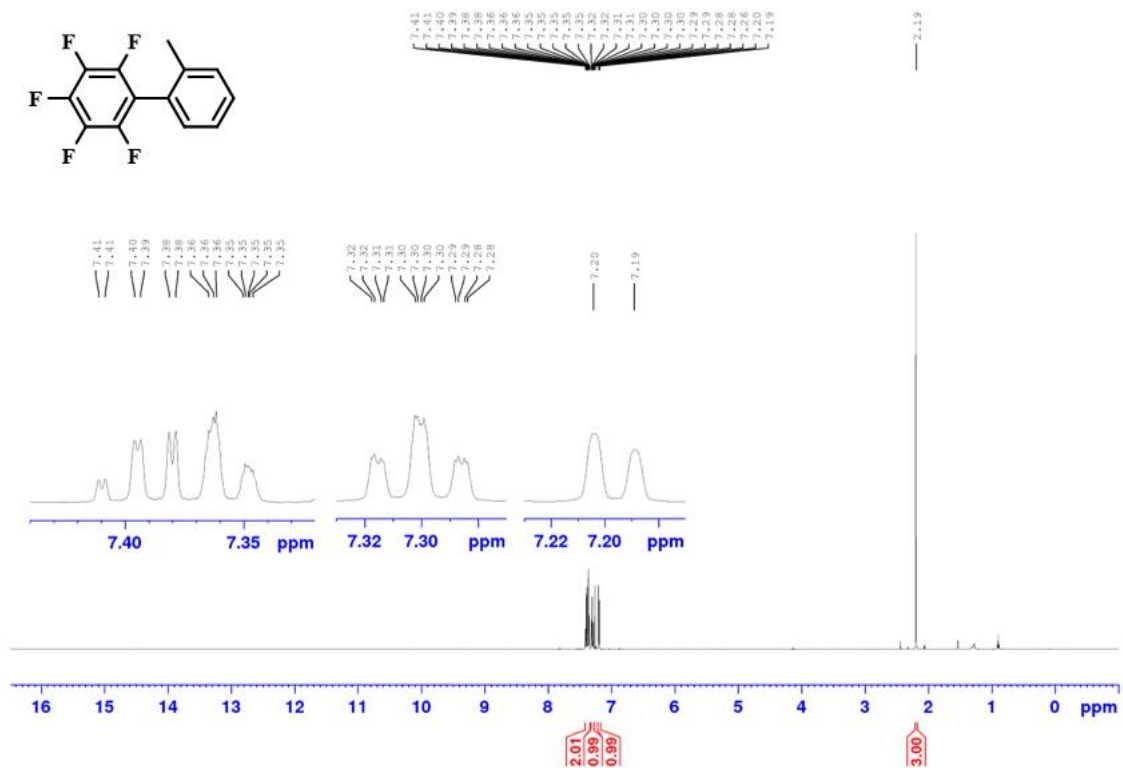
^1H NMR Spectrum of 2_3c (500 MHz, CDCl_3) $^{13}\text{C}\{^1\text{H}\}$ NMR Spectrum of 2_3c (126 MHz, CDCl_3)

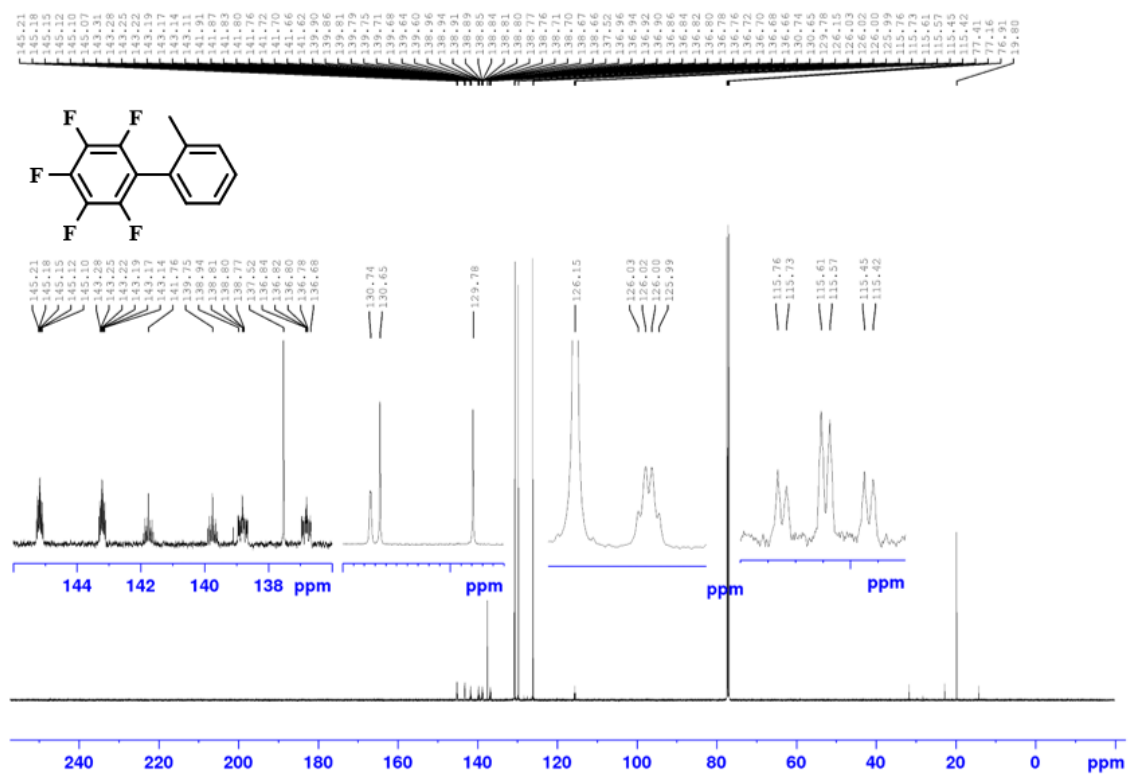
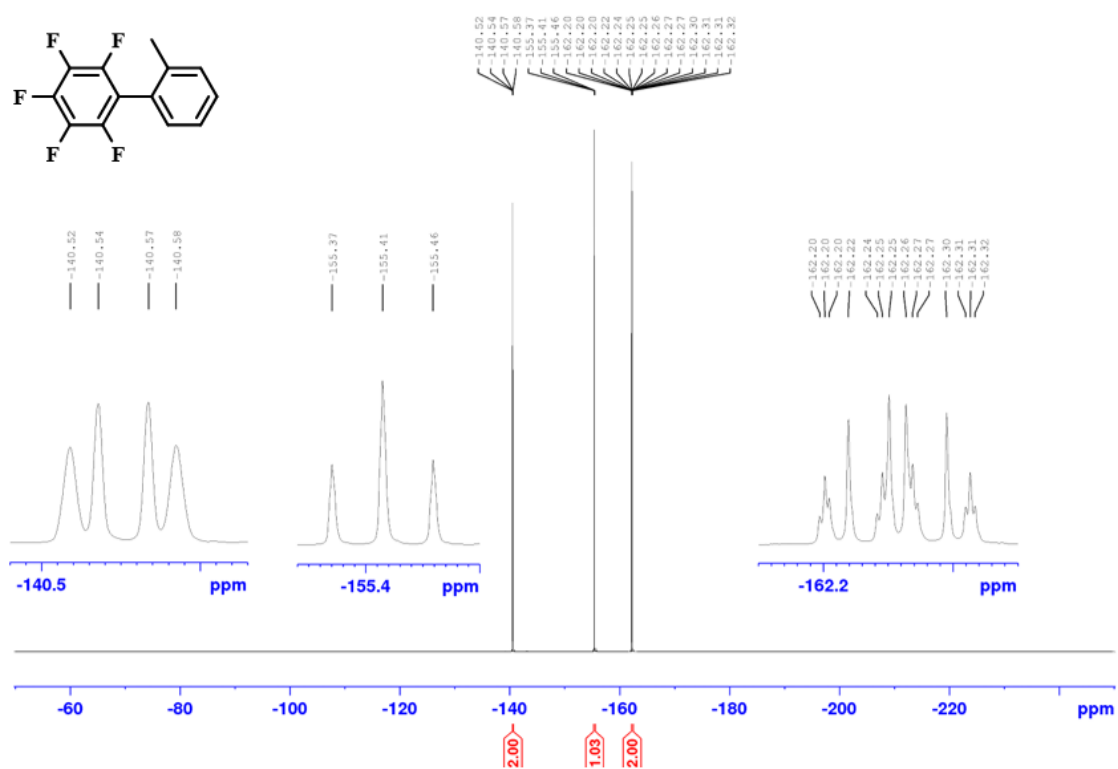
^{19}F NMR Spectrum of 2_3c (470 MHz, CDCl_3)**GC-MS of 2_3c**

Appendix

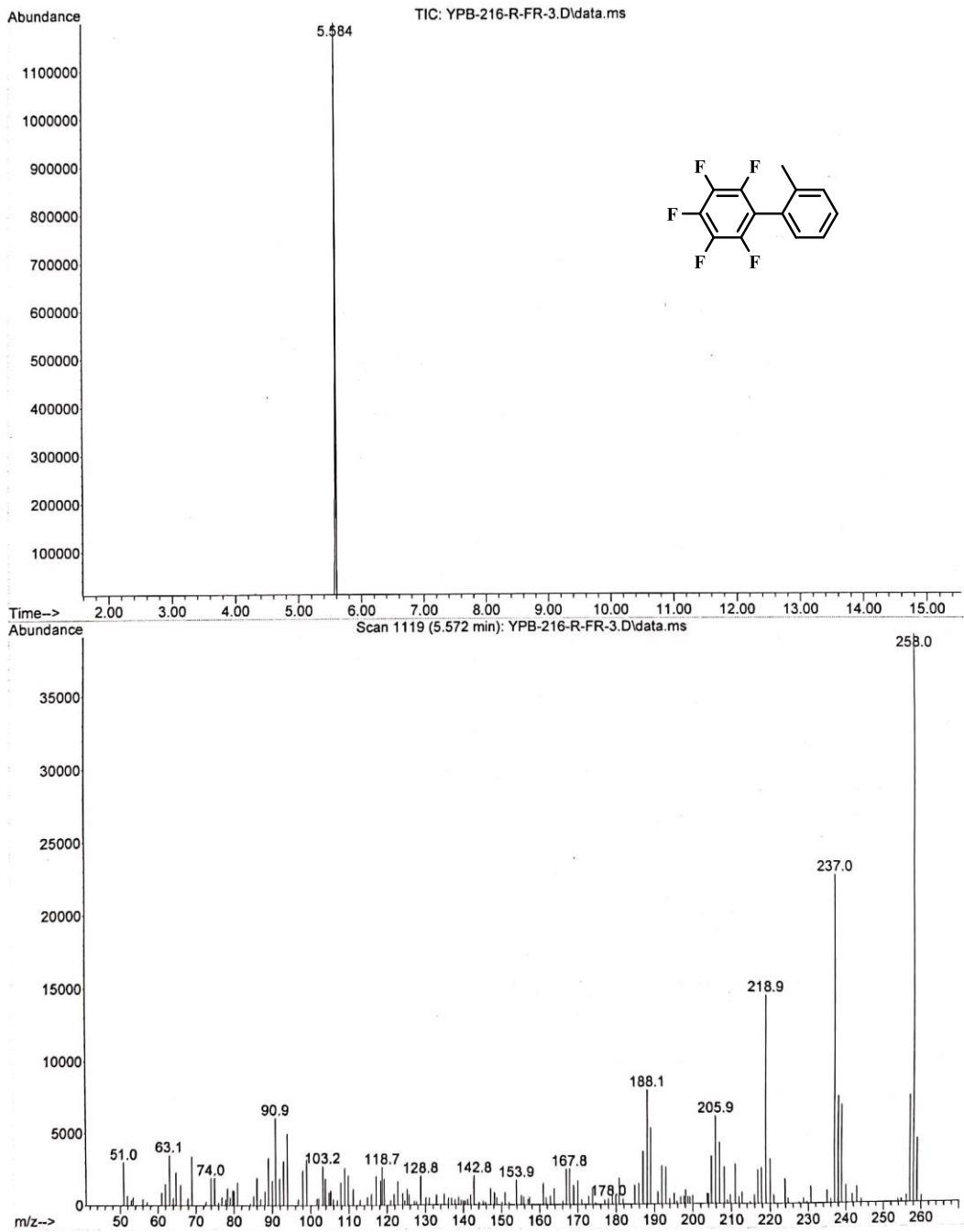


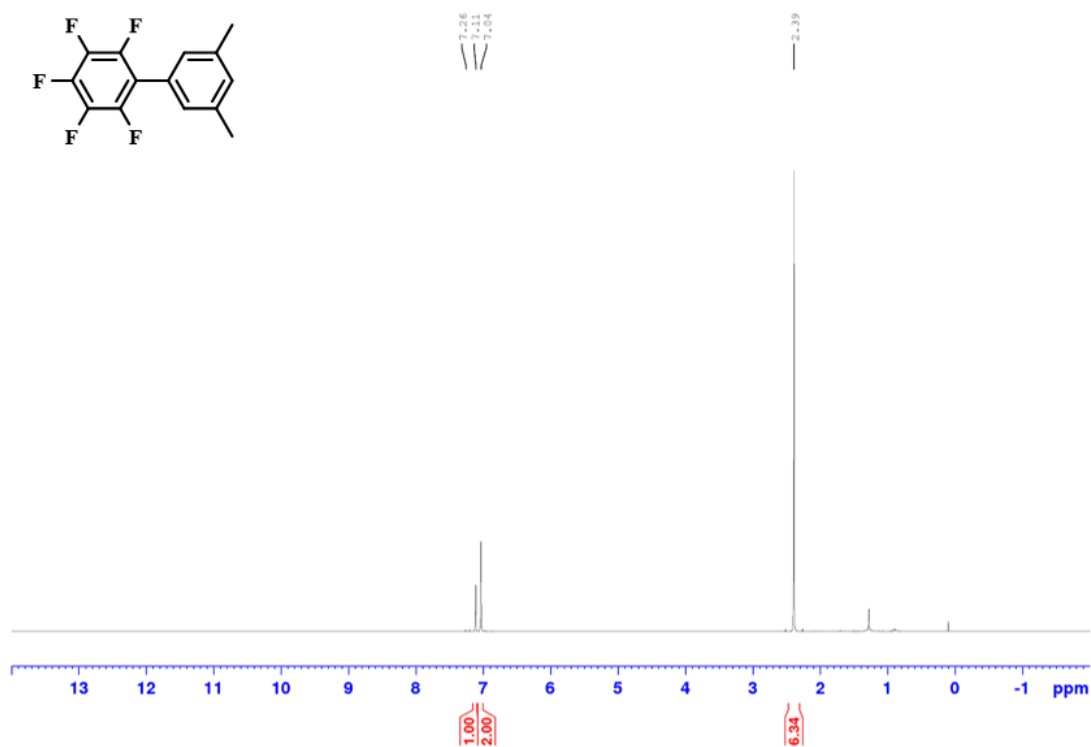
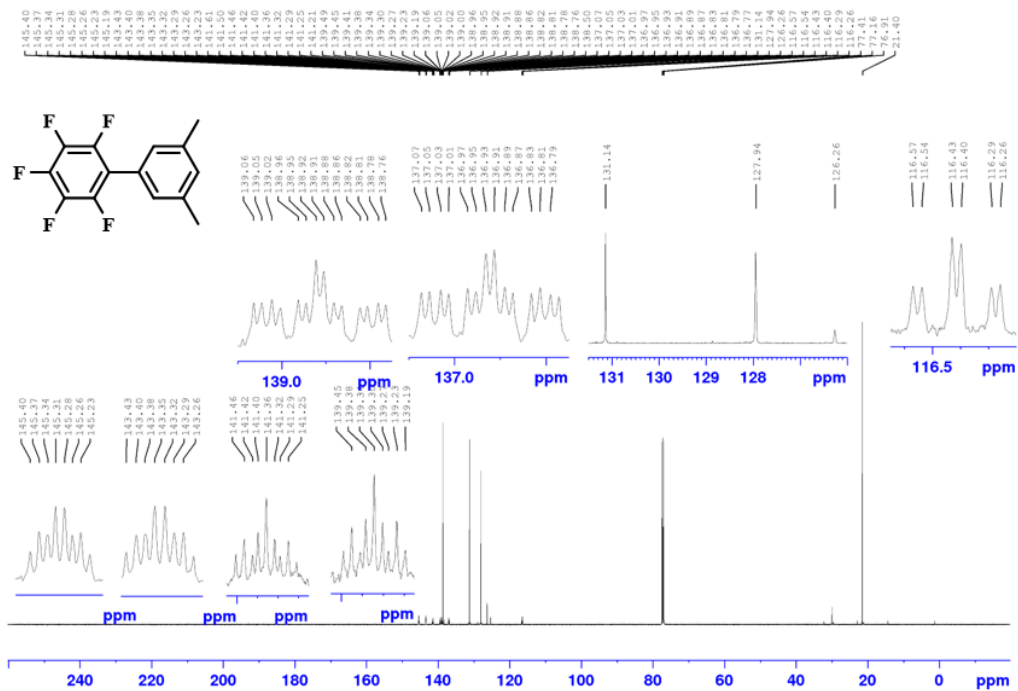
¹H NMR Spectrum of 2_3d (500 MHz, CDCl₃)

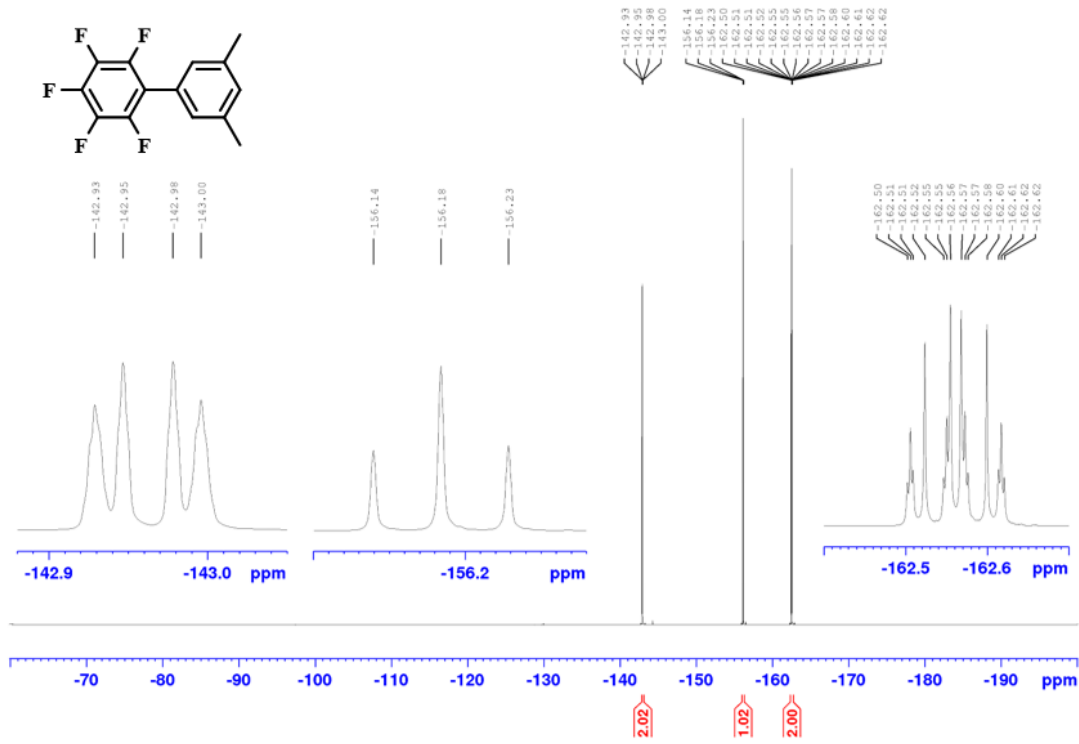
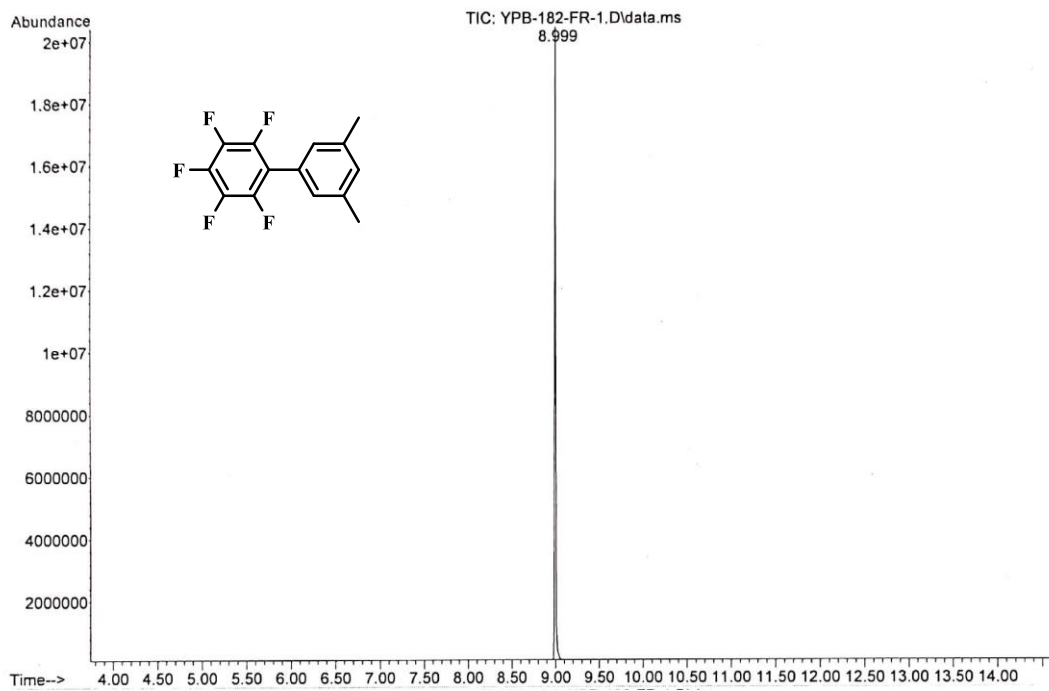


$^{13}\text{C}\{^1\text{H}\}$ NMR Spectrum of 2_3d (126 MHz, CDCl_3) ^{19}F NMR Spectrum of 2_3d (470 MHz, CDCl_3)

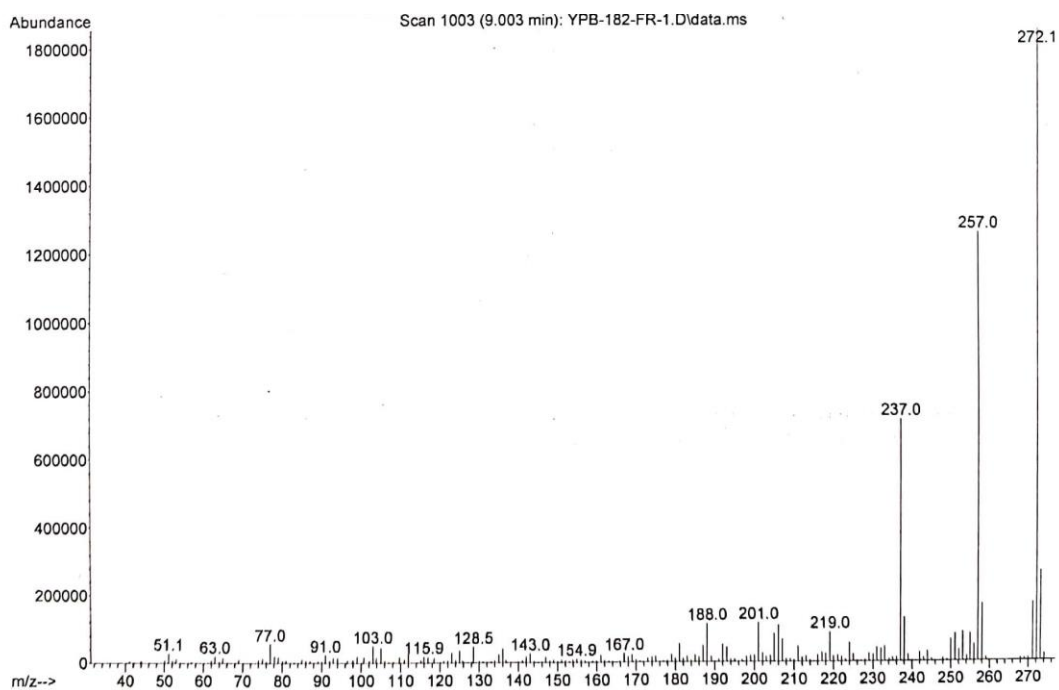
GC-MS of 2_3d



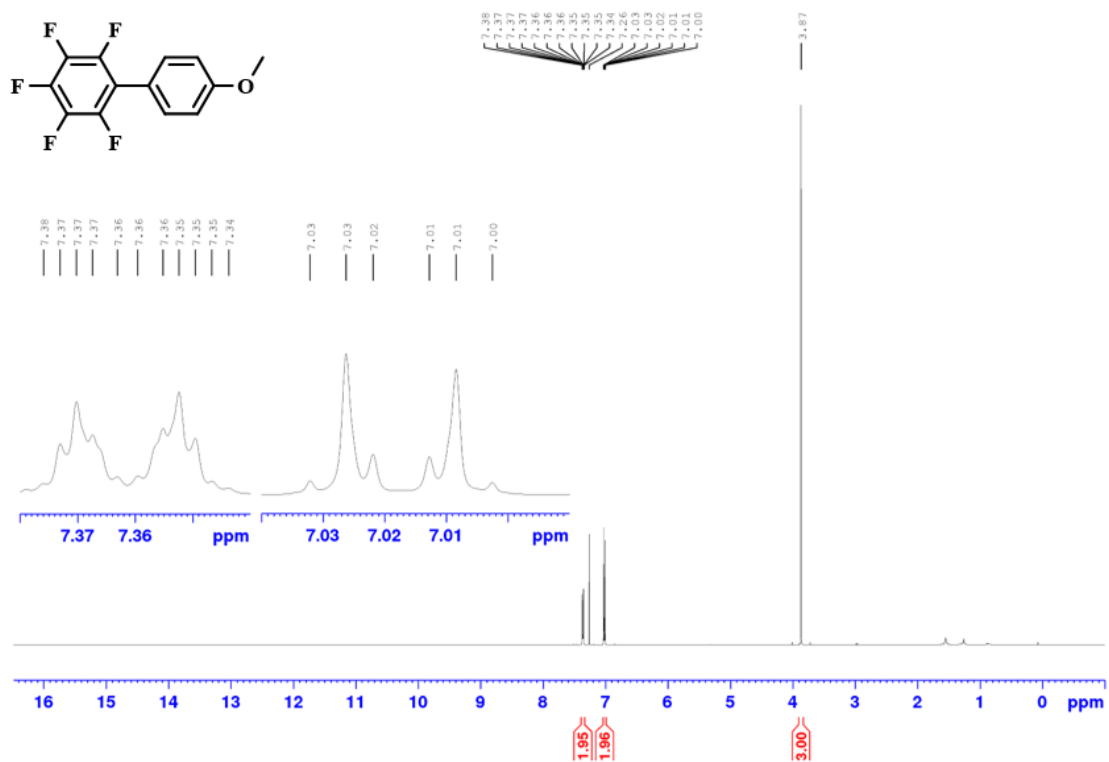
^1H NMR Spectrum of 2_3e (500 MHz, CDCl_3) $^{13}\text{C}\{^1\text{H}\}$ NMR Spectrum of 2_3e (126 MHz, CDCl_3)

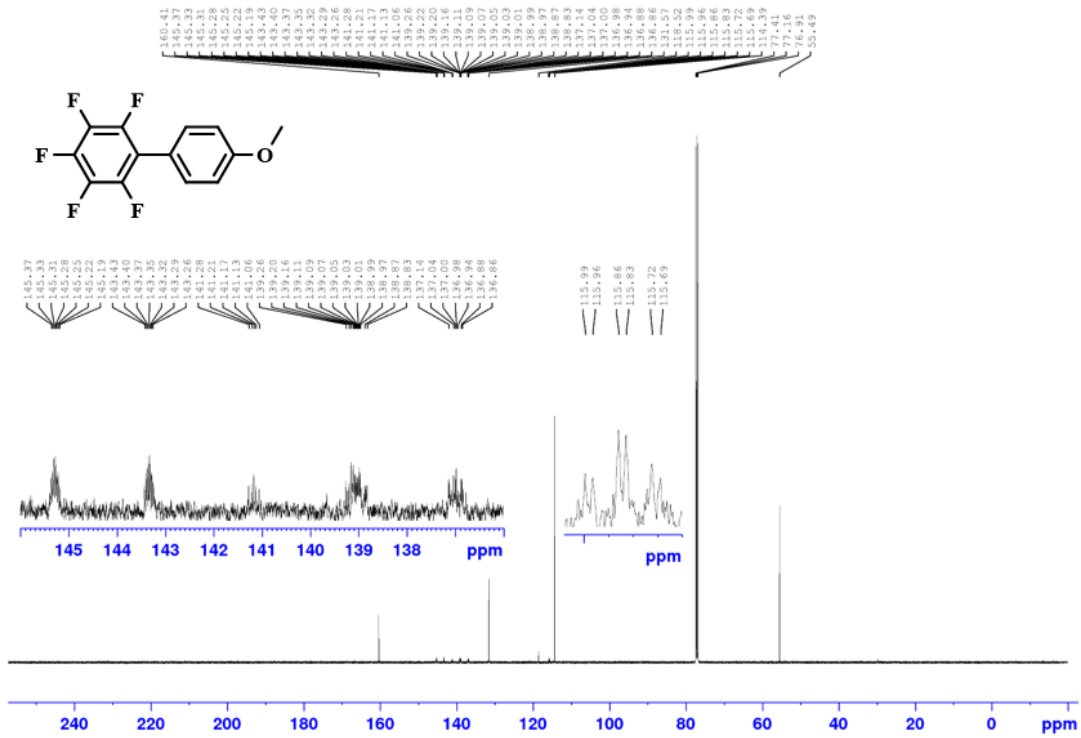
^{19}F NMR Spectrum of 2_3e (470 MHz, CDCl_3)**GC-MS of 2_3e**

Appendix

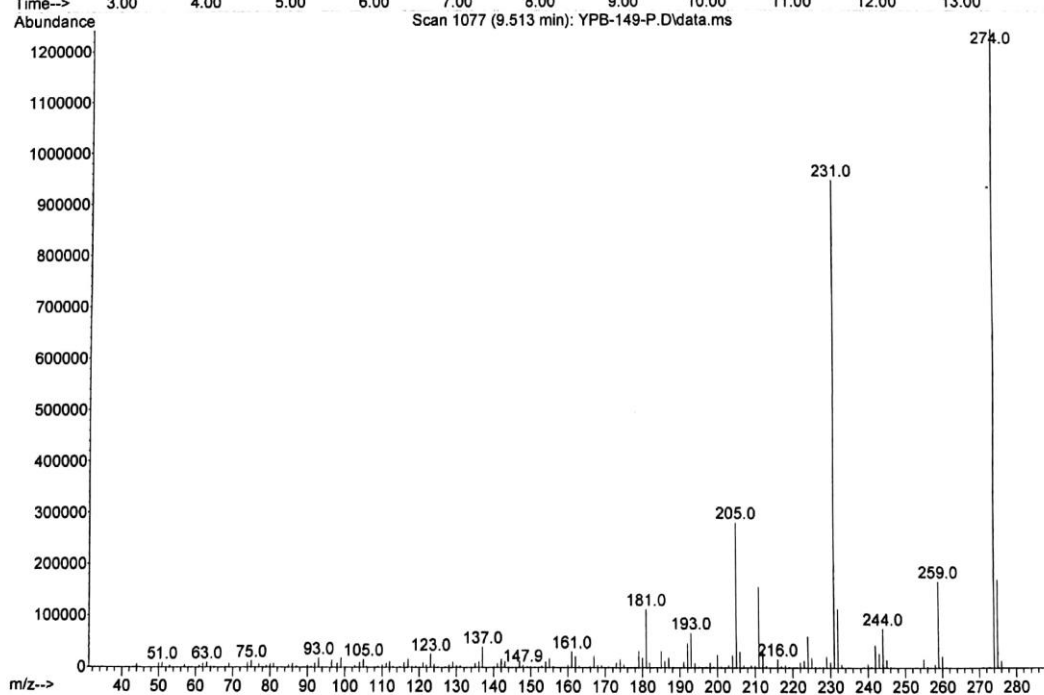
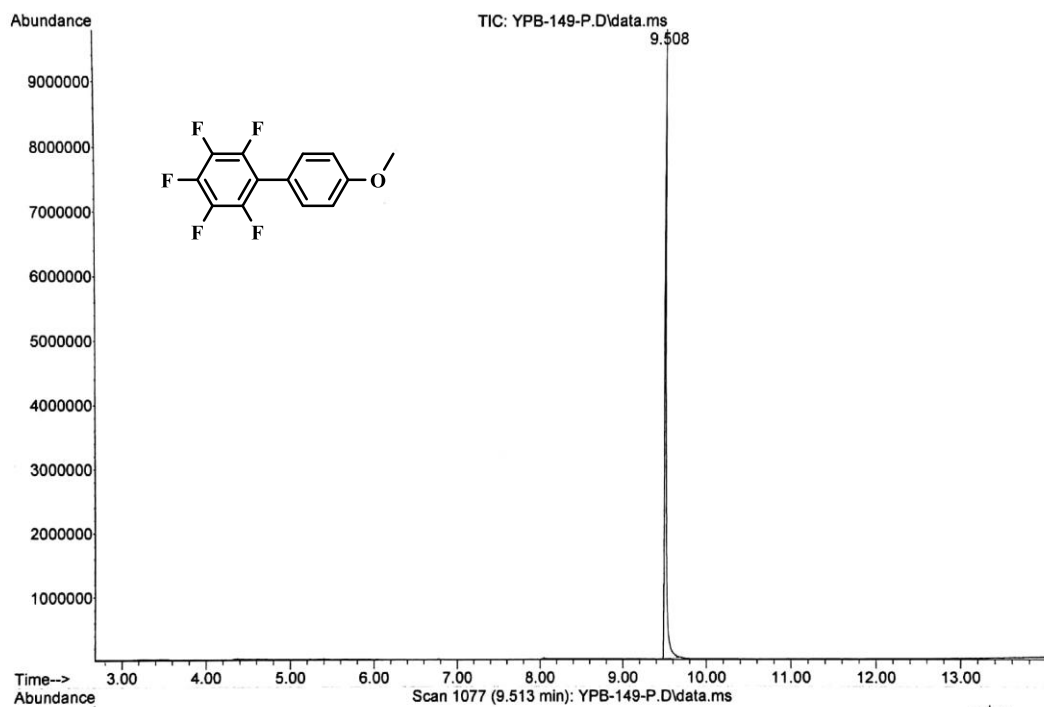


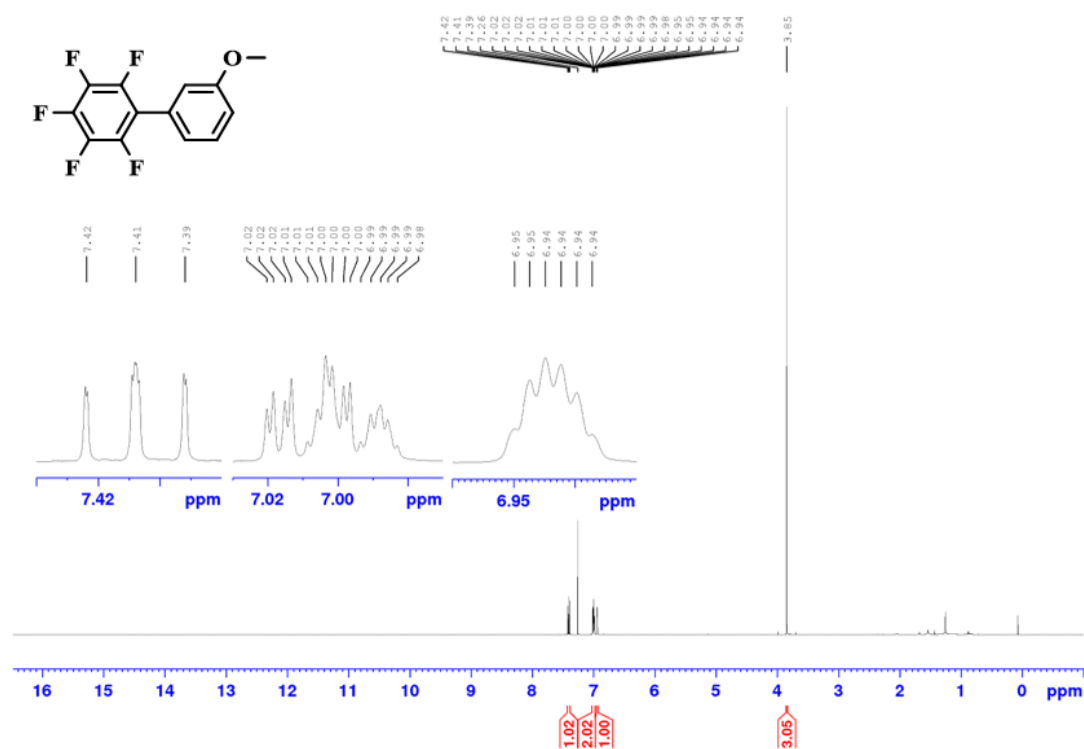
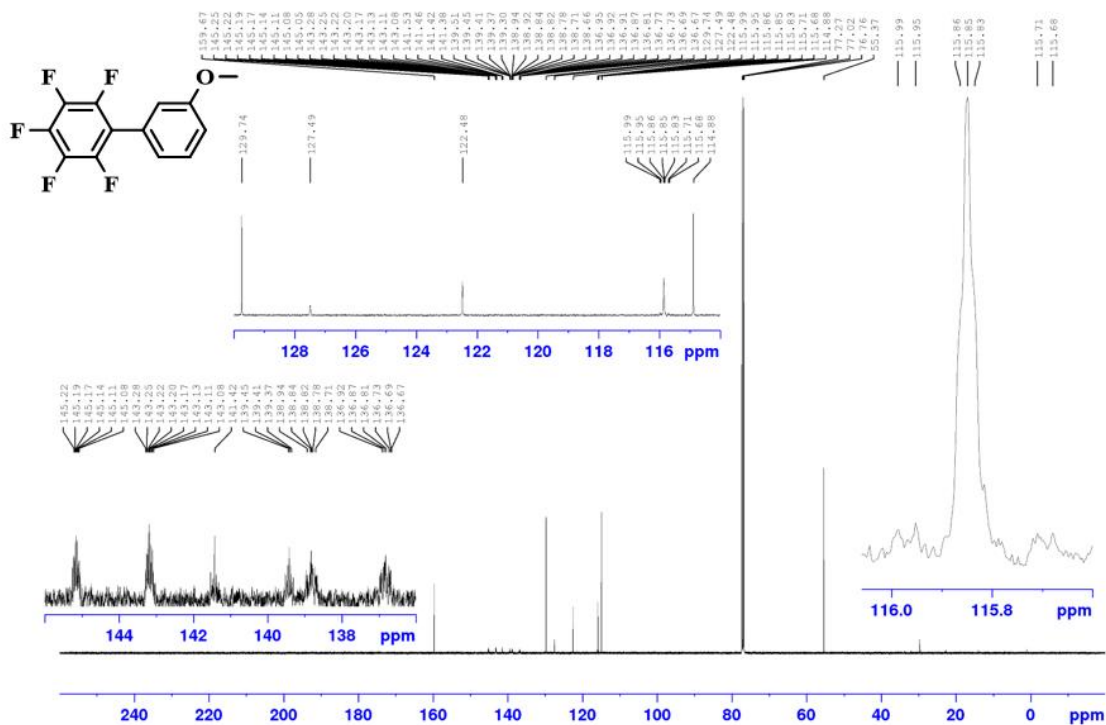
¹H NMR Spectrum of 2_3f (500 MHz, CDCl₃)

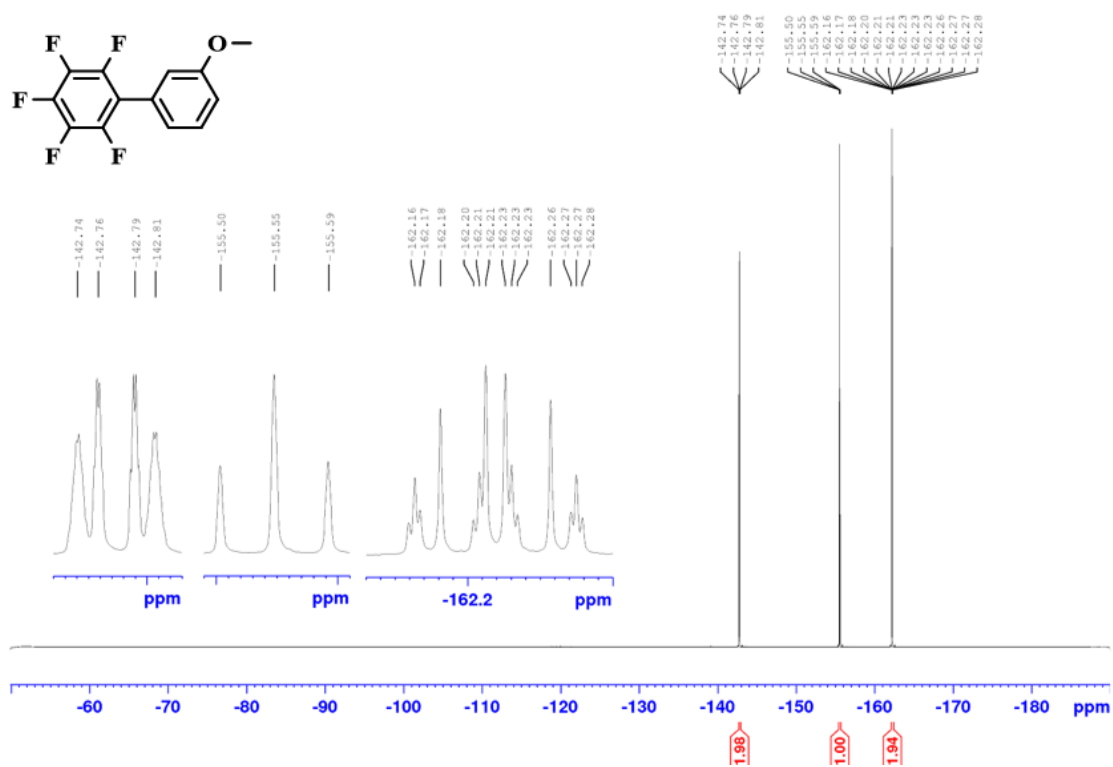
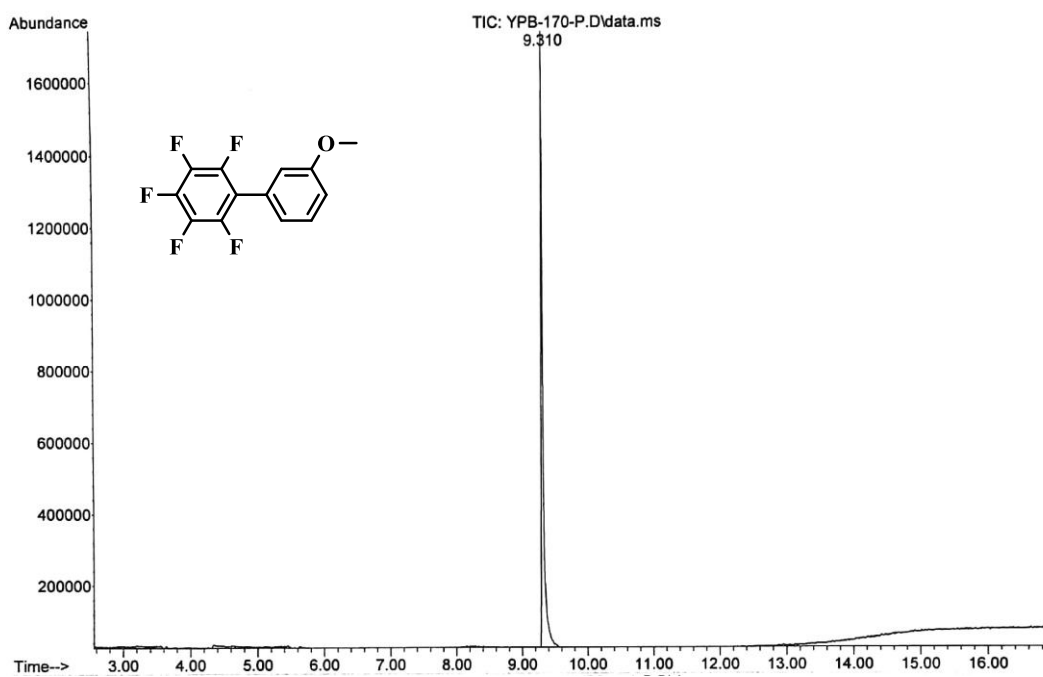


$^{13}\text{C}\{^1\text{H}\}$ NMR Spectrum of 2_3f (126 MHz, CDCl_3)

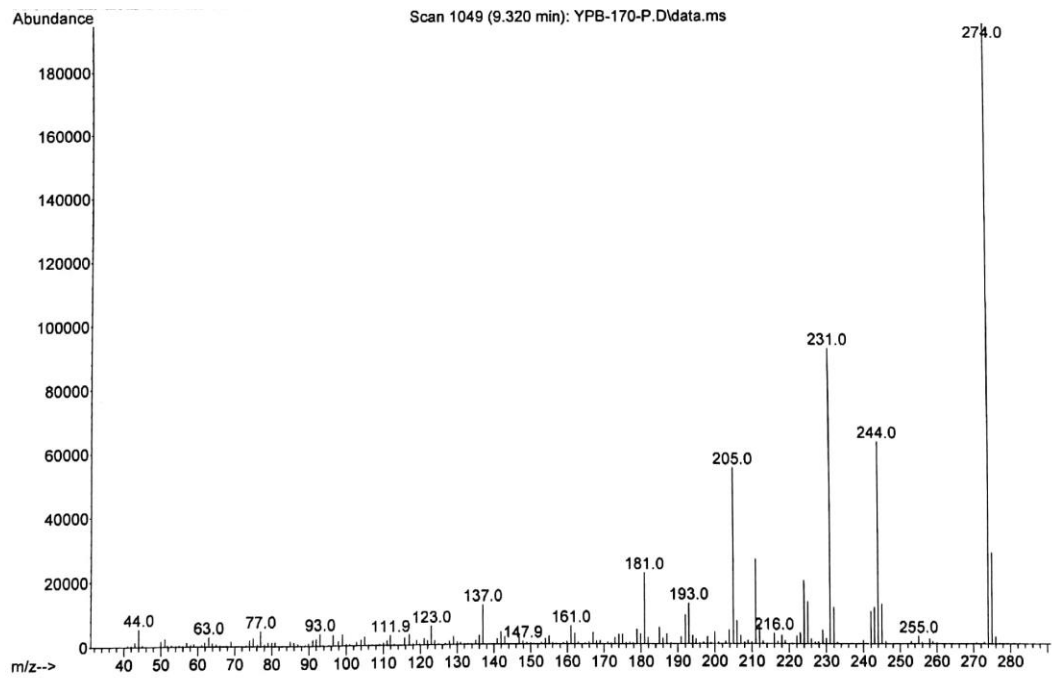
GC-MS of 2_3f



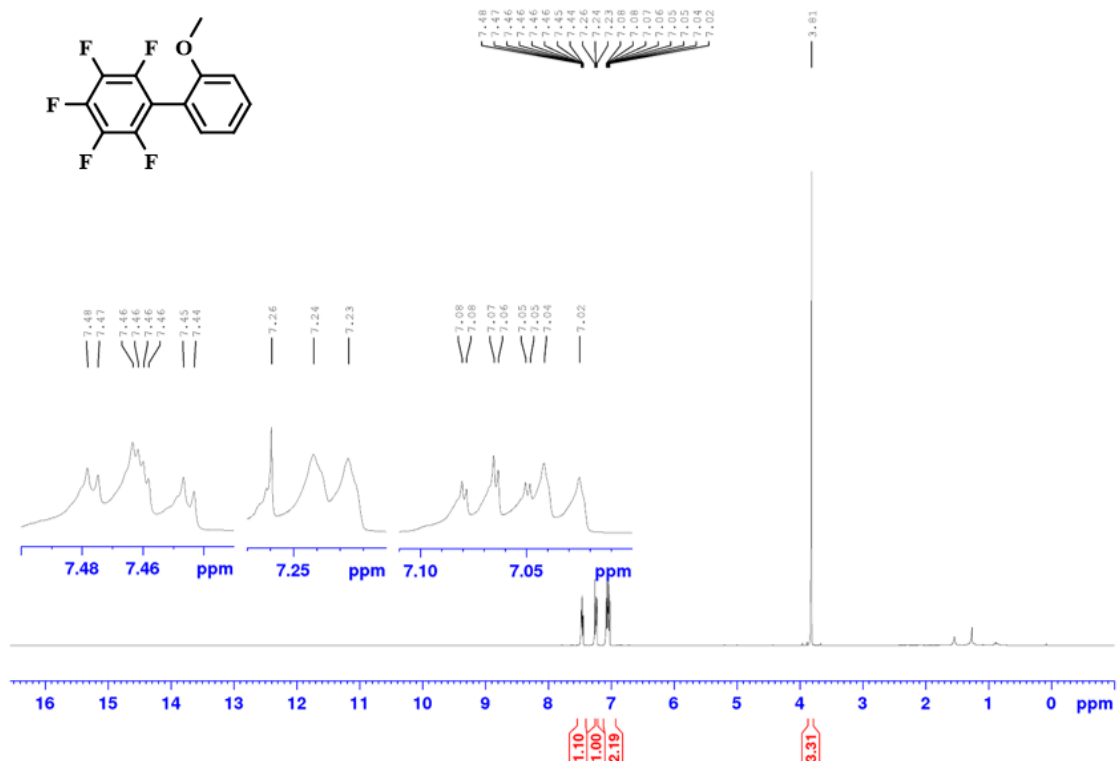
^1H NMR Spectrum of 2_3g (500 MHz, CDCl_3) $^{13}\text{C}\{^1\text{H}\}$ NMR Spectrum of 2_3g (126 MHz, CDCl_3)

¹⁹F NMR Spectrum of 2_3g (470 MHz, CDCl₃)**GC-MS of 2_3g**

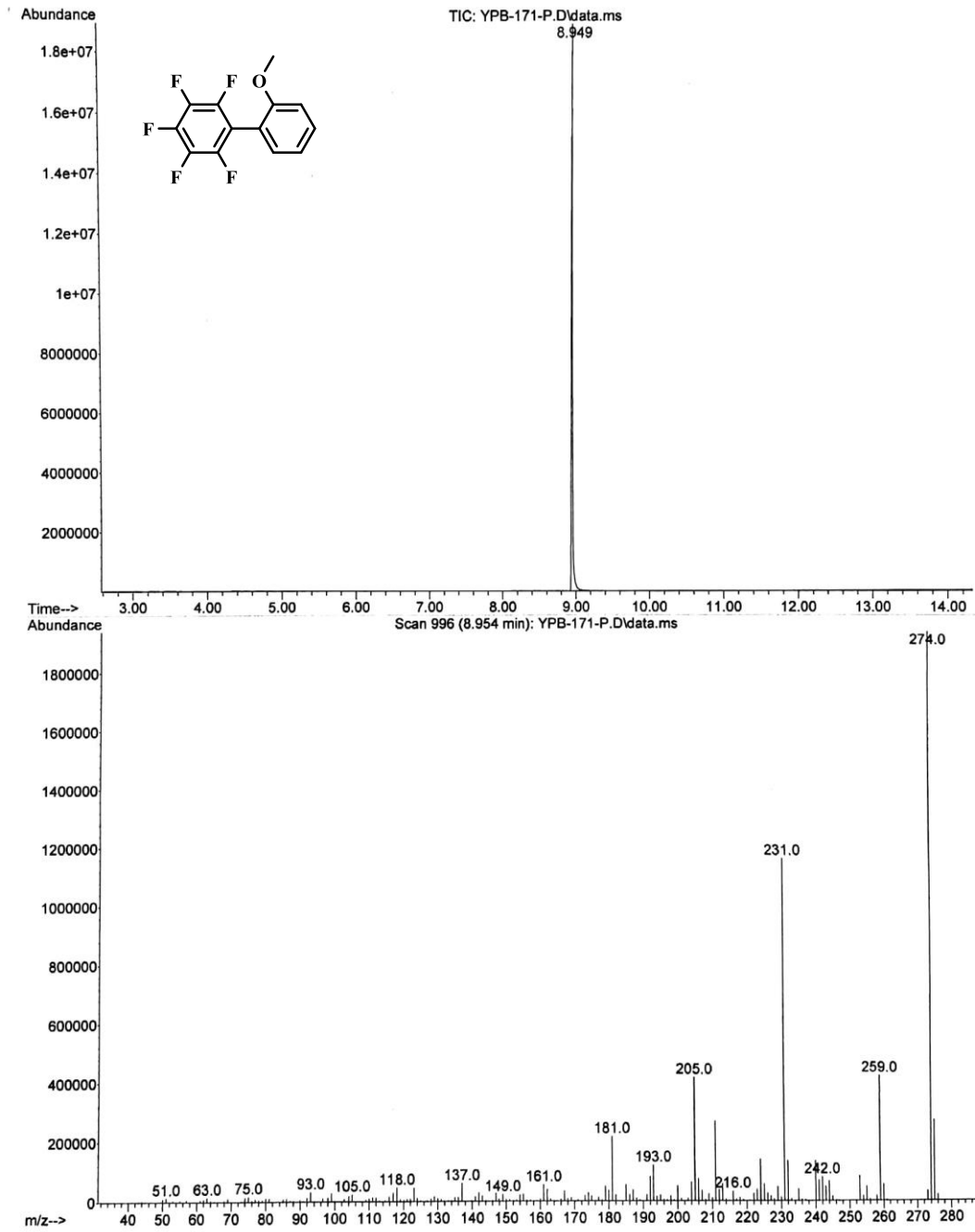
Appendix

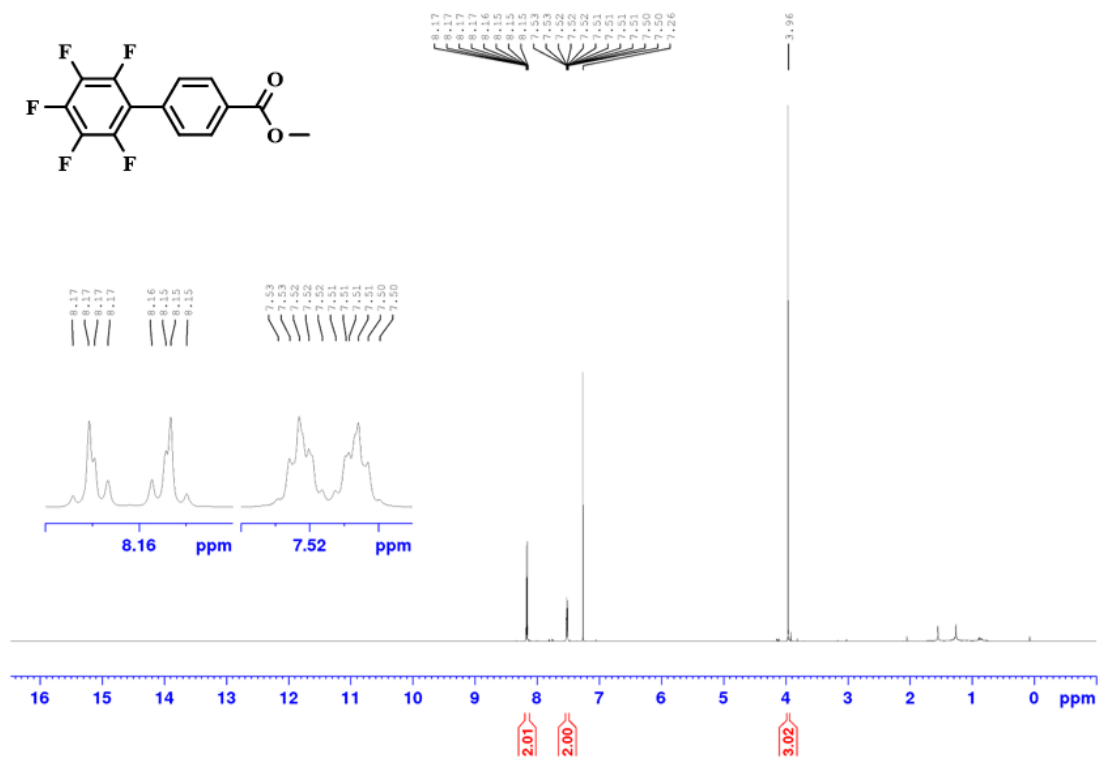
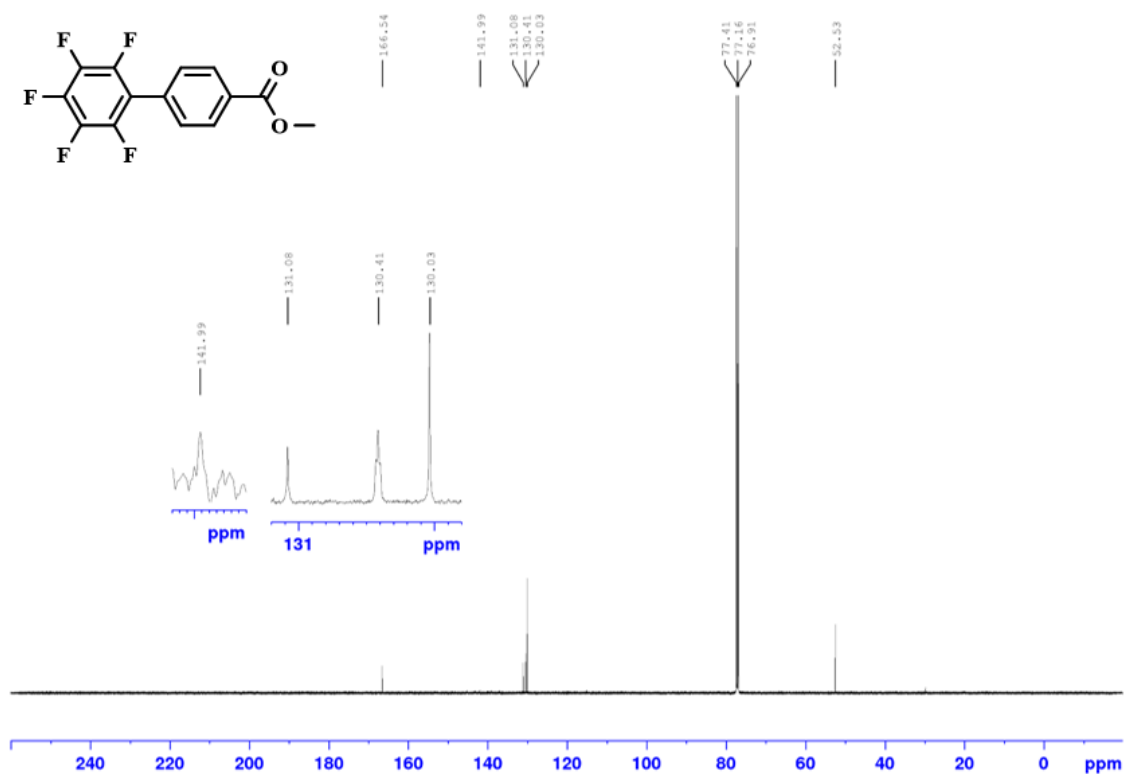


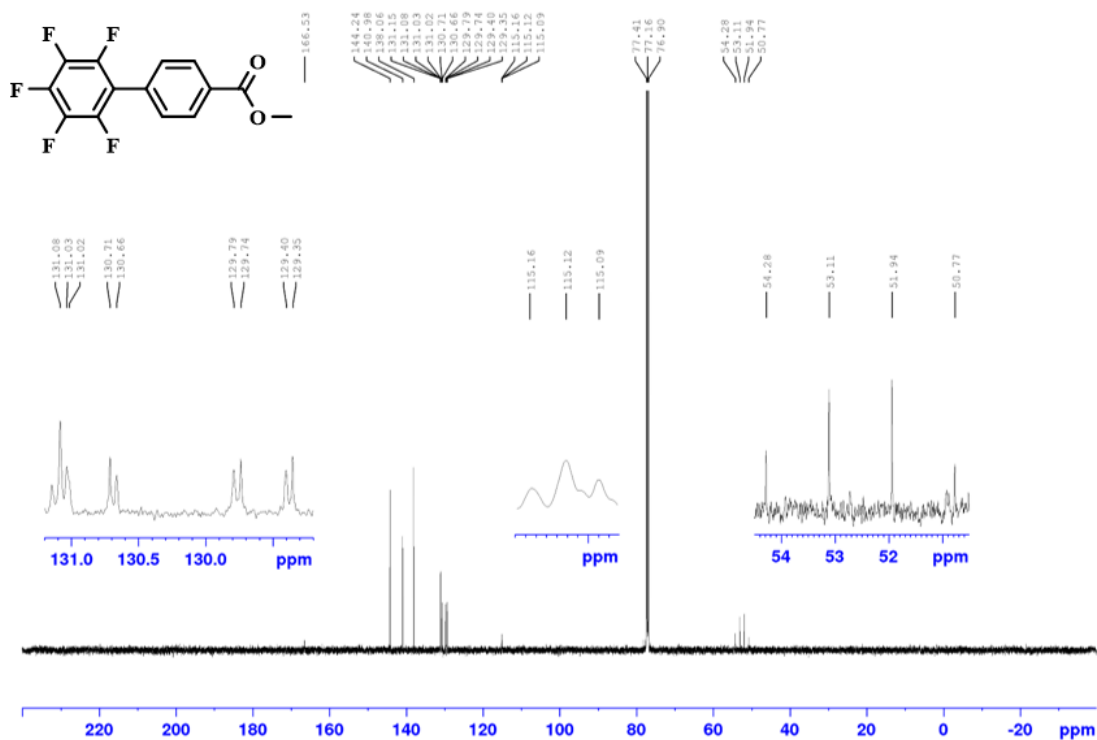
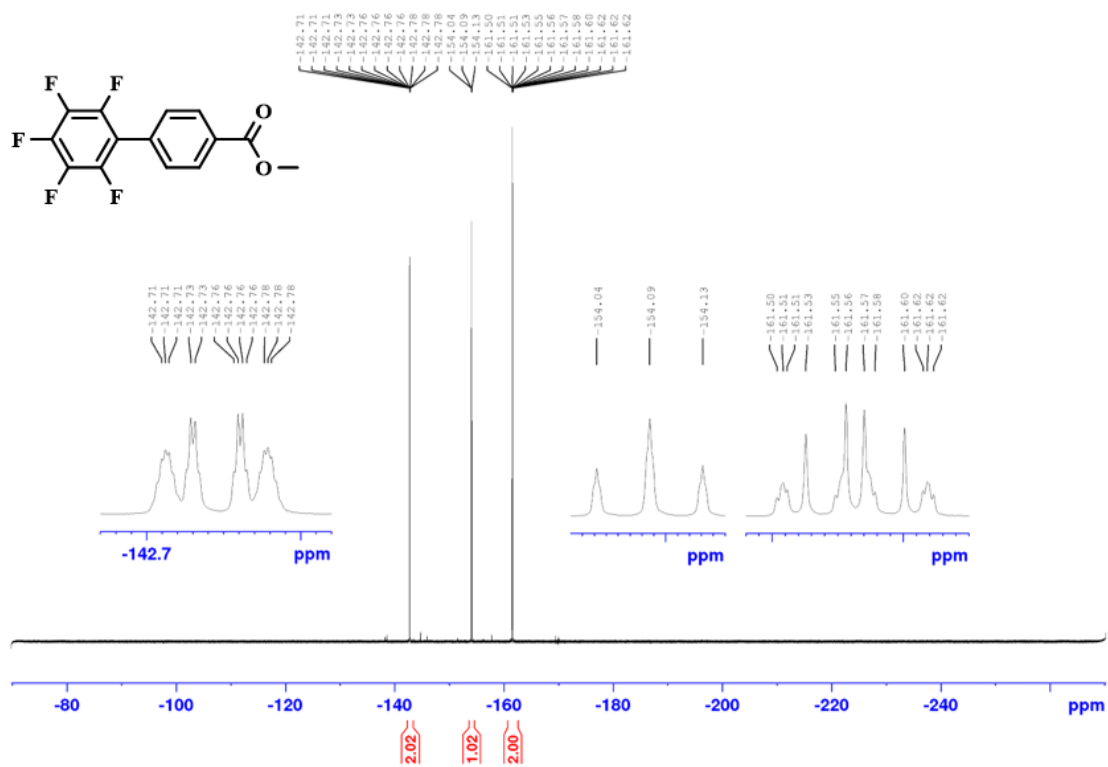
¹H NMR Spectrum of 2_3h (500 MHz, CDCl₃)



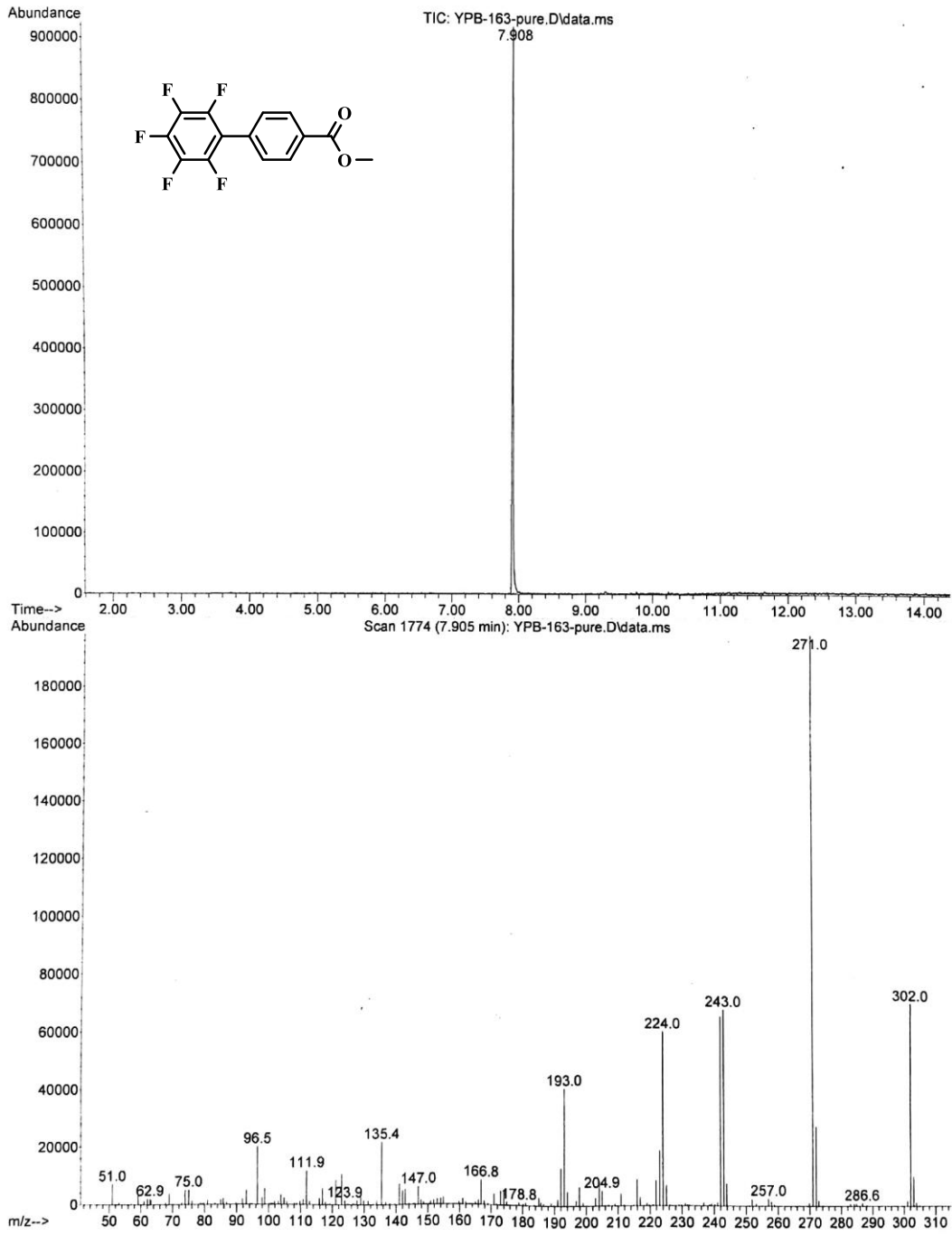
GC-MS of 2_3h

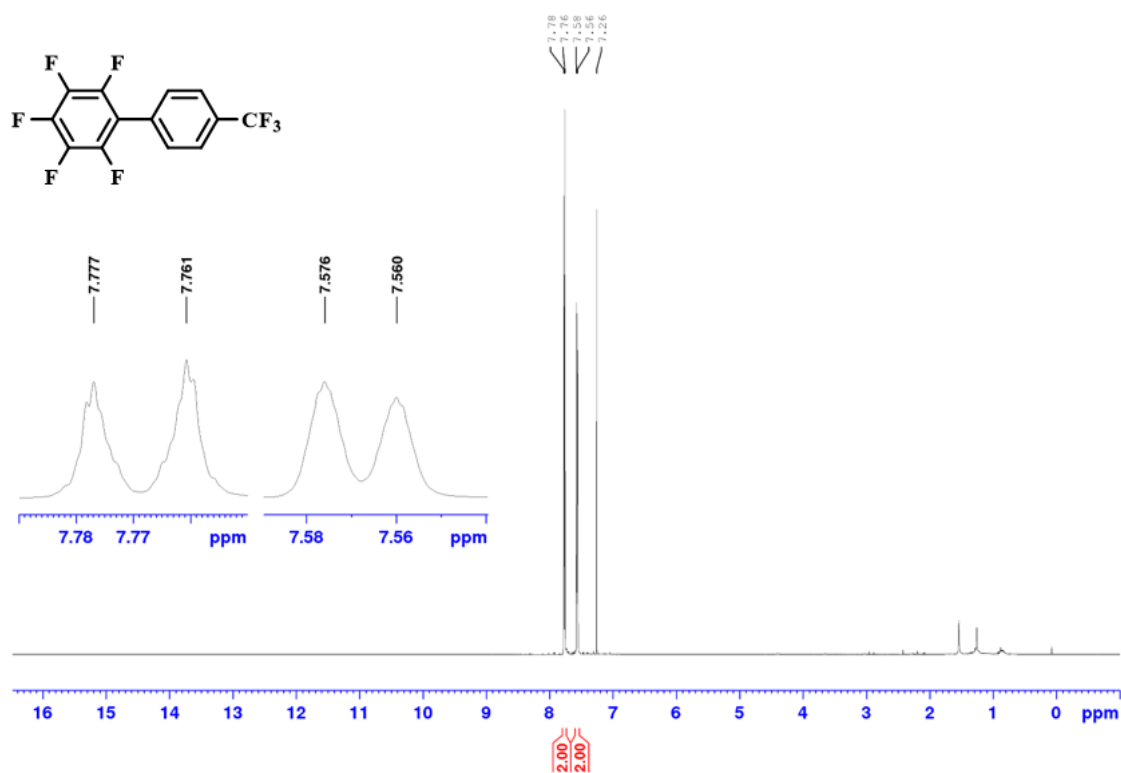
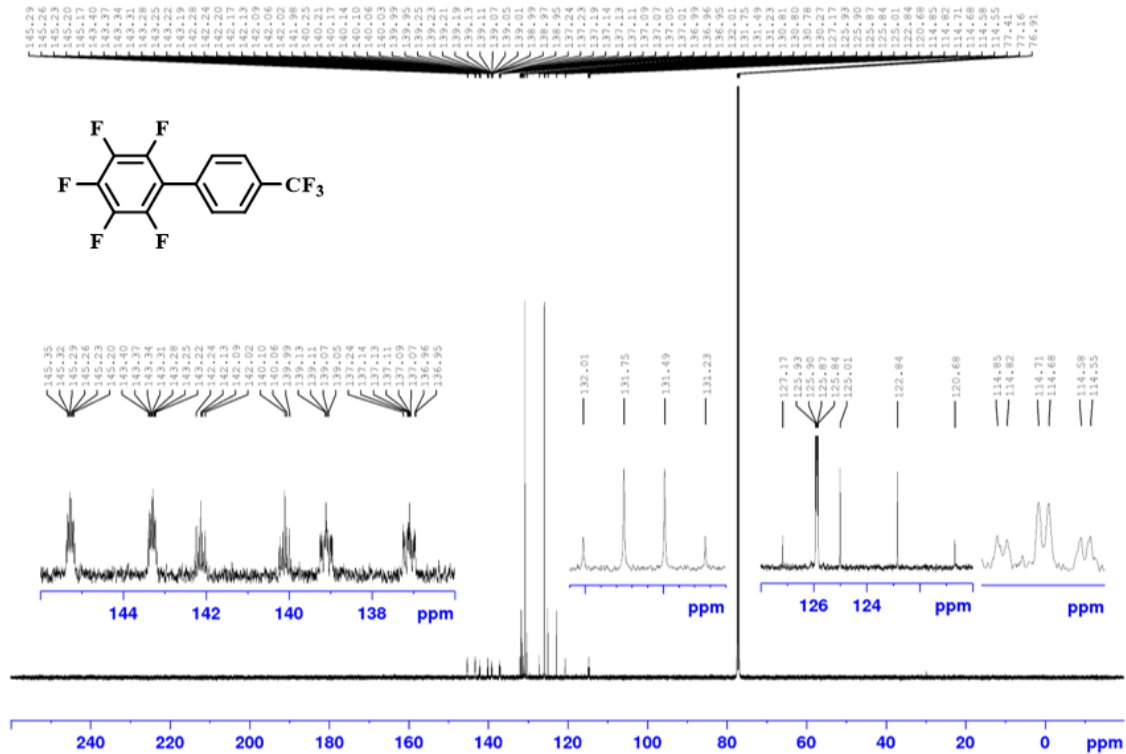


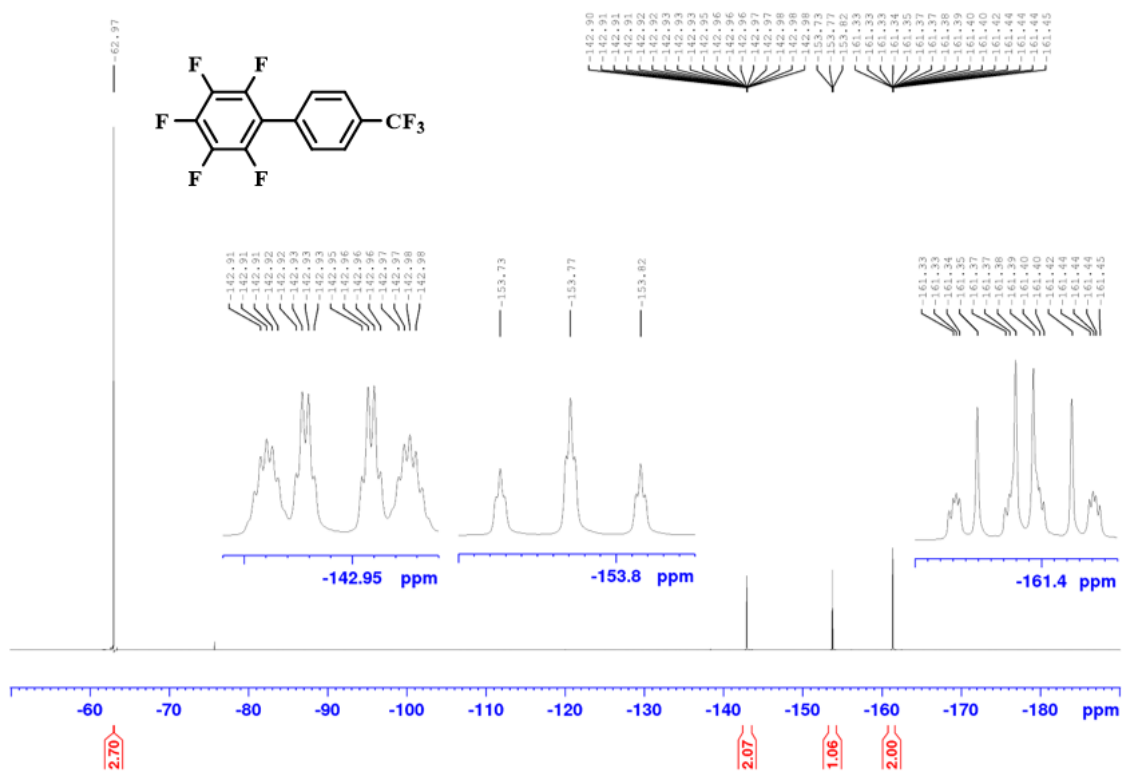
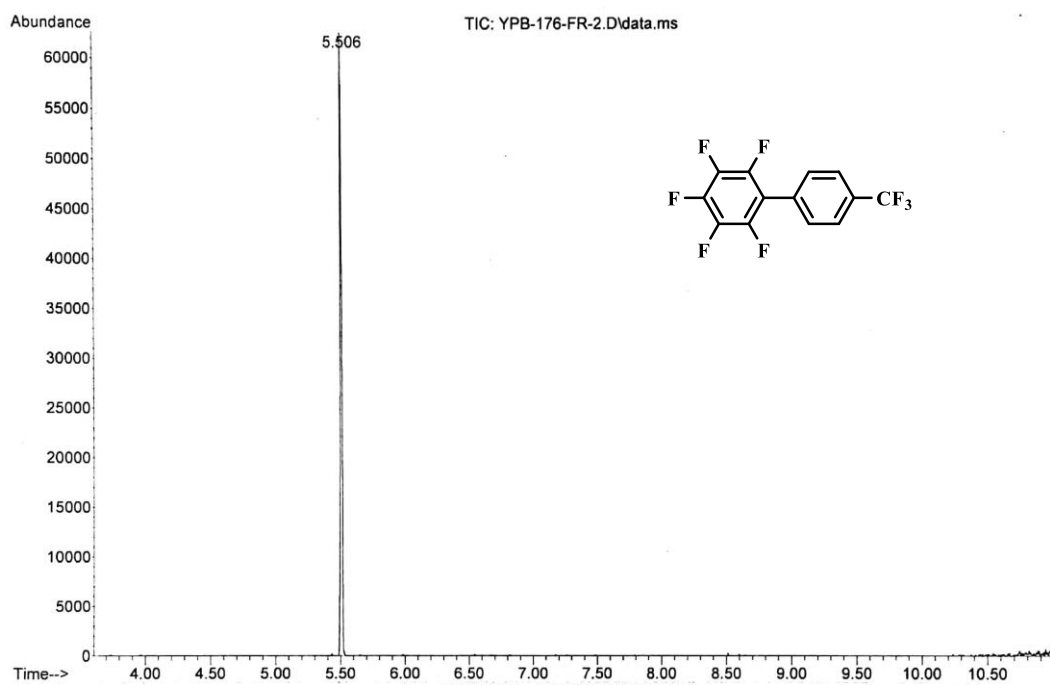
^1H NMR Spectrum of 2_3i (500 MHz, CDCl_3) $^{13}\text{C}\{^1\text{H}\}$ NMR Spectrum of 2_3i (126 MHz, CDCl_3)

$^{13}\text{C}\{^{19}\text{F}\}$ NMR Spectrum of 2_3i (126 MHz, CDCl_3 , (for C_6F_5)) ^{19}F NMR Spectrum of 2_3i (470 MHz, CDCl_3)

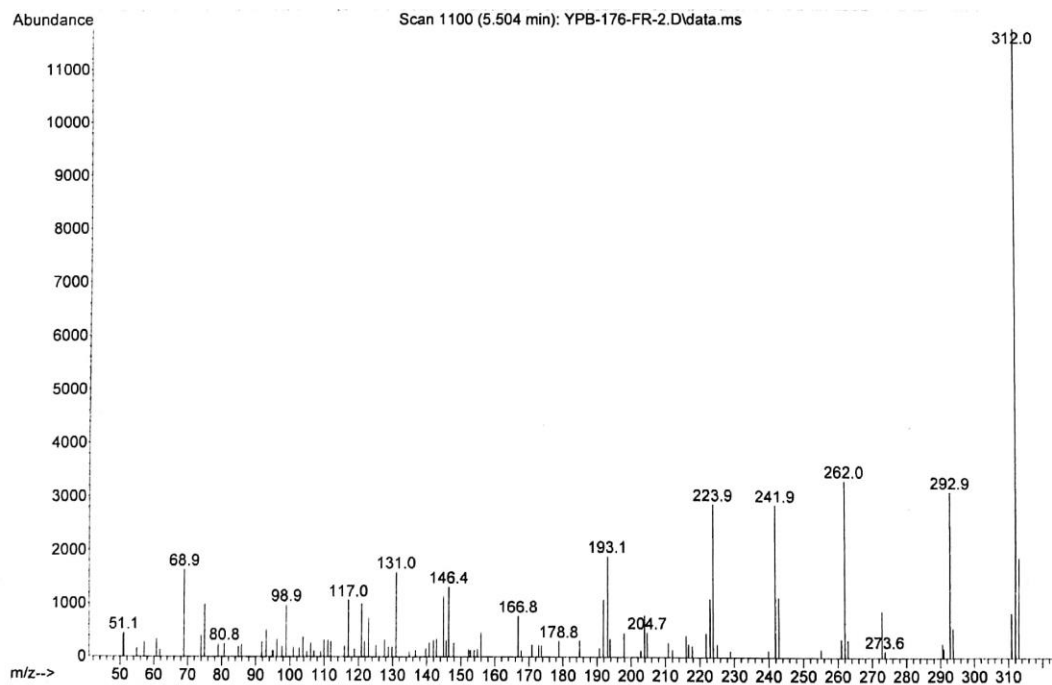
GC-MS of 2_3i



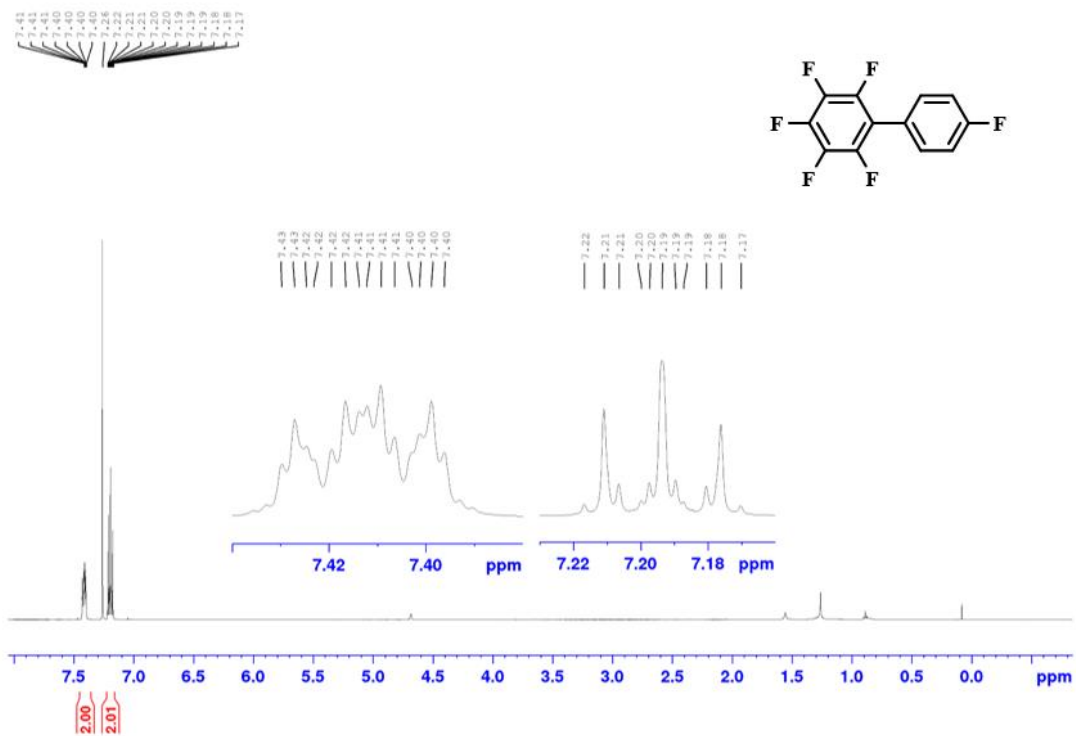
¹H NMR Spectrum of 2_3j (500 MHz, CDCl₃)**¹³C{¹H} NMR Spectrum of 2_3j (126 MHz, CDCl₃)**

^{19}F NMR Spectrum of 2_3j (470 MHz, CDCl_3)**GC-MS of 2_3j**

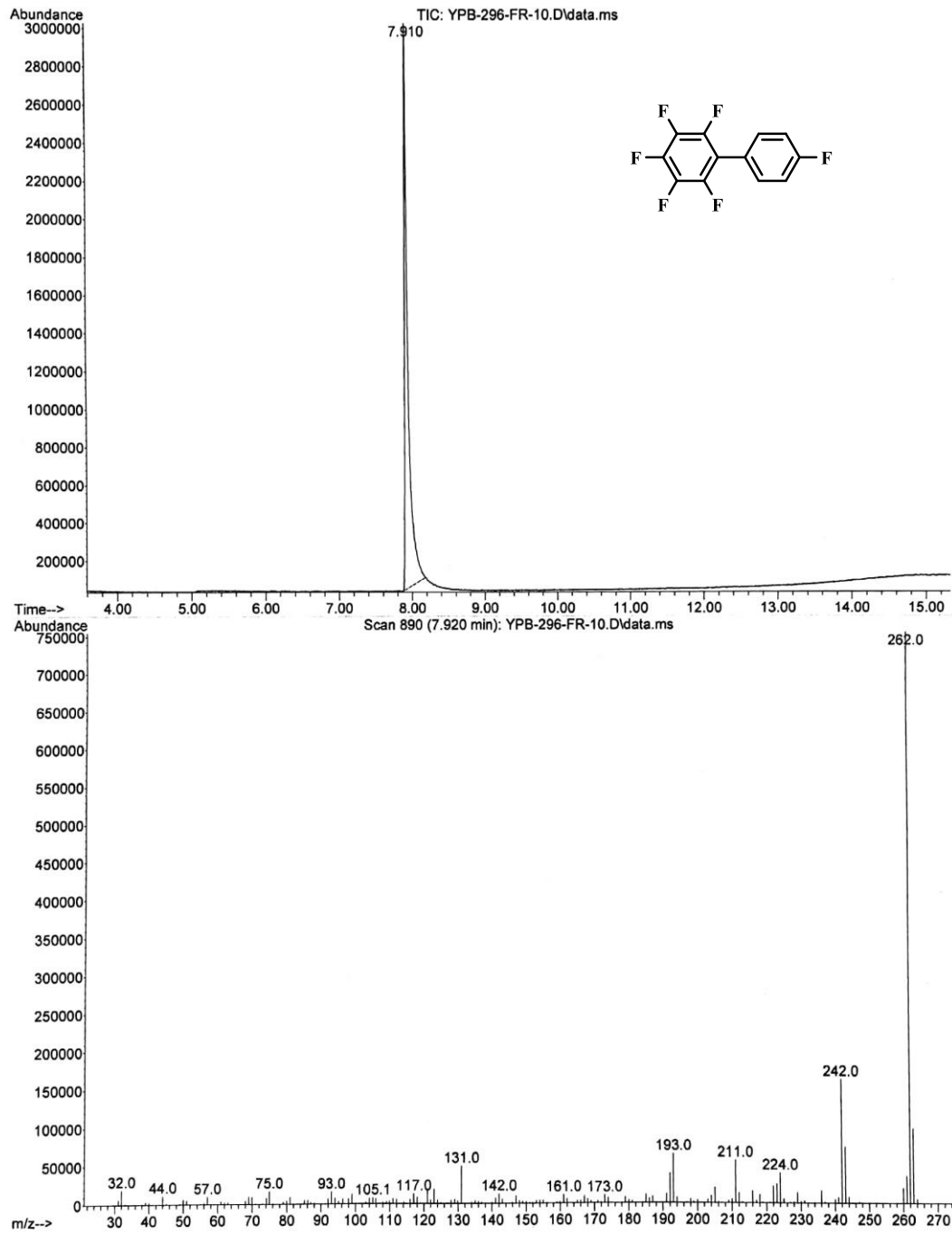
Appendix

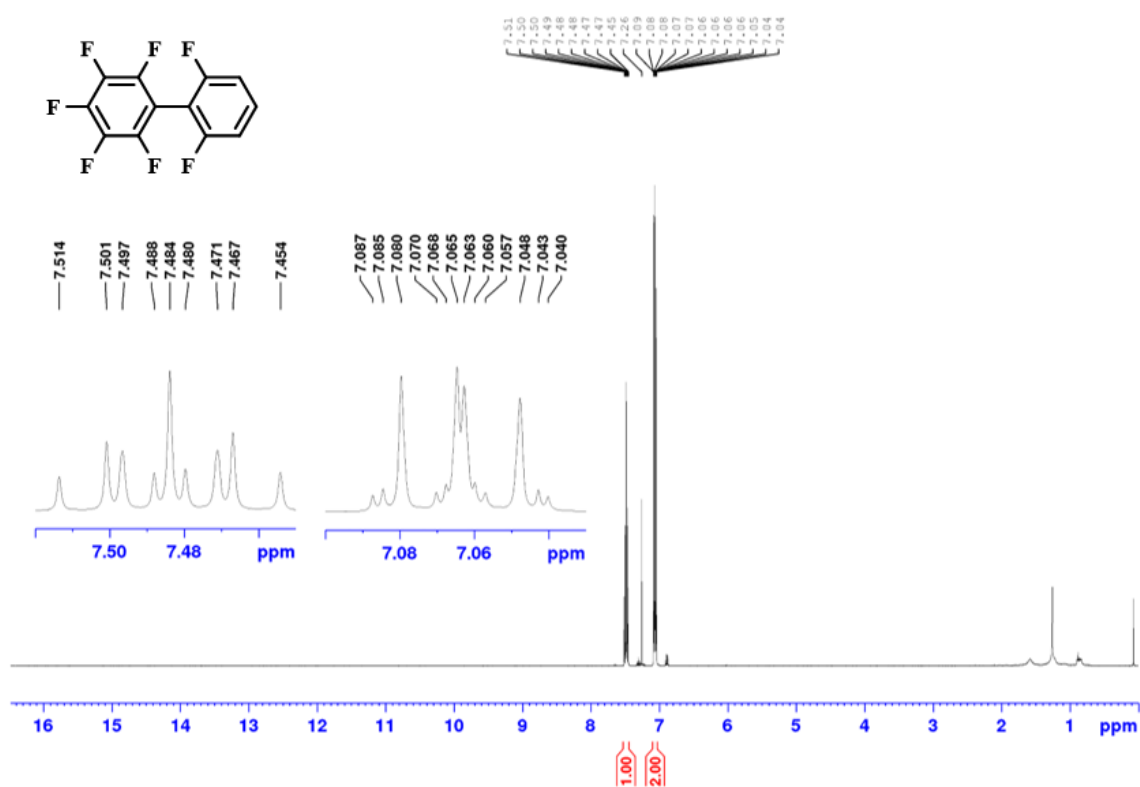
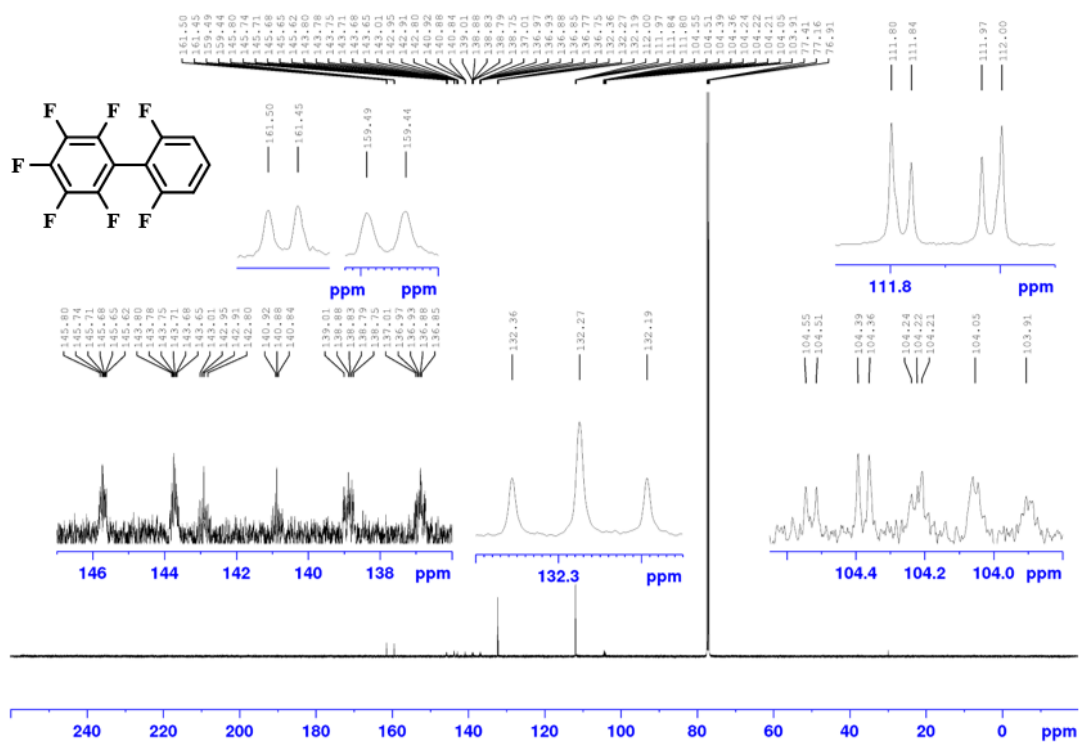


¹H NMR Spectrum of 2_3k (500 MHz, CDCl₃)

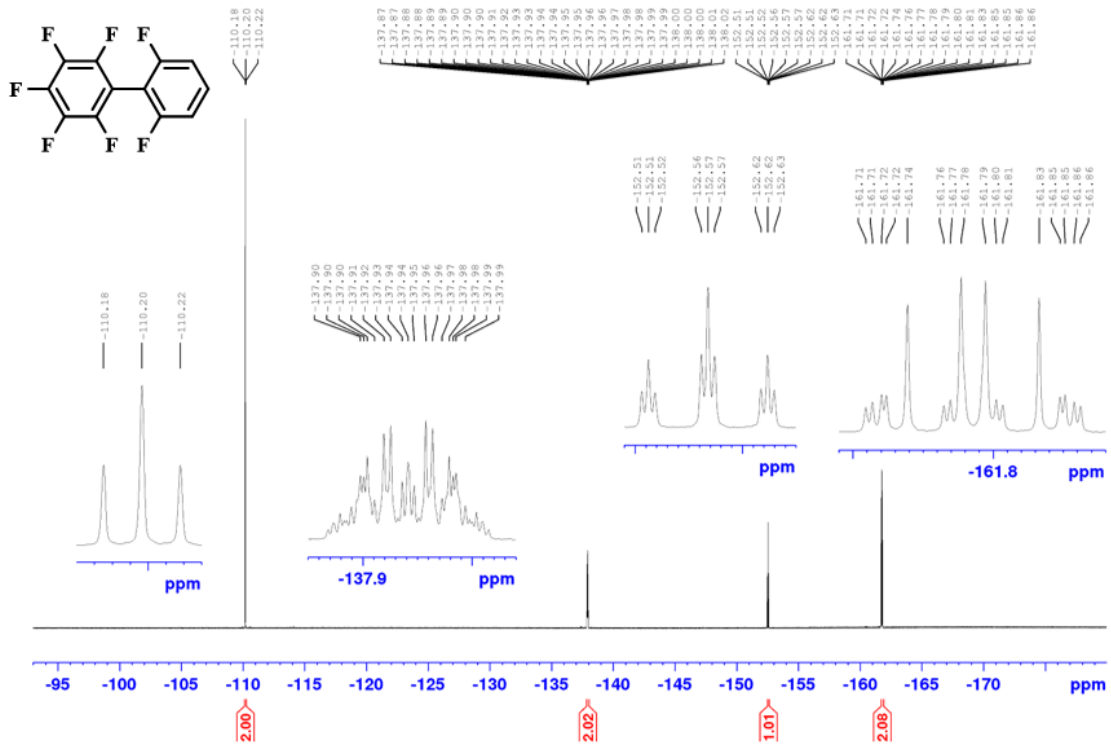


GC-MS of 2_3k

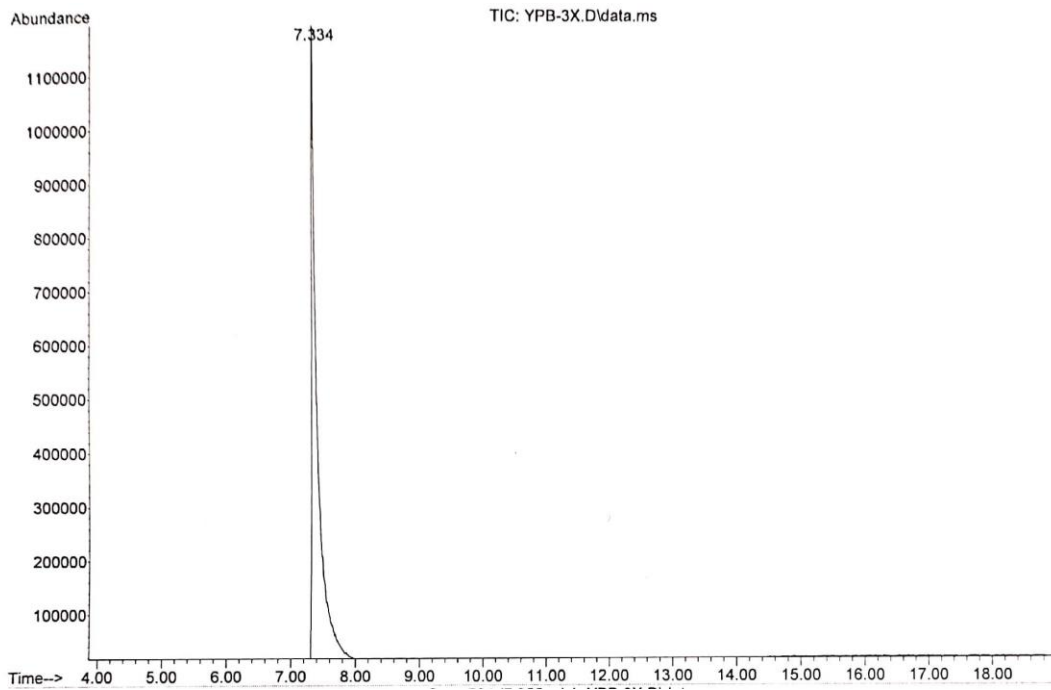


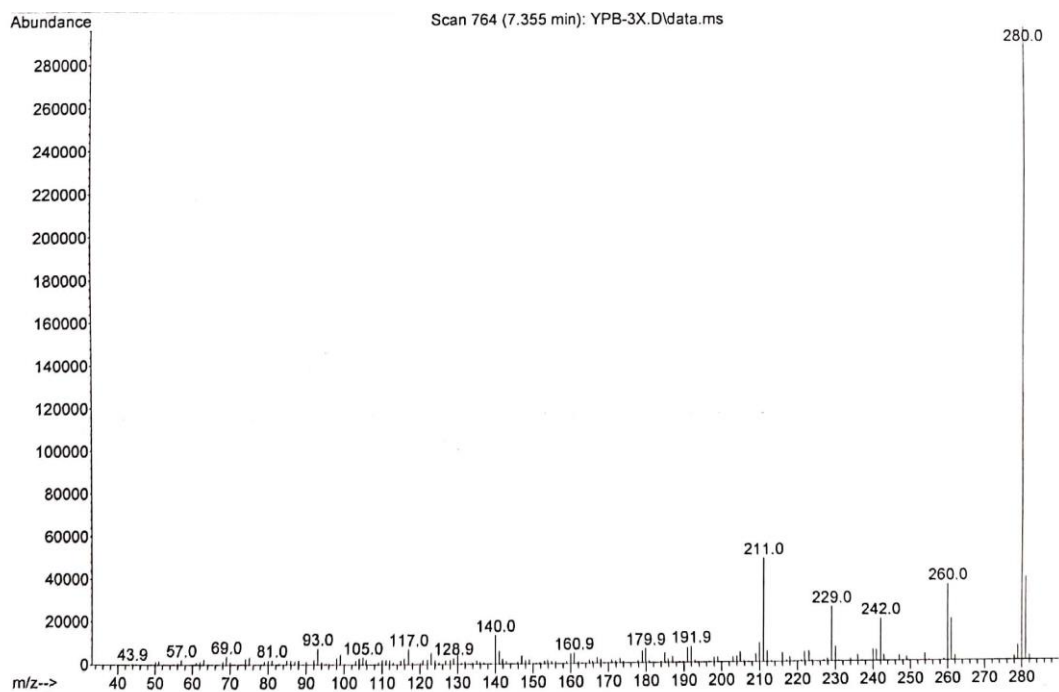
^1H NMR Spectrum of 2_3I (500 MHz, CDCl_3) $^{13}\text{C}\{^1\text{H}\}$ NMR Spectrum of 2_3I (126 MHz, CDCl_3)

$^{19}\text{F}\{^1\text{H}\}$ NMR Spectrum of 2_31 (376 MHz, CDCl_3)

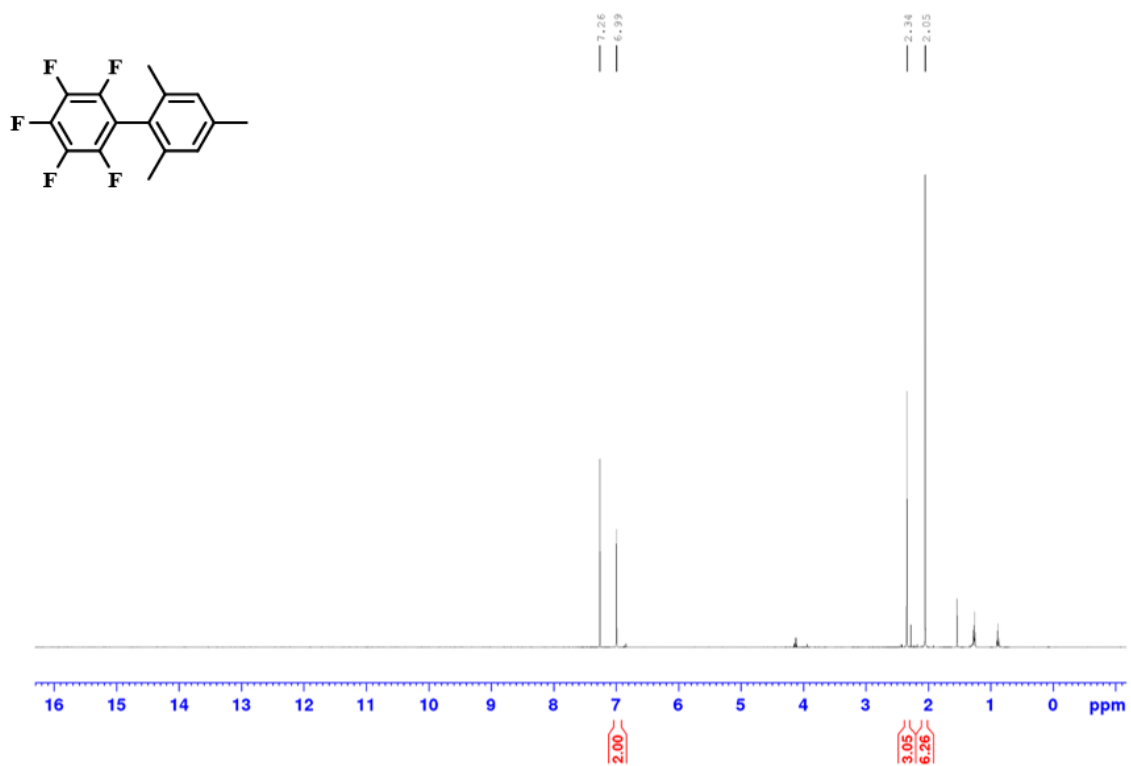


GC-MS of 2_31

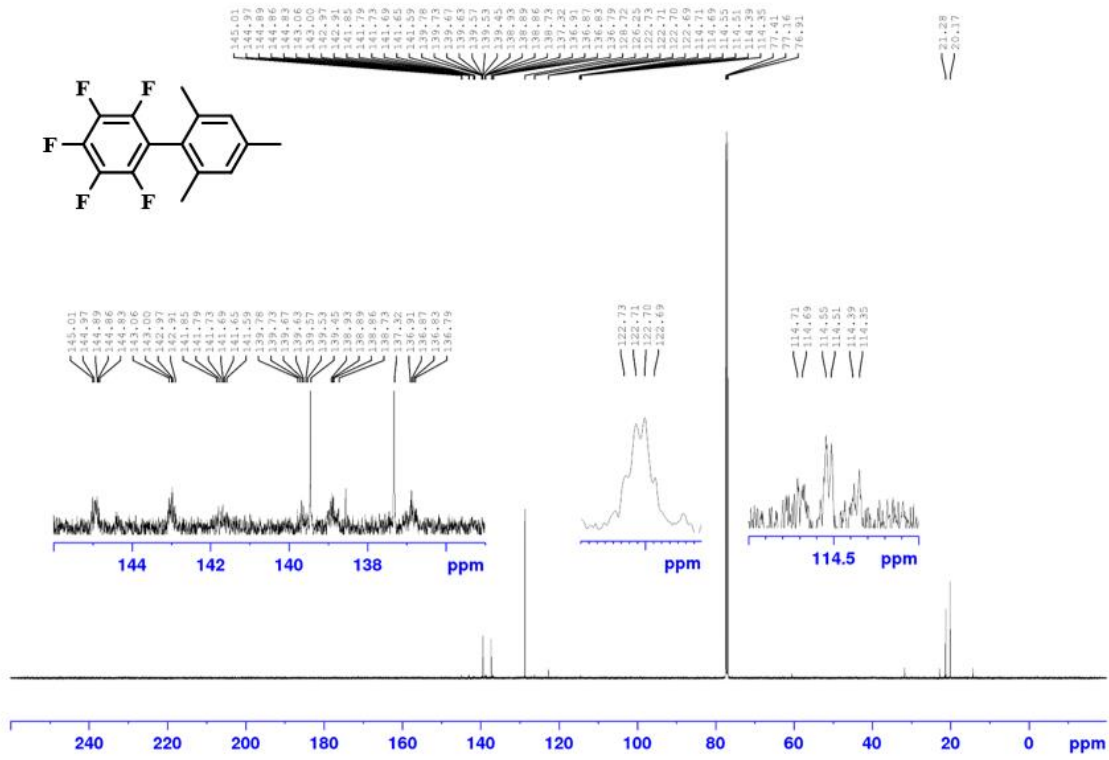




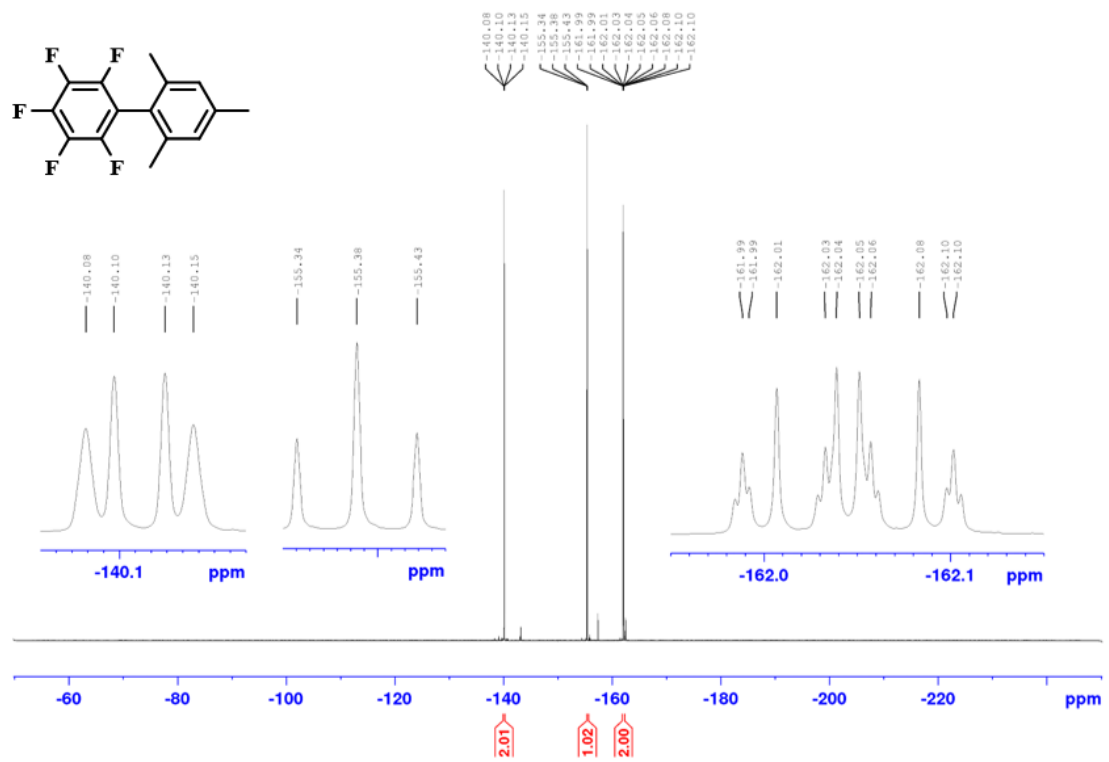
^1H NMR Spectrum of 2_3m (500 MHz, CDCl_3)



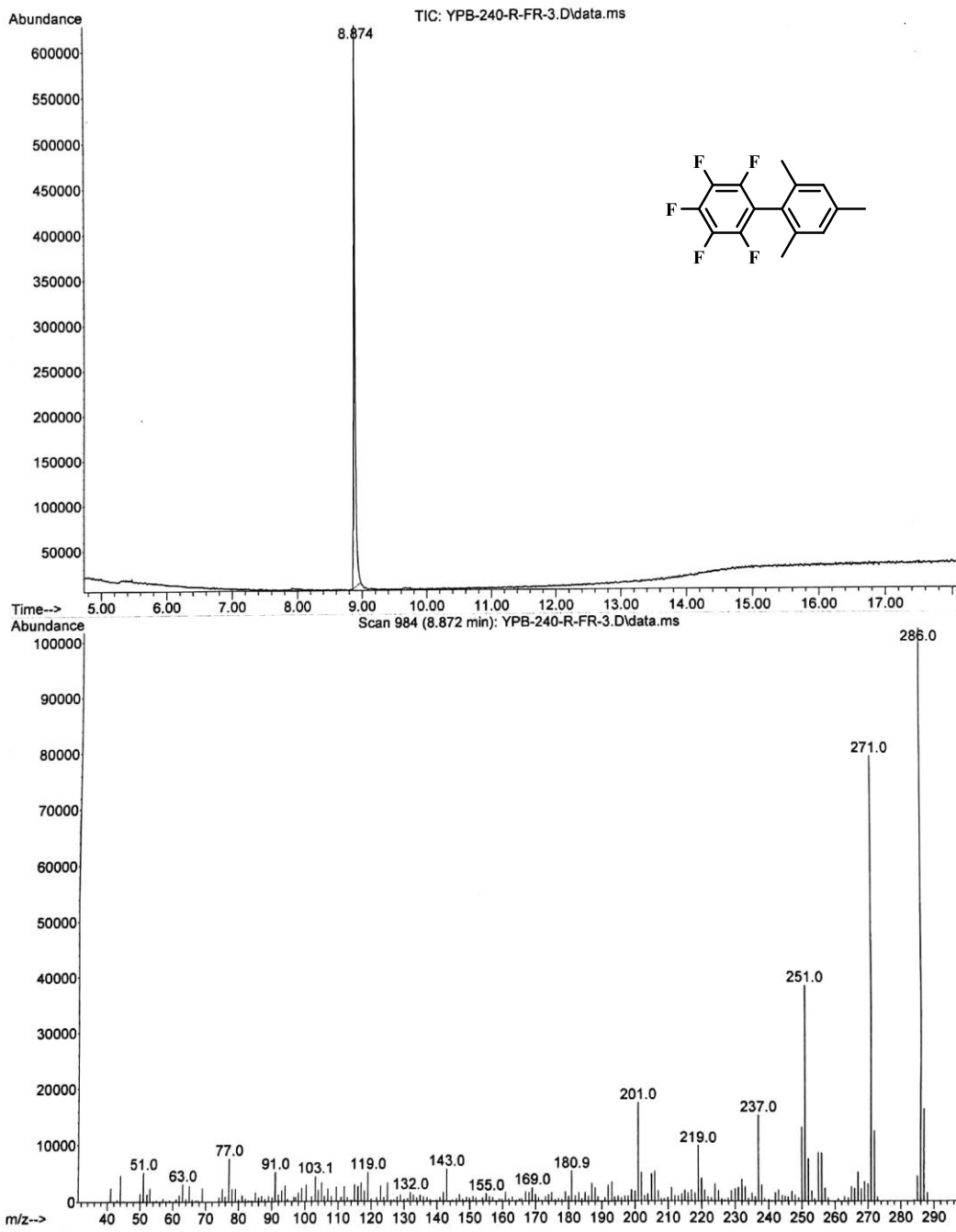
$^{13}\text{C}\{^1\text{H}\}$ NMR Spectrum of 2_3m (126 MHz, CDCl_3)

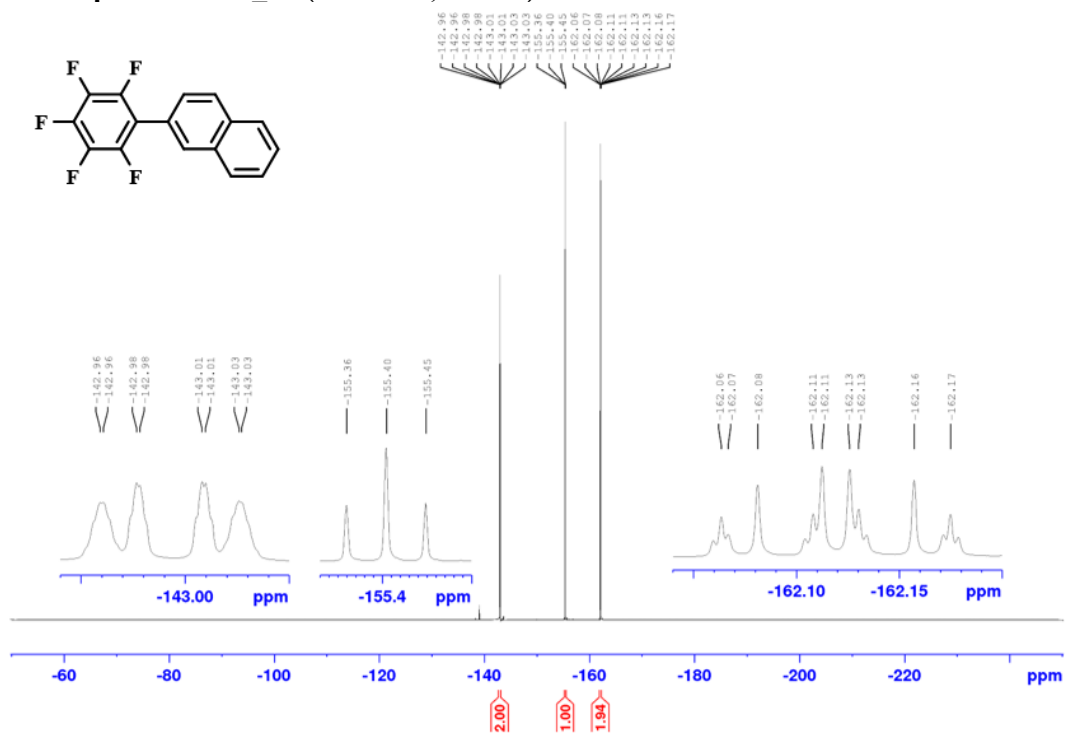
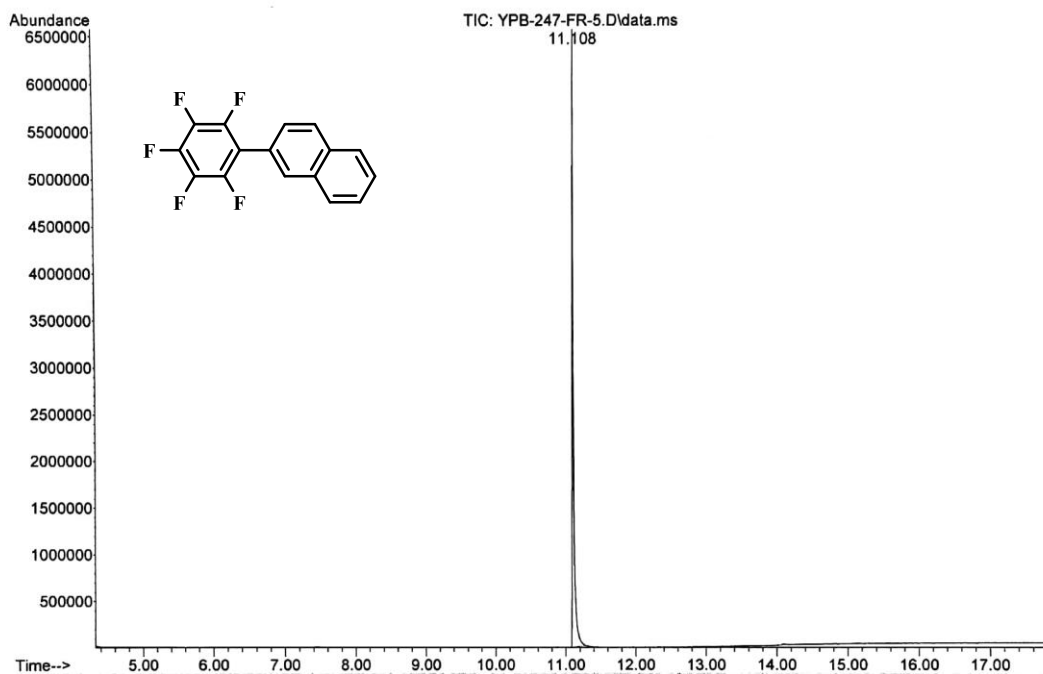


^{19}F NMR Spectrum of 2_3m (470 MHz, CDCl_3)

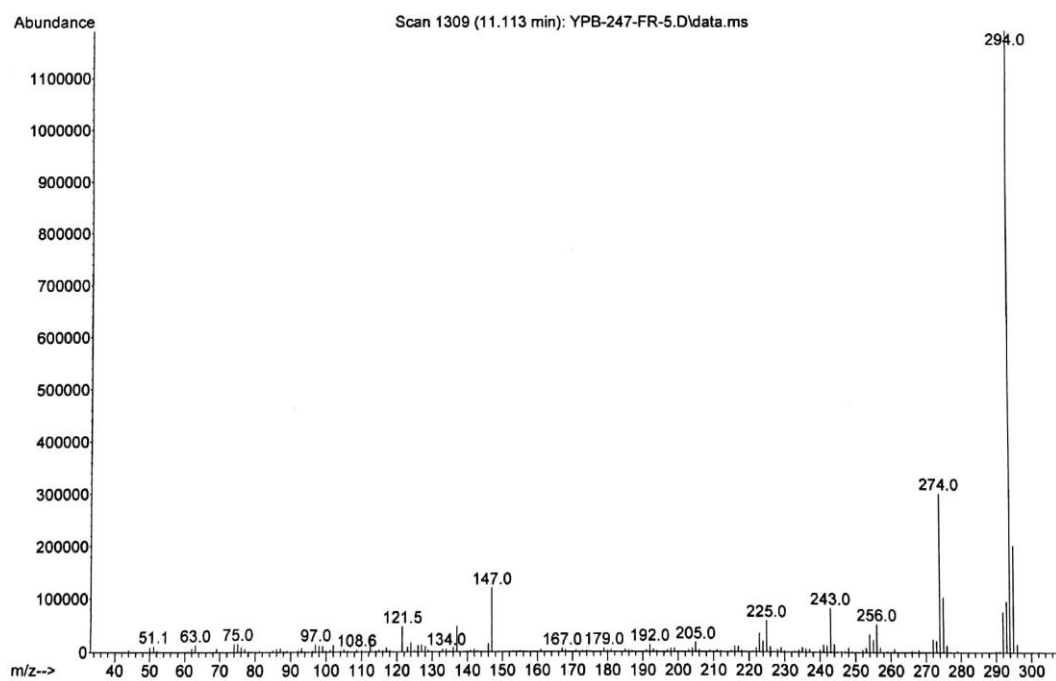


GC-MS of 2_3m

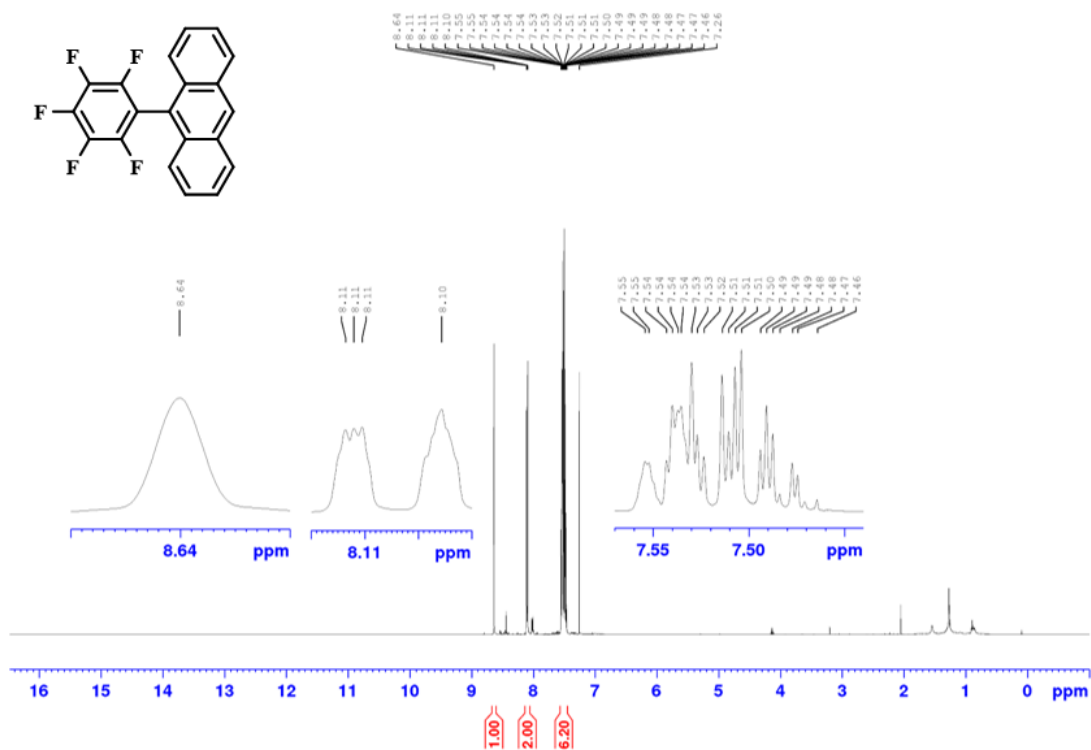


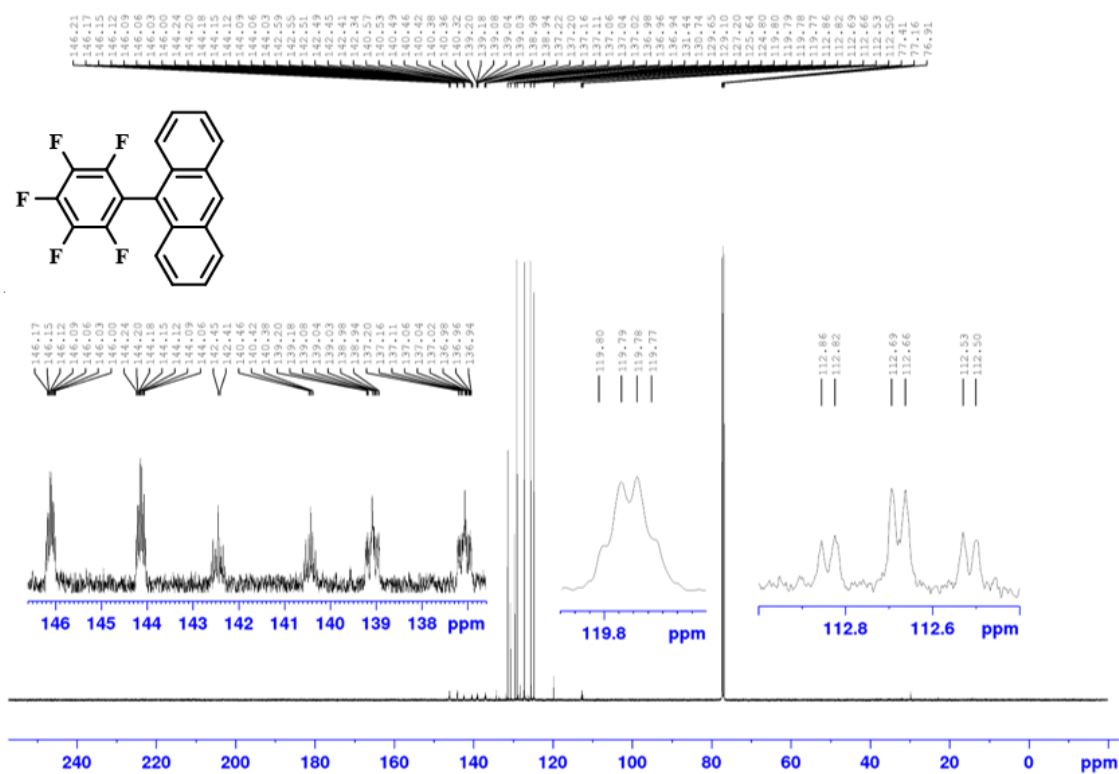
^{19}F NMR Spectrum of 2_3n (470 MHz, CDCl_3)**GC-MS of 2_3n**

Appendix

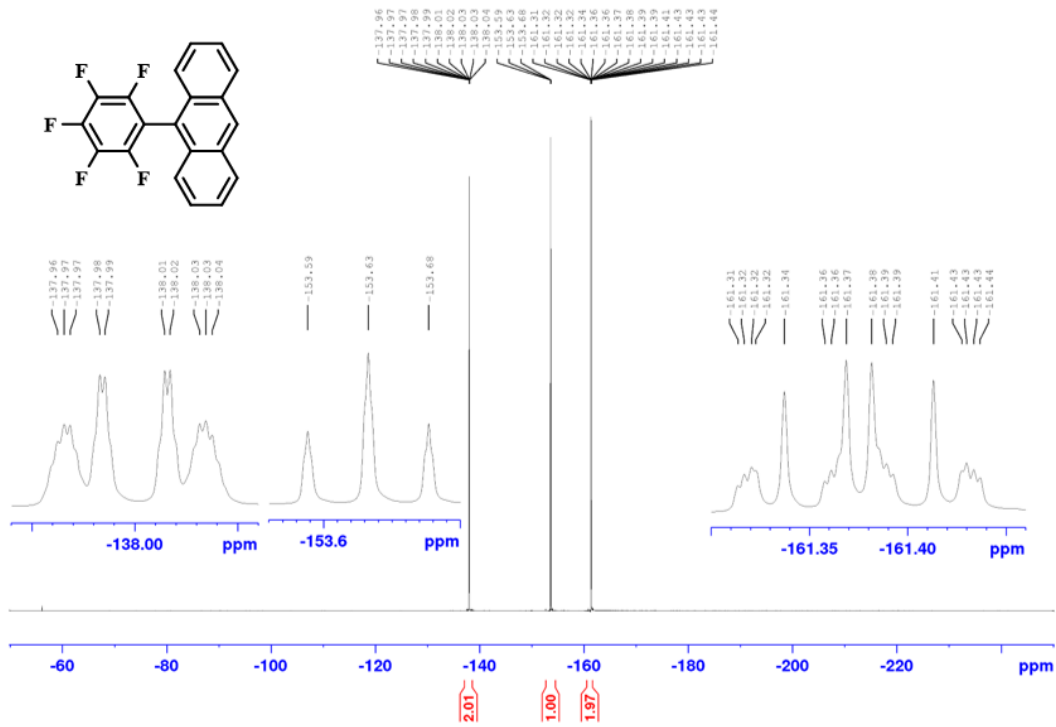


¹H NMR Spectrum of 2_3o (500 MHz, CDCl₃)

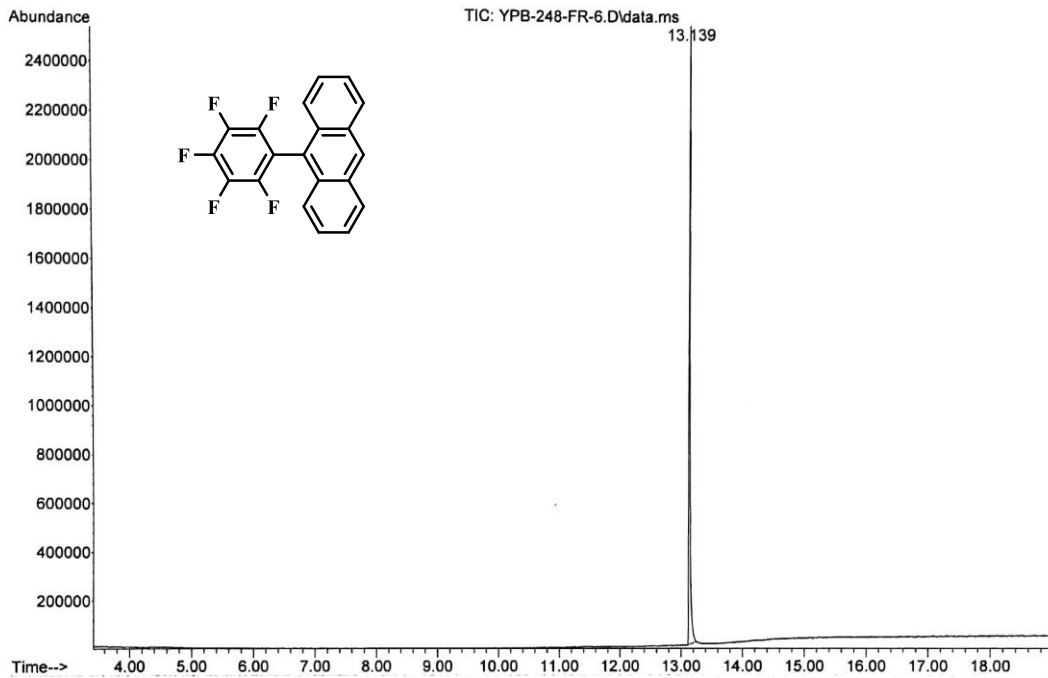


$^{13}\text{C}\{^1\text{H}\}$ NMR Spectrum of 2_3o (126 MHz, CDCl_3)

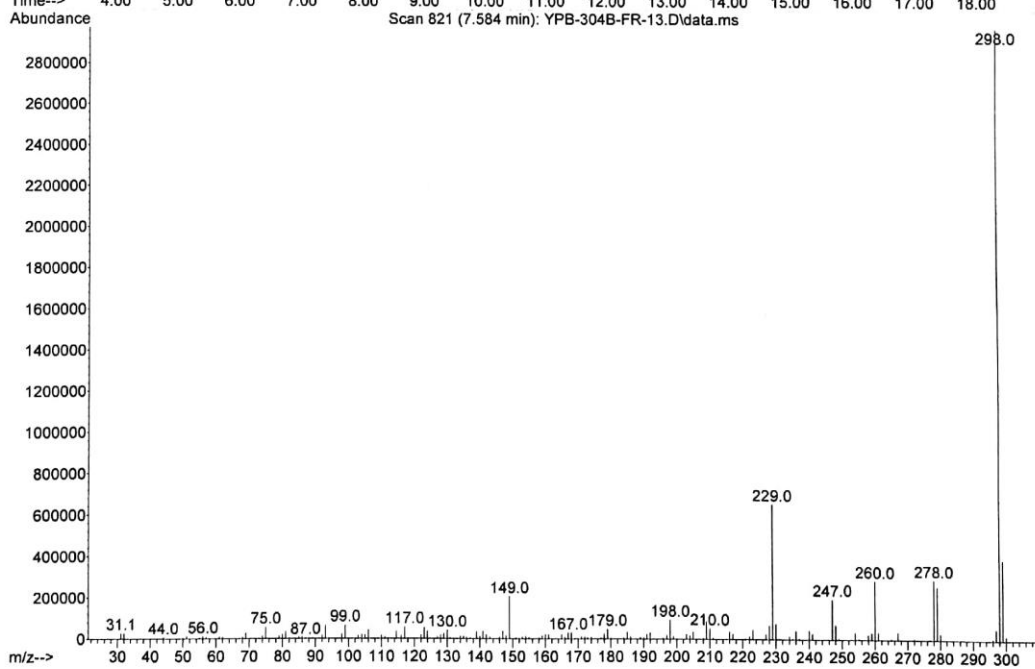
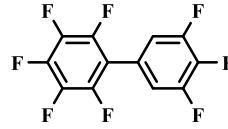
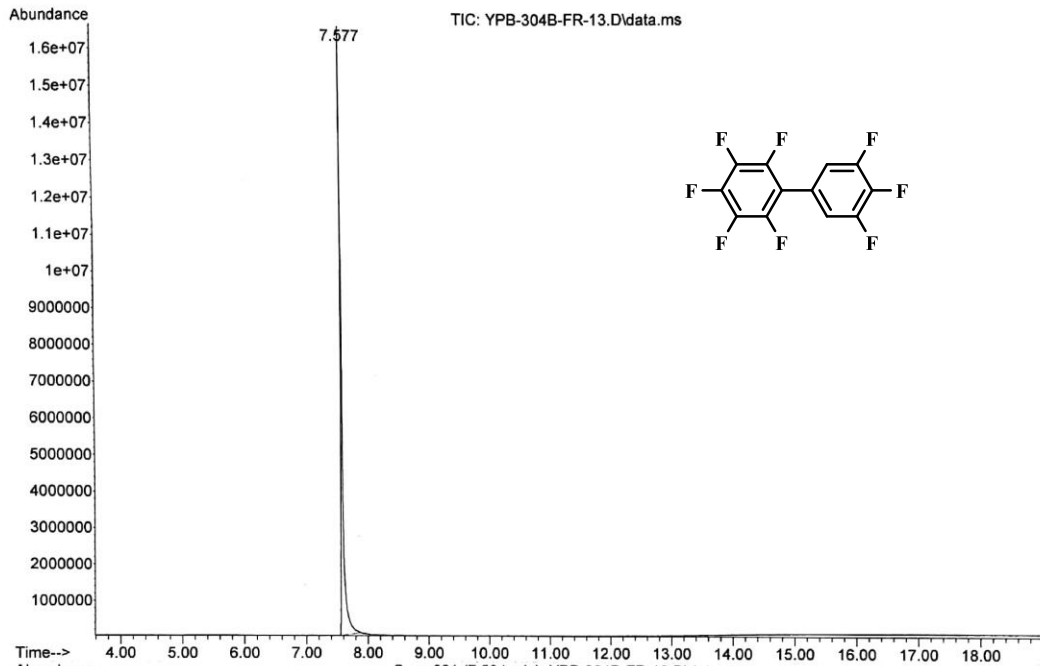
¹⁹F NMR Spectrum of 2_3o (470 MHz, CDCl₃)

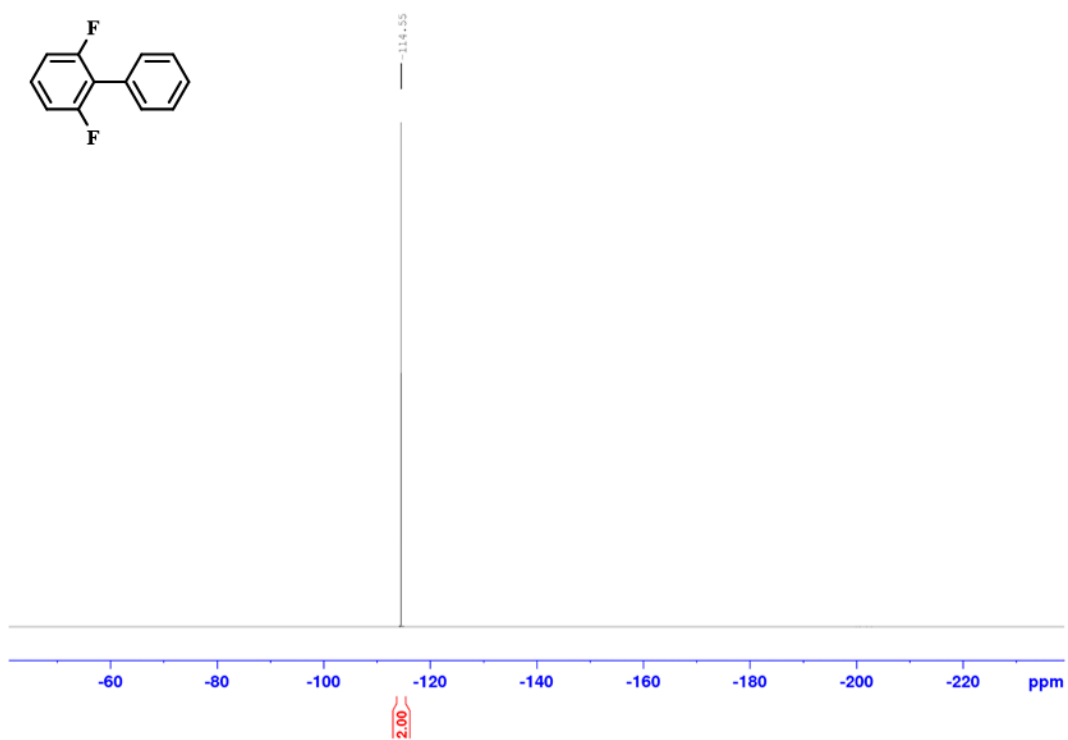


GC-MS of 2_3o

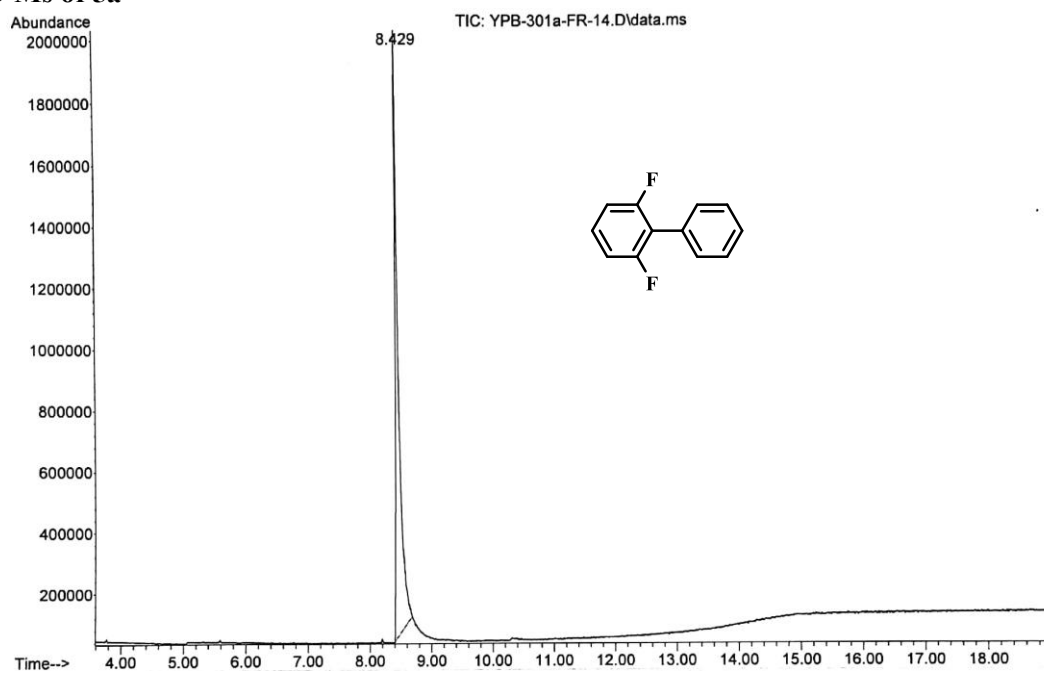


GC-MS of 2_3p

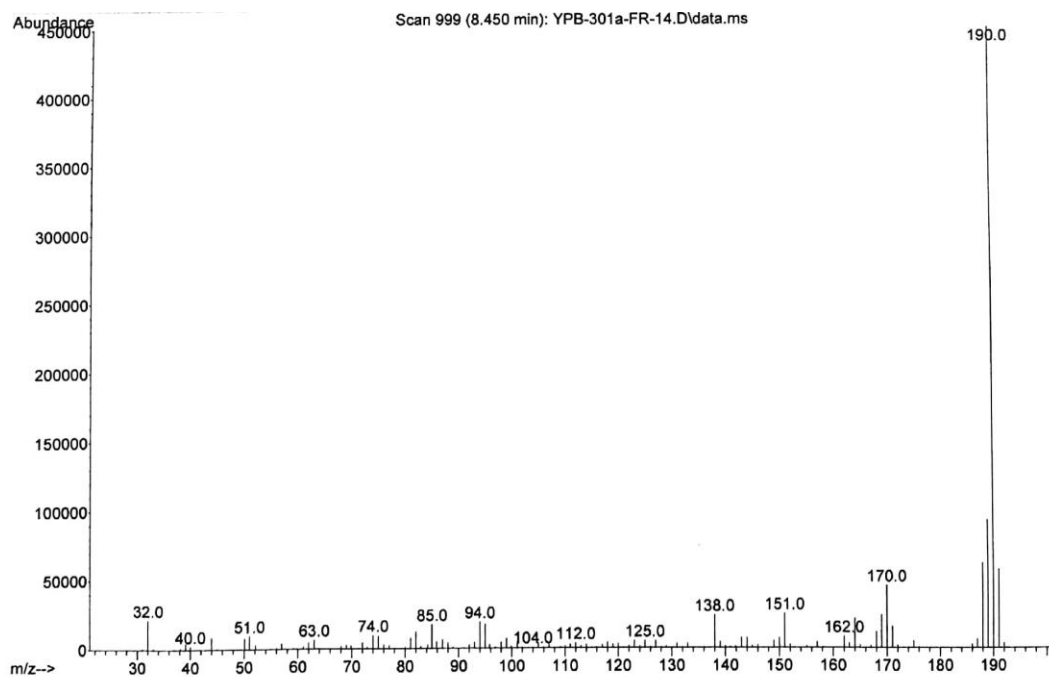


$^{19}\text{F}\{^1\text{H}\}$ NMR Spectrum of 2_5a (376 MHz, CDCl_3)

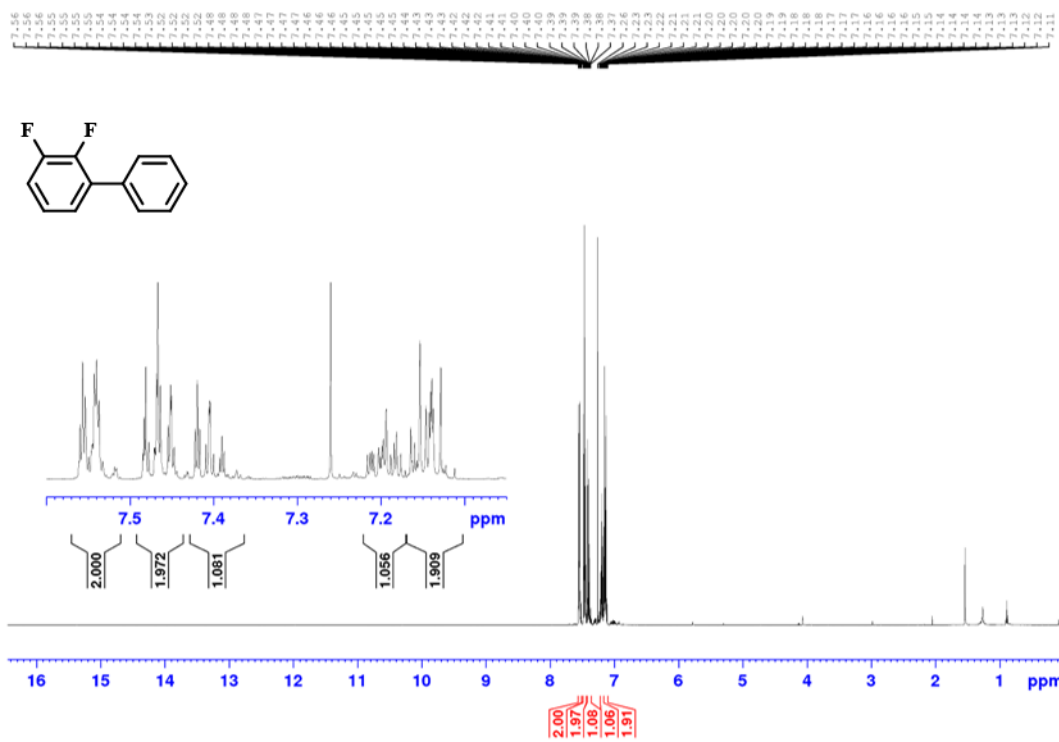
GC-MS of 5a

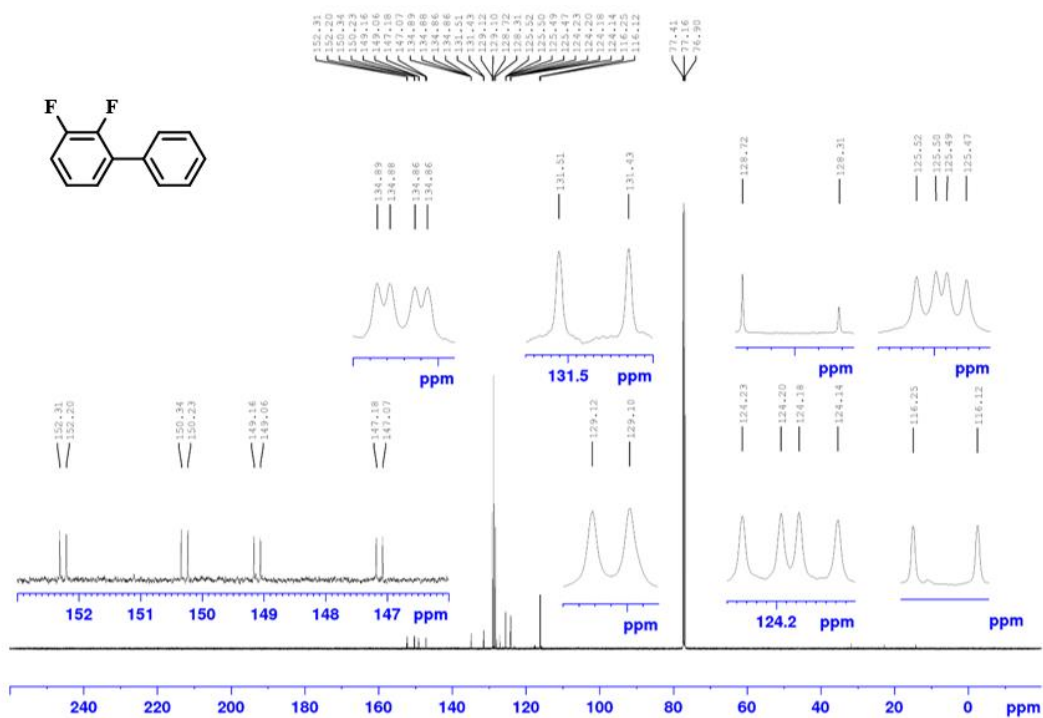
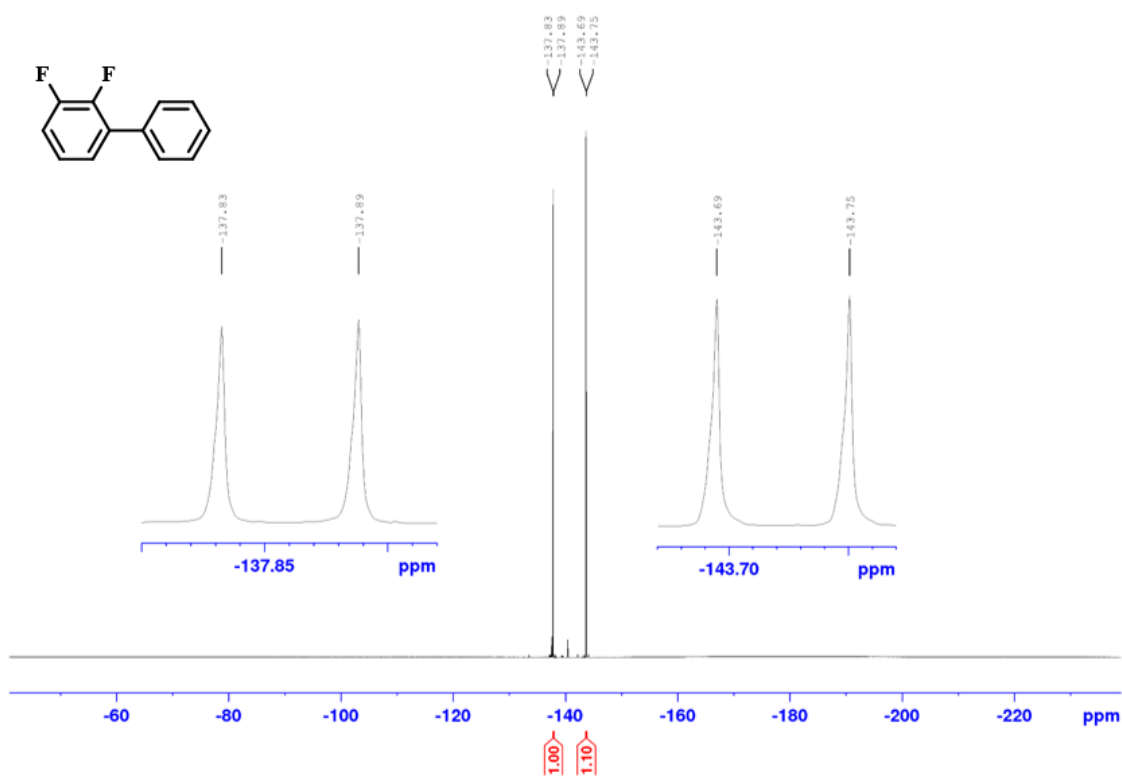


Appendix

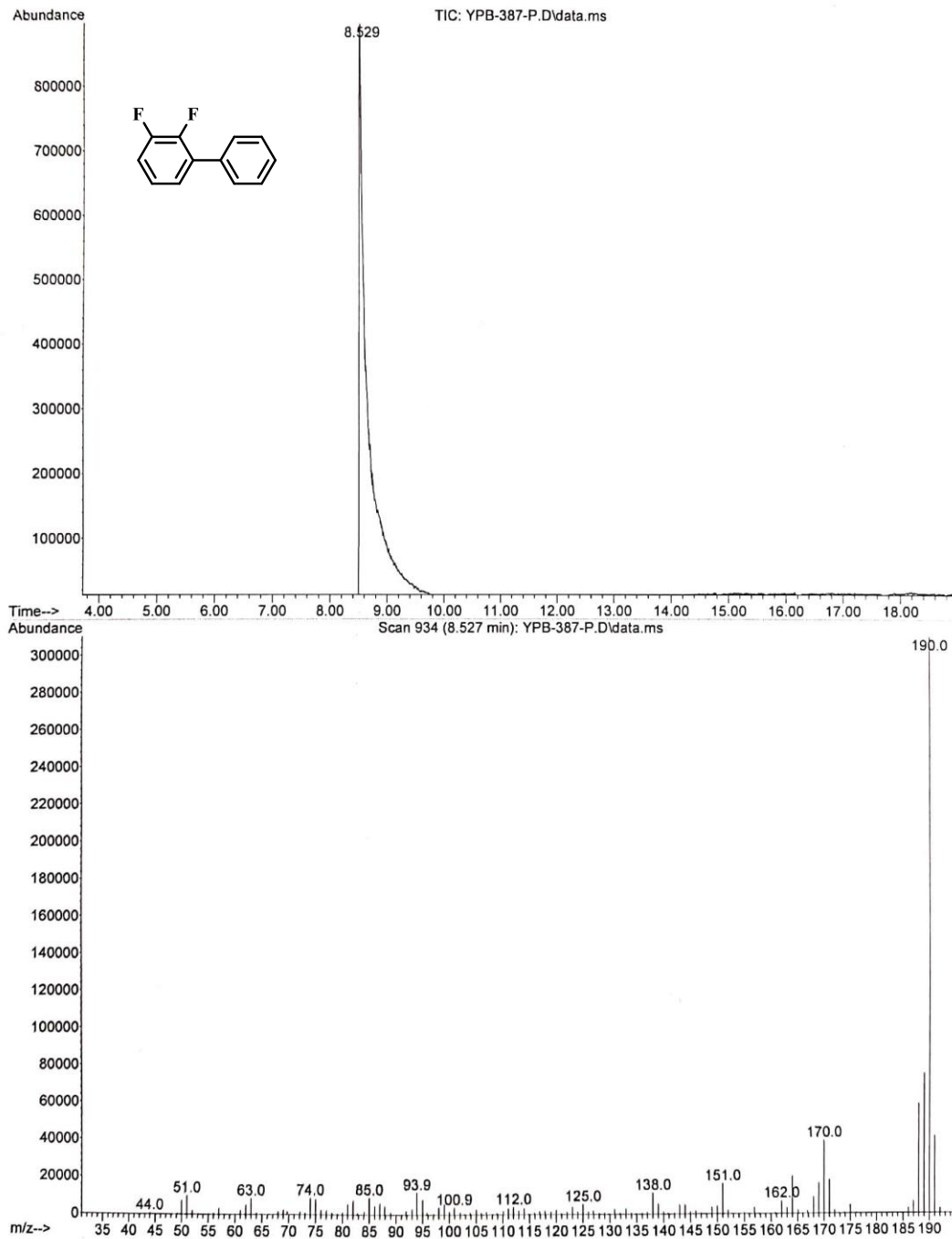


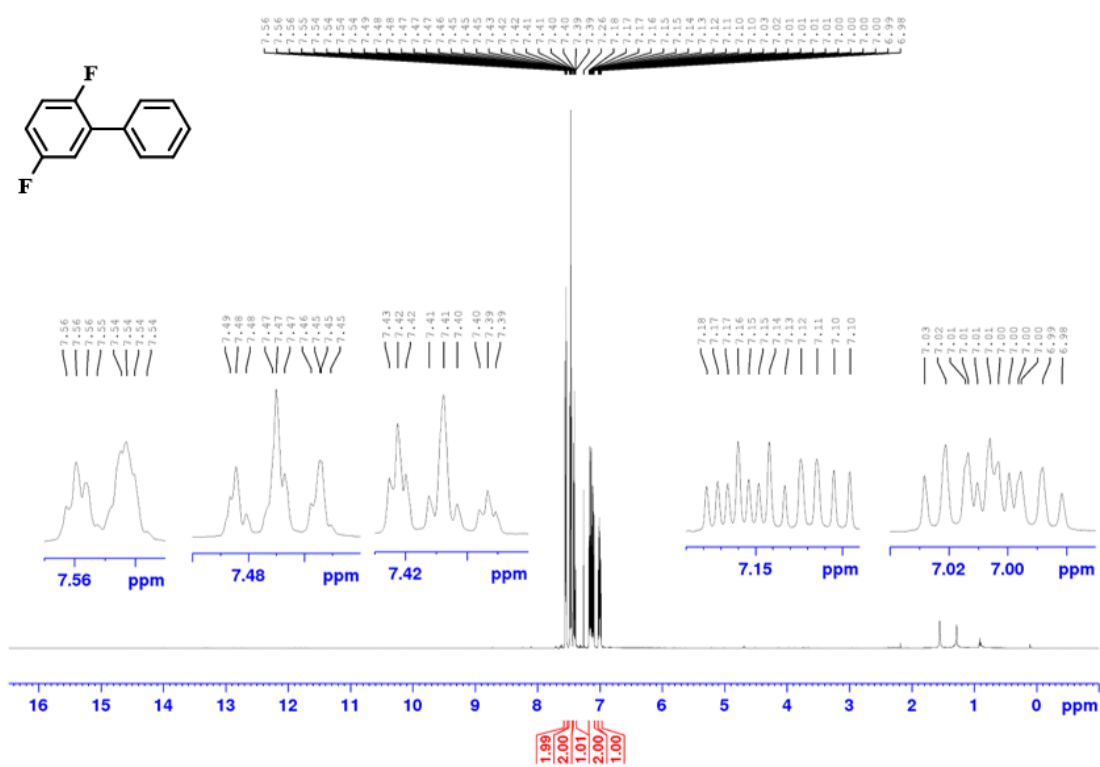
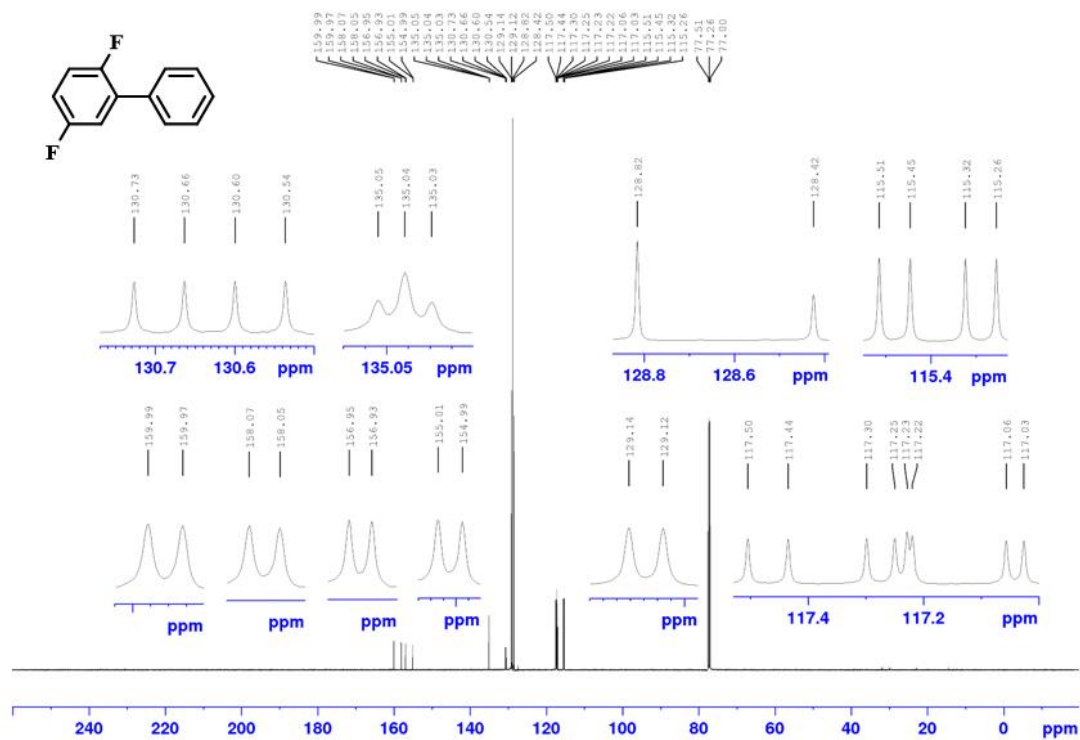
¹H NMR Spectrum of 2_5b (500 MHz, CDCl₃)

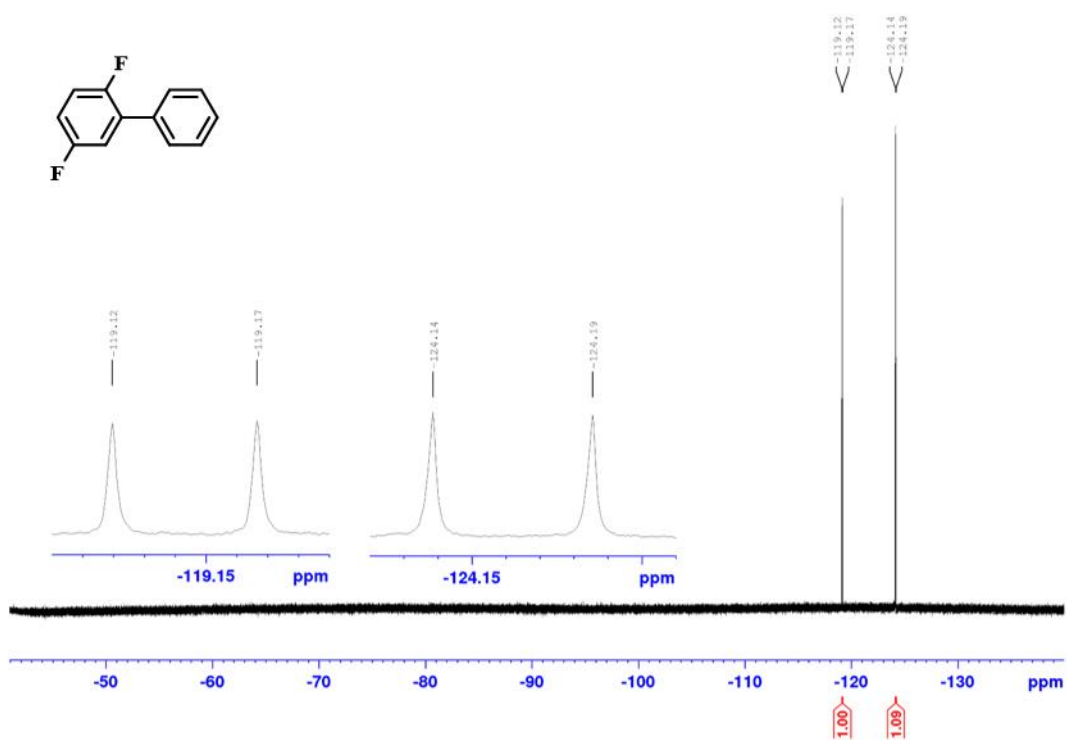


$^{13}\text{C}\{^1\text{H}\}$ NMR Spectrum of 2_5b (126 MHz, CDCl_3) $^{19}\text{F}\{^1\text{H}\}$ NMR Spectrum of 2_5b (376 MHz, C_6D_6)

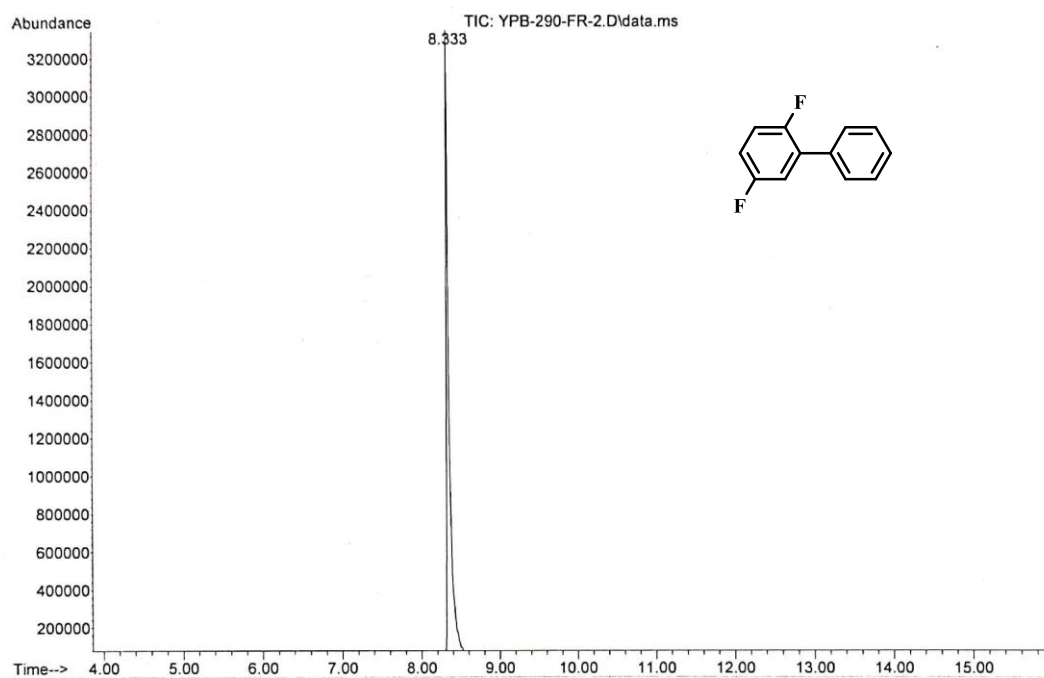
GC-MS of 2_5b

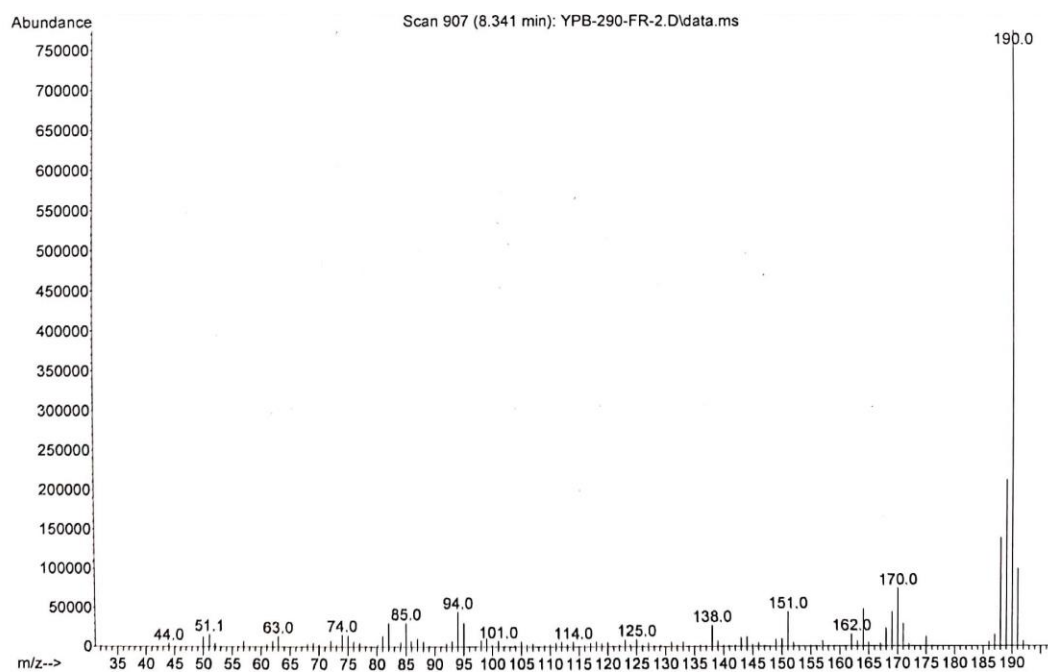


^1H NMR Spectrum of 2_5c (500 MHz, CDCl_3) $^{13}\text{C}\{^1\text{H}\}$ NMR Spectrum of 2_5c (126 MHz, CDCl_3)

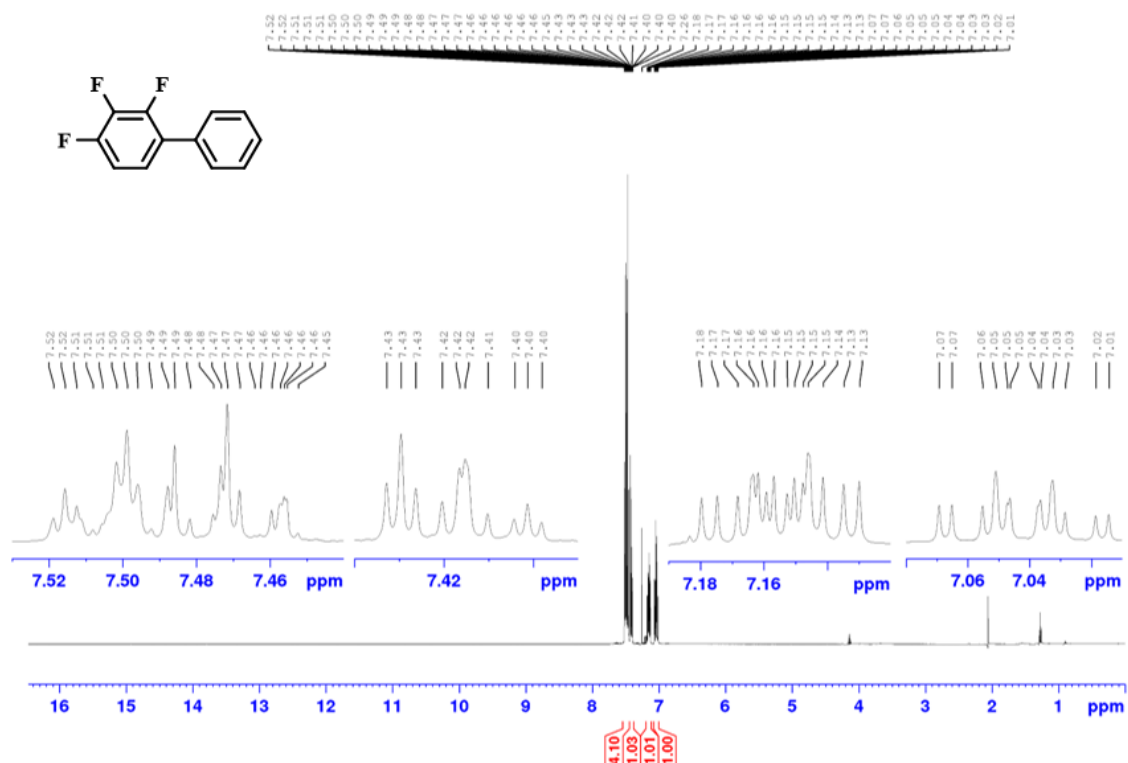
$^{19}\text{F}\{^1\text{H}\}$ NMR Spectrum of 2_5c (376 MHz, CDCl_3)

GC-MS of 2_5c

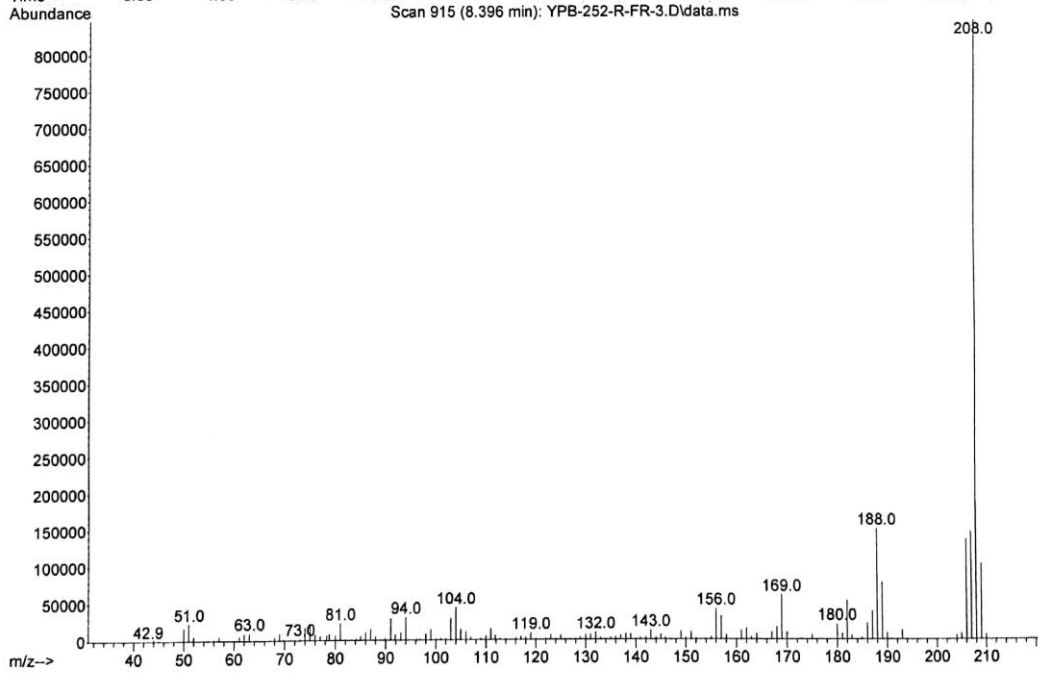
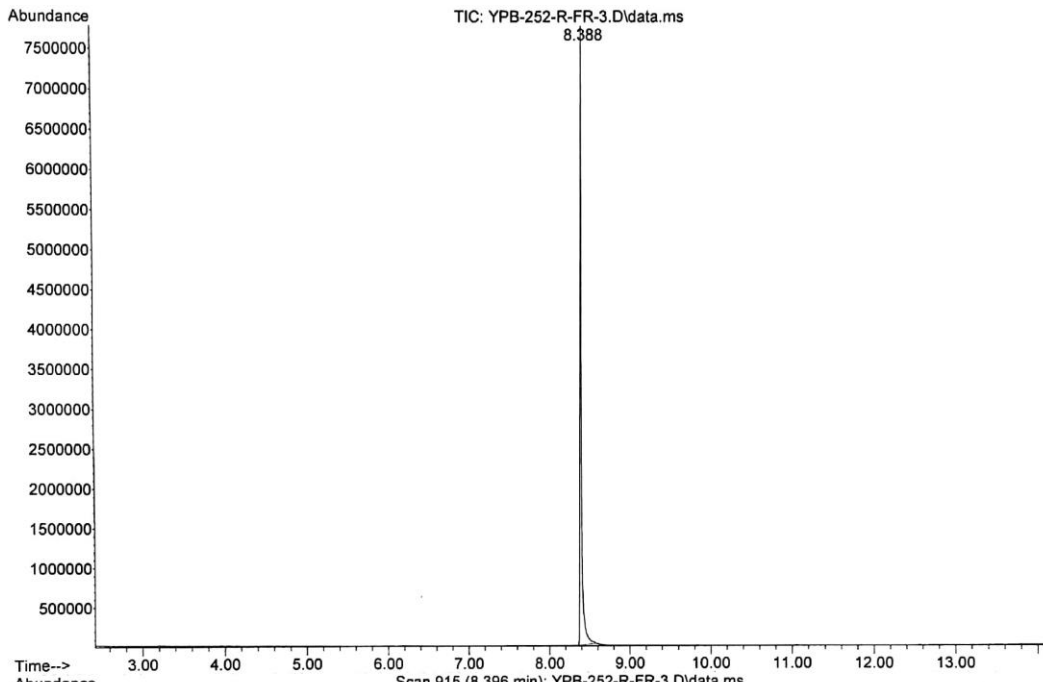


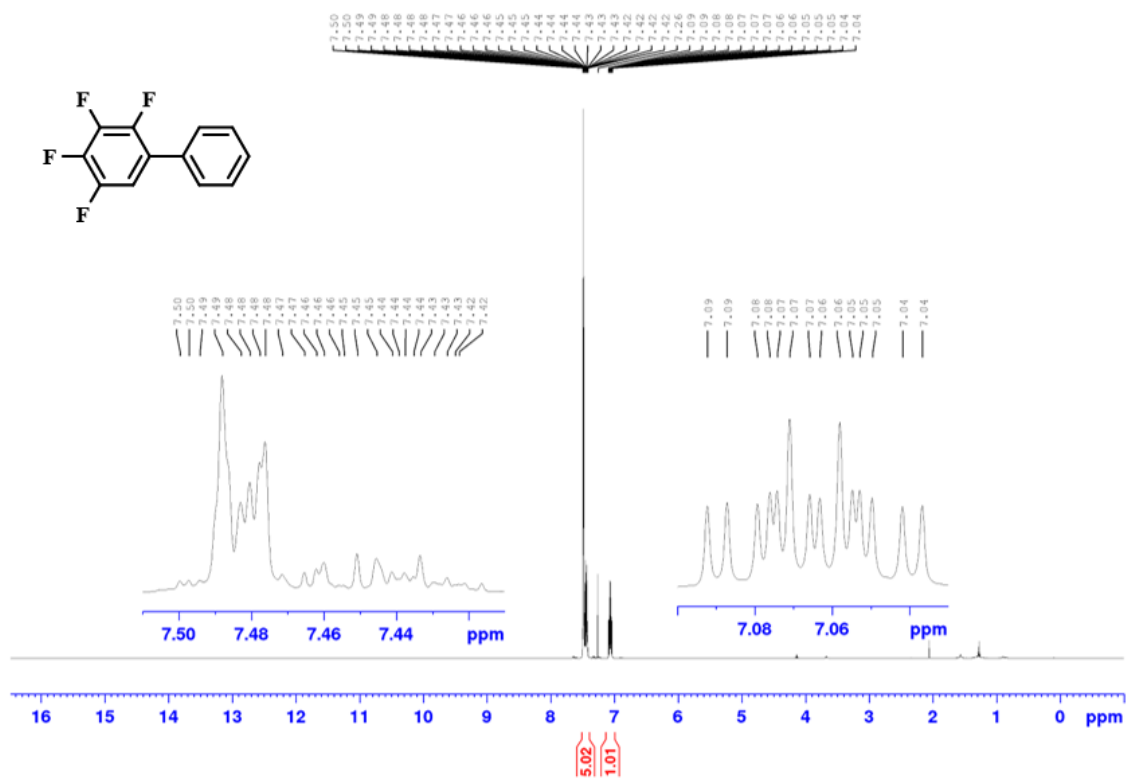
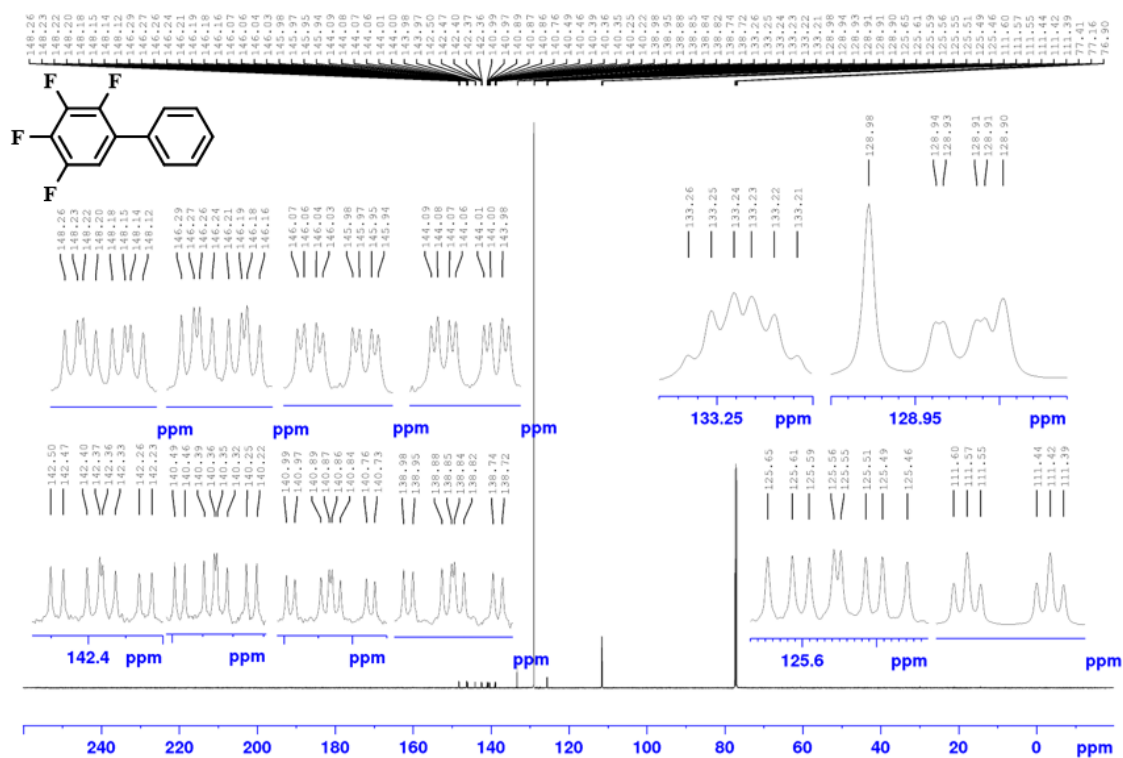


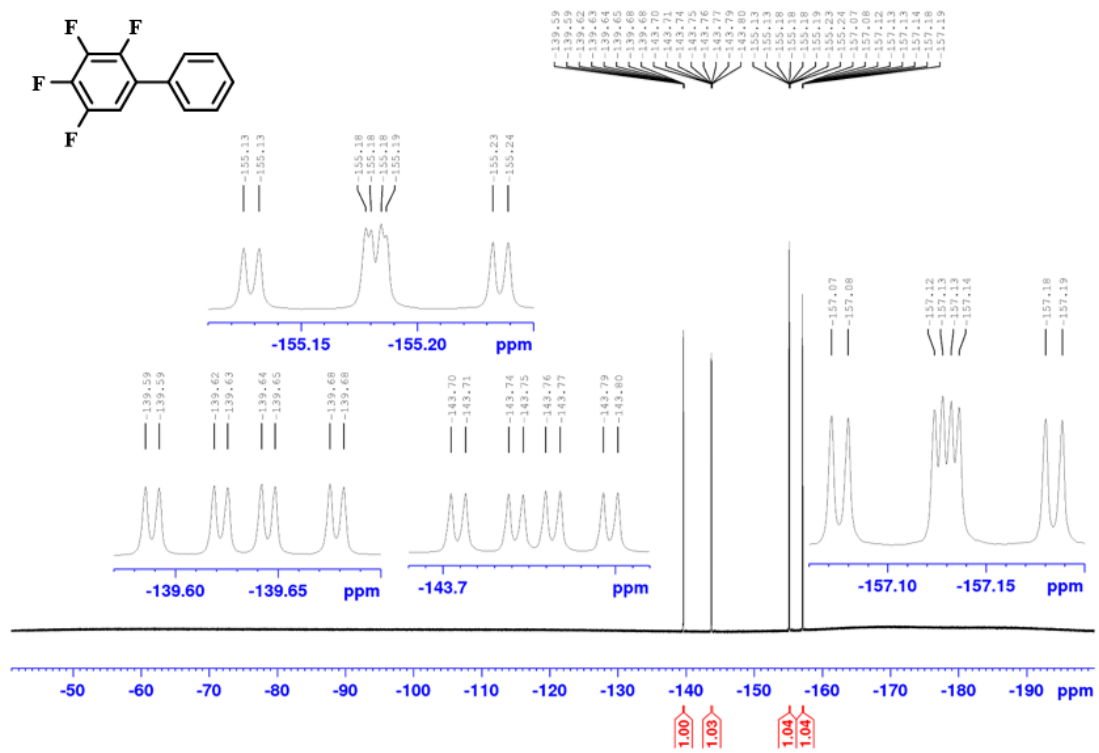
^1H NMR Spectrum of 2_5d (500 MHz, CDCl_3)



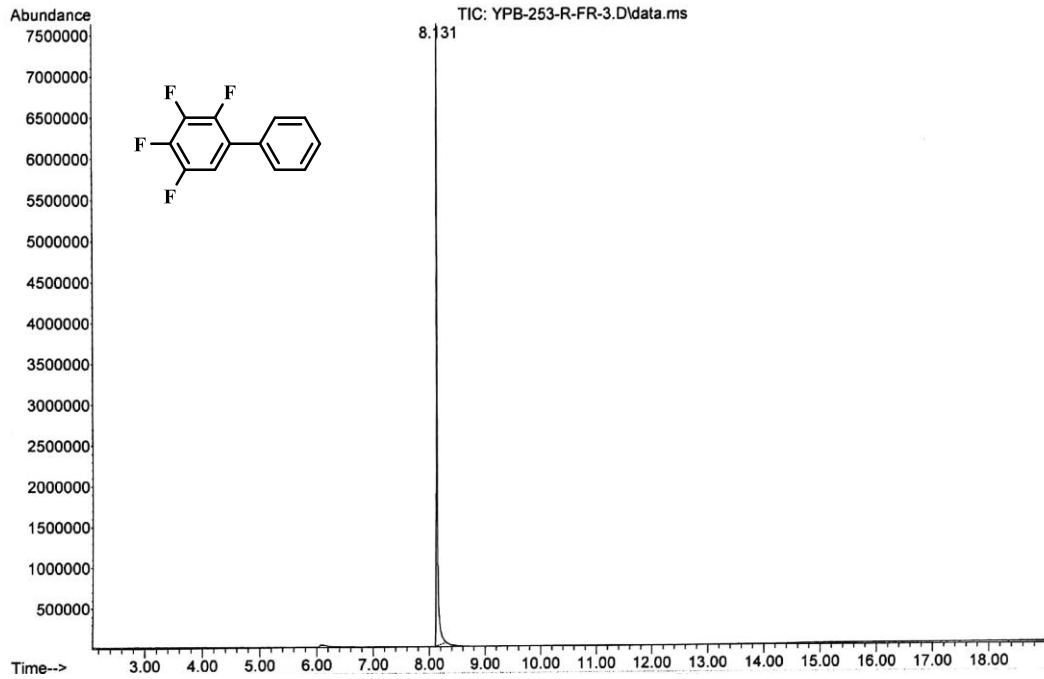
GC-MS of 2_5d



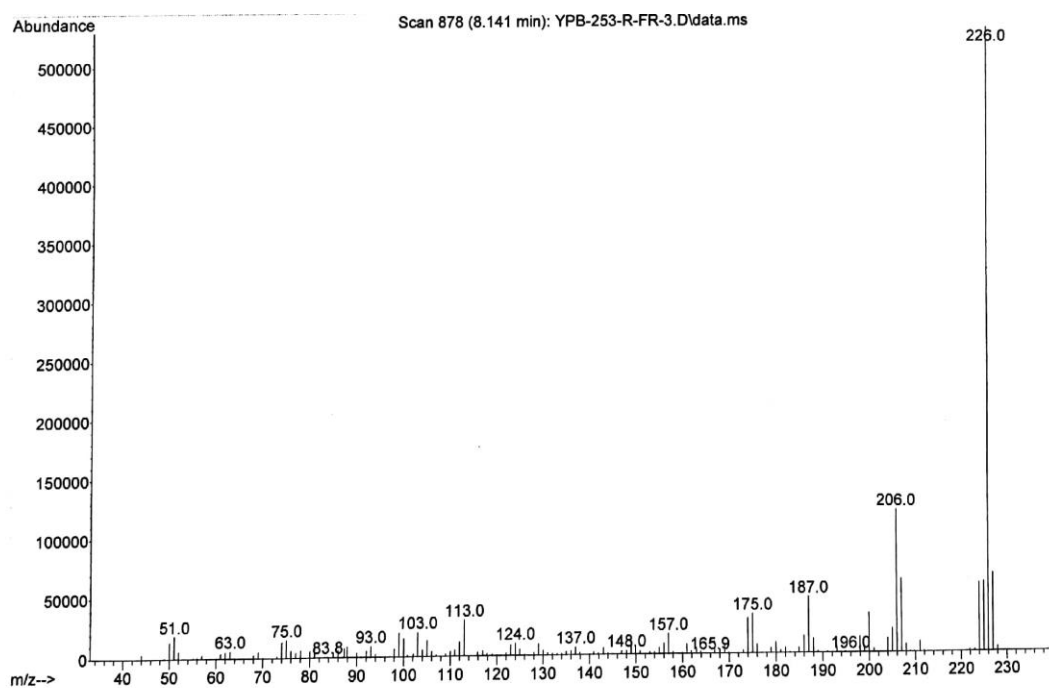
¹H NMR Spectrum of 2_5e (500 MHz, CDCl₃)**¹³C{¹H} NMR Spectrum of 2_5e (126 MHz, CDCl₃)**

$^{19}\text{F}\{^1\text{H}\}$ NMR Spectrum of 2_5e (376 MHz, CDCl_3)

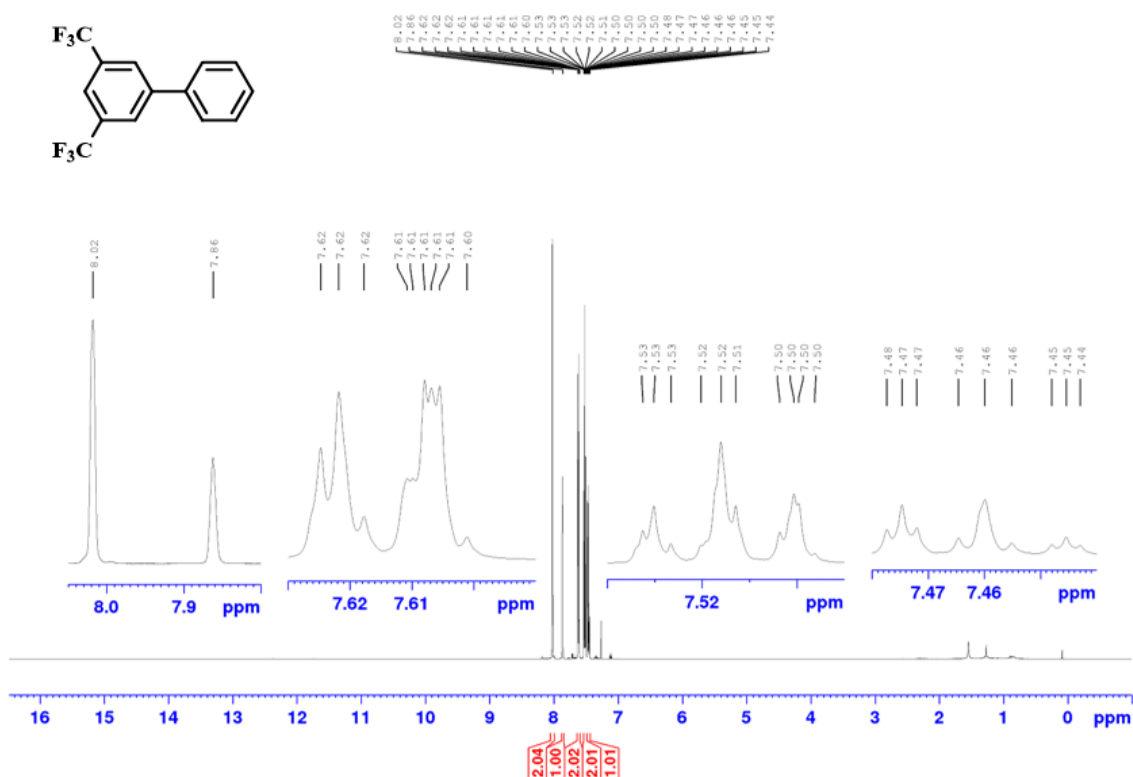
GC-MS of 2_5e

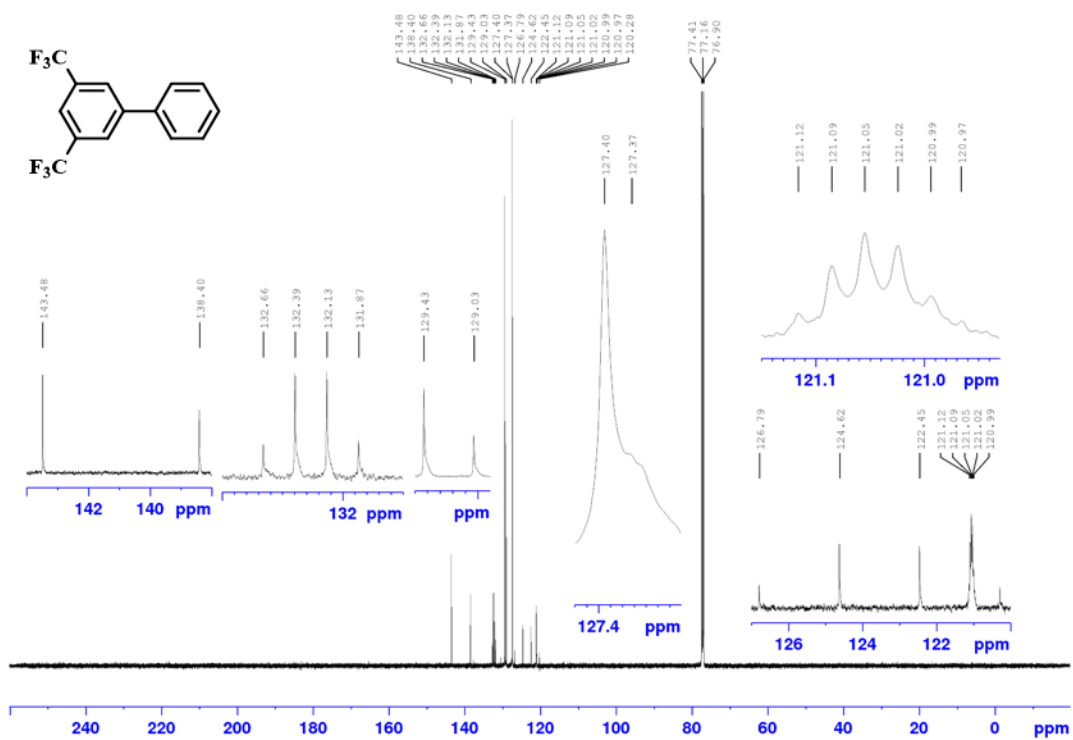
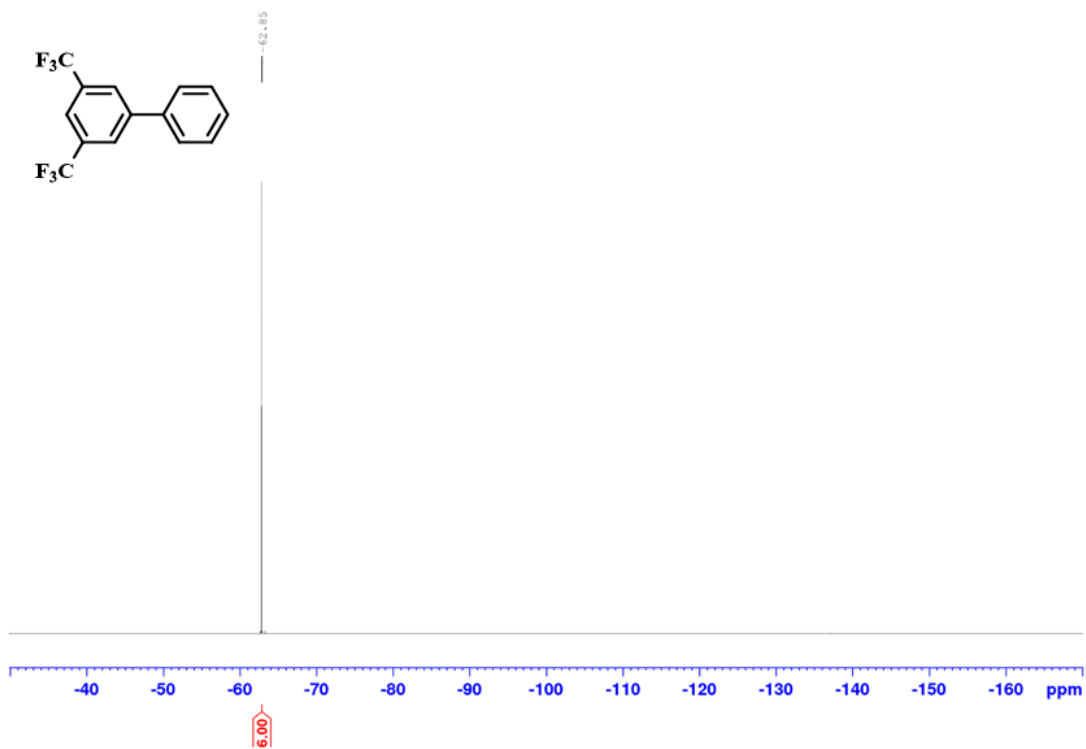


Appendix

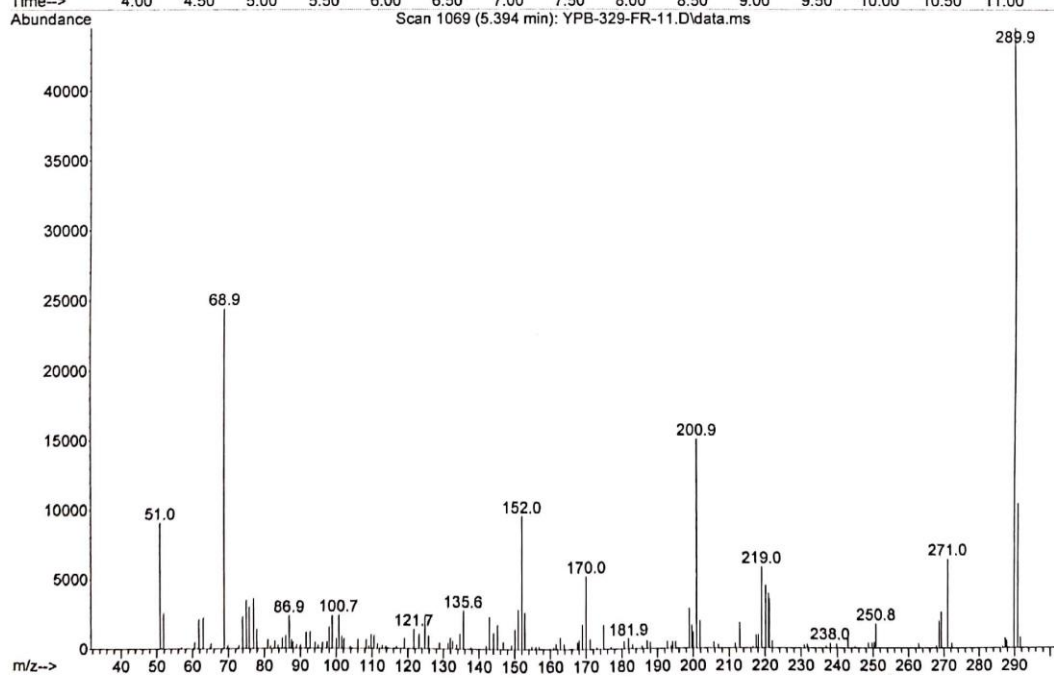
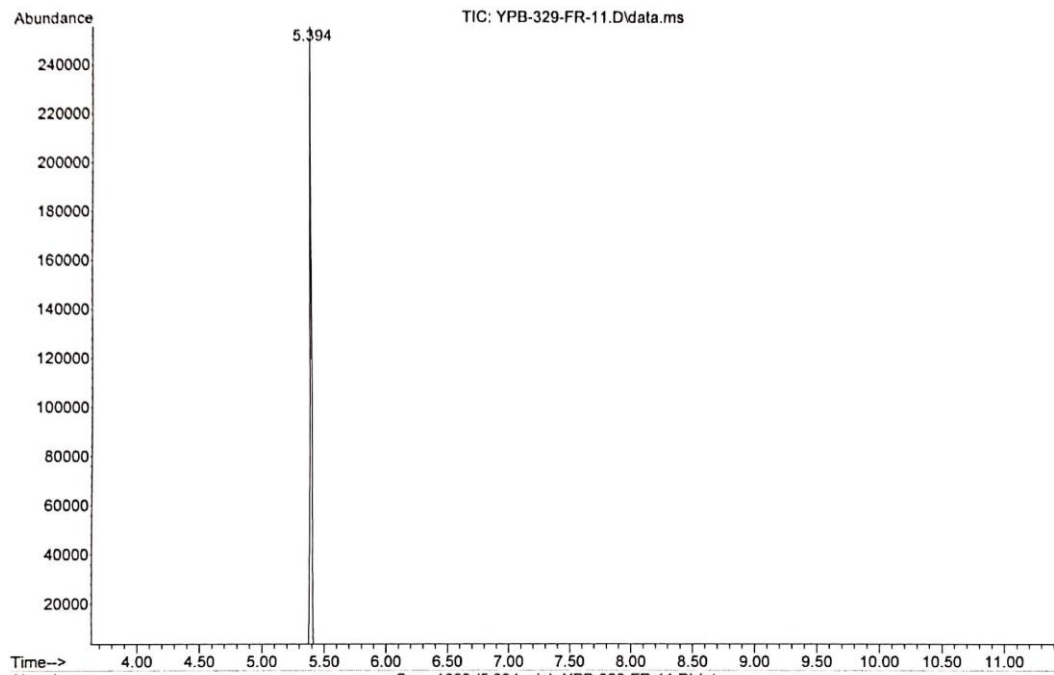


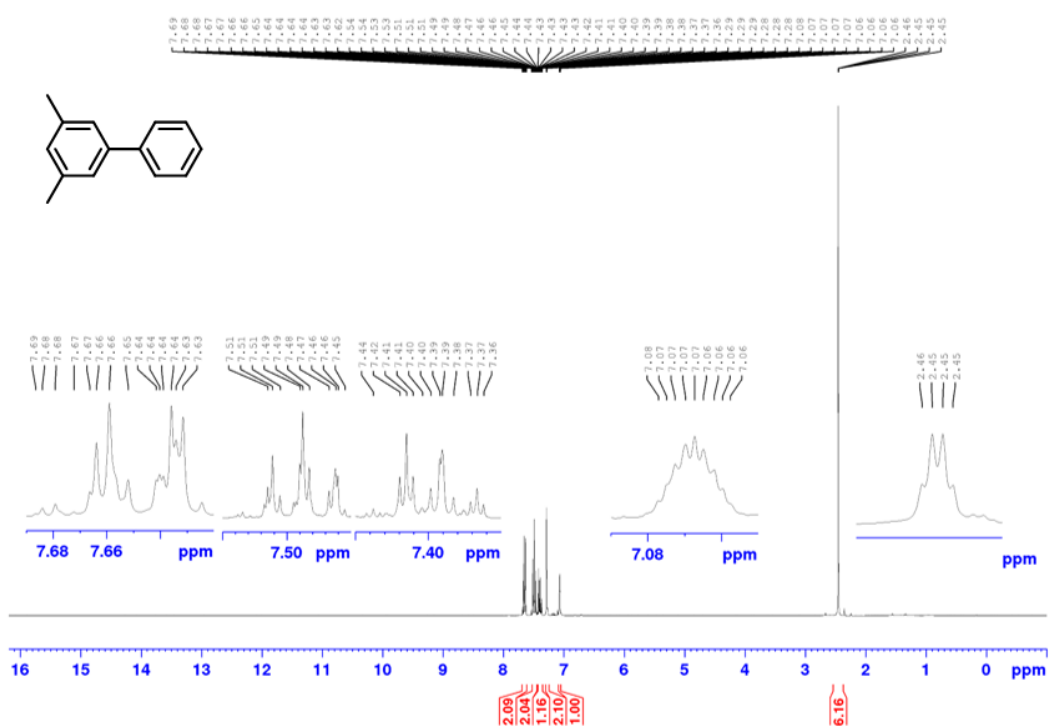
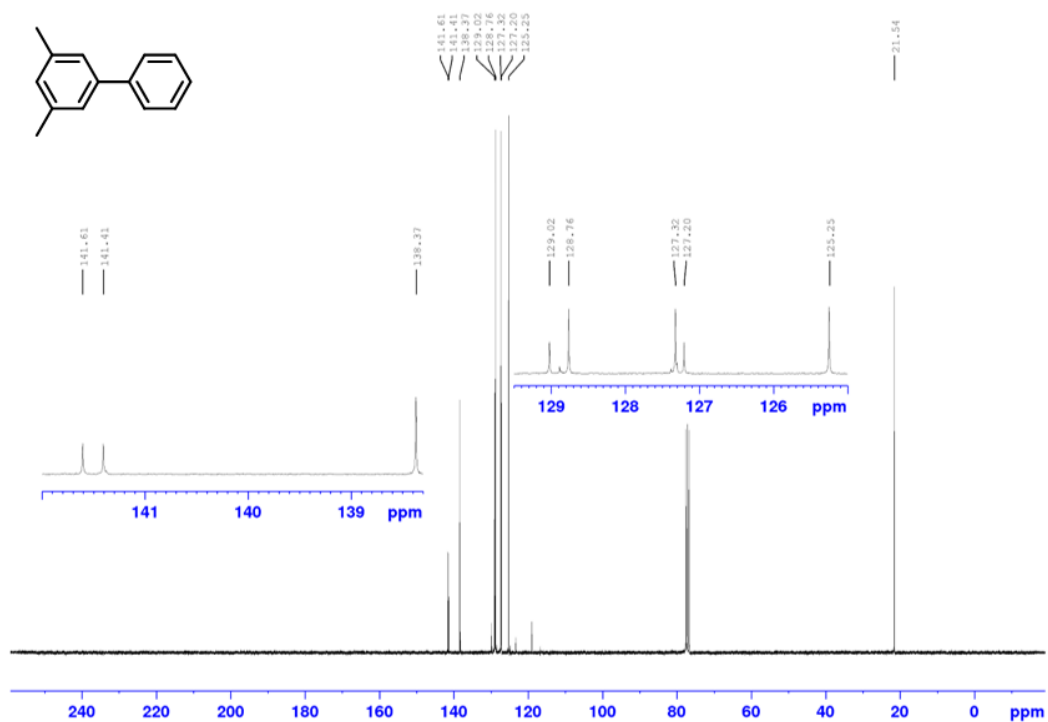
¹H NMR Spectrum of 2_5f (500 MHz, CDCl₃)



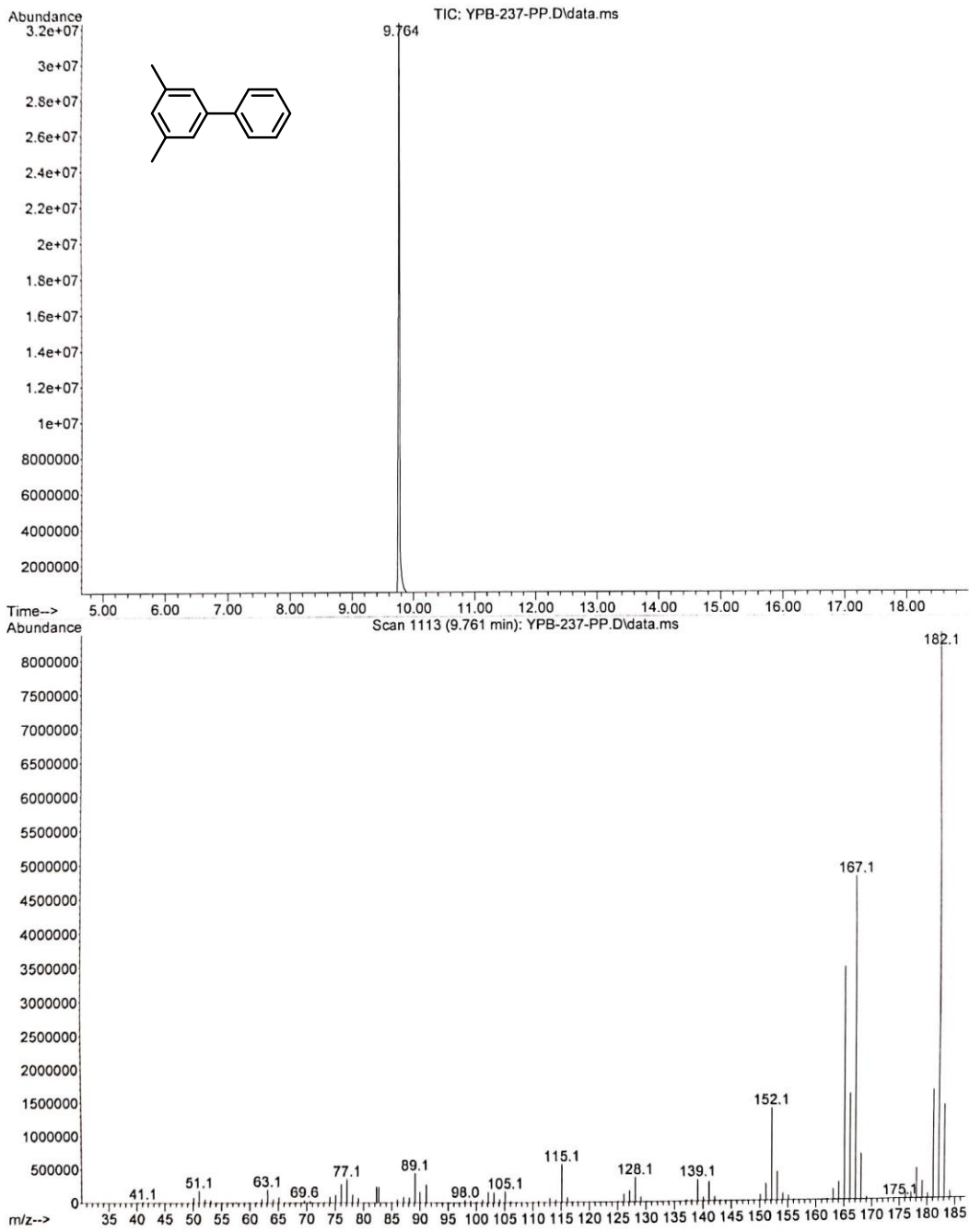
$^{13}\text{C}\{^1\text{H}\}$ NMR Spectrum of 2_5f (126 MHz, CDCl_3) ^{19}F NMR Spectrum of 2_5f (470 MHz, CDCl_3)

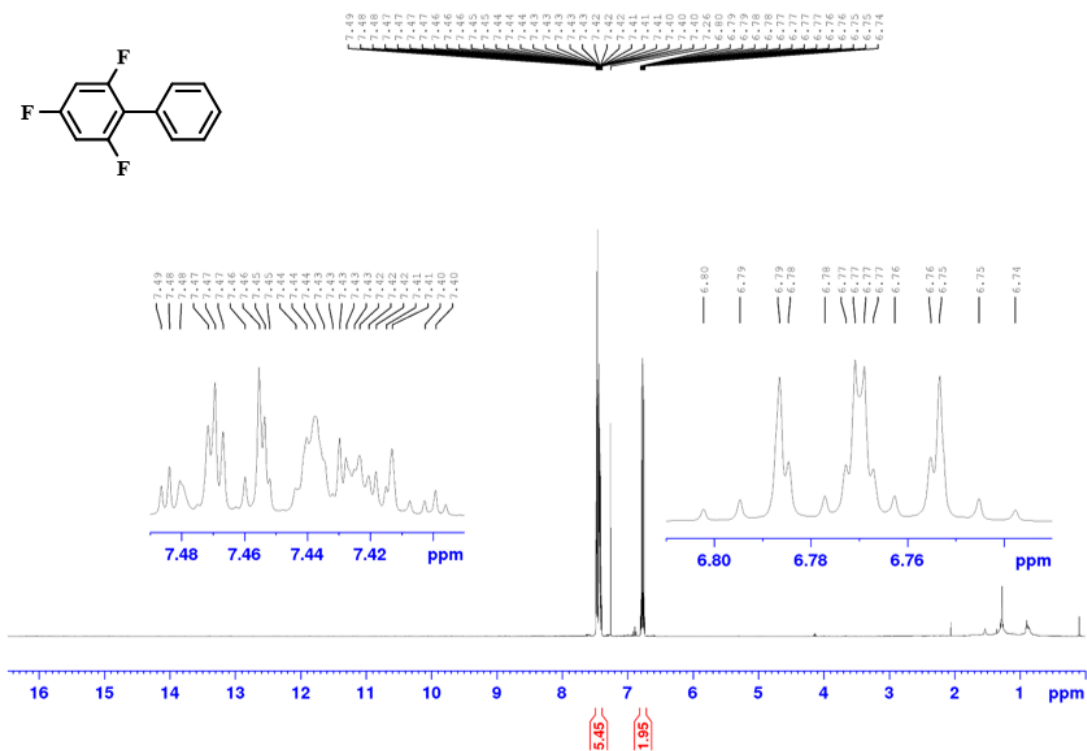
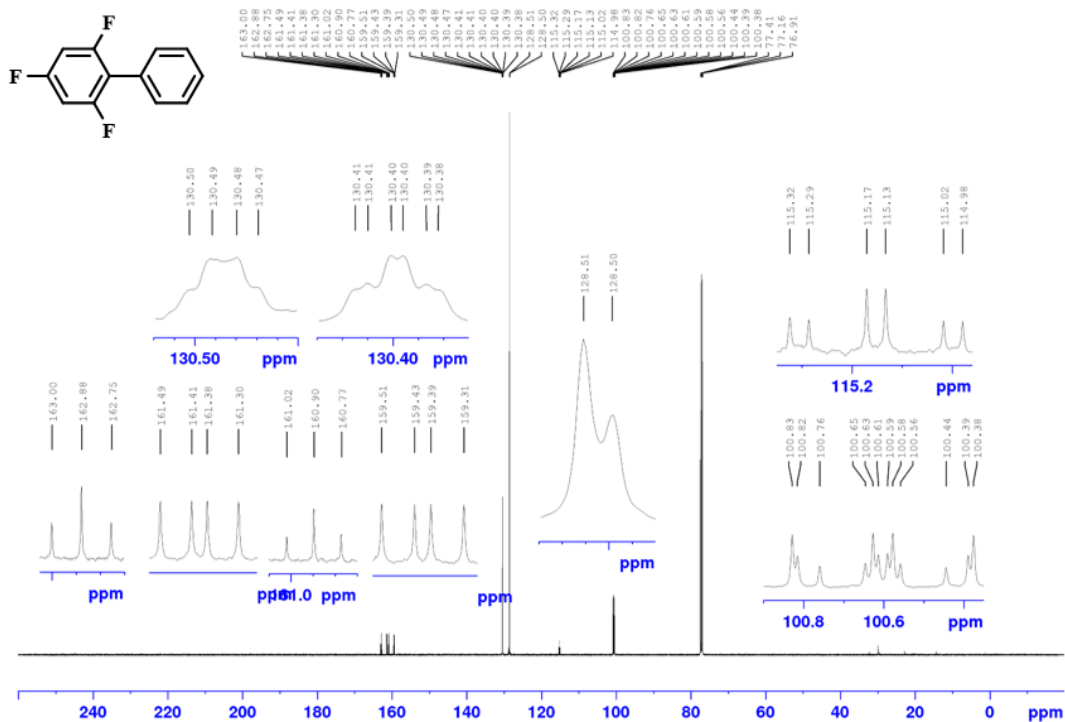
GC-MS of 2_5f

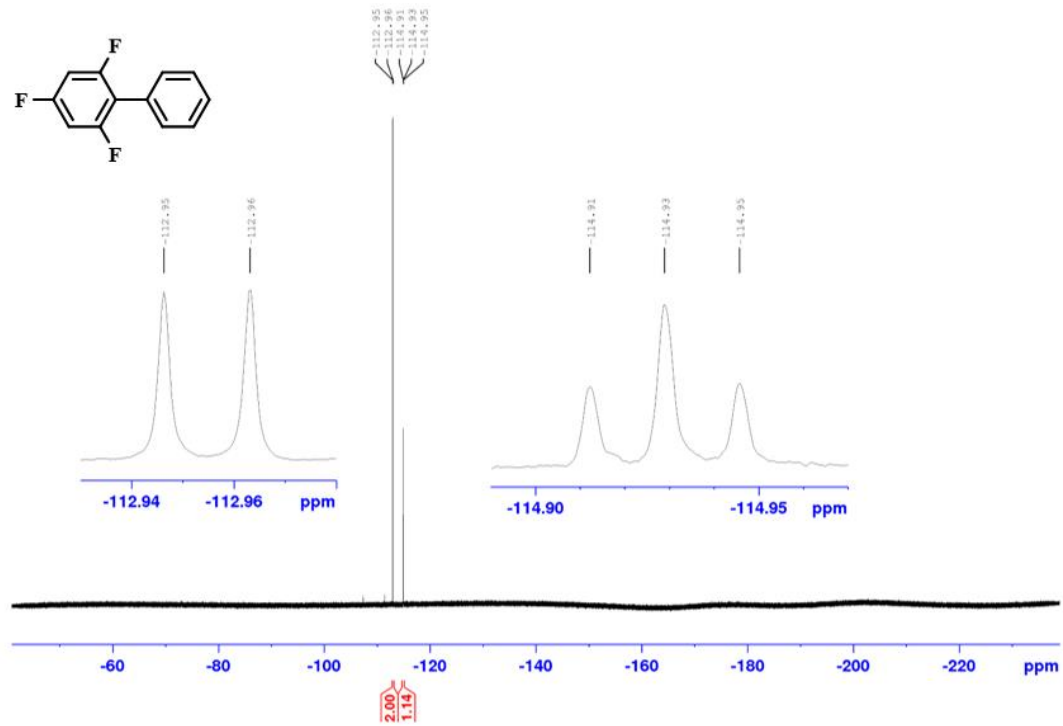


^1H NMR Spectrum of 2_5g (300 MHz, CDCl_3) $^{13}\text{C}\{^1\text{H}\}$ NMR Spectrum of 2_5g (126 MHz, CDCl_3)

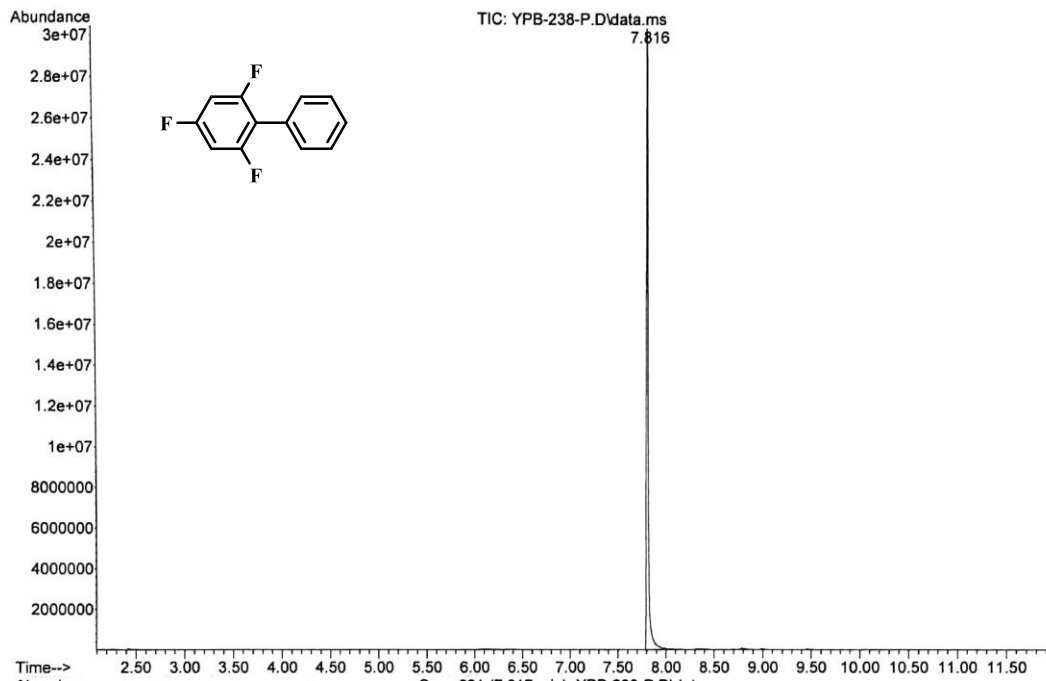
GC-MS of 2_5g



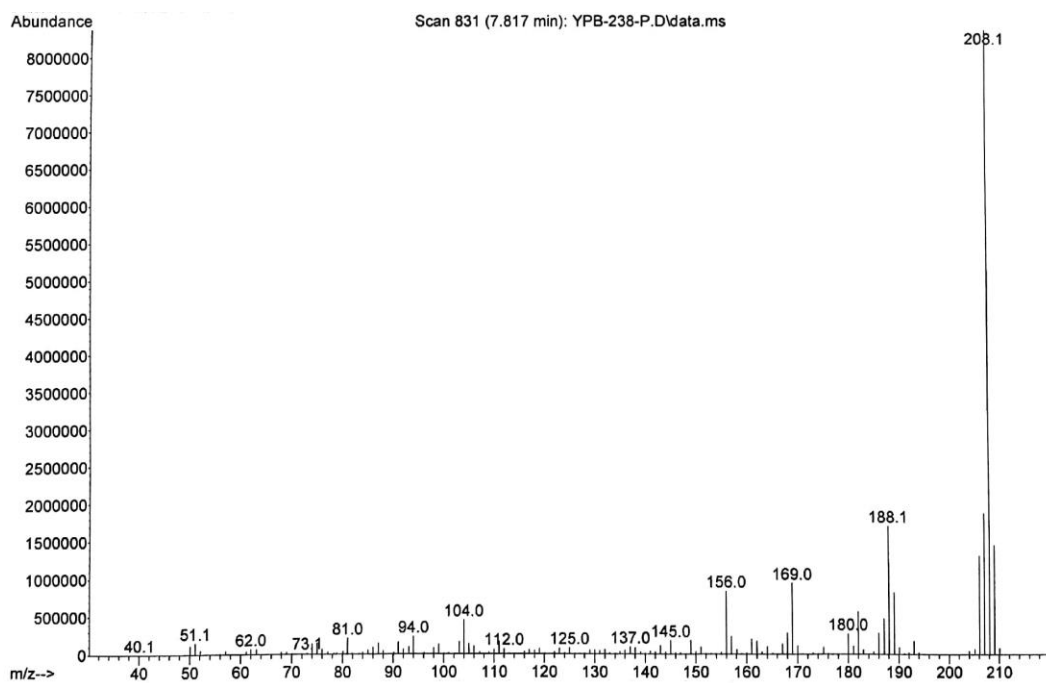
^1H NMR Spectrum of 2_5h (500 MHz, CDCl_3) $^{13}\text{C}\{^1\text{H}\}$ NMR Spectrum of 2_5h (126 MHz, CDCl_3)

$^{19}\text{F}\{^1\text{H}\}$ NMR Spectrum of 2_5h (376 MHz, C_6D_6)

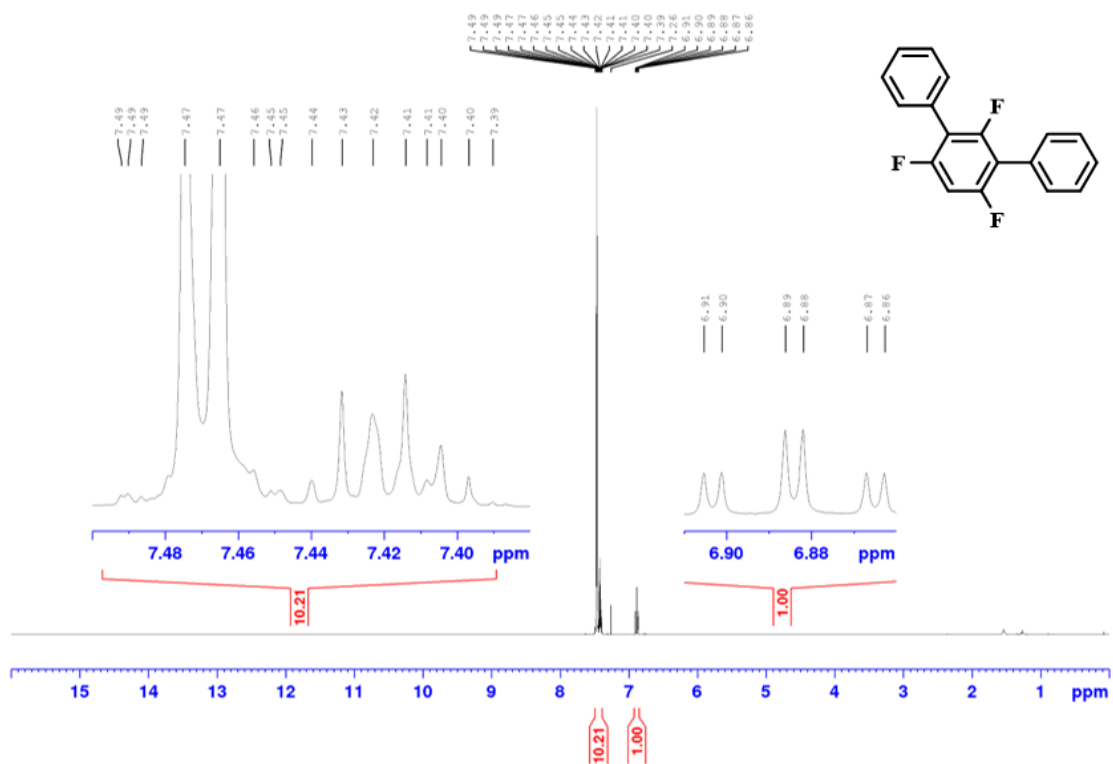
GC-MS of 2_5h

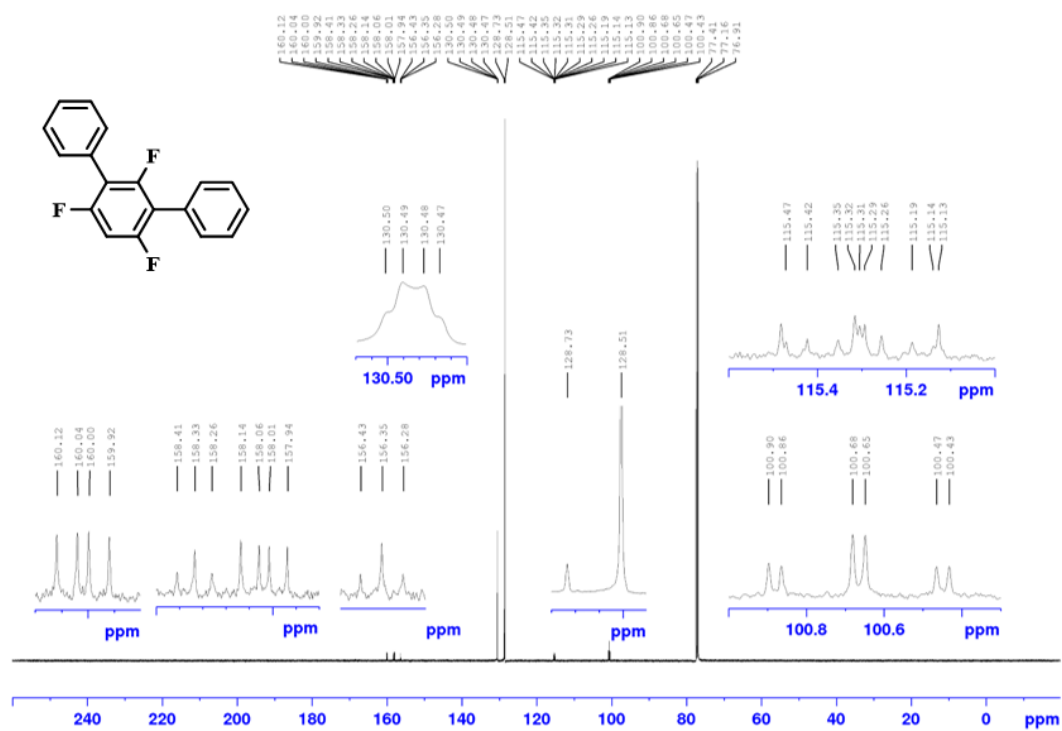
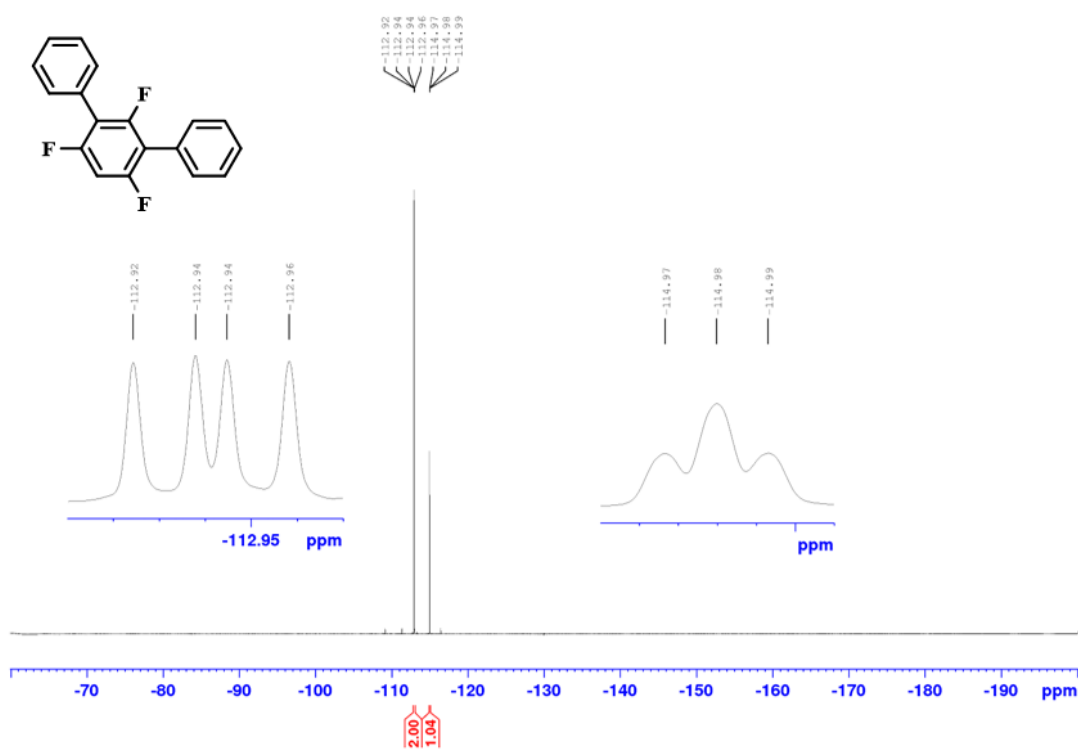


Appendix

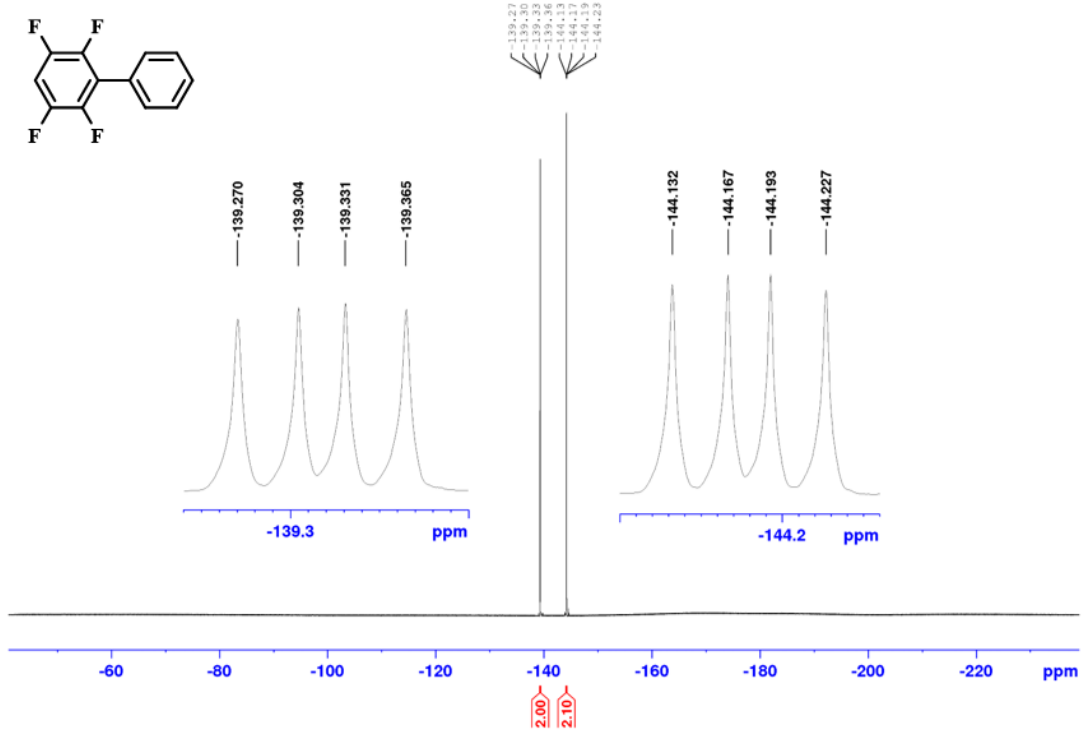


¹H NMR Spectrum of 2_5h' (500 MHz, CDCl₃)

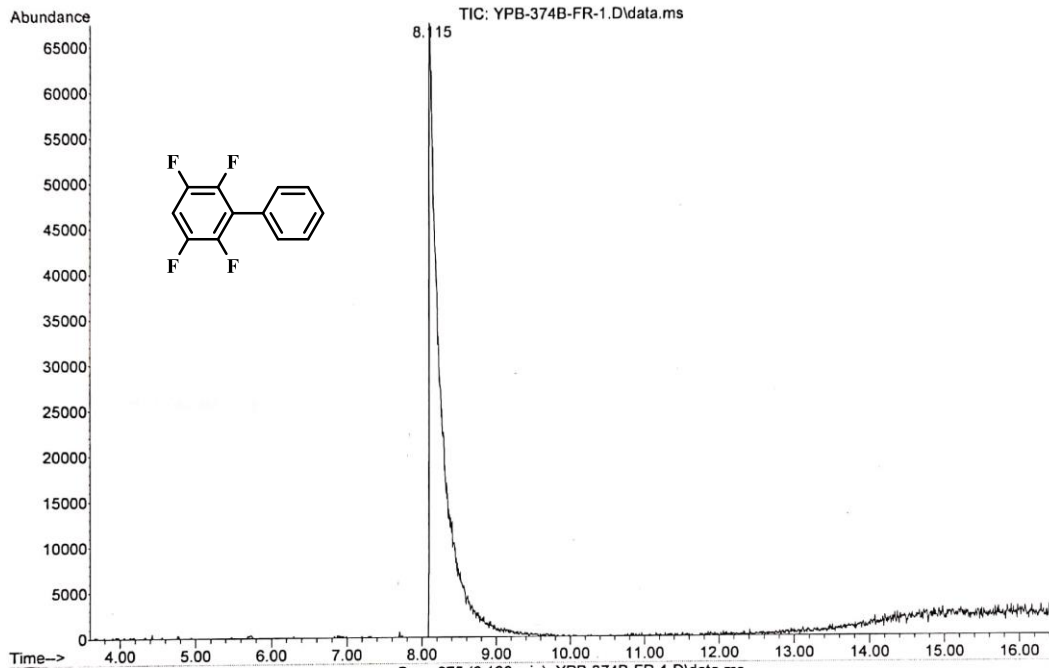


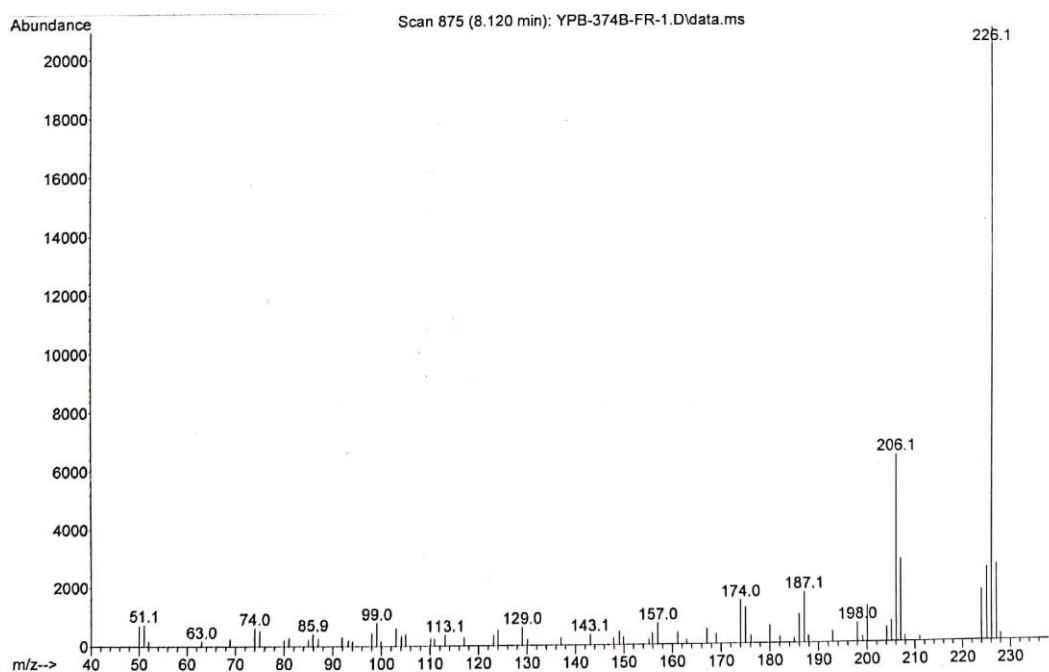
$^{13}\text{C}\{^1\text{H}\}$ NMR Spectrum of 2_5h' (126 MHz, CDCl_3) ^{19}F NMR Spectrum of 2_5h' (470 MHz, CDCl_3)

$^{19}\text{F}\{^1\text{H}\}$ NMR Spectrum of 2_5i (376 MHz, C_6D_6)

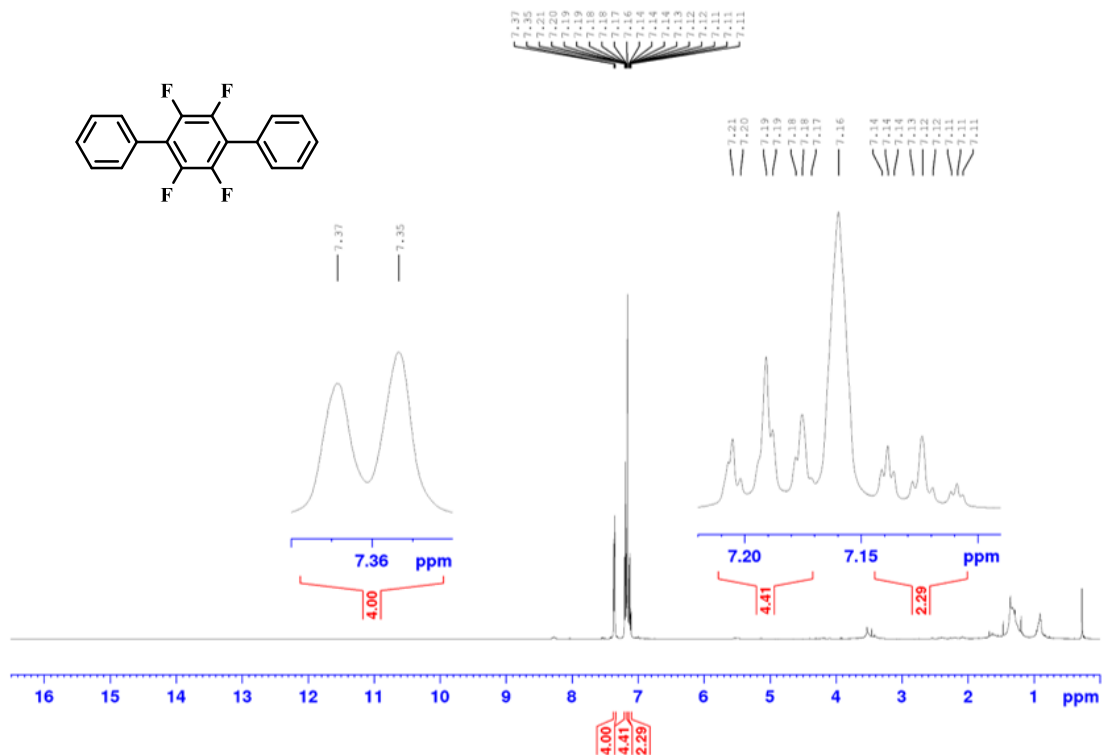


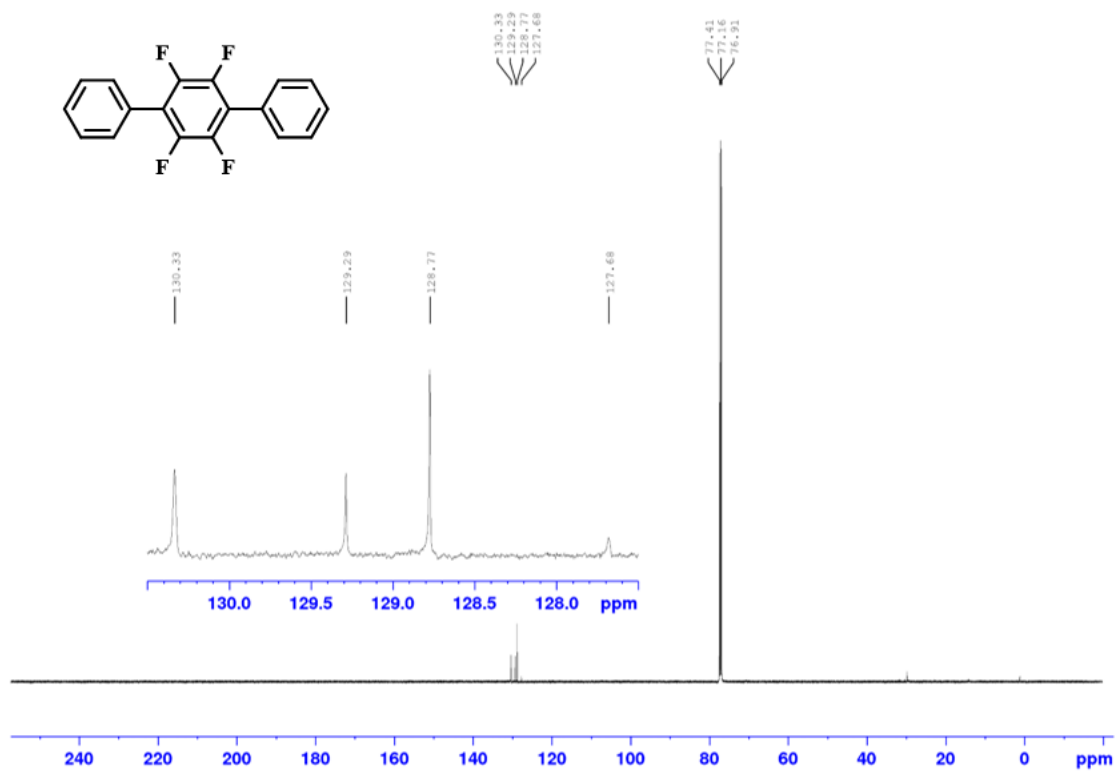
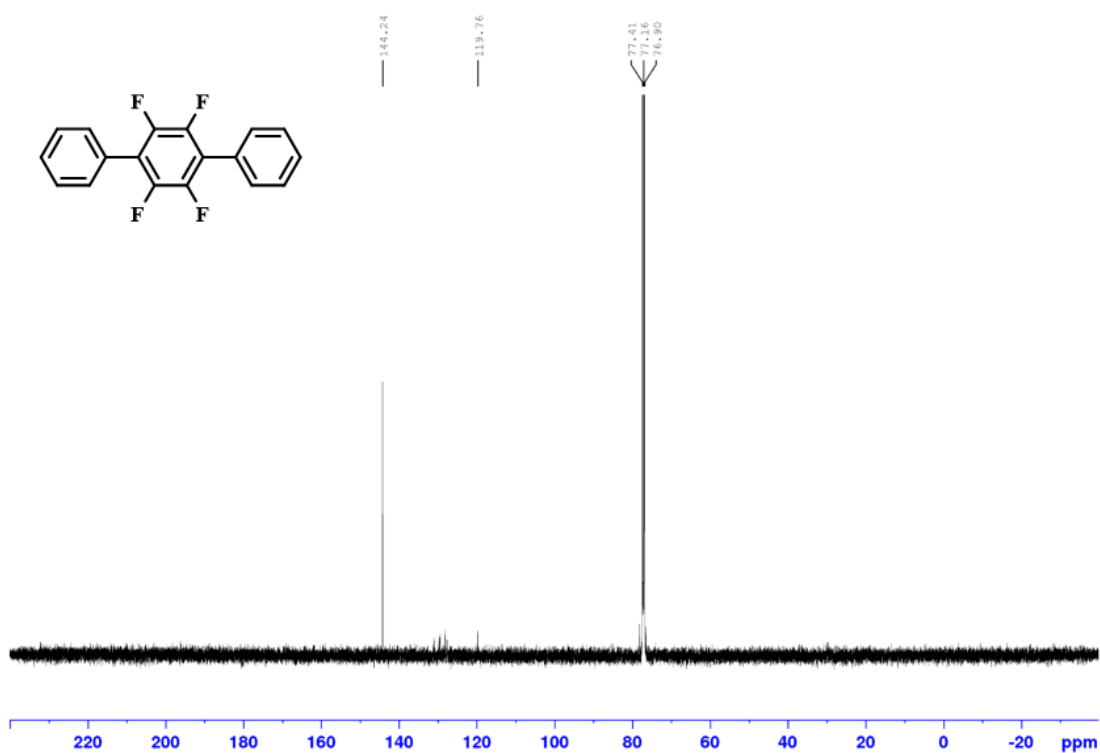
GC-MS of 2_5i

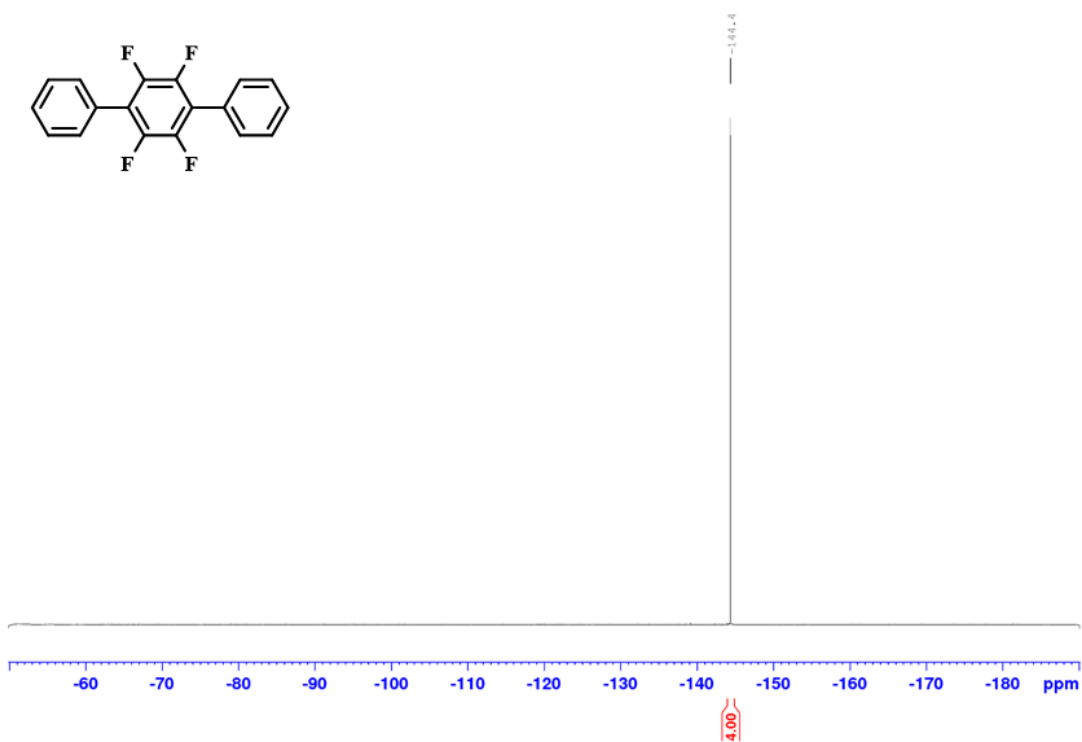
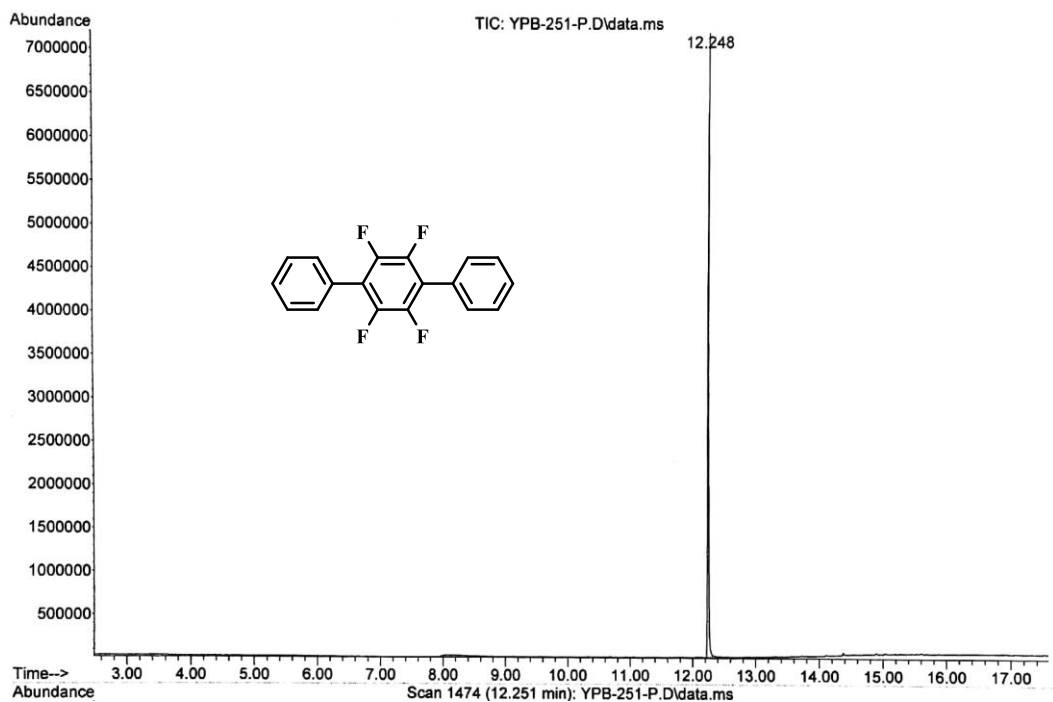




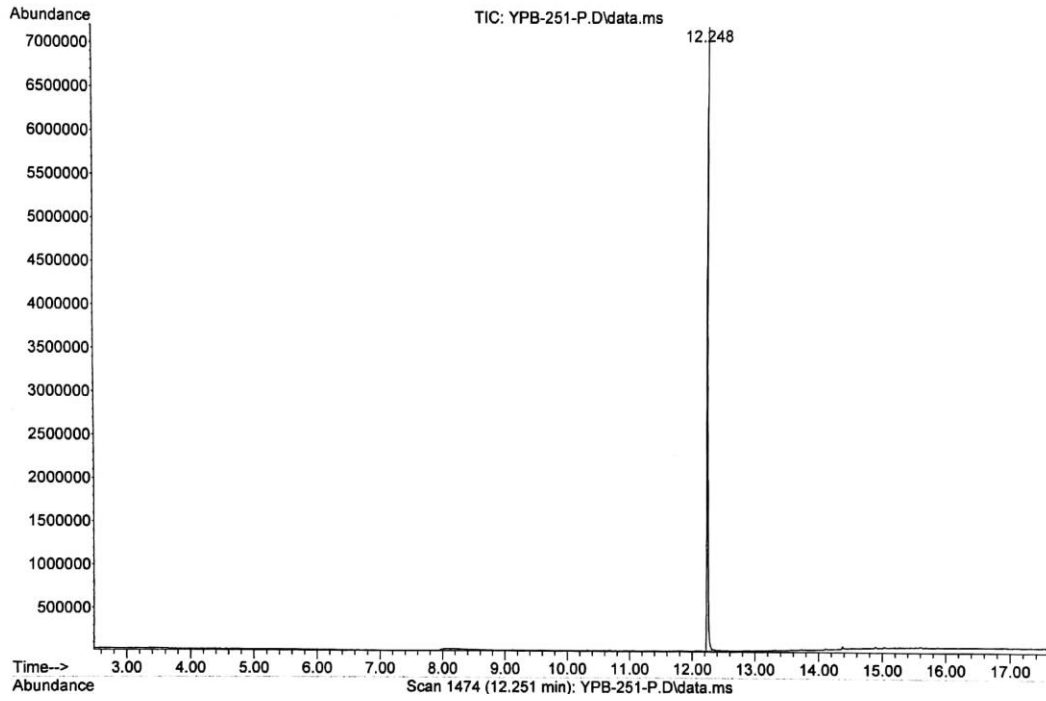
^1H NMR Spectrum of 2_5i' (500 MHz, CDCl_3)



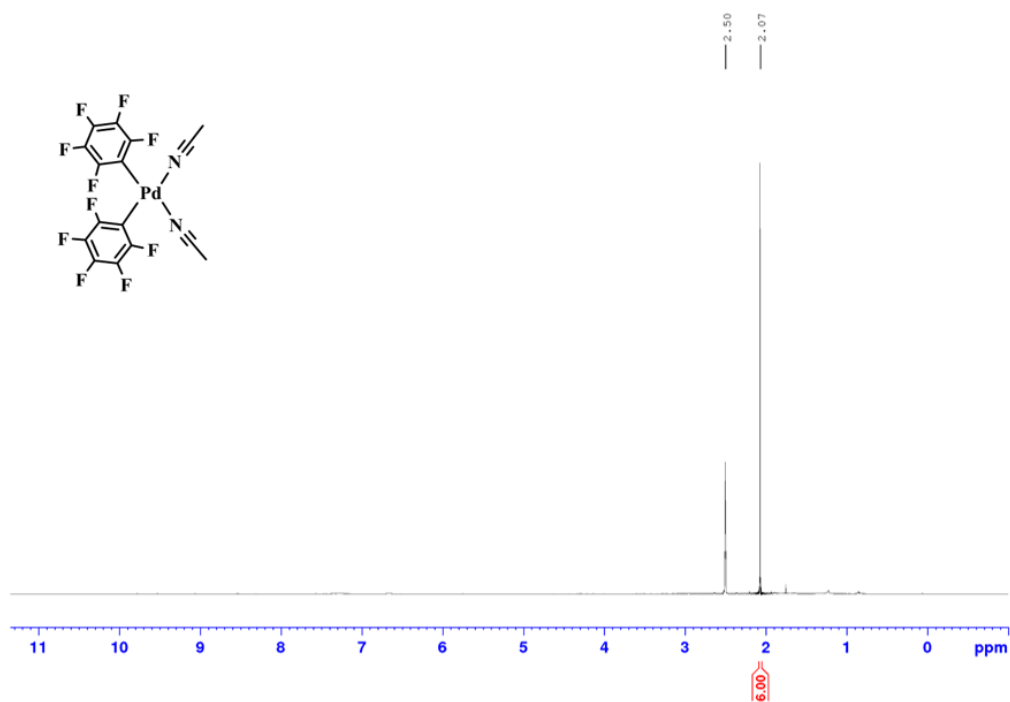
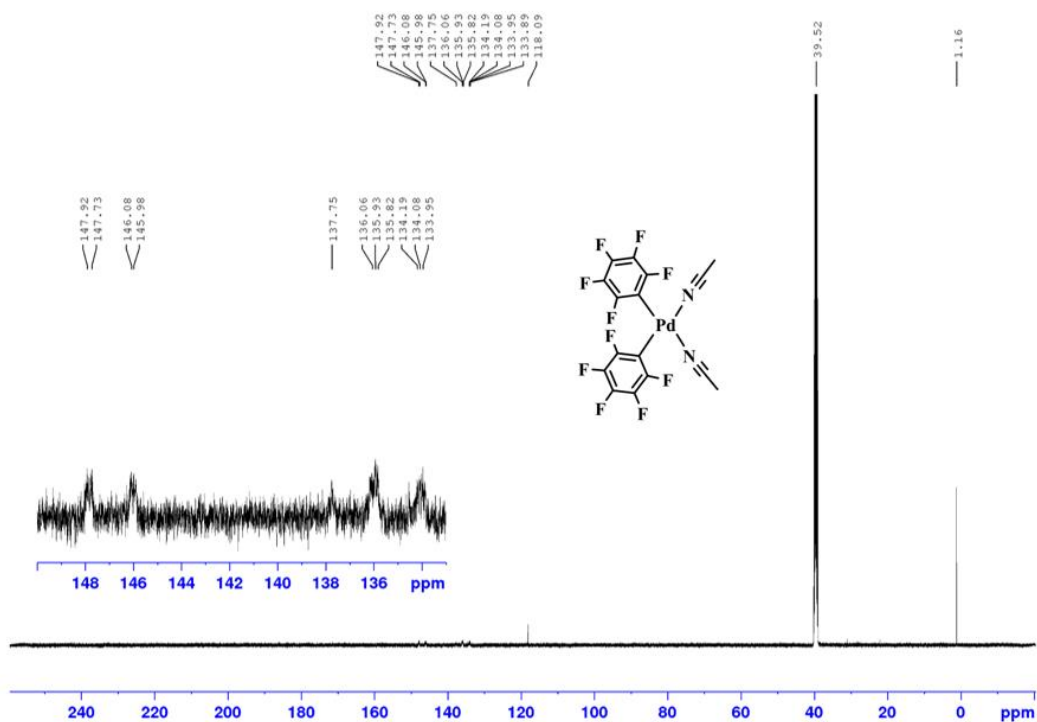
$^{13}\text{C}\{^1\text{H}\}$ NMR Spectrum of 2_5i' (126 MHz, CDCl_3) $^{13}\text{C}\{^{19}\text{F}\}$ NMR Spectrum of 2_5i' (126 MHz, CDCl_3 , (for C_6F_4))

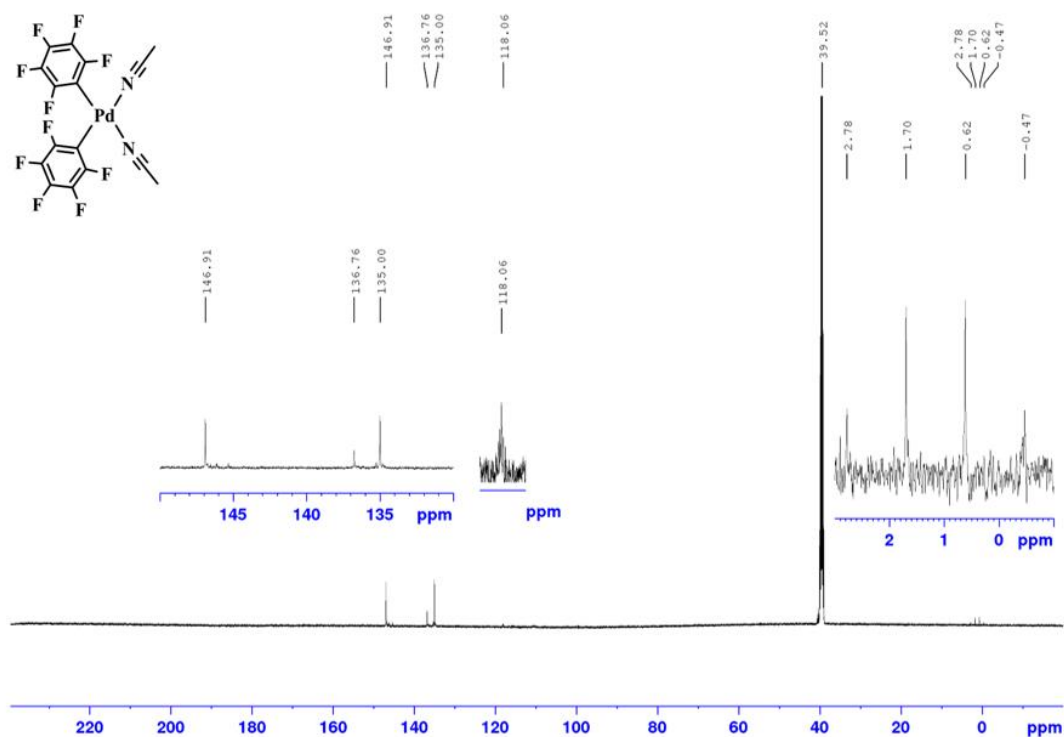
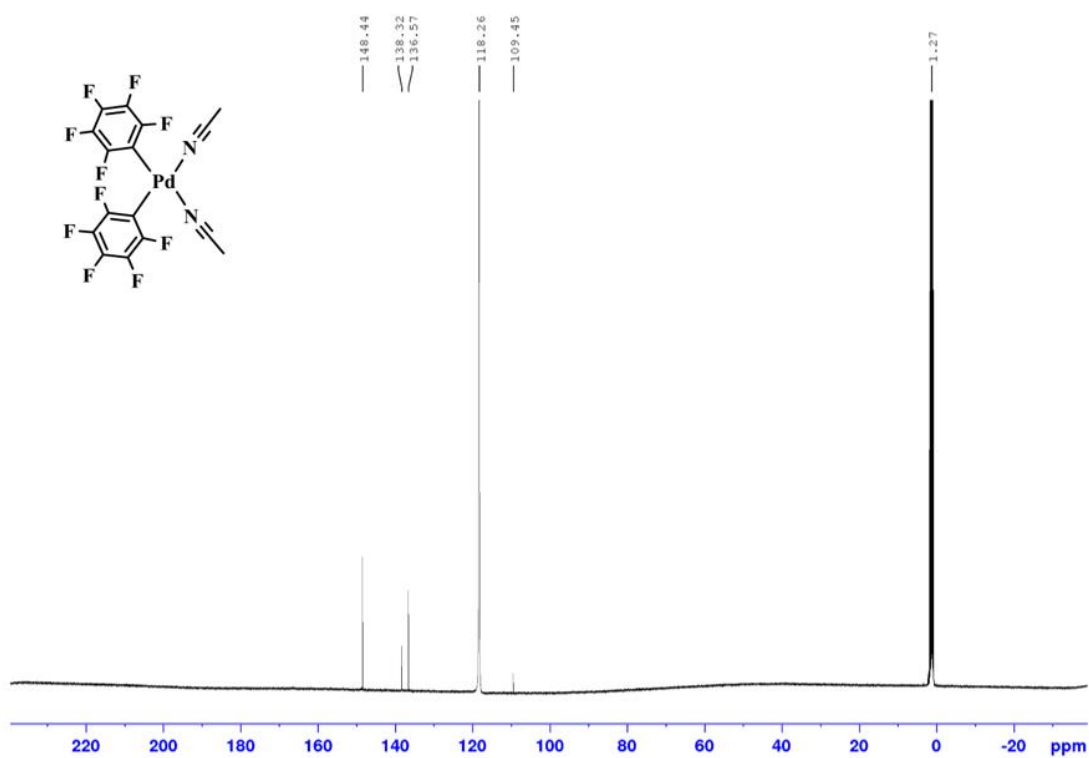
^{19}F NMR Spectrum of 2_5i' (470 MHz, CDCl_3)**GC-MS of 2_5i'**

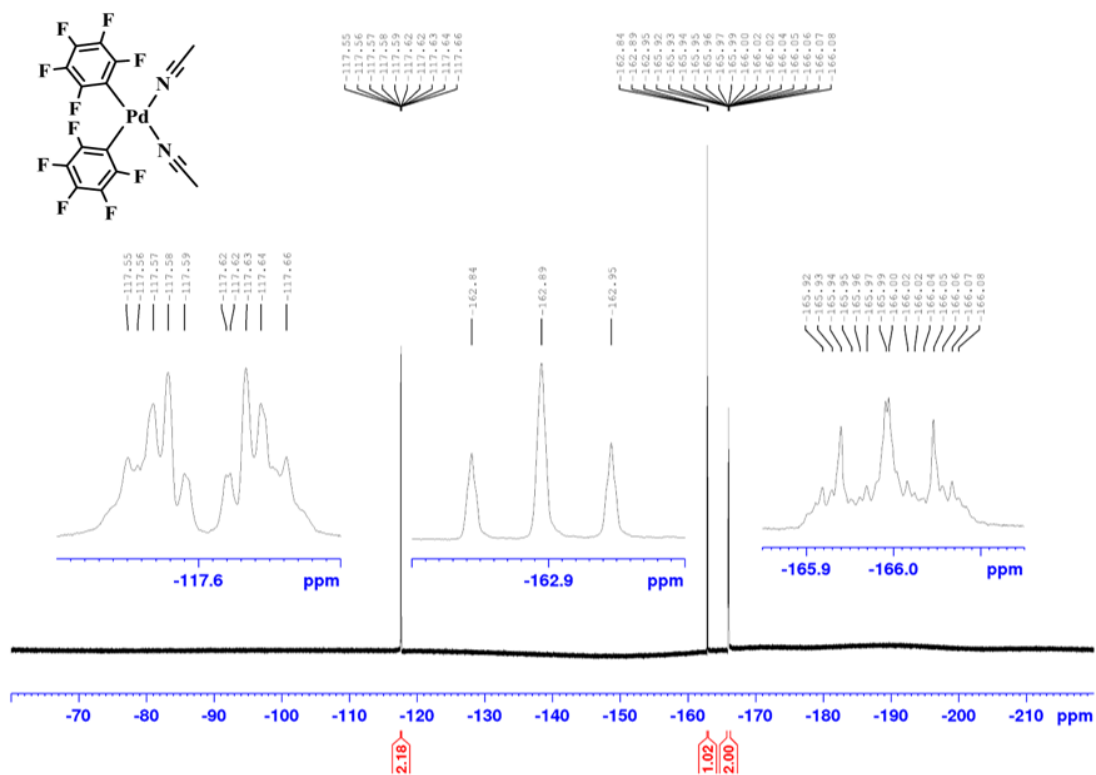
Appendix



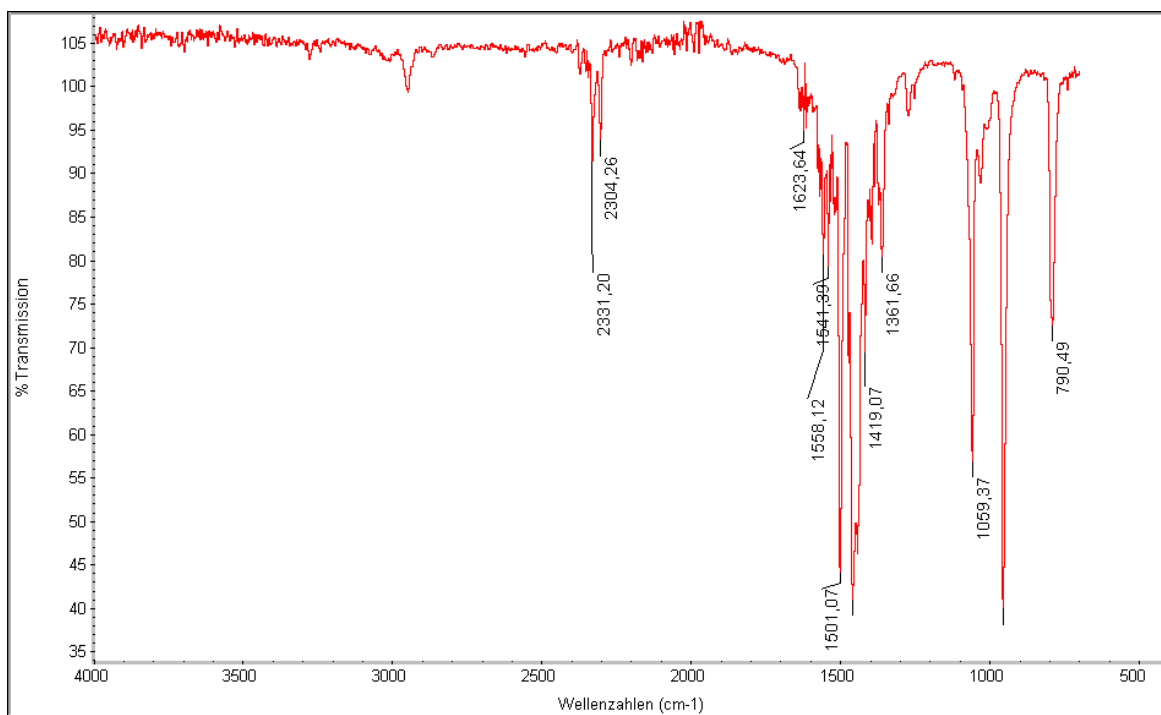
7.2 NMR Spectra for Chapter 3

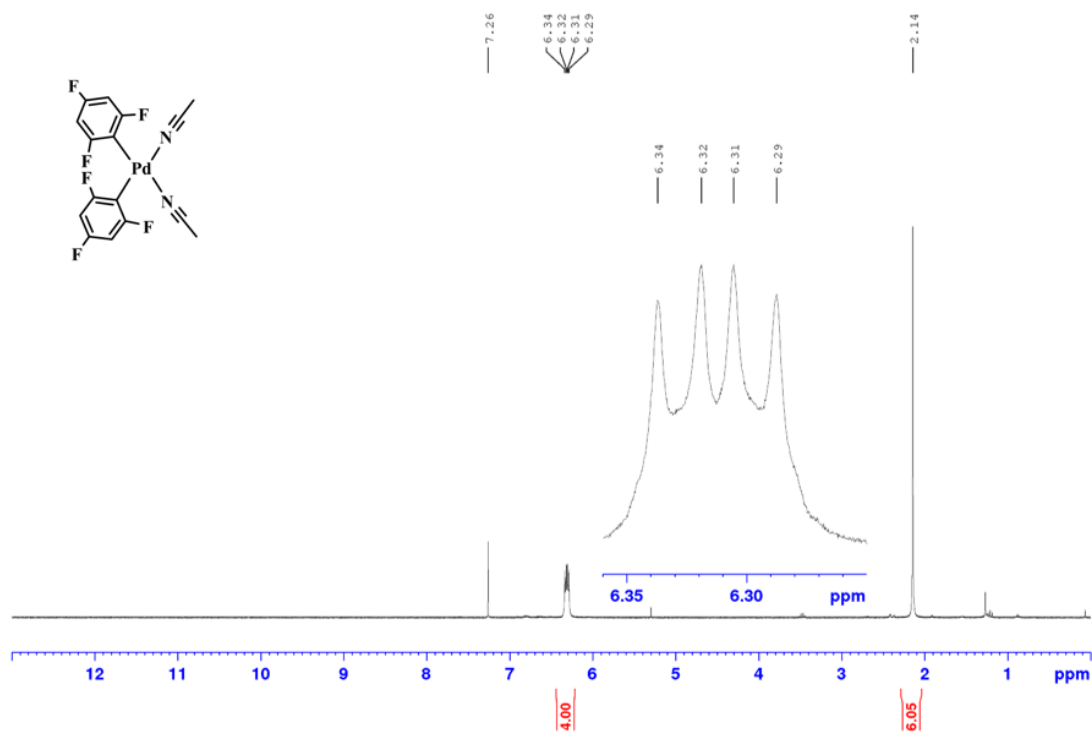
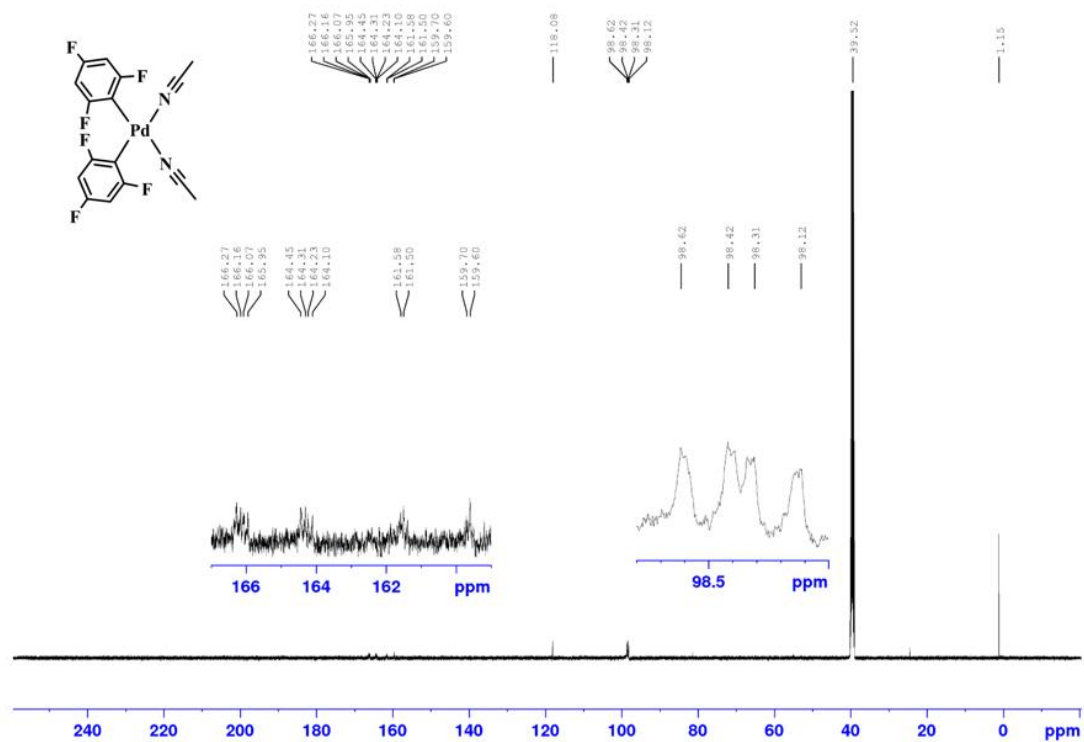
 ^1H NMR spectrum of 3_3a (500 MHz, DMSO- d_6) $^{13}\text{C}\{^1\text{H}\}$ NMR spectrum of 3_3a (125 MHz, DMSO- d_6)

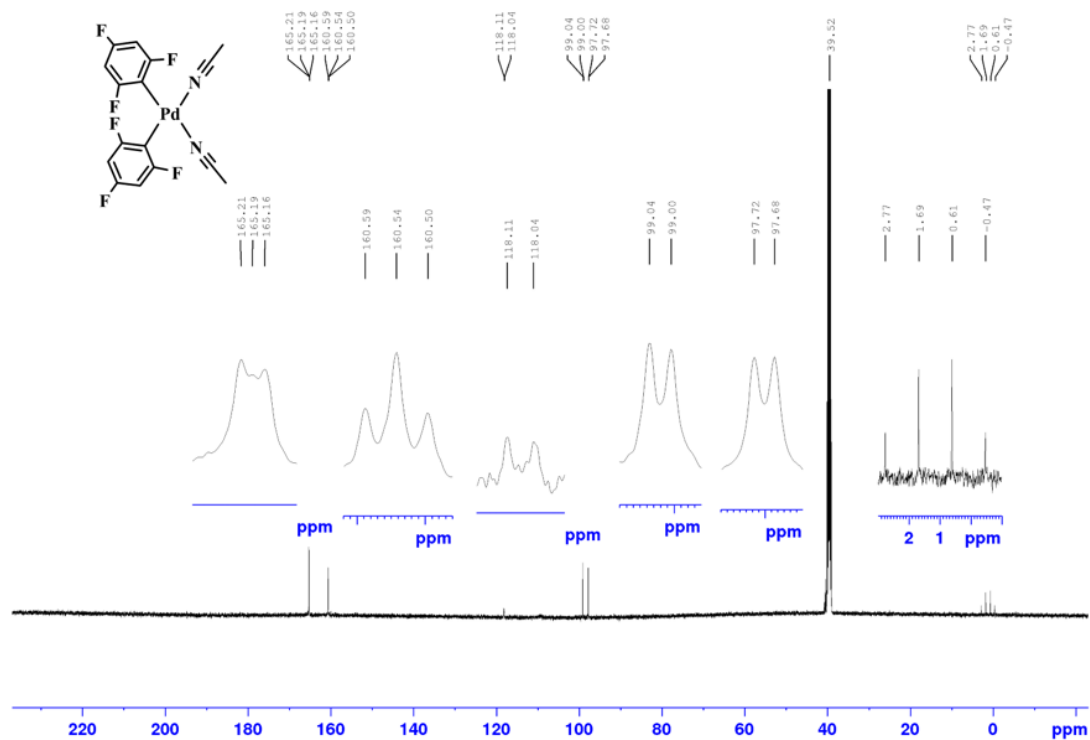
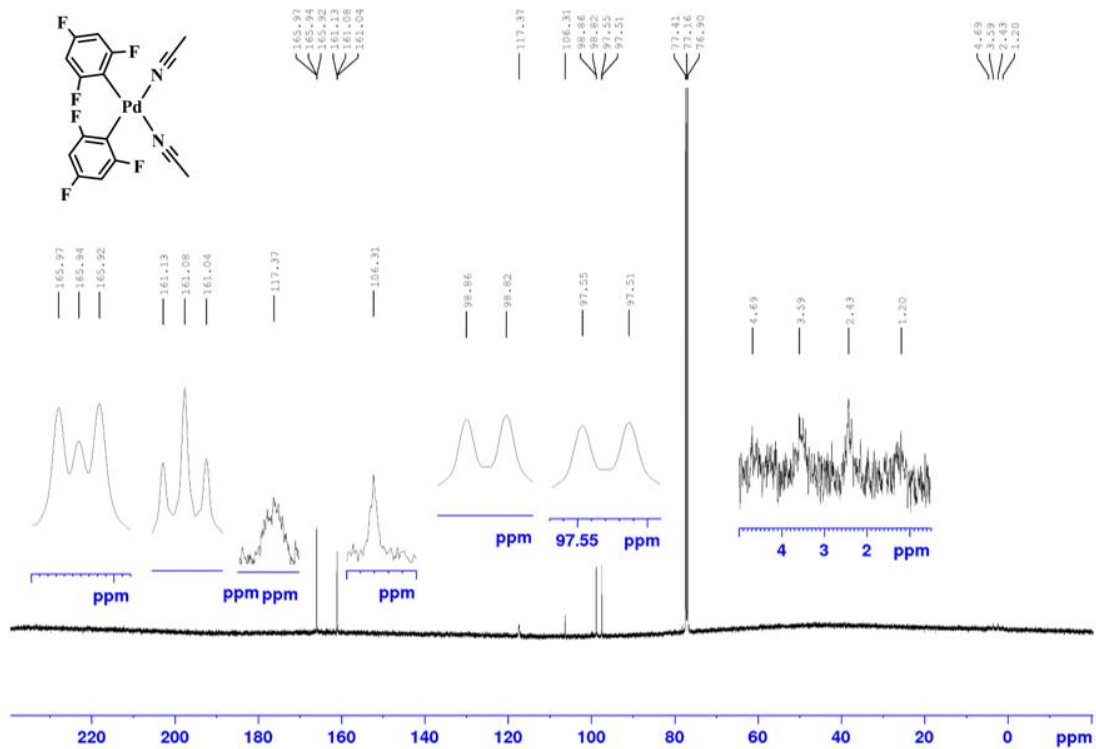
$^{13}\text{C}\{^{19}\text{F}\}$ NMR spectrum of 3_3a (125 MHz, $\text{DMSO-}d_6$) $^{13}\text{C}\{^{19}\text{F}\}$ NMR spectrum of 3_3a (125 MHz, CD_3CN)

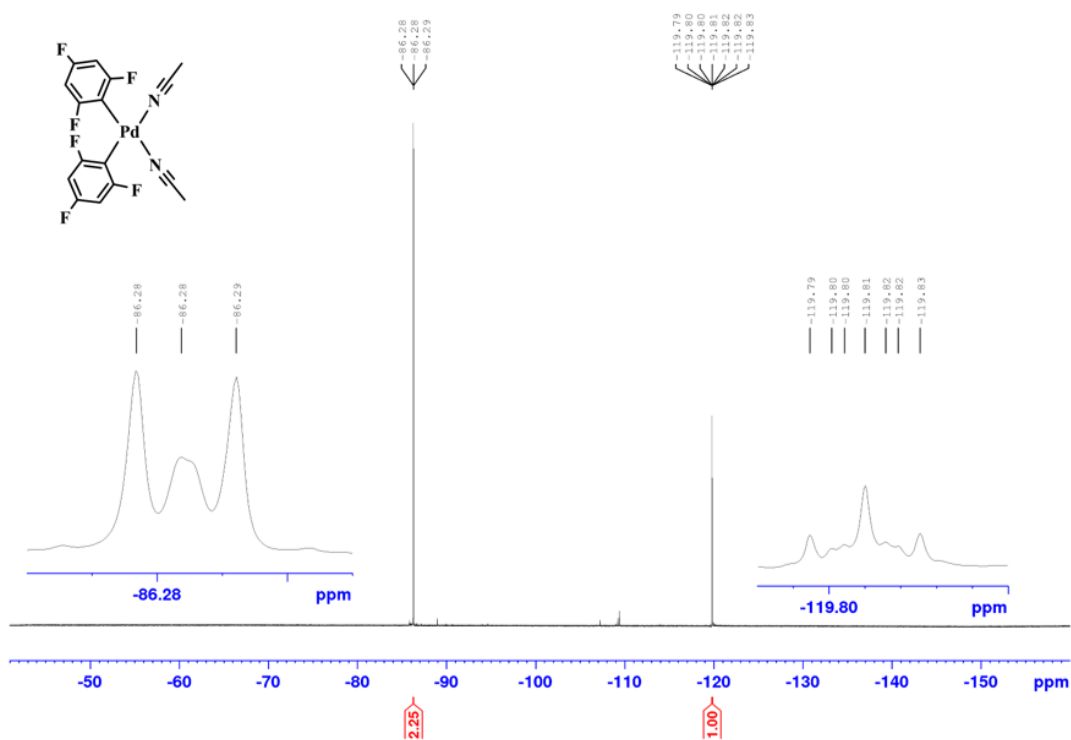
$^{19}\text{F}\{^1\text{H}\}$ NMR spectrum of 3_3a (376 MHz, CD_3CN)

IR spectrum of 3_3a in the solid-state

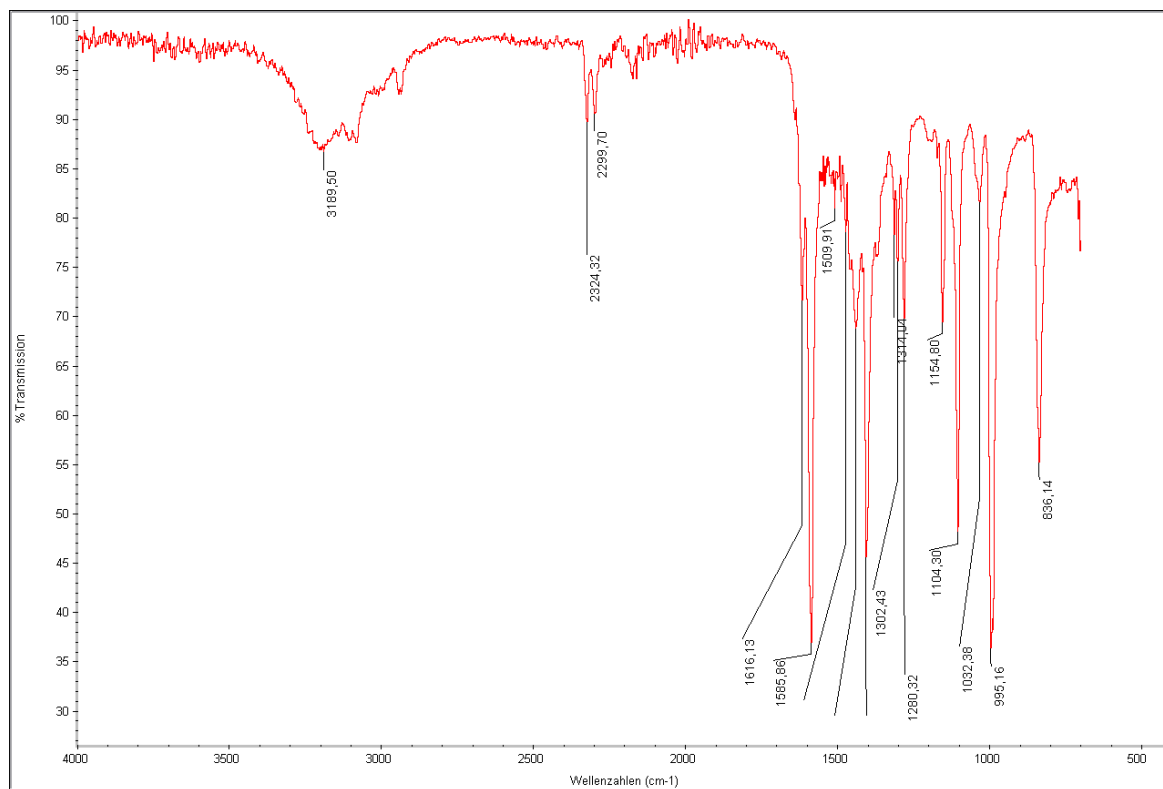


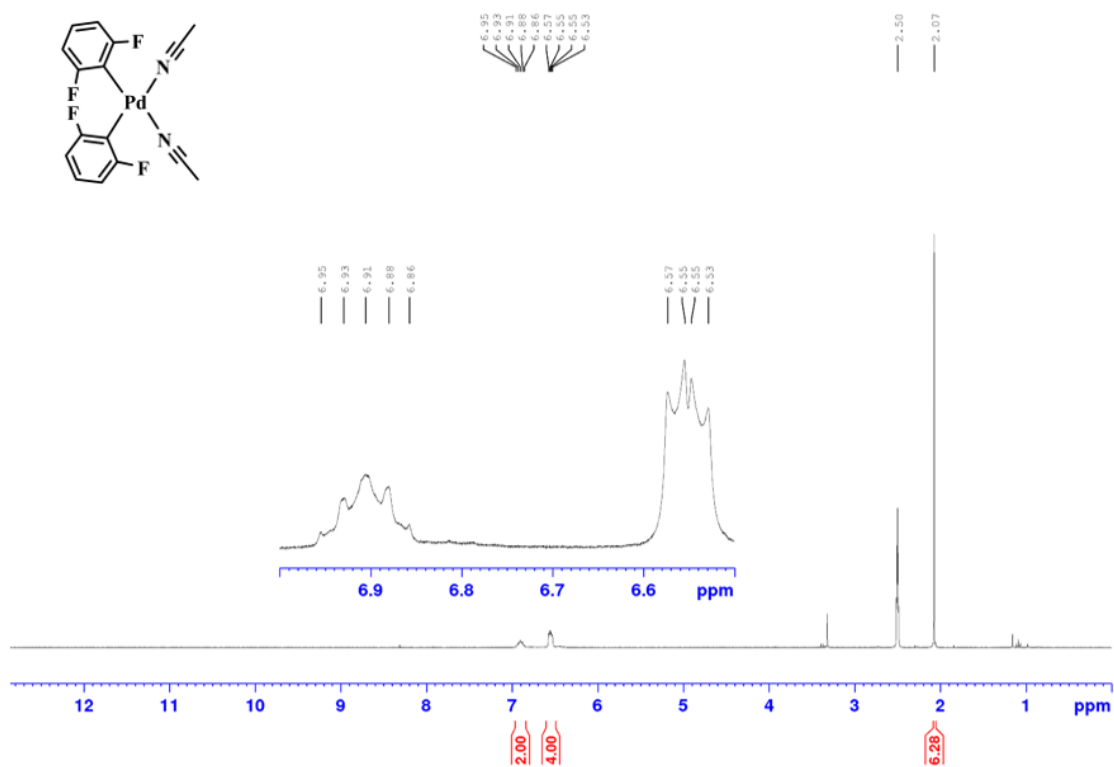
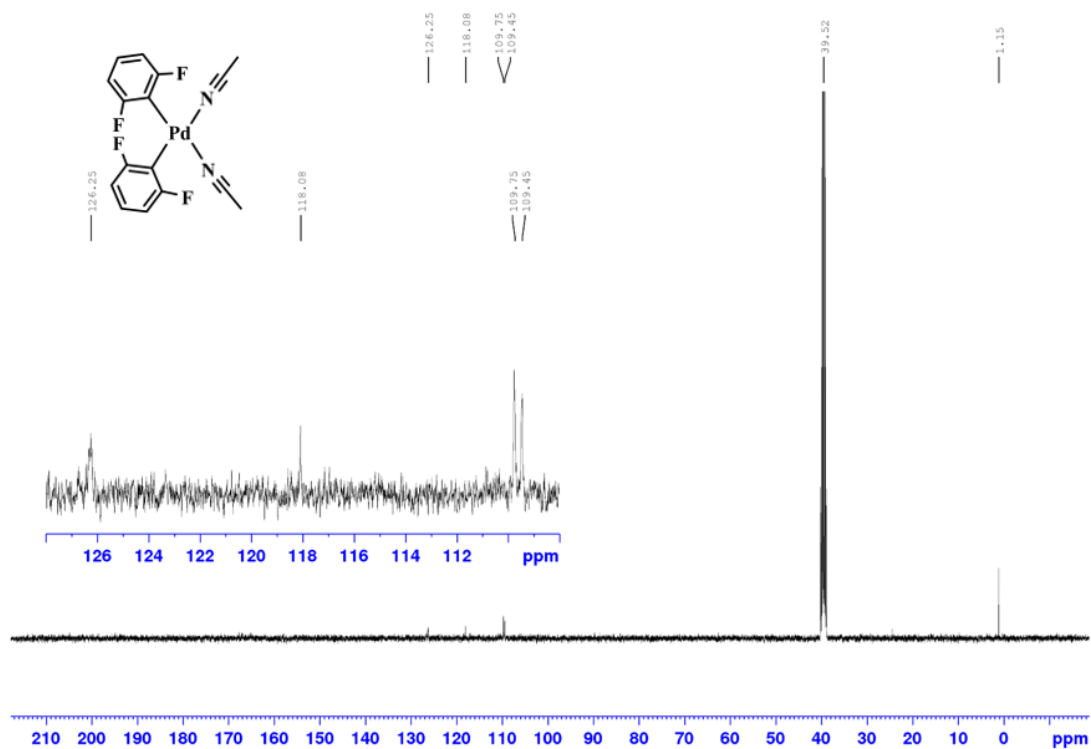
^1H NMR spectrum of 3_3b (300 MHz, CDCl_3) **$^{13}\text{C}\{^1\text{H}\}$ NMR spectrum of 3_3b (125 MHz, $\text{DMSO}-d_6$)**

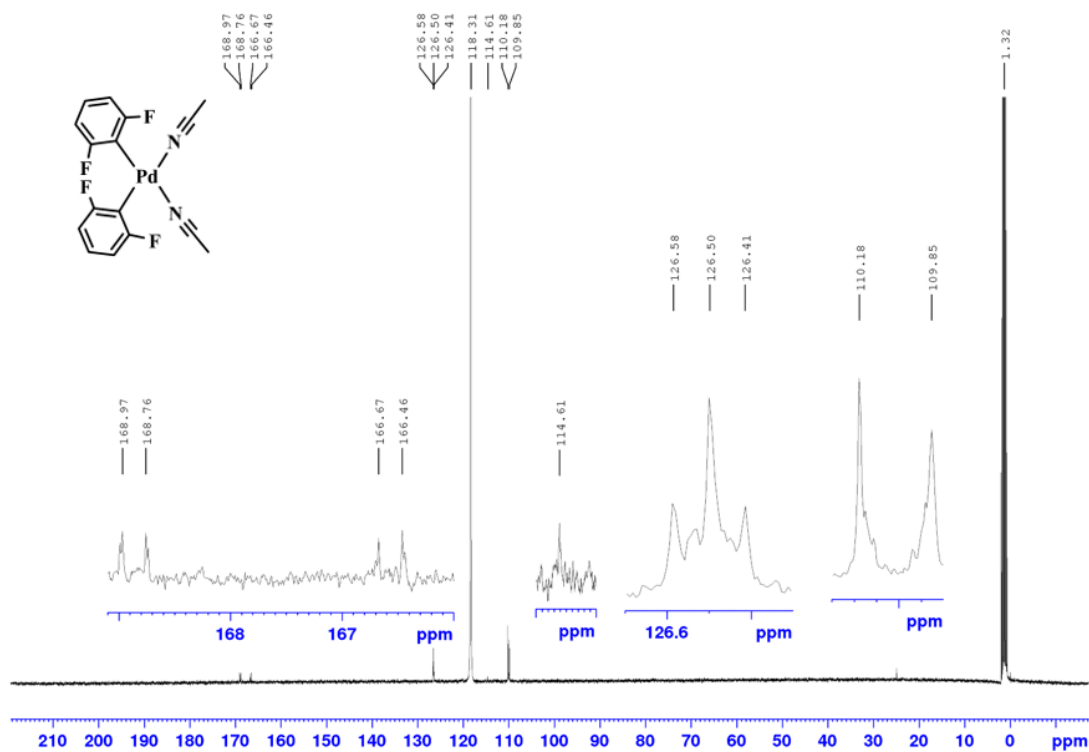
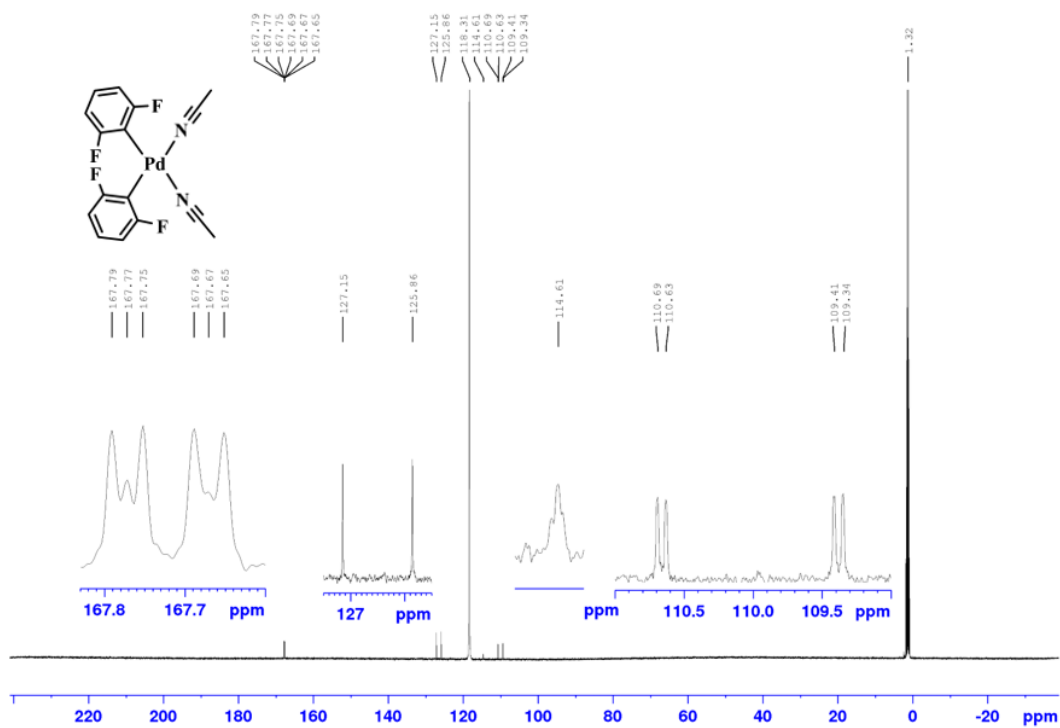
$^{13}\text{C}\{^{19}\text{F}\}$ NMR spectrum of 3_3b (125 MHz, DMSO- d_6) $^{13}\text{C}\{^{19}\text{F}\}$ NMR spectrum of 3_3b (125 MHz, CDCl_3)

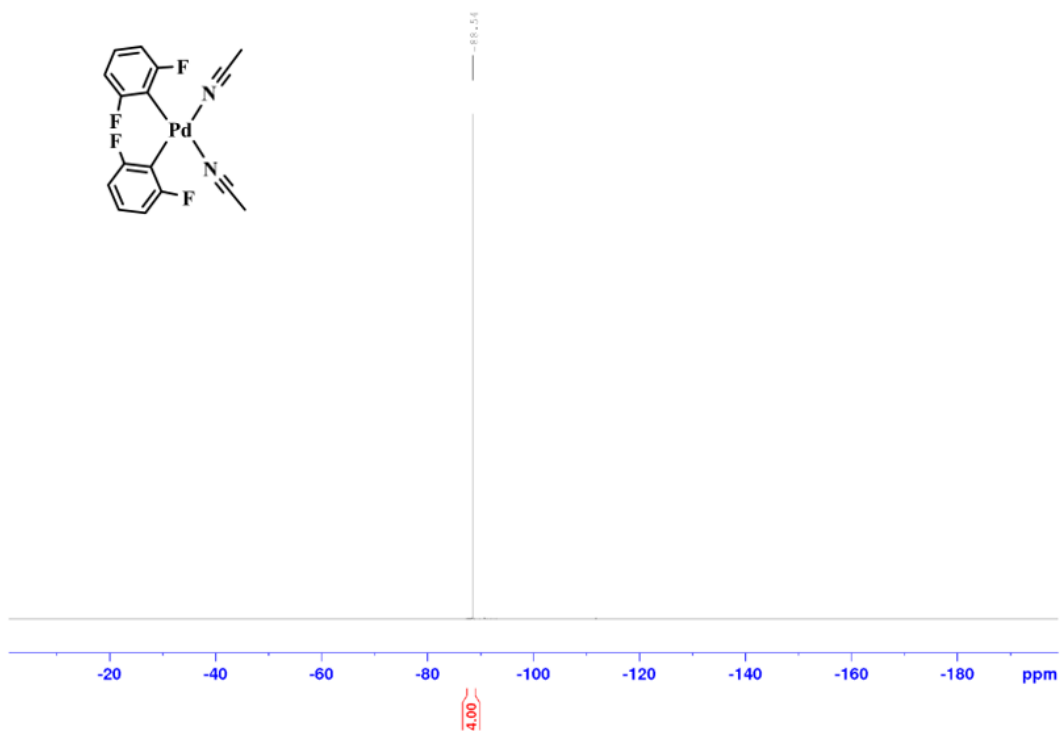
$^{19}\text{F}\{^1\text{H}\}$ NMR spectrum of 3_3b (376 MHz, CD_3CN)

IR spectrum of 3_3b in the solid-state

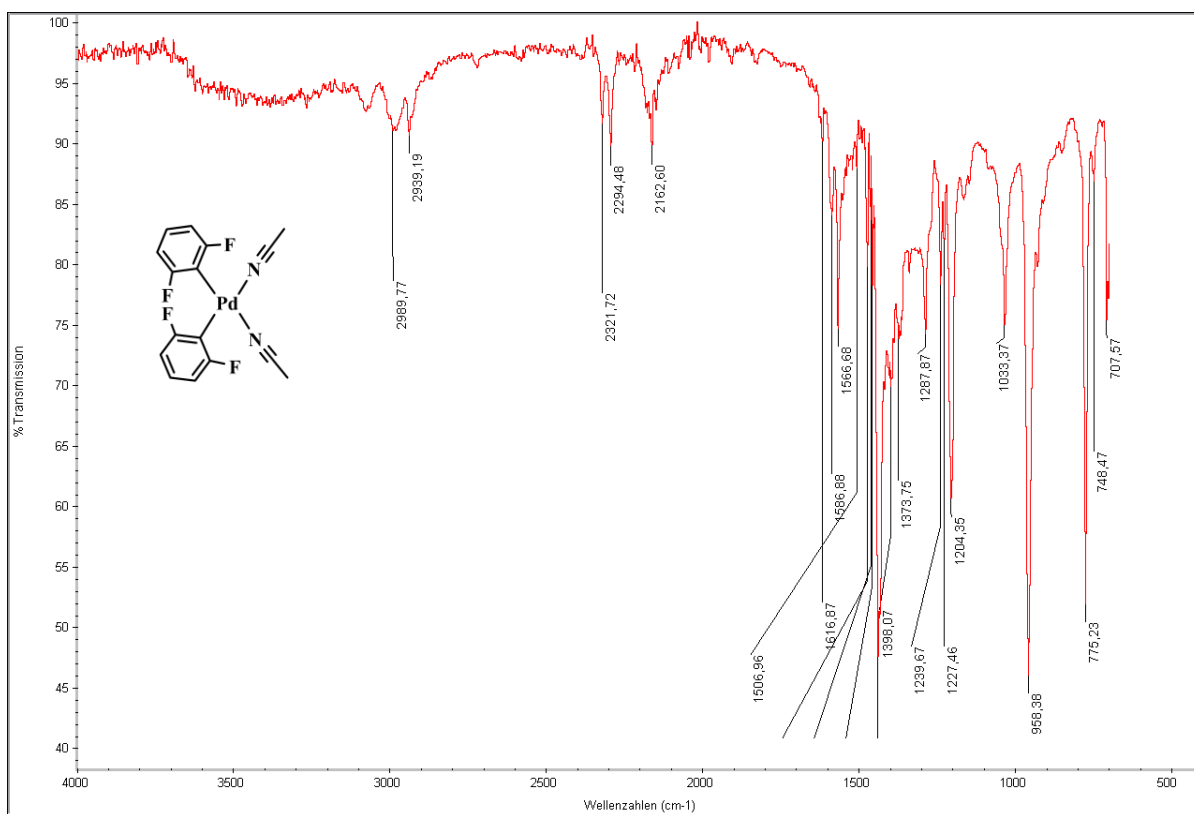


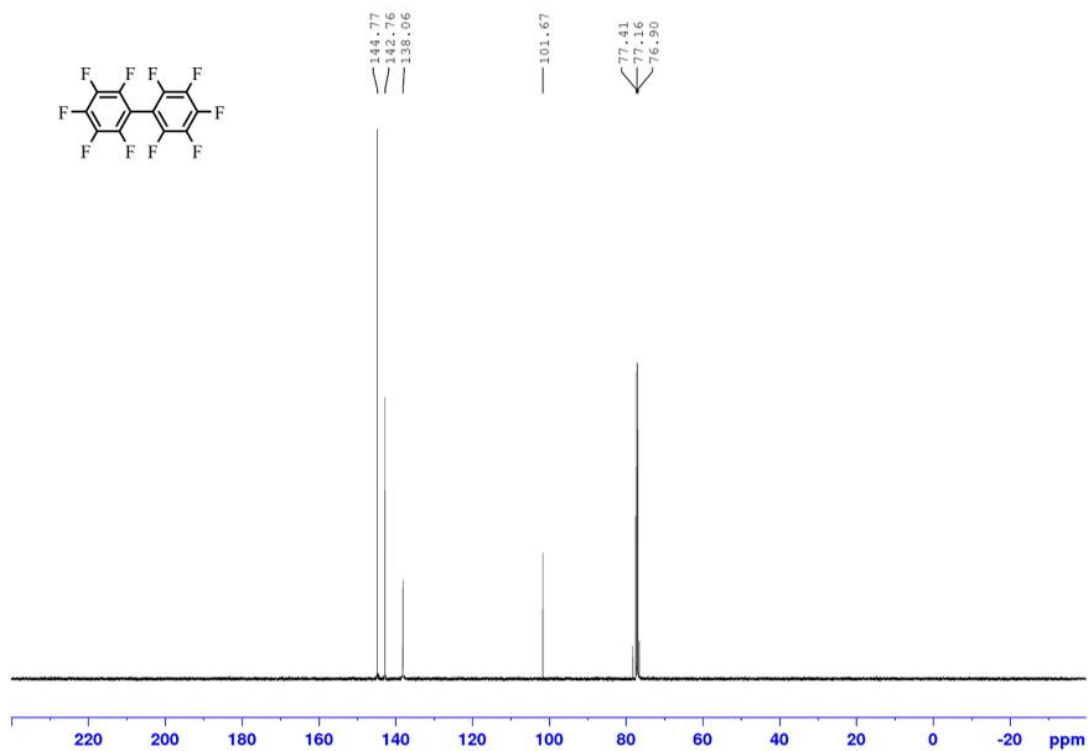
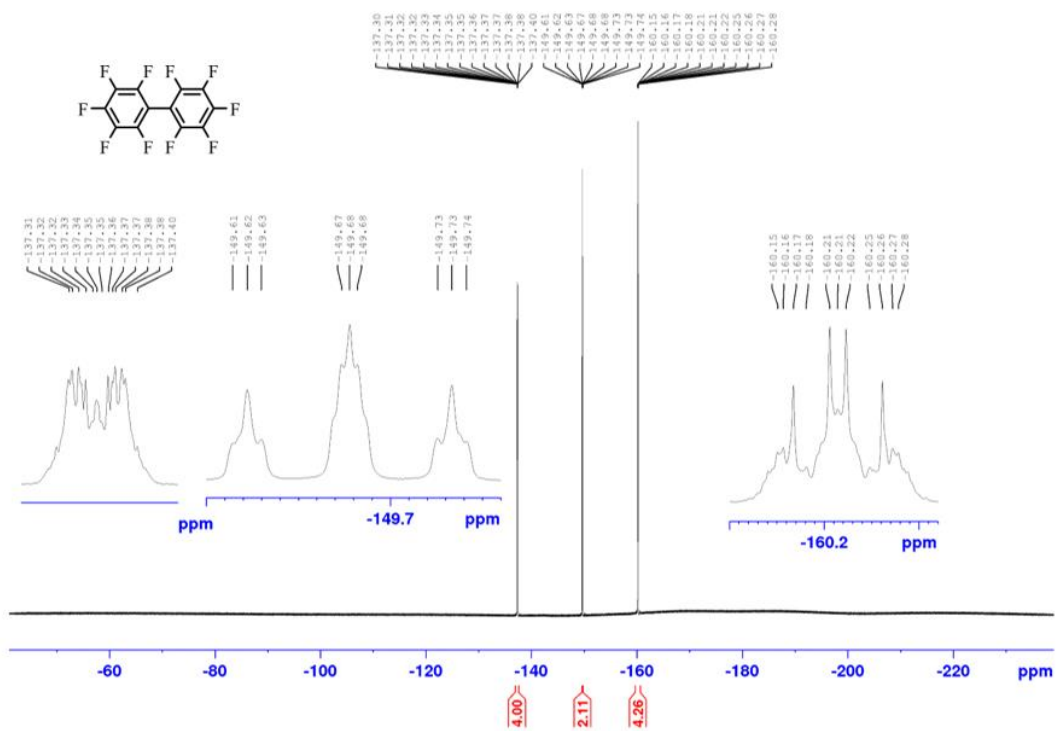
^1H NMR spectrum of 3_3e (300 MHz, DMSO- d_6) $^{13}\text{C}\{^1\text{H}\}$ NMR spectrum of 3_3e (101 MHz, DMSO- d_6)

$^{13}\text{C}\{^1\text{H}\}$ NMR spectrum of 3_3e (101 MHz, CD_3CN) $^{13}\text{C}\{^{19}\text{F}\}$ NMR spectrum of 3_3e (126 MHz, CD_3CN)

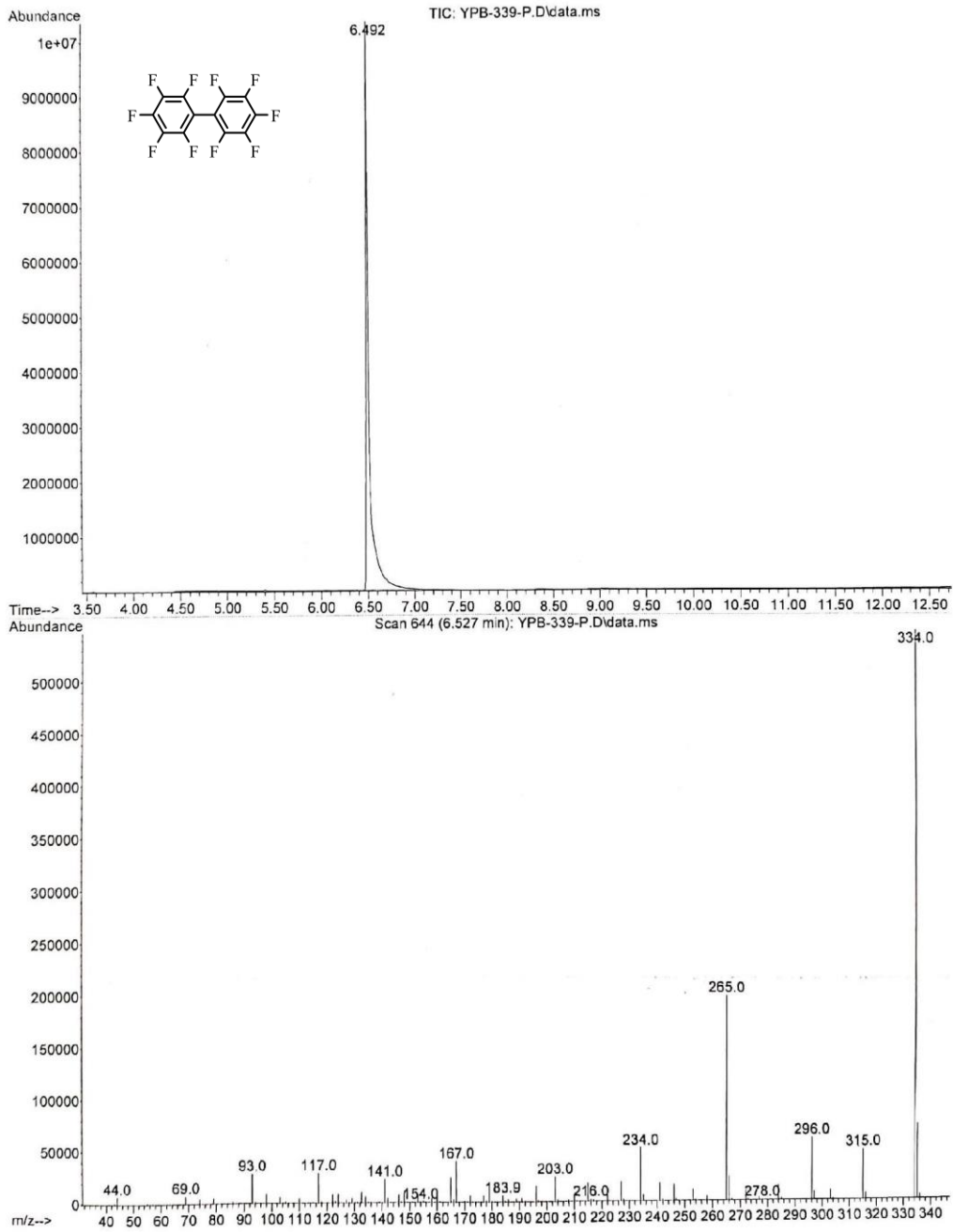
$^{19}\text{F}\{^1\text{H}\}$ NMR spectrum of 3_3e (376 MHz, CD_3CN)

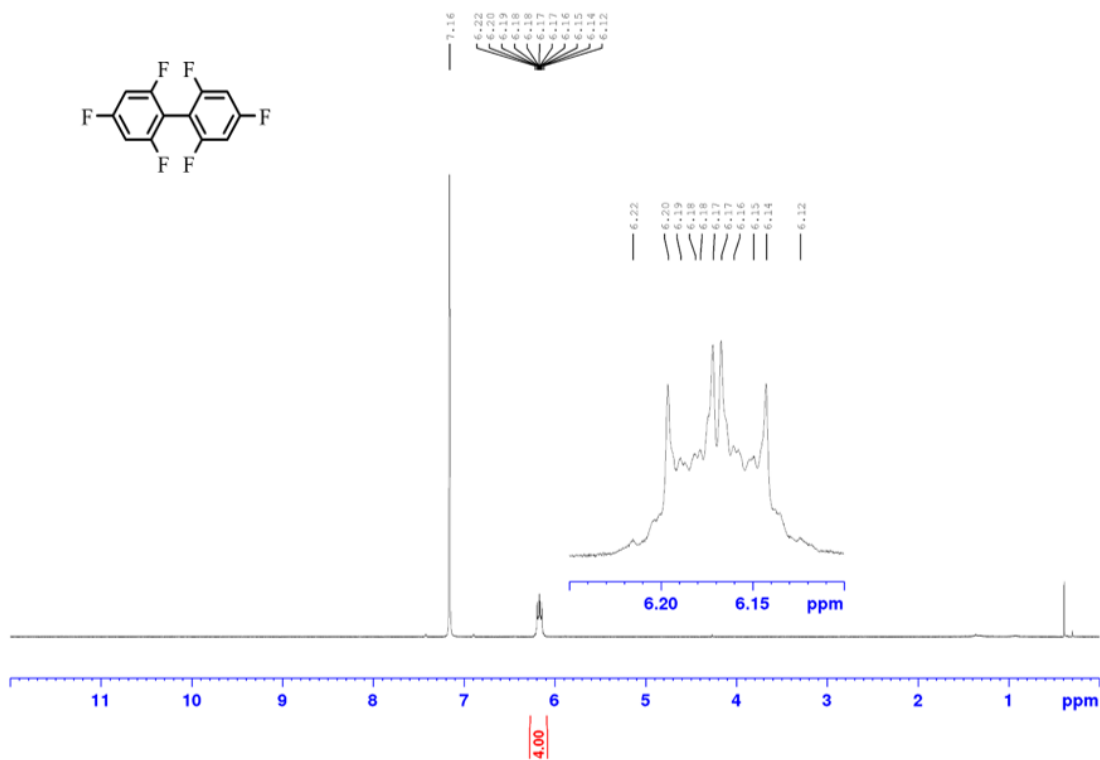
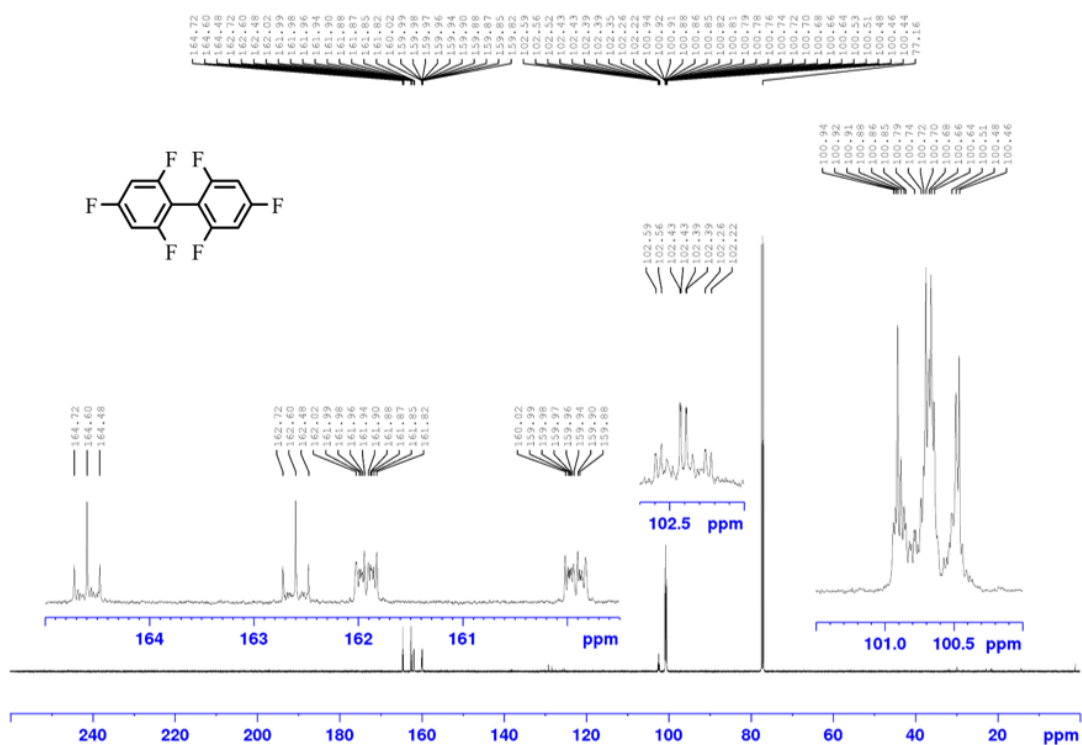
IR spectrum of 3_3e in the solid-state

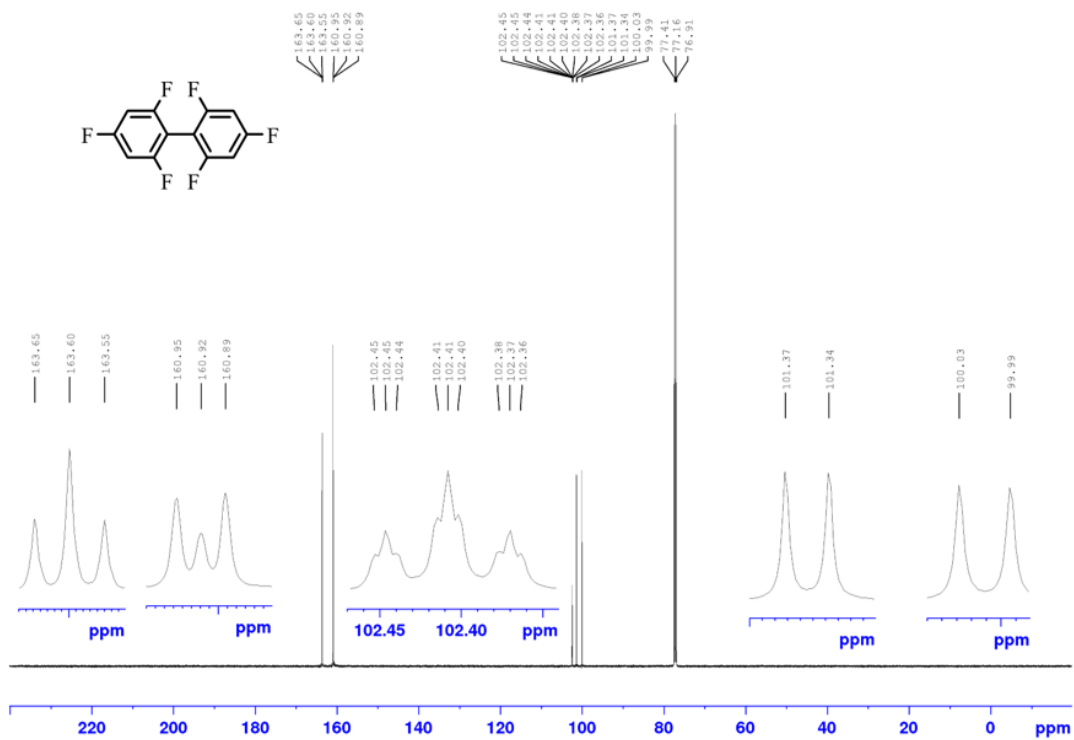
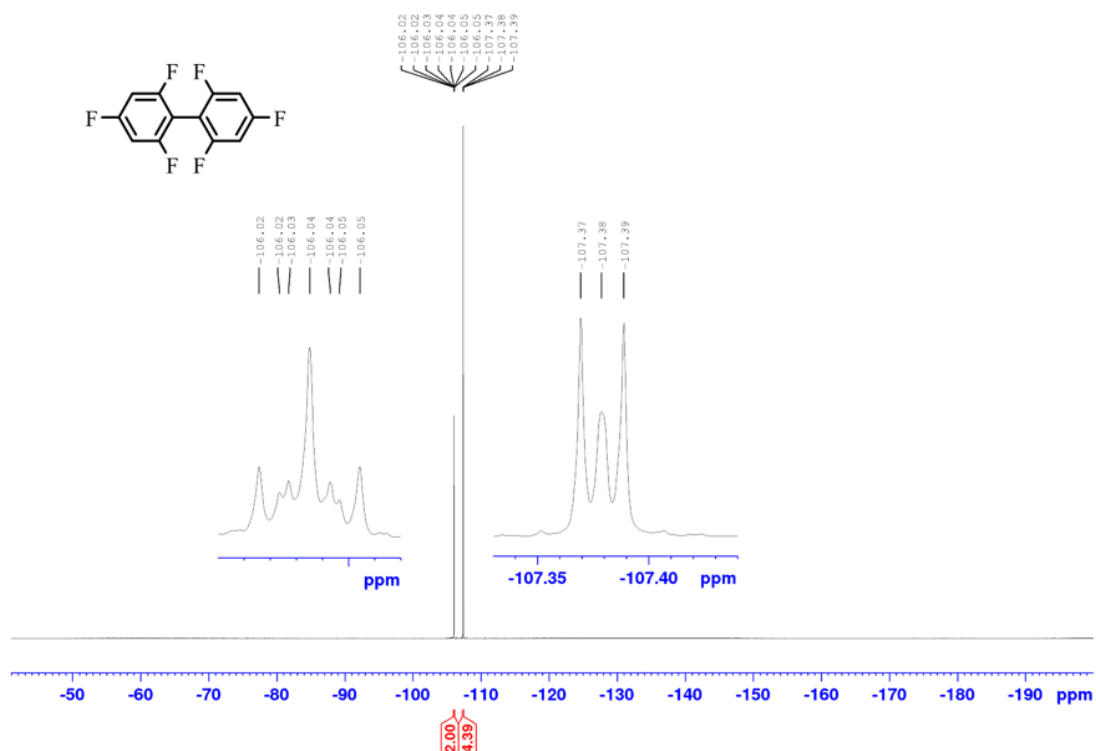


$^{13}\text{C}\{^{19}\text{F}\}$ NMR spectrum of 3_2a (125 MHz, CDCl_3) $^{19}\text{F}\{^1\text{H}\}$ NMR spectrum of 3_2a (376 MHz, CDCl_3)

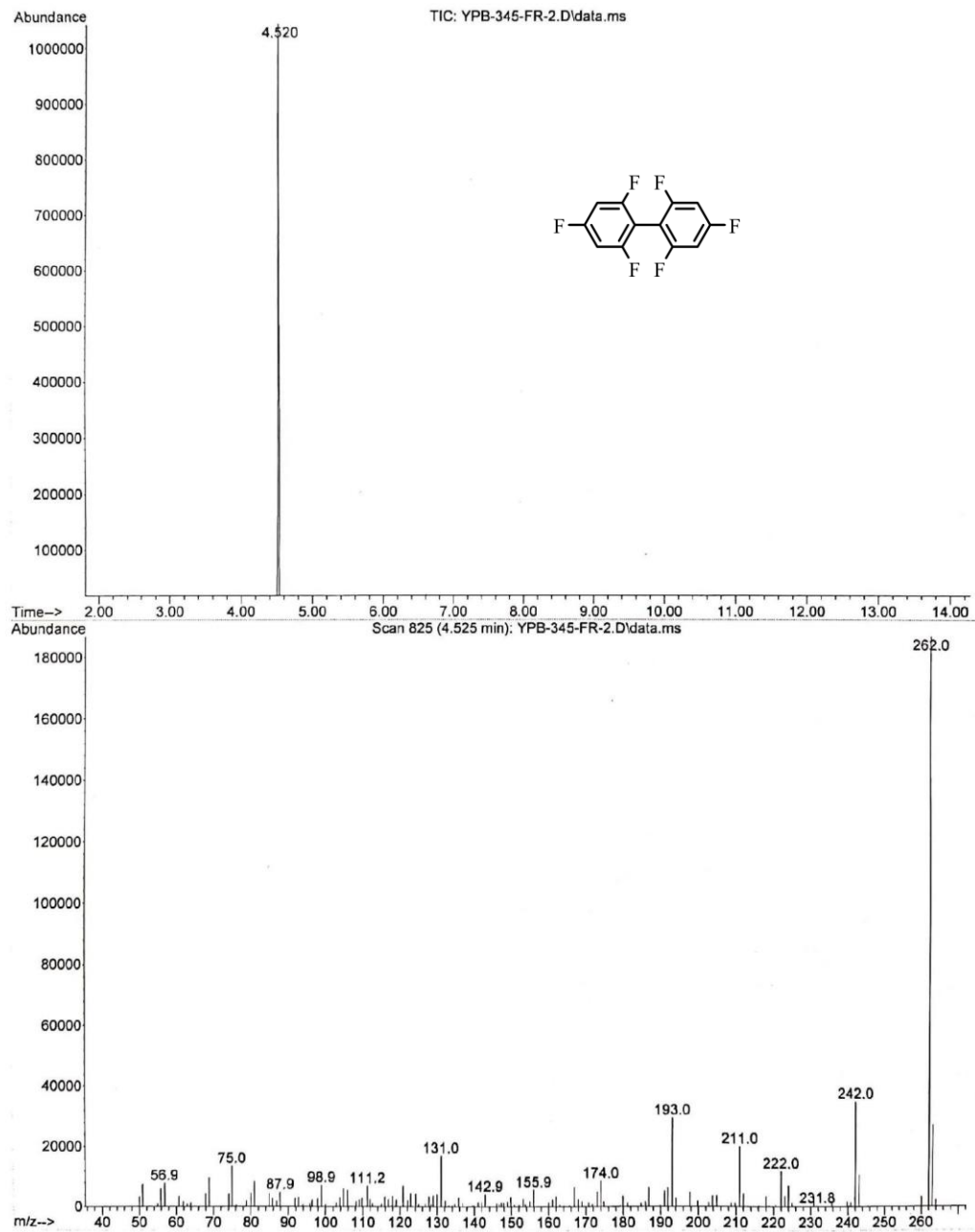
GC-MS of 3_2a

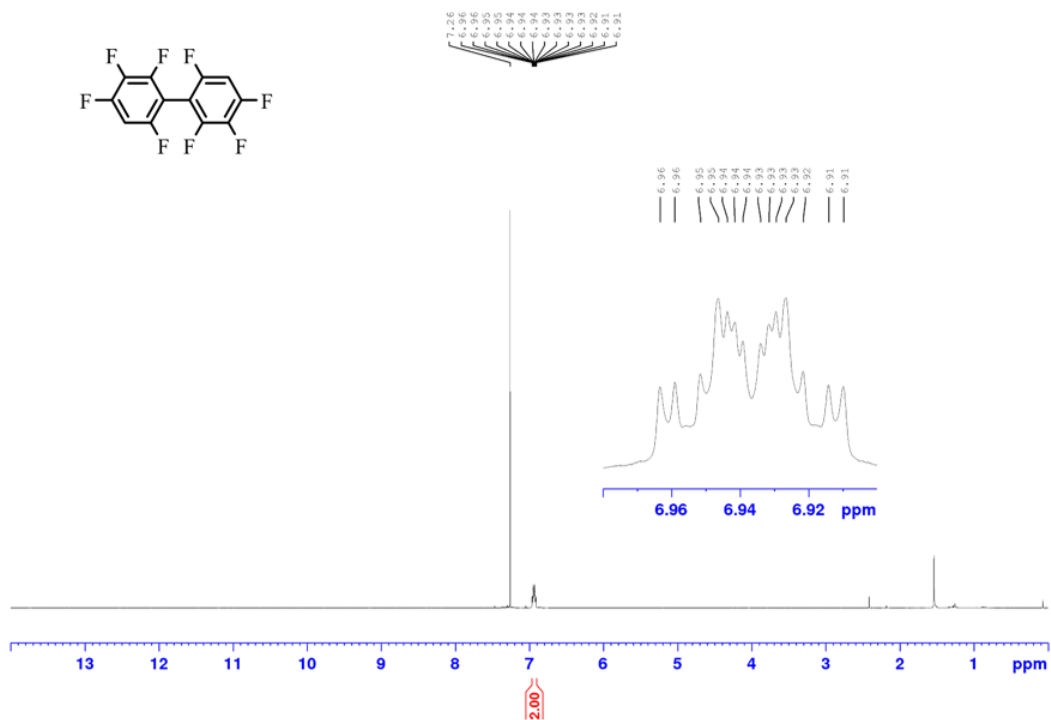
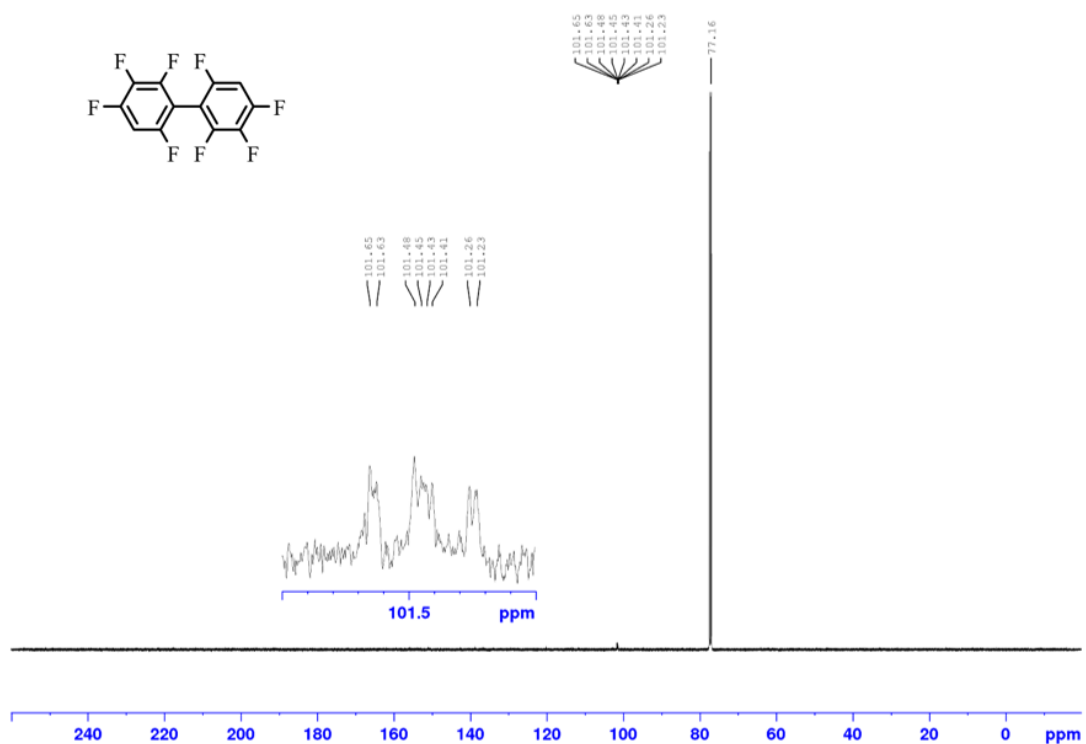


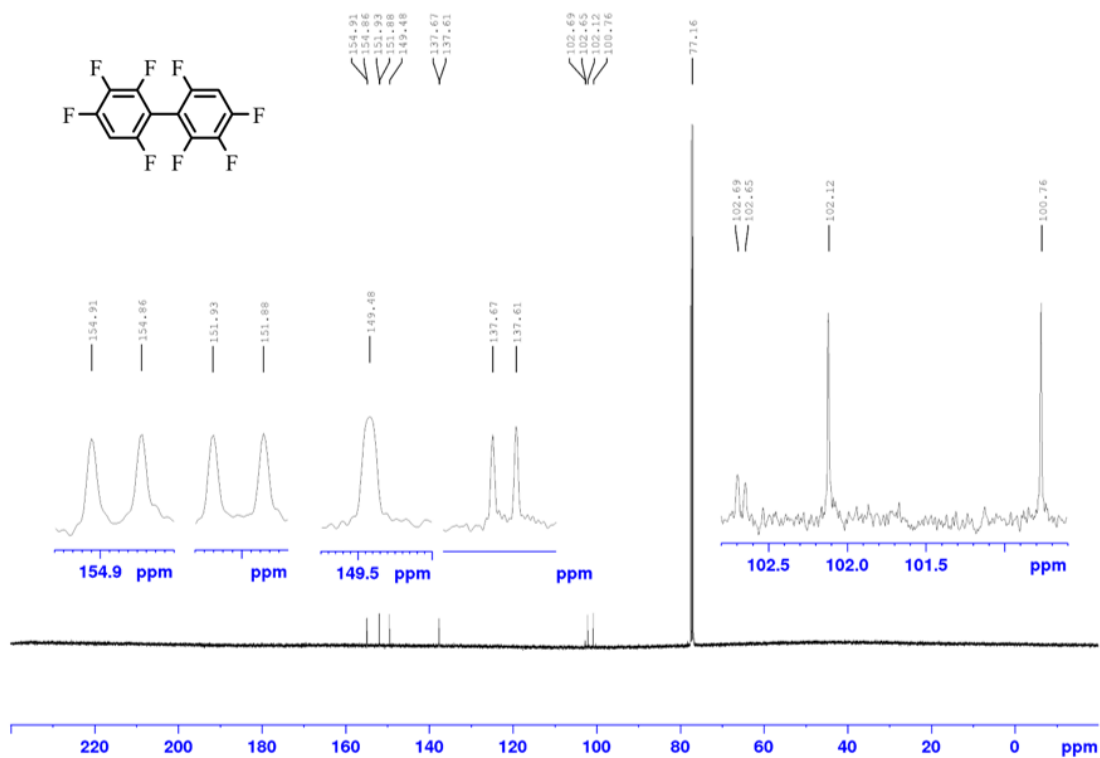
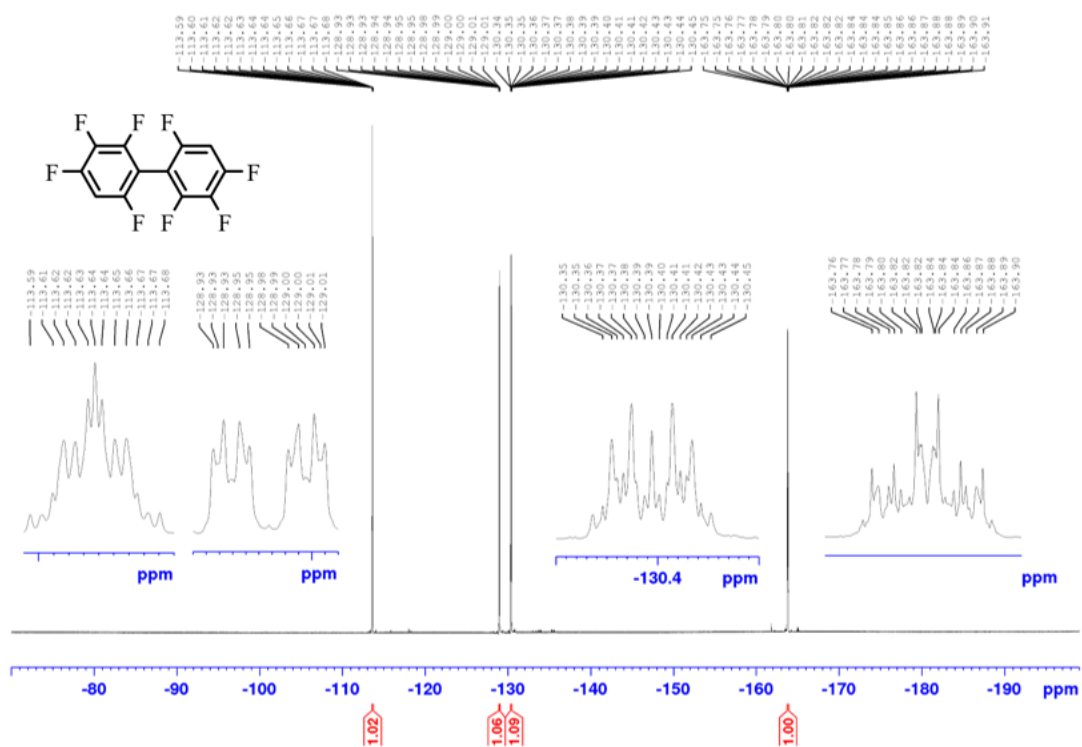
^1H NMR spectrum of 3_2b (300 MHz, C_6D_6) **$^{13}\text{C}\{^1\text{H}\}$ NMR spectrum of 3_2b (125 MHz, CDCl_3)**

$^{13}\text{C}\{^{19}\text{F}\}$ NMR spectrum of 3_2b (125 MHz, CDCl_3) $^{19}\text{F}\{^1\text{H}\}$ NMR spectrum of 3_2b (376 MHz, CDCl_3)

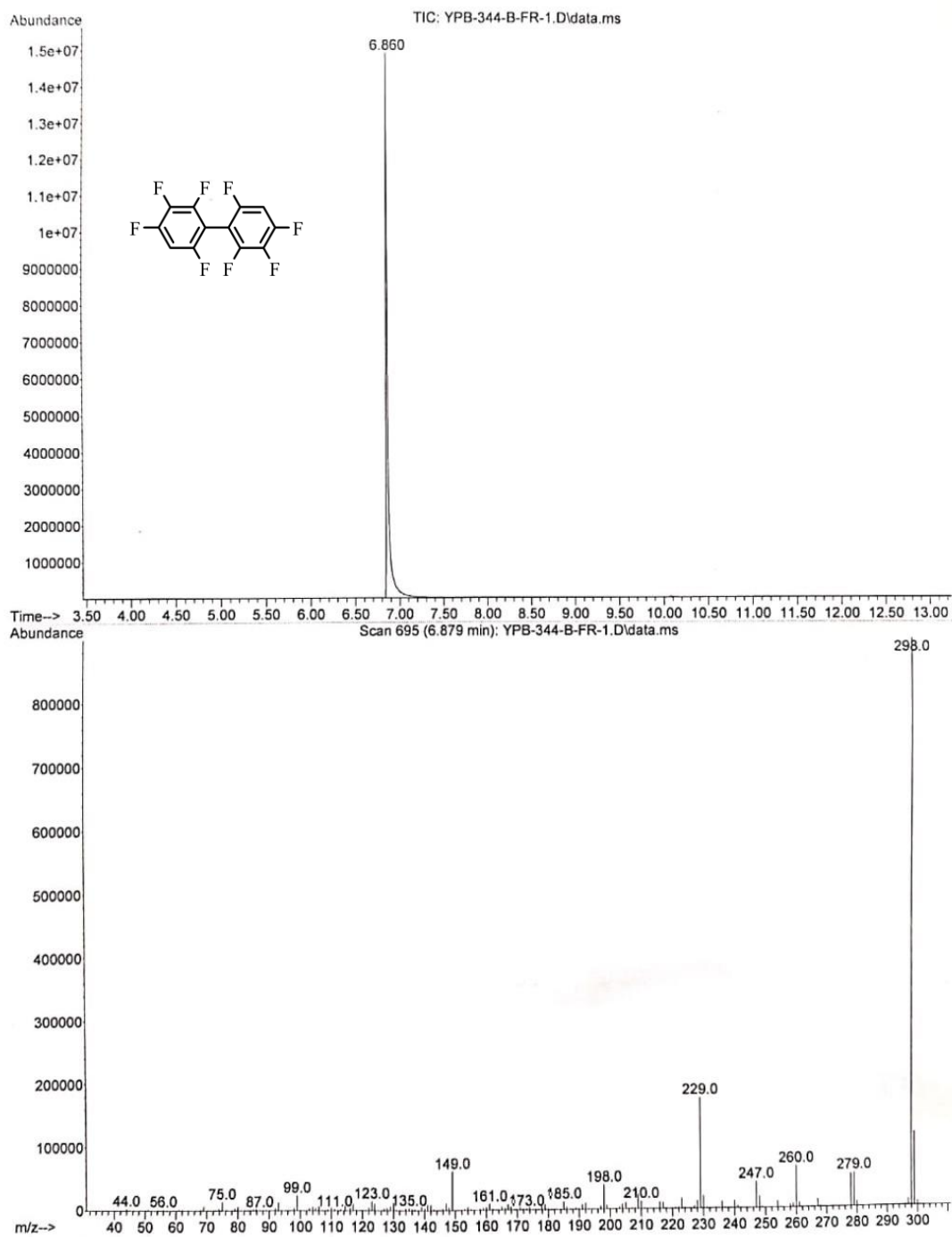
GC-MS of 3_2b

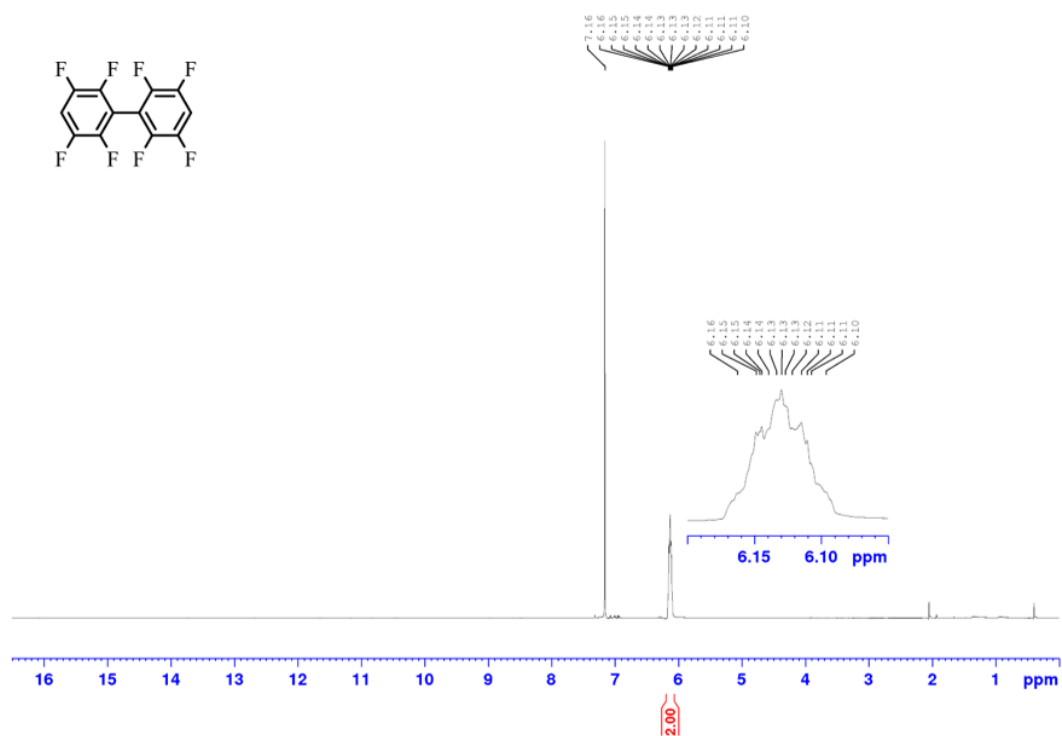
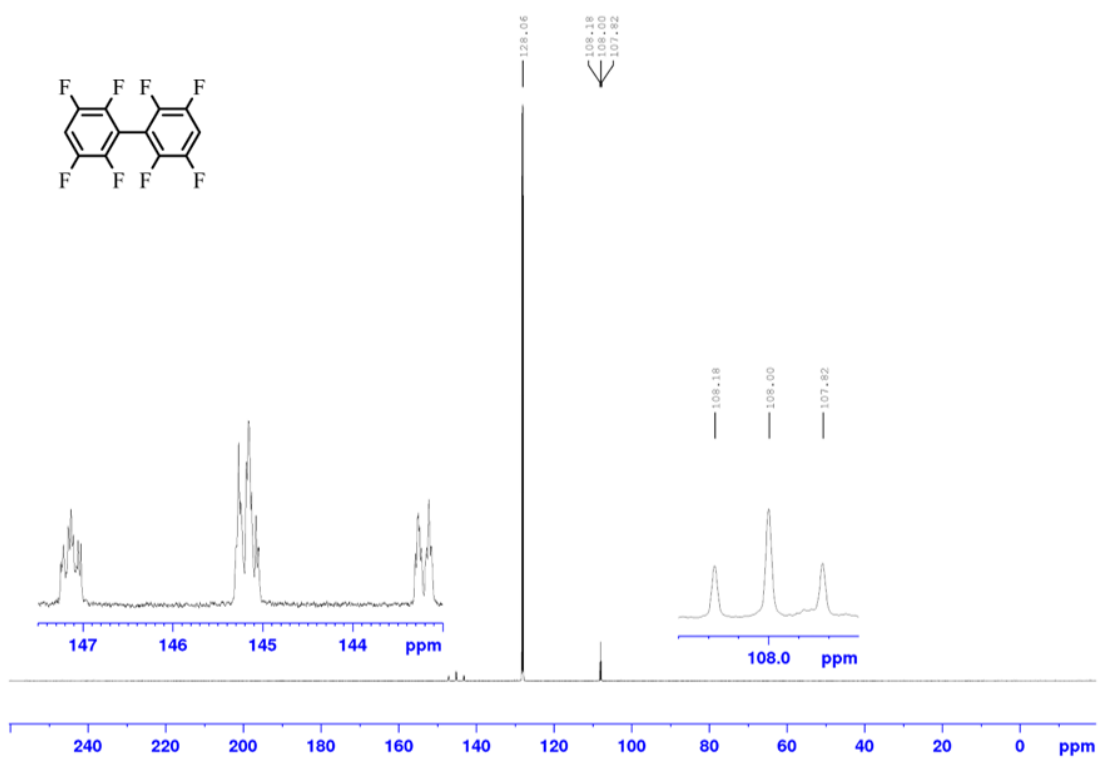


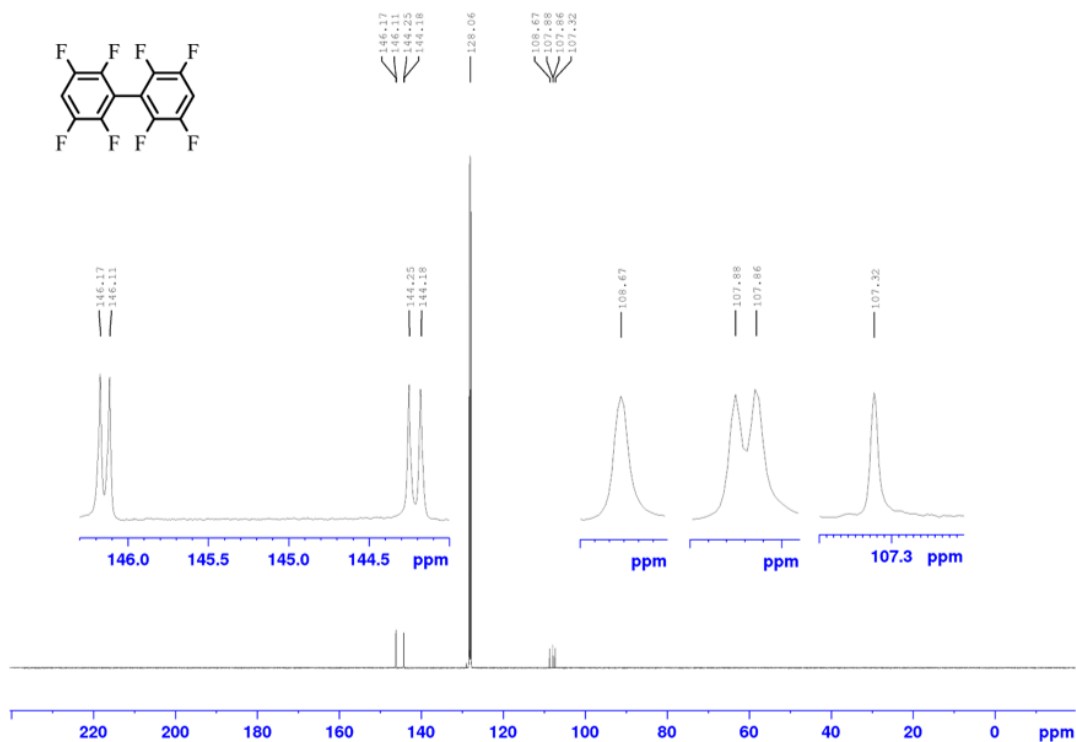
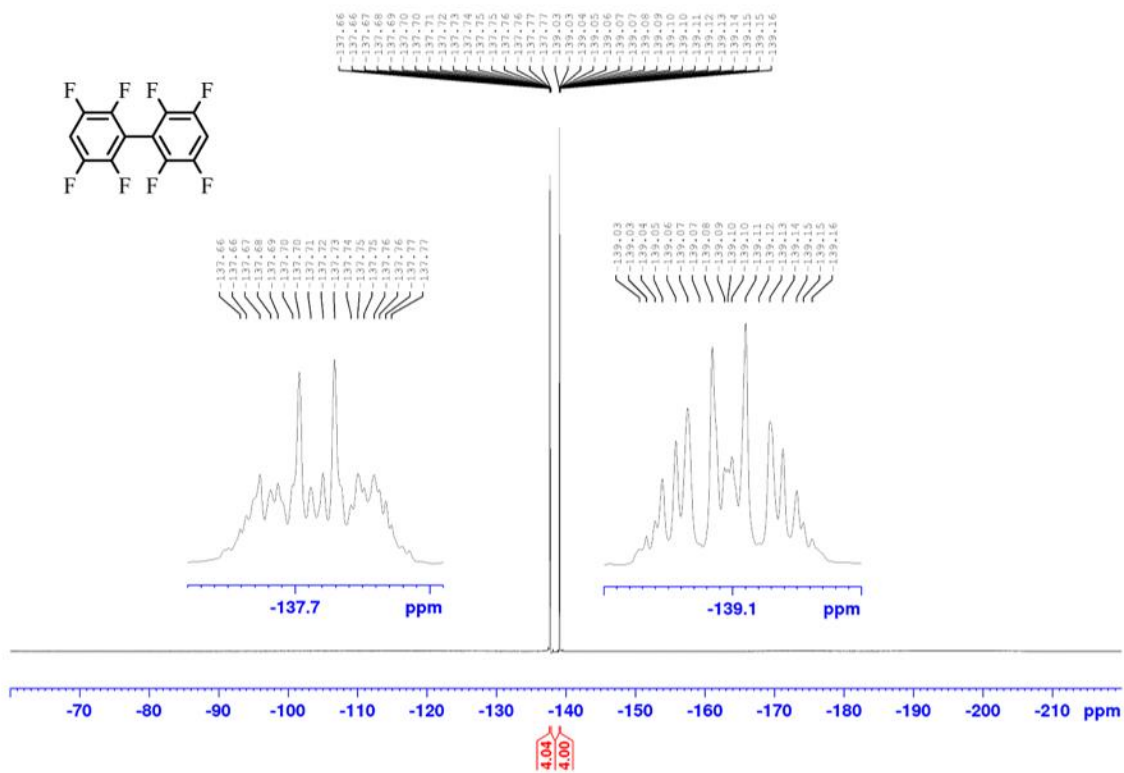
^1H NMR spectrum of 3_2c (500 MHz, CDCl_3) **$^{13}\text{C}\{^1\text{H}\}$ NMR spectrum of 3_2c (125 MHz, CDCl_3)**

$^{13}\text{C}\{^{19}\text{F}\}$ NMR spectrum of 3_2c (125 MHz, CDCl_3) $^{19}\text{F}\{^1\text{H}\}$ NMR spectrum of 3_2c (376 MHz, CDCl_3)

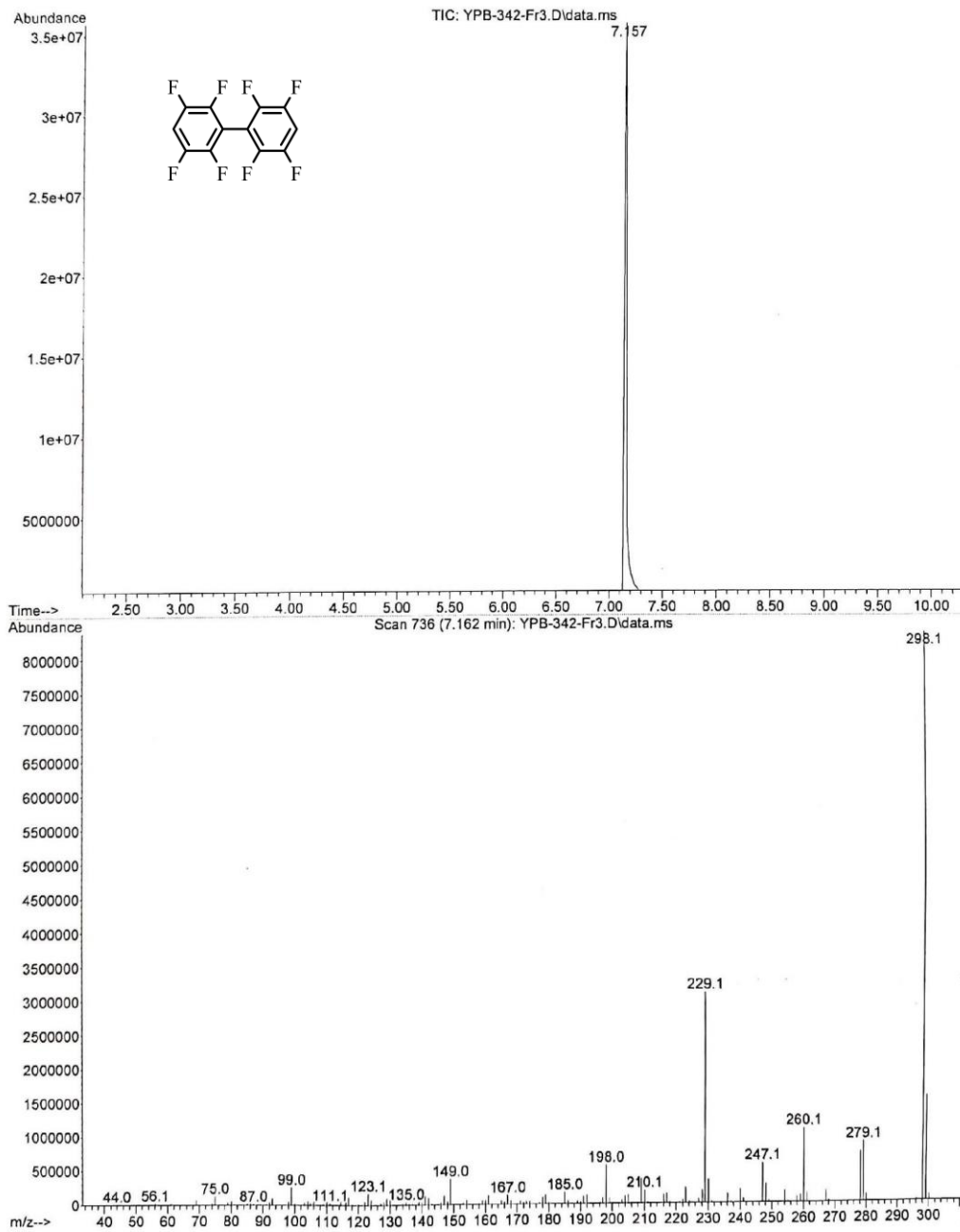
GC-MS of 3_2c

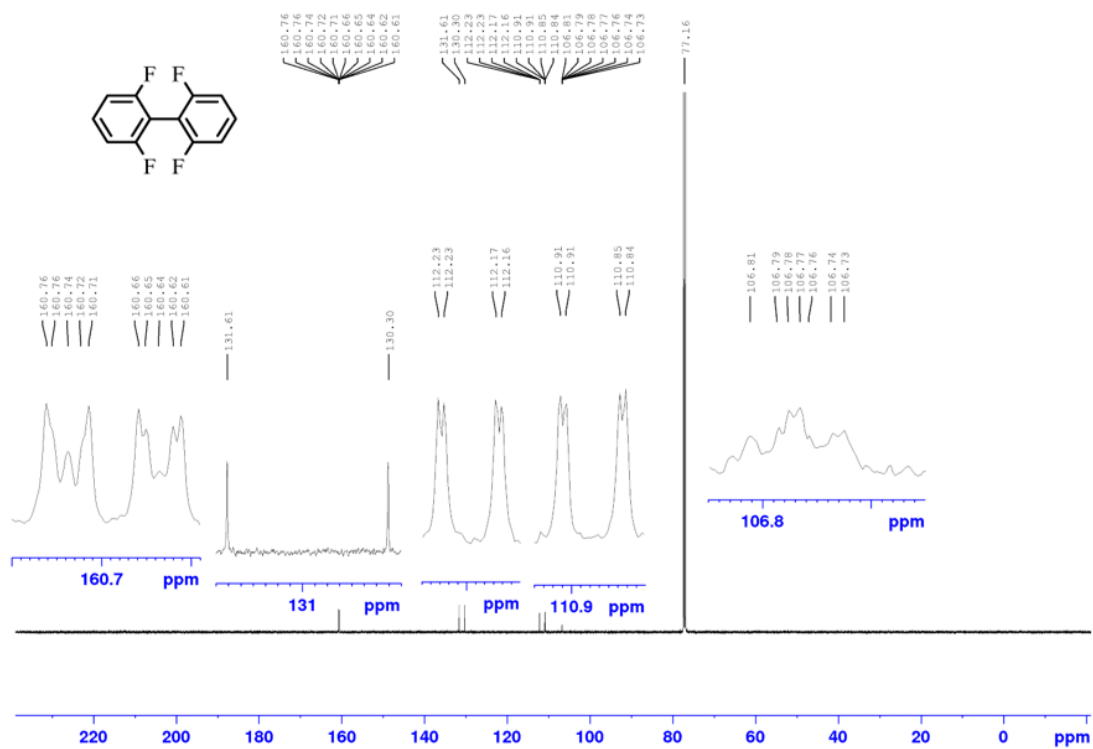
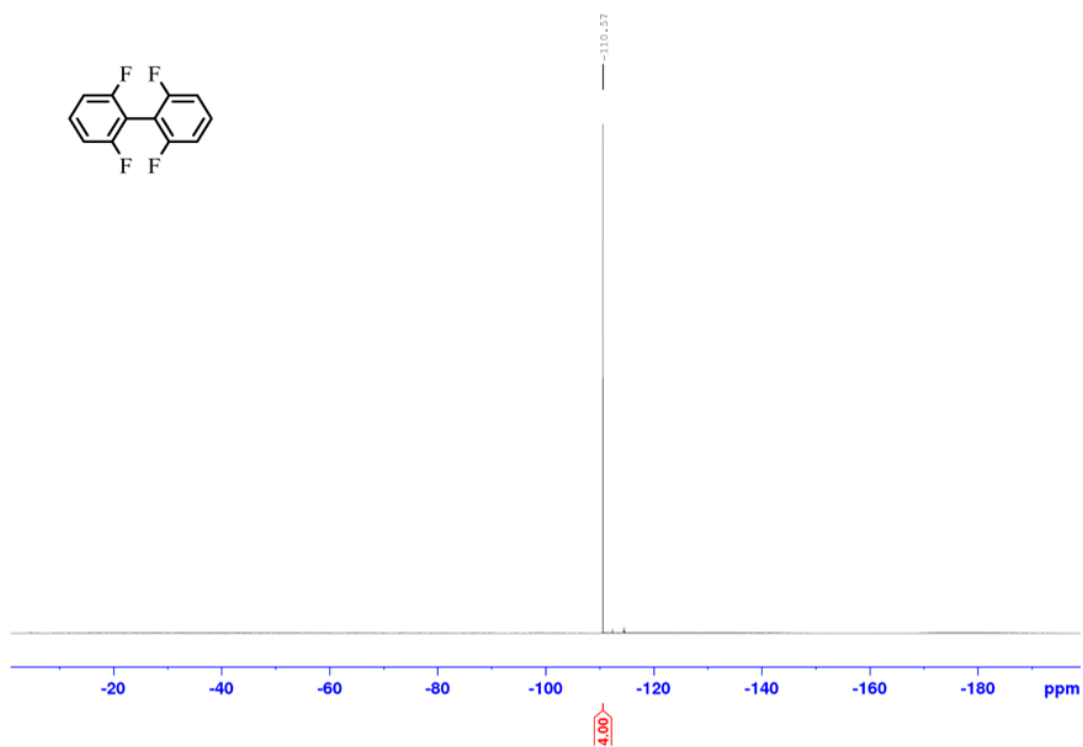


^1H NMR spectrum of 3_2d (500 MHz, C_6D_6) **$^{13}\text{C}\{^1\text{H}\}$ NMR spectrum of 3_2d (125 MHz, C_6D_6)**

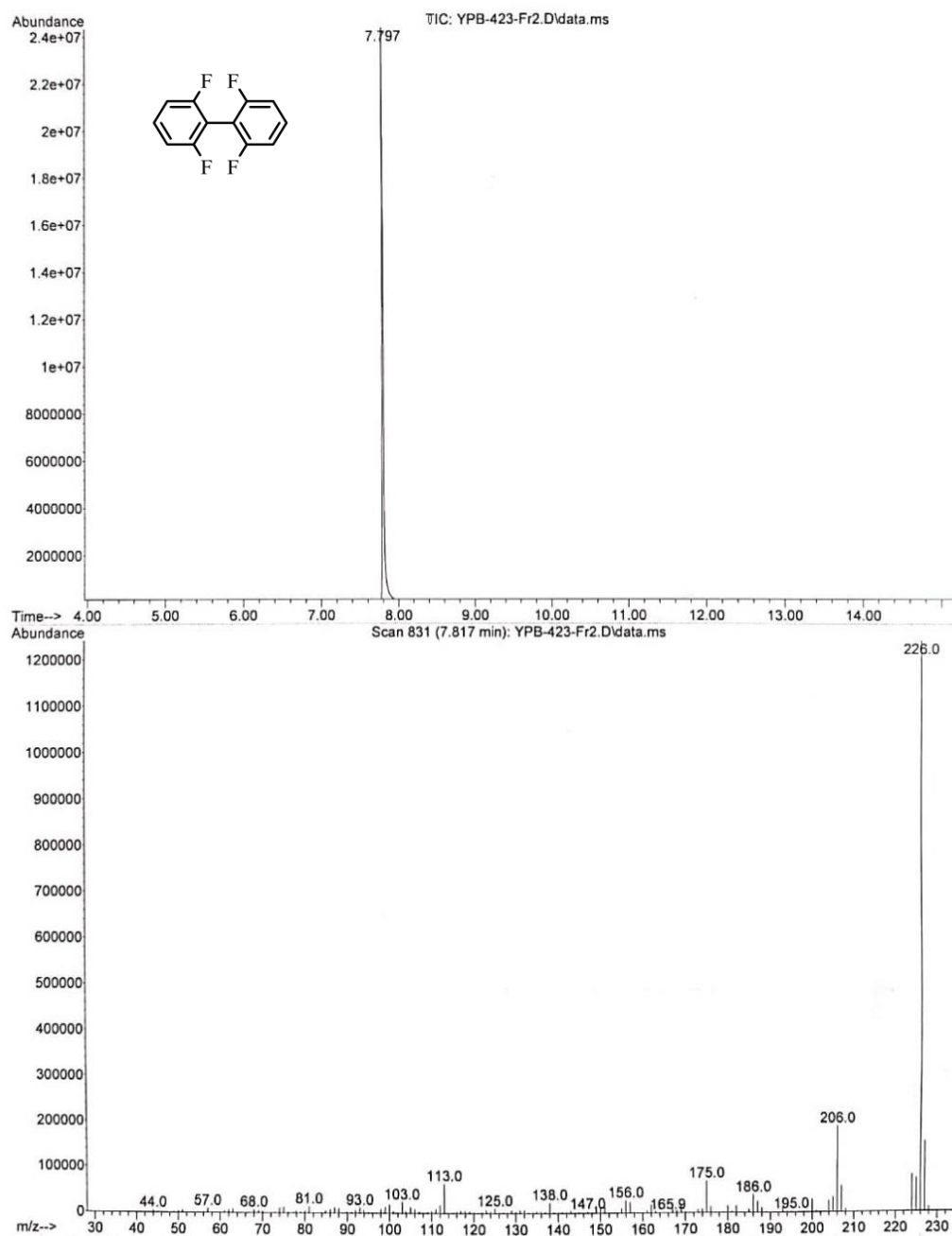
$^{13}\text{C}\{^{19}\text{F}\}$ NMR spectrum of 3_2d (125 MHz, C_6D_6) $^{19}\text{F}\{^1\text{H}\}$ NMR spectrum of 3_2d (376 MHz, C_6D_6)

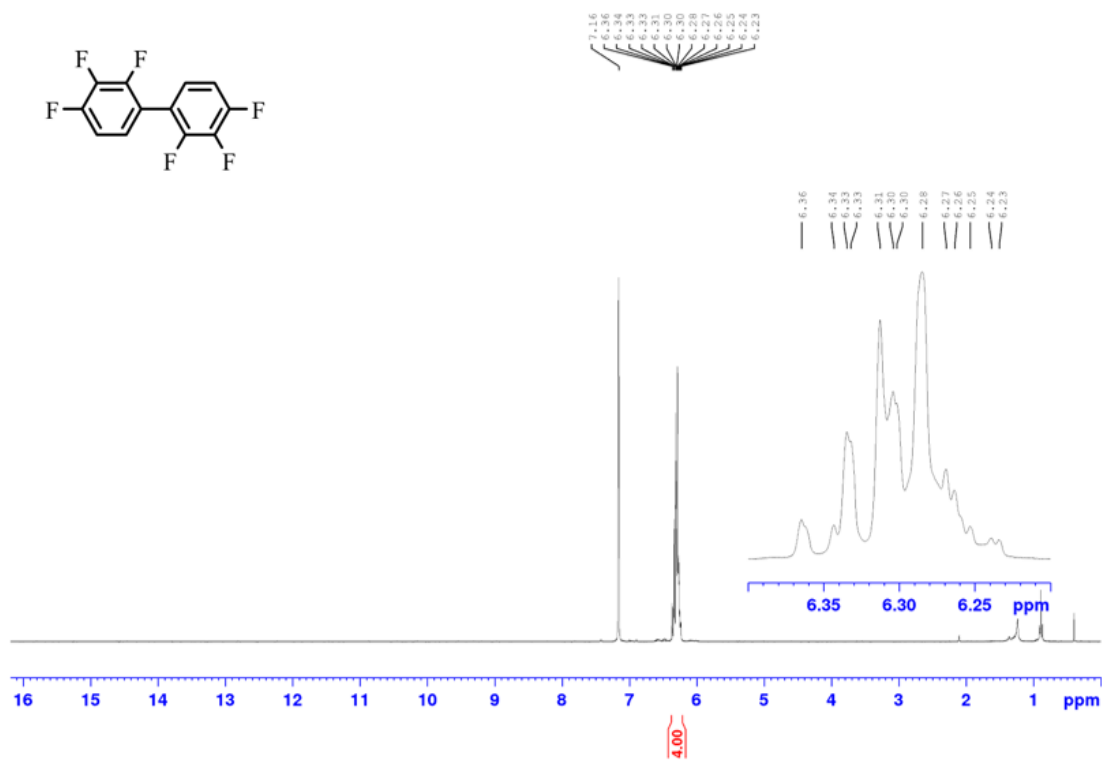
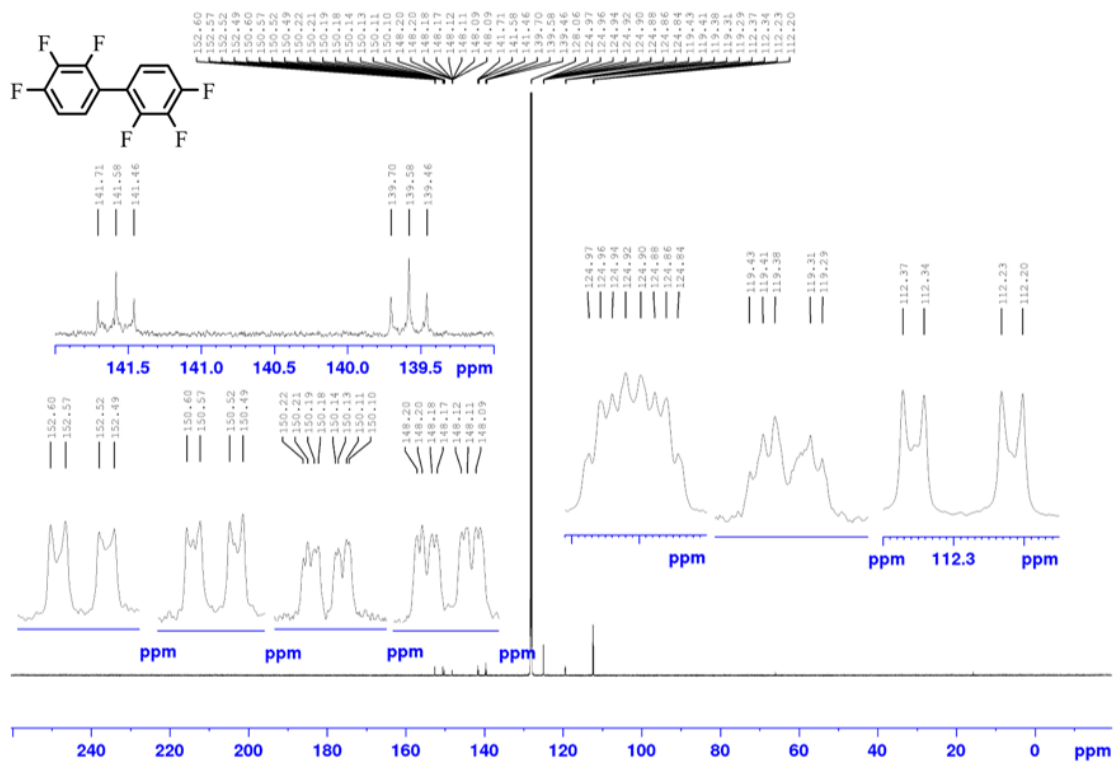
GC-MS of 3_2d

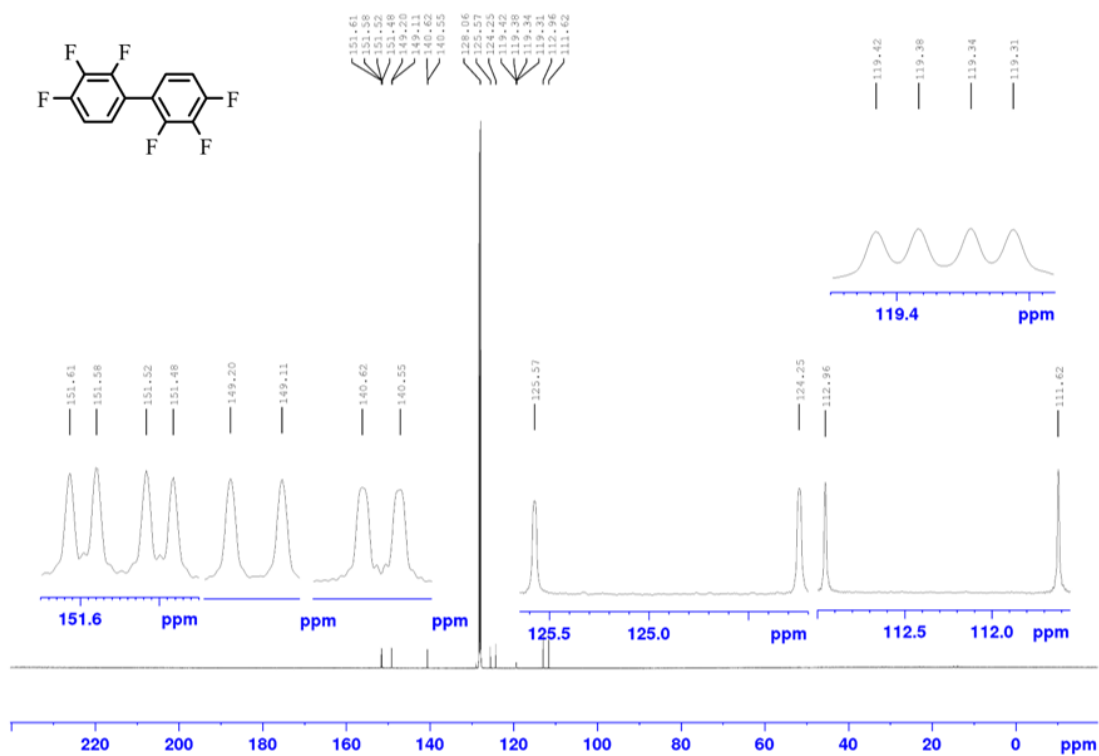
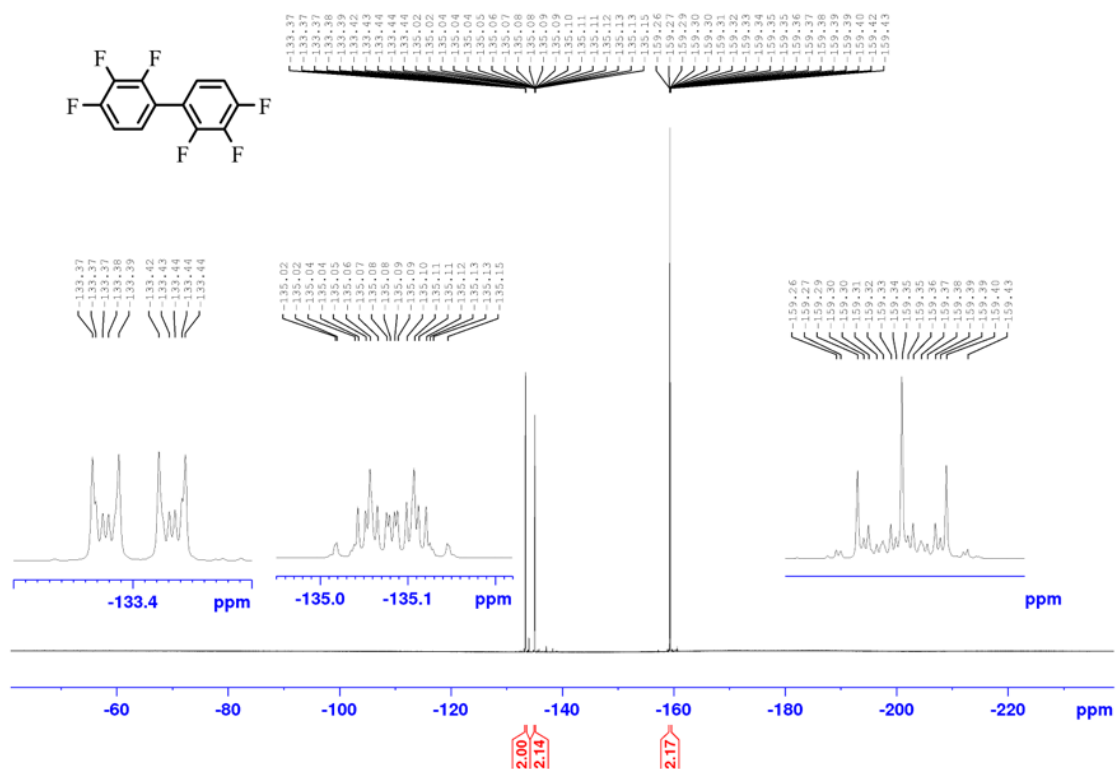


$^{13}\text{C}\{^1\text{F}\}$ NMR spectrum of 3_2e (125 MHz, CDCl_3) $^{19}\text{F}\{^1\text{H}\}$ NMR spectrum of 3_2e (376 MHz, CDCl_3)

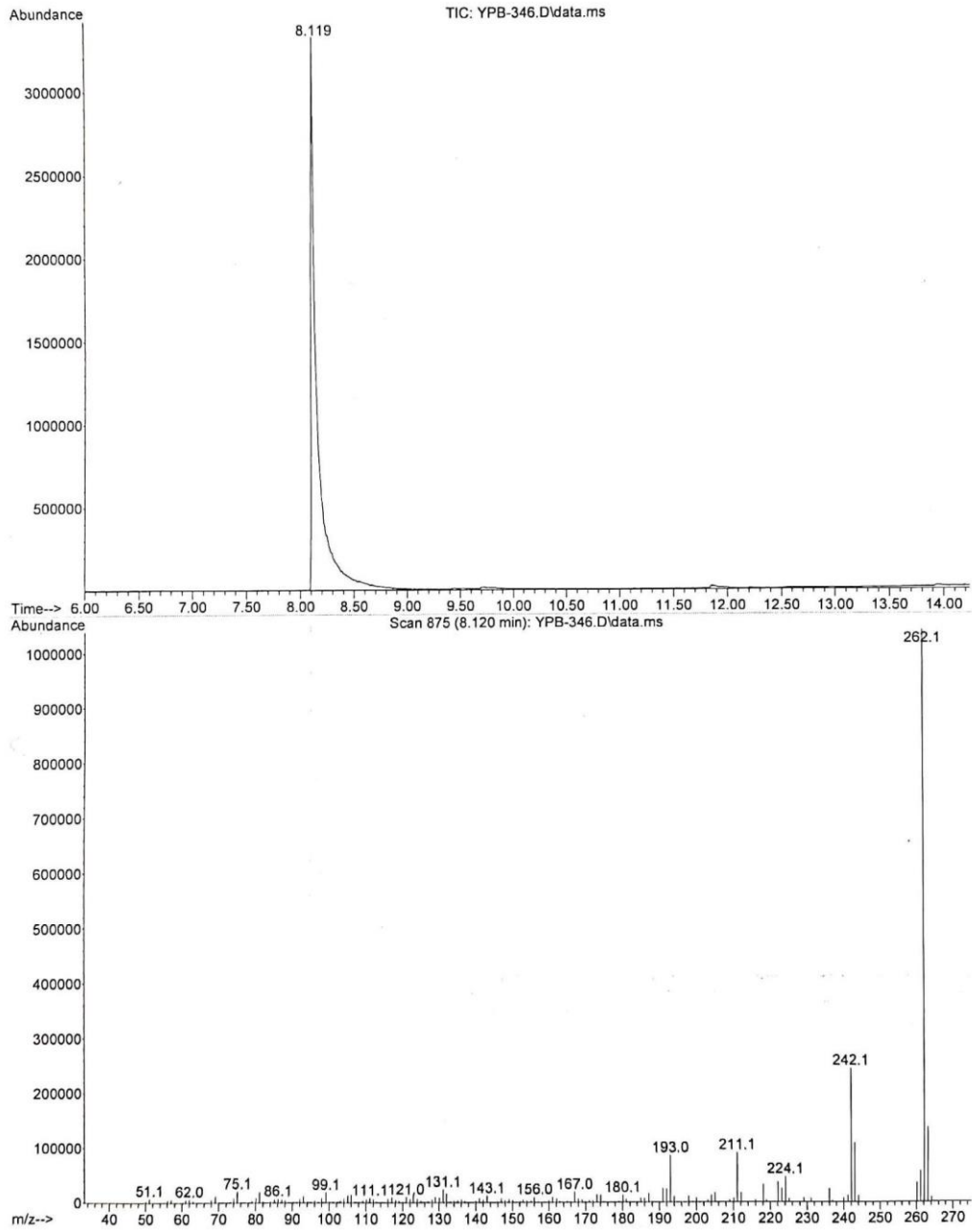
GC-MS of 3_2e

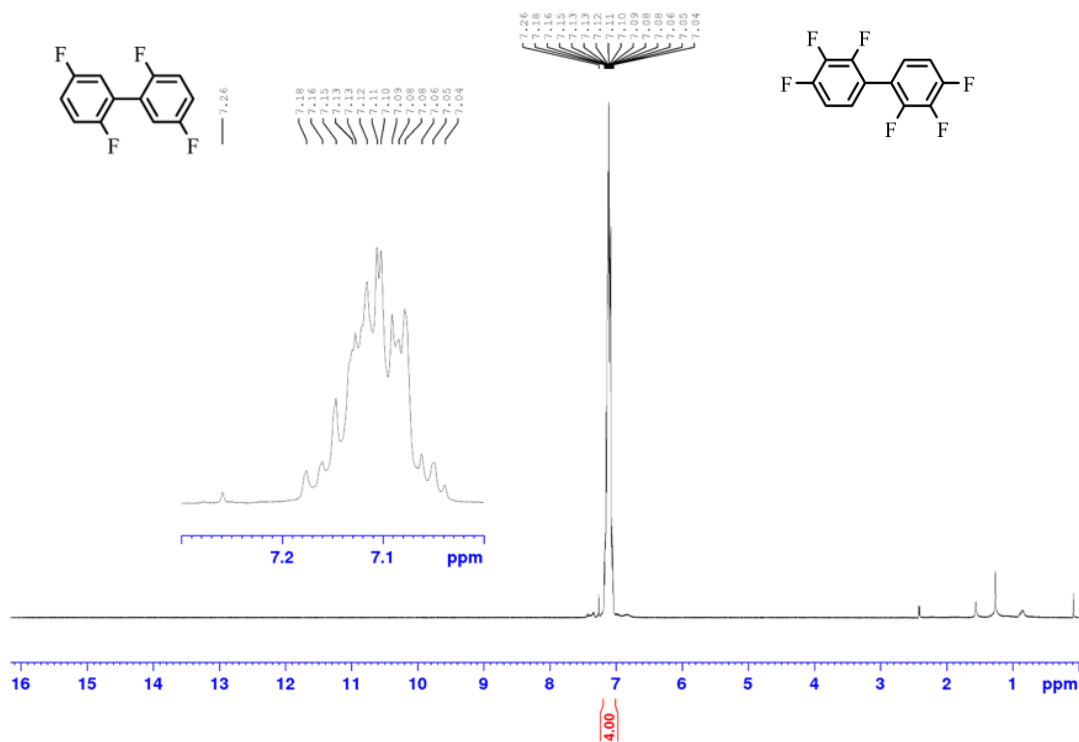
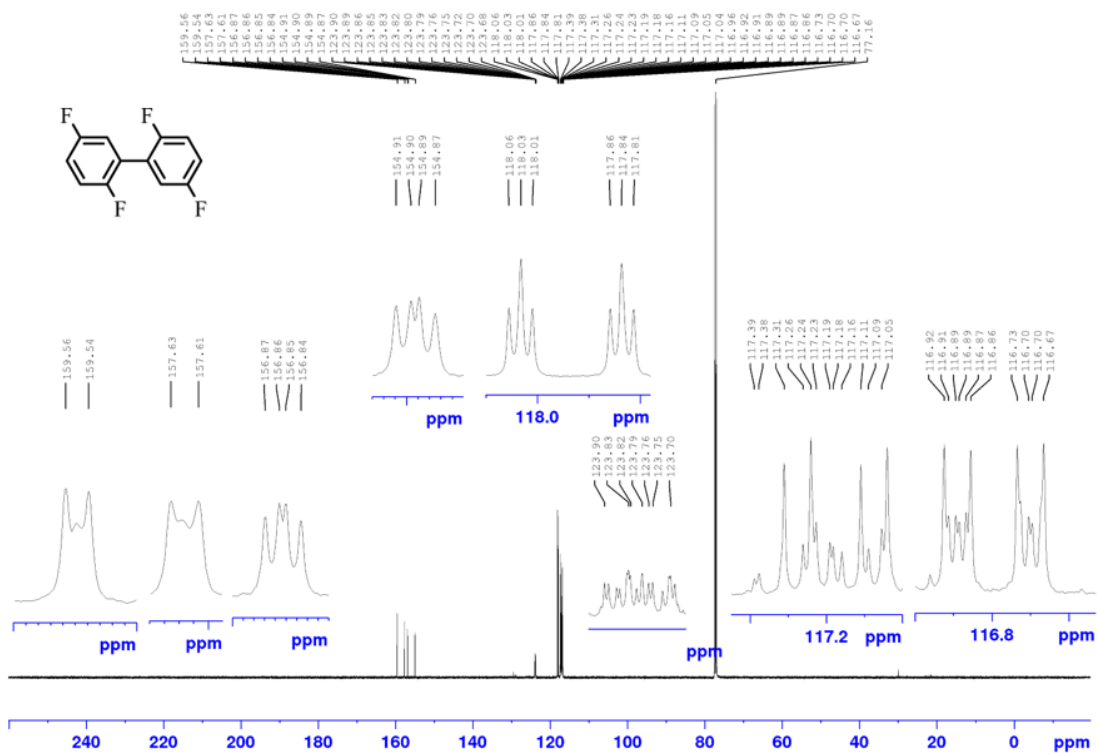


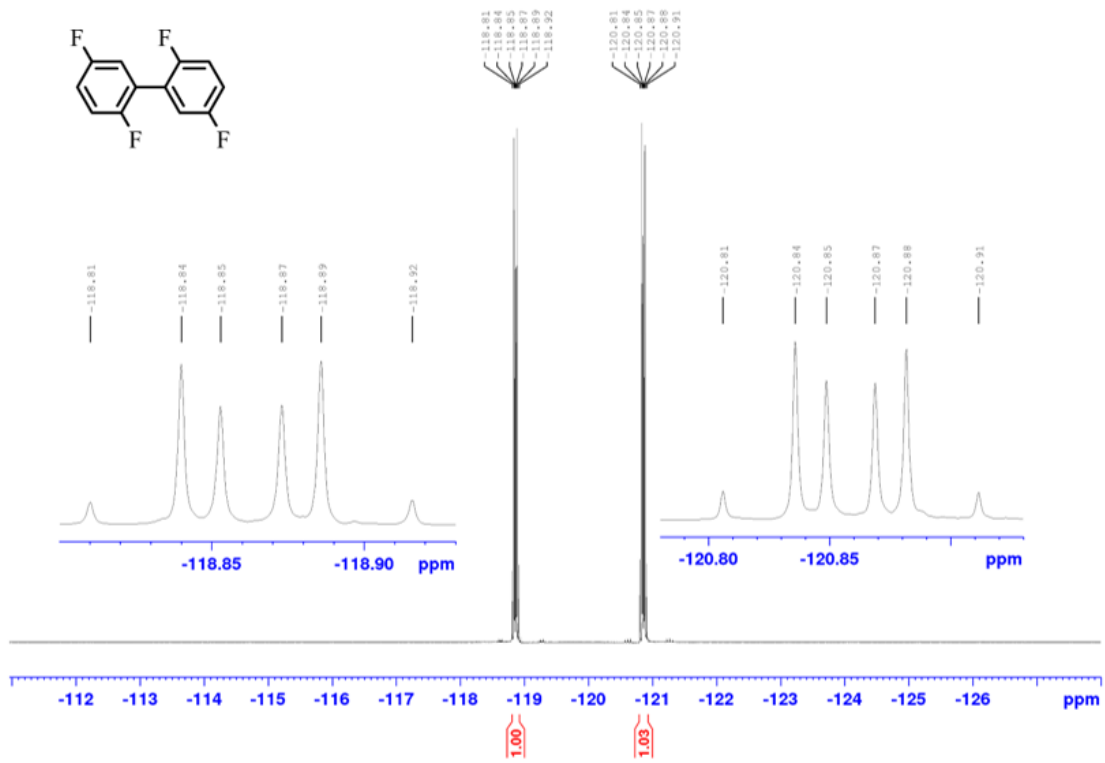
^1H NMR spectrum of 3_2f (300 MHz, C_6D_6) $^{13}\text{C}\{^1\text{H}\}$ NMR spectrum of 3_2f (125 MHz, C_6D_6)

$^{13}\text{C}\{^{19}\text{F}\}$ NMR spectrum of 3_2f (125 MHz, C_6D_6) $^{19}\text{F}\{^1\text{H}\}$ NMR spectrum of 3_2f (376 MHz, C_6D_6)

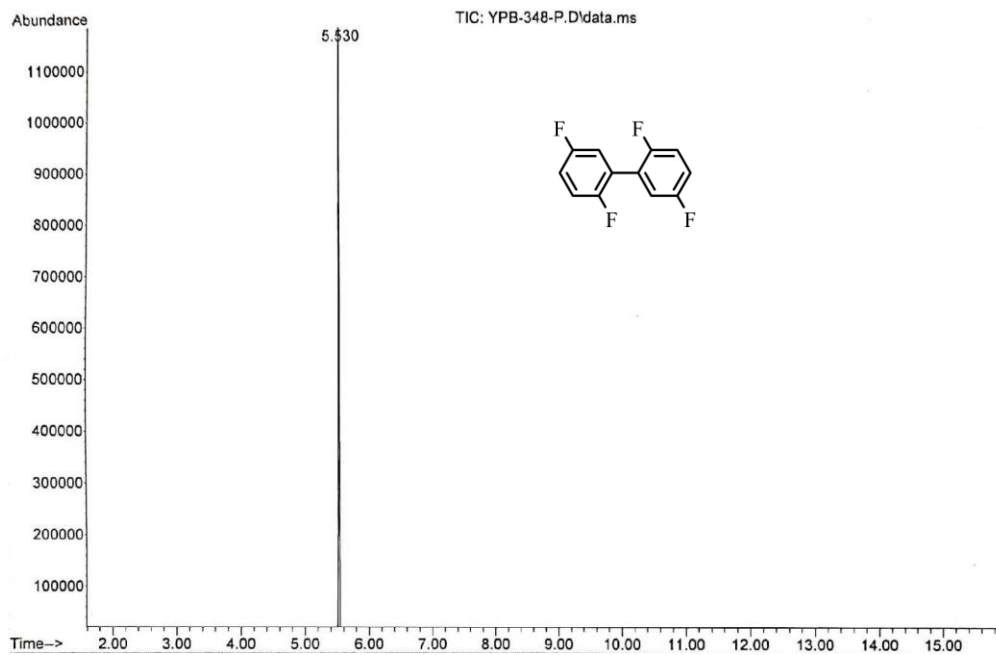
GC-MS of 3_2f

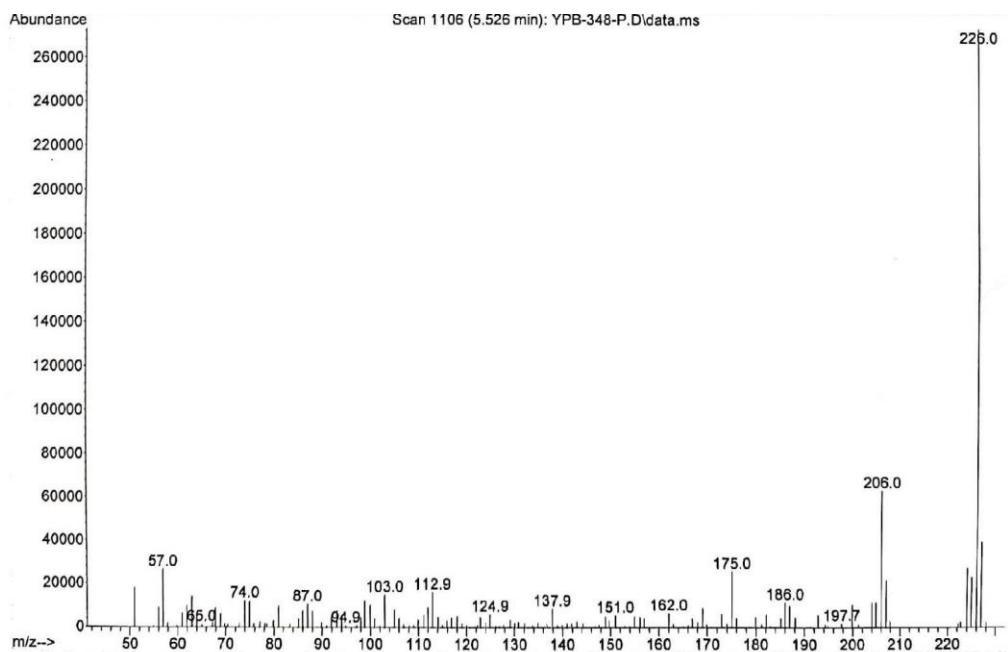


^1H NMR spectrum of 3_2g (300 MHz, CDCl_3) $^{13}\text{C}\{^1\text{H}\}$ NMR spectrum of 3_2g (125 MHz, CDCl_3)

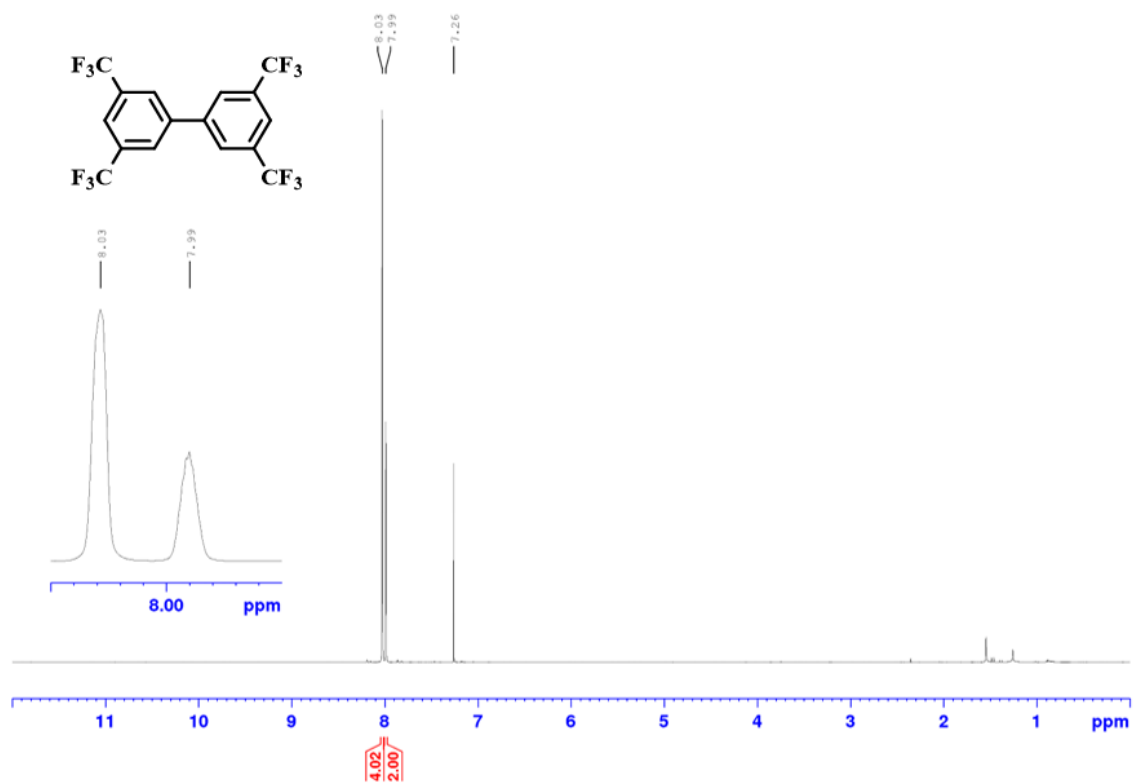
$^{19}\text{F}\{^1\text{H}\}$ NMR spectrum of 3_2g (376 MHz, CDCl_3)

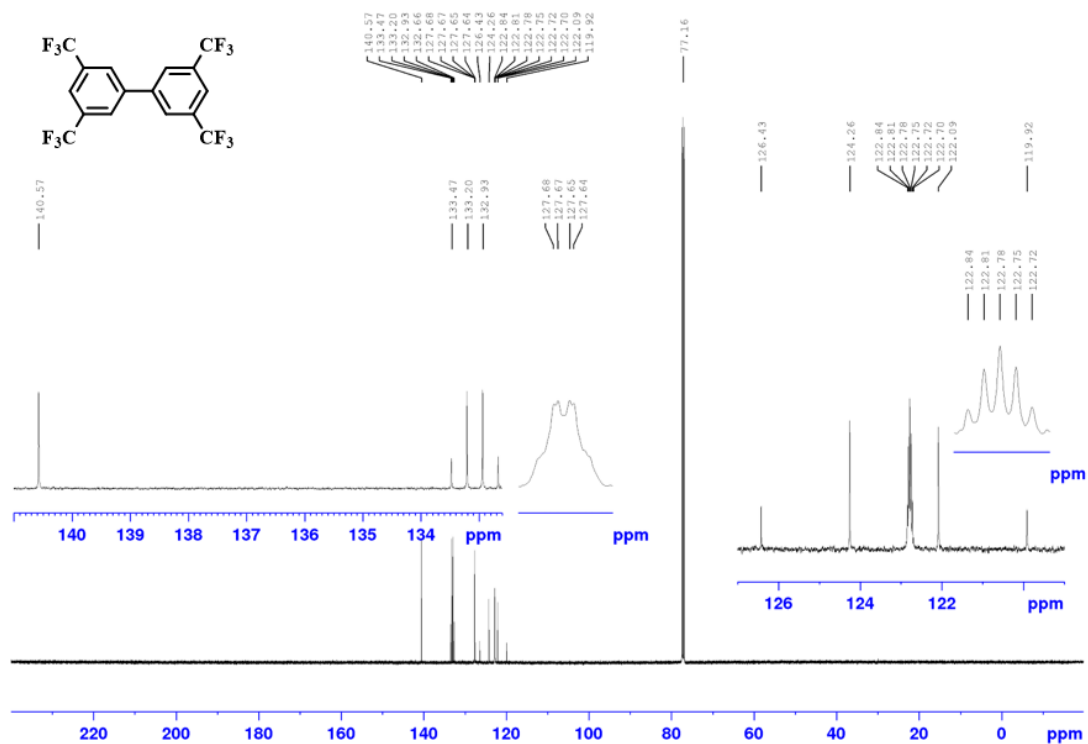
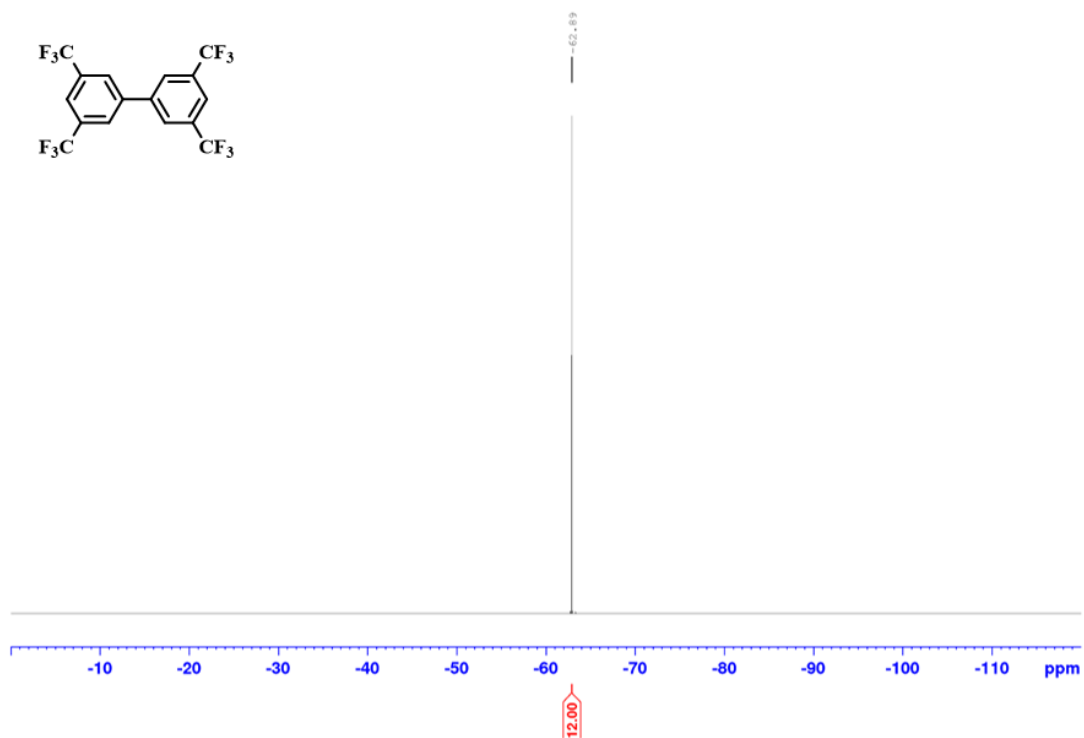
GC-MS of 2g



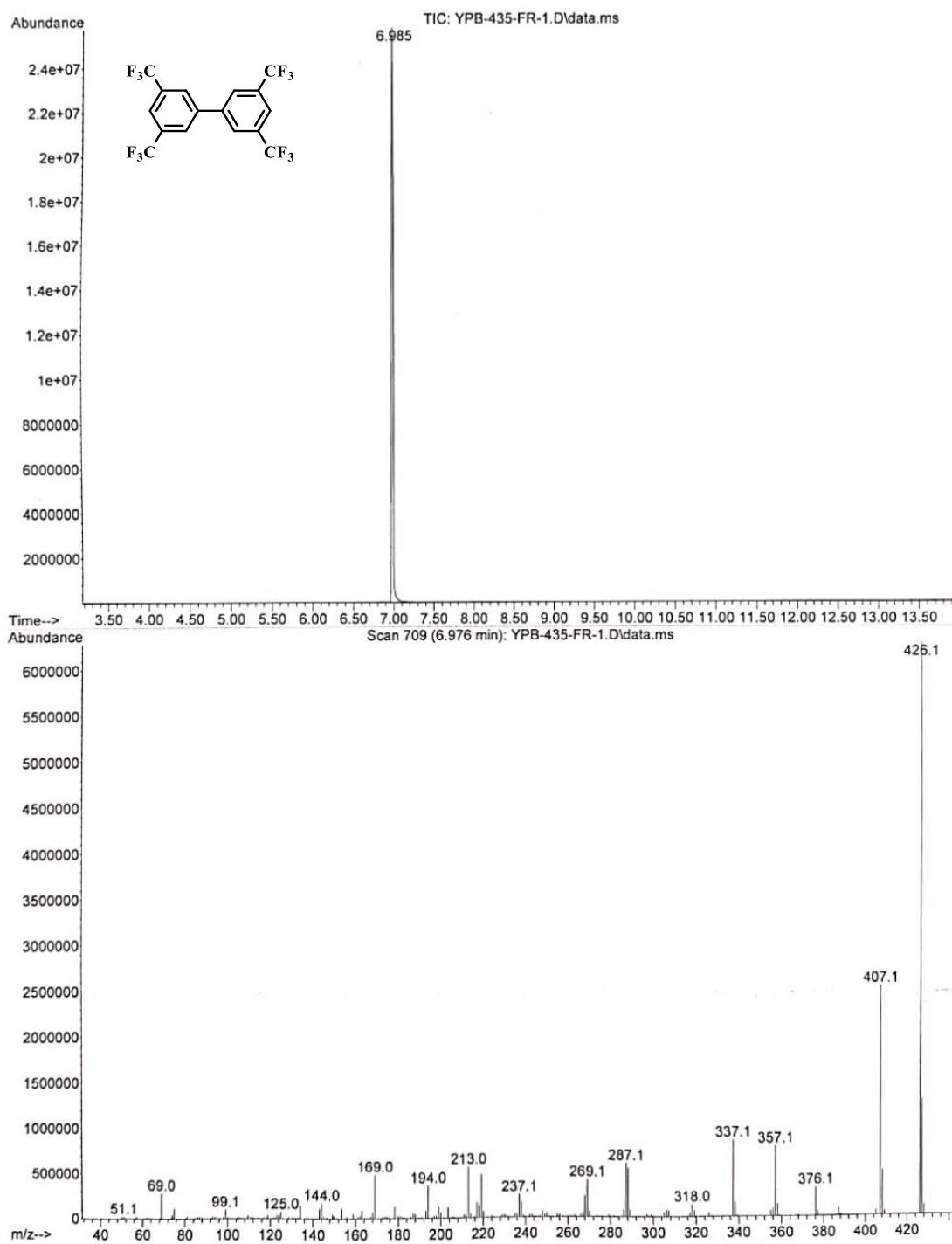


^1H NMR spectrum of 3_2h (500 MHz, CDCl_3)



$^{13}\text{C}\{^1\text{H}\}$ NMR spectrum of 3_2h (125 MHz, CDCl_3) ^{19}F NMR spectrum of 3_2h (470 MHz, CDCl_3)

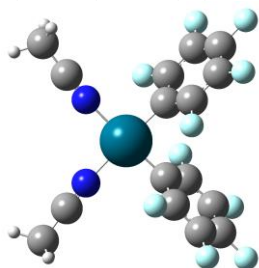
GC-MS of 3_2h



7.3 XYZ Coordinates for Chapter 3

Optimized Structures, Cartesian Coordinates, and Energies

1) [Pd(MeCN)₂(C₆F₅)₂] (3_3a)



Number of imaginary frequencies = 0

$E_{\text{total}} = -1849.14566484$ a.u

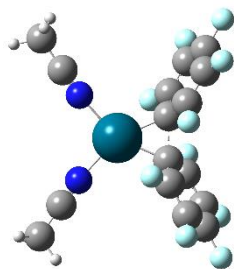
$G_{\text{correction}} = 0.127629$ a.u

Cartesian coordinates:

Pd	0.00000000	0.00000000	1.32741100
F	-2.19119000	0.81516600	-0.87967600
N	0.03252500	-1.50791000	2.79180400
C	0.00000000	1.37137200	-0.13507300
C	-1.07063100	1.56851100	-0.99658300
F	-2.11945800	2.68987700	-2.81927700
C	0.06552700	3.32714200	-2.17497700
F	2.24848900	3.93062200	-1.49086100
C	-1.05979700	2.52655300	-2.00769700
F	0.09504100	4.25838200	-3.14136100
C	1.15884300	3.15902600	-1.33056500
F	2.19672000	2.06619000	0.46203900
C	1.10451300	2.19045800	-0.33221500
C	0.05059700	-2.37578700	3.55406300
C	0.07038300	-3.47280700	4.50747700
H	0.07311300	-3.07720200	5.52596900
H	0.96710700	-4.07768100	4.35205100
H	-0.81503300	-4.09714800	4.36456100
F	2.19119000	-0.81516600	-0.87967600
N	-0.03252500	1.50791000	2.79180400
C	0.00000000	-1.37137200	-0.13507300
C	1.07063100	-1.56851100	-0.99658300
F	2.11945800	-2.68987700	-2.81927700
C	-0.06552700	-3.32714200	-2.17497700
F	-2.24848900	-3.93062200	-1.49086100
C	1.05979700	-2.52655300	-2.00769700
F	-0.09504100	-4.25838200	-3.14136100
C	-1.15884300	-3.15902600	-1.33056500
F	-2.19672000	-2.06619000	0.46203900
C	-1.10451300	-2.19045800	-0.33221500
C	-0.05059700	2.37578700	3.55406300
C	-0.07038300	3.47280700	4.50747700
H	-0.07311300	3.07720200	5.52596900
H	-0.96710700	4.07768100	4.35205100

H	0.81503300	4.09714800	4.36456100
---	------------	------------	------------

2) TS[(3_3a)-4]



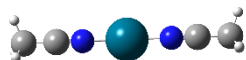
Number of imaginary frequencies = 1 ($i94.30 \text{ cm}^{-1}$)

$E_{\text{total}} = -1849.09234227 \text{ a.u.}$

$G_{\text{correction}} = 0.123003 \text{ a.u.}$

Cartesian coordinates:

Pd	-0.00001200	1.39323900	0.00020900
C	-0.83692600	-0.55872700	-0.05326400
C	-1.36419400	-1.23633400	-1.18117700
C	-1.69333400	-0.61314200	1.08386400
C	-2.57999400	-1.90377100	-1.18551000
C	-2.91338100	-1.26722300	1.09490200
C	-3.36597200	-1.93443700	-0.03993100
C	0.83686200	-0.55876000	0.05329400
C	1.36411500	-1.23663500	1.18105100
C	1.69326800	-0.61293500	-1.08384700
C	2.57989900	-1.90410400	1.18522700
C	2.91330000	-1.26704100	-1.09503900
C	3.36587500	-1.93452800	0.03964000
F	-0.65751700	-1.29709700	-2.32507400
F	-1.41058400	0.09977300	2.19868600
F	-3.69339600	-1.22109100	2.18754800
F	-4.54156700	-2.57534400	-0.03289700
F	-2.99519100	-2.53599900	-2.29456900
F	0.65743800	-1.29765300	2.32493300
F	1.41053600	0.10025300	-2.19850000
F	3.69331600	-1.22067100	-2.18767300
F	2.99508000	-2.53660000	2.29414000
F	4.54145500	-2.57546000	0.03245900
N	-1.64558300	2.84417700	-0.24031400
N	1.64566800	2.84402400	0.24093700
C	2.58579400	3.51379900	0.34271700
C	-2.58552200	3.51416300	-0.34241600
C	-3.76813000	4.35313300	-0.47064400
H	-4.65415600	3.72652600	-0.60022100
H	-3.88839600	4.96276800	0.42834700
H	-3.66363900	5.01035000	-1.33751000
C	3.76867400	4.35246600	0.47041500
H	3.66564400	5.00829500	1.33850800
H	4.65485100	3.72556400	0.59750400
H	3.88754500	4.96354400	-0.42778000

3) [Pd(MeCN)₂]

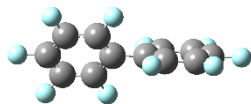
Number of imaginary frequencies = 0

$E_{\text{total}} = -393.51885011$ a.u

$G_{\text{correction}} = 0.057706$ a.u

Cartesian coordinates:

Pd	0.00000000	-0.00147000	0.00005400
N	-1.98346900	-0.00081700	0.00016000
N	1.98347100	-0.00085600	-0.00003200
C	3.14351400	0.00090000	-0.00004000
C	-3.14351400	0.00094400	0.00001400
C	-4.59811600	0.00354000	-0.00019400
H	-4.96854400	0.65999000	-0.79197800
H	-4.97178800	-1.00923300	-0.17235300
H	-4.96951200	0.36199100	0.96348100
C	4.59811500	0.00357800	-0.00012200
H	4.97187700	-1.02320900	-0.03201200
H	4.96882600	0.54560700	-0.87409400
H	4.96913300	0.49042800	0.90563700

4) (C₆F₅)₂

Number of imaginary frequencies = 0

$E_{\text{total}} = -1455.61804677$ a.u

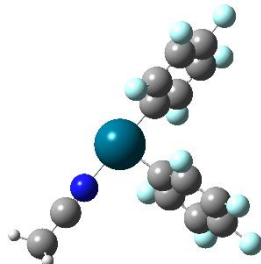
$G_{\text{correction}} = 0.052999$ a.u

Cartesian coordinates:

C	-0.73798700	0.00002600	0.00000400
C	-1.46513700	-1.06525900	0.53906800
C	-1.46516000	1.06528800	-0.53907200
C	-2.85502500	-1.07765000	0.53886400
C	-2.85505200	1.07764900	-0.53886500
C	-3.55159400	-0.00000400	0.00000500
C	0.73798900	0.00002600	0.00000200
C	1.46516000	1.06527800	0.53908600
C	1.46513700	-1.06526000	-0.53907500
C	2.85505700	1.07764400	0.53888100
C	2.85502100	-1.07764700	-0.53887100
C	3.55159100	-0.00000300	0.00000100
F	-0.82257300	-2.10602500	1.08483000
F	-0.82263200	2.10604200	-1.08489600
F	-3.52380700	2.11044900	-1.06384500
F	-4.88636100	-0.00002700	0.00000100
F	-3.52376300	-2.11047500	1.06381700
F	0.82263500	2.10603500	1.08491300
F	0.82256700	-2.10600900	-1.08485600

F	3.52377300	-2.11045600	-1.06383800
F	3.52380200	2.11044500	1.06386400
F	4.88636000	-0.00003700	-0.00000800

5) [Pd(MeCN)(C₆F₅)₂] (5)



Number of imaginary frequencies = 0

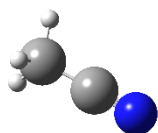
E_{total} = -1716.34277731 a.u

G_{correction} = 0.085593 a.u

Cartesian coordinates:

Pd	0.39189600	-1.61610800	-0.16760200
C	-1.40001400	-0.73594900	-0.26405500
C	-2.35464700	-1.01442600	0.70898800
C	-1.78343300	0.15008500	-1.26489800
C	-3.63042700	-0.45903400	0.69790100
C	-3.04963900	0.72744300	-1.31421200
C	-3.97790100	0.41989100	-0.32400800
C	1.11052300	0.19587000	0.14330100
C	1.91366000	0.80029400	-0.81610900
C	0.86883400	0.91023400	1.30958400
C	2.46586200	2.06471600	-0.63061600
C	1.40641000	2.17699900	1.52629900
C	2.20878400	2.75702700	0.54895600
F	-2.06087800	-1.86074100	1.72637000
F	-0.91825200	0.49086300	-2.24852600
F	-3.38827200	1.57255100	-2.30265000
F	-5.20347200	0.96287700	-0.35759700
F	-4.52713100	-0.75714500	1.65340400
F	2.18971900	0.16796300	-1.97833700
F	0.09337400	0.39263600	2.28750000
F	1.16051500	2.84174700	2.66697900
F	3.24033000	2.62254600	-1.57531700
F	2.73539800	3.97458000	0.74447300
N	2.28869700	-2.50857300	-0.05898900
C	3.35448500	-2.95241100	-0.00177000
C	4.69442200	-3.51019500	0.06757900
H	5.13233800	-3.29378000	1.04506600
H	4.64944600	-4.59246400	-0.07691600
H	5.31660300	-3.06695000	-0.71387300

6) MeCN



Number of imaginary frequencies = 0

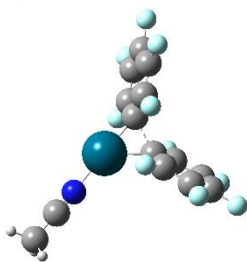
$E_{\text{total}} = -132.77158285$ a.u

$G_{\text{correction}} = 0.021432$ a.u

Cartesian coordinates:

C	0.27806500	-0.00030500	-0.00055000
C	-1.17994800	0.00007300	0.00012800
H	-1.55441200	0.10906900	-1.02068800
H	-1.55393400	-0.93856600	0.41643300
H	-1.55357900	0.82990400	0.60509900
N	1.43903100	0.00014100	0.00024100

7) TS(5-6)



Number of imaginary frequencies = 1 ($i249.64$ cm⁻¹)

$E_{\text{total}} = -1716.30592047$ a.u

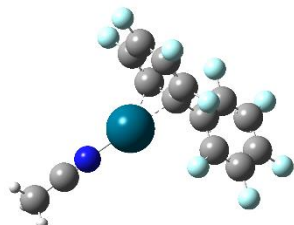
$G_{\text{correction}} = 0.087126$ a.u

Cartesian coordinates:

Pd	0.60653700	1.54468500	-0.14541600
C	-1.00519900	0.28053900	-0.13189100
C	-1.70292600	-0.21872100	-1.25334600
C	-1.84041700	0.67587200	0.94409600
C	-3.08330200	-0.35701400	-1.29502800
C	-3.22178200	0.54805600	0.92011400
C	-3.85408800	0.02032300	-0.20099800
C	0.58807100	-0.52554300	0.10160900
C	0.65199900	-1.25364600	1.30539600
C	1.33040400	-1.09178300	-0.96084700
C	1.35083400	-2.44635200	1.44159100
C	2.03750300	-2.27969600	-0.84480800
C	2.04351900	-2.97554500	0.35968500
F	-1.03480800	-0.63946000	-2.33992900
F	-1.33065200	1.27806200	2.03897800
F	-3.95905400	0.97314500	1.95679000
F	-5.18451900	-0.10040200	-0.23513600
F	-3.67848700	-0.85714200	-2.38749400
F	-0.01090000	-0.83024500	2.39601600
F	1.47032800	-0.44201900	-2.13612900

F	2.75388700	-2.74340000	-1.88053600
F	1.35022000	-3.09555800	2.61551700
F	2.72065300	-4.12317300	0.47929700
N	2.26852000	2.82424100	-0.07730400
C	3.16727500	3.55254400	-0.02328800
C	4.30166300	4.45919900	0.04838800
H	5.13516800	4.05295900	-0.53009200
H	4.02201700	5.43372900	-0.35956900
H	4.61114300	4.58044300	1.08953400

8) Intermediate-6



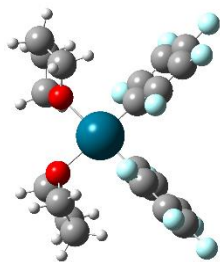
Number of imaginary frequencies = 0

$E_{\text{total}} = -1716.34874631$ a.u

$G_{\text{correction}} = 0.083376$ a.u

Cartesian coordinates:

Pd	1.39799300	0.92695600	-0.08849400
C	-0.01570900	-0.66915700	0.18777000
C	0.37724000	-1.35775900	1.38180300
C	0.79071000	-0.90654900	-0.98271800
C	1.42726700	-2.24201600	1.40833000
C	1.84977400	-1.85869900	-0.94004400
C	2.17077800	-2.49305400	0.23497500
C	-1.42456900	-0.20068600	0.07465400
C	-2.33622100	-0.86427700	-0.75106200
C	-1.90918700	0.87840100	0.81744900
C	-3.65852600	-0.44911500	-0.87030100
C	-3.22767800	1.30678700	0.72057200
C	-4.10610000	0.63997000	-0.12909500
F	-0.35515600	-1.17664400	2.49268100
F	0.27280300	-0.66581200	-2.21960200
F	2.53842800	-2.11056200	-2.06240500
F	3.21842000	-3.32470900	0.29900700
F	1.78824900	-2.85316200	2.54719300
F	-1.94971000	-1.94313400	-1.44678500
F	-1.09069100	1.55340600	1.64151200
F	-3.65536900	2.35388800	1.43576400
F	-4.50390600	-1.10214600	-1.67619300
F	-5.37521100	1.04303500	-0.22980300
N	2.68273100	2.52954000	-0.33174100
C	3.38035200	3.44988700	-0.42483100
C	4.26044900	4.60074700	-0.54596600
H	4.00195800	5.34343700	0.21302100
H	5.29809000	4.28804300	-0.40419600
H	4.15096200	5.04743100	-1.53744800

9) [Pd(THF)₂(C₆F₅)₂] (7)

Number of imaginary frequencies = 0

$E_{\text{total}} = -2048.56768273$ a.u

$G_{\text{correction}} = 0.270449$ a.u

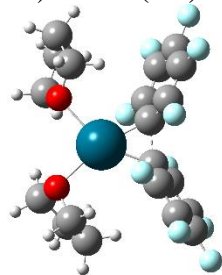
Cartesian coordinates:

Pd	-0.10781500	0.96359500	-0.29143900
C	-1.27552700	-0.62958800	-0.07896500
C	-1.43704800	-1.59758400	-1.06339700
C	-2.04170200	-0.79247200	1.06974600
C	-2.32053700	-2.66654200	-0.93311600
C	-2.93674800	-1.84493000	1.24083800
C	-3.07461000	-2.79114200	0.22976200
C	1.44488500	-0.25623700	-0.06050100
C	1.85979200	-0.69511600	1.19057700
C	2.21577300	-0.67193800	-1.13959500
C	2.99042300	-1.48485300	1.38001500
C	3.35185300	-1.46447800	-0.99769000
C	3.73978000	-1.87635000	0.27404100
F	-0.74038400	-1.51847900	-2.22127800
F	-1.95440100	0.10402100	2.08625600
F	-3.66515900	-1.95912900	2.36431200
F	-3.93218300	-3.81281300	0.37268800
F	-2.45700000	-3.57431900	-1.91421300
F	1.18143300	-0.32104900	2.30434500
F	1.90673900	-0.26894000	-2.39803600
F	4.07825100	-1.83173400	-2.06629700
F	3.36839400	-1.87044600	2.61009900
F	4.83195300	-2.63820900	0.43334200
O	-1.83152100	2.28512300	-0.53994100
C	-2.43695200	2.91331400	0.63274100
C	-2.85972600	1.94372200	-1.51567200
C	-3.93956400	2.72850500	0.45052900
H	-2.04043300	2.42124200	1.51996300
H	-2.14414000	3.96795600	0.62706100
C	-4.08818000	2.73175000	-1.07805300
H	-2.47289200	2.20985200	-2.50091400
H	-3.03332400	0.86471000	-1.47053500
H	-4.51340800	3.51638800	0.94291200
H	-4.25147500	1.76308800	0.86214300
H	-4.04943500	3.75493800	-1.46511300
H	-5.01490400	2.26629900	-1.42059200
O	1.13060000	2.79203800	-0.40587400
C	1.31986000	3.43111200	0.88272800
C	2.45450100	2.74359700	-1.00230400

Appendix

C	2.61088100	2.82274500	1.43297300
H	1.41382900	4.51020700	0.71167000
H	0.43187300	3.23331200	1.48260500
C	3.42807900	2.47471500	0.15964500
H	2.43434200	1.97440200	-1.77085300
H	2.63891900	3.71949700	-1.46501900
H	2.38209600	1.92105100	2.00372200
H	3.13330000	3.52089400	2.09044800
H	3.74015900	1.42953200	0.17504000
H	4.32215500	3.09445300	0.06341100

10) TS(7-8)



Number of imaginary frequencies = 1 ($i111.30 \text{ cm}^{-1}$)

$E_{\text{total}} = -2048.51462478 \text{ a.u.}$

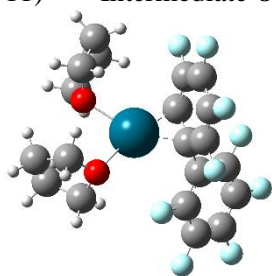
$G_{\text{correction}} = 0.269660 \text{ a.u.}$

Cartesian coordinates:

Pd	-0.04239100	1.04020300	-0.46326300
C	-0.63838000	-0.88648900	-0.00607500
C	-1.10708300	-1.86040800	-0.92441500
C	-1.50341500	-0.70897500	1.11319700
C	-2.28977800	-2.56958100	-0.76727100
C	-2.69491200	-1.39541100	1.27497900
C	-3.09941300	-2.34413300	0.34005600
C	1.03486500	-0.68020300	0.04222500
C	1.64269500	-0.97151800	1.28892000
C	1.89010800	-0.92113200	-1.06998800
C	2.93264500	-1.46238700	1.42537700
C	3.18300600	-1.40535900	-0.95410500
C	3.71562400	-1.69504300	0.29939400
F	-0.38153800	-2.16452800	-2.01548600
F	-1.27589100	0.26121500	2.03113000
F	-3.50914700	-1.09079100	2.30088200
F	-4.25008200	-3.00915600	0.49470600
F	-2.65365700	-3.47972000	-1.68300300
F	0.95239500	-0.80386500	2.43232700
F	1.51904200	-0.56147000	-2.32170700
F	3.95169500	-1.54613600	-2.04563500
F	3.42753300	-1.72499200	2.64440400
F	4.96086600	-2.16975700	0.41948500
O	-2.04679300	2.23134500	-0.79174500
C	-2.58605800	2.85644100	0.40567500
C	-3.08351600	1.45248800	-1.44759500
C	-3.92989000	2.17758700	0.65797900
H	-1.86997700	2.71129400	1.21618600

H	-2.70103400	3.92870000	0.20944900
C	-4.39322000	1.84650600	-0.76815200
H	-3.04893600	1.67953500	-2.51577300
H	-2.86127900	0.39009600	-1.30319400
H	-4.62462700	2.82629900	1.19639800
H	-3.79248500	1.26357100	1.24315300
H	-4.82425800	2.73312200	-1.24415800
H	-5.13213400	1.04268700	-0.80508500
O	1.23718400	2.97254700	-0.68915200
C	1.34910300	3.65561400	0.57869600
C	2.60039700	2.67031100	-1.06454200
C	2.40093300	2.85835300	1.35762100
H	1.67996500	4.68615400	0.39274700
H	0.35803700	3.67070100	1.03252700
C	3.30908600	2.27116200	0.24293800
H	2.56407600	1.88442000	-1.81836400
H	3.04478800	3.57347000	-1.50178100
H	1.92039300	2.05432000	1.92041700
H	2.94843500	3.48974200	2.06096800
H	3.37470600	1.18673100	0.33300600
H	4.32345200	2.67460000	0.27735600

11) Intermediate-8



Number of imaginary frequencies = 0

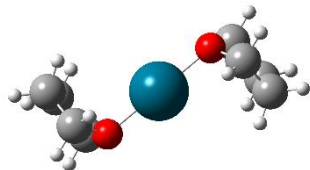
$E_{\text{total}} = -2048.55171606 \text{ a.u.}$

$G_{\text{correction}} = 0.269902 \text{ a.u.}$

Cartesian coordinates:

Pd	0.98133300	0.35790100	0.08063600
C	-0.73361100	-0.81744600	0.45191900
C	-0.66398700	-1.42537400	1.75593500
C	0.15870500	-1.37414400	-0.56900500
C	0.14029300	-2.49266100	2.03162400
C	0.91880300	-2.55759300	-0.25718300
C	0.94449200	-3.06509800	1.00771200
C	-2.03947700	-0.21277900	0.05827500
C	-2.94292400	-0.92700800	-0.73470500
C	-2.44349100	1.05331200	0.48587600
C	-4.16296400	-0.39098400	-1.13372600
C	-3.66107900	1.60867900	0.10748500
C	-4.52468000	0.88331800	-0.70797300
F	-1.46225400	-0.93151500	2.72310500
F	-0.23365400	-1.31380900	-1.89425800
F	1.64088300	-3.13125000	-1.24095200
F	1.75171400	-4.09041800	1.32904200

F	0.22884500	-3.00385200	3.27428300
F	-2.65036900	-2.17680400	-1.12470000
F	-1.64510400	1.78853400	1.27711700
F	-4.00775500	2.83296700	0.52610300
F	-4.99829400	-1.10042100	-1.90329500
F	-5.69832800	1.40664900	-1.07596100
O	3.01608200	0.84990400	-0.90756200
C	2.97851400	0.90134300	-2.34886400
C	4.08193500	-0.06883500	-0.56872900
C	3.17840700	-0.54816200	-2.78534900
H	2.02038600	1.33689100	-2.63493400
H	3.79424300	1.54846400	-2.69938400
C	4.13286100	-1.11421600	-1.70374500
H	5.01667900	0.50075500	-0.49961300
H	3.84317600	-0.48822600	0.40933400
H	3.59099100	-0.62101100	-3.79428000
H	2.22371600	-1.07683200	-2.76193400
H	5.15324100	-1.21990600	-2.07964300
H	3.79319000	-2.09208500	-1.36215300
O	1.37609000	2.31539100	1.25483500
C	2.73334100	2.61725900	1.64657900
C	0.86874300	3.51958600	0.64395200
C	3.28073100	3.60578800	0.59536400
H	2.70955500	3.06701400	2.64690400
H	3.27465600	1.67277700	1.69246400
C	2.02759100	4.02995800	-0.21166800
H	-0.03217500	3.25313900	0.09339600
H	0.60890300	4.23503400	1.43639200
H	4.01382500	3.12295600	-0.05170100
H	3.75773600	4.46045800	1.08148800
H	2.01629200	3.53543900	-1.18609000
H	1.97254100	5.10894800	-0.37469100

12) [Pd(THF)₂] (9)

Number of imaginary frequencies = 0

$E_{\text{total}} = -592.89886036$ a.u

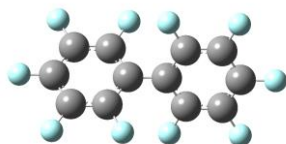
$G_{\text{correction}} = 0.194714$ a.u

Cartesian coordinates:

Pd	0.00000100	0.17509400	-0.00001700
O	-1.95177500	0.18539700	0.92082900
C	-2.64541200	-1.08594400	0.84514100
C	-2.88208400	1.12634700	0.32498300
C	-3.27483300	-1.10710100	-0.55302300
H	-1.91278800	-1.86893000	1.03401900
H	-3.41180800	-1.09507600	1.63152800
C	-3.45501000	0.39869600	-0.89893200

H	-3.66152700	1.33881500	1.06861200
H	-2.32712900	2.03633800	0.10289700
H	-4.21930100	-1.65636600	-0.55649700
H	-2.59522100	-1.58256000	-1.26420500
H	-4.50045000	0.66885300	-1.06563200
H	-2.88567000	0.65658200	-1.79492800
O	1.95179700	0.18538200	-0.92084300
C	2.88210200	1.12634100	-0.32499800
C	2.64542100	-1.08596600	-0.84510300
C	3.45492900	0.39872800	0.89897800
H	3.66158800	1.33875100	-1.06859700
H	2.32715200	2.03635200	-0.10298700
C	3.27486300	-1.10708000	0.55305800
H	1.91277900	-1.86894600	-1.03393700
H	3.41180500	-1.09514500	-1.63149800
H	2.88545800	0.65659100	1.79489800
H	4.50033500	0.66893700	1.06581800
H	2.59531500	-1.58260800	1.26425400
H	4.21938200	-1.65626000	0.55650400

13) (C₆F₅)₂



Number of imaginary frequencies = 0

$E_{\text{total}} = -1455.61737333 \text{ a.u}$

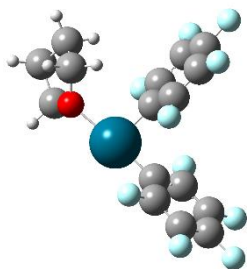
$G_{\text{correction}} = 0.053037 \text{ a.u}$

Cartesian coordinates:

C	0.73801000	0.00002600	-0.00000400
C	1.46499400	-1.06537200	-0.53935700
C	1.46501700	1.06540000	0.53936100
C	2.85504900	-1.07785900	-0.53905400
C	2.85507700	1.07785800	0.53905400
C	3.55160500	-0.00000400	-0.00000500
C	-0.73801100	0.00002600	-0.00000100
C	-1.46501700	1.06539000	-0.53937500
C	-1.46499500	-1.06537300	0.53936500
C	-2.85508100	1.07785300	-0.53907100
C	-2.85504600	-1.07785600	0.53906100
C	-3.55160300	-0.00000300	-0.00000100
F	0.82214600	-2.10543600	-1.08546600
F	0.82220400	2.10545200	1.08553100
F	3.52374200	2.11025800	1.06400800
F	4.88606600	-0.00002700	-0.00000100
F	3.52369900	-2.11028400	-1.06398100
F	-0.82220700	2.10544500	-1.08554700
F	-0.82214000	-2.10542000	1.08549200
F	-3.52370800	-2.11026400	1.06400200
F	-3.52373600	2.11025400	-1.06402800

F -4.88606600 -0.00003600 0.00000800

14) [Pd(THF)(C₆F₅)₂] (**10**)



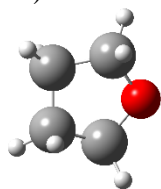
Number of imaginary frequencies = 0

$E_{\text{total}} = -1816.05032820$ a.u

$G_{\text{correction}} = 0.157324$ a.u

Cartesian coordinates:

Pd	0.22582100	-1.42524500	-0.07732900
C	-1.61754600	-0.74518900	0.17999700
C	-2.02824300	-0.01061900	1.28779100
C	-2.58918200	-1.01098100	-0.78065800
C	-3.33808800	0.43428300	1.44830100
C	-3.90779500	-0.58455100	-0.65762800
C	-4.28225900	0.14531000	0.46731000
C	0.81304100	0.45246200	-0.16653100
C	0.44790500	1.30478200	-1.20277000
C	1.69096800	0.95919600	0.78518600
C	0.94117900	2.60399000	-1.30324200
C	2.20646300	2.24973900	0.71235700
C	1.82482600	3.07858500	-0.33867100
F	-1.15001700	0.30420000	2.26715800
F	-2.26791800	-1.71104600	-1.89571800
F	-4.81911300	-0.86473100	-1.60360900
F	-5.54858200	0.56125900	0.60860200
F	-3.70248300	1.13417100	2.53518200
F	-0.39697100	0.89064000	-2.17123500
F	2.10025300	0.19096800	1.82286500
F	3.06404300	2.70071100	1.64094800
F	0.57800000	3.39948300	-2.32091000
F	2.31156200	4.32378600	-0.42501200
O	2.21064600	-2.26471500	-0.36305700
C	3.21228300	-1.60899800	-1.20044900
C	2.85617300	-2.85277200	0.81569500
C	4.39767000	-1.38578500	-0.27390100
H	3.45563100	-2.28675000	-2.02521900
H	2.76656400	-0.69634500	-1.59369200
C	4.35518200	-2.64564800	0.60368000
H	2.48898400	-2.31690200	1.69314900
H	2.55453800	-3.90070000	0.86841300
H	4.23697200	-0.49129900	0.33526300
H	5.33560500	-1.27449800	-0.82193900
H	4.88329900	-2.52624300	1.55193200
H	4.79104600	-3.49605300	0.07045100

15) **THF**

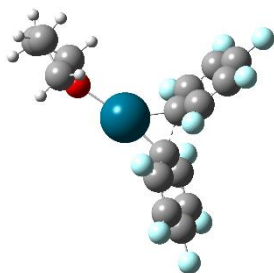
Number of imaginary frequencies = 0

$E_{\text{total}} = -232.47855000$ a.u

$G_{\text{correction}} = 0.088513$ a.u

Cartesian coordinates:

C	-1.16703200	-0.42677400	-0.13274100
O	-0.00030300	-1.25435600	-0.00064300
C	1.16656400	-0.42742800	0.13362200
C	0.73167200	0.99417700	-0.23125900
C	-0.73086600	0.99487500	0.23081300
H	-1.53186900	-0.47331900	-1.16931600
H	-1.95290400	-0.81779100	0.52237400
H	1.52943300	-0.47356200	1.17094100
H	1.95341300	-0.81926200	-0.51979400
H	1.34384500	1.75882500	0.25300600
H	0.78793300	1.14476200	-1.31472200
H	-0.78693100	1.14656400	1.31412900
H	-1.34253000	1.75952800	-0.25408200

16) **TS(10-11)**

Number of imaginary frequencies = 1 ($i214.60$ cm⁻¹)

$E_{\text{total}} = -1816.00895341$ a.u

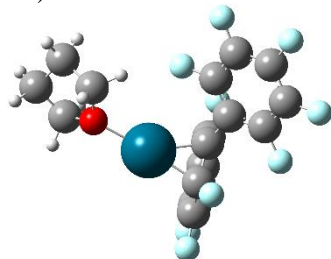
$G_{\text{correction}} = 0.155601$ a.u

Cartesian coordinates:

Pd	-0.87768100	-0.96888500	-0.13783100
C	1.11394700	-0.48845700	-0.13819900
C	1.95620600	-0.31872200	-1.25993100
C	1.70864500	-1.21390300	0.92744200
C	3.26446500	-0.77948200	-1.31219800
C	3.01318200	-1.68459500	0.89207700
C	3.80667700	-1.46166200	-0.22884200
C	0.01209200	0.88028600	0.10945200
C	0.25211400	1.56913200	1.31709700
C	-0.45752700	1.70451900	-0.94386200
C	0.08065800	2.93934900	1.46412300

C	-0.63878000	3.07381700	-0.81514200
C	-0.35944200	3.70642500	0.39203600
F	1.52829900	0.36274200	-2.33563900
F	0.99689200	-1.55586200	2.02244900
F	3.50407500	-2.39537700	1.91824100
F	5.06289900	-1.91626300	-0.27216400
F	4.01218700	-0.56215600	-2.40385300
F	0.71175900	0.91344200	2.39699300
F	-0.84518900	1.17527000	-2.12456700
F	-1.12532800	3.79013800	-1.84009000
F	0.34930800	3.52854000	2.63870900
F	-0.53142400	5.02623800	0.52449500
O	-2.89338600	-1.81238300	-0.14249100
C	-3.55900000	-2.25767000	1.07688700
C	-3.87377600	-1.48283100	-1.16439500
C	-5.05129600	-2.05191000	0.82079600
H	-3.30341300	-3.31141300	1.22491500
H	-3.16878400	-1.67011800	1.91035600
C	-5.15111600	-2.17656200	-0.70772600
H	-3.98980800	-0.39375000	-1.19824400
H	-3.48053500	-1.83517900	-2.11961700
H	-5.35932300	-1.05109700	1.13970300
H	-5.66202300	-2.78448800	1.35262800
H	-6.04617900	-1.70430400	-1.11822200
H	-5.14313300	-3.22866500	-1.01025100

17) Intermediate-11



Number of imaginary frequencies = 0

$E_{\text{total}} = -1816.05127966$ a.u

$G_{\text{correction}} = 0.157863$ a.u

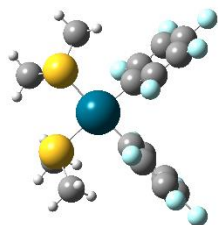
Cartesian coordinates:

Pd	1.34897000	0.22862200	-0.69322100
C	-0.21400900	-0.91131300	0.22786900
C	0.23075100	-1.40315900	1.49727200
C	0.34769900	-1.54305200	-0.94982300
C	1.11667700	-2.44309500	1.61187900
C	1.24726200	-2.64795000	-0.79362900
C	1.63794900	-3.06428300	0.45291800
C	-1.52800100	-0.21272600	0.17184100
C	-2.66149800	-0.86483800	-0.32150300
C	-1.69958200	1.09499900	0.63267200
C	-3.89857500	-0.23324600	-0.40321200
C	-2.92589900	1.74527500	0.56546900
C	-4.03107400	1.07729500	0.04478600

Appendix

F	-0.28305500	-0.85069100	2.61106800
F	-0.36609000	-1.54488500	-2.12076100
F	1.70219200	-3.26725100	-1.89349900
F	2.54210300	-4.04403500	0.59812700
F	1.54457700	-2.86000700	2.81473500
F	-2.57749100	-2.14095300	-0.72326400
F	-0.65775100	1.78161400	1.13414800
F	-3.05011100	3.00613400	0.99768600
F	-4.96197000	-0.88373700	-0.88954700
F	-5.21481600	1.69229400	-0.02101200
O	2.44876400	2.12148900	-0.66948300
C	1.72608400	3.38938400	-0.73748600
C	3.65042500	2.27041800	0.13654900
C	2.49314800	4.34428800	0.17759300
H	1.73505400	3.71372800	-1.78247300
H	0.69891500	3.21044900	-0.41723100
C	3.91777500	3.76980800	0.15221000
H	3.45025300	1.88156400	1.14130000
H	4.43412200	1.67383800	-0.33383900
H	2.08792800	4.30485500	1.19379200
H	2.43953300	5.37727800	-0.17260400
H	4.51714500	4.07281800	1.01352600
H	4.44121400	4.07373800	-0.75999400

18) [Pd(SMe₂)₂(C₆F₅)₂] (12)



Number of imaginary frequencies = 0

$E_{\text{total}} = -2539.68864396 \text{ a.u.}$

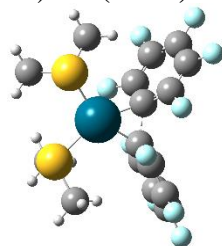
$G_{\text{correction}} = 0.189460 \text{ a.u.}$

Cartesian coordinates:

Pd	-0.03722900	1.16920400	-0.27910000
C	1.35261100	-0.26964200	0.00536200
C	1.67148000	-0.76914200	1.25944000
C	2.06319400	-0.80129000	-1.06281100
C	2.64314700	-1.74638700	1.46273000
C	3.04017900	-1.78116900	-0.90968600
C	3.32864000	-2.25964900	0.36563800
C	-1.38739200	-0.32991400	-0.15545500
C	-1.65957800	-1.20205100	-1.19953300
C	-2.10256100	-0.53793700	1.01576800
C	-2.59466800	-2.23019100	-1.10202100
C	-3.04520000	-1.55144100	1.16103500
C	-3.28898300	-2.40780800	0.09111600
F	1.04293700	-0.28900400	2.36304800
F	1.85330100	-0.33611000	-2.31995200
F	3.71447500	-2.26194700	-1.96788500

F	4.27050000	-3.19967700	0.53695500
F	2.92845700	-2.19673600	2.69627700
F	-1.01939300	-1.06561200	-2.38569800
F	-1.93484800	0.29841000	2.07479800
F	-3.72575700	-1.70928000	2.30935000
F	-2.83620800	-3.04929100	-2.13957900
F	-4.19467900	-3.39123400	0.20558300
S	-1.75232200	2.80829200	-0.79838600
S	1.65192500	2.91970800	-0.18730000
C	-1.58360000	4.15848000	0.41885000
H	-1.59808000	3.75838100	1.43382900
H	-0.63457000	4.65883100	0.22302200
H	-2.39984900	4.86883300	0.27742100
C	-3.38549900	2.16652500	-0.30517400
H	-4.13351300	2.93926600	-0.48859400
H	-3.59014500	1.29388300	-0.92447200
H	-3.37271600	1.87793100	0.74552500
C	3.26153600	2.25364500	-0.72178500
H	3.51597300	1.37596500	-0.12794700
H	3.16292000	1.97067700	-1.76960600
H	4.01797400	3.03184400	-0.61061200
C	1.93986500	3.03882200	1.61195300
H	2.78719700	3.70119000	1.79708900
H	1.03854700	3.46323500	2.05520000
H	2.11704700	2.04781500	2.03009900

19) TS(12-13)



Number of imaginary frequencies = 1 ($i121.48 \text{ cm}^{-1}$)

$E_{\text{total}} = -2539.63909494 \text{ a.u.}$

$G_{\text{correction}} = 0.188612 \text{ a.u.}$

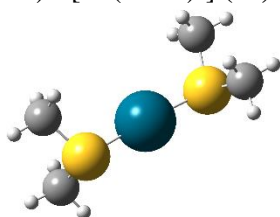
Cartesian coordinates:

Pd	-0.10418400	1.24493700	-0.40035500
C	0.89881000	-0.57367200	-0.00182400
C	1.51151100	-0.96156600	1.21429200
C	1.71454400	-0.81377300	-1.14284500
C	2.75913200	-1.56347100	1.29641800
C	2.96229600	-1.41174400	-1.08317000
C	3.49353200	-1.81051000	0.14106700
C	-0.79049900	-0.73613900	-0.04959000
C	-1.28176500	-1.67389700	-0.98874200
C	-1.60260400	-0.62747700	1.11301900
C	-2.42709100	-2.43395300	-0.79837400
C	-2.75026900	-1.37382700	1.32065800
C	-3.17008000	-2.29947600	0.36941500

Appendix

F	0.86417000	-0.77772500	2.38200800
F	1.35186600	-0.34032900	-2.35688200
F	3.69593200	-1.55550600	-2.19793700
F	4.69748500	-2.39191300	0.20712300
F	3.25848500	-1.91637100	2.49062300
F	-0.61568000	-1.88845600	-2.13761000
F	-1.36849400	0.33790800	2.03462500
F	-3.50228200	-1.16118600	2.41249300
F	-2.81650900	-3.30920100	-1.73743600
F	-4.27636100	-3.02704500	0.56470400
S	-2.02213400	2.54022900	-1.16089300
S	1.59113700	2.96748900	0.11482500
C	-2.12767800	4.02727300	-0.10618500
H	-2.11922100	3.74392400	0.94806000
H	-1.25007400	4.63666900	-0.32762500
H	-3.03344800	4.59010400	-0.34070900
C	-3.48986100	1.63491400	-0.56301100
H	-4.39881800	2.18129200	-0.82179300
H	-3.48812500	0.66422500	-1.06102900
H	-3.42658300	1.48865100	0.51653500
C	3.20495300	2.16162600	-0.15354900
H	3.21268700	1.18120200	0.32534900
H	3.33375300	2.04273500	-1.23003500
H	4.00483700	2.78681200	0.24783500
C	1.54431200	2.92268700	1.94098600
H	2.35860500	3.52560200	2.34823600
H	0.58607800	3.34280100	2.24927200
H	1.61573900	1.89185200	2.29252000

20) [Pd(SMe₂)₂] (13)



Number of imaginary frequencies = 0

$E_{\text{total}} = -1084.04647072$ a.u

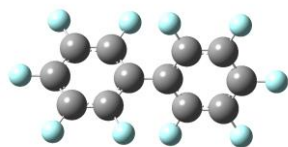
$G_{\text{correction}} = 0.114020$ a.u

Cartesian coordinates:

Pd	-0.00000700	0.17186500	0.00000700
S	2.26943100	0.25181700	0.43419800
S	-2.26946800	0.25189300	-0.43414700
C	3.16451200	0.64285300	-1.11482200
H	2.89184500	-0.06202900	-1.90147300
H	2.87034500	1.65071800	-1.40931600
H	4.24089000	0.61146900	-0.92934000
C	2.89190600	-1.44997200	0.69722100
H	3.97630600	-1.42262500	0.82834900
H	2.42035900	-1.82765000	1.60504400
H	2.62571100	-2.08859700	-0.14616600
C	-3.16465800	0.64261800	1.11488400

H	-2.89198700	-0.06237800	1.90143300
H	-2.87058100	1.65045500	1.40957300
H	-4.24102400	0.61119400	0.92933600
C	-2.89166800	-1.44996900	-0.69739700
H	-3.97607700	-1.42279500	-0.82849600
H	-2.42007400	-1.82744200	-1.60528000
H	-2.62534700	-2.08865900	0.14589900

21) (C₆F₅)₂



Number of imaginary frequencies = 0

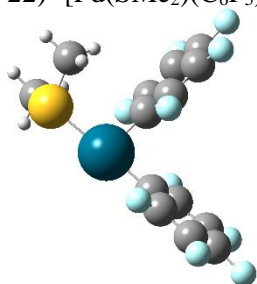
E_{total} = -1455.61715120 a.u

G_{correction} = 0.053058 a.u

Cartesian coordinates:

C	0.73801600	0.00002600	-0.00000400
C	1.46494300	-1.06539300	-0.53948300
C	1.46496500	1.06542100	0.53948600
C	2.85505300	-1.07790500	-0.53916100
C	2.85508000	1.07790300	0.53916100
C	3.55160500	-0.00000400	-0.00000500
C	-0.73801800	0.00002600	-0.00000200
C	-1.46496500	1.06541100	-0.53950000
C	-1.46494300	-1.06539300	0.53949100
C	-2.85508400	1.07789800	-0.53917800
C	-2.85504900	-1.07790100	0.53916800
C	-3.55160300	-0.00000300	-0.00000100
F	0.82200000	-2.10521900	-1.08571600
F	0.82205800	2.10523600	1.08578000
F	3.52371600	2.11015200	1.06415000
F	4.88596800	-0.00002700	-0.00000100
F	3.52367300	-2.11017800	-1.06412300
F	-0.82206100	2.10522900	-1.08579700
F	-0.82199400	-2.10520400	1.08574200
F	-3.52368300	-2.11015800	1.06414500
F	-3.52371000	2.11014900	-1.06417100
F	-4.88596700	-0.00003600	0.00000800

22) [Pd(SMe₂)(C₆F₅)₂] (**14**)



Number of imaginary frequencies = 0

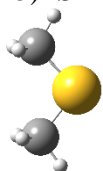
$E_{\text{total}} = -2061.60974416 \text{ a.u}$

$G_{\text{correction}} = 0.117140 \text{ a.u}$

Cartesian coordinates:

Pd	-0.22117200	-1.54748700	-0.16254800
C	1.55890200	-0.60863200	-0.24748600
C	1.92650400	0.30835100	-1.22553500
C	2.51028500	-0.88169200	0.72951300
C	3.17762900	0.91946400	-1.25042600
C	3.77148400	-0.29366100	0.74376000
C	4.10395300	0.61588300	-0.25657200
C	-1.02233400	0.23067600	0.11037400
C	-0.94782600	0.87824500	1.33702300
C	-1.73076100	0.86732800	-0.90120400
C	-1.56783500	2.10420600	1.56626000
C	-2.36520700	2.09126200	-0.70479100
C	-2.27990700	2.71404000	0.53745800
F	1.06281300	0.64408200	-2.21117100
F	2.22865800	-1.76104100	1.72343700
F	4.66736900	-0.58903500	1.69988300
F	5.31425500	1.19123400	-0.26724200
F	3.50421900	1.79273000	-2.21732100
F	-0.27494900	0.31940500	2.36615100
F	-1.85007400	0.29585700	-2.12185800
F	-3.05415000	2.67446200	-1.69714500
F	-1.49095300	2.69935200	2.76596600
F	-2.88666100	3.89046200	0.74400100
S	-2.31317200	-2.75581900	0.06095100
C	-3.23303300	-2.59018200	-1.50680800
H	-4.22390300	-3.03037500	-1.38321500
H	-3.30177200	-1.54327800	-1.79917100
H	-2.67577500	-3.14639600	-2.26160200
C	-3.37983700	-1.78828500	1.17934700
H	-3.50848600	-0.77559100	0.79614900
H	-4.34261600	-2.29225000	1.27450600
H	-2.87964500	-1.75420600	2.14752600

23) **SMe₂**



Number of imaginary frequencies = 0

$E_{\text{total}} = -478.03511113 \text{ a.u}$

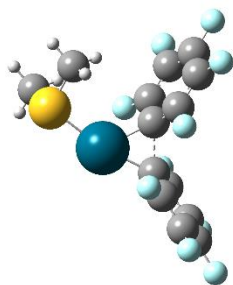
$G_{\text{correction}} = 0.049080 \text{ a.u}$

Cartesian coordinates:

C	1.39257100	-0.51597100	-0.00000900
H	1.36890800	-1.14417200	0.89380000

H	1.36882000	-1.14426000	-0.89375300
H	2.31391600	0.06945000	-0.00008000
C	-1.39257100	-0.51597100	-0.00000400
H	-1.36885500	-1.14422100	-0.89377800
H	-1.36887400	-1.14421200	0.89377600
H	-2.31391600	0.06945000	-0.00001700
S	0.00000000	0.66435100	0.00000800

24) TS(14-15)



Number of imaginary frequencies = 1 ($i250.02 \text{ cm}^{-1}$)

$E_{\text{total}} = -2061.57323865 \text{ a.u.}$

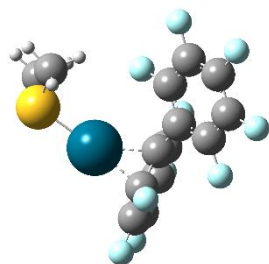
$G_{\text{correction}} = 0.117148 \text{ a.u.}$

Cartesian coordinates:

Pd	0.33257200	-1.58779900	0.00994600
C	-1.19996500	-0.19367400	0.11314700
C	-1.83802400	0.29095000	1.27318100
C	-2.07287000	-0.46428000	-0.96812500
C	-3.20408000	0.52658900	1.34953000
C	-3.44133500	-0.23867000	-0.91198600
C	-4.01544300	0.26868600	0.24956700
C	0.47078000	0.46981100	-0.09010500
C	0.59784900	1.26110100	-1.24893800
C	1.27442200	0.89589800	0.99468200
C	1.41470000	2.38248100	-1.32368000
C	2.10071200	2.00875900	0.93884100
C	2.16696500	2.77324800	-0.22240700
F	-1.12188600	0.59488500	2.36808300
F	-1.62223600	-1.03840300	-2.10315800
F	-4.22365700	-0.54772000	-1.95599100
F	-5.33213200	0.48408700	0.31550400
F	-3.74645100	1.00491200	2.47806500
F	-0.10864700	0.96722300	-2.35497800
F	1.36098400	0.15759300	2.12455700
F	2.87378700	2.32958500	1.98741600
F	1.47359100	3.09611300	-2.45766900
F	2.95869900	3.85015600	-0.28420700
S	2.37420800	-2.85024400	-0.26860200
C	3.20625100	-2.78163700	1.35831000
H	4.23371600	-3.13639400	1.25581400
H	3.18458800	-1.76468600	1.75135900
H	2.65555400	-3.44336600	2.02810600
C	3.41107100	-1.66417600	-1.19453700
H	3.38106500	-0.68618800	-0.71068900

H	4.43588400	-2.03650000	-1.25100400
H	2.98886200	-1.58663200	-2.19693200

25) Intermediate-15



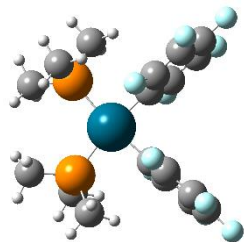
Number of imaginary frequencies = 0

$E_{\text{total}} = -2061.61611623$ a.u

$G_{\text{correction}} = 0.118200$ a.u

Cartesian coordinates:

Pd	1.22787300	0.91515600	-0.66754500
C	0.22723900	-0.81892900	0.23308100
C	0.85547100	-1.06992600	1.48899200
C	0.97909200	-1.16779400	-0.94414600
C	2.10538400	-1.63647700	1.58624600
C	2.26280100	-1.77187500	-0.82004400
C	2.82038600	-1.97935900	0.42128400
C	-1.24824300	-0.64121400	0.19281900
C	-2.07542600	-1.62183600	-0.36260700
C	-1.87566400	0.48605800	0.73155100
C	-3.45679800	-1.46778200	-0.43144200
C	-3.25258100	0.66069800	0.67574200
C	-4.04793300	-0.32215800	0.09187900
F	0.18147200	-0.77809100	2.61369200
F	0.33467300	-1.38003000	-2.12567800
F	2.91355700	-2.14274500	-1.93021300
F	4.05432200	-2.48508200	0.53993500
F	2.68224000	-1.82698700	2.78166400
F	-1.54417100	-2.75600600	-0.83879600
F	-1.14837200	1.46439600	1.29839700
F	-3.81560600	1.76515600	1.17965600
F	-4.21784600	-2.42273600	-0.97695700
F	-5.37268300	-0.16636700	0.03815500
S	1.47815200	3.28551400	-0.72008600
C	1.80687100	3.77484600	1.01115700
H	1.79290200	4.86396700	1.08885400
H	1.06256200	3.33234600	1.67428200
H	2.79790300	3.39945800	1.26834700
C	-0.22424200	3.93166500	-0.90199800
H	-0.88082000	3.46563200	-0.16709200
H	-0.21437100	5.01696400	-0.78084900
H	-0.55719700	3.67713600	-1.90886100

26) [Pd(PMe₃)₂(C₆F₅)₂] (16)

Number of imaginary frequencies = 0

$E_{\text{total}} = -2505.92212439$ a.u

$G_{\text{correction}} = 0.260071$ a.u

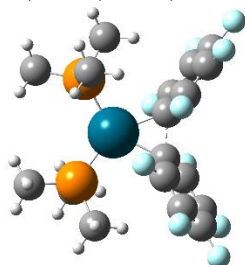
Cartesian coordinates:

Pd	0.00012100	1.00214300	0.00005100
C	1.39492700	-0.50641200	-0.08773600
C	2.18768300	-0.81099700	1.00794700
C	1.59409300	-1.28397600	-1.21706800
C	3.13778800	-1.82881600	1.00247900
C	2.52983700	-2.31410600	-1.27529900
C	3.30608600	-2.58878300	-0.15235200
C	-1.39482600	-0.50635900	0.08761000
C	-2.18752500	-0.81119700	-1.00803100
C	-1.59406800	-1.28369800	1.21709800
C	-3.13766100	-1.82898900	-1.00238400
C	-2.52982800	-2.31379600	1.27552100
C	-3.30604900	-2.58869200	0.15260200
F	2.08286300	-0.07424900	2.14809600
F	0.87556500	-1.04019600	-2.34246300
F	2.70024500	-3.03974700	-2.39371000
F	4.21528800	-3.57544400	-0.18428700
F	3.89306300	-2.08535800	2.08441900
F	-2.08251600	-0.07485100	-2.14842900
F	-0.87557900	-1.03969500	2.34248000
F	-2.70029400	-3.03919600	2.39407700
F	-3.89284600	-2.08576700	-2.08433100
F	-4.21526200	-3.57533300	0.18469600
C	-3.25821400	1.86797300	1.05342000
H	-3.66726700	1.06664500	0.43666500
H	-2.99294900	1.44632800	2.02566000
H	-4.00836300	2.65293200	1.18507700
C	-2.37292500	3.26008100	-1.30967500
H	-3.20011800	3.95322500	-1.13045500
H	-1.56428800	3.78285700	-1.82463700
H	-2.70946200	2.43949400	-1.94699200
C	3.25871000	1.86841700	-1.05242400
H	3.66796100	1.06766300	-0.43505000
H	2.99390000	1.44600000	-2.02445100
H	4.00854500	2.65362000	-1.18439500
C	2.37211600	3.26231600	1.30908400
H	3.19886900	3.95582500	1.12924900
H	1.56309800	3.78506300	1.82346000
H	2.70922800	2.44263700	1.94726400
P	1.74355300	2.54515500	-0.26220600

Appendix

P	-1.74363600	2.54490300	0.26223800
C	-1.40530400	4.01189400	1.32472700
H	-0.59079700	4.60998100	0.91280500
H	-2.29541000	4.64165800	1.41428100
H	-1.11043100	3.66659300	2.31909100
C	1.40437200	4.01085800	-1.32617100
H	0.58885200	4.60828700	-0.91530300
H	2.29379400	4.64159500	-1.41570000
H	1.11052700	3.66434100	-2.32041200

27) TS(16-17)



Number of imaginary frequencies = 1 ($i166.00\text{ cm}^{-1}$)

$E_{\text{total}} = -2505.86659944\text{ a.u}$

$G_{\text{correction}} = 0.258635\text{ a.u}$

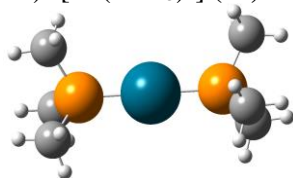
Cartesian coordinates:

Pd	-0.04586900	1.15699600	-0.08477800
C	0.88592100	-0.77733200	-0.04180800
C	1.55550300	-1.39453000	1.03966200
C	1.58285600	-0.89115600	-1.27475100
C	2.75265000	-2.08406900	0.91716700
C	2.77742400	-1.57518800	-1.42204400
C	3.37065100	-2.19695500	-0.32518900
C	-0.82782100	-0.84890300	0.01896400
C	-1.43241300	-1.61825100	-1.00053700
C	-1.52451400	-0.90369500	1.25563300
C	-2.57687900	-2.38162900	-0.81920100
C	-2.66973500	-1.65445300	1.45886900
C	-3.20275500	-2.41824600	0.42316500
F	1.03132700	-1.32399700	2.27956800
F	1.16991700	-0.18814700	-2.35476000
F	3.40337600	-1.59327000	-2.60923100
F	4.51764800	-2.87477000	-0.46025100
F	3.31884500	-2.64761000	1.99548400
F	-0.89311900	-1.63958600	-2.23388300
F	-1.17601300	-0.08198900	2.27347000
F	-3.30876800	-1.60427000	2.63837300
F	-3.08212200	-3.09065200	-1.84026600
F	-4.30176600	-3.15860800	0.61474300
C	-3.55180800	1.55409500	-0.14110000
H	-3.57606000	0.54388200	-0.55777200
H	-3.58605000	1.47214700	0.94834800
H	-4.42722400	2.11061600	-0.49017000
C	-2.21695900	2.56936500	-2.46465400
H	-3.15445700	3.08738300	-2.69177100

Appendix

H	-1.38021400	3.13505200	-2.88226900
H	-2.22547200	1.58181600	-2.93307700
C	3.42873700	1.86040200	-0.04749900
H	3.53313600	0.79745200	0.18289100
H	3.46558000	1.97840800	-1.13356700
H	4.25926900	2.41064300	0.40577600
C	2.03635000	2.29727900	2.41228800
H	2.94524100	2.81098600	2.74262100
H	1.17213100	2.72330100	2.92806700
H	2.09818500	1.23889800	2.67746900
P	1.79585100	2.44258200	0.58691700
P	-1.97273500	2.36623200	-0.64662200
C	-2.20087600	4.08865000	-0.02476500
H	-1.36861200	4.70597400	-0.37329000
H	-3.14343700	4.52765400	-0.36779300
H	-2.18546200	4.07909900	1.06847000
C	1.89783200	4.26718900	0.32608800
H	1.01105600	4.73936000	0.75742900
H	2.79346700	4.69380700	0.78933100
H	1.91323200	4.48015000	-0.74623000

28) [Pd(PMe₃)₂] (17)



Number of imaginary frequencies = 0

$E_{\text{total}} = -1050.27777395$ a.u

$G_{\text{correction}} = 0.182638$ a.u

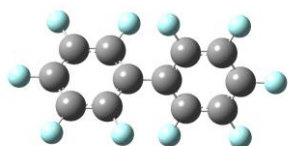
Cartesian coordinates:

Pd	-0.00001000	0.00151700	0.00019300
C	3.13637900	-0.47475400	1.57917000
H	2.82601600	0.20986600	2.37250300
H	2.82833700	-1.48468200	1.86157600
H	4.22698100	-0.44327200	1.47939700
C	3.13706100	1.60400700	-0.38007300
H	4.22758400	1.50166700	-0.35629700
H	2.82759500	1.94736400	-1.37037800
H	2.82862500	2.35448500	0.35209500
C	-3.13681200	1.59123900	0.42947100
H	-2.82981500	1.90194500	1.43137200
H	-2.82620100	2.36543300	-0.27664900
H	-4.22735200	1.49029700	0.39976700
C	-3.13568100	-1.16852500	1.16407200
H	-4.22623300	-1.09613200	1.08878700
H	-2.82446600	-2.19089100	0.93495400
H	-2.82825600	-0.94087000	2.18782700

Appendix

P	-2.29756100	-0.00054500	-0.00039900
P	2.29773400	-0.00041800	-0.00027000
C	3.13649600	-1.13217800	-1.19954200
H	2.82664100	-0.87489200	-2.21559700
H	4.22698400	-1.05940800	-1.12378300
H	2.82857100	-2.16170900	-1.00045300
C	-3.13759200	-0.42559600	-1.59315500
H	-2.82778600	-1.42501100	-1.90878500
H	-4.22804900	-0.39985700	-1.49046800
H	-2.83039600	0.28518800	-2.36437900

29) $(C_6F_5)_2$



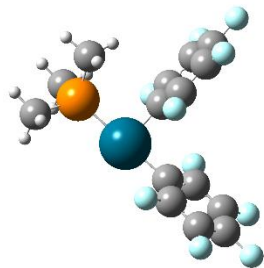
Number of imaginary frequencies = 0

$E_{\text{total}} = -1455.61597898 \text{ a.u.}$

$G_{\text{correction}} = 0.053206 \text{ a.u.}$

Cartesian coordinates:

C	0.73804500	0.00001000	0.00000000
C	1.46466400	-1.06542100	-0.54029900
C	1.46467200	1.06543100	0.54029800
C	2.85505900	-1.07802400	-0.53995000
C	2.85507100	1.07802100	0.53995000
C	3.55159100	-0.00000200	-0.00000100
C	-0.73804600	0.00001000	-0.00000200
C	-1.46467100	1.06542200	-0.54031000
C	-1.46466500	-1.06542000	0.54031000
C	-2.85507400	1.07801700	-0.53996500
C	-2.85505600	-1.07801900	0.53995900
C	-3.55158800	0.00000100	-0.00000300
F	0.82124900	-2.10397800	-1.08726300
F	0.82127400	2.10398700	1.08728100
F	3.52354200	2.10938900	1.06534900
F	4.88545600	-0.00001400	-0.00000100
F	3.52352900	-2.10939800	-1.06533800
F	-0.82127600	2.10397800	-1.08730000
F	-0.82124400	-2.10396400	1.08728700
F	-3.52353800	-2.10938000	1.06535800
F	-3.52353600	2.10938500	-1.06537100
F	-4.88545500	-0.00002200	0.00000500

30) [Pd(PMe₃)(C₆F₅)₂] (**18**)

Number of imaginary frequencies = 0

$E_{\text{total}} = -2044.71825905$ a.u

$G_{\text{correction}} = 0.152695$ a.u

Cartesian coordinates:

Pd	-0.29890000	-1.37438700	-0.25690900
C	1.60432200	-0.63535900	-0.29651300
C	2.07977900	0.31819700	-1.18820500
C	2.51410500	-1.10183300	0.64469100
C	3.39247500	0.78313500	-1.16468200
C	3.83473200	-0.66906700	0.70819100
C	4.27296800	0.28495100	-0.20723400
C	-0.92243500	0.46569000	0.09801200
C	-0.77921900	1.03944900	1.35431800
C	-1.54901000	1.22220900	-0.88383100
C	-1.24863200	2.31990800	1.63826800
C	-2.03117200	2.50433800	-0.63181400
C	-1.87654700	3.05657000	0.63736700
F	1.26455400	0.83790900	-2.13523900
F	2.12369900	-2.03463600	1.55280700
F	4.68701000	-1.15217200	1.62668700
F	5.54113400	0.71564800	-0.17247800
F	3.82290000	1.69791600	-2.04866800
F	-0.19079200	0.35239400	2.35606700
F	-1.74118400	0.71516000	-2.12274800
F	-2.64232200	3.20906000	-1.59487500
F	-1.10787300	2.84607800	2.86329600
F	-2.33672500	4.28729300	0.89580800
P	-2.52478000	-2.15059500	-0.12122100
C	-3.49166100	-2.06672200	-1.68124800
H	-3.01199600	-2.69306600	-2.43761200
H	-4.51920500	-2.40843000	-1.52558100
H	-3.49342100	-1.03688200	-2.04216100
C	-3.56313500	-1.23676200	1.08652100
H	-4.56565400	-1.66941800	1.14635000
H	-3.08835100	-1.27330600	2.06979100
H	-3.63529000	-0.19132300	0.77980700
C	-2.68798400	-3.90618500	0.40606300
H	-2.22789600	-4.03574400	1.38885400
H	-3.74042500	-4.20055900	0.45901300
H	-2.17176000	-4.55352700	-0.30768100

31) **PMe₃**

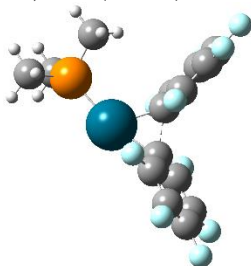
Number of imaginary frequencies = 0

$E_{\text{total}} = -461.13081969$ a.u

$G_{\text{correction}} = 0.083723$ a.u

Cartesian coordinates:

C	0.64436700	-1.50598000	0.28050100
H	0.05787200	-2.38203400	-0.01112000
H	1.68338900	-1.68592100	-0.01030800
H	0.59635600	-1.39501800	1.36957900
C	-1.62648300	0.19514200	0.28062200
H	-1.50697000	0.17920200	1.36974100
H	-2.09097800	1.14198700	-0.00962200
H	-2.30248300	-0.61356200	-0.01195100
P	-0.00013900	-0.00004200	-0.60624700
C	0.98234600	1.31090800	0.28043800
H	0.61828600	2.30078600	-0.00965100
H	0.91107300	1.21333500	1.36951200
H	2.03415400	1.24143400	-0.01184400

32) **TS(18-19)**

Number of imaginary frequencies = 1 ($i279.53$ cm⁻¹)

$E_{\text{total}} = -2044.68525615$ a.u

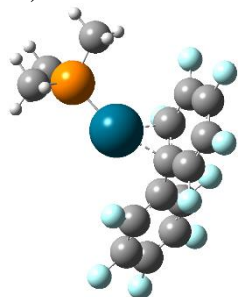
$G_{\text{correction}} = 0.152850$ a.u

Cartesian coordinates:

Pd	-0.49495600	-1.38282900	-0.19761700
C	1.28248000	-0.28077700	-0.14902400
C	2.02717600	0.21029800	-1.23721700
C	2.05450700	-0.79223200	0.91796300
C	3.41607000	0.23179100	-1.25866500
C	3.44348900	-0.78325500	0.91744800
C	4.13313700	-0.26015100	-0.17241500
C	-0.30068700	0.65375900	0.09074700
C	-0.32346000	1.32973900	1.32355900
C	-0.95232600	1.32915100	-0.96474600
C	-0.91519300	2.57524300	1.49714400
C	-1.55346200	2.57067800	-0.81141000

C	-1.52742000	3.21246700	0.42380800
F	1.40879800	0.72689500	-2.31032300
F	1.47284200	-1.39416300	1.97536200
F	4.12700900	-1.31187500	1.94135900
F	5.46832600	-0.25087600	-0.18518300
F	4.06977300	0.72530800	-2.31863700
F	0.25235200	0.78448000	2.40951900
F	-1.12627400	0.73138300	-2.16277100
F	-2.19840500	3.14003300	-1.84049700
F	-0.89160000	3.16883200	2.69900500
F	-2.09840000	4.41247300	0.57949100
P	-2.71079700	-2.10445200	-0.07300500
C	-3.59036300	-2.36585400	-1.67204500
H	-3.12935400	-3.19825200	-2.20988200
H	-4.65138700	-2.58273100	-1.51249100
H	-3.49150400	-1.46621400	-2.28444600
C	-3.73736100	-0.80677400	0.73999200
H	-4.79546800	-1.08501200	0.76547100
H	-3.37593300	-0.65335100	1.75986300
H	-3.62079700	0.13314800	0.19452700
C	-3.15205900	-3.61991200	0.88100200
H	-2.77598300	-3.52678800	1.90292000
H	-4.23611300	-3.76992200	0.90733600
H	-2.68050200	-4.49139500	0.41938800

33) Intermediate-19



Number of imaginary frequencies = 0

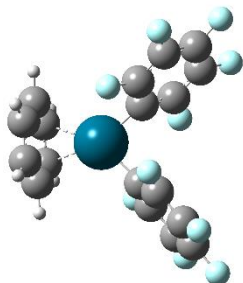
$E_{\text{total}} = -2044.73094521$ a.u

$G_{\text{correction}} = 0.152703$ a.u

Cartesian coordinates:

Pd	1.13905800	-0.73809000	-0.31932000
C	-0.40652200	0.86291300	-0.16852700
C	-0.12529500	1.76486200	-1.23677400
C	0.49998000	0.88246500	0.94801300
C	0.92293800	2.65541100	-1.19182500
C	1.54159900	1.84937800	1.00180100
C	1.76190500	2.69593200	-0.05807300
C	-1.76095200	0.26592100	-0.04951000
C	-2.64597600	0.68834400	0.94633000
C	-2.21557400	-0.71845700	-0.92995600
C	-3.91786900	0.13986700	1.07948500
C	-3.48451900	-1.27518100	-0.82375100
C	-4.33869300	-0.84353000	0.18843800
F	-0.94665000	1.77460400	-2.29811100

F	0.09711200	0.37752200	2.14475700
F	2.34835200	1.87179700	2.07396800
F	2.80711800	3.53184400	-0.05581900
F	1.18115400	3.47294600	-2.22333200
F	-2.28097200	1.65644800	1.79702800
F	-1.40733100	-1.17256000	-1.90350500
F	-3.88492000	-2.22405900	-1.67694600
F	-4.74178000	0.56286800	2.04409000
F	-5.55898200	-1.37212200	0.30310100
P	2.97618200	-2.01602200	0.18616200
C	3.76553500	-3.10055800	-1.08245300
H	4.05208300	-2.49792300	-1.94807000
H	4.65324700	-3.60088000	-0.68174500
H	3.04616700	-3.85457000	-1.41233700
C	2.76627100	-3.17595300	1.60539400
H	3.70968600	-3.67227500	1.85579900
H	2.40870200	-2.61685800	2.47353300
H	2.01726200	-3.93027700	1.35175000
C	4.39389900	-0.97430000	0.74577000
H	4.05986600	-0.32749000	1.56077000
H	5.23631900	-1.58665000	1.08398000
H	4.71898400	-0.33692000	-0.08063400

34) [Pd(C₆H₆)(C₆F₅)₂] (20)

Number of imaginary frequencies = 0

$E_{\text{total}} = -1815.83598343 \text{ a.u.}$

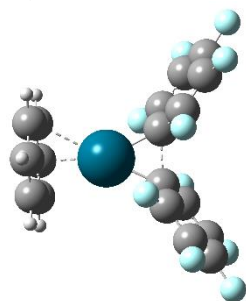
$G_{\text{correction}} = 0.139543 \text{ a.u.}$

Cartesian coordinates:

Pd	0.00015600	1.35136400	-0.00064100
C	1.33792000	-0.09891300	-0.21526400
C	2.36542600	-0.21497200	0.71410700
C	1.33360800	-1.00672000	-1.26716000
C	3.36174000	-1.18078600	0.60880600
C	2.31389200	-1.98746800	-1.40437600
C	3.33181400	-2.07448500	-0.45879600
C	-1.33803100	-0.09842300	0.21488000
C	-2.36548600	-0.21483700	-0.71449600
C	-1.33401700	-1.00553400	1.26737800
C	-3.36204100	-1.18034600	-0.60863900
C	-2.31455900	-1.98593800	1.40517800
C	-3.33242000	-2.07333400	0.45956500
F	2.42858300	0.63187700	1.76841800
F	0.36851300	-0.96363100	-2.21014400

F	2.29087800	-2.84408300	-2.43666100
F	4.28452500	-3.00816800	-0.57991200
F	4.34445200	-1.26232700	1.51890200
F	-2.42832800	0.63131900	-1.76937900
F	-0.36897500	-0.96207100	2.21040100
F	-2.29184400	-2.84186900	2.43803600
F	-4.34470100	-1.26226900	-1.51875800
F	-4.28537500	-3.00669600	0.58123900
C	0.10531100	3.61160100	-1.40979600
C	1.26103100	3.56308200	-0.60827900
C	1.15792600	3.58606300	0.79939900
C	-0.10400900	3.61222900	1.40992700
C	-1.25978500	3.56394800	0.60843100
C	-1.15672300	3.58630900	-0.79924200
H	0.19055200	3.61487800	-2.49017500
H	2.24028100	3.52942800	-1.07286500
H	2.05596400	3.56381700	1.40543200
H	-0.18927700	3.61604300	2.49030200
H	-2.23904200	3.53105800	1.07305400
H	-2.05476600	3.56442000	-1.40528500

35) **TS(20-21)**



Number of imaginary frequencies = 1 ($i264.41 \text{ cm}^{-1}$)

$E_{\text{total}} = -1815.80674228 \text{ a.u.}$

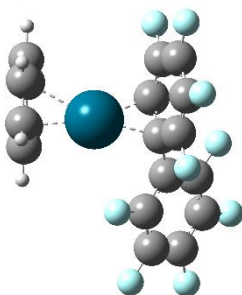
$G_{\text{correction}} = 0.140908 \text{ a.u.}$

Cartesian coordinates:

Pd	-0.44568900	1.24318500	-0.51061500
C	-0.64003900	-0.78018200	-0.17269500
C	-0.62728400	-1.81557500	-1.12500800
C	-1.56088900	-0.95384800	0.88457700
C	-1.43062600	-2.94507400	-1.02659700
C	-2.37416700	-2.07355200	0.99907600
C	-2.30562200	-3.08471000	0.04545700
C	1.05198400	-0.05389000	0.05520400
C	1.53414400	-0.28002700	1.35708500
C	2.03871300	-0.05630500	-0.95549900
C	2.87239200	-0.52908700	1.63687500
C	3.38049600	-0.30203600	-0.69691100
C	3.80479700	-0.55033700	0.60529200
F	0.20767600	-1.76809300	-2.17515100
F	-1.75916900	0.01452600	1.80104000
F	-3.25592900	-2.16925400	2.00374500

F	-3.08474900	-4.16530100	0.14721000
F	-1.36109100	-3.90487800	-1.95866600
F	0.69169400	-0.30178600	2.40206400
F	1.73205200	0.26508800	-2.22823400
F	4.28039700	-0.25961100	-1.68881500
F	3.26725300	-0.75545200	2.89698300
F	5.09457900	-0.78464600	0.86295700
C	-2.86140700	3.17522800	0.32846800
C	-2.45827200	2.83651800	-0.97106600
C	-1.16717200	3.19645100	-1.42608400
C	-0.27800600	3.84699200	-0.53770800
C	-0.69980200	4.17660600	0.75822900
C	-1.99195500	3.85775900	1.18270500
H	-3.85886600	2.91185400	0.66479200
H	-3.15275700	2.35386300	-1.65026900
H	-0.89797700	3.06327700	-2.46965200
H	0.70704200	4.14176400	-0.88349000
H	-0.01816300	4.69113900	1.42769700
H	-2.31572700	4.12666700	2.18262400

36) Intermediate-21



Number of imaginary frequencies = 0

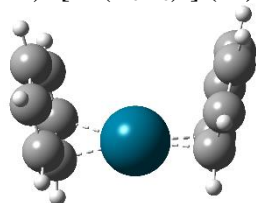
$E_{\text{total}} = -1815.85117254$ a.u

$G_{\text{correction}} = 0.140755$ a.u

Cartesian coordinates:

Pd	-1.14939900	-0.68832200	-0.56346900
C	1.68993300	0.23784600	0.14704800
C	2.69978000	1.03388600	-0.40111500
C	2.06043400	-1.02127200	0.62558200
C	4.01293500	0.58652900	-0.50844800
C	3.36690900	-1.48766500	0.53405500
C	4.34749800	-0.67931800	-0.03576600
C	0.29638300	0.74837600	0.24653300
C	-0.19668500	1.15427300	1.52383000
C	-0.38884200	1.27002800	-0.90672300
C	-1.24946300	2.02819200	1.66024600
C	-1.45568100	2.19934600	-0.74262300
C	-1.88778600	2.54916100	0.51550700
F	2.41660200	2.27119700	-0.82951700
F	1.14295600	-1.83444300	1.17205900
F	3.68528300	-2.70500300	0.98790100

F	5.60525100	-1.11670800	-0.12603400
F	4.95474500	1.37060700	-1.04304600
F	0.42312700	0.69722800	2.62297100
F	0.24663400	1.30049100	-2.10948600
F	-2.04347300	2.71001000	-1.83196600
F	-1.71479400	2.36289500	2.87198800
F	-2.94426300	3.35522300	0.67280800
C	-2.07873900	-3.01634100	0.23611000
C	-2.09276500	-2.63571500	-1.12868600
C	-3.17313400	-1.85955700	-1.61767800
C	-4.23575500	-1.52337800	-0.76476400
C	-4.23090000	-1.94274800	0.56682000
C	-3.14778200	-2.67054600	1.07049800
H	-1.26186800	-3.62041400	0.61577300
H	-1.35374800	-3.03946400	-1.81523700
H	-3.20909600	-1.58843700	-2.66745700
H	-5.06850700	-0.94477700	-1.15153300
H	-5.06393200	-1.69311100	1.21599700
H	-3.13717400	-2.98103900	2.11036500

37) [Pd(C₆H₆)₂] (22)

Number of imaginary frequencies = 0

$E_{\text{total}} = -592.51722559$ a.u

$G_{\text{correction}} = 0.158618$ a.u

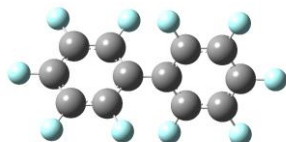
Cartesian coordinates:

Pd	-0.01545600	-0.70586400	0.00436100
C	2.09076200	-0.79849600	0.76968300
C	2.34825700	0.44093900	1.41138500
C	2.12105300	-0.86363300	-0.65194600
C	2.64267000	1.57240700	0.66479000
C	2.40950400	0.31212900	-1.39315500
C	2.67360200	1.50780900	-0.74143200
C	-2.27790100	-0.30641900	1.19002800
C	-2.19399900	-0.99432200	-0.04837700
C	-2.24554900	-0.24402400	-1.25163000
C	-2.44027100	1.14261000	-1.20868900
C	-2.57317500	1.79910500	0.01763900
C	-2.47166700	1.08120300	1.21196100
H	-2.27320100	-0.87042900	2.11689500
H	-2.25651000	-2.07921200	-0.07710800
H	-2.21231200	-0.76009600	-2.20547200
H	-2.50005100	1.70354700	-2.13622000
H	-2.74335200	2.87092800	0.04275300
H	-2.55606100	1.59445600	2.16487400

Appendix

H	2.07033300	-1.71111900	1.35882800
H	2.12364600	-1.82646000	-1.15545800
H	2.45117900	0.25721100	-2.47678800
H	2.90968400	2.39762700	-1.31723200
H	2.85519400	2.51163800	1.16652800
H	2.34273400	0.48578500	2.49626900

38) (C₆F₅)₂



Number of imaginary frequencies = 0

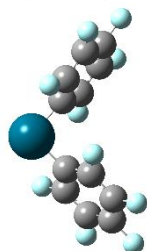
$E_{\text{total}} = -1455.61597898$ a.u

$G_{\text{correction}} = 0.053206$ a.u

Cartesian coordinates:

C	0.73804500	0.00001000	0.00000000
C	1.46466400	-1.06542100	-0.54029900
C	1.46467200	1.06543100	0.54029800
C	2.85505900	-1.07802400	-0.53995000
C	2.85507100	1.07802100	0.53995000
C	3.55159100	-0.00000200	-0.00000100
C	-0.73804600	0.00001000	-0.00000200
C	-1.46467100	1.06542200	-0.54031000
C	-1.46466500	-1.06542000	0.54031000
C	-2.85507400	1.07801700	-0.53996500
C	-2.85505600	-1.07801900	0.53995900
C	-3.55158800	0.00000100	-0.00000300
F	0.82124900	-2.10397800	-1.08726300
F	0.82127400	2.10398700	1.08728100
F	3.52354200	2.10938900	1.06534900
F	4.88545600	-0.00001400	-0.00000100
F	3.52352900	-2.10939800	-1.06533800
F	-0.82127600	2.10397800	-1.08730000
F	-0.82124400	-2.10396400	1.08728700
F	-3.52353800	-2.10938000	1.06535800
F	-3.52353600	2.10938500	-1.06537100
F	-4.88545500	-0.00002200	0.00000500

39) [Pd(C₆F₅)₂] (**23**)



Number of imaginary frequencies = 0

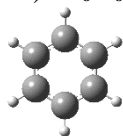
$E_{\text{total}} = -1583.52090997 \text{ a.u.}$

$G_{\text{correction}} = 0.046148 \text{ a.u.}$

Cartesian coordinates:

Pd	-0.00514400	2.04145700	0.11334000
C	-1.34404800	0.60803900	0.23149100
C	-2.31657200	0.50550900	-0.75995300
C	-1.38211800	-0.31383200	1.27346600
C	-3.31654300	-0.46142500	-0.71035700
C	-2.37084200	-1.29211100	1.34781500
C	-3.33960800	-1.36494400	0.34971800
C	1.34052300	0.63804800	-0.16412100
C	2.29187900	0.41015100	0.82642900
C	1.40408400	-0.13894900	-1.31663900
C	3.29802700	-0.53902000	0.67259800
C	2.39976500	-1.09620100	-1.49703300
C	3.34787200	-1.29579000	-0.49618300
F	-2.32237300	1.36095100	-1.80294100
F	-0.45821900	-0.28668900	2.25190600
F	-2.39970100	-2.16091700	2.36665100
F	-4.29690600	-2.29540100	0.41373300
F	-4.25214500	-0.53186300	-1.66593300
F	2.26689100	1.12270800	1.97107100
F	0.49915000	0.01390800	-2.30140200
F	2.45563100	-1.82398200	-2.62001200
F	4.21398800	-0.73209200	1.63036200
F	4.31169500	-2.20705300	-0.66088500

40) C_6H_6



Number of imaginary frequencies = 0

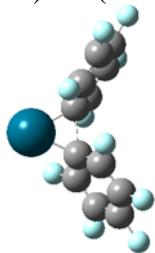
$E_{\text{total}} = -232.27814567 \text{ a.u.}$

$G_{\text{correction}} = 0.073222 \text{ a.u.}$

Cartesian coordinates:

C	1.06383300	-0.90425300	-0.00000500
C	-0.25133100	-1.37329800	-0.00006700
C	-1.31506700	-0.46915300	0.00005500
C	-1.06375600	0.90434200	-0.00000800
C	0.25121500	1.37331700	-0.00006100
C	1.31510700	0.46904700	0.00005600
H	1.89119200	-1.60781000	0.00006500
H	-0.44663500	-2.44167100	-0.00007700
H	-2.33801000	-0.83396700	0.00014800
H	-1.89128800	1.60768700	-0.00000900
H	0.44676800	2.44163800	-0.00001400
H	2.33796800	0.83411400	0.00005900

41) TS(23-24)



Number of imaginary frequencies = 1 ($i267.61 \text{ cm}^{-1}$)

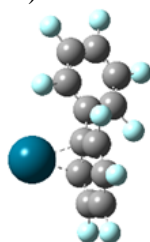
$E_{\text{total}} = -1583.49220244 \text{ a.u.}$

$G_{\text{correction}} = 0.048602 \text{ a.u.}$

Cartesian coordinates:

Pd	-0.00006100	0.00023900	2.16002400
C	-0.91885400	-0.12247100	0.32900700
C	-1.84145000	0.94429700	0.23314800
C	-1.28209900	-1.28736200	-0.37411000
C	-3.00388000	0.87050400	-0.52280000
C	-2.43962800	-1.38023000	-1.13709700
C	-3.30552900	-0.29470400	-1.22180100
C	0.91889400	0.12255400	0.32902900
C	1.84148200	-0.94424200	0.23340900
C	1.28215400	1.28729000	-0.37433100
C	3.00391500	-0.87061400	-0.52255300
C	2.43967400	1.37998700	-1.13735100
C	3.30557100	0.29443900	-1.22181000
F	-1.66969200	2.07649400	0.94462800
F	-0.48075000	-2.36343900	-0.37168400
F	-2.72189600	-2.50953400	-1.79884100
F	-4.42348500	-0.37734600	-1.94667200
F	-3.85923500	1.90039300	-0.55167900
F	1.66968300	-2.07631200	0.94507200
F	0.48080000	2.36336500	-0.37215500
F	2.72193100	2.50913700	-1.79936100
F	3.85926200	-1.90051600	-0.55122100
F	4.42352700	0.37690700	-1.94670100

42) Intermediate-24



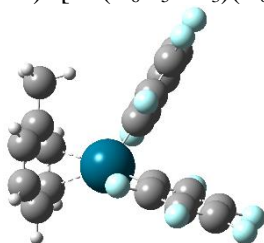
Number of imaginary frequencies = 0

$E_{\text{total}} = -1583.53477720 \text{ a.u.}$

$G_{\text{correction}} = 0.049145 \text{ a.u.}$

Cartesian coordinates:

Pd	1.19815500	-1.49563800	-1.12346400
C	-1.05092900	0.14037800	0.15902200
C	-1.87166300	-0.97530700	0.33562500
C	-1.68006700	1.37593600	-0.01534600
C	-3.25829600	-0.88115200	0.30852600
C	-3.06593000	1.49486500	-0.05262800
C	-3.85709400	0.36147600	0.11402000
C	0.43357300	0.04493000	0.20144600
C	1.24560700	0.58905000	-0.86467300
C	1.06594200	-0.11538900	1.47282000
C	2.58442700	1.00491300	-0.59549600
C	2.36762300	0.26643200	1.69826800
C	3.13333200	0.82537100	0.65310800
F	-1.32648500	-2.19195600	0.50378900
F	-0.94413000	2.48812800	-0.14012700
F	-3.63984100	2.68929900	-0.22770900
F	-5.18713100	0.46515300	0.08701500
F	-4.01634300	-1.97160900	0.46359000
F	0.64107900	1.20362700	-1.91887100
F	0.33928500	-0.60325200	2.49048600
F	2.94316300	0.08044400	2.89396500
F	3.29347800	1.57789000	-1.57609100
F	4.40867500	1.15231100	0.88964300

43) [Pd(C₆H₅CH₃)(C₆F₅)₂] (25)

Number of imaginary frequencies = 0

$E_{\text{total}} = -1855.16575508$ a.u

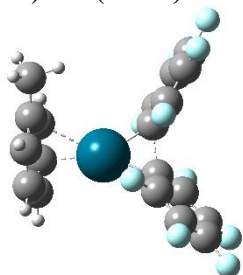
$G_{\text{correction}} = 0.165795$ a.u

Cartesian coordinates:

Pd	0.24471800	1.21677600	0.01529500
C	-1.46447300	0.23001000	-0.20820300
C	-1.72645000	-0.64488900	-1.25522300
C	-2.48469500	0.42998300	0.71506000
C	-2.95359300	-1.29013400	-1.39447500
C	-3.72305900	-0.19562000	0.60819800
C	-3.95584600	-1.06412400	-0.45525300
C	1.11342100	-0.55535300	0.20269000
C	0.85615700	-1.43186200	1.25033800
C	2.07212600	-0.94951300	-0.72426900
C	1.53073100	-2.64335400	1.38812500
C	2.76883700	-2.14910200	-0.61700800
C	2.49126600	-3.00325000	0.44696900
F	-0.78745200	-0.89904500	-2.19226500
F	-2.29677100	1.26227300	1.76639700

F	-4.68974300	0.02403300	1.51297900
F	-5.14284600	-1.67303600	-0.57798800
F	-3.18153800	-2.12164200	-2.42276700
F	-0.06363800	-1.12893500	2.19115000
F	2.37224300	-0.15310700	-1.78003200
F	3.69592200	-2.49280400	-1.52419900
F	1.27006500	-3.46320200	2.41743800
F	3.15320700	-4.16117400	0.56960500
C	0.29470900	3.56838500	1.19191300
C	-0.34479300	3.77121900	-0.04445700
C	0.36877100	3.57913900	-1.24792500
C	1.68480400	3.11110500	-1.21303100
C	2.31120600	2.81007900	0.02128700
C	1.60945200	3.07910700	1.22130600
H	-0.24239200	3.74007900	2.11738500
H	-1.37581900	4.10521500	-0.07300700
H	2.09040600	2.87771600	2.17259300
H	-0.11691900	3.76481700	-2.19927900
H	2.22094400	2.92881000	-2.13790200
C	3.71394200	2.26287600	0.04971300
H	3.94541400	1.82041000	1.02086300
H	3.84266700	1.50035200	-0.72105900
H	4.43853600	3.06245300	-0.14054500

44) TS(25-26)



Number of imaginary frequencies = 1 ($i259.13 \text{ cm}^{-1}$)

$E_{\text{total}} = -1855.13405430 \text{ a.u}$

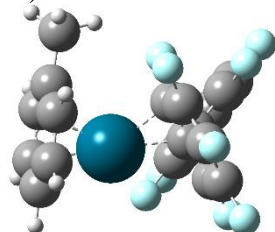
$G_{\text{correction}} = 0.164140 \text{ a.u}$

Cartesian coordinates:

Pd	-0.75822800	-0.85654300	-0.67552700
C	1.13933700	-0.24664000	-0.15379400
C	2.16626200	0.20197500	-1.00490900
C	1.56823300	-1.06356400	0.91708500
C	3.50689400	-0.09946700	-0.79940200
C	2.90216800	-1.37884200	1.13768300
C	3.88427700	-0.88739200	0.28293400
C	-0.20392100	1.00994200	0.00162300
C	-0.29923500	1.50254100	1.31608500
C	-0.51005900	1.94903400	-1.00900000
C	-0.63240600	2.81914900	1.61079300
C	-0.84593900	3.26791100	-0.73572400
C	-0.90021500	3.71478800	0.58147000
F	1.88672000	0.98961800	-2.05552100

F	0.67873000	-1.65719500	1.73826100
F	3.24853700	-2.18903100	2.14754700
F	5.17042900	-1.18642900	0.48685500
F	4.44032300	0.37182000	-1.63713900
F	-0.02712300	0.70779400	2.36386500
F	-0.57528900	1.57990000	-2.30428400
F	-1.16287300	4.10682600	-1.73159800
F	-0.69009000	3.23086000	2.88475900
F	-1.22668300	4.98175700	0.85296600
C	-1.78079400	-3.80429800	0.05554400
C	-1.51085000	-3.31905500	-1.23079600
C	-2.24997400	-2.22038600	-1.72763100
C	-3.20131400	-1.58869600	-0.89353900
C	-3.45808800	-2.07249800	0.40487500
C	-2.75413700	-3.19860900	0.85222700
H	-1.23352500	-4.66307200	0.43063100
H	-0.78715100	-3.81671000	-1.86692200
H	-2.95788100	-3.59232400	1.84345300
H	-2.15494200	-1.92089900	-2.76706600
H	-3.78562600	-0.76044800	-1.28237500
C	-4.45038700	-1.37257400	1.29595900
H	-5.27560900	-0.94551400	0.71919500
H	-4.86479300	-2.05409600	2.04319600
H	-3.96525100	-0.54915100	1.83384600

45) Intermediate-26



Number of imaginary frequencies = 0

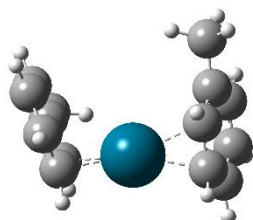
$E_{\text{total}} = -1855.17850248$ a.u

$G_{\text{correction}} = 0.167396$ a.u

Cartesian coordinates:

Pd	0.91795600	-0.91539800	-0.48106600
C	-0.48052600	0.74213700	-0.19734700
C	-0.17953700	1.68110900	-1.23254900
C	0.45934500	0.66411900	0.89022500
C	0.92322700	2.50107600	-1.18487100
C	1.56885000	1.55335800	0.94346800
C	1.80833800	2.42914600	-0.08810800
C	-1.88040400	0.26741300	-0.03579800
C	-2.68115100	0.75524200	1.00005000
C	-2.46084200	-0.65120500	-0.91273200
C	-3.99362700	0.32913500	1.17788700
C	-3.77226000	-1.08661200	-0.76101200
C	-4.54131500	-0.59324900	0.29048500
F	-1.03524800	1.79126300	-2.26061700
F	0.06774800	0.13507400	2.08149900

F	2.40831000	1.47937700	1.98529800
F	2.90539400	3.19482300	-0.09036700
F	1.20116200	3.34486300	-2.18921500
F	-2.18960100	1.66784900	1.84903700
F	-1.74263300	-1.16114900	-1.92779600
F	-4.29565400	-1.97642200	-1.61102300
F	-4.73381600	0.81151300	2.18137000
F	-5.80147500	-1.00425200	0.44641800
C	4.35505700	-0.93308400	-0.79487900
C	3.46548600	-1.70200100	-1.53790700
C	2.49458100	-2.49063300	-0.87218400
C	2.41834800	-2.44870400	0.54207800
C	3.32308200	-1.65702800	1.29229500
C	4.28981000	-0.92339700	0.60695700
H	5.11222700	-0.34264400	-1.30134500
H	3.53217100	-1.73372700	-2.62043100
H	4.99654400	-0.32216600	1.17136200
H	1.91524200	-3.22559100	-1.42670000
H	1.74530000	-3.12218000	1.06509700
C	3.20354900	-1.59703600	2.79266700
H	4.10544400	-1.17894200	3.24645000
H	2.35958100	-0.96177700	3.08077100
H	3.02978600	-2.58984500	3.22001600

46) $[\text{Pd}(\text{C}_6\text{H}_5\text{CH}_3)_2]$ (27)

Number of imaginary frequencies = 0

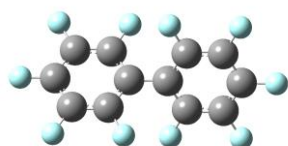
$E_{\text{total}} = -671.17130088$ a.u

$G_{\text{correction}} = 0.211236$ a.u

Cartesian coordinates:

Pd	-0.00000100	1.04075700	-0.00000400
C	1.61821600	0.10292700	-1.27948500
C	1.80801500	-1.21187900	-0.76912800
C	2.15468600	1.22371500	-0.59378200
C	2.55351400	-1.37511200	0.39337300
C	2.88331000	1.01821400	0.60789300
C	3.08659000	-0.26857100	1.08209300
C	-3.08660600	-0.26857300	-1.08207800
C	-2.88332300	1.01821100	-0.60787700
C	-2.15468300	1.22371100	0.59378800
C	-1.61820100	0.10292100	1.27948200
C	-1.80800600	-1.21188400	0.76912400
C	-2.55351900	-1.37511500	-0.39336800
H	-3.66385300	-0.42820200	-1.98791200
H	-3.30904100	1.87176200	-1.12601700
H	-2.72578500	-2.37764400	-0.77609200

H	-2.17277200	2.19909700	1.07383000
H	-1.20950400	0.22240100	2.27975700
C	-1.19567500	-2.38391800	1.49029200
H	-1.55596200	-3.33394200	1.08700800
H	-0.10411600	-2.36521500	1.39096600
H	-1.42358100	-2.35787900	2.56169300
H	1.20952800	0.22240900	-2.27976400
H	2.17277800	2.19910300	-1.07382000
H	3.30902000	1.87176500	1.12604100
H	3.66382600	-0.42820100	1.98793300
H	2.72577900	-2.37764200	0.77609500
C	1.19568800	-2.38391200	-1.49030000
H	1.55604100	-3.33393700	-1.08707500
H	0.10413400	-2.36526000	-1.39090200
H	1.42352100	-2.35782300	-2.56171500

47) (C₆F₅)₂

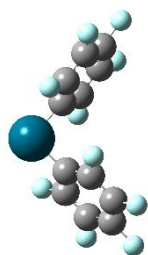
Number of imaginary frequencies = 0

 $E_{\text{total}} = -1455.61604973$ a.u $G_{\text{correction}} = 0.053196$ a.u

Cartesian coordinates:

C	0.73804600	0.00001000	-0.00000100
C	1.46468000	-1.06542000	-0.54025600
C	1.46468800	1.06543100	0.54025500
C	2.85505700	-1.07801700	-0.53990600
C	2.85506900	1.07801500	0.53990600
C	3.55158300	-0.00000200	-0.00000100
C	-0.73804700	0.00001100	-0.00000200
C	-1.46468800	1.06542100	-0.54026700
C	-1.46468000	-1.06541900	0.54026600
C	-2.85507300	1.07801100	-0.53992000
C	-2.85505300	-1.07801300	0.53991500
C	-3.55158100	0.00000000	-0.00000300
F	0.82129100	-2.10404700	-1.08717800
F	0.82131600	2.10405600	1.08719800
F	3.52355900	2.10942900	1.06527600
F	4.88547700	-0.00001400	0.00000000
F	3.52354600	-2.10943800	-1.06526400
F	-0.82131900	2.10404700	-1.08721700
F	-0.82128500	-2.10403300	1.08720200
F	-3.52355400	-2.10942000	1.06528500
F	-3.52355400	2.10942300	-1.06529700
F	-4.88547600	-0.00002200	0.00000600

48) [Pd(C₆F₅)₂] (28)



Number of imaginary frequencies = 0

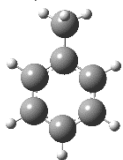
$E_{\text{total}} = -1583.52151770$ a.u

$G_{\text{correction}} = 0.046166$ a.u

Cartesian coordinates:

Pd	-0.00509100	2.04249000	0.11226900
C	-1.34342100	0.60846300	0.23083700
C	-2.31582800	0.50443200	-0.76053800
C	-1.38180300	-0.31234300	1.27372600
C	-3.31546700	-0.46281200	-0.71024000
C	-2.37015100	-1.29091100	1.34894100
C	-3.33861800	-1.36521300	0.35072500
C	1.34001000	0.63825100	-0.16437500
C	2.29135100	0.41016300	0.82610600
C	1.40368100	-0.13921800	-1.31655700
C	3.29706000	-0.53955600	0.67280700
C	2.39885200	-1.09705100	-1.49656200
C	3.34675400	-1.29680900	-0.49561100
F	-2.32194100	1.35867600	-1.80463700
F	-0.45830800	-0.28388600	2.25269300
F	-2.39897800	-2.15862100	2.36883600
F	-4.29567200	-2.29601600	0.41544700
F	-4.25079100	-0.53460700	-1.66612700
F	2.26681800	1.12307000	1.97066200
F	0.49910000	0.01371400	-2.30181200
F	2.45447300	-1.82525400	-2.61939400
F	4.21283500	-0.73271300	1.63087000
F	4.31020600	-2.20868900	-0.65986300

49) $\text{C}_6\text{H}_5\text{CH}_3$



Number of imaginary frequencies = 0

$E_{\text{total}} = -271.60402628$ a.u

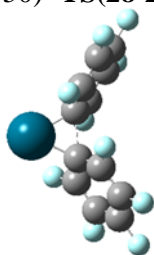
$G_{\text{correction}} = 0.097438$ a.u

Cartesian coordinates:

C	1.90333900	-0.00011500	0.00841600
C	1.19968700	-1.20522300	0.00196600
C	-0.19510300	-1.20219900	-0.00926800

C	-0.91319500	0.00016700	-0.01173900
C	-0.19490300	1.20231500	-0.00923900
C	1.19996300	1.20507100	0.00199300
H	2.98899800	-0.00024100	0.01396400
H	1.73676100	-2.14918900	0.00143400
H	-0.73601800	-2.14497100	-0.01807100
H	-0.73561900	2.14519400	-0.01800500
H	1.73718900	2.14895000	0.00148400
C	-2.42199800	0.00006900	0.00994500
H	-2.80111700	-0.00814400	1.03923000
H	-2.82842500	0.88987700	-0.47929800
H	-2.82850700	-0.88197800	-0.49319000

50) TS(28-29)



Number of imaginary frequencies = 1 ($i266.85 \text{ cm}^{-1}$)

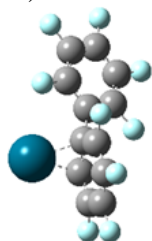
$E_{\text{total}} = -1583.49262377 \text{ a.u.}$

$G_{\text{correction}} = 0.048596 \text{ a.u.}$

Cartesian coordinates:

Pd	-0.00006800	0.00030400	2.15988600
C	-0.91779200	-0.12225000	0.32824600
C	-1.84055200	0.94455400	0.23258200
C	-1.28206300	-1.28712600	-0.37456900
C	-3.00345500	0.87081800	-0.52257300
C	-2.44006000	-1.37996000	-1.13678000
C	-3.30585600	-0.29437900	-1.22120200
C	0.91783500	0.12235600	0.32826800
C	1.84058600	-0.94448300	0.23290700
C	1.28212600	1.28703600	-0.37485900
C	3.00349000	-0.87096300	-0.52226800
C	2.44011300	1.37964700	-1.13711100
C	3.30590100	0.29403700	-1.22122400
F	-1.66854600	2.07702000	0.94376100
F	-0.48098200	-2.36351500	-0.37270400
F	-2.72290300	-2.50943000	-1.79815200
F	-4.42435200	-0.37694000	-1.94538500
F	-3.85873500	1.90089800	-0.55095100
F	1.66853600	-2.07677900	0.94433800
F	0.48104400	2.36342400	-0.37330600
F	2.72294900	2.50892400	-1.79881600
F	3.85876000	-1.90106000	-0.55037500
F	4.42439500	0.37637700	-1.94543600

51) Intermediate-29



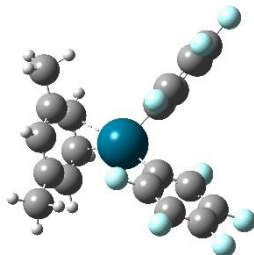
Number of imaginary frequencies = 0

$E_{\text{total}} = -1583.53510775$ a.u

$G_{\text{correction}} = 0.049147$ a.u

Cartesian coordinates:

Pd	1.19825800	-1.49613700	-1.12326700
C	-1.05080800	0.13981600	0.15875300
C	-1.87215200	-0.97528500	0.33619700
C	-1.67940800	1.37555100	-0.01627000
C	-3.25872800	-0.88045800	0.30907800
C	-3.06520300	1.49513700	-0.05362300
C	-3.85693800	0.36229100	0.11375200
C	0.43368200	0.04353100	0.20109600
C	1.24603700	0.58706400	-0.86532700
C	1.06575100	-0.11534800	1.47294300
C	2.58455600	1.00410100	-0.59556500
C	2.36698700	0.26738900	1.69864200
C	3.13291900	0.82593600	0.65331400
F	-1.32766800	-2.19212500	0.50532900
F	-0.94303300	2.48743300	-0.14165000
F	-3.63853600	2.68980400	-0.22943500
F	-5.18697400	0.46660700	0.08669700
F	-4.01732800	-1.97048100	0.46494500
F	0.64157400	1.20232100	-1.91953700
F	0.33885900	-0.60272100	2.49080400
F	2.94226800	0.08266900	2.89478900
F	3.29383500	1.57665200	-1.57641000
F	4.40810700	1.15361600	0.89028300

52) $[\text{Pd}(\text{C}_6\text{H}_4(\text{CH}_3)_2)(\text{C}_6\text{F}_5)_2]$ (30)

Number of imaginary frequencies = 0

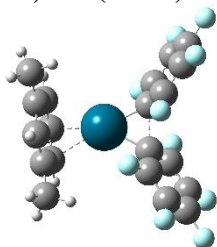
$E_{\text{total}} = -1894.49387213$ a.u

$G_{\text{correction}} = 0.192649$ a.u

Cartesian coordinates:

Pd	-0.03769000	1.08923600	-0.37389400
C	-1.36532100	-0.38929500	-0.28862400
C	-1.42257800	-1.41930700	-1.22010700
C	-2.31048700	-0.41632800	0.73103500
C	-2.38716800	-2.42284200	-1.16455900
C	-3.29088300	-1.40015400	0.81930900
C	-3.32568000	-2.41224700	-0.13632200
C	1.33588300	-0.27532400	0.03406400
C	1.42586100	-0.91536900	1.26434300
C	2.31325800	-0.57577500	-0.90791200
C	2.44905700	-1.81343800	1.56039300
C	3.35031800	-1.46707900	-0.64628900
C	3.41496800	-2.09094700	0.59707600
F	-0.53220900	-1.47643700	-2.23450200
F	-2.30756600	0.53949600	1.69298300
F	-4.19439500	-1.38902500	1.81181100
F	-4.26300200	-3.36718600	-0.07088300
F	-2.42437300	-3.39600500	-2.08771100
F	0.51605900	-0.67424000	2.23248200
F	2.29118900	0.01194400	-2.12562000
F	4.28495100	-1.73000000	-1.57249100
F	2.51727700	-2.40785400	2.76127400
F	4.40831600	-2.94762200	0.86826200
C	-1.28547100	3.51154100	0.10163700
C	-1.05011000	3.35780900	-1.28633200
C	0.25680500	3.21809900	-1.78108600
C	1.33356700	3.13495200	-0.88231500
C	1.12269600	3.28593000	0.51428000
C	-0.18416800	3.51208500	0.97815600
H	0.42966900	3.11794100	-2.84656600
H	-0.35499400	3.63052200	2.04354300
H	-1.88957500	3.37158400	-1.97317900
H	2.33943500	2.97623000	-1.25604300
C	-2.68628300	3.66087800	0.63450900
H	-2.99555500	2.74201000	1.14032800
H	-2.73857300	4.47458300	1.36375500
H	-3.39770900	3.86745600	-0.16800100
C	2.28821700	3.20194400	1.46341100
H	1.95326000	3.18911100	2.50234100
H	2.86582100	2.29163900	1.27714600
H	2.96083500	4.05562800	1.32735500

53) TS(30-31)



Number of imaginary frequencies = 1 ($i253.33\text{ cm}^{-1}$)

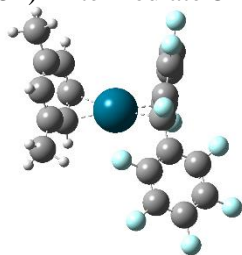
$E_{\text{total}} = -1894.46039993\text{ a.u.}$

$G_{\text{correction}} = 0.190924 \text{ a.u.}$

Cartesian coordinates:

Pd	-0.89550700	-0.69278100	-0.36230700
C	1.13227600	-0.42579500	-0.09982100
C	2.11395500	-0.27314400	-1.09747800
C	1.52377900	-1.22436600	0.99967600
C	3.38430700	-0.82717000	-1.00366400
C	2.78705800	-1.78934200	1.11059400
C	3.73231600	-1.58435700	0.10999100
C	0.08865000	1.07200700	0.05726500
C	0.24066300	1.68527400	1.31521600
C	-0.16014500	1.96511500	-1.01049900
C	0.19229700	3.06153200	1.50074700
C	-0.21244200	3.34228700	-0.84634100
C	-0.02573600	3.90175600	0.41461500
F	1.86527600	0.46469700	-2.19146000
F	0.64425700	-1.55401400	1.96739200
F	3.09059500	-2.56826500	2.15828500
F	4.95037400	-2.12523200	0.20727400
F	4.27982700	-0.62972100	-1.98082600
F	0.48228400	0.94560700	2.40989100
F	-0.44851200	1.50874900	-2.24651600
F	-0.48713000	4.13875500	-1.88891800
F	0.36313800	3.58358100	2.72304000
F	-0.07799900	5.22644000	0.58246800
C	-2.36863700	-3.28048200	0.58367300
C	-2.11358500	-2.95842400	-0.75717500
C	-2.68376900	-1.79555300	-1.33606500
C	-3.42827800	-0.93502100	-0.48852100
C	-3.67055300	-1.25097200	0.86309700
C	-3.15732000	-2.44904600	1.37881600
H	-1.53880800	-3.63541800	-1.38122700
H	-3.35072100	-2.71277000	2.41382600
H	-3.87932500	-0.04316400	-0.91483500
C	-4.44270000	-0.29880500	1.73858900
H	-3.76572900	0.43342800	2.19477000
H	-5.18983800	0.25750100	1.16576900
H	-4.94959400	-0.82734400	2.55003100
C	-2.63897300	-1.56698700	-2.82963500
H	-3.48273000	-2.07462000	-3.31252200
H	-2.70266600	-0.50378700	-3.07207100
H	-1.71728700	-1.96268000	-3.26311500
H	-1.94794800	-4.18965400	1.00133300

54) Intermediate-31

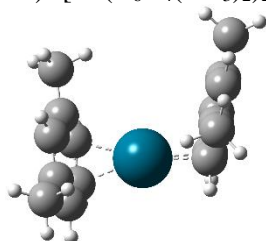


Number of imaginary frequencies = 0

$E_{\text{total}} = -1894.50440132 \text{ a.u.}$ $G_{\text{correction}} = 0.190946 \text{ a.u.}$

Cartesian coordinates:

Pd	-0.93972700	-0.44953300	-0.67713400
C	1.92602200	0.24137800	0.17167000
C	2.99842000	1.00636600	-0.29597600
C	2.20628200	-1.06531500	0.57825400
C	4.28514300	0.48636200	-0.39735200
C	3.48444100	-1.60490000	0.49192200
C	4.52866900	-0.82488200	0.00104800
C	0.56156900	0.82728100	0.26172700
C	0.05156300	1.18460000	1.54812600
C	-0.05060500	1.46268700	-0.87704900
C	-0.94876400	2.11327700	1.70873900
C	-1.06384700	2.44618400	-0.68344900
C	-1.51568700	2.74311400	0.58063100
F	2.80413200	2.28385900	-0.64957000
F	1.22600200	-1.85316700	1.04872700
F	3.71539900	-2.86571500	0.87516000
F	5.75999200	-1.33322900	-0.08375300
F	5.28816800	1.24302500	-0.85491900
F	0.60580300	0.62185300	2.63391100
F	0.62924300	1.53623500	-2.05432200
F	-1.58705200	3.05584300	-1.75523400
F	-1.43669500	2.39908000	2.92489700
F	-2.52992400	3.59880100	0.75822300
C	-2.24166100	-2.70921200	-0.00191900
C	-2.02583600	-2.31058100	-1.34759300
C	-2.90955100	-1.38622000	-1.95642500
C	-4.00463600	-0.88412100	-1.24023100
C	-4.23661600	-1.27772500	0.08292100
C	-3.34450000	-2.17904900	0.68184900
H	-2.77289300	-1.11983700	-2.99927200
H	-3.51683900	-2.48745400	1.71025300
H	-1.26987100	-2.81574500	-1.94331400
H	-4.67932400	-0.18098500	-1.71961200
C	-1.36642700	-3.75861400	0.63663300
H	-0.35989800	-3.74985300	0.21454000
H	-1.28379300	-3.59995500	1.71494000
H	-1.79081900	-4.75786800	0.48003400
C	-5.38773800	-0.70292200	0.86819600
H	-5.75952500	-1.41312300	1.61212600
H	-5.07490700	0.20061900	1.40617200
H	-6.21773900	-0.42277300	0.21387800

55) $[\text{Pd}(\text{C}_6\text{H}_4(\text{CH}_3)_2)_2]$ (32)

Number of imaginary frequencies = 0

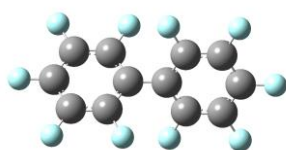
$E_{\text{total}} = -749.82250306 \text{ a.u.}$

$G_{\text{correction}} = 0.262171 \text{ a.u.}$

Cartesian coordinates:

Pd	-0.00032900	-1.19308200	-0.00040100
C	-1.20776100	-0.33059700	-1.70579300
C	-1.37827800	1.04564900	-1.38243800
C	-1.98836500	-1.31423300	-1.04901600
C	-2.33768600	1.39667800	-0.44234100
C	-2.93158600	-0.91148500	-0.06651300
C	-3.11841700	0.43165900	0.23458100
C	3.11862200	0.43180200	-0.23440300
C	2.93177200	-0.91179700	0.06462200
C	1.98853000	-1.31605100	1.04646200
C	1.20819700	-0.33343900	1.70507300
C	1.37861200	1.04329200	1.38370700
C	2.33786500	1.39576900	0.44400600
H	3.53702000	-1.66616100	-0.42995400
H	2.48841100	2.44857300	0.21442000
H	2.00280500	-2.33921800	1.41319500
H	0.60894800	-0.60183200	2.57143600
C	0.50891700	2.07753800	2.04923600
H	0.90753600	3.08587000	1.90840600
H	-0.50124400	2.05173800	1.62385900
H	0.41546900	1.89137500	3.12463300
H	-0.60800200	-0.59774800	-2.57218600
H	-2.00271800	-2.33679200	-1.41740400
H	-3.53697100	-1.66655900	0.42680600
H	-2.48830400	2.44912300	-0.21116700
C	-0.50857800	2.08092200	-2.04635900
H	-0.90725200	3.08902500	-1.90403900
H	0.50158900	2.05457900	-1.62103400
H	-0.41513400	1.89636800	-3.12203000
C	4.11870300	0.87227200	-1.27418400
H	3.61494300	1.28790400	-2.15545600
H	4.78071200	1.65403000	-0.88554200
H	4.74003300	0.03768900	-1.60969200
C	-4.11849100	0.87049200	1.27507000
H	-3.61474300	1.28448700	2.15711800
H	-4.78032700	1.65305000	0.88774500
H	-4.74000900	0.03544000	1.60906300

56) $(\text{C}_6\text{F}_5)_2$



Number of imaginary frequencies = 0

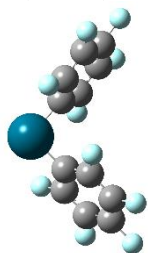
$E_{\text{total}} = -1455.61603218 \text{ a.u.}$

$G_{\text{correction}} = 0.053198 \text{ a.u.}$

Cartesian coordinates:

C	0.73804600	0.00001000	-0.00000100
C	1.46467600	-1.06542000	-0.54026700
C	1.46468400	1.06543100	0.54026600
C	2.85505700	-1.07801900	-0.53991700
C	2.85506900	1.07801700	0.53991700
C	3.55158500	-0.00000200	-0.00000100
C	-0.73804700	0.00001100	-0.00000200
C	-1.46468300	1.06542100	-0.54027800
C	-1.46467600	-1.06541900	0.54027700
C	-2.85507300	1.07801300	-0.53993100
C	-2.85505400	-1.07801500	0.53992600
C	-3.55158300	0.00000000	-0.00000300
F	0.82128000	-2.10403000	-1.08719900
F	0.82130500	2.10403800	1.08721800
F	3.52355400	2.10941900	1.06529400
F	4.88547200	-0.00001400	0.00000000
F	3.52354100	-2.10942800	-1.06528200
F	-0.82130800	2.10403000	-1.08723700
F	-0.82127500	-2.10401600	1.08722300
F	-3.52355000	-2.10941000	1.06530300
F	-3.52354900	2.10941400	-1.06531500
F	-4.88547100	-0.00002200	0.00000600

57) $[\text{Pd}(\text{C}_6\text{F}_5)_2]$ (**33**)



Number of imaginary frequencies = 0

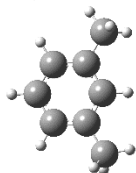
$E_{\text{total}} = -1583.52136677 \text{ a.u.}$

$G_{\text{correction}} = 0.046162 \text{ a.u.}$

Cartesian coordinates:

Pd	-0.00510700	2.04223500	0.11259500
C	-1.34357400	0.60834900	0.23101000
C	-2.31600500	0.50470900	-0.76039000
C	-1.38188100	-0.31274300	1.27365200
C	-3.31572500	-0.46246100	-0.71029100
C	-2.37032100	-1.29124400	1.34862700
C	-3.33885700	-1.36516200	0.35043400
C	1.34013800	0.63821000	-0.16428700
C	2.29147000	0.41012400	0.82621200
C	1.40379100	-0.13909300	-1.31658500
C	3.29728400	-0.53945900	0.67275200
C	2.39908600	-1.09677800	-1.49671700
C	3.34702500	-1.29654200	-0.49578800

F	-2.32203900	1.35927100	-1.80419600
F	-0.45829000	-0.28463100	2.25249300
F	-2.39915900	-2.15924700	2.36824000
F	-4.29597000	-2.29588200	0.41495600
F	-4.25111300	-0.53390000	-1.66610700
F	2.26681700	1.12289600	1.97081800
F	0.49913400	0.01386800	-2.30172200
F	2.45477700	-1.82482900	-2.61961600
F	4.21309300	-0.73264100	1.63074300
F	4.31056600	-2.20826700	-0.66017900

58) $C_6H_4(CH_3)_2$ 

Number of imaginary frequencies = 0

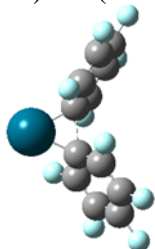
$E_{total} = -310.92982518$ a.u

$G_{correction} = 0.121323$ a.u

Cartesian coordinates:

C	-0.00613700	1.82296300	0.00135500
C	1.20760200	1.13174600	-0.00547100
C	1.22675000	-0.26532300	-0.00705000
C	0.00319200	-0.94965100	-0.00543500
C	-1.22020900	-0.27617700	0.00125000
C	-1.21093200	1.12633100	0.00520900
H	-0.00867300	2.90914800	0.00142000
H	2.14490400	1.68143700	-0.01039100
H	0.00682400	-2.03761400	-0.01053600
H	-2.15265000	1.66906800	0.00877400
C	-2.52536800	-1.03349100	0.00027400
H	-3.13363600	-0.77786500	0.87508600
H	-3.12291900	-0.79425100	-0.88661300
H	-2.35971500	-2.11394600	0.01103600
C	2.52812800	-1.02893900	0.00549100
H	2.70134900	-1.50056800	0.98010600
H	2.52890600	-1.82827400	-0.74282600
H	3.37745300	-0.37188300	-0.19979400

59) TS(33-34)



Number of imaginary frequencies = 1 ($i267.04$ cm^{-1})

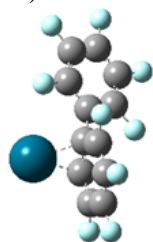
$E_{\text{total}} = -1583.49251934 \text{ a.u.}$

$G_{\text{correction}} = 0.048598 \text{ a.u.}$

Cartesian coordinates:

Pd	-0.00006600	0.00028800	2.15992200
C	-0.91805500	-0.12230500	0.32843600
C	-1.84077500	0.94448900	0.23272200
C	-1.28207100	-1.28718500	-0.37445400
C	-3.00355900	0.87074000	-0.52263100
C	-2.43995000	-1.38002800	-1.13685900
C	-3.30577200	-0.29446100	-1.22135300
C	0.91809700	0.12240500	0.32845900
C	1.84080800	-0.94442200	0.23303200
C	1.28213200	1.28709900	-0.37472700
C	3.00359400	-0.87087600	-0.52234100
C	2.44000200	1.37973200	-1.13717100
C	3.30581600	0.29413700	-1.22137200
F	-1.66883200	2.07688900	0.94397700
F	-0.48092400	-2.36349700	-0.37244800
F	-2.72265000	-2.50945700	-1.79832300
F	-4.42413300	-0.37704100	-1.94570900
F	-3.85885800	1.90077200	-0.55113500
F	1.66882200	-2.07666200	0.94452100
F	0.48098300	2.36341000	-0.37301700
F	2.72269300	2.50897800	-1.79895200
F	3.85888300	-1.90092400	-0.55058800
F	4.42417600	0.37650900	-1.94575400

60) Intermediate-34



Number of imaginary frequencies = 0

$E_{\text{total}} = -1583.53502571 \text{ a.u.}$

$G_{\text{correction}} = 0.049147 \text{ a.u.}$

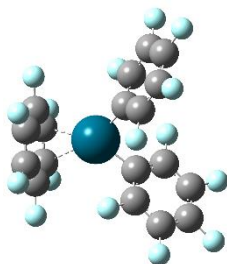
Cartesian coordinates:

Pd	1.19823400	-1.49600600	-1.12332600
C	-1.05083800	0.13995400	0.15882000
C	-1.87203100	-0.97529200	0.33605200
C	-1.67957200	1.37564600	-0.01603600
C	-3.25862100	-0.88063200	0.30893900
C	-3.06538400	1.49506900	-0.05337100
C	-3.85697700	0.36208800	0.11382000
C	0.43365500	0.04387700	0.20118300
C	1.24593000	0.58756200	-0.86516100
C	1.06579800	-0.11536800	1.47291200
C	2.58452400	1.00430700	-0.59554000

Appendix

C	2.36714400	0.26714100	1.69855200
C	3.13302100	0.82579200	0.65327000
F	-1.32737500	-2.19208500	0.50494000
F	-0.94330600	2.48760500	-0.14126300
F	-3.63886000	2.68967900	-0.22899700
F	-5.18701300	0.46624500	0.08677800
F	-4.01708400	-1.97076300	0.46460300
F	0.64145200	1.20265600	-1.91936500
F	0.33896400	-0.60286900	2.49072100
F	2.94248900	0.08209900	2.89458600
F	3.29374700	1.57697000	-1.57632000
F	4.40824700	1.15328700	0.89013400

61) [Pd(C₆F₆)(C₆F₅)₂] (35)



Number of imaginary frequencies = 0

$E_{\text{total}} = -2411.16082538 \text{ a.u.}$

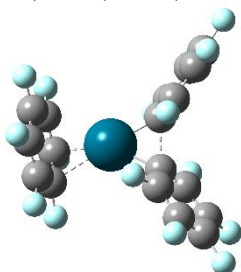
$G_{\text{correction}} = 0.080266 \text{ a.u.}$

Cartesian coordinates:

Pd	-0.72044900	0.00002100	0.00000100
C	0.71573800	-1.33618800	-0.20886400
C	1.62354800	-1.34809400	-1.26000600
C	0.79745400	-2.36128500	0.72656400
C	2.57727200	-2.35534800	-1.39147500
C	1.73679600	-3.38212400	0.62360000
C	2.63304000	-3.37394000	-0.44326100
C	0.71578400	1.33618100	0.20886900
C	1.62360900	1.34804700	1.25999800
C	0.79752100	2.36128600	-0.72654900
C	2.57736700	2.35526800	1.39146400
C	1.73689900	3.38209300	-0.62358900
C	2.63315600	3.37386800	0.44326000
F	1.60465000	-0.37994700	-2.19708500
F	-0.05839000	-2.39127200	1.77275700
F	1.79034200	-4.36525700	1.53194100
F	3.54003700	-4.34964100	-0.56159300
F	3.43653800	-2.35684800	-2.41931200
F	1.60469200	0.37989200	2.19706900
F	-0.05833800	2.39131200	-1.77273000
F	1.79046300	4.36523300	-1.53192100
F	3.43664800	2.35673100	2.41929000
F	3.54018700	4.34953700	0.56159000
C	-3.00747600	-1.38418000	-0.18490000
C	-3.04539500	-0.53089300	-1.30312800
C	-3.04935400	0.85607500	-1.11824700

C	-3.00749400	1.38424300	0.18489700
C	-3.04542600	0.53095600	1.30312400
C	-3.04936700	-0.85601200	1.11824300
F	-2.99360400	2.69978400	0.36223200
F	-3.06080500	1.04492700	2.52560200
F	-3.07247100	-1.67104000	2.16266700
F	-2.99356900	-2.69972100	-0.36223500
F	-3.06075300	-1.04486500	-2.52560600
F	-3.07244700	1.67110300	-2.16267100

62) TS(35-36)



Number of imaginary frequencies = 1 ($i288.94 \text{ cm}^{-1}$)

$E_{\text{total}} = -2411.13920377 \text{ a.u.}$

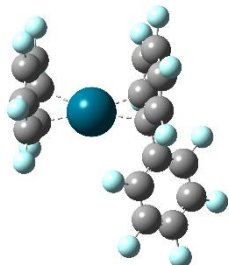
$G_{\text{correction}} = 0.085283 \text{ a.u.}$

Cartesian coordinates:

Pd	0.10956600	-1.29746700	-0.32903600
C	0.14529700	0.72459600	0.03750900
C	0.03681600	1.32585300	1.30266400
C	-0.54036000	1.38301900	-1.00341900
C	-0.68531500	2.49341300	1.52134900
C	-1.27178200	2.54763600	-0.80446900
C	-1.33945900	3.11695500	0.46335800
C	1.81676700	-0.13691200	-0.20064200
C	2.54442600	0.45560200	-1.24706500
C	2.58893400	-0.62238000	0.87639900
C	3.92746500	0.58825200	-1.22022000
C	3.97167100	-0.50105900	0.92230000
C	4.64791600	0.11489600	-0.12759800
F	0.64226800	0.78155700	2.36915700
F	-0.62298300	0.83529800	-2.23295800
F	-1.95310900	3.09450200	-1.81697900
F	-2.04682600	4.22951800	0.66851300
F	-0.75611300	3.01879800	2.74941400
F	1.91381300	0.96116400	-2.31640600
F	2.01679200	-1.30470500	1.88762600
F	4.66398700	-1.00720100	1.94929900
F	4.56972500	1.17289100	-2.23806800
F	5.97630300	0.23051000	-0.09627700
C	-2.54086200	-0.99535300	1.40798100
C	-1.92238700	-2.16623800	0.95354500
C	-1.90376300	-2.46454500	-0.42822300
C	-2.53694200	-1.58491700	-1.33457800
C	-3.13615300	-0.42171900	-0.86943900

C	-3.13438100	-0.12900300	0.49827000
F	-2.56751300	-1.89319100	-2.62871400
F	-3.66287500	0.45257400	-1.72666400
F	-3.64897700	1.02638100	0.91971600
F	-2.50814500	-0.69004700	2.70479700
F	-1.46431200	-3.06217700	1.82924000
F	-1.55730000	-3.69976900	-0.83843600

63) Intermediate-36



Number of imaginary frequencies = 0

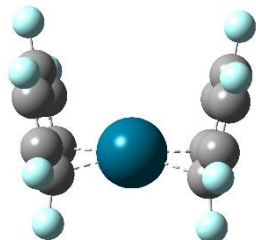
$E_{\text{total}} = -2411.18552022$ a.u

$G_{\text{correction}} = 0.085107$ a.u

Cartesian coordinates:

Pd	-0.49783900	-0.65868800	-0.46142000
C	2.40484800	0.22943000	0.22825000
C	3.53668900	0.99760400	-0.06157200
C	2.60179100	-1.13218700	0.46245900
C	4.80697500	0.43386500	-0.12590200
C	3.85912600	-1.71948900	0.41246100
C	4.96784700	-0.92844700	0.11709400
C	1.06476300	0.86730400	0.30746400
C	0.36288400	0.94491600	1.53944200
C	0.60069800	1.71295200	-0.73392600
C	-0.69613100	1.82689300	1.72972900
C	-0.44687600	2.61512500	-0.54046100
C	-1.09514200	2.66841100	0.68996900
F	3.41061800	2.31242200	-0.27561000
F	1.54129900	-1.92553600	0.71792700
F	4.00866500	-3.02677400	0.63259500
F	6.18006200	-1.47681900	0.06268800
F	5.86960200	1.19167800	-0.40420500
F	0.78374300	0.21055100	2.57491400
F	1.25489700	1.73841600	-1.89960400
F	-0.85813300	3.38652600	-1.54736900
F	-1.34933900	1.85138200	2.89385800
F	-2.13350900	3.48168500	0.86074800
C	-2.83758600	-2.32941700	0.02144900
C	-2.15645800	-1.83470800	-1.13211500
C	-2.34821500	-0.45877400	-1.50565200
C	-3.21727900	0.35584200	-0.72136700
C	-3.81983500	-0.14836200	0.40615400
C	-3.62995000	-1.49917000	0.77965900
F	-3.40448400	1.63111200	-1.08823400
F	-4.54378800	0.64448300	1.20380200

F	-4.19025500	-1.93703600	1.91334600
F	-2.69420000	-3.61892800	0.34369900
F	-1.81235700	-2.73739600	-2.08324600
F	-2.15707900	-0.09366200	-2.79569600

64) [Pd(C₆F₆)₂] (37)

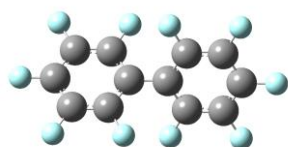
Number of imaginary frequencies = 0

$E_{\text{total}} = -1783.19104704$ a.u

$G_{\text{correction}} = 0.045590$ a.u

Cartesian coordinates:

Pd	0.00002500	-0.73478100	-0.01062700
C	2.10877000	-1.02791100	0.68265100
C	2.34468100	0.16773200	1.40331100
C	2.09913800	-0.99176600	-0.74136200
C	2.55416200	1.36159000	0.72998500
C	2.32516800	0.23950100	-1.40297800
C	2.54419100	1.39734200	-0.67241200
F	2.39445300	0.12429300	2.73529200
F	2.23463100	-2.13355600	-1.43663900
F	2.35641900	0.26499500	-2.73597800
F	2.71675000	2.49706600	1.41267400
F	2.69730200	2.56609900	-1.29881400
C	-2.33696100	0.17738600	1.40991300
C	-2.10459200	-1.02333800	0.69649600
C	-2.10275100	-0.99730500	-0.72779200
C	-2.33276300	0.22914800	-1.39692000
C	-2.54830700	1.39207900	-0.67342100
C	-2.55048700	1.36632100	0.72923500
F	-2.37132700	0.24503300	-2.72988200
F	-2.70532500	2.55631700	-1.30722000
F	-2.70979900	2.50657500	1.40471400
F	-2.37946900	0.14352300	2.74242700
F	-2.24390500	-2.19446800	1.34018000
F	-2.24165700	-2.14401800	-1.41420500
F	2.25163200	-2.20349900	1.31729400

65) (C₆F₅)₂

Number of imaginary frequencies = 0

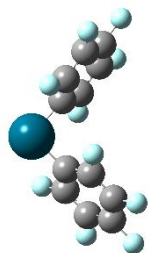
$E_{\text{total}} = -1455.61579449$ a.u

$G_{\text{correction}} = 0.053233$ a.u

Cartesian coordinates:

C	0.73804900	0.00001400	-0.00000700
C	1.46461200	-1.06542400	-0.54046100
C	1.46462000	1.06544100	0.54045500
C	2.85506000	-1.07803400	-0.54012700
C	2.85507000	1.07803700	0.54012700
C	3.55159100	0.00000000	0.00000000
C	-0.73804900	0.00001200	-0.00000600
C	-1.46462300	1.06543000	-0.54047500
C	-1.46460900	-1.06542400	0.54046400
C	-2.85507600	1.07802700	-0.54014100
C	-2.85505500	-1.07803300	0.54013500
C	-3.55159000	-0.00000400	0.00000000
F	0.82109400	-2.10371700	-1.08760800
F	0.82111600	2.10372600	1.08763200
F	3.52352700	2.10922600	1.06565100
F	4.88537600	-0.00001200	0.00000600
F	3.52351300	-2.10923500	-1.06563100
F	-0.82112500	2.10371800	-1.08765700
F	-0.82108400	-2.10370400	1.08762600
F	-3.52351100	-2.10922300	1.06565800
F	-3.52353000	2.10921600	-1.06566500
F	-4.88537600	-0.00002100	0.00001100

66) $[\text{Pd}(\text{C}_6\text{F}_5)_2]$ (38)



Number of imaginary frequencies = 0

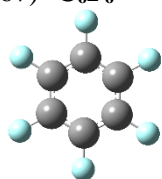
$E_{\text{total}} = -1583.51933230$ a.u

$G_{\text{correction}} = 0.046096$ a.u

Cartesian coordinates:

Pd	-0.00543300	2.03824700	0.11714600
C	-1.34585200	0.60646100	0.23251100
C	-2.31874500	0.50827700	-0.75902800
C	-1.38321700	-0.31824800	1.27209500
C	-3.31991200	-0.45753900	-0.71107000
C	-2.37323700	-1.29541300	1.34431400
C	-3.34291600	-1.36400800	0.34661200
C	1.34218200	0.63751200	-0.16296600
C	2.29337900	0.40969800	0.82788000

C	1.40584800	-0.13747000	-1.31687500
C	3.30082600	-0.53782400	0.67221700
C	2.40305600	-1.09291500	-1.49868900
C	3.35143200	-1.29257500	-0.49796800
F	-2.32363100	1.36685500	-1.79898900
F	-0.45807100	-0.29482800	2.24898500
F	-2.40240900	-2.16718700	2.36027100
F	-4.30112500	-2.29328700	0.40881300
F	-4.25637800	-0.52413500	-1.66572400
F	2.26695200	1.12061400	1.97311900
F	0.50027700	0.01574800	-2.30049400
F	2.46005000	-1.81887900	-2.62248700
F	4.21712900	-0.73124300	1.62923400
F	4.31641000	-2.20200300	-0.66416300

67) **C₆F₆**

Number of imaginary frequencies = 0

$E_{\text{total}} = -827.61889216$ a.u

$G_{\text{correction}} = 0.016070$ a.u

Cartesian coordinates:

C	-0.76235900	1.16565700	-0.00002200
C	0.62825500	1.24305900	-0.00001300
C	1.39040200	0.07739700	-0.00001800
C	0.76233300	-1.16567400	-0.00001000
C	-0.62822800	-1.24307400	-0.00002600
C	-1.39040300	-0.07736700	-0.00000700
F	-1.23134600	-2.43502600	0.00000300
F	2.72411400	0.15158600	0.00001000
F	1.49407000	-2.28324700	0.00001600
F	1.23126300	2.43506700	0.00001400
F	-1.49399200	2.28329800	0.00000700
F	-2.72410900	-0.15167800	0.00001500

68) **TS(38-39)**

Number of imaginary frequencies = 1 ($i269.85$ cm⁻¹)

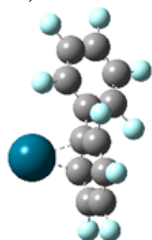
$E_{\text{total}} = -1583.49109841$ a.u

$$G_{\text{correction}} = 0.048613 \text{ a.u.}$$

Cartesian coordinates:

Pd	-0.00003200	0.00000800	2.16029600
C	-0.92164900	-0.12305100	0.33092600
C	-1.84380500	0.94364300	0.23465300
C	-1.28224000	-1.28794100	-0.37302000
C	-3.00506200	0.86971800	-0.52326900
C	-2.43861000	-1.38087500	-1.13793500
C	-3.30480100	-0.29549200	-1.22325400
C	0.92167100	0.12305300	0.33094900
C	1.84382600	-0.94364200	0.23468400
C	1.28226300	1.28793800	-0.37300500
C	3.00509100	-0.86971000	-0.52322700
C	2.43863000	1.38087200	-1.13792200
C	3.30482800	0.29549500	-1.22322200
F	-1.67261400	2.07512500	0.94691200
F	-0.48017400	-2.36319300	-0.36926100
F	-2.71941600	-2.50971100	-1.80069000
F	-4.42140500	-0.37831800	-1.94983400
F	-3.86061400	1.89911100	-0.55335600
F	1.67260800	-2.07514600	0.94689500
F	0.48018300	2.36317800	-0.36927200
F	2.71942000	2.50969800	-1.80070200
F	3.86064500	-1.89910200	-0.55331600
F	4.42143700	0.37831400	-1.94979700

69) Intermediate-39



Number of imaginary frequencies = 0

$$E_{\text{total}} = -1583.53391677 \text{ a.u.}$$

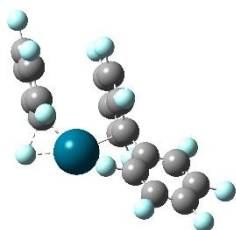
$$G_{\text{correction}} = 0.049136 \text{ a.u.}$$

Cartesian coordinates:

Pd	1.19780100	-1.49475900	-1.12342800
C	-1.05122500	0.14191000	0.15969900
C	-1.87036600	-0.97526700	0.33428100
C	-1.68175800	1.37696800	-0.01320400
C	-3.25714600	-0.88286700	0.30720400
C	-3.06779600	1.49418300	-0.05033400
C	-3.85747200	0.35940900	0.11461600
C	0.43330500	0.04865100	0.20236000
C	1.24447800	0.59392500	-0.86318500
C	1.06648000	-0.11497500	1.47253800
C	2.58408900	1.00680600	-0.59571500
C	2.36932300	0.26453900	1.69715800

C	3.13443100	0.82412400	0.65221800
F	-1.32337400	-2.19138300	0.50013600
F	-0.94694900	2.48993700	-0.13663400
F	-3.64321100	2.68797600	-0.22373600
F	-5.18751200	0.46142100	0.08772000
F	-4.01375600	-1.97442000	0.46036200
F	0.63974000	1.20641500	-1.91751600
F	0.34046100	-0.60376500	2.48988000
F	2.94556700	0.07566700	2.89172800
F	3.29252800	1.58054500	-1.57587400
F	4.41018500	1.14921300	0.88747400

70) TS(36-40)



Number of imaginary frequencies = 1 ($i336.88 \text{ cm}^{-1}$)

$E_{\text{total}} = -2411.14641075 \text{ a.u}$

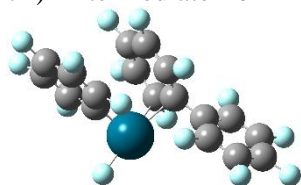
$G_{\text{correction}} = 0.087444 \text{ a.u}$

Cartesian coordinates:

Pd	-0.06779400	-0.25764600	-1.45184000
C	2.41378800	0.14466600	0.29951400
C	3.38566700	1.11844400	0.55345900
C	2.85702600	-1.15294100	0.02954000
C	4.74401000	0.82493600	0.51152800
C	4.21038500	-1.46978200	-0.01459800
C	5.15582900	-0.47593100	0.22949800
C	0.97089300	0.49745900	0.38137700
C	0.19397800	0.02357300	1.47880400
C	0.45272100	1.62491900	-0.33258600
C	-0.99701200	0.61678400	1.82927900
C	-0.73240700	2.27587200	0.08387200
C	-1.45895600	1.75083000	1.13010900
F	3.01176700	2.36642300	0.86025400
F	1.97240900	-2.12691600	-0.22980000
F	4.60531500	-2.71377000	-0.29111000
F	6.45402300	-0.76817800	0.19021200
F	5.64986900	1.77385400	0.75550900
F	0.64079500	-1.02227200	2.17674800
F	1.25649600	2.29657700	-1.18154400
F	-1.15935800	3.34983900	-0.57635200
F	-1.75046300	0.11767700	2.81126200
F	-2.62803700	2.28622700	1.47628500
C	-2.21494500	-1.79234100	-0.11034500
C	-2.01204000	-0.77802800	-1.05186000
C	-2.98742100	0.21464300	-1.18394100
C	-4.07550800	0.26143600	-0.32009000

C	-4.24577900	-0.72995400	0.64464600
C	-3.29982200	-1.74813600	0.75686200
F	-4.95630100	1.26347400	-0.40874200
F	-5.28848100	-0.68407100	1.48160000
F	-3.43621000	-2.68138800	1.70485900
F	-1.29764200	-2.76658600	0.03255800
F	-1.48165200	-1.38040900	-2.57411000
F	-2.81963300	1.20207500	-2.08382400

71) Intermediate-40



Number of imaginary frequencies = 0

$E_{\text{total}} = -2411.18671470$ a.u

$G_{\text{correction}} = 0.087562$ a.u

Cartesian coordinates:

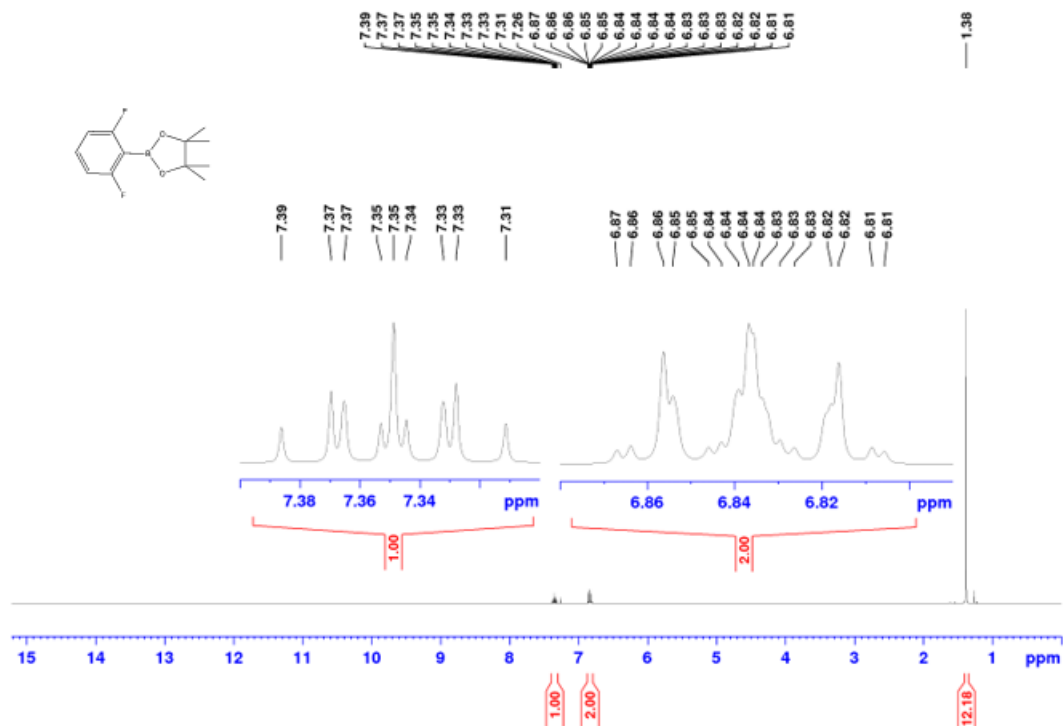
Pd	-0.06063000	-0.13884200	-1.44228100
C	2.36767400	0.12656700	0.35227300
C	3.40233800	1.06329300	0.47204400
C	2.72838400	-1.20809200	0.12737600
C	4.73651800	0.69975500	0.33067700
C	4.05761200	-1.59167400	-0.01361600
C	5.06365000	-0.63315500	0.08853800
C	0.95218400	0.54171600	0.53374200
C	0.22014100	0.05977100	1.65603800
C	0.42344500	1.68949200	-0.13101100
C	-0.94231900	0.66521300	2.07285400
C	-0.73845300	2.34203100	0.33944700
C	-1.42538300	1.81053000	1.40827700
F	3.11893200	2.33929000	0.75534500
F	1.78581400	-2.14960200	0.01621200
F	4.37106300	-2.86643200	-0.24421300
F	6.33804300	-0.99000400	-0.04288200
F	5.70126900	1.61321200	0.44705300
F	0.68690200	-0.99327800	2.32334300
F	1.18510000	2.35931800	-1.01660800
F	-1.18042100	3.42495400	-0.28988400
F	-1.64782500	0.16486000	3.08494900
F	-2.57385000	2.34771800	1.80503000
C	-2.10951300	-1.60340200	0.05913500
C	-1.85871300	-0.50029000	-0.74511000
C	-2.91434400	0.33690000	-1.07981800
C	-4.19482000	0.11816300	-0.57589700
C	-4.42655500	-0.97842200	0.25193900
C	-3.38167700	-1.84074300	0.57668500
F	-5.19836100	0.94773000	-0.87992400
F	-5.64933800	-1.19689600	0.74308400
F	-3.60615200	-2.88860100	1.37641800

Appendix

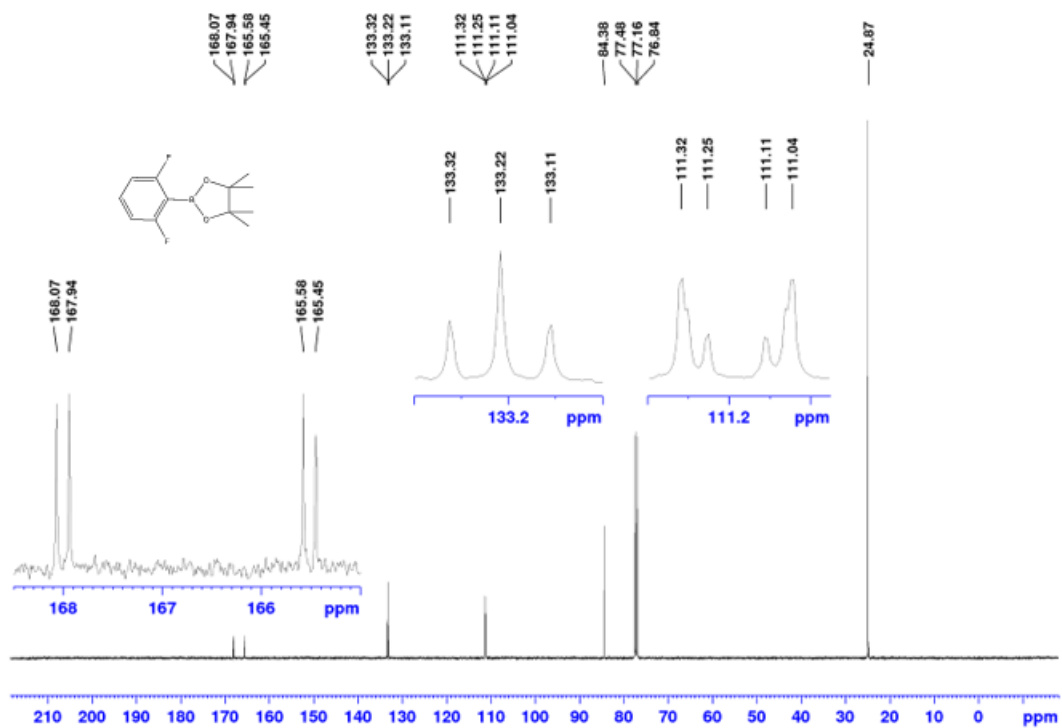
F	-1.11740900	-2.44581700	0.39880800
F	-0.49801900	-1.10005600	-3.05589600
F	-2.71264300	1.41147300	-1.86489000

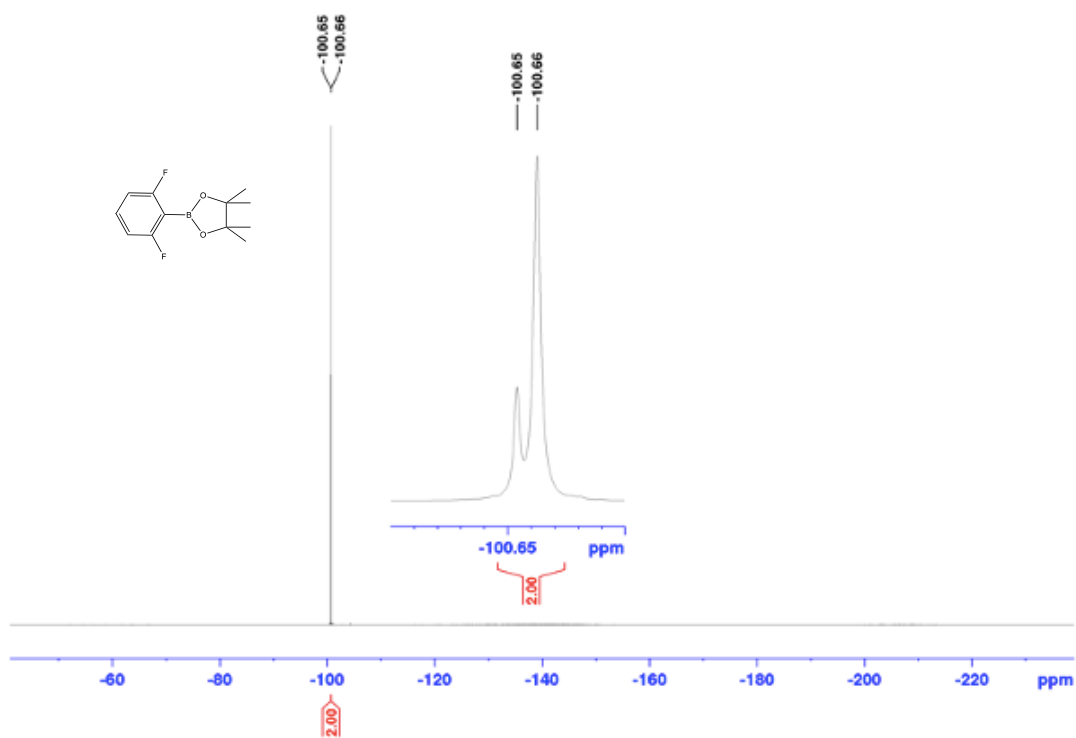
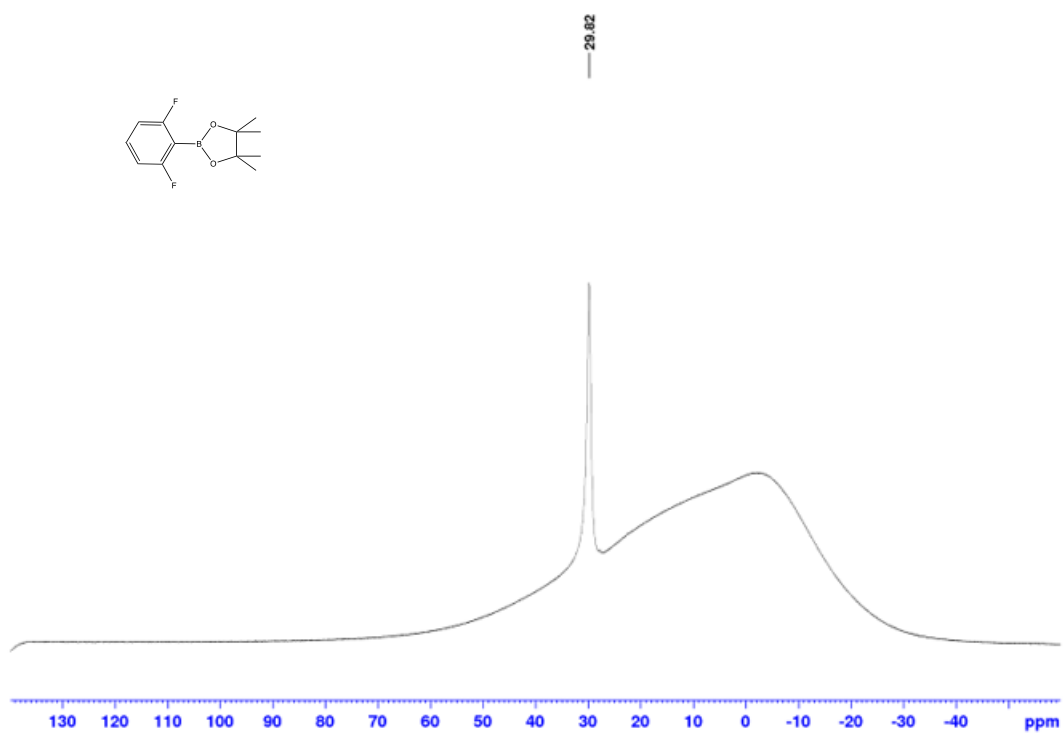
7.4 NMR Spectra for Chapter 4

^1H NMR spectrum of 4_2a (CDCl_3 , 500 MHz)

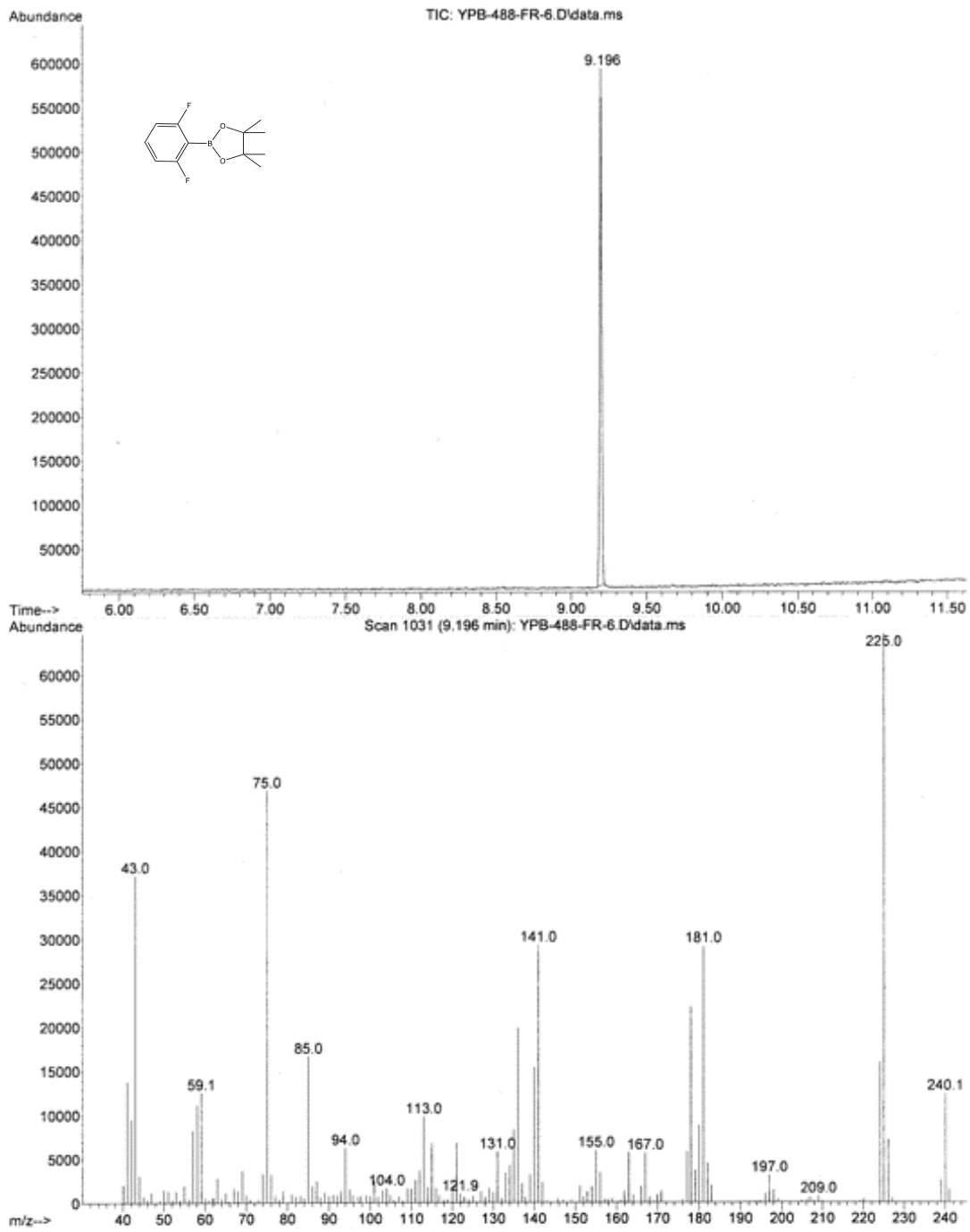


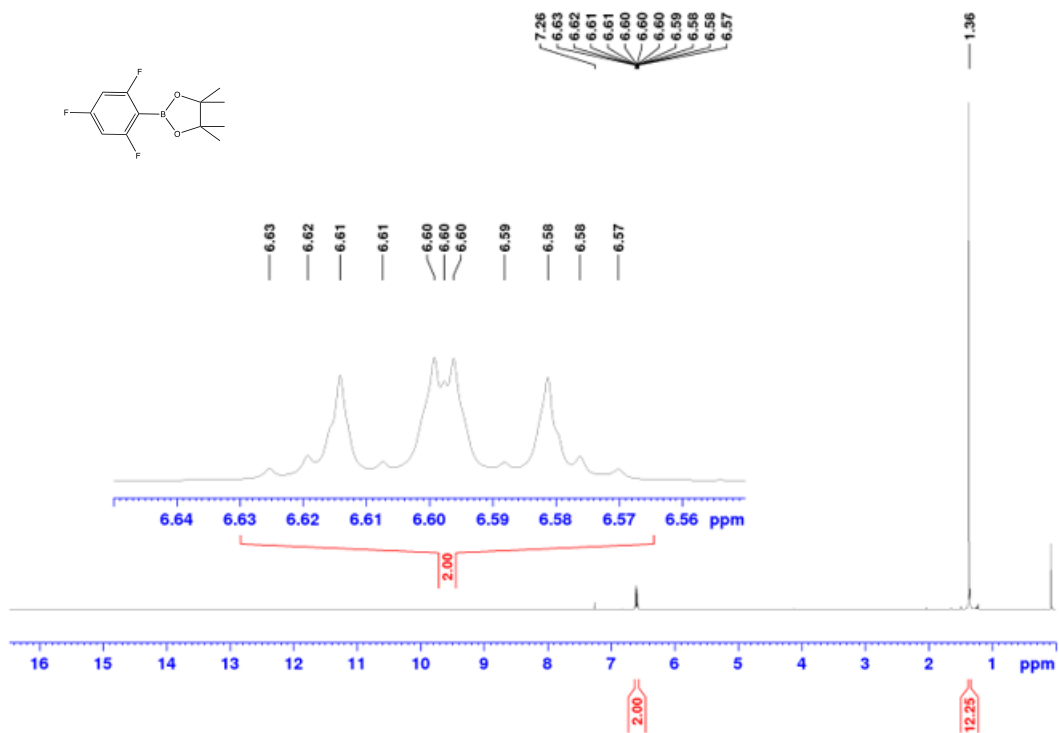
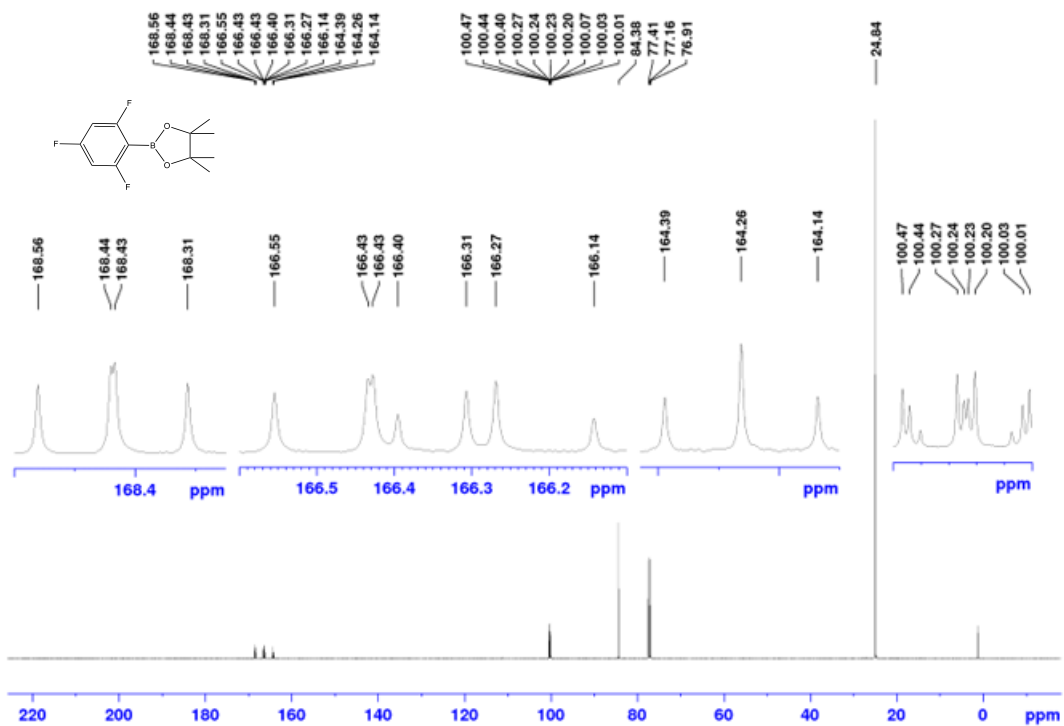
$^{13}\text{C}\{^1\text{H}\}$ NMR spectrum of 4_2a (CDCl_3 , 100 MHz)

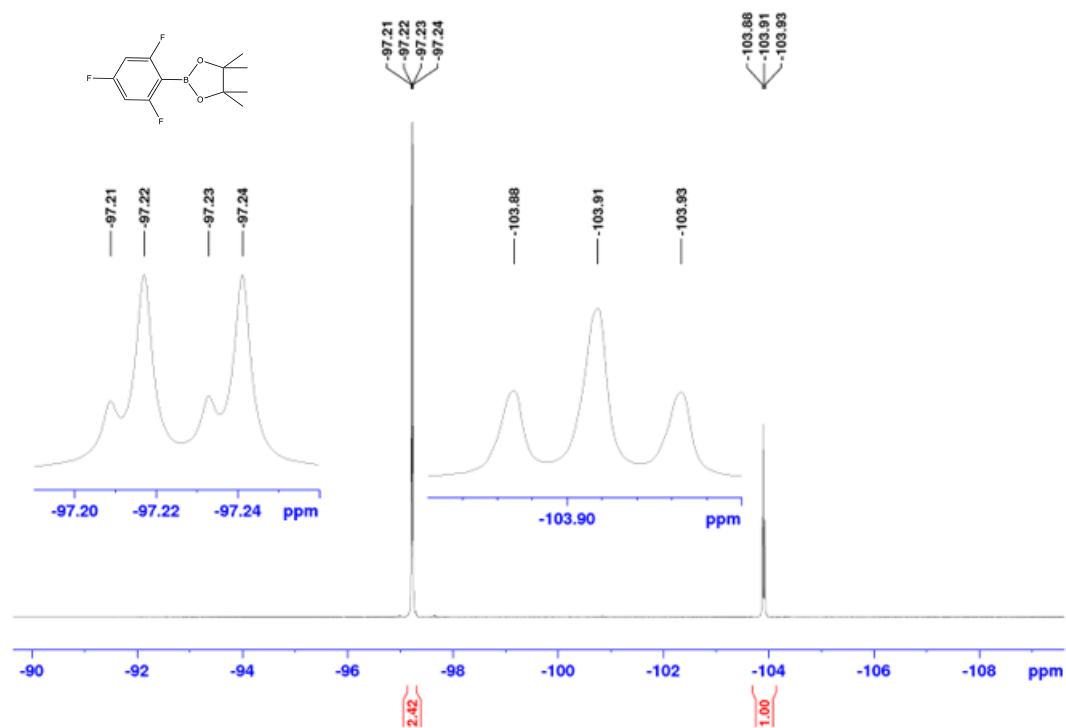
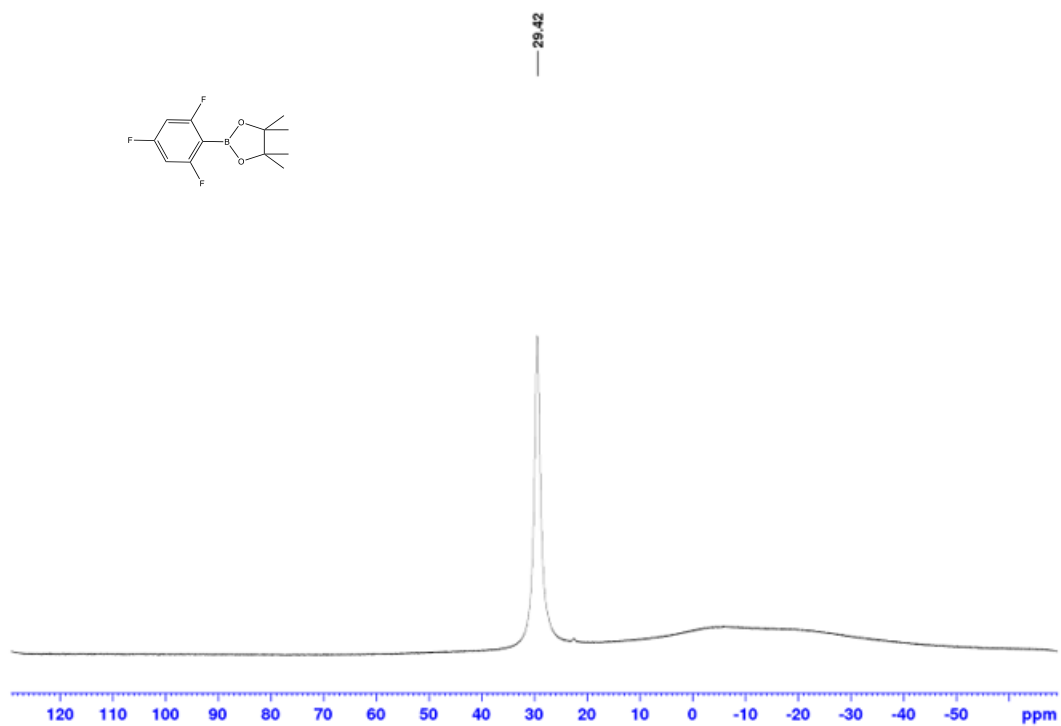


$^{19}\text{F}\{^1\text{H}\}$ NMR spectrum of 4_2a (CDCl_3 , 377 MHz) $^{11}\text{B}\{^1\text{H}\}$ NMR spectrum of 4_2a (160 MHz, CDCl_3)

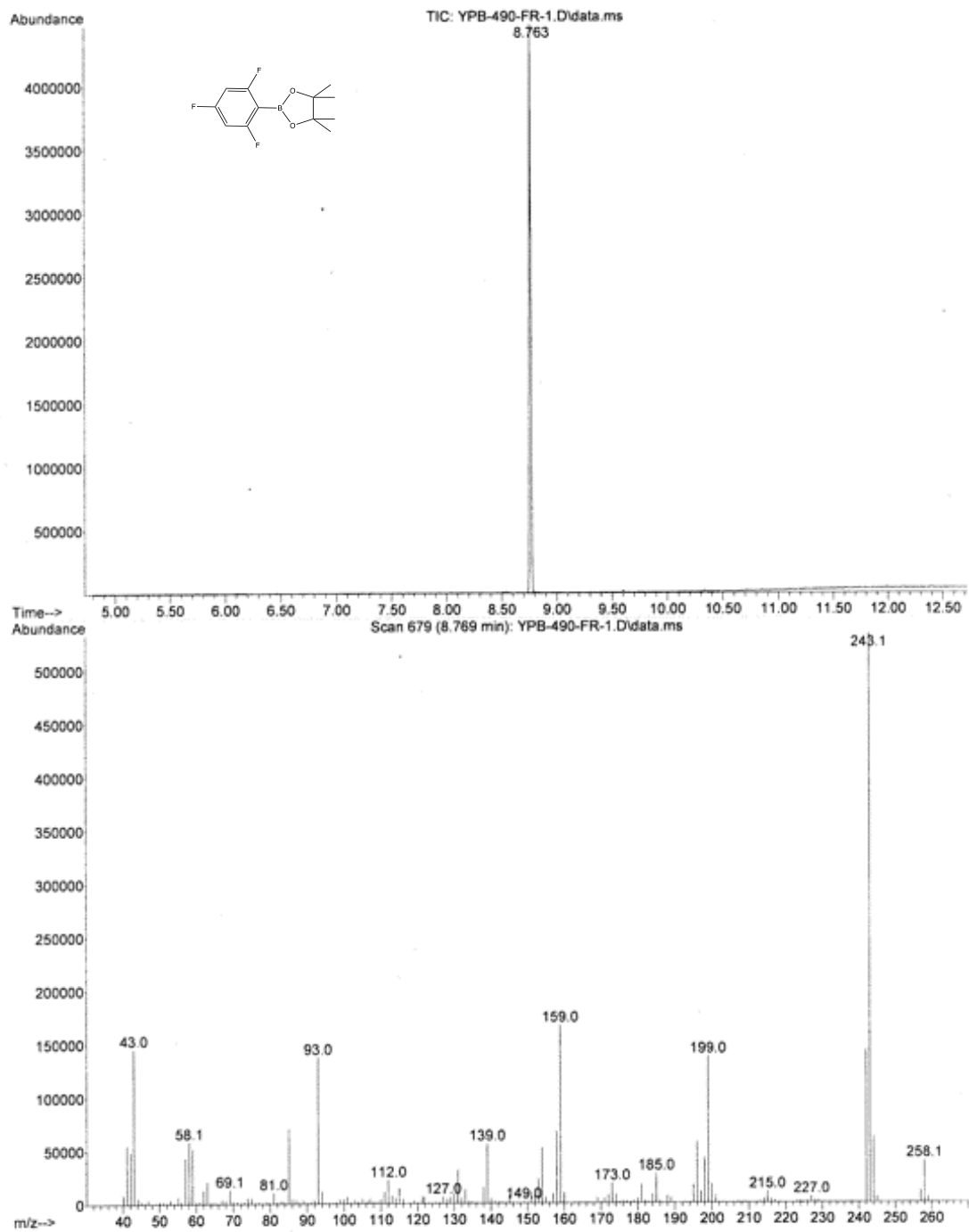
GC-MS of 4_2a

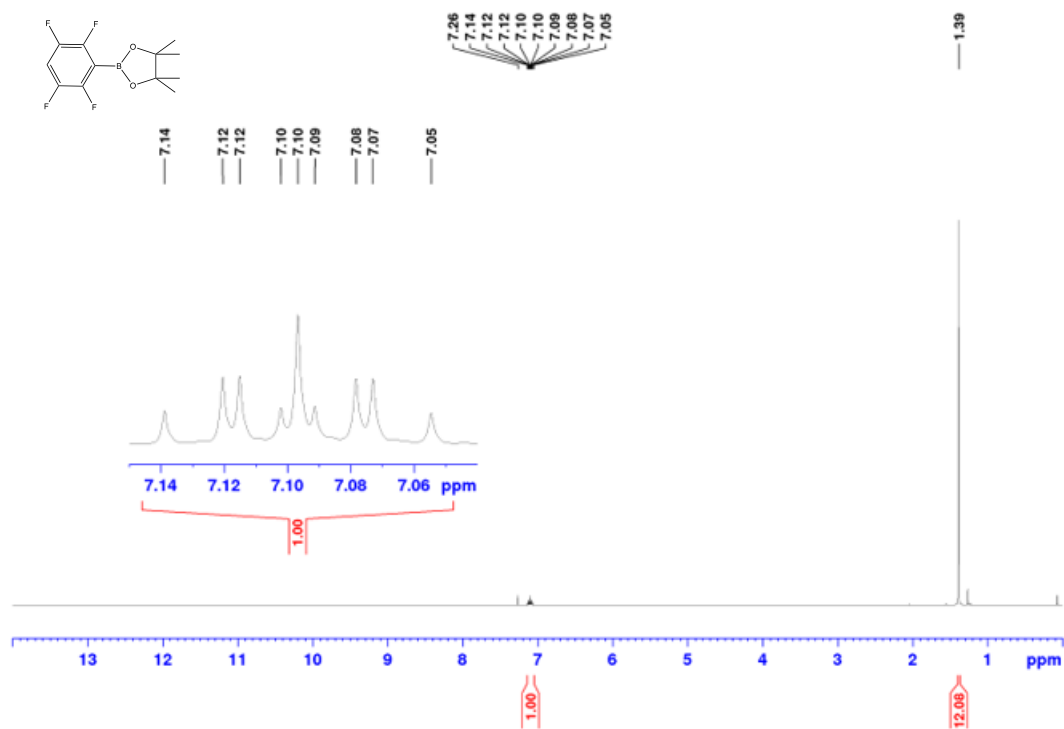
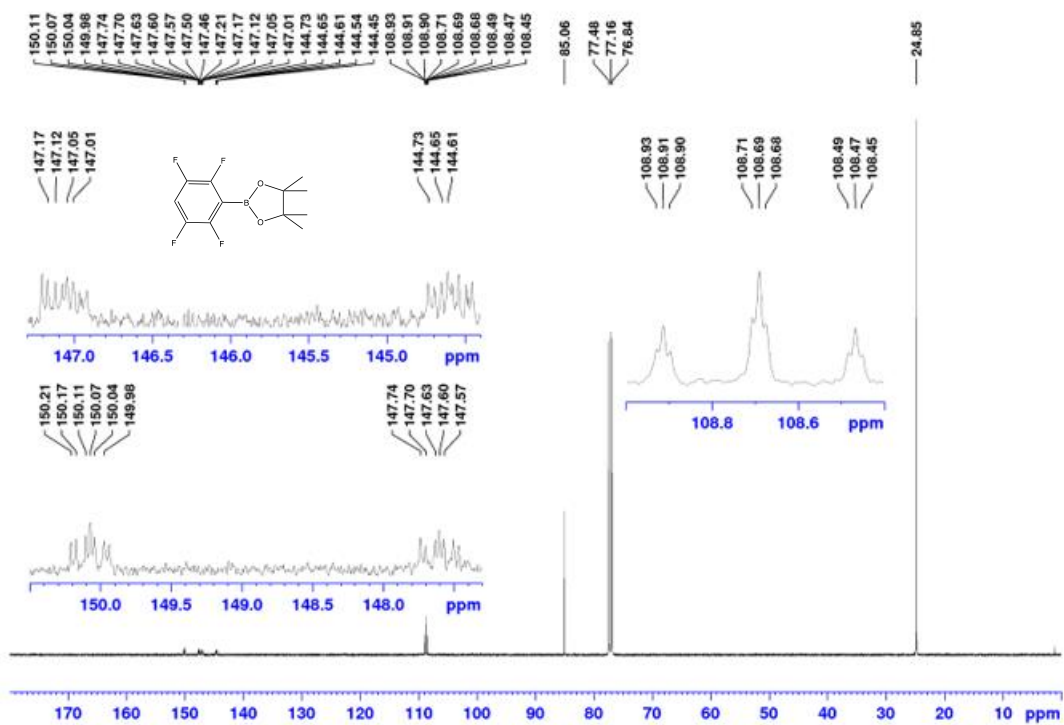


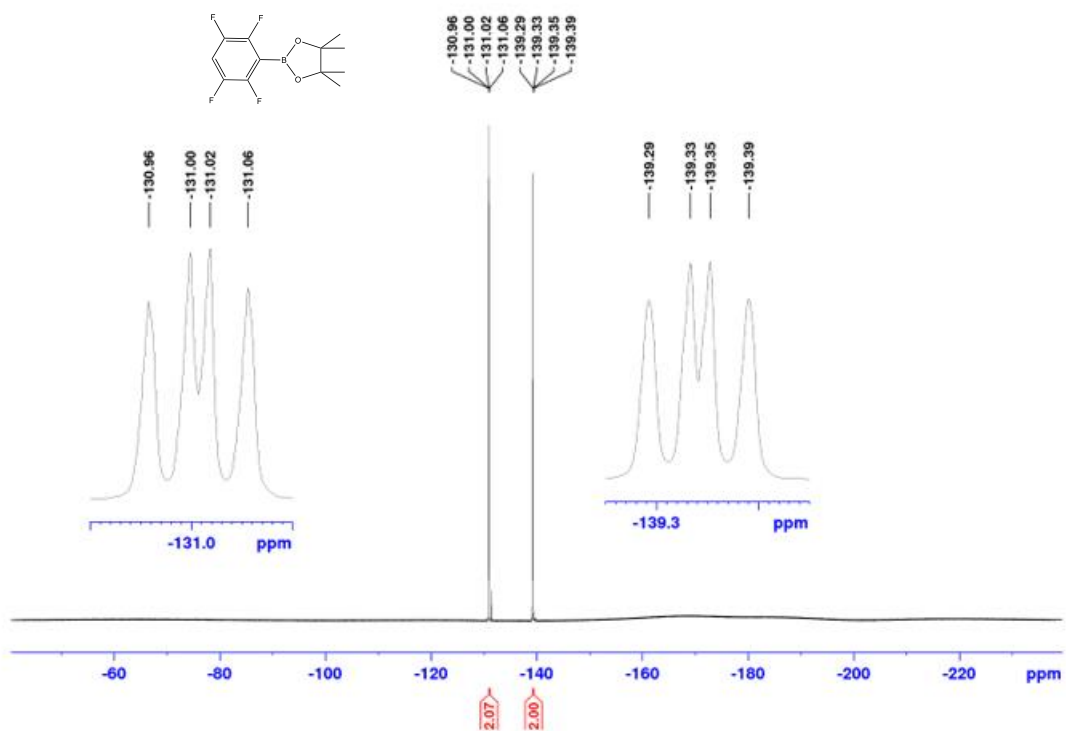
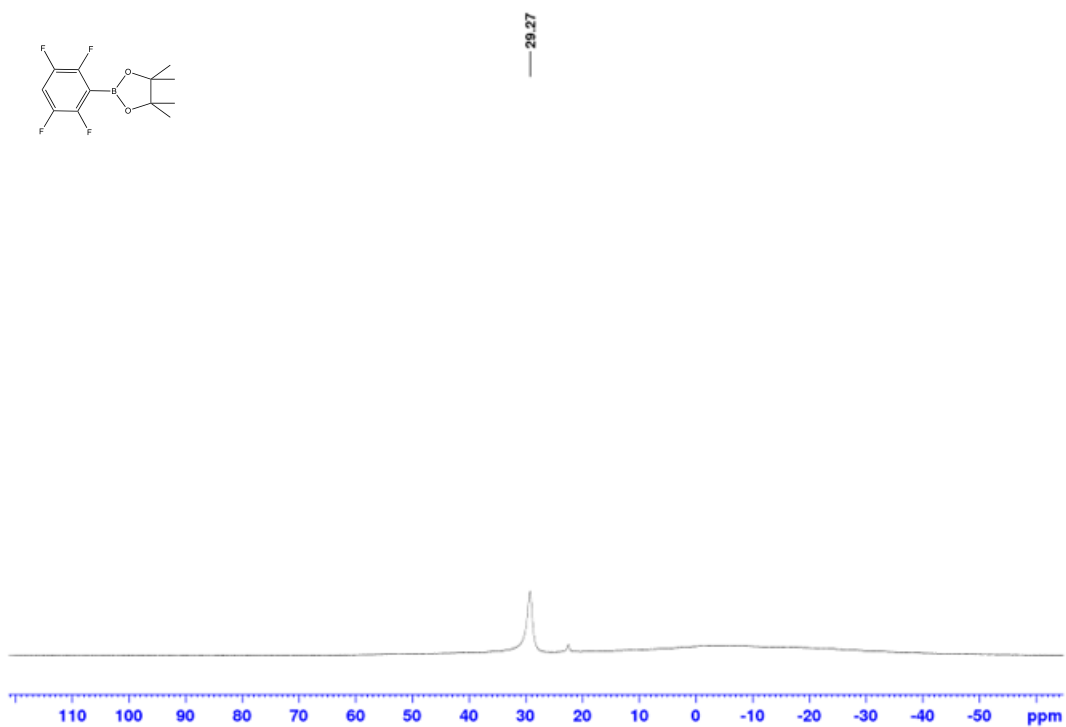
^1H NMR spectrum of 4_2b (CDCl_3 , 500 MHz) $^{13}\text{C}\{^1\text{H}\}$ NMR spectrum of 4_2b (CDCl_3 , 126 MHz)

$^{19}\text{F}\{^1\text{H}\}$ NMR spectrum of 4_2b (CDCl_3 , 377 MHz) $^{11}\text{B}\{^1\text{H}\}$ NMR spectrum of 4_2b (128 MHz, CDCl_3)

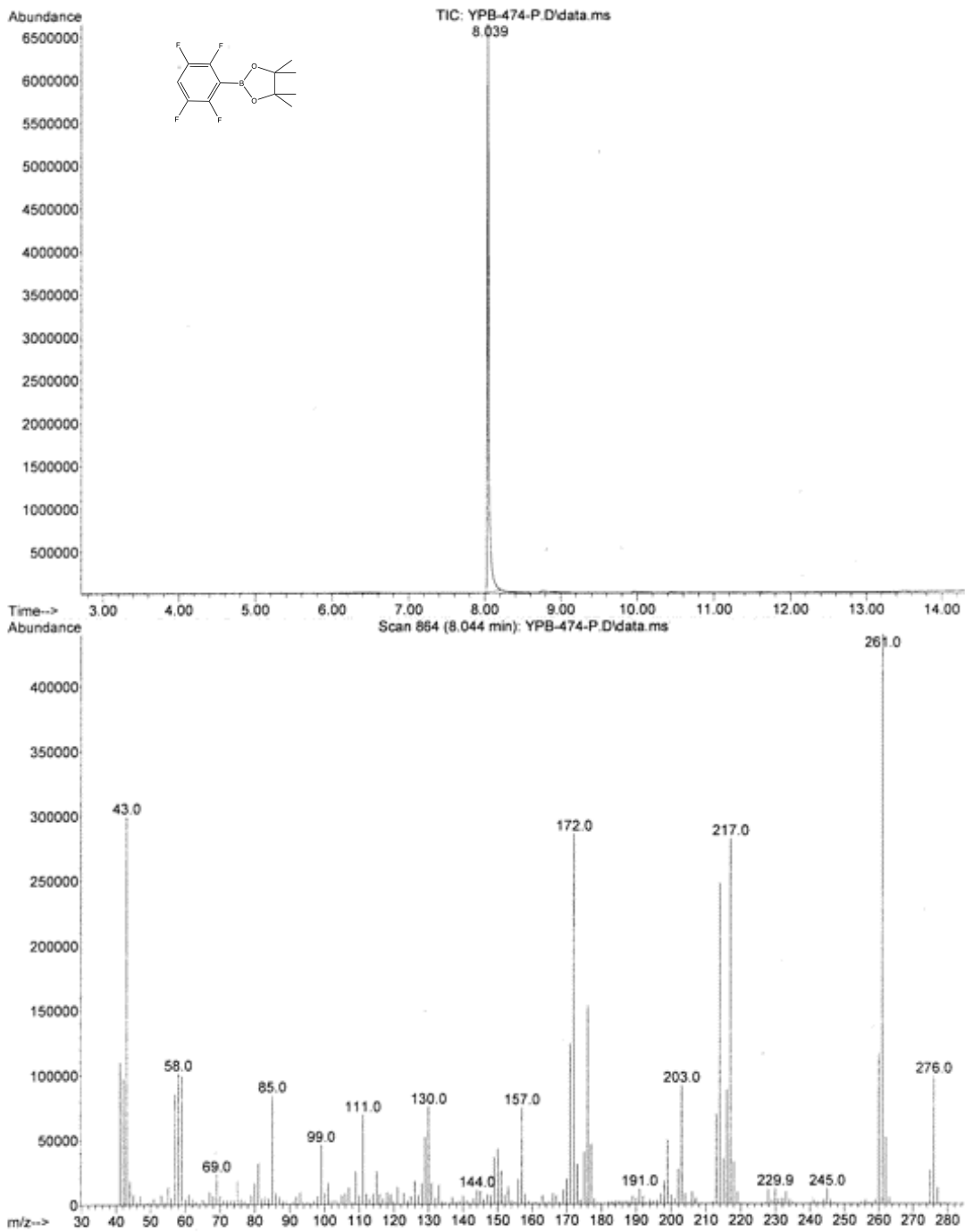
GC-MS of 4_2b

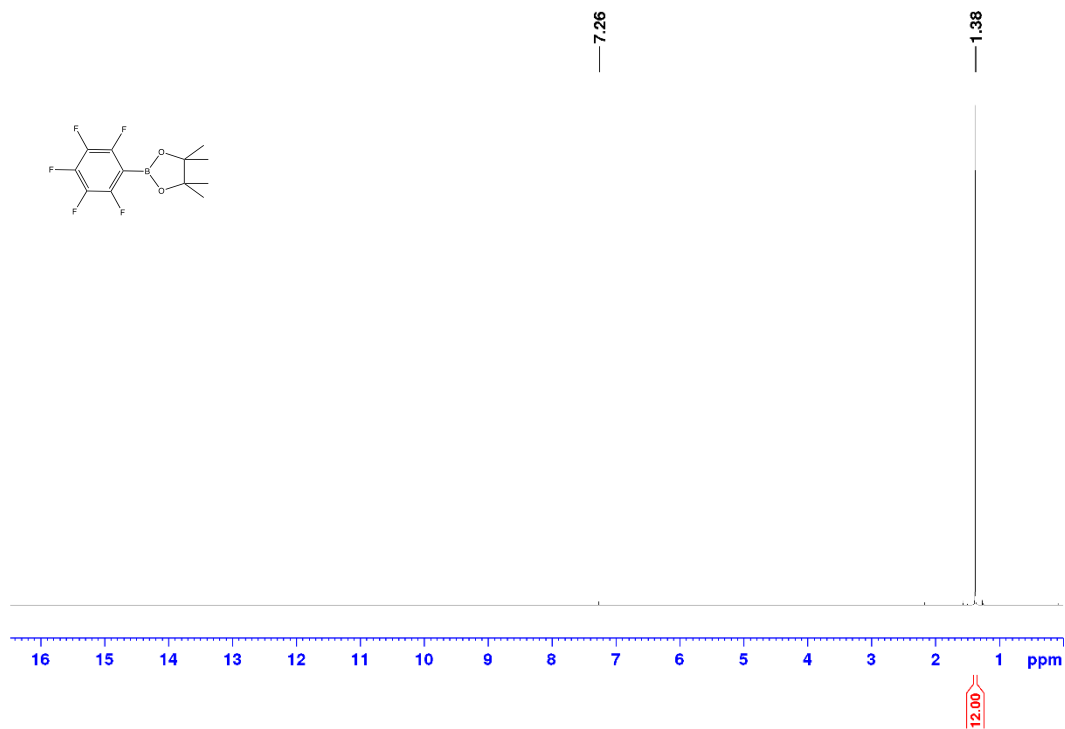
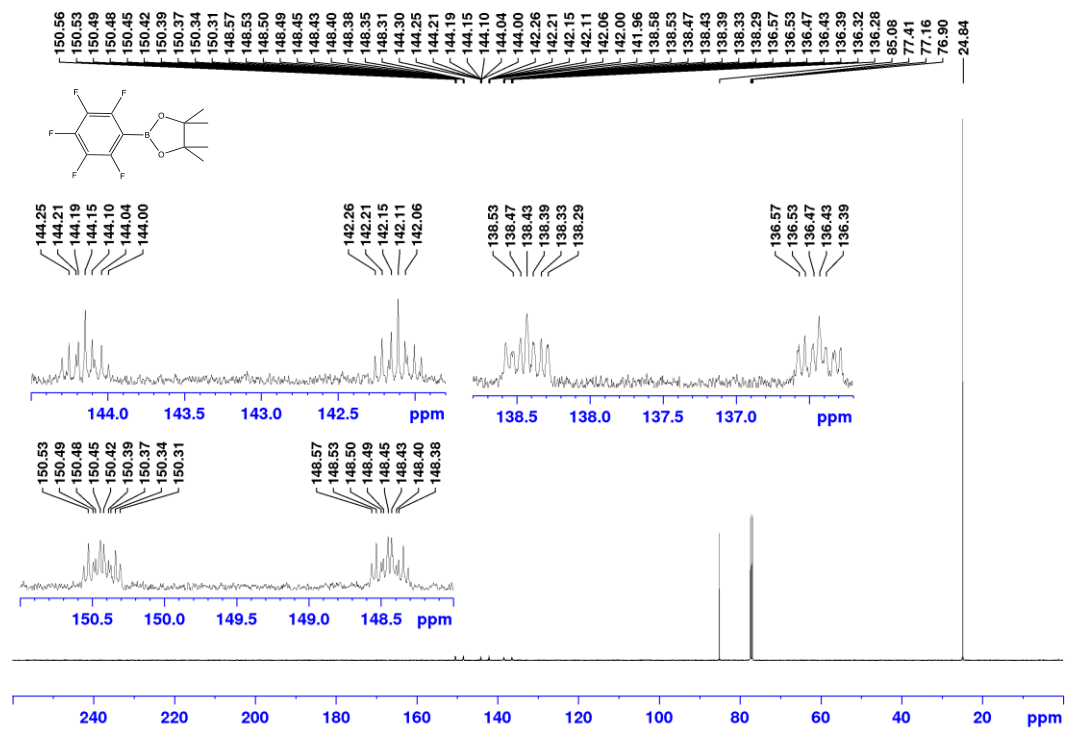


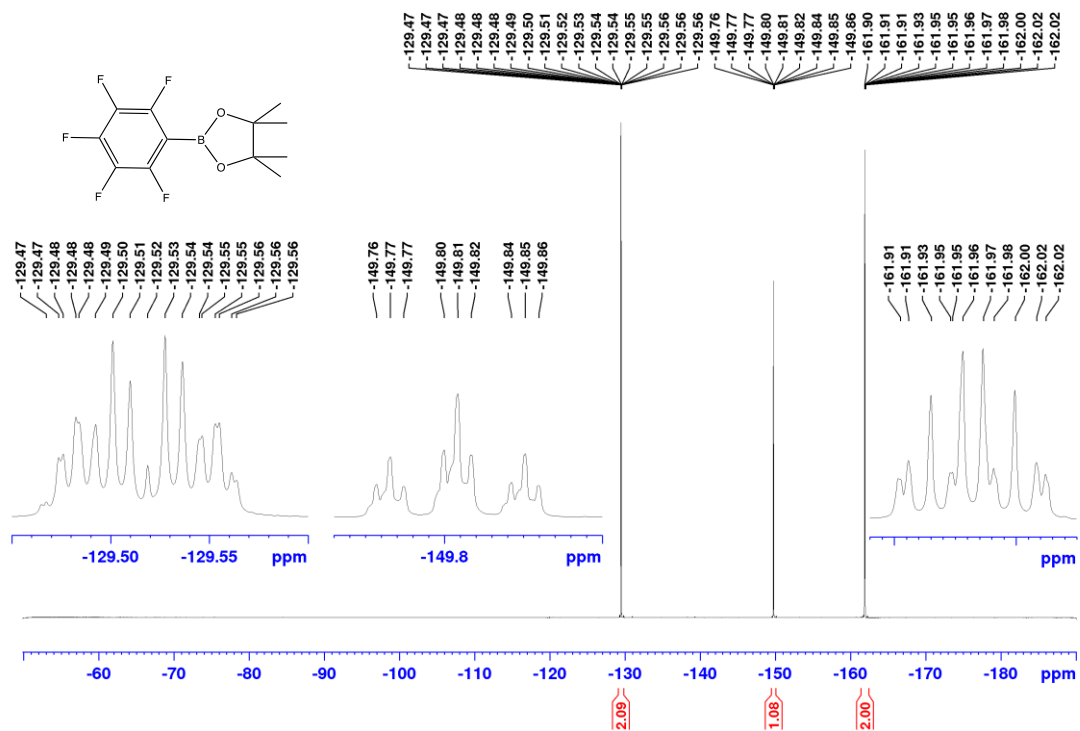
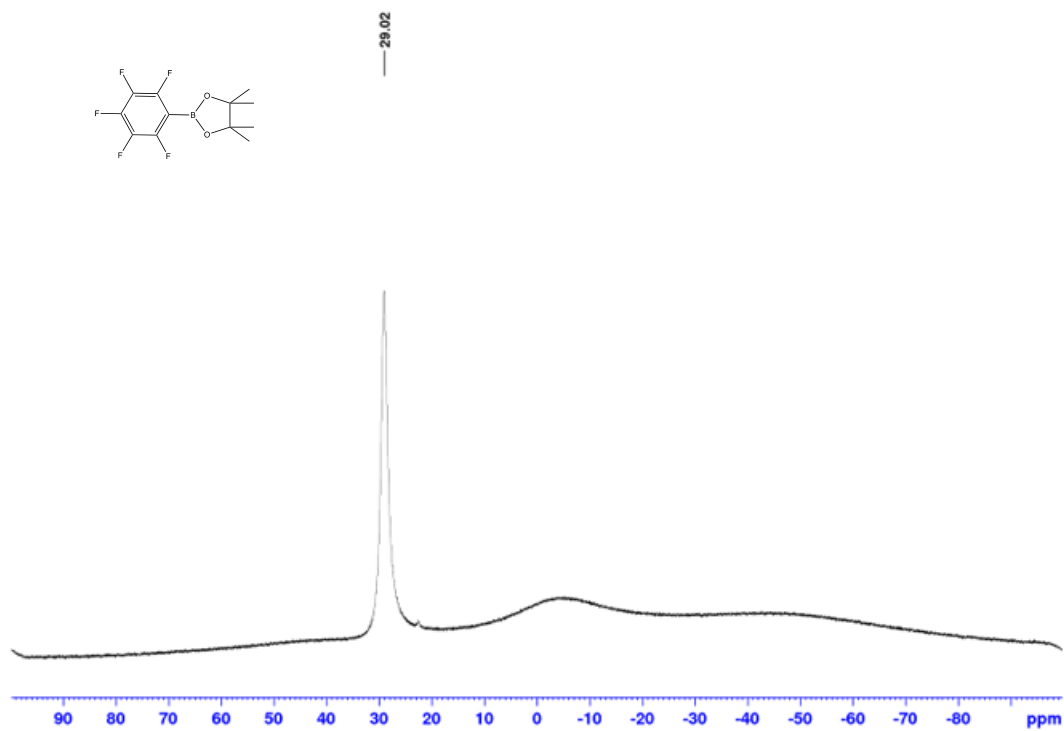
^1H NMR spectrum of 4_2c (CDCl_3 , 400 MHz) $^{13}\text{C}\{^1\text{H}\}$ NMR spectrum of 4_2c (CDCl_3 , 126 MHz)

$^{19}\text{F}\{^1\text{H}\}$ NMR spectrum of 4_2c (CDCl_3 , 377 MHz) $^{11}\text{B}\{^1\text{H}\}$ NMR spectrum of 4_2c (CDCl_3 , 128 MHz)

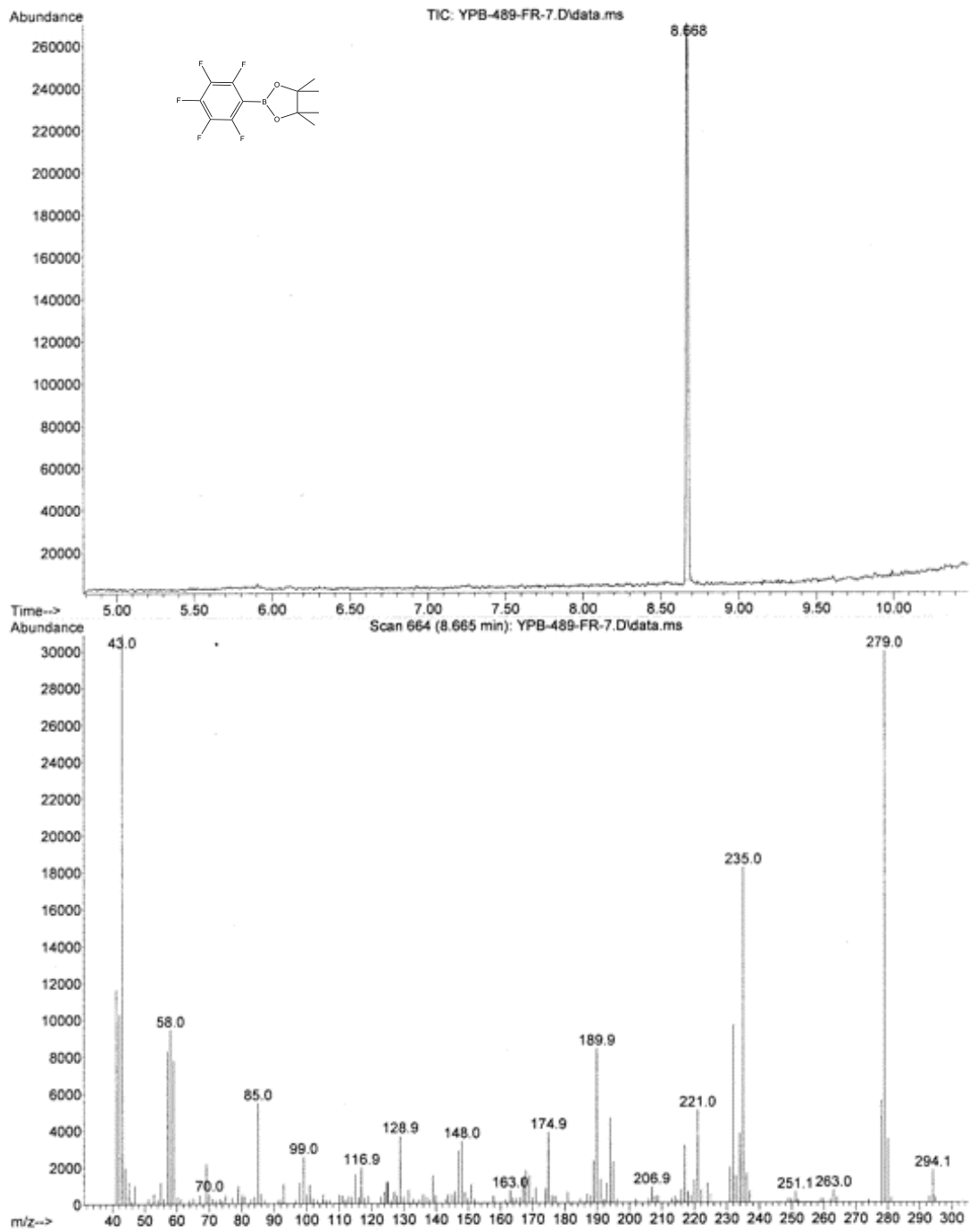
GC-MS of 4_2c

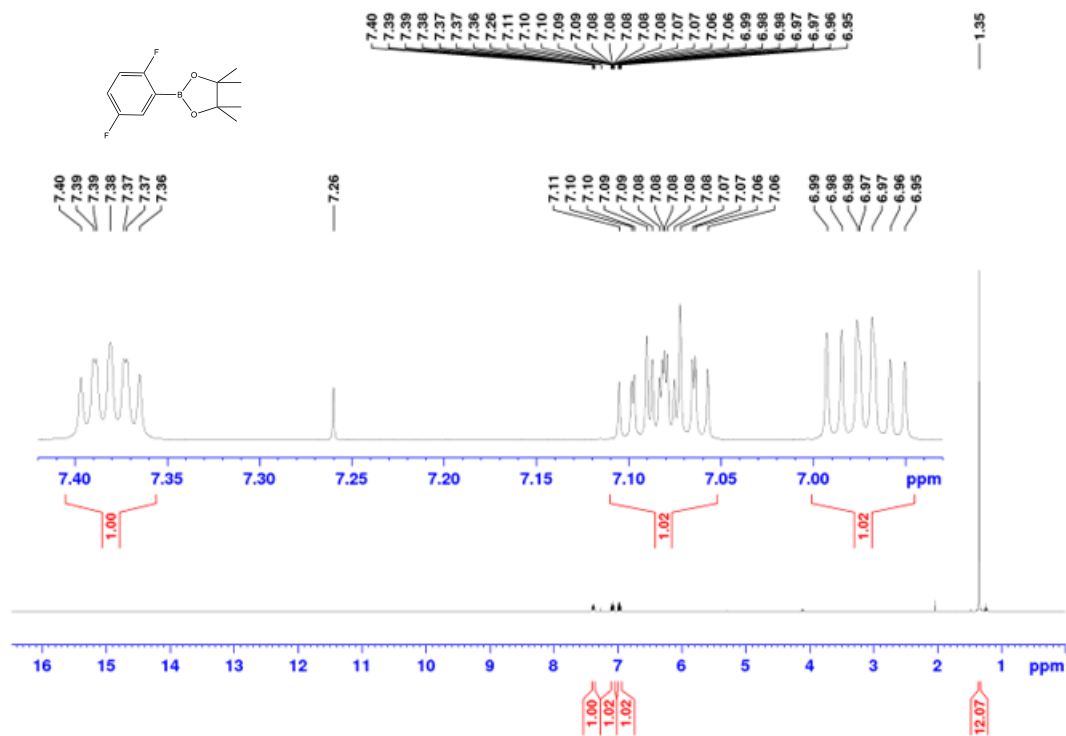
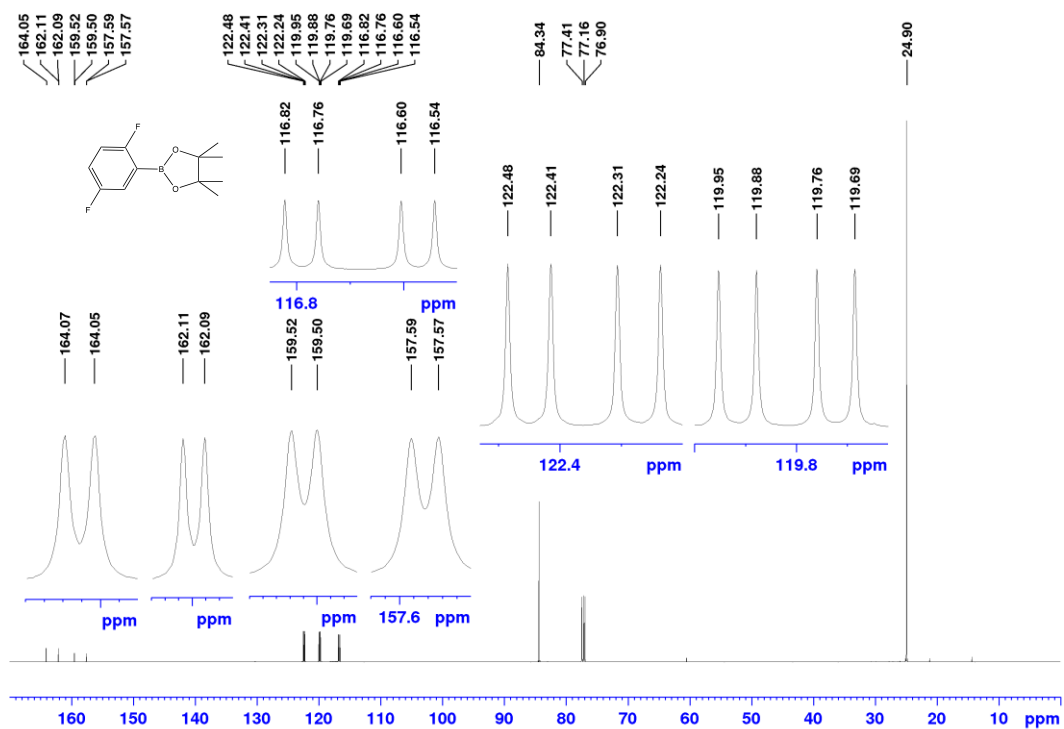


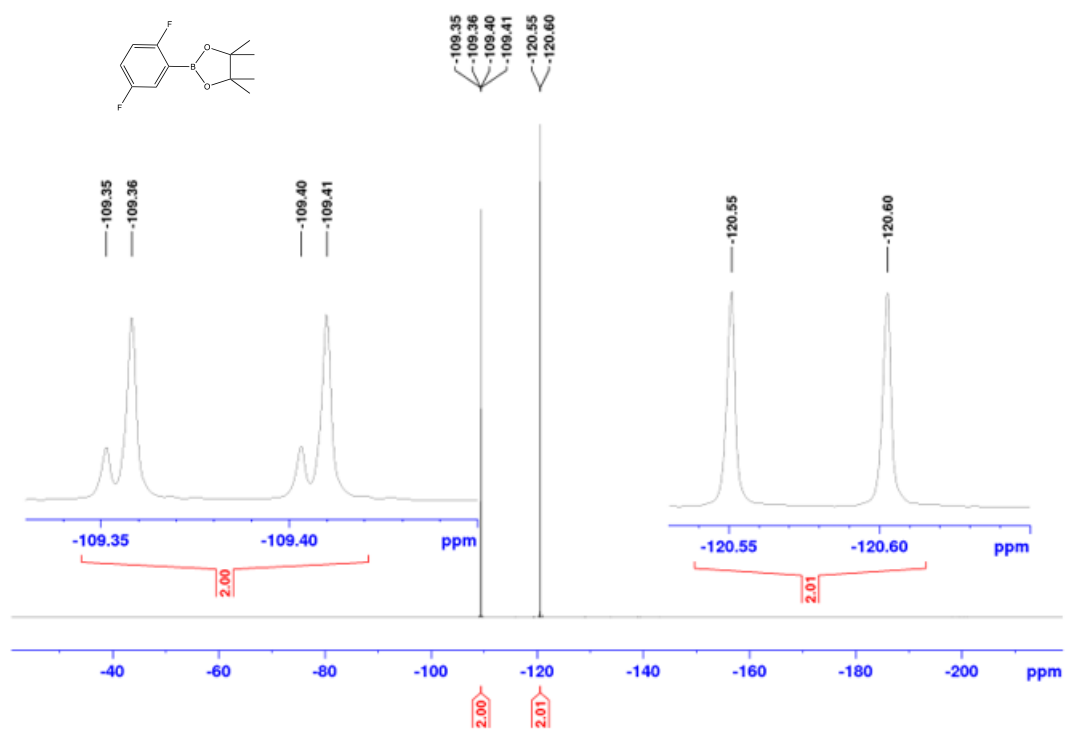
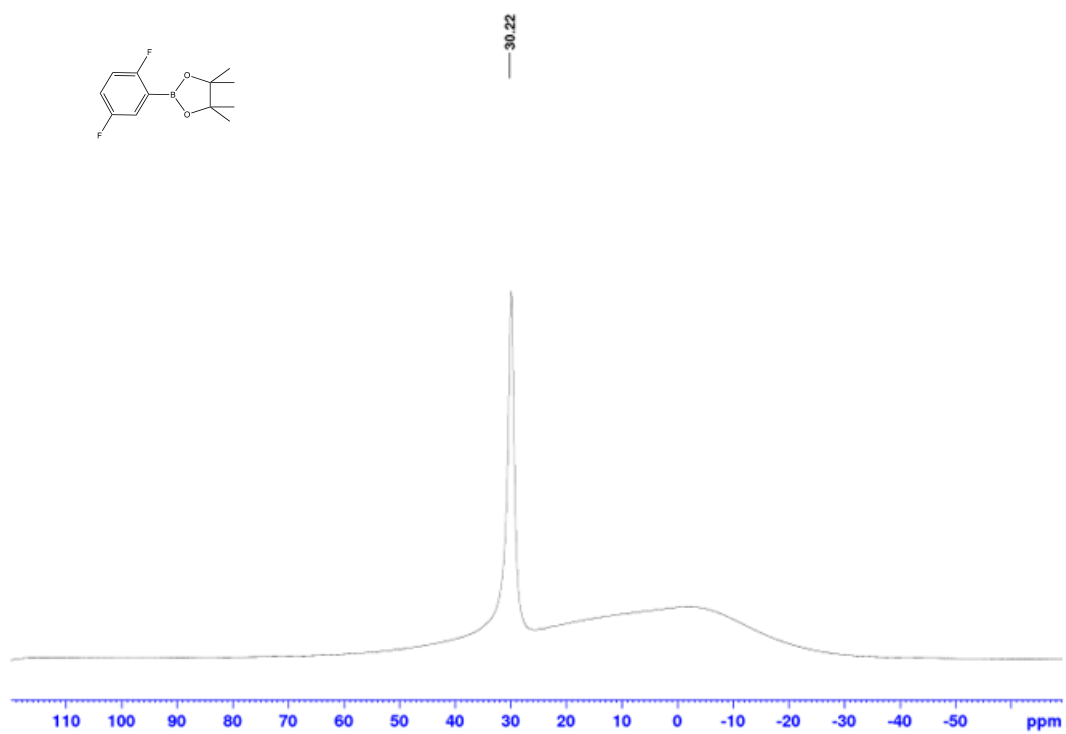
^1H NMR spectrum of 4_2d (CDCl_3 , 500 MHz) $^{13}\text{C}\{^1\text{H}\}$ NMR spectrum of 4_2d (CDCl_3 , 126 MHz)

^{19}F NMR spectrum of 4_2d (CDCl_3 , 471 MHz) $^{11}\text{B}\{^1\text{H}\}$ NMR spectrum of 4_2d (CDCl_3 , 96 MHz)

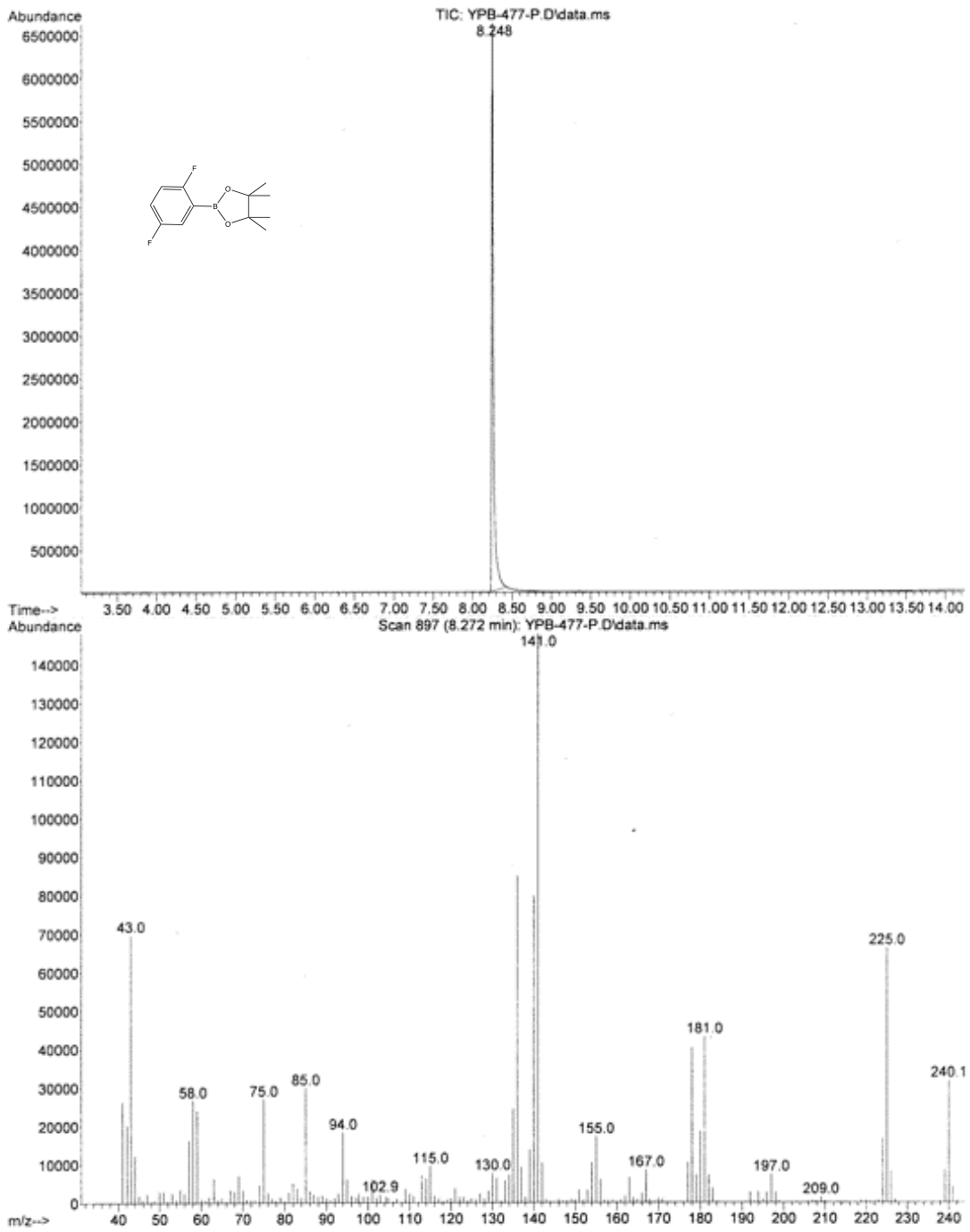
GC-MS of 4_2d

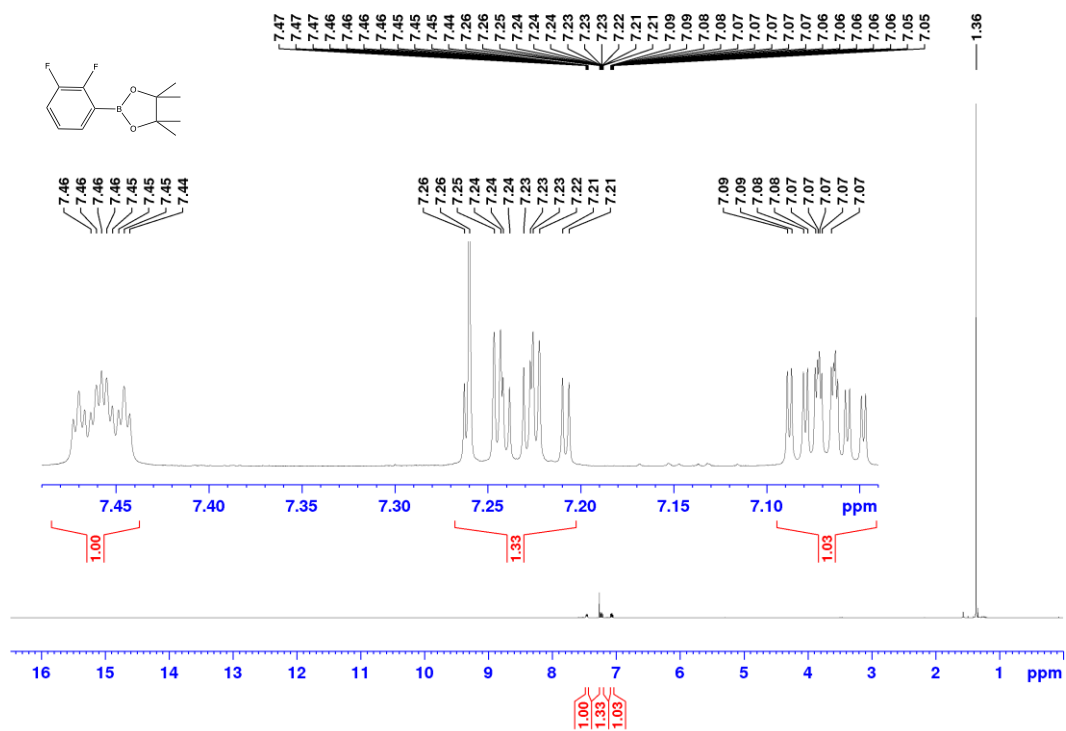
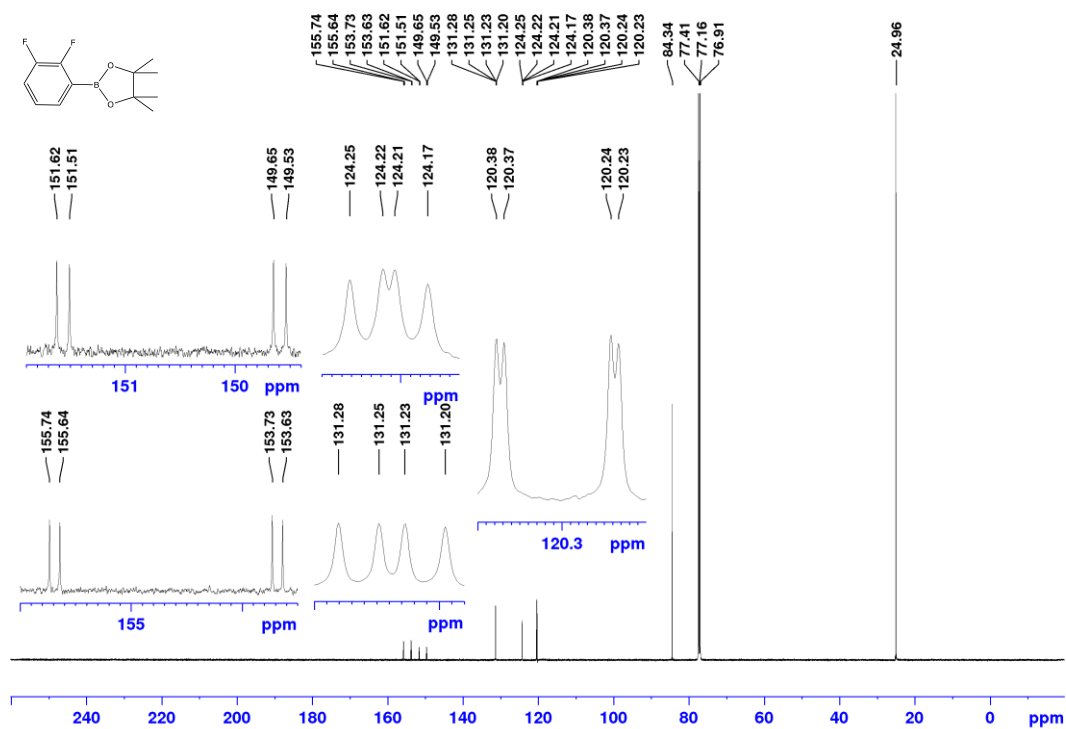


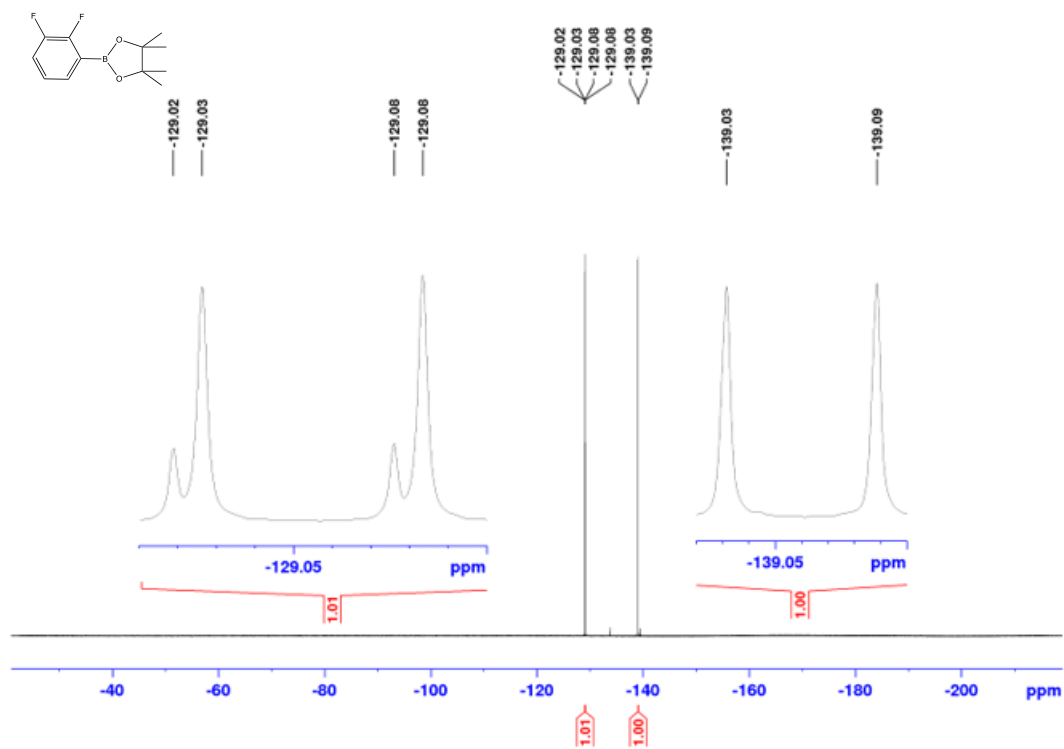
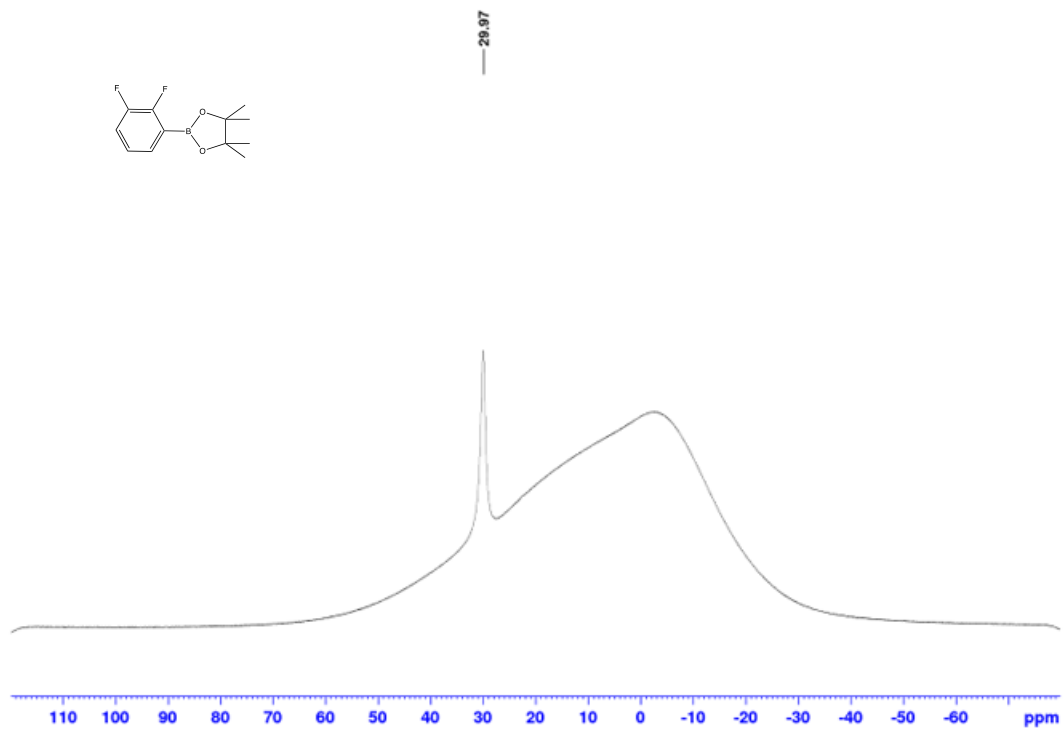
^1H NMR spectrum of 4_2e (CDCl_3 , 500 MHz) $^{13}\text{C}\{^1\text{H}\}$ NMR of 4_2e (CDCl_3 , 126 MHz)

$^{19}\text{F}\{^1\text{H}\}$ NMR 4_2e (CDCl_3 , 377 MHz) $^{11}\text{B}\{^1\text{H}\}$ NMR spectrum of 4_2e (CDCl_3 , 160 MHz)

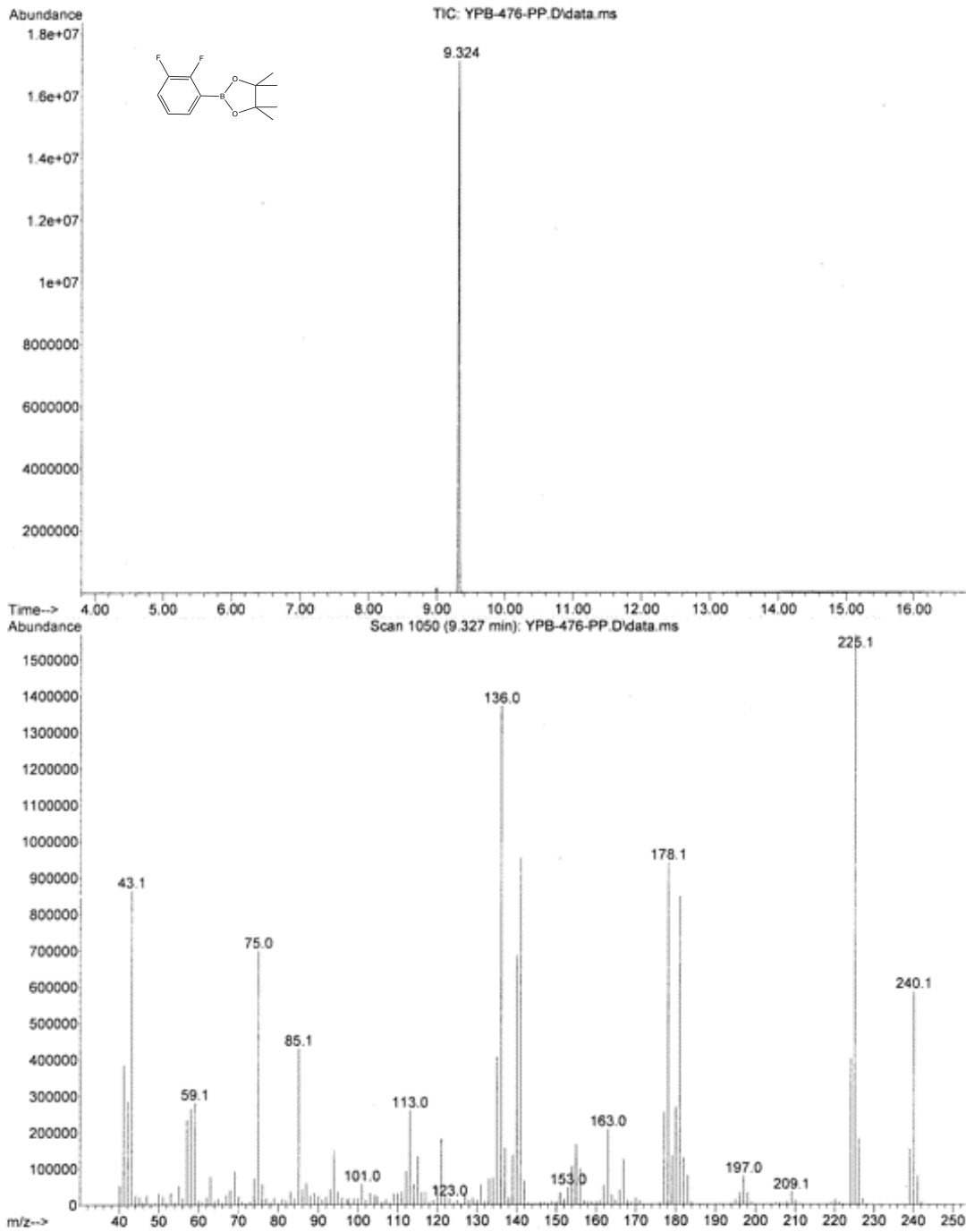
GC-MS of 4_2e

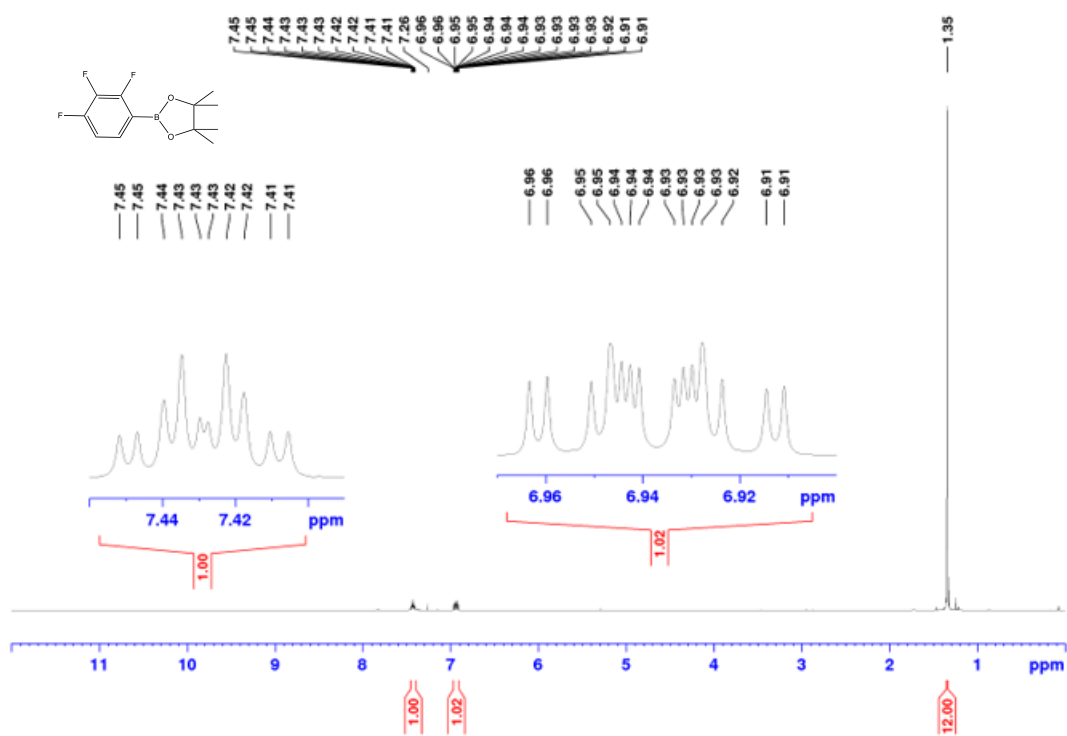
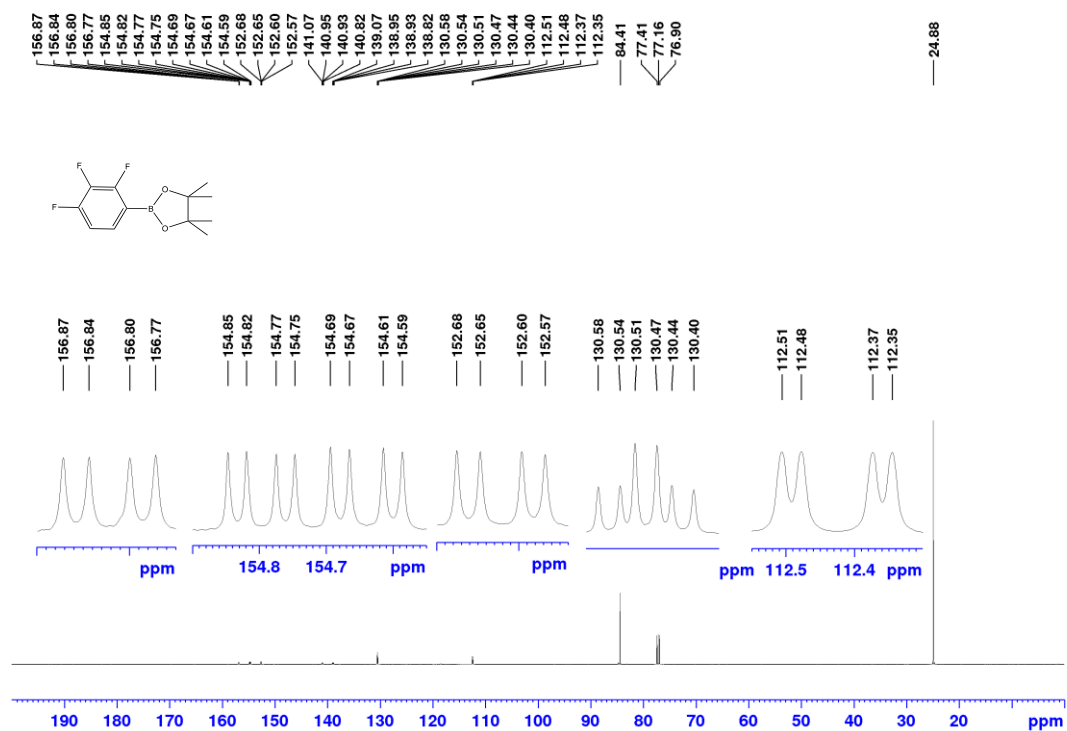


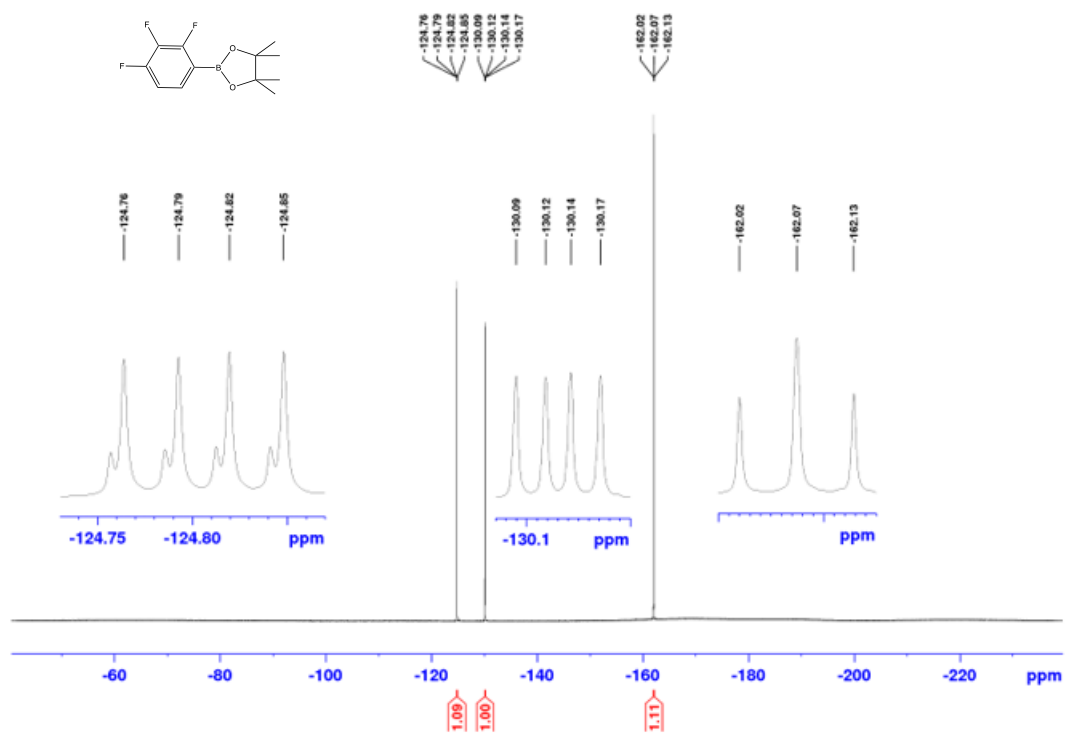
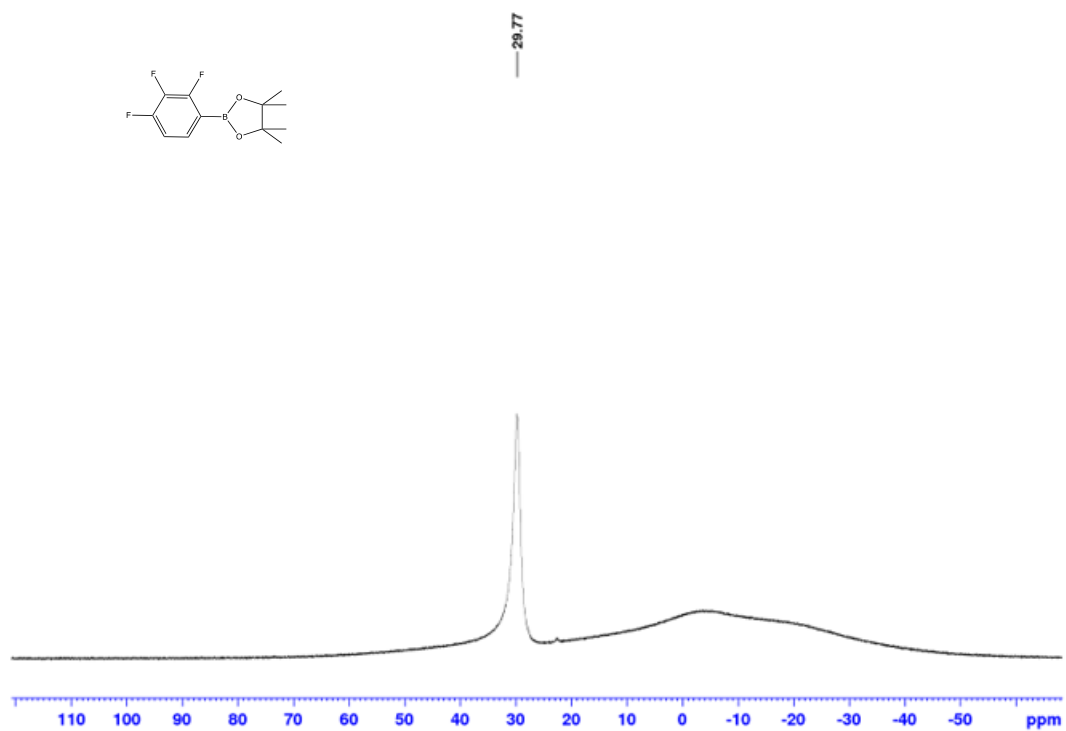
^1H NMR spectrum of 4_2f (CDCl₃, 500 MHz) $^{13}\text{C}\{^1\text{H}\}$ NMR of 4_2f (CDCl₃, 126 MHz)

$^{19}\text{F}\{^1\text{H}\}$ NMR 4_2f (CDCl_3 , 377 MHz) $^{11}\text{B}\{^1\text{H}\}$ NMR spectrum of 4_2f (CDCl_3 , 160 MHz)

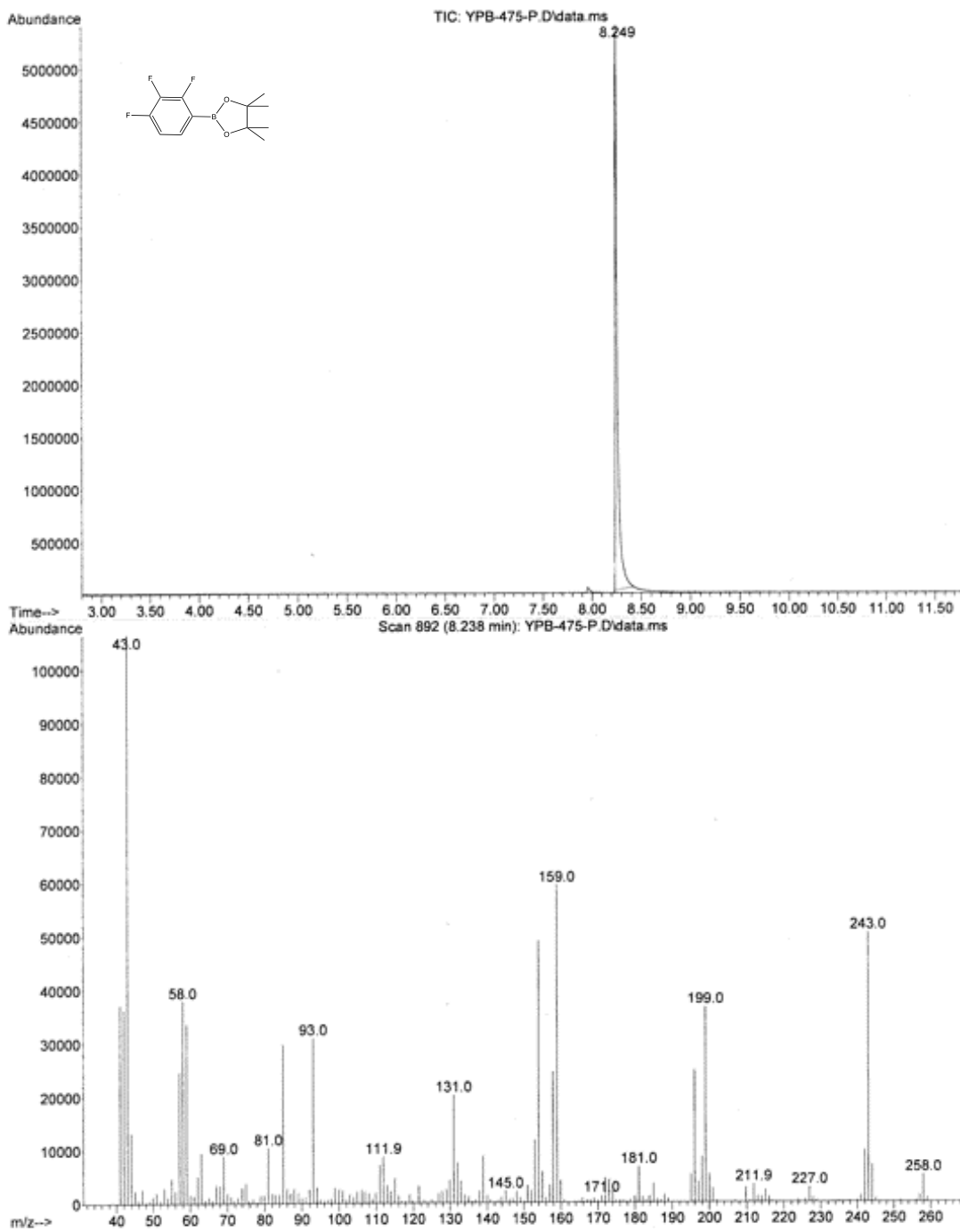
GC-MS of 4_2f

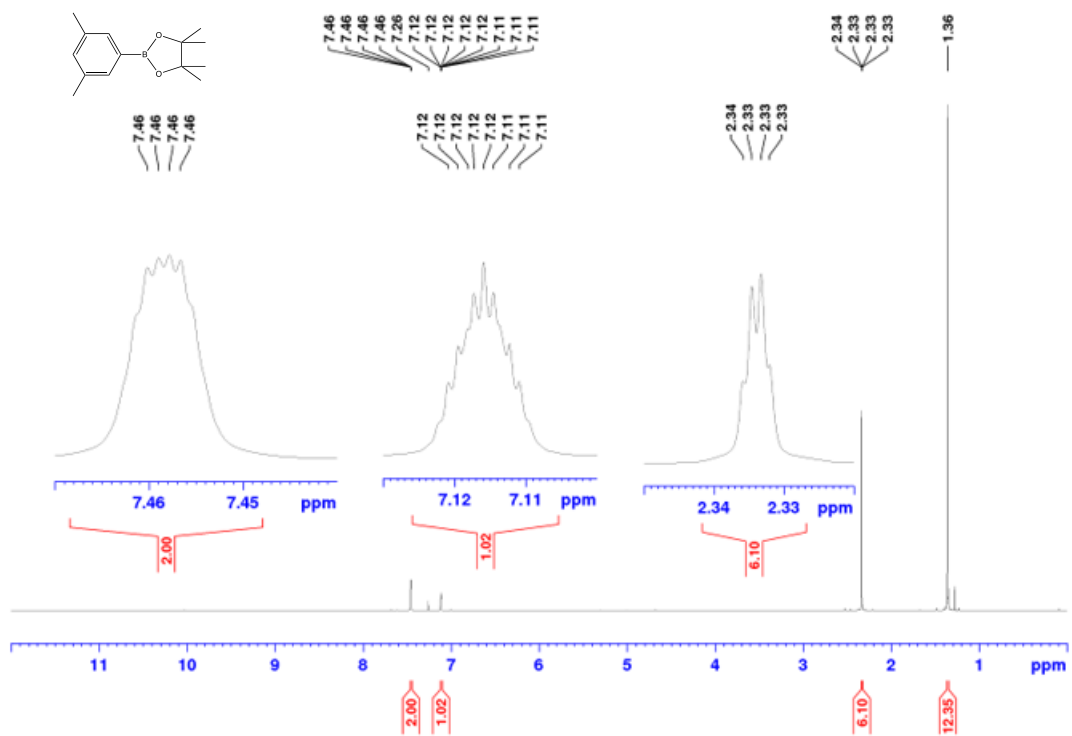
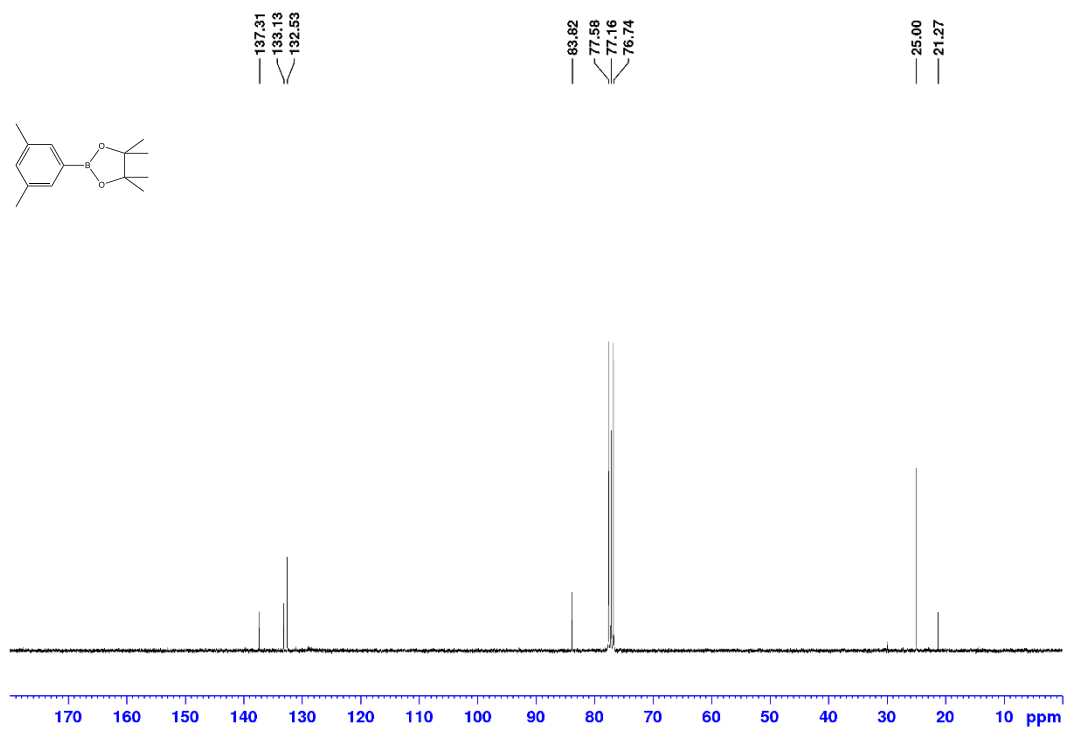


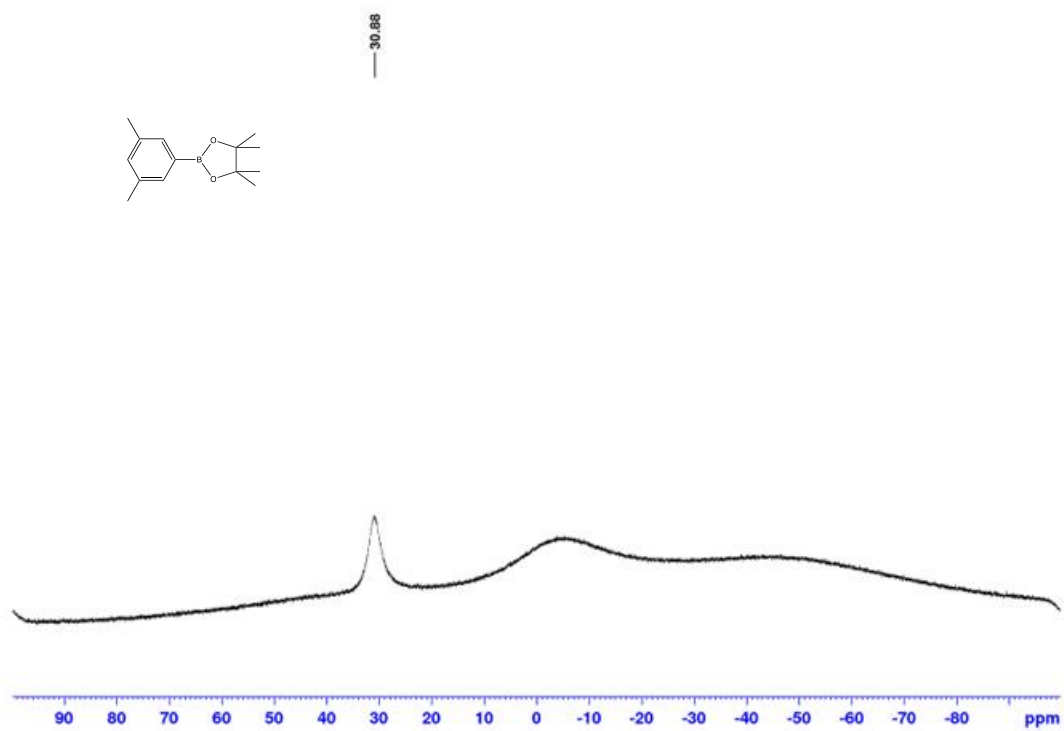
^1H NMR spectrum of 4_2g (CDCl_3 , 500 MHz) $^{13}\text{C}\{^1\text{H}\}$ NMR of 4_2g (CDCl_3 , 126 MHz)

$^{19}\text{F}\{^1\text{H}\}$ NMR of 4_2g (CDCl_3 , 377 MHz) $^{11}\text{B}\{^1\text{H}\}$ NMR of 4_2g (CDCl_3 , 128 MHz)

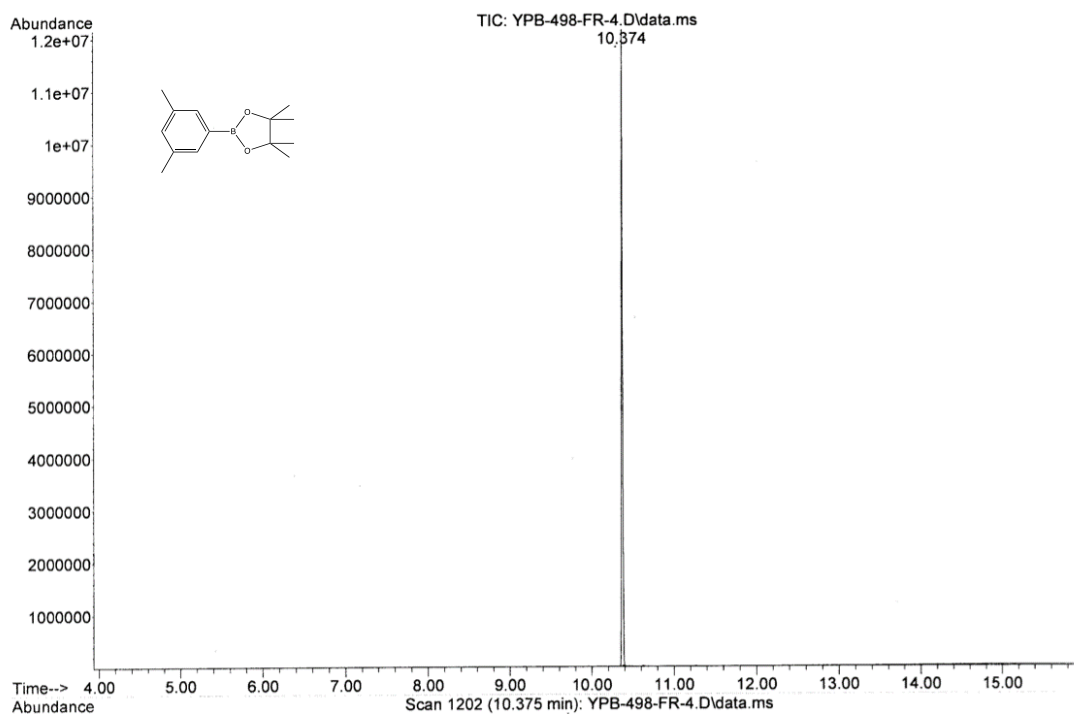
GC-MS of 4_2g



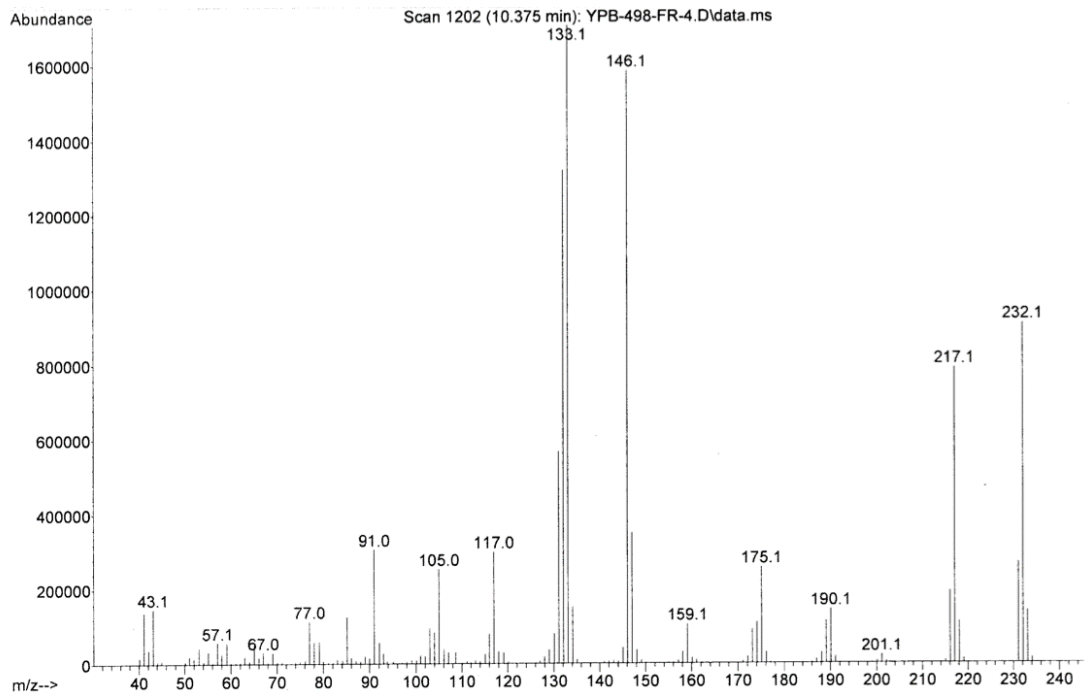
^1H NMR spectrum of 4_2h (CDCl_3 , 500 MHz) $^{13}\text{C}\{^1\text{H}\}$ NMR of 4_2h (CDCl_3 , 75 MHz)

$^{11}\text{B}\{^1\text{H}\}$ NMR of 4_2h (96 MHz, CDCl_3)

GC-MS of 4_2h



Appendix



Permission of Wiley-VCH

RightsLink[®]?
Help✉
Email Support**Copper-Catalysed Suzuki-Miyaura Cross-Coupling of Highly Fluorinated Aryl Boronate Esters with Aryl Iodides and Bromides and Fluoroarene-Arene π -Stacking Interactions in the Products**

Author: Yudha P. Budiman, Alexandra Friedrich, Udo Radius, et al

Publication: ChemCatChem

Publisher: John Wiley and Sons

Date: Aug 8, 2019

©201x The Authors. Published by Wiley-VCH Verlag GmbH & Co. KGaA.

Open Access Article

This is an open access article distributed under the terms of the [Creative Commons CC BY](#) license, which permits unrestricted use, distribution, and reproduction in any medium, provided the original work is properly cited.

You are not required to obtain permission to reuse this article.

For an understanding of what is meant by the terms of the Creative Commons License, please refer to [Wiley's Open Access Terms and Conditions](#).


Permission is not required for this type of reuse.

Wiley offers a professional reprint service for high quality reproduction of articles from over 1400 scientific and medical journals. Wiley's reprint service offers:

- Peer reviewed research or reviews
- Tailored collections of articles
- A professional high quality finish
- Glossy journal style color covers
- Company or brand customisation
- Language translations
- Prompt turnaround times and delivery directly to your office, warehouse or congress.

Please contact our Reprints department for a quotation. Email corporatesaleseurope@wiley.com or corporatesalesusa@wiley.com or corporatesalesDE@wiley.com.

Permission of American Chemical Society



RightsLink[®]


[Home](#)

[Help](#)

[Email Support](#)

[Sign in](#)

[Create Account](#)



ACS Publications
Most Trusted. Most Cited. Most Read.

Palladium-Catalyzed Homocoupling of Highly Fluorinated Arylboronates: Studies of the Influence of Strongly vs Weakly Coordinating Solvents on the Reductive Elimination Process

Author: Yudha P. Budiman, Arumugam Jayaraman, Alexandra Friedrich, et al
 Publication: Journal of the American Chemical Society
 Publisher: American Chemical Society
 Date: Apr 1, 2020

Copyright © 2020, American Chemical Society

Quick Price Estimate

This service provides permission for reuse only. If you do not have a copy of the portion you are using, you may copy and paste the content and reuse according to the terms of your agreement. Please be advised that obtaining the content you license is a separate transaction not involving RightsLink.

TM Permission for this particular request is granted for print and electronic formats, and translations, at no charge. Figures and tables may be modified. Appropriate credit should be given. Please print this page for your records and provide a copy to your publisher. Requests for up to 4 figures require only this record. Five or more figures will generate a printout of additional terms and conditions. Appropriate credit should read: "Reprinted with permission from {COMPLETE REFERENCE CITATION}. Copyright {YEAR} American Chemical Society." Insert appropriate information in place of the capitalized words.

I would like to... ?	reuse in a Thesis/Dissertation ▼	Will you be translating? ?	No ▼
Requestor Type ?	Author (original work) ▼	Select your currency	EUR - € ▼
Portion ?	Full article ▼	Quick Price	Click Quick Price
Format ?	Print and Electronic ▼		

QUICK PRICE

CONTINUE

To request permission for a type of use not listed, please contact [the publisher](#) directly.

© 2020 Copyright - All Rights Reserved | [Copyright Clearance Center, Inc.](#) | [Privacy statement](#) | [Terms and Conditions](#)
 Comments? We would like to hear from you. E-mail us at customercare@copyright.com



RightsLink®



Home



Help



Email Support



Sign in



Create Account

Palladium-Catalyzed Homocoupling of Highly Fluorinated Arylboronates: Studies of the Influence of Strongly vs Weakly Coordinating Solvents on the Reductive Elimination Process



Author: Yudha P. Budiman, Arumugam Jayaraman, Alexandra Friedrich, et al

Publication: Journal of the American Chemical Society

Publisher: American Chemical Society

Date: Apr 1, 2020

Copyright © 2020, American Chemical Society

PERMISSION/LICENSE IS GRANTED FOR YOUR ORDER AT NO CHARGE

This type of permission/license, instead of the standard Terms & Conditions, is sent to you because no fee is being charged for your order. Please note the following:

- Permission is granted for your request in both print and electronic formats, and translations.
- If figures and/or tables were requested, they may be adapted or used in part.
- Please print this page for your records and send a copy of it to your publisher/graduate school.
- Appropriate credit for the requested material should be given as follows: "Reprinted (adapted) with permission from (COMPLETE REFERENCE CITATION). Copyright (YEAR) American Chemical Society." Insert appropriate information in place of the capitalized words.
- One-time permission is granted only for the use specified in your request. No additional uses are granted (such as derivative works or other editions). For any other uses, please submit a new request.

BACK

CLOSE WINDOW

Affidavit

I hereby confirm that my theses entitled “*Applications of Fluorinated Aryl Boronates in Organic Synthesis*” is the result of my own work. I did not receive any help or support from commercial consultants. All sources and/or materials applied are listed and specified in the thesis. Furthermore, I confirm that this thesis has not yet been submitted as part of another examination process neither in identical nor similar form.

Würzburg, 26.10.2020

Signature

Eidesstaatliche Erklärung

Hiermit erkläre ich an Eides statt, die Dissertation „*Applications of Fluorinated Aryl Boronates in Organic Synthesis*” eigenständig, d.h. insbesondere selbstständig und ohne Hilfe eines kommerziellen Promotionsberaters angefertigt und keinen anderen als die von mir angegebenen Quellen und Hilfsmittel verwendet zu haben. Ich erkläre außerdem, dass die Dissertation weder in gleicher noch ähnlicher Form bereits in einem anderen Prüfungsverfahren vorgelegen hat.

Würzburg, 26.10.2020

Unterschrift